TRANSPORTATION RESEARCH
RECORD

No. 1286

Highway and Facility Design

Design and Evaluation of Rigid and Flexible Pavements 1990

A peer-reviewed publication of the Transportation Research Board

TRANSPORTATION RESEARCH BOARD
NATIONAL RESEARCH COUNCIL
WASHINGTON, D.C. 1990

Transportation Research Record 1286
Price: $40.00

Subscriber Category
IIA highway and facility design

Modes
1 highway transportation
3 rail transportation

Subject Areas
24 pavement design and performance
63 soil and rock mechanics

TRB Publications Staff
Director of Publications: Nancy A. Ackerman
Senior Editor: Naomi C. Kassabian
Associate Editor: Alison G. Tobias
Assistant Editors: Luanne Crayton, Kathleen Solomon, Norman Solomon
Graphics Coordinator: Diane L. Ross
Production Coordinator: Karen S. Waugh
Office Manager: Phyllis D. Barber
Production Assistant: Betty L. Hawkins

Printed in the United States of America

Library of Congress Cataloging-in-Publication Data
National Research Council. Transportation Research Board.

Design and evaluation of rigid and flexible pavements.
p. cm.—(Transportation research record, ISSN 0361-1981 ; no. 1286)
Papers prepared for the 69th Annual Meeting of the Transportation Research Board.
"A peer-reviewed publication of the Transportation Research Board."
ISBN 0-309-05070-7
1. Pavements—Performance. 2. Flexible pavements—Design and construction. 3. Pavements, Concrete—Design and construction. I. National Research Council (U.S.). Transportation Research Board. Meeting (69th : 1990 : Washington, D.C.) II. Series. III. Series: Transportation research record ; 1286.
TE251.5.D47 1990
625.8—dc20 91-10115
CIP

Sponsorship of Transportation Research Record 1286

GROUP 2—DESIGN AND CONSTRUCTION OF TRANSPORTATION FACILITIES
Chairman: Raymond A. Forsyth, Sacramento, California

Pavement Management Section
Chairman: R. G. Hicks, Oregon State University

Committee on Rigid Pavement Design
Chairman: Walter P. Kilareski, Penn State University
Don R. Alexander, Ernest J. Barenberg, Brian T. Bock, Kathleen Theresa Hall, Amir N. Hanna, John E. Hunt, Michael P. Jones, Starr D. Kohn, Roger Larson, Jo A. Lary, Robert R. Long, Jr., Richard A. McComb, B. Frank McCullough, Theodore L. Neff, Mauricio R. Poblete, Gary Wayne Sharpe, Shiraz D. Tayabji, Mang Tia, James H. Woodstrom, William A. Yrjanson, John P. Zaniewski, Terrence L. Zoller, Dan G. Zollinger

Committee on Flexible Pavement Design
Chairman: Joe P. Mahoney, Department of Civil Engineering, University of Washington
Secretary: Chris A. Bell, Department of Civil Engineering, Oregon State University
Douglas I. Anderson, Uno Arebratt, Jaques Bonnot, Elton R. Brow, James L. Brown, Stephen F. Brown, George R. Cochran, N. F. Coetzee, David C. Esch, C. R. Freeme, Wilbur Charles Greer, Jr., Newton Jackson, W. N. Lofroos, Kenneth H. McGhee, Carl L. Monismith, William A. Nokes, John L. Rice, James A. Scherocman, Peter Sebaaly, James A. Sherwood, James F. Shook, Herbert F. Southgate, T. Paul Teng, Marshall R. Thompson, Harry H. Ulery, Jr.

Geology and Properties of Earth Materials Section
Chairman: William Lovell, Purdue University

Committee on Frost Action
Chairman: Thomas C. Kinney, University of Alaska–Fairbanks
Kenneth O. Anderson, Richard L. Berg, Frederick M. Boyce, Edwin J. Chamberlain, George R. Cochran, Barry J. Dempsey, Denis E. Donnelly, David C. Esch, Wilbur M. Haas, Neil F. Hawks, Larry K. Heinig, Ira J. Huddleston, Newton Jackson, Ronald H. Jones, Hiroshi Kubo, C. William Lovell, Joe P. Mahoney, Melvin W. Morgan, Mary Rutherford, John A. Shuster, Ted S. Vinson, Gary C. Whited, Chen Xiaobai, Qiang Zhu

Committee on Environmental Factors Except Frost
Chairman: Robert L. Lytton, Texas A & M University
Warren T. Bennett, Michael L. Bunting, Samuel H. Carpenter, Fu Hua Chen, Koon Meng Chua, Judith B. Corley, Barry J. Dempsey, Gary L. Fitts, Donald G. Fohs, Donald J. Janssen, Lawrence D. Johnson, Amos Komornik, C. William Lovell, Joseph Massucco, Said Ossama Mazen, R. Gordon McKeen, Thomas M. Petry, Miguel Picornell, Rogel H. Prysock, Albert C. Ruckman, Larry A. Scofield, Malcolm L. Steinberg, Jacob Uzan, Gdalyah Wiseman

George W. Ring III, Transportation Research Board staff

Sponsorship is indicated by a footnote at the end of each paper. The organizational units, officers, and members are as of December 31, 1989.

Transportation Research Record 1286

Contents

Foreword	**vii**
Field Investigation of Punchout Distress in Continuously Reinforced Concrete Pavement in Illinois *Dan G. Zollinger and Ernest J. Barenberg*	1
Aggregate Interlock: A Pure-Shear Load Transfer Mechanism *Anastasios M. Ioannides and George T. Korovesis*	14
Mechanistic Design Considerations for Punchout Distress in Continuously Reinforced Concrete Pavement *Dan G. Zollinger and Ernest J. Barenberg*	25
Prestressed Concrete Pavement: Instrumentation, Behavior, and Analysis of Horizontal Movements *Elliott David Mandel, Ned H. Burns, and B. Frank McCullough*	38
Control of Faulting Through Joint Load Transfer Design *Anastasios M. Ioannides, Ying-Haur Lee, and Michael I. Darter*	49
Effect of Lane Widening on Lateral Distribution of Truck Wheels *Rahim F. Benekohal, Kathleen T. Hall, and Harlan W. Miller*	57
Validation of Concrete Pavement Responses Using Instrumented Pavements *Ernest J. Barenberg and Dan G. Zollinger*	67
Evaluation of the Subbase Drag Formula by Considering Realistic Subbase Friction Values *Mehmet M. Kunt and B. Frank McCullough*	78

Field Performance and Evaluation of Thin Bonded Overlays 84
David G. Peshkin and Amy L. Mueller

Heavily Loaded Trailers: An Approach to Evaluate Their Interaction with Asphalt Concrete Pavements 95
Jorge B. Sousa, Jim McGhie, and Bob Shepard

Overlay Design Method for Flexible Pavements in Arizona 112
Michael S. Mamlouk, John P. Zaniewski, William N. Houston, and Sandra L. Houston

MICH-PAVE: A Nonlinear Finite Element Program for Analysis of Flexible Pavements 123
Ronald S. Harichandran, Ming-Shan Yeh, and Gilbert Y. Baladi

Extension of Load Equivalency Factors for Various Pavement Conditions 132
Jacob Uzan and Arieh Sidess

Influence of Axle Group Spacing on Pavement Damage 138
J. J. Hajek and A. C. Agarwal

Fatigue Damage Properties of Asphaltic Concrete Pavements 150
Kuo-Hung Tseng and Robert L. Lytton

Assessment of Damage Caused to Pavements by Heavy Trucks in New England 164
K. Wayne Lee and Wendy L. Peckham

Effect of Fracture Healing on Laboratory-to-Field Shift Factor 173
Adli Al-Balbissi and Dallas N. Little

Probabilistic Modeling of Flexible Pavements 184
Philippe L. Bourdeau

Computer Simulation of Load Equivalence Factors 192
W. J. Kenis and C. M. Cobb

AASHTO Flexible Pavement Design Method: Fact or Fiction? 206
B. J. Coree and T. D. White

Thaw Weakening of Pavement Structures in Seasonal Frost Areas 217
Vincent C. Janoo and Richard L. Berg

Prediction of Damage to Flexible Pavements in Seasonal Frost Areas 234
W. Allen, R. Berg, and S. Bigl

Evaluation of Variables Affecting Flexible Pavement Thawing for Timing Spring Load Restrictions 248
Mary Rutherford

Integrated Computer Model to Estimate Moisture and Temperature Effects Beneath Pavements 259
D. E. Pufahl, R. L. Lytton, and H. S. Liang

Foreword

Of the 24 papers in this Record, 9 deal with rigid pavements, 11 with flexible pavements, 3 with seasonal frost damage, and 1 with temperature and moisture effects.

Zollinger and Barenberg review factors related to punchout distress and discuss a possible cause. Ioannides and Korovesis demonstrate that in jointed or cracked concrete pavement systems equipped with a pure-shear load transfer mechanism, deflection load transfer efficiency is related to stress load transfer efficiency, and that this relationship is sensitive to the size of the applied loading. Zollinger and Barenberg outline how pavement thickness, percent reinforcement, and crack spacing may be considered with respect to pavement spalling and loss of load transfer in the process of punchout development. McCullough et al. discuss the evaluation of the performance of a prestressed concrete pavement overlay; horizontal slab displacement because of temperature change was closely monitored and recommendations are made. Ioannides et al. describe and evaluate mechanistic-empirical algorithms for more realistic estimates of anticipated faulting in concrete pavements. Benekohal et al. suggest that lane widening is likely to be a very cost-effective design improvement for concrete highway pavements that would otherwise be vulnerable to transverse fatigue cracking as a predominant mode of failure. Barenberg and Zollinger describe two instrumented pavement sections constructed in Illinois to validate the mathematical models used in the development of a mechanistic-based pavement design procedure for jointed concrete pavements. Typical results and the significance of results with respect to the analysis models used and the design procedure developed using the models are presented. McCullough and Kunt present a reinforcement formula modified in accordance with the experimental results obtained concerning subbase frictional resistance. Peshkin and Mueller found that bonded concrete overlays showed mixed success, and in general debonding was a cause for concern on many of the projects.

Sousa et al. compared some aspects of the dynamic behavior of a new super-heavy-haul vehicle trailer equipped with a hydraulic cylinder-nitrogen suspension with the behavior of four other currently used semitrailer types. On the basis of the data obtained, the dynamic component of the loads induced by the new trailer at normal highway operations is within the same range of magnitude produced by the other trailers studied, and from a dynamic point of view the effect of suspension type appears to be more significant than the number of axles. Mamlouk et al. developed a rational overlay design method for flexible pavements in Arizona that includes roughness, fatigue, and plastic deformation models. The three design models are incorporated in a microcomputer program for determining the optimum overlay thickness, estimating the remaining life of an existing pavement, evaluating the life of a user-specified overlay, and performing economic analysis. Harichandran et al. describe a nonlinear mechanistic finite-element program called Mich-Pave that has been developed for use on personal computers to aid in the analysis and design of flexible pavements. Uzan and Sidess found that the load equivalency factors of all load configurations depend on the pavement condition. Hajek and Agarwal evaluated the damage effects of dual and triple axles on flexible pavements and found that axle spacing has a significant influence on pavement damage. Tseng and Lytton describe the development of material property relations for the two fatigue damage properties K_1 and K_2, which can be used to predict the fatigue life of asphalt concrete pavements. Lee and Peckham observed that in all cases heavy trucks caused more damage than benchmark trucks and that more damage due to heavy trucks is predicted when there is a higher legal weight limit. Al-Balbissi and Little investigated the healing mechanism in asphalt concrete and introduced a theoretical hypothesis for the shift factor, which accounts for the effects of residual stresses and healing in the field that does not occur in the laboratory. Bourdeau presents a probabilistic approach to the deterioration processes of flexible pavements with unbound granular layers under the effect of traffic. Kenis and Cobb evaluated the AASHTO load equivalency factors with a computational model for predicting flexible pavement response. Coree and White reviewed the 1986 AASHTO *Guide for Design of*

Pavement Structures and revealed a number of opportunities for re-examining the AASHTO Road Test results.

Janoo and Berg discuss the development of a nondestructive pavement evaluation procedure for seasonal frost areas using a falling weight deflectometer. Allen et al. discuss the work being done by the U.S. Army Engineer Cold Regions Research and Engineering Laboratory in developing a mechanistic pavement design method for use in seasonal frost areas. Five fatigue equations were used to determine the cumulative damage for the pavement sections at Springfield, Missouri, and Rochester, Minnesota, and although all of the equations predicted failure during the design life for each pavement section modeled, significant jumps occurred during the spring, indicating that the thaw period is crucial in the fatigue life of a pavement. Rutherford performed a finite-element analysis of pavement freezing and thawing on four flexible pavement structures developed to represent typical pavements that receive spring load restrictions because of thaw weakening.

Pufahl et al. provide an overview of a computer model that estimates moisture and temperature effects beneath pavements.

Field Investigation of Punchout Distress in Continuously Reinforced Concrete Pavement in Illinois

DAN G. ZOLLINGER AND ERNEST J. BARENBERG

Most maintenance activities on continuously reinforced concrete (CRC) pavements are related in one way or another to punchout distress. Over several years of observation of CRC pavement, several symptoms related to the structural aspects of punchout distress have been noted. These symptoms include, but are not limited to, close crack spacing, surface widening and spalling of transverse cracks, development of longitudinal cracking, loss of load transfer, and subbase and subgrade pumping. Literature reviews have elaborated on punchout-related factors with respect to pavement performance. However, the punchout mechanism relating the various factors is not completely defined. Some questions exist concerning the sequence of events leading to the loss of load transfer across transverse cracks as a prerequisite to the development of a punchout. This sequence of events relates to the role reinforcement plays in the punchout process and whether the loss of aggregate interlock requires rupturing of the steel. If rupturing of the steel occurs, the question is whether rupturing occurs before or after the loss of aggregate interlock. Factors related to punchout distress as noted by this investigation and others are reviewed and a possible mechanism of punchout distress is addressed.

Punchout distress is regarded as the most severe performance-related problem that continuously reinforced concrete (CRC) pavements develop. Defined as a structural failure, punchout distress typically is associated with close transverse cracking and is bounded by a longitudinal crack on one side and a longitudinal edge joint on the other (Figure 1). Characteristically, the pavement pushes or punches downward under traffic loading, causing permanent deformation or faulting. The punchout can also, and frequently does, develop at Y-cracking, which is the development of closely spaced cracks that meet 2 to 3 ft from the pavement edge and form one crack. This type of cracking may also develop at an interior position in the pavement, but perhaps not as frequently.

Several investigators have noted problems associated with CRC pavement that have been the result of improper construction or easily identified design defects (*1*). In some instances failures have occurred at construction joints caused by the lack of consolidation. In other cases pavement failure has been attributed to improper lapping of the reinforcement (*2*,*3*). Problems such as these have given CRC pavement performance the reputation of being particularly sensitive to construction practice.

D. G. Zollinger, Department of Civil Engineering and Texas Transportation Institute, Texas A&M University, College Station, Tex. 77843. E. J. Barenberg, Department of Civil Engineering, University of Illinois, Urbana-Champaign, Ill. 61801.

Poor support conditions coupled with short cracking intervals have shown a strong correlation to a high frequency of punchout distress. Performance surveys have shown that the crack spacing distribution may include a wide range of cracking intervals from project to project. This range frequently includes crack intervals less than 2 ft. Factors related to environment and materials are known to influence crack spacing irregularities. However, the variabilities associated with these make difficult prediction and control of crack spacing within certain limits. Given the sometimes uncertain performance of CRC pavement in the past, it is necessary to improve the understanding of the failure mechanism associated with punchout distress, thus allowing CRC pavement design procedures to address the factors that influence the punchout process directly.

NATURE OF PUNCHOUT DISTRESS IN ILLINOIS CRC PAVEMENT

A field investigation was undertaken to further study a method of analysis on which to base a mechanistically oriented thickness design procedure for CRC pavements and to gain further knowledge of the mechanism related to the punchout distress as demonstrated by CRC pavements in Illinois. It is reasonable that design analysis should focus on the punchout mechanism, since punchout distress is recognized as the predominant distress type in CRC pavement (*4*,*5*). In this study, loss of support was found to be the primary cause of the punchout, which, incidentally, was recognized by previous investigators (*5*,*6*). This investigation examines factors associated with steel rupture, which is related to concrete fracture development around the reinforcement. Faulting occurred in most instances in which loss of support was indicated. Various loss-of-support mechanisms and failure modes are proposed based on the field observations.

CRC Pavement Survey

Several observation sections that represent the performance of CRC pavement within the state of Illinois were selected to study punchout development. The survey results from selected sections are presented in this paper. The sections selected for observation were chosen on the basis of performance, pavement thickness, subbase type, percent of reinforcement, and particularly susceptibility to D-cracking. It was important to

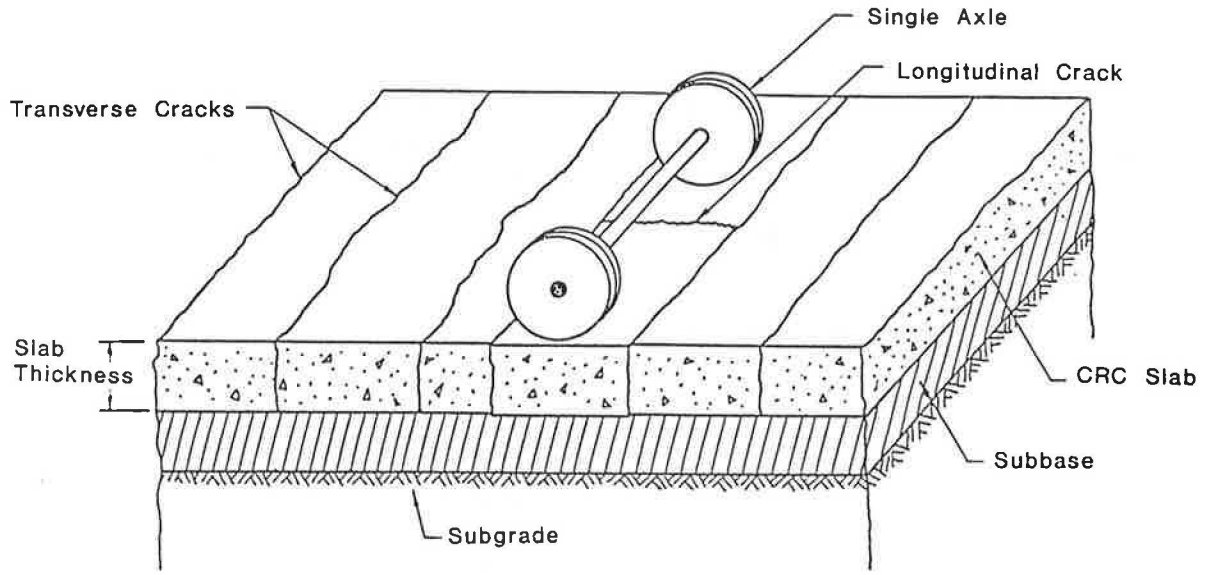

FIGURE 1 Formation of longitudinal crack between two transverse cracks; intermediate state of edge punchout (*6*).

TABLE 1 OBSERVATION AND SAMPLING SECTION DATA

Route	Thickness*	Reinforcement % Steel	Reinforcement Method	Subbase Type	Aggregate Source	Average** Traffic ESAL [1]	Average Crack Spacing	Punchouts (Per Mile)	Year Const.
I-72WB [4]									
MP41.9-48.5	8	0.59(#5)	Tube	CAM I	Thornton Pit [2]	2.97	4.8	11	1976
MP48.5-53.5	8	0.59(#5)	Tube	CAM I	Covington Pit	2.87	5.4	<1	1976
MP58.1-62.9	8	0.59(#5)	Tube	CAM II	Fairmount Quarry	2.87	6.0	9	1976
I-55NB [4]									
MP223.0-224.0	9	0.59(#5)	Tube	CAM I	Westowe Quarry	7.10	4.7	<1	Fall 1977
I-55SB [4]									
MP223.0-225.0	9	0.59(#5)	Tube	CAM I	Westowe Quarry	7.10	5.9	10	Spring 1978
I-39NB,SB [4]									
MP118.0-130.5	10	0.71(#6)	Tube	CAM II	Mulford Quarry [2]	4.7	7.4	NB:9 [3] SB:16	1981-82
MP130.5-139.0	10	0.71(#6)	Tube	CAM I	Mulford Quarry [2]	4.7	7.4	NB:2 [3] SB:7	1981-82
I-57NB [4]									
MP250.5-256.0	7	0.59(#5)	Tube	BAM	Fairmount Quarry	8.77	1.8	<1	1970
I-57SB [4]									
MP324.1-330.5	8	0.59(#5)	Chairs	BAM	2	11.1	4	27	1968
MP275.5-279.6	8	0.59(#5)	Tube	BAM	Lehigh Quarry	8.84	3.0	13	1970
FA 409 [4,5]									
STA3153-3199	7	0.70(#6)	Chair	CAM II	2	0.04	5.5	0	1986
STA3014-3153	8	0.73(#6)	Chair	CAM II	2	0.04	5.1	0	1986
STA2989-3014	9	0.72(#6)	Chair	CAM II	2	0.04	6.0	0	1986
US 50 [4]									
STA2767-2789	8	0.60(#6)	Tube	BAM	Columbia Quarry	0.04	6.0	0	1980

* Thickness in inches
** Average Crack Spacing in feet
[1] In the driving lane (in millions)
[2] Low D-cracked susceptible aggregate
[3] Total punchouts per mile
[4] 4 or 6 inch pipe edge drains
[5] Some sections with no edge drains

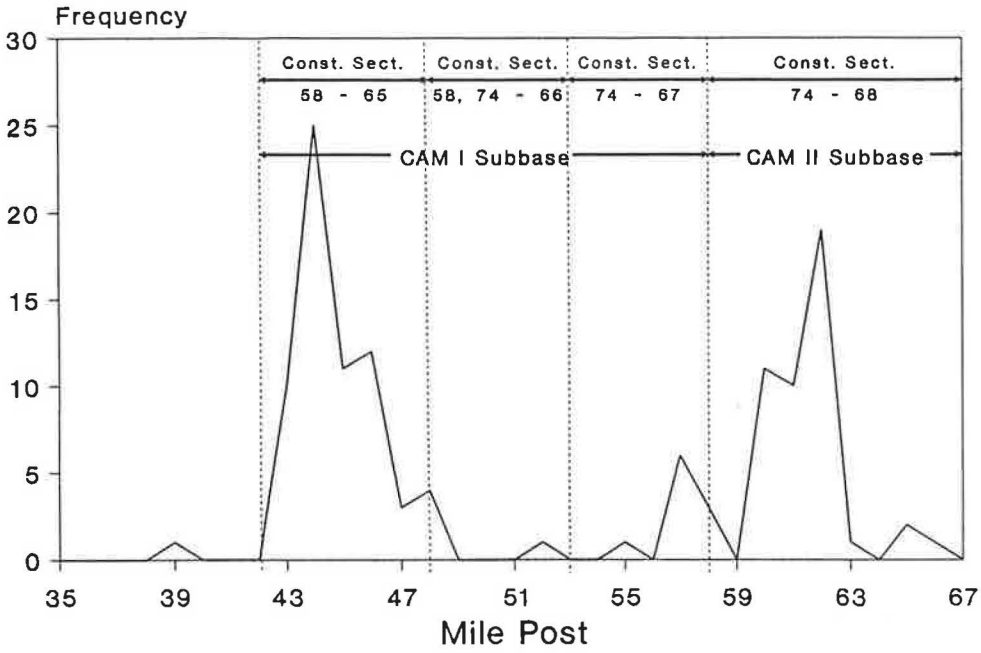

FIGURE 2 I-72WB CRC pavement survey of punchouts and patches in driving lane.

study the structural failure aspects related to punchout distress independent of D-cracking susceptible concrete. This type of study could not be done for some of the survey sections. Recent surveys have indicated that over 50 percent of the pavement mileage in Illinois has either a low, intermediate, or severe level of D-cracking (*7*). This percentage is even greater when the pavement mileage that contains D-cracking susceptible aggregate that is not currently showing visible signs of D-cracking is included. Table 1 summarizes the observation sections and pertinent data (including subbase data) relative to the punchout performance survey conducted in this study. The D-cracking information is based on core examinations and available quarry D-cracking evaluations. All the pavements included in this study have a bituminous shoulder except the FA-409 pavement sections.

The nature of punchout distress is then described by the factors affecting the punchout rate and performance from a few selected sites. Results of a survey of patches and punchouts in the truck lane from the I-72 westbound sites are shown in Figure 2. The approximate construction boundaries of each project are shown, delineating where different contractors and aggregate sources were used for construction of the pavement. Significantly different punchout rates are evidenced from construction section to construction section, which suggests that punchouts may be related to construction practice.

A similar pattern of punchout frequency was noted at another observation section on I-55. The punchout rate recorded for the southbound driving lane was as high as 20 punchouts per mile, as contrasted with the northbound lanes, which had a punchout rate near zero. Significant performance differences exist, similar to those in the sections on I-72 between the northbound and the southbound lanes, both of which have cement aggregate mixture (CAM) I type subbases. As shown by the data in Table 1, little difference is apparent in traffic level, aggregate source, and steel reinforcement between the northbound and southbound lanes, which, in this case, were constructed by the same contractor.

An observation section on I-39, with 4.7 18-kip equivalent single axle loads (in millions based on unpublished data from the Illinois Department of Transportation, 1983, traffic factor equations), is experiencing a relatively high punchout rate. The cracking pattern on I-39 is not uniform but divided between groups of wide and narrow crack intervals with a crack space distribution made up of a combination of the short and long crack spacings. Other factors leading to the formation of punchouts on I-39 will be discussed later, but the crack pattern in CRC pavement appears to be a factor in the punchout development. Nonuniform crack spacing distributions may lead to a greater tendency to punchout. In fact, the data from this study indicated that maintaining an average crack spacing within the limits designated in the literature is no guarantee that punchouts will not develop.

Close cracking intervals have been characteristic of good-performing CRC pavements in Illinois. The average cracking interval, which is now less than 2 ft, was noted on 0.7 percent and 1.0 percent reinforcement sections of the well-known Vandalia CRC pavement (constructed in 1947). It has been pointed out previously that the cracking intervals of the Vandalia pavement have shown some dependence on the percent of reinforcement (*8*). The percent of reinforcement also has had a profound effect on the punchout performance of the pavement, as indicated by the data shown in Figure 3. This effect may be indirectly related to the cracking intervals associated with the percent of reinforcement. Other pavement sections on the heavily traveled Stevenson (I-55) and the Dan Ryan (I-57) in the Chicago area have average crack spacing reported to be 3 ft or less (unpublished data, Illinois Department of Transportation, 1987).

A comparison between the northbound section on I-57 (Table 1) and the site on I-39 shows much better performance on I-57. This particular section is 3 in. less in thickness and has

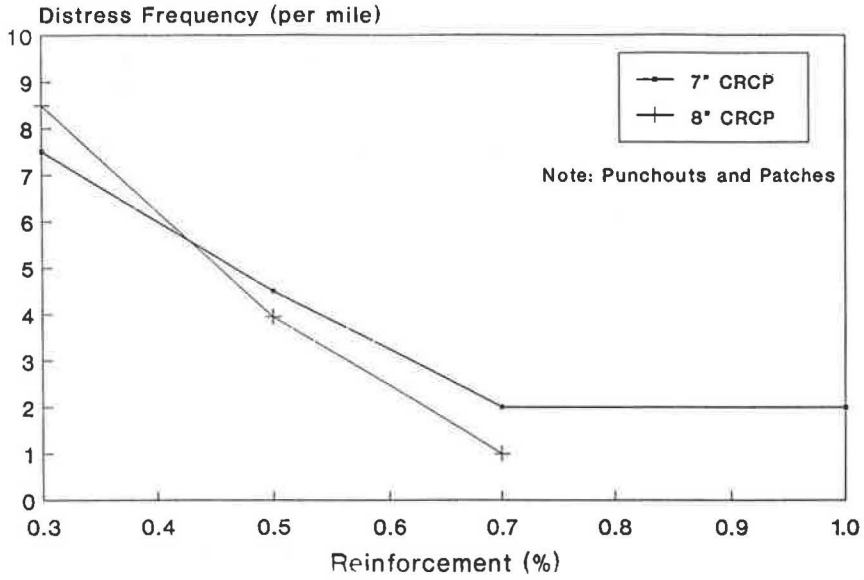

FIGURE 3 Effect of reinforcement on performance of Vandalia CRC pavement (US-40).

carried more than twice the traffic of I-39. A factor much more significant than pavement thickness is contributing to the markedly better performance of the I-57NB section over the I-39 section. The I-57 section contains a greater percentage of D-cracking susceptible aggregate, a bituminous aggregate mixture (BAM) subbase, and an average crack spacing of less than 2 ft with a uniform cracking pattern.

Although no significant distinctions could be made in the crack spacing distributions between the adjacent good- and the bad-performing sections of I-72WB (shown in Figure 2), the apparent differences lie in whether the coarse aggregate was D-cracking susceptible. The pavement thicknesses are equivalent and the average crack spacing is similar. The construction section containing the low percentage non–D-cracking susceptible aggregate source (Thornton Pit) is the one with the highest rate of distress.

The subbase types used on I-72WB are CAM I and CAM II. CAM I subbase is roller compacted and usually contains an 8 percent cement content, an aggregate blend of 75 percent coarse aggregate, and 25 percent natural sand (*9*). CAM II subbase type is equivalent to a lean concrete subbase. Two of the construction sections with high rates of distress had different subbase types, so the source of the distress may not be strictly attributable to the type of subbase. A standard procedure was followed on each construction section, making little difference in construction procedure between the sections. Especially with regard to the construction of the CAM I subbase, the standard procedure called for the trimming of the CAM I material with an autograder. This meant that the stabilized subbase was trimmed before placement of the 8-in. CRC pavement. The subbase material was not roller compacted again after the trimming operation was completed.

A limited survey of Y-cracking from selected pavements indicated that the pavement sections in which the reinforcement was placed using a tube device incur a higher incidence of Y-cracking (12 cracks per 100 ft) than pavements in which the reinforcement was placed using chairs (4 per 100 ft). The incidence of Y-cracking may be tied to the variability of the depth of reinforcement cover, which is largely a function of the placement method (*4*). Field data indicate that for a tube type placement method a trend of greater average rebar cover

FIGURE 4 Type 1 spalling, I-39SB.

and variation occurs as the thickness of the pavement increases. The standard deviation of rebar cover is lower for chair placement (2.2 in. versus 4.2 in. for tube placement).

Spall development was investigated on the I-57 sites, in which two types of spalls were noted. Spalling developing as a result of a spall mechanism suggested by McCullough et al. (*10*) is classified as a Type 1 spall (Figure 4). A Type 1 spall develops into an advanced stage when the pavement is broken out within the boundaries of the cracking. Although not in all cases, it was noted that Type 1 spalls tend to coincide with the longitudinal reinforcement in the pavement and can extend to a considerable depth into the pavement. Spalling of this nature that extends to the depth of the reinforcement severely reduces the aggregate interlock and may lead directly to punchout distress. It may also contribute to the Type 2 form of spalling shown in Figure 5 and can be classified as either minor or severe spalling as noted previously. These spalls tend to develop abruptly into a severe condition of spalling in a period of a few months. McCullough et al. (*11*) indicated that Type 2 spalling increases with crack spacing because of an increase in crack width. A low-severity form of Type 1 spall or concrete wearing also leads to widening of the crack width. The formation of longitudinal cracking is associated with spall development and concomitant loss of load transfer.

CRC Pavement Removal and Coring Program

As a part of this study, several pavement cores and slab sections containing punchouts in various stages of development were removed from the field and relocated to the Newmark Civil Engineering Laboratory for examination (*4*). A brief summary of the results of the laboratory examination is presented regarding the condition and performance of the steel in the pavement with respect to punchout distress. The condition of the reinforcement will be discussed later after factors related to the loss of subbase support are presented.

FIGURE 5 Type 2 spalling, I-39.

Loss of Subbase Support

In an effort to preserve the details of the punchout distress, short sections of CRC pavement were carefully lifted and removed from in-service pavements. On removal of the sections from pavements with CAM I subbase, severe erosion was noted in the surface of the subbase. The approximate area of surface erosion is shown in Figure 6. The most extensive erosion occurred along the shoulder where disintegrated subbase extended to a depth of 1 to 2 in. into the subbase. In the figure, the subbase surface was eroded approximately 24 in. along the pavement edge. The erosion extended another 12 in. in the vicinity of the punchout. Some of the erosion may have occurred while the punchout was developing because of slab rocking and other related motion under loads. However, the uniformly eroded 24-in. area shown in the diagram appears to have developed by other than load-associated means.

At other sample sections, punchout information was obtained during punchout repair operations in which erosion of the

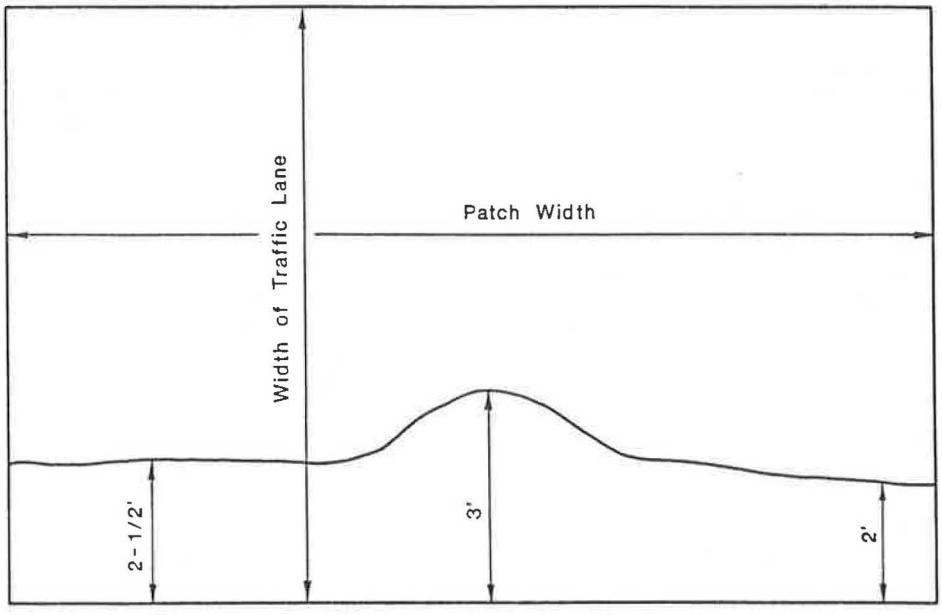

FIGURE 6 Diagram of subbase surface erosion at punchout repair site, I-72WB MP57.

TABLE 2 I-39SB: UNCONFINED COMPRESSIVE STRENGTH (CORRELATED TO DCP)

Station	Subbase Type	Initial* Penetration (inches)	Unconfined Compressive Strength: First Drop (psi)	Unconfined Compressive Strength: Average of First Five Drops (psi)	Subbase$^{\Delta}$ Average (psi)
2209+00	CAM I	0.5	33	135	240
2141+50	"	"	33	84	200
2131+00	"	"	46	120	95
Patch #113	CAM II	0.4	20	53	90
1851+00+	"	0.2	33	118	155
1851+00	"	0.0	46	161	340
1841+50+	"	0.5	33	83	200
1841+50+	"	-	-	38	55
1841+50	"	0.0	-	110	290

* Penetration of the cone under the weight of the 8 kg hammer
\+ Measurements were made in the eroded area of the subbase
Δ over the full depth

same nature was noted in the CAM I subbase on I-39. While the punchouts on I-39 were being repaired, in situ strength tests were made on the subbase. The strength of the CAM I and CAM II subbases was found to be low. A summary of unconfined compressive strength determined from tests taken using the dynamic cone penetrometer (*12*) is shown in Table 2. Obviously, the measured subbase strengths are very low. The lowest-strength material is in the upper portion of the subbase. The eroded areas showed a lower strength than the noneroded areas. Some damage from slab rocking may have decreased the strength in the eroded areas. A stabilized, nonerodible subbase should have a compressive strength of 1,000 psi (*13*). It would be difficult to drive a dynamic cone penetrometer through a stabilized subbase of normal strength.

A coring program was instigated to obtain further information on the development of subbase erosion. Most cores obtained for the study were taken from transverse cracks. The descriptions of the various classification systems for transverse crack conditions and other core-related data are given in Table 3. A variety of sample sections, subbase types, crack conditions, and spacings were cored to obtain punchout information about the subbase performance in punched-out and nonpunched-out areas.

A series of cores were obtained at the I-55 sections, which also had a CAM I subbase. All cored cracks on I-55 had some erosion at the pavement longitudinal edge joint. However, a significant difference exists between the erosion data from the northbound lanes and the erosion data from the southbound lanes. The extent of the erosion in the northbound lanes was much less than that in the southbound lanes. The punchout rate in the southbound driving lane was much higher than that in the northbound driving lane, as noted in Table 1. A slight amount of erosion under the northbound lanes was noted 22 in. from the pavement edge, but the support conditions were considerably better than those for the southbound lanes. The southbound lanes had wider longitudinal edge joints, which may be an indication of greater pumping susceptibility, compared with the longitudinal joint on the northbound lane, which was very narrow and tight. The crack classification was nearly the same on all cracks cored in this series and no faulting was noted. The cracking interval associated with the cored cracks ranged from 2 to 6 ft. Little or no shoulder staining was visible at the I-55 sections.

The information obtained from the field cores on CAM I subbase suggests that subbase erosion and loss of support must develop before the development of punchout distress. A series of cores obtained from a pavement with a BAM subbase taken from a sample section on I-57NB that exhibited a low punchout rate showed that subbase erosion was almost nonexistent. This conclusion emphasizes the need for nonerodible subbases under CRC pavements as a primary step toward improved pavement performance. The BAM type subbase may be a good candidate for a low-erodible, uniform supporting subbase, as long as drainage is provided.

A problem related to lean concrete subbases was noted in cores obtained from the pavement sample section on I-72WB, between MP 58.1 and MP 62.9. This section, which has a CAM II subbase, indicated a failure mode similar to that experienced in Wisconsin and Pennsylvania on CRC pavement overlays on jointed concrete pavement. This failure mode, illustrated in Figure 7, developed at a crack in the CAM II subbase. A 6-in.-diameter core was taken on a faulted crack in which the subbase portion included the crack in the subbase displaced approximately 3 in. from the crack in the pavement. On removal of the subbase core it was noted that the subbase crack face was spalled (the strength of this subbase was great

TABLE 3 CRC PAVEMENT CLASSIFICATION SYSTEMS

CRCP Crack Classification (Modified AASHO Road Test-Report 5)

C-1: Fine crack not visible under dry surface conditions at a distance of 15 feet. (Tight)

C-2: A crack that can be seen at 15 feet, but exhibits only minor spalling. The opening at the surface is 1/32" or less. (Open)

C-3: The crack is opened at the surface 1/32" or more for any portion of the crack length. The crack exhibits low to medium spalling. Amount of faulting is noted.

C-4: The crack is either very wide (>1/16") or sealed and exhibits medium to severe spalling. Amount of faulting is noted.

IDOT Rebar Corrosion Rating

1: Clear or free of rust

2: Slight rust with no appreciable reduction in cross-sectional area.

3: Moderate rust with no substantial reduction in cross-sectional area.

4: Heavy rust with a marked reduction in cross-sectional area.

Diamond Void Size Classification

Small: Radius of the void (from the surface of the rebar) is less than the diameter of the rebar.

Large: Radius of the void is greater than the diameter of the rebar.

Number of D-Cracking Aggregate

Number of aggregates on the surface of a 4 inch diameter core showing signs of D-Cracking. Other core diameters are listed along with the pavement thickness.

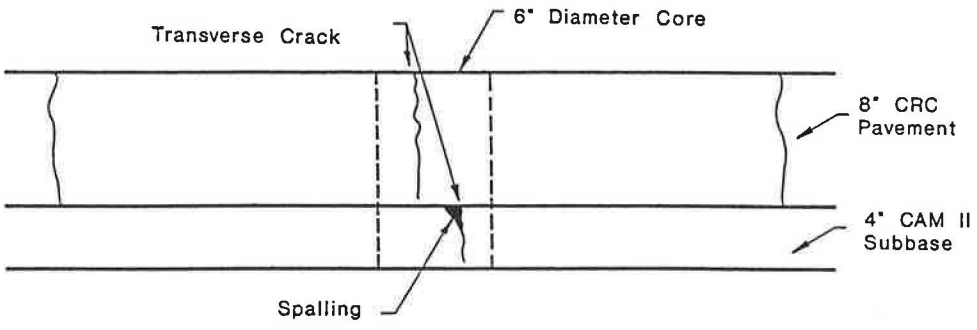

FIGURE 7 Spalling on crack face of CAM II subbase.

enough that a dynamic cone penetrometer could not be driven through it). A loss of load transfer in the subbase can lead to an unsupported condition in the CRC pavement, which can cause faulting and punchout distress.

Results from this investigation indicate that unsupported conditions are the main factor in the development of punchout distress and faulting of CRC pavements in Illinois. Loss of support conditions may result from soft and wet soil conditions in the case of BAM subbases, surface erosion caused by low strength in the case of CAM I and CAM II subbases, and unequal deflection characteristic between the pavement and the subbase in the case of high-strength CAM II subbases.

Subbase erosion has been identified as the primary cause of punchout-related distress in CRC pavements with CAM I subbases. It provides an explanation for the varying punchout rates evident in the data of Table 1, particularly for the various levels of performance between the I-39 and I-57NB sections. Apparently small amounts of subbase erosion can extend up to 24 in. from the pavement edge and still have adequate performing CRC pavement in Illinois. CRC pavement with CAM I and BAM subbases showing good performance show less erosion than those with a poor performance. The difference in the varying erosion rates between pavement sections noted in this paper under apparently identical traffic and climatic conditions was found to be dependent on whether the aggregate in the pavement was susceptible to D-cracking. D-cracking had an effect on the pavement behavior under load and is elaborated further elsewhere (*4*).

Condition of the Reinforcement

The factors related to the performance of the reinforcement in CRC pavement during punchout development are apparently secondary or consequential in nature. Details regarding the condition and behavior of the reinforcement in punchout distress are explained on the basis of the laboratory examination of slabs and cores removed from actual pavement. Cores taken from the slab specimens were split at the level of the reinforcement to allow examination of the rebar and the surrounding concrete. Examination of the cores showed that diamond-shaped fractures and voids were noted around the reinforcement in several of the cores. Voids around the reinforcement have been noted by other investigators (*6*) but were being attributed to expansive forces from corrosion. Figure 8 illustrates a diamond-shaped fracture pattern around the reinforcement found in several cores. A direct correlation between these fractures and corrosive forces is doubtful. However, it is apparent that the voids around the rebar are an end result of the diamond-shaped fracturing that can form from 0.5 to 1.0 in. from the crack face. The voids and fractures were found in the portion of the punched-out areas that had no faulting.

Bond studies of bars in tension (*14,15*) noted that secondary cracks similar to those in the fracturing shown in Figure 8 formed at the loaded face of the specimen at a threshold steel stress between 14 and 18 ksi. These fractures caused by pullout forces form the diamond-shaped configuration around the steel shown in Figure 8. Measured strains in the reinforcement at the crack face (*4*) predicted that steel stresses from climatic effects can exceed the threshold levels for a broad range of environmental conditions leading to the formation of the pullout cone. Once the fractures around the steel have formed, bearing stresses may crush the concrete in the immediate vicinity of the bar, which leads to a void, as shown in Figure 8. The cone pullout fractures will also lead to reduced bond stiffness as indicated by Mains (*16*).

Laboratory analysis of a slab section containing punchouts in the initial stages of development indicated void development around the steel before the crack developed faulting. The void apparently forms with the development of the punchout and may develop before permanent faulting. Consequently, some voids were present around the steel on nonfaulted cracks. The effect of these voids on load transfer is discussed later in this paper, but one would expect load transfer to decrease. As a result, participation of the reinforcement in the transfer of load across the transverse crack is minimized because of the pullout fracturing.

The field data indicate that 80 percent of the cores taken in the field study had either cone pullout fracture or a rebar void. Although one would expect a high correlation between rebar voids and pavement nonsupport, the data suggest that

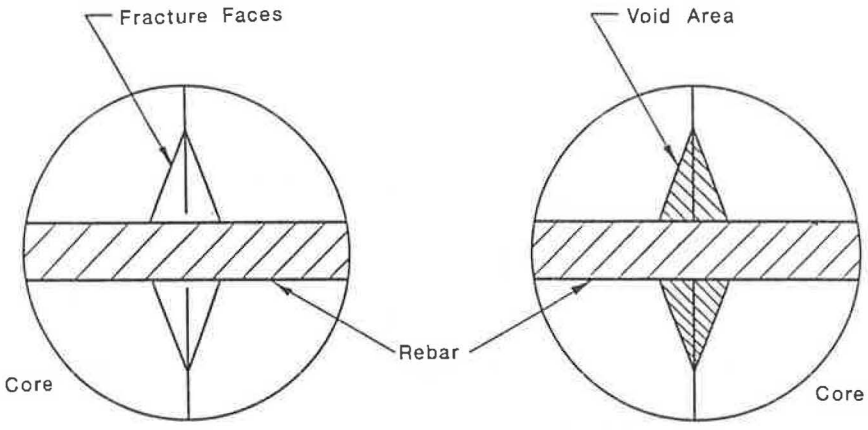

FIGURE 8 State development of void area around reinforcement.

unsupported conditions are coincidental with voids around the rebar only 55 percent of the time. A high correlation was found between the number of cores with either a rebar void or pullout fracture and subbase nonsupport. It is expected that cone pullout fracture may have some dependence on the length of crack spacing and climatic conditions at the time of construction, but strong correlations in this regard were not apparent in the data. At the I-39 site, where the cracking pattern tended to change from a long crack spacing to a short crack spacing, 100 percent of the cores that had rebar in them indicated pullout fracture. Examination of the cores taken at the I-57NB site revealed that 42 percent showed pullout fracture. This pavement had a closely spaced and uniformly distributed cracking pattern. Two sites on route US-50 were investigated for cone pullout fracture as a function of time and traffic. Although they are 6 years apart in age, these two sites were opened to traffic at the same time. Pullout fracture was noted in both of the cores obtained from the older site, whereas it was indicated in only two of the seven cores taken in the newer section. At the time of coring, the newer section had been through one winter since construction.

Sections on I-57NB near MP 320 containing punchouts at further stages of development were visited and several instances of broken reinforcement were found. It was noted that tensile type breaks in the reinforcement were located at a small distance from the crack face (ranges from 1 to 2 in.). The steel breaks were straight across the bar cross section and orthogonal to the axis of the bar. Other punchouts with broken steel were also noted to be displaced from the crack face. Large diamond-shaped voids were also found around the reinforcement along with faulting on the crack face. In one instance, breaks in the rebar were found at the crack face where transverse steel coincided with the transverse crack. Otherwise, no other breaks were found at the crack face.

The bar breakages were noted at two locations, where one break occurred at the crack face and another break occurred approximately 2 in. from the crack face. A closer look at the rebar revealed several fractures of partial depth on one side of the steel. These fractures were found to correlate with the tensile side of the rebar from the bending stress that the bar underwent during the process of fault development of the punchout. This process (which may develop under 3 months) is illustrated in Figure 9. Once the void forms around the reinforcement either by cone pullout fracture or bearing failure, vertical displacement or faulting in the pavement will not put the bar under immediate shear stress. Further faulting applies a bending strain in the rebar on the under and top sides as shown in Figure 9*b*. The resulting fracturing is caused by the fatigue strain of several repeated loadings, since rebar is commonly bent to radii much shorter than those that occur in the faulted case without tensile fracture. Once the fracture has progressed through the rebar, as seen in Figure 9*c*, further faulting can develop. Eventually, the voided area will begin to make repeated contact with the rebar, which will either fracture the concrete or cause a shear-type failure in the reinforcement. This leads to short segments of broken steel resulting from the punchout process.

CRC Pavement NDT Program

Nondestructive testing (NDT) was conducted on several test sites to gain further insight into CRC pavement behavior leading to punchout-related distress. During the testing process, data relative to the slab deflection, load transfer efficiency, pavement stiffness, and crack width were obtained. The falling weight deflectometer (FWD) used for the field testing was the Dynatest Model 8000, which is widely used in the United States. Most of the testing was conducted in the outer wheel path, with the center of the loaded plate varying between 36 and 42 in. from the pavement edge. The FWD, which was calibrated monthly, has been shown to yield repeatable data (*17*). The crack openings were measured, but results with respect to crack width measurements are reported elsewhere (*4*).

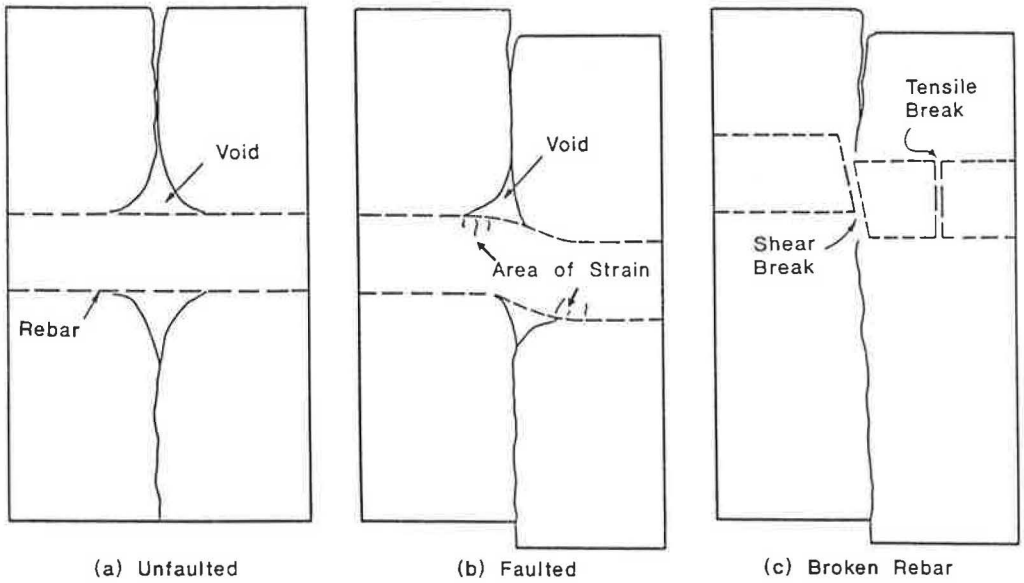

FIGURE 9 Broken reinforcement mechanism.

The results of the FWD field measurements are described in terms of the plate deflection (D_0), the load transfer efficiency (LTE), and the deflection basin area. The LTE is equal to the change in deflection on the unloaded side of the joint divided by the change in deflection of the loaded side of the joint. The basin area has been shown to be useful in interpreting measured deflection profiles by the FWD and is calculated from the sensor deflections (*18*).

FWD load transfer data were obtained from several transverse cracks for each group of crack classification (Table 3). The results indicate that significant differences in load transfer efficiency measured during the early hours of the day can exist between the C-1,2 and the C-3,4 classifications of cracks. However, these load transfer differences between the two groups are much fewer and tend to disappear if determined from results found during the afternoon. The closing of the cracks because of an increase in the pavement temperature can cause a dramatic increase in LTE.

The NDT results are also useful in backcalculating material properties of the pavement system, such as the modulus of elasticity (E) and the modulus of subgrade reaction (K). Particular interest lies in backcalculated E values and the radius of relative stiffness (l_k) at the transverse cracks, which is a function of E and K. [Note that $l_k = \{Eh^3/[12(1 - \mu)^2K]\}^{1/4}$ where h and μ are the pavement thickness and Poisson ratio, respectively.] A method of backcalculation of these parameters based on ILLI-SLAB modeling of the deflection basin [iterative calculation with various values of concrete modulus (E) and foundation modulus (K) to match the deflection basin measured by the FWD for a given load condition] has been discussed by others for jointed concrete pavements (*17–19*); however, little information is available about application of these methods to CRC pavement. A suggested procedure for CRC pavement, which is described elsewhere (*4*), is based on determining an effective radius of relative stiffness from modeling the measured deflection basin of the CRC pavement using a 100-ft continuous slab without joints.

This backcalculation procedure can be accomplished for a range of thicknesses and load positions. The calculations for l_k using ILLI-SLAB analysis at the wheel path locations were found to be similar to those of the closed form curve obtained from the theoretical solution (*19*) of a case of a circular load and a dense liquid foundation for an interior loading condition. Consequently, the theoretical curve could possibly be used in place of the ILLI-SLAB generated curves. As stated earlier, the FWD wheel path testing position varied anywhere from 36 to 42 in. from the pavement edge. Given the deflection basin area from the FWD test results, the radius of relative stiffness can be obtained from Figure 10 for either the edge load or wheel path load positions for any pavement thickness.

The determination of unique E and K values is discussed elsewhere (*19*) from l_k values obtained from Figure 10 and Westergaard solutions (*20*) for slab-on-grade deflections at the edge and interior load positions. The theoretical interior loading solution is applied to the wheel path load position in the actual pavement since the load behavior between the two positions was shown to be similar.

The l_k can be useful in determining potential punchout areas in CRC pavement. On the basis of the field data (*4*), if voids are present, the LTE and the l_k values are low (usually below 70 percent and 25.0, respectively) and if they are not, the l_k values are high. The l_k values at which rebar voids may be beginning to develop are not clearly defined. The data (*4*) indicated the ranges of l_k where problems may and may not be developing. This approach to CRC pavement evaluation can be useful as an indicator of potential punchout since subbase erosion and rebar voids tend to lead to lower l_k values. Comparisons between the l_k values from the NDT data (using Figure 10) and calculated l_k values (using the backcalculated K value, a range of concrete modulus, and the pavement thickness, h) may provide a basis for evaluation.

Calculated l_k values for a range of E values between 3 and 4 million psi are plotted as shaded-in evaluation limits to be

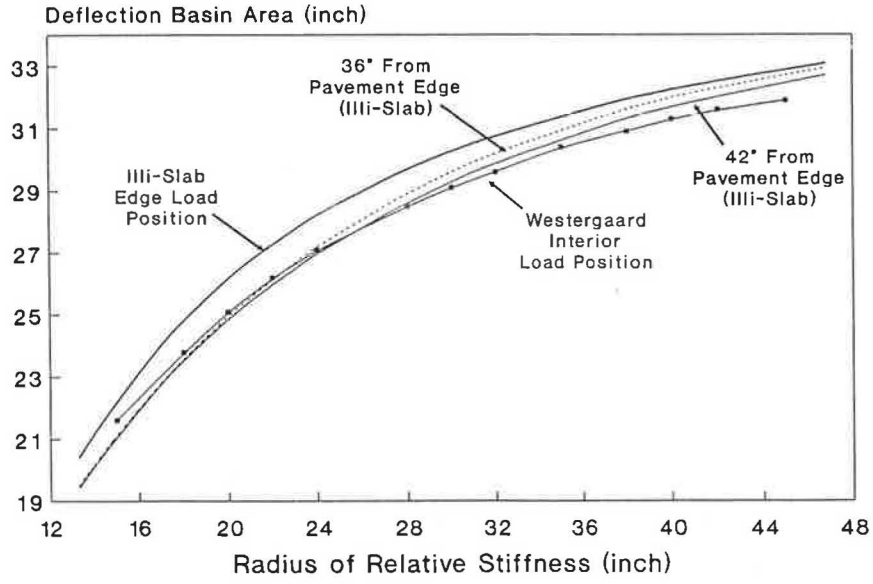

FIGURE 10 Variation of deflection basin area with l_k.

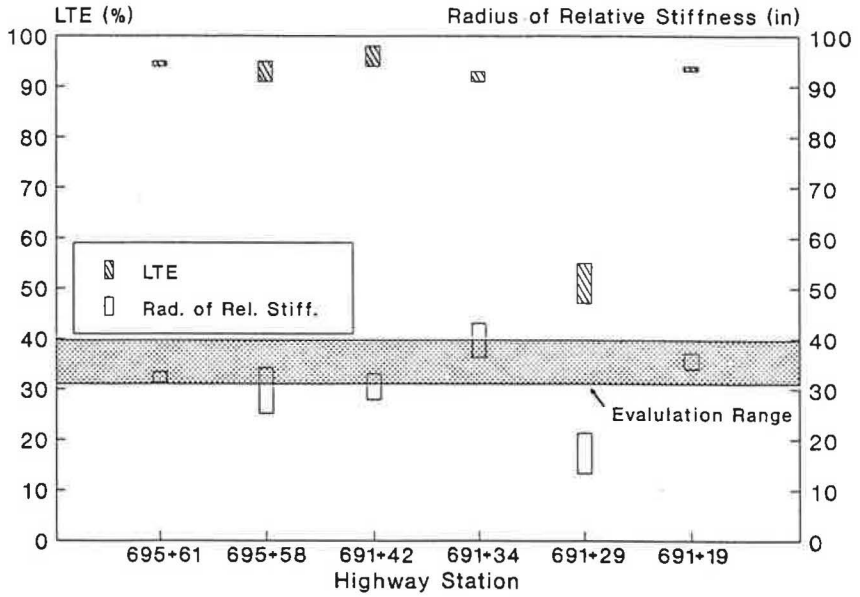

FIGURE 11 Comparison of LTE and l_k for I-55NB.

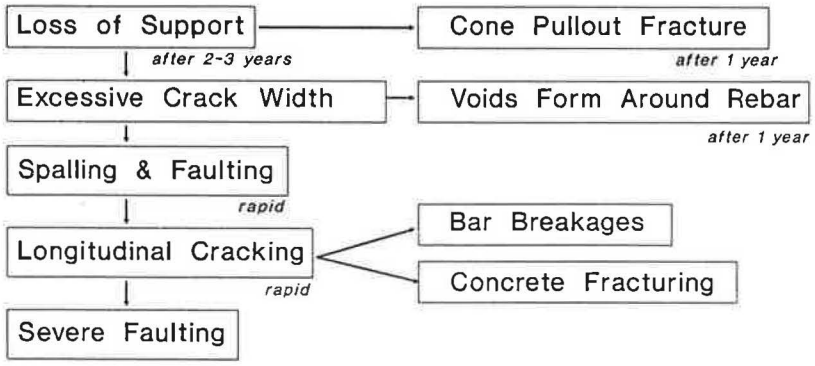

FIGURE 12 Morphology of punchout distress.

compared with l_k values from the NDT data illustrated in Figure 11. Figure 11 shows a comparison of LTEs and l_k values determined for the same test locations on I-55SB (approach and leave data are illustrated). At two test locations low l_k values were determined; these values had corresponding LTEs over 90 percent, suggesting that the radius of relative stiffness may be more effective in terms of CRC pavement evaluation than LTE. The shaded area is the limit range below which problems may exist. Evidently, potential punchout-related distress in CRC pavement may be evaluated from a combination of transverse crack observation, load transfer efficiency, and pavement radius of relative stiffness values.

Punchout Mechanism

Based on an appraisal of the previously noted factors, a punchout mechanism is postulated. A schematic diagram of the formation of punchout distress is shown in Figure 12. This diagram may apply to premature punchouts and those that occur at the end of the pavement life, depending on the cause of loss of load transfer. A noted prerequisite to punchout formation is the loss of subbase support. (This is particularly true in the case of premature punchout distress.) Support loss can develop in a number of ways. Support loss normally will develop if the subbase is susceptible to erosion when the necessary moisture conditions or discontinuities of load transfer or faulting in the subbase exist, all of which cause a nonuniform support condition in the pavement system. Stabilized subbases may also erode if they become or are weakened in the upper surface. Weakening may occur from poor compaction or poor strength gain. Wet subgrade conditions can also contribute to nonuniform support. Loss of support, depending on its nature, can develop as early as 2 to 3 years. The time for punchout development may be more dependent on the length of time associated with the development of unsupported conditions rather than the given pavement thickness (within the range of thicknesses, subbases and levels of traffic

included in this study) due to the intensity of the stresses associated with it. Time to punchout from erosion of CAM I subbases ranged from 3 to 8 years in Illinois. CAM II subbases that are low in strength usually lead to punchouts by the third year after construction. The CAM II subbases of normal strength may lead to punchouts more gradually over time and more in the 5- to 8-year range.

Punchout distress may be related to the loss of bond such as that caused by cone pullout fracture around the reinforcement. These fractures appear to form from a poor combination of long and short cracking intervals and a large drop in pavement temperature. In these instances, this distress can begin to form within 1 year after construction and may be mitigated if a uniform crack pattern develops (where steel and bond stresses are low). The likelihood that this distress will develop within the first 24 hr after construction was not supported by the strain data collected under this study. The data indicate that either pullout fractures or loss of support leads to a reduction in pavement bending stiffness.

Excessive crack widths can also lead to reduced bending stiffness in the vicinity of the transverse crack. Crack widths tend to open under loading repetitions, particularly when fracturing associated with Type 1 spalling developed at the time of initial drying shrinkage. Widened cracks can also occur with poor combinations of short and long cracking intervals. A combination of a short segment of pavement between two long segments is particularly susceptible to punchout distress because the stresses that cause longitudinal cracking increase significantly as the crack spacing decreases after load transfer across the crack is lost. These stresses are discussed and elaborated on elsewhere (*4*). Because the crack width affects the bending stiffness and load transfer efficiency, wide cracks will also increase the pumping potential of the pavement.

The bending stiffness is also reduced when bar looseness increases or the concrete within the pullout fracture disintegrates, leaving a void around the reinforcement. Rebar voids are instigated by bearing stresses on the concrete and can form quickly, at least within 1 year after poor support conditions have formed. The looseness around the steel may also be affected by the crack width since the aggregate interlock decreases as the transverse cracks widen.

A reduction in bending stiffness at the transverse cracks can cause spalling and faulting, leading to a loss of load transfer. After load transfer is lost, longitudinal cracking can form quickly—possibly simultaneously. The formation of a longitudinal crack should not be considered as the cause of the punchout but only a consequence of it. Type 2 spalling leads to a significant reduction in load transfer across the transverse cracks, which, as pointed out above, dramatically increases the stresses that lead to longitudinal cracking. Rebar breakages and pavement delamination are consequences of the above processes and are the result of loss of load transfer. Rebar breakages can occur either at the crack face or displaced from it. The breaks at the crack face are usually a consequence of corrosion, which reduces the cross-sectional area of the bar. This corrosion weakens the bar and makes it susceptible to an abrupt tensile failure caused by temperature contraction or wheel load-induced shear stress. This process may begin on the pavement edge, leading to a widened crack there, and proceeding to the next bar until the entire lane is encompassed. Consequently, a wide and faulted crack develops. The bar breakages displaced from the crack face are load induced and fatigue related. Stresses forming this break are not great enough until most of the load transfer from aggregate interlock is lost. Once the bar has failed, the faulting can progress rapidly to a severe level since the reinforcement was transferring most of the load before failure. If the crack spacing is short, as in the case of a Y-crack, the rebar may not fail, which may lead to delamination and deep spalling of the concrete pavement above the reinforcement.

SUMMARY

The fundamental cause of punchout distress has been identified as loss of subbase support. The probability of punchout is enhanced when loss of support and nonuniformly distributed crack spacing combine under load to destroy the load transfer across the transverse crack. There are instances, reported in the literature and found in this study, where nonuniform support has precipitated localized short crack spacing, leading ultimately to punchout failure. Whether the punchout is at the pavement edge or in the wheel path, the cause is still the same. Pavement faulting, which is characteristic of the punchout distress, cannot develop unless the support underneath that portion of the pavement is lost. Therefore, definitions in the literature appraising various causes to edge and interior punchout are unnecessary.

ACKNOWLEDGMENT

This paper is based on the results of a cooperative study between the Illinois Department of Transportation (DOT) and the University of Illinois sponsored by the Division of Highways of the Illinois DOT and FHWA.

REFERENCES

1. G. P. York. *Continuously Reinforced Concrete Pavements—The State of the Art*. Technical Report No. AFWL-TR-71-102. Air Force Weapons Laboratory, October 1971.
2. T. C. Paul Teng and J. O. Coley. Continuously Reinforced Concrete Pavements in Mississippi. In *Transportation Research Record 485*, TRB, National Research Council, Washington, D.C., pp. 25–38, 1974.
3. F. C. Witkoski and R. K. Shaffer. Continuously Reinforced Concrete Pavements in Pennsylvania. *Bulletin 238*. HRB, National Research Council, Washington, D.C., 1960.
4. D. G. Zollinger. *Investigation of Punchout Distress of Continuously Reinforced Concrete Pavement*. Ph.D. thesis. Department of Civil Engineering, University of Illinois at Champaign-Urbana, 1989.
5. *NCHRP Synthesis 60: Failure and Repair of Continuously Reinforced Concrete Pavement*. TRB, National Research Council, Washington, D.C., July 1979.
6. S. A. La Coursiere, M. I. Darter, and S. A. Smiley. Performance of Continuously Reinforced Concrete Pavement in Illinois. Civil Engineering Studies, Transportation Engineering Series 10. University of Illinois, Urbana, 1978.
7. D. J. Janssen. *The Effect of Asphalt Concrete Overlays on the Progression of Durability Cracking in Portland Cement Concrete*. Ph.D. thesis. University of Illinois, Urbana-Champaign, 1985.
8. J. D. Lindsay. A Ten-Year Report on the Illinois Continuously Reinforced Pavement. *Bulletin 214*. HRB, National Research Council, Washington, D.C., 1959.

9. D. R. Schwartz. *Effect of Subbase Type and Subsurface Drainage on Behavior of CRC Pavements*. Physical Research Report No. 83. Bureau of Materials and Physical Research, Illinois Department of Transportation, May 1979.
10. B. F. McCullough, A. Abou-Ayyash, W. R. Hudson, and J. P. Randall. *Design of Continuously Reinforced Concrete Pavements for Highways. NCHRP Project 1-15*. TRB, National Research Council, Washington, D.C., Aug. 1975.
11. B. F. McCullough, J. C. M. Ma, and C. S. Noble. *Limiting Criteria for the Design of CRCP*. Research Report 177-17. Center for Transportation Research, University of Texas, Aug. 1979.
12. E. G. Kleyne and P. F. Savage. The Application of the Pavement DCP to Determine the Bearing Properties and Performance of Road Pavements. Presented at the International Symposium on Bearing Capacity of Roads and Airfields, Trondheim, Norway, June 1982.
13. Adrian J. Van Wijk. *Rigid Pavement Pumping: (1) Subbase Erosion; (2) Economic Modeling*. Ph.D. thesis. School of Civil Engineering, Purdue University, West Lafayette, Ind., 1985.
14. D. H. Jiang, S. P. Shah, and A. T. Andonian. Study of the Transfer of Tensile Forces by Bond. *ACI Journal*, Proceedings Vol. 81, No. 3, May–June 1984, pp. 251–259.
15. Y. Goto. "Cracks Formed in Concrete Around Deformed Tension Bars. *ACI Journal*, Proceedings Vol. 68, No. 4, April 1971, pp. 244–251.
16. R. M. Mains. Measurement of the Distribution of Tensile Stresses Along Reinforcing Bars. *ACI Journal*, Proceedings Vol. 48, Nov. 1951, pp. 225–252.
17. P. T. Foxworthy. *Concepts for the Development of a Nondestructive Testing and Evaluation System for Rigid Airfield Pavements*. Ph.D. thesis. Department of Civil Engineering, University of Illinois, Urbana-Champaign, 1985.
18. M. S. Hoffman and M. R. Thompson. *Mechanistic Interpretation of Nondestructive Pavement Testing Deflections*. Civil Engineering Studies, Transportation Engineering Series 32, Illinois Cooperative Highway and Transportation Research Program Series No. 190, University of Illinois, Urbana, 1981.
19. A. M. Ioannides. Dimensional Analysis in NDT Rigid Pavement Evaluation. *Journal of Transportation Engineering*, ASCE, Vol. 116, No. 1, Jan.–Feb. 1990, pp. 23–26.
20. A. M. Ioannides, M. R. Thompson, and E. J. Barenberg. The Westergaard Solutions Reconsidered. Presented at the 1985 Annual Meeting of the Transportation Research Board, Washington, D.C., January, 1985.

Publication of this paper sponsored by Committee on Rigid Pavement Design.

Aggregate Interlock: A Pure-Shear Load Transfer Mechanism

ANASTASIOS M. IOANNIDES AND GEORGE T. KOROVESIS

A finite element investigation was made of the behavior of jointed or cracked pavement systems equipped with a pure-shear load transfer mechanism, such as aggregate interlock. Dimensional analysis was used in the interpretation of the data, leading to a general definition of the relative joint stiffness of the pavement system in terms of its structural characteristics. Results obtained in this study were verified by comparisons with earlier published field, laboratory, and analytical information. The investigation demonstrated that deflection load transfer efficiency is related to stress load transfer efficiency and that this relationship is sensitive to the size of the applied loading (or to the gear configuration). A simple back calculation procedure is outlined to evaluate the in situ joint stiffness of such pavements. Pure-shear load transfer devices are shown to be particularly desirable under a combined externally applied and thermal loading condition, since they offer no additional restraint to longitudinal curling.

Aggregate interlock is a natural mechanism effective in transferring loads across discontinuities, such as joints and cracks, in plain or reinforced Portland cement concrete pavement systems. Only a shear action is operative in this mechanism. In contrast, load transfer devices such as dowel bars also involve bending, thus creating an interest to investigate load transfer by aggregate interlock. This mechanism is easier to model and analyze than, say, a doweled system. Furthermore, its study can provide useful information on alleviating certain ill side effects resulting from the use of bending action load transfer mechanisms, such as additional restraint to longitudinal curling. Finally, interpretation of numerical results obtained from the simpler shear-only devices can suggest methods for handling data pertaining to the more complex case of doweled pavement systems. A finite element investigation is presented to provide a better understanding of the most significant aspects of load transfer in slab-on-grade pavements, when this does not involve bending action.

Because of its questionable long-term endurance record, aggregate interlock is not relied on as a primary load transfer mechanism, except perhaps in low-volume roads. Abrasion and attrition of the aggregates, coupled with temperature variations causing a fluctuation in the size of the opening at the discontinuity, can result in a significant decrease in the effectiveness of this mechanism over time. This deterioration, however, does not detract from the value of a research effort such as is described below. Even for doweled pavement, "the current concept [is] that load is transferred across a joint principally by shear . . . [whereas] moment transfer across joints with visible openings is negligible" (*1*,*2*).

The finite element computer program ILLI-SLAB (*3*,*4*) was used in this study. This program has been thoroughly checked for accuracy and reliability. It has been adapted recently to permit analysis of multiple-slab systems under combined externally applied and thermal loads (*5*). Aggregate interlock (or any pure-shear device, in general) is modeled in ILLI-SLAB by a set of linear springs, acting at each node along the discontinuity. The spring constant assigned, therefore, is indicative of the stiffness of the joint, which is itself a function of joint width, as well as aggregate angularity and hardness. This model is similar to that employed in comparable codes, such as J-SLAB (*6*) and WESLIQID (*7*).

Numerical data are interpreted by using the principles of dimensional analysis (*8*). This approach offers an attractive, often superior, alternative to the more conventional statistical interpretation techniques. As demonstrated in this paper, the considerable progress achieved in understanding load transfer systems, and in compromising apparently conflicting evidence in the technical literature, confirms the validity of this assertion.

EFFICIENCY AND ENDURANCE OF JOINTS

Aggregate interlock was first recognized as a beneficial load transfer mechanism in the early 1900s, when the popularity of Portland cement concrete as a paving material was beginning to increase. The first major field tests and other investigations seeking to provide a better understanding of pavement behavior, thereby leading to improved designs, also date from that time. The Bates Road Test, conducted near Bates, Ill., between 1921 and 1923 (*9*), led to the conclusion that once cracks had formed in plain concrete, they tended to propagate rapidly and deteriorate badly under a small number of load repetitions (*10*). In contrast, cracks developing in reinforced concrete pavement sections remained tight, deteriorated slowly, and exhibited overall much better behavior.

The issue of long-term endurance of natural aggregate interlock has been addressed by subsequent studies as well. In an extensive field investigation conducted by the Michigan State Highway Department in the early 1930s, the superior performance of reinforced sections (in which cracks were held tight) was confirmed, under both a single, as well as repeated, load applications. Therefore it was concluded that "when roughened edges of two slabs are held firmly together the aggregate interlock may be expected to function perfectly and permanently as a load-transfer medium" (*11*). Seasonal variations

A. M. Ioannides, Department of Civil Engineering, University of Illinois, 205 N. Mathews Ave., Urbana, Ill. 61801. G. T. Korovesis, PCS/Law Engineering, 12240 Indian Creek Ct., Suite 120, Beltsville, Md. 20705-1242.

in the efficiency of load transfer at the cracks were also noted. These were the result of expansion of the slabs in the summer and their corresponding contraction in the winter. Joint opening was clearly established as a major determinant of aggregate interlock and efficiency of load transfer. The recommendation to use short slabs with reinforcement to keep tight any cracks that may develop (*10*) aimed at ensuring both initial load transfer efficiency (by "lessening the probability of erratic cracking") and better long-term endurance of the joints.

The Arlington load tests (*12*), on the other hand, led to the conclusion that

> aggregate interlock cannot be depended upon to control load stresses. Even when joints are held closed by bonded steel bars there is a wide variation in the value of the critical stress caused by a given load, from side to side of the joint and from point to point along it. For this reason it appears necessary to provide independent means for load transfer.

This constituted an implicit call for the use of dowels as load transfer devices, in view of the unreliability and variability of aggregate interlock. A fresh look at the Arlington conclusions is offered by the data obtained in this study.

The importance of achieving a satisfactory degree of load transfer at first loading, as well as maintaining this standard over a large number of load applications, was a primary motivation for the comprehensive laboratory study by Colley and Humphrey (*13*). These investigators introduced the Endurance Index (*EI*) as a descriptor of long-term joint performance. Expressed as a percentage, this value was defined as the ratio of the area under the curve of joint effectiveness (*Eff*) versus the number of repetitions (N) to the corresponding area under the curve obtained by setting *Eff* equal to 100 percent for $N = 1 \times 10^6$ cycles. The joint effectiveness was defined as follows:

$$Eff = \frac{2\,\Delta_U}{\Delta_U + \Delta_L} * 100 \text{ percent} \qquad (1)$$

where Δ_U and Δ_L are the deflections on the unloaded and the loaded side of the joint or crack, respectively.

Their laboratory tests examined five factors considered important to both *EI* and *Eff*, namely, joint width (ω); slab thickness (h); load magnitude (P); foundation type and subgrade modulus (k); and shape of aggregate. Slabs were tested on an unprotected silty-clayey soil (k = 89 psi/in.), as well as on the same subgrade covered with a 6-in. base, consisting of either sandy gravel (k = 145 psi/in.) or a cement-treated material (k = 452 psi/in.). The composite subgrade modulus values quoted were averages from 24-in.-diameter plate load tests. Results confirmed that *Eff* decreases as ω increases, or as N increases, with about 90 percent of the loss occurring during the first 500,000 repetitions. In addition, *EI* is improved considerably as k increases. Both *Eff* and *EI* deteriorate as P increases above some critical value, suggesting that "light loads cause little or no wear and probably do not need to be considered." More angular aggregates resulted in better long-term performance, as expected. Similarly, thicker slabs exhibited higher *Eff* and *EI* values than thinner ones.

Following the advent of nondestructive testing (NDT) methods in recent years, attention has also been directed to field evaluation of the load transfer performance of joints and cracks. The falling weight deflectometer (FWD) has been a popular choice for this purpose, with the recommendation for more sensitive sensors to detect small differences in deflection across the discontinuity tested (*14*). Results to date (*15*) suggest that an increase in ambient temperature improves the efficiency of joints or cracks that are free to open or close. This had also been the conclusion of earlier studies not involving the FWD (*11*,*16*).

ENGINEERING INDEPENDENT VARIABLES

The preceding discussion shows that the number of parameters involved in the problem under investigation is large. A factorial designed on the basis of the assumption that the effects of each of these is independent of the others would be prohibitively extensive. It is true that in a finite element investigation such as is described below several factors that are important in the field cannot be explicitly accounted for. Using the Aggregate Interlock Option in ILLI-SLAB, for example, it is not possible to study the effect of the number of load applications (N) on long-term endurance or the effect of aggregate characteristics on joint effectiveness. Even joint width can be incorporated only indirectly in the selection of the spring constant (AGG) used to represent the shear stiffness per unit length of the joint. This constant is also commonly referred to as the aggregate interlock factor (AIF). Empirical relations are, therefore, necessary to fill these and other analytical gaps. Yet, even for an idealized and simplified problem, such as is posed by an ILLI-SLAB run, a methodology is required for designing a short but effective factorial of runs and for interpreting the results obtained so that broad conclusions may be reached. Previous investigations at the University of Illinois have demonstrated the efficacy of dimensional analysis for this purpose.

In previous analytical studies involving a single slab under a single-wheel load, the following nondimensional engineering independent variables have been established:

1. The load size ratio (a/l), where a is the radius of the applied load and l is the radius of relative stiffness of the slab-foundation system (*17*);
2. The slab size ratios (L/l and W/l), where L and W are the length and width of the slab, respectively (*18*,*19*); and
3. The temperature differential parameter ($\alpha\Delta T$) in which α is the coefficient of linear expansion of the slab material and ΔT is the temperature differential between the top and the bottom of the slab (*20*).

The effect of dual-wheel loads (and, by implication, of multiple-wheel loads, in general) may be quantified by the spacing ratio S/a, where S is the distance between the wheels (*21*). This gives rise to the equivalent single axle radius (ESAR) concept, which would allow the application of results obtained from single-wheel load studies to cases involving more complex gear configurations (*20*). Recent efforts have shown that it is possible to derive with reasonable accuracy an ESAR for any arbitrary loading gear configuration simply as a function of its geometry (size and spacing of tire prints). The loss of accuracy involved in such a transformation from a multiple- to a single-wheel load is the topic of an ongoing investigation at the University of Illinois.

It is essential to establish the form of the nondimensional engineering independent variable(s) governing the behavior of a two-slab system equipped with a pure-shear load transfer mechanism, such as aggregate interlock. A procedure suggested by Langhaar (*22*) may be used for this purpose. The only additional input parameter entering a typical ILLI-SLAB run involving aggregate interlock is AGG, whose dimensions are FL^{-2}. To form a nondimensional product (π), AGG must be combined with one or more other input parameters, which include force (F) and length (L) in their dimensions. To reduce the number of choices further, it is pertinent to recall that AGG is a stiffness term. It is, therefore, reasonable to consider, at least to begin with, other stiffness terms. Clearly, the subgrade modulus (k) and the radius of relative stiffness (l) are ideal choices, since they also possess the necessary dimensions.

Now, any product (π) of these three parameters will have the following form:

$$\pi = k^{m1} l^{m2} \text{AGG}^{m3} \tag{2}$$

The corresponding dimensions of π are

$$\pi = (FL^{-3})^{m1} (L)^{m2} (FL^{-2})^{m3} \tag{3}$$

To obtain a dimensionless product, the exponents of F and L must be zero. Thus

$$m_1 + m_3 = 0 \tag{4}$$

$$-3m_1 + m_2 - 2m_3 = 0 \tag{5}$$

Assuming that $m_3 = 1$, a solution of the above system of equations is obtained for $m_1 = m_2 = -1$. Thus, the resulting dimensionless variable is AGG/kl. This variable expresses the relative stiffness of the joint itself to the stiffness of the pavement system in which it is installed. It is interesting to observe that $1/kl$ was identified as a pertinent lumped variable form by Tabatabaie and Barenberg (*3*).

Note that the formal procedure outlined by Langhaar (*22*) and applied above in writing and in solving equations 2 through 5 guarantees neither the uniqueness nor the suitability of the derived dimensionless variable. Like many other engineering aids (e.g., computers, statistics, and the finite element method), dimensional analysis is merely a tool. Fruitful implementation of this type of analysis demands considerable engineering judgment, imagination, and experience. It is primarily on the basis of engineering intuition that the three parameters in Equation 2 were selected in the first place. Furthermore, the weight of the numerical evidence presented below confirms the correctness and adequacy of the dimensionless variable selected. Although the formal derivation outlined above is the most appropriate way of presenting results in a paper, it is rare that one arrives at the most suitable form of the dimensionless variable a priori. More often than not, this is a painstaking trial-and-error procedure, concealed perhaps by the brevity demanded by technical journals. The satisfaction of finally establishing the most general form, and the resulting immense simplification of the problem, provide the fuel that sustains the student of dimensional analysis.

DIMENSIONLESS RESPONSE VARIABLES

The three primary response parameters in the analysis of slab-on-grade pavement systems are deflection (δ), bending stress (σ), and subgrade stress (q). When the dense liquid foundation model is adopted, the latter may be eliminated because

$$q = k\delta \tag{6}$$

Several dimensionless combinations of the first two response parameters have been proposed in the technical literature as measures of the load transfer efficiency developing in multiple-slab systems. The large number of definitions for the term joint effectiveness is because some definitions may not be appropriate or even correct, particularly when field measurements are considered. In the analytical study presented in this paper no such complications arose, since each definition may be transformed in an algebraically exact manner into any other. Nonetheless, the results justify to a considerable extent the concerns expressed by previous investigators about some definitions. Most of these pertain to the sensitivity of field measuring devices and the impact of relatively minor changes in measured responses.

The definitions adopted in the interpretation of the finite element data presented below are as follows:

- Deflection load transfer efficiency (LTE_δ) (often abbreviated simply load transfer efficiency or LTE):

$$\text{LTE}_\delta = \text{LTE} = \frac{\Delta_U}{\Delta_L} \times 100 \text{ percent} \tag{7}$$

- Stress load transfer efficiency (LTE_σ):

$$\text{LTE}_\sigma = \frac{\sigma_U}{\sigma_L} \times 100 \text{ percent} \tag{8}$$

- Transferred load efficiency (TLE):

$$\text{TLE} = \frac{P_T}{P} \times 100 \text{ percent} \tag{9}$$

where

σ_U, σ_L = slab bending stress on the unloaded and on the loaded side of a joint or crack, respectively;
P_T = total load transferred from the loaded to the unloaded side of a joint or crack, along its entire length; and
P = total externally applied load.

FINITE ELEMENT INVESTIGATION

The problem under investigation is fairly complex, even after the simplifying assumptions of linear elasticity, plate theory, and dense liquid foundation have been adopted. The purpose of these idealizations is to reduce the number of variables involved and thus improve the engineer's ability to understand, if not solve, the problem. Nonetheless, even in the idealized model there is a prohibitively large number of pos-

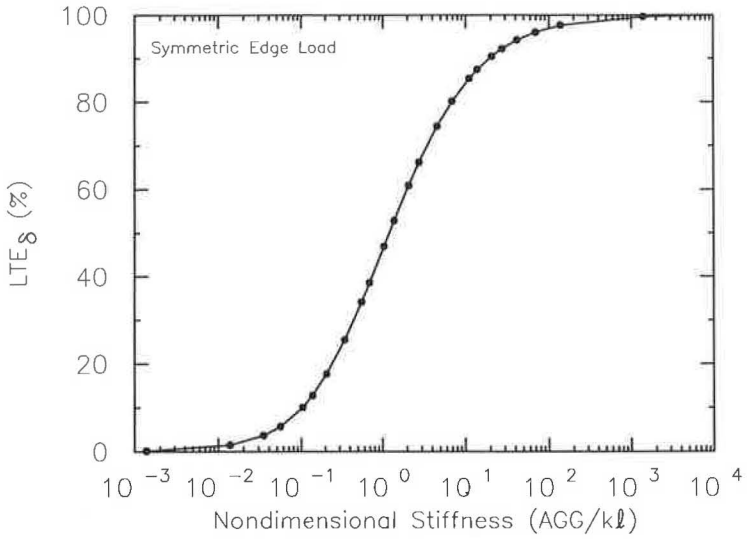

FIGURE 1 LTE_δ as a function of dimensionless joint stiffness (AGG/*kl*).

sible interconnections between the input parameters, so that to describe it completely would require an enormous number of analytical or experimental data. Dimensional analysis offers "a method to reduce the number of quantities which are related to each other [with] no sacrifice in accuracy. The simplification obtainable by dimensional analysis is pure gain" (*23*). The validity of these comments is clearly illustrated by the finite element runs presented below.

The major relationship established in this study is depicted in the form of the nondimensional plot of LTE_δ versus AGG/*kl* shown in Figure 1. Twenty-five executions of the ILLI-SLAB code were more than enough to define the S-shaped curve obtained with considerable precision. These runs were carefully designed to conform with user guidelines developed in previous investigations involving the use of ILLI-SLAB (*24*). To ensure the generality of the conclusions reached, the relationship described by Figure 1 was later verified and confirmed by a number of additional finite element runs, involving input parameters (such as slab modulus E, h, and k) that are substantially different from those used in the original form. It is apparent that "dimensional analysis leads to organization of the results of an analytical or experimental investigation so that is possible to present them more compactly and at the same time more generally than if the same information is presented in dimensional form" (*23*). In Figure 1, "the objectives of making the subject easier to grasp as a whole, or more compatible with related problems" (*23*) have all been achieved.

LTE_δ is extremely sensitive and deteriorates rapidly as the independent variable (AGG/*kl*) falls below 10. Also interesting is that other things being equal, an increase in the subgrade modulus (k) or the slab stiffness (Eh^3) will yield a lower LTE_δ. Experimental data presented by Teller and Cashell (*25*) as well as numerical results by Kilareski et al. and Ozbeki et al. (*26,27*) also pointed to the same conclusion, although this was not explicitly stated as such. Perhaps this was because such a conclusion would be in apparent contradiction to the intuitive speculation that a stronger subgrade or stiffer slab should improve pavement response. However, in this respect, a lower LTE_δ does not indicate a poorer pavement system, because absolute deflections and stresses will also be decreased as k or Eh^3 increases. Thus, the lower LTE_δ will be sustained over a longer period of time, leading to a higher endurance index, as reported by Colley and Humphrey (*13*).

The sensitivity of the relationship between LTE_δ and AGG/*kl* was also investigated for a range of values of the three other independent variables, *a/l*, *L/l*, and *W/l*, set in developing Figure 1 at values of 0.156, 5.0 and 3.9, respectively. These were considered to be representative of "typical" in situ conditions.

Effect of Size of Loaded Area

Thirty-two additional ILLI-SLAB runs, in which (*a/l*) ranged between 0.047 and 0.584, showed that the maximum change in LTE_δ was only 6 percent (from 84 to 90 percent). Thus, it may be concluded safely that the effect of the load size ratio on LTE_δ is not pronounced. Combining this result with the ESAR concept, it may be postulated that the relationship in Figure 1 also holds with adequate accuracy for multiple-wheel loads.

The load size ratio (*a/l*) influences significantly LTE_σ, however, as suggested by Figure 2. This plot shows the pronounced sensitivity of the relationship between LTE_δ and LTE_σ to changes in *a/l*. At any value of LTE_δ, much higher LTE_σ values are obtained as *a/l* increases, i.e., as the load becomes less concentrated. An additional benefit may also be expected from increased values of *a/l*, since the absolute value of pavement responses will also decrease as the load is distributed over a larger contact area.

Note that for any given (*a/l*) value, a small change in LTE_δ can result in a significant change in LTE_σ, particularly when more concentrated loads are considered. This would explain why Teller and Sutherland (*12*) concluded that LTE_δ is "not a usable measure of the stress conditions that accompany them." Their field measurements indicated that even when $\Delta_U - \Delta_L$, "as nearly as can be judged by visual examination," LTE_σ was only 50 percent. This conclusion was reiterated by Kelley (*28*). The latter also adopted an alternative definition

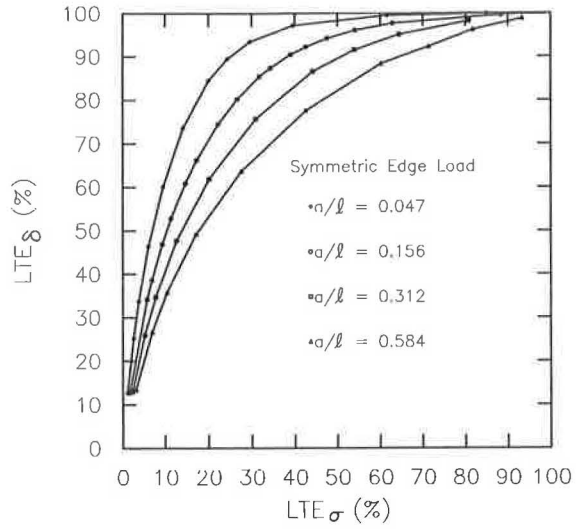

FIGURE 2 Relationship between LTE_δ and LTE_σ.

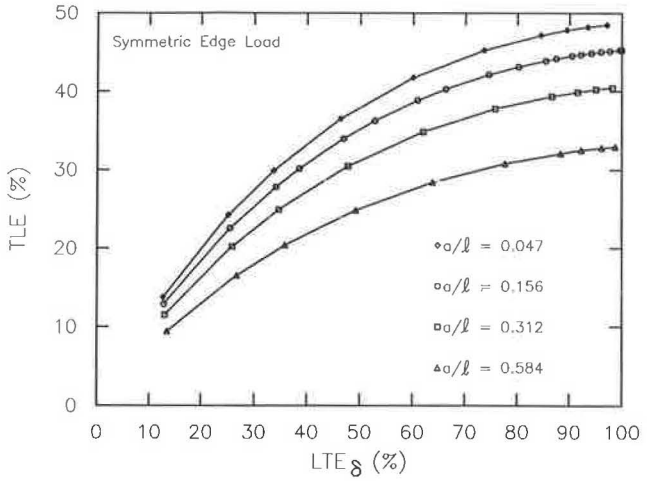

FIGURE 3 Relationship between LTE_δ and TLE.

of LTE_σ, suggested by Teller and Sutherland (*12*), hoping to overcome this difficulty. The Arlington data corresponded to *a/l* values between the upper two curves in Figure 2. In this range, LTE_δ is about 95 percent for LTE_σ of 40 percent. The measured deflections on each side of the joint were about 5 mils; i.e., an accuracy of 0.25 mils would have been necessary to discern any deviation in LTE_δ from the ideal value of 100 percent. Therefore, it is evident that the concerns of Teller and Sutherland (*12*) should be interpreted as a commentary on the accuracy of their measurements, coupled with the sensitivity of the relationship depicted in Figure 2. Most surprising, however, is that recently their presumption of no usable relationship between LTE_δ and LTE_σ has been replaced by the erroneous assumption of a unique correlation between these two response ratios.

Referring to the ESAR concept once again, it may be anticipated that individual curves similar to those in Figure 2 will be obtained for each specific multiple-wheel gear configuration. The single LTE_δ versus LTE_σ curve presented by Barenberg and Arntzen (*29*) should, therefore, be interpreted as pertaining to one loading configuration (i.e., one aircraft type). Similarly, unique relationships, such as those presented in the AASHTO Guide (*30*), by Bush et al. (*31*), by Korbus and Barenberg (*32*), and others, must be viewed as incomplete interpretations of a limited amount of data.

The sensitivity of LTE_σ to *a/l* exhibited in Figure 2 constitutes a significant finding of this study. A consequence of the faulty conception that the relationship between LTE_δ and LTE_σ is unique is encountered in the current design procedure of the Federal Aviation Administration (FAA) (*33*). This accounts for load transfer at the joints by reducing the free edge stresses by 25 percent. This is tantamount to assuming an LTE_σ of 33 percent. As indicated in Figure 2, this corresponds to 95 percent LTE_δ for a fairly concentrated load (*a/l* = 0.047), whereas for a more distributed load (*a/l* = 0.584) the concomitant LTE_δ is only 63 percent. The corresponding AGG/*kl* values from Figure 1 are about 50 and 2, respectively. Thus, the degree of conservatism in the FAA recommendation will vary widely as a function of the size (or configuration) of the applied loading considered, i.e., with aircraft type. It is regrettable that the uniqueness assumption is retained and made even more prominent in the envisaged "unified" design procedure, under development for the FAA by the U.S. Army Corps of Engineers (*34,35*).

The effect of *a/l* is also pronounced when considering the relationship between TLE and LTE_δ. As illustrated in Figure 3, TLE approaches its maximum theoretical value of 50 percent only for rather concentrated loads. Its limit value becomes progressively smaller as *a/l* increases, approaching 40 percent for *a/l* of about 0.5.

Effect of Slab Length and Slab Width

In both the original 25 runs and the additional 32 runs to investigate the effect of *a/l*, the slab length ratio (*L/l*) was maintained at 5.0, whereas the slab width ratio (*W/l*) was kept at 3.9. Under full contact conditions, *L/l* = 5.0 has been shown to result in infinite-slab responses (*18*). This value is also close to the shortest slab length encountered in practice (around 15 ft). On the other hand, *W/l* of 3.9 corresponds to (*L/W*) of about 1.25, which is the value usually recommended for this parameter [e.g., see AASHTO Guide (*30*)].

Setting *a/l* at 0.156, *W/l* at 3.9, and AGG/*kl* at 13.84, an additional series of five ILLI-SLAB runs was conducted in which *L/l* ranged from 1 to 9. For *L/l* in excess of about 4.0, TLE as well as LTE_δ and LTE_σ were found to be practically insensitive to slab length. Even for shorter slabs, LTE_δ and LTE_σ increase, whereas TLE decreases by only about 1.5 percent per unit decrease in (*L/l*).

Similarly, keeping *a/l* constant at 0.156, *L/l* at 5.0, and AGG/*kl* at 13.84, a series of five finite element runs was performed with *W/l* varying between 1 and 7. TLE was found to be insensitive to *W/l* throughout the range, whereas LTE_δ and LTE_σ were affected only for *W/l* below 4. The value of LTE_δ increases by 3 percent, whereas LTE_σ decreases by 8 percent per unit decrease in *W/l*. Both the slab length and slab width investigations, therefore, suggest that slab size effects on TLE, LTE_δ, and LTE_σ are not overly significant.

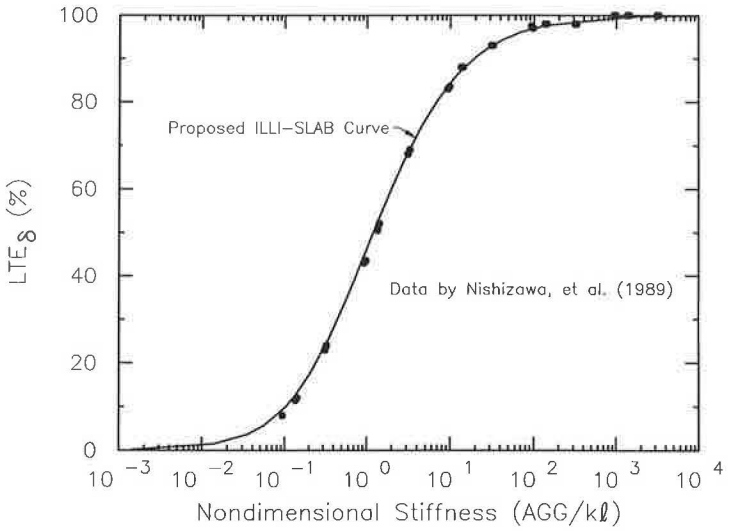

FIGURE 4 Verification of proposed curve using data by Nishizawa et al. (*36*).

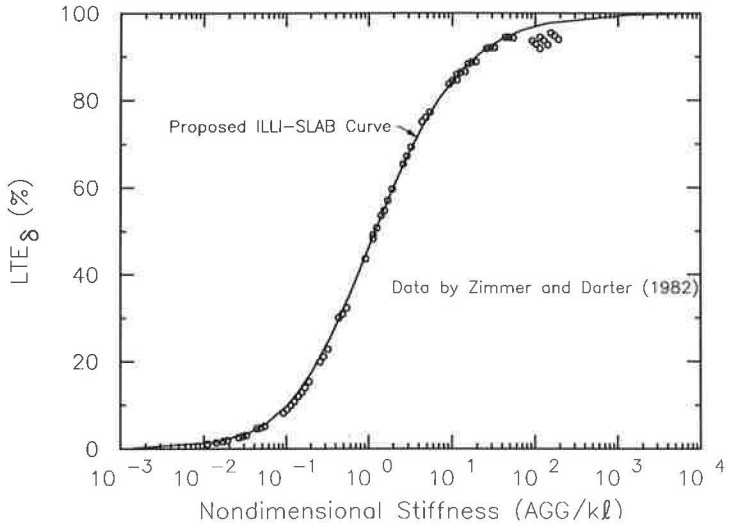

FIGURE 5 Verification of proposed curve using data by Zimmer and Darter (*37*).

RE-INTERPRETATION OF PREVIOUS STUDIES

Previous studies have also produced data describing the variation of LTE_δ as a function of the parameters entering the analysis of multiple-slab pavement systems with aggregate interlock. Implicit in the application of dimensional analysis described previously is the assertion that the resulting interpretation of the data is general. Thus, the S-shaped curve in Figure 1 should be valid with no regard to the individual input parameters assumed. It is, therefore, interesting to examine whether the proposed relationship between LTE_δ and AGG/*kl* can be reproduced from results presented in the technical literature.

Nishizawa et al. (*36*) presented data obtained from the execution of a new finite element code in the form of LTE_δ versus κ/k, where κ represents the joint spring stiffness per unit area of shear in the cross-section of the slab. This parameter, therefore, corresponds to *AGG/h* as used in ILLI-SLAB, or AGG/*kl* = (κ/k) × (*h*/*l*). Figure 4 presents the data by Nishizawa et al. (*36*) replotted in terms of AGG/*kl* and superimposed on the ILLI-SLAB curve from Figure 1. Despite the fact that results from two different computer programs are compared, the scatter in Figure 4 is impressively narrow. In fact, it is significantly less than that exhibited by the original plot presented by those investigators.

Similarly, Figure 5 presents a re-interpretation of a data base generated using ILLI-SLAB by Zimmer and Darter (*37*). In the partial factorial of 64 finite element runs performed, *k* ranged from 50 to 400 psi/in., *h* from 6 to 8 in., and AGG from 10^2 to 10^6 psi. The data obtained had been presented as LTE_δ versus AGG for various *k* and *h* values in a total of 15 separate curves. These, however, are usable only for the pavement systems employed in their derivation. The same data, plotted against the proposed independent variable (AGG/*kl*)

allow the consolidation of the original 15 curves into one. This not only confirms the generality and validity of the Figure 1 curve (solid line in Figure 5), but more importantly it permits the application of the data base to cases outside the range considered in its development. According to Taylor (*23*) "perhaps [the] most important use [of dimensional analysis] to the engineer is as a means of developing the ability to generalize from experience and thus to apply knowledge to a new situation. Although always perilous, generalization is essential to bring an element of order into an otherwise chaotic world." The minor scatter in Figure 5 can be attributed to the coarseness of the finite element mesh used to perform these runs.

Plots of LTE_δ versus AGG/*kl* were also prepared for ILLI-SLAB data presented by Tabatabaie and Barenberg (*3*) and by Korbus and Barenberg (*32*). These also confirmed the generality of the proposed S-shaped curve in Figure 1 (*5*), but are not presented in this paper for the sake of brevity.

PRACTICAL APPLICATIONS

The S-shaped curve shown in Figure 1 offers the possibility of determining the in situ stiffness of joints and cracks. Nondestructive testing (NDT) data may be used for this purpose, in conjunction with a procedure to backcalculate *k* and *l*, e.g., program ILLI-BACK (*15*,*38*). The value of LTE_δ can also be obtained using the FWD, for example, with sensors located on either side of the discontinuity. Thus, knowing these three parameters, the in situ stiffness of the joint or crack, AGG, may be readily determined from Figure 1. Periodical measurements of this important characteristic of the pavement system can provide useful insights into a study of the time history of joint deterioration. In addition, through carefully designed experiments, the factors influencing AGG may be investigated. These include the joint (or crack) width, ambient temperature, aggregate shape, and resistance to polishing.

The proposed backcalculation approach may also be used in interpreting experimental results published in the literature. Consider, for example, the data presented by Colley and Humphrey (*13*). These investigators tested slabs whose effective length may be considered infinite, since they restrained the upward movement of the slab ends when the joint was loaded. The slab width, however, was only 46 in., or less than 2.0 *l*. Accordingly, their reported *Eff* values were first converted to LTE_δ, and these were then adjusted by decreasing them by 3 percent per unit change of *W*/*l* when the latter was less than 4.0. Both the data reported by Colley and Humphrey (*13*), and the results of the backcalculations conducted in this study are given in Table 1.

A word of caution is in order concerning the numerical accuracy of the backcalculated AGG values. These values are based on data read off the figures in the original paper, which themselves consist of best-fit curves to the actual experimental

TABLE 1 BACKCALCULATION OF JOINT STIFFNESS FROM DATA BY COLLEY AND HUMPHREY (*13*)

h in.	k psi/in.	ℓ in.	(a/ℓ)	(W/ℓ)	ω in.	Eff %	LTE_δ %	(AGG/kℓ)	AGG psi
7	89	35.1	0.228	1.31	0.035	89	72	4.1	1.3E+04
9	89	42.3	0.189	1.09	0.035	92	76	5.4	2.0E+04
7	145	31.0	0.258	1.48	0.065	82	62	2.2	1.0E+04
7	145	31.0	0.258	1.48	0.045	88	70	3.7	1.7E+04
7	145	31.0	0.258	1.48	0.035	88	71	3.8	1.7E+04
7	145	31.0	0.258	1.48	0.025	93	78	6.2	2.8E+04
7	145	31.0	0.258	1.48	0.015	98	88	14.2	6.4E+04
9	145	37.5	0.213	1.23	0.085	40	17	0.2	1.1E+03
9	145	37.5	0.213	1.23	0.065	78	56	1.6	8.9E+03
9	145	37.5	0.213	1.23	0.045	98	88	14.6	8.0E+04
9	145	37.5	0.213	1.23	0.035	99	89	16.8	9.1E+04
9	145	37.5	0.213	1.23	0.025	99	90	19.0	1.0E+05
9	452	28.2	0.284	1.63	0.085	84	65	2.7	3.4E+04
9	452	28.2	0.284	1.63	0.065	92	78	6.1	7.7E+04
9	452	28.2	0.284	1.63	0.035	98	89	17.4	2.2E+04

Note: E = 4.6 x 10^6 psi (based on unconfined compressive stress data); μ = 0.15; a = 8 in.; W = 46 in.
Eff values are as reported by Colley and Humphrey.
LTE_δ = (Eff/(200-Eff)) x 100%. LTE_δ values given are adjusted for slab width.

results. In addition, Figure 1 was used in the backcalculation, using LTE_δ values adjusted as noted above. For these reasons, the backcalculated AGG values may be considered as approximate (perhaps within ±30 percent), giving a fairly good picture only of the order of magnitude of this parameter for the test conditions investigated.

Of particular interest to users of ILLI-SLAB or of similar finite element codes is the fact that Figure 1 provides the opportunity to determine a priori the value of AGG to be provided as input to the program to achieve a desired level of LTE_δ. Until now, guidelines for the selection of AGG had been scarce, and this process has often been one of trial and error.

Nishizawa et al. (*36*) outlined a method that may be used to relate joint stiffness to the joint opening. This method involves using the following simple empirical equation, which expresses LTE_δ as a linear function of a ω:

$$LTE_\delta \text{ (percent)} = 100 - 25\,\omega \text{ (millimeters)} \quad (10)$$

Equation 10 appears to be a best-fit straight line through the data by Colley and Humphrey (*13*), reproduced in Table 1. A logarithmic expression may also be fitted to the relation between LTE_δ and relative joint stiffness (such as that shown in Figure 1). Thus, combining these two equations, a third may be obtained relating the joint stiffness to ω. Such a procedure is treacherous, however, because it involves combining an empirical relation with a mathematically exact function. The accuracy and reliability of its outcome are often hard to establish and rarely can be used successfully in a quantitative, as opposed to a merely qualitative, manner.

It may be reasonable to postulate that a curve similar to that in Figure 1, relating LTE_δ and the relative joint stiffness of the pavement system, should also exist for pavements fitted with dowels as the primary load transfer mechanism. In consequence, the relationships depicted in Figures 2 and 3 would also hold for doweled pavements. The pertinent questions that need to be answered are how to define the relative joint stiffness of a doweled pavement system, and how to relate this to such factors as dowel spacing, joint opening, and the modulus of dowel support. Research in this direction is continuing at the University of Illinois.

AGGREGATE INTERLOCK EFFECTS IN CURLING ANALYSIS

One of the primary concerns in designing load transfer mechanisms for a pavement system is the possibility of a detrimental effect when external loads and a temperature differential are considered simultaneously. With respect to doweled joints, in particular, Kelley (*28*) cautioned that "dowels that are too stiff may cause more distress in the pavement slab than would result from their complete omission," due to an increased "restraint to longitudinal warping." In recent years, there has been considerable interest in devices that would "take up the shear forces due to the passage of vehicles by preventing vertical movements, while allowing longitudinal movements created by thermal changes" (*39*). Such a shear-only load transfer mechanism can be modeled using the Aggregate Interlock Option in ILLI-SLAB. This program was, therefore, used to examine the response of a two-slab system with aggregate interlock, under combined externally applied and thermal loading conditions.

A partial factorial of 16 ILLI-SLAB runs was performed for this purpose. The governing independent variable ($\alpha\Delta T$) was set at 1.5×10^{-4}, which corresponds to a daytime temperature differential of about 30°F. Daytime conditions are often considered to be critical when combined with an externally applied edge load (*20*,*40*). To reduce the number of runs required, *a*/*l* was fixed at 0.23, since its effect on LTE_δ was found to be small. Under a temperature differential the effect of the load size ratio most likely will be more pronounced, particularly with respect to slab bending stresses (*20*). This outcome, however, should not influence the broad conclusions sought here with respect to the impact of aggregate interlock on curling responses. Setting L equal to W, two values of the slab size ratio, L/l, were considered, namely, 4.1 and 14.8, simulating the behavior of a short and an infinite slab, respectively. Finally, the joint stiffness ratio AGG/*kl* was set to 1.0 for a low efficiency joint and at 10.0 for a high efficiency joint. These inputs gave rise to four runs for each of the following three loading conditions: external load only, curling only, and combined curling and external loading. In addition, four extra runs were performed to examine the corresponding single-slab case: two for external loading only, and two for combined loading (one for each of the two L/l values). The response of a single slab under curling-only conditions was identical to that of each of two slabs connected by aggregate interlock, and it was not repeated.

The results obtained by finite element are presented in Table 2. Under curling-only conditions, joint stiffness caused by a pure-shear mechanism does not affect the response of either a short or a long slab. In contrast, a mechanism that involves bending as well may be expected to increase the curling-only stresses, particularly in shorter slabs. Thus, a pure-shear load transfer system would reduce edge stresses caused by the load, without increasing the curling-only stresses. This response would be especially desirable during the early life of the pavement system when the slab strength has not yet developed fully.

For either of the two levels of AGG/*kl* considered, very similar LTE_δ and LTE_σ values are obtained for both the short and long slabs if the external load is considered alone. In contrast, under combined external load plus temperature differential conditions, a substantial improvement in load transfer efficiency is obtained in either slab size level, as AGG/*kl* increases. It is also interesting to observe that the principle of superposition (conventionally used to obtain the maximum combined stress) applies fairly well in the case of long two-slab systems, but leads to considerable underestimates when short slabs are analyzed.

The maximum combined stresses in the two-slab systems are also lower than the corresponding stresses in the single slabs, especially for the higher AGG/*kl* value. Thus, aggregate interlock (and by implication, pure-shear devices) perform best when needed the most, without increasing curling-only stresses. A manufactured shear-only load transfer mechanism, installed either during or after pavement construction, would also largely eliminate the durability and deterioration problems experienced when relying on natural aggregate interlock alone.

TABLE 2 AGGREGATE INTERLOCK EFFECTS IN CURLING ANALYSIS

RUN	(L/ℓ)	(AGG/kℓ)	Δ_L mils	Δ_U mils	LTE_δ %	σ_L psi	σ_U psi	LTE_σ %	P_T kips	TLE %
(a) Load Only: Two Slabs										
1	14.8	1.0	8.5	3.6	42	314	40	13	3.2	32
2	14.8	10.0	6.6	5.4	83	257	96	37	4.2	42
3	4.1	1.0	9.5	4.4	46	310	34	11	3.2	32
4	4.1	10.0	7.5	6.3	85	252	92	36	4.1	41
(b) Curling Only: Two Slabs, or One Slab										
5	14.8	1.0	14.9	14.9	100	311	311	100	0	0
6	14.8	10.0	14.9	14.9	100	311	311	100	0	0
7	4.1	1.0	1.2	1.2	100	68	68	100	0	0
8	4.1	10.0	1.2	1.2	100	68	68	100	0	0
(c) Load + Curling: Two Slabs										
9	14.8	1.0	23.9	18.8	79	628	354	56	3.5	35
10	14.8	10.0	21.9	20.8	95	571	411	72	4.5	45
11	4.1	1.0	14.9	9.2	62	417	132	32	3.6	36
12	4.1	10.0	12.7	11.5	91	356	194	55	4.4	44
(d) Load Only: One Slab										
13	14.8	-	12.1	-	-	354	-	-	-	-
14	4.1	-	13.9	-	-	344	-	-	-	-
(e) Load + Curling: One Slab										
15	14.8	-	27.8	-	-	669	-	-	-	-
16	4.1	-	20.5	-	-	461	-	-	-	-

Note: $E = 4 \times 10^6$ psi; $\mu = 0.15$; h = 8 in.; k = 500 psi/in.; $\ell = 24.3$ in.; P = 10 kips; p = 100 psi; $\alpha = 5 \times 10^{-6}$ in./in.°F; $\Delta T = +30$ °F; L = W

CONCLUSIONS

The study of the behavior of joints and cracks in slab-on-grade systems is the primary justification for the development of all analytical procedures pertaining to so-called "rigid pavement." Were it not for the presence of such discontinuities, the contributions of pioneers like Westergaard, Bradbury, and Pickett would hardly have commanded the respect they have enjoyed for decades among pavement engineers. Extensive laboratory and field studies of joint performance have also been undertaken since the early 1900s, involving a great investment of both time and money. Investigators such as Older, Teller and Sutherland, Kelley, or Benkelman owe a significant portion of their well-deserved reputations to such investigations. It is unfortunate that in more recent years—following the rise to prominence of the personal computer—the very complex phenomena occurring at such discontinuities have largely been ignored, as a result of a tendency to think wishfully that Westergaard is dead.

This paper is intended as a constructive contribution to the debate surrounding the adoption by some agencies of a "unified" analysis and design approach. Unfortunately, this often means that the particular identifying characteristics of "rigid" pavement systems (with joint behavior topping the list) are entirely disregarded, but not without potential penalties.

In this investigation, it has been shown how a sophisticated analytical tool (the finite element method) and a time-honored numerical data interpretation approach (dimensional analysis) can be combined to yield a simple description of the complex problem at hand. This explanation can easily be incorporated into a personal computer algorithm for routine application. The methodology described also offers the following possibilities:

1. Back calculation of in situ joint stiffness using NDT data;
2. Reinterpretation and compromise of available laboratory and field test results, which may have been apparently contradictory;
3. Abandonment of long-held false perceptions, such as those pertaining to the uniqueness of the relationship between LTE_δ and LTE_σ, or to the futility of searching for such a relationship altogether;
4. An improved understanding of more complex load transfer mechanisms, such as doweled systems;
5. Evaluation of the desirability of pure-shear devices; and
6. An approach for analyzing the effect of multiple-wheel loads, when results obtained are combined with the ESAR concept.

REFERENCES

1. Y. H. Huang. Discussion: Finite-Element Analysis of Jointed or Cracked Concrete Pavements, by A. M. Tabatabaie and E. J. Barenberg. In *Transportation Research Board Record 671*, TRB, National Research Council, Washington, D.C., 1978, pp. 17–18.
2. American Concrete Institute. Structural Design Considerations for Pavement Joints. *Journal of the American Concrete Institute*, Vol. 28, No. 1, July 1956, pp. 1–28.
3. A. M. Tabatabaie and E. J. Barenberg. Structural Analysis of Concrete Pavement Systems. *Transportation Engineering Journal*, ASCE, Vol. 106, No. TE5, Sept. 1980, pp. 493–506.
4. A. M. Ioannides, M. R. Thompson, and E. J. Barenberg. Finite Element Analysis of Slabs-On-Grade Using a Variety of Support Models. *Proc., 3rd International Conference on Concrete Pavement Design and Rehabilitation*, Purdue University, West Lafayette, Ind., April 23–25, 1985, pp. 309–324.
5. G. T. Korovesis. *Analysis of Slab-on-Grade Pavement Systems Subjected to Wheel and Temperature Loadings*. Ph.D. thesis. University of Illinois, Urbana, 1990.
6. S. D. Tayabji and B. E. Colley. *Analysis of Jointed Concrete Pavements*. Report FHWA/RD-86/041. FHWA, U.S. Department of Transportation, 1986.
7. Y. T. Chou. *Structural Analysis Computer Programs for Rigid Multicomponent Pavement Structures with Discontinuities—WESLIQID and WESLAYER: Report 2: Manual for the WESLIQID Finite Element Program*. Technical Report GL-81-6. U.S. Army Engineer Waterways Experiment Station, Vicksburg, Miss., May 1981.
8. P. W. Bridgman. *Dimensional Analysis*, 2nd ed. Yale University Press, New Haven, Conn., 1931.
9. C. Older. Highway Research in Illinois. *Transactions*, ASCE, Vol. 87, Paper 1546, 1924, pp. 1180–1224.
10. R. D. Bradbury. *Reinforced Concrete Pavements*. Wire Reinforcement Institute, Washington, D.C., 1938.
11. A. C. Benkelman. Tests of Aggregate Interlock at Joints and Cracks. *Engineering News Record*, Vol. 111, No. 8, Aug. 24, 1933, pp. 227–232.
12. L. W. Teller and E. C. Sutherland. The Structural Design of Concrete Pavements. *Public Roads*, Vol. 16, No. 8, Oct. 1935, pp. 145–158; Vol. 16, No. 9, Nov. 1935, pp. 169–197; Vol. 16, No. 10, Dec. 1935, pp. 201–221; Vol. 17, No. 7, Sept. 1936, pp. 175–192; Vol. 23, No. 8, April, May, June 1943, pp. 167–212.
13. B. E. Colley and H. A. Humphrey. Aggregate Interlock at Joints in Concrete Pavements. *Bulletin 189*, HRB, National Research Council, Washington, D.C., 1967, pp. 1–18.
14. E. B. Owusu-Antwi, A. H. Meyer, and W. R. Hudson. Preliminary Evaluation of Procedures for the Assessment of Load Transfer Across Joints and Cracks in Rigid Pavements Using the Falling Weight Deflectometer. *Proc., 4th International Conference on Concrete Pavement Design and Rehabilitation*, Purdue University, W. Lafayette, Ind., April 18–20, 1989, pp. 697–708.
15. A. M. Ioannides, E. J. Barenberg, and J. A. Lary. Interpretation of Falling Weight Deflectometer Results Using Principles of Dimensional Analysis. *Proc., 4th International Conference on Concrete Pavement Design and Rehabilitation*, Purdue University, W. Lafayette, Ind., April 18–20, 1989, pp. 231–247.
16. M. Poblete, J. Blanco, R. Salsilli, R. Valenzuela, and P. Sprätz. Slab Behavior of Plain Undoweled Concrete Pavements. Presented at 5th Symposium on Concrete Pavements, Aachen, W. Germany, June 2–4, 1986.
17. A. M. Ioannides. Discussion: Response and Performance of Alternate Launch and Recovery Surfaces that Contain Layers of Stabilized Material, by R. R. Costigan and M. R. Thompson. In *Transportation Research Record 1095*, TRB, National Research Council, Washington, D.C., pp. 70–71, 1986.
18. A. M. Ioannides, M. R. Thompson, and E. J. Barenberg. Westergaard Solutions Reconsidered. In *Transportation Research Record 1043*, TRB, National Research Council, Washington, D.C., 1985, pp. 13–23.
19. A. M. Ioannides and R. A. Salsilli-Murua. *Slab Length, Slab Width and Widened Lanes Effects in Rigid Pavements*. Prepared for the FHWA, U.S. Department of Transportation. Contract No. DTFH61-85-C-00103, University of Illinois, Urbana, Ill., December 1988.
20. A. M. Ioannides and R. Salsilli-Murua. Temperature Curling in Rigid Pavements: An Application of Dimensional Analysis. In *Transportation Research Record 1227*, TRB, National Research Council, Washington, D.C., 1989, pp. 1–11.
21. A. M. Ioannides. Discussion: Thickness Design of Roller-Compacted Concrete Pavements, by S. D. Tayabji and D. Halpenny. In *Transportation Research Record 1136*, TRB, National Research Council, Washington, D.C., 1988, pp. 31–32.
22. H. L. Langhaar. *Dimensional Analysis and Theory of Models*. John Wiley and Sons, Inc., New York, 1951.
23. E. S. Taylor. Dimensional Analysis for Engineers. Clarendon Press, Oxford, England, 1974.
24. A. M. Ioannides. *Analysis of Slabs-on-Grade for a Variety of Loading and Support Conditions*. Ph.D. thesis. University of Illinois, Urbana, 1984.
25. L. W. Teller and H. D. Cashell. Performance of Dowels Under Repetitive Loading. *Public Roads*, Vol. 30, No. 1, April 1958, pp. 1–24.
26. W. P. Kilareski, M. A. Ozbeki, and D. A. Anderson. *Fourth Cycle of Pavement Research at the Pennsylvania Transportation Research Facility—Vol. 4: Rigid Pavement Joint Evaluation and Full Depth Patch Designs*. Report FHWA/PA-84-026. The Pennsylvania Transportation Institute, The Pennsylvania State University, University Park, December 1984.
27. M. A. Ozbeki, W. P. Kilareski, and D. A. Anderson. Computer Simulation and Field Evaluation of Transverse Joints in Rigid Pavements. *Proc., 3rd International Conference on Concrete Pavement Design and Rehabilitation*. Purdue University, W. Lafayette, Ind., April 23–25, 1985, pp. 577–586.
28. E. F. Kelley. Application of the Results of Research to the Structural Design of Concrete Pavements. *Public Roads*, Vol. 20, No. 5, July 1939, pp. 83–104; Vol. 20, No. 6, August 1939, pp. 107–126.
29. E. J. Barenberg and D. M. Arntzen. Design of Airport Pavements as Affected by Load Transfer and Support Conditions. *Proc., 2nd International Conference on Concrete Pavement Design and Rehabilitation*. Purdue University, W. Lafayette, Ind., April 14–16, 1981, pp. 161–170.
30. *AASHTO Guide for Design of Pavement Structures*. American Association of State Highway and Transportation Officials, Washington, D.C., 1986.
31. A. J. Bush, III, R. W. Brown, and C. E. Bailey. An Evaluation Procedure for Rigid Airfield Pavements. *Proc., 4th International Conference on Concrete Pavement Design and Rehabilitation*. Purdue University, W. Lafayette, Ind., April 18–20, 1989, pp. 419–429.
32. L. Korbus and E. J. Barenberg. *Longitudinal Joint Systems in Slip-Formed Rigid Pavements: Vol. IV—Recommendations for Alternate Joint Systems and for Strengthening Existing Joints*. Report No. DOT/FAA/RD-79/4, IV, FAA, U.S. Department of Transportation, November 1981.

33. Federal Aviation Administration. *Airport Pavement Design and Evaluation*. Advisory Circular AC 150/5320-6C. U.S. Department of Transportation, Dec. 7, 1978.
34. J. L. Rice. FAA Sponsored Project for Mechanistic Pavement Design. Presented at ASCE/ATD Airfield Pavement Committee Meeting, Washington, D.C., Jan. 26, 1989.
35. Y. T. Chou. Rigid Pavement Design for Roads and Streets Elastic Layered Method. *Proc., 4th International Conference on Concrete Pavement Design and Rehabilitation*. Purdue University, W. Lafayette, Ind., April 18–20, 1989, pp. 267–278.
36. T. Nishizawa, T. Fukuda, and S. Matsuno. A Refined Model of Doweled Joints for Concrete Pavement Using FEM Analysis. *Proc., 4th International Conference on Concrete Pavement Design and Rehabilitation*. Purdue University, W. Lafayette, Ind., April 18–20, 1989, pp. 735–745.
37. T. D. Zimmer and M. I. Darter. *Load Transfer Efficiency with Various Subgrade Modulus and Aggregate Interlock Factor Values*. ERES Consultants, Inc. Champaign, Ill., March 1982.
38. A. M. Ioannides. Dimensional Analysis in NDT Rigid Pavement Evaluation. *Journal of Transportation Engineering*, ASCE, Vol. 116, No. 1, Jan./Feb. 1990, pp. 23–36.
39. J. P. Christory, J. L. Nissoux, P. Orsat, and F. Verheé. Load Transfer Restoration at Joints. *Proc., 4th International Conference on Concrete Pavement Design and Rehabilitation*. Purdue University, W. Lafayette, Ind., April 18–20, 1989, pp. 709–724.
40. G. T. Korovesis and A. M. Ioannides. Discussion: Effect of Concrete Overlay Debonding on Pavement Performance, by T. Van Dam, E. Blackmon, and M. Y. Shahin. In *Transportation Research Record 1136*, TRB, National Research Council, Washington, D.C., 1987, pp. 129–132.

Publication of this paper sponsored by Committee on Rigid Pavement Design.

Mechanistic Design Considerations for Punchout Distress in Continuously Reinforced Concrete Pavement

DAN G. ZOLLINGER AND ERNEST J. BARENBERG

A study was undertaken at the University of Illinois to develop a mechanistic design approach for continuously reinforced concrete (CRC) pavements to account for punchout distress. A mechanism relating to the loss of load transfer and the progressive development of punchout-related distress is presented. Analysis procedures, demonstrated to implement the mechanism as a rationally based thickness design procedure for CRC pavement, suggest that the optimal crack interval is between 3 and 4 ft. Present CRC design methodologies focus on limiting to certain design criteria cracking intervals, crack width, and stress in the reinforcements. Load transfer mechanisms have not been considered in the limiting design criteria and consequently are not included in these design procedures. These methods attempted to determine the design pavement thickness based on the combined effects of environmental and load-related stress on the final crack spacing, which must be limited to the design cracking criteria. However, past experience has indicated that a certain percentage of crack spacing usually falls below the specified minimum crack interval. These data suggest a greater tendency for punchouts to develop within this lower range of crack spacing. How pavement thickness, percent reinforcement, and crack spacing may be considered with respect to pavement spalling and loss of load transfer in the process of punchout development are outlined.

Continuously reinforced concrete (CRC) pavements exhibit distinctive cracking patterns induced by the restraint to volumetric strains in the concrete material caused by the reinforcing steel. This type of pavement, in which the longitudinal reinforcement is placed in a continuous configuration, can be considered as an alternative to jointed concrete pavement in some instances. Once the transverse cracks develop, the role of the reinforcement is to maintain the crack width below certain levels so that, in combination with the pavement thickness, a high degree of load transfer efficiency can be achieved throughout the design life. The primary pavement distress in CRC pavements is the punchout and faulting between closely spaced transverse cracks. This distress is a manifestation of the loss of load transfer across the transverse cracks. Therefore, there is evident need for thickness design analysis of CRC pavement based on punchout failure mechanisms to improve the reliability against premature punchout development.

D. G. Zollinger, Department of Civil Engineering and Texas Transportation Institute, Texas A&M University, College Station, Tex. 77843. E. J. Barenberg, Department of Civil Engineering, University of Illinois, Urbana-Champaign, Ill. 61801.

Present thickness design procedures for CRC pavements are either based on a thickness ratio between CRC pavement and jointed concrete design thickness (*1*,*2*) or are indirectly related to limiting design criteria for calculated structural response parameters (*3*), or both. Neither of these methods for selection of the design thickness of CRC pavement considers load transfer across the transverse cracks directly. The latter method, which has been adopted into the 1986 AASHTO Design Guide (*3*) and into the Concrete Reinforcing Steel Institute (CRSI) design manual (*4*) for CRC pavement, approaches the design of CRC pavements by focusing on the prediction of crack spacing, crack width, and steel stress as a function of wheel load and environmentally induced contraction. The design crack width and steel stress are dependent on the design crack spacing, which is a function of the percentage of reinforcement and wheel load stress. Therefore, the percentage of reinforcement (and the wheel load stress as input) is determined so that the limiting design criterion applied to crack spacing, crack width, and steel stress indirectly produces a design pavement thickness. The design thickness is derived from this procedure because the percent of reinforcement and the wheel load stress are a function of the pavement thickness.

Present procedures recommend that crack spacing should be selected so that the crack width is small enough to minimize the entrance of surface water and to provide the necessary load transfer through aggregate interlock (*5*). The cracking design criteria have evolved over time to include shorter cracking intervals. Intervals initially were set between 5 and 8 ft based on deflection test results and steel corrosion studies (*6*). Most recently minimum crack spacing has changed to as low as 3 ft based on an arbitrary load transfer and pavement stiffness relationship. Field performance has suggested that the maximum crack spacing is a function of pavement spalling and should range between 6 and 8 ft (*7*). Frequently, punchout distress shows up in pavement sections with crack spacing of 1 to 2 ft. In spite of the limiting design criteria, a certain percentage of crack spacing usually falls below the specified minimum crack interval. A short cracking interval has been recognized as an undesirable feature (*6*).

Correlations between CRC pavement thickness and jointed pavement thickness are taken from present serviceability index ratings for jointed concrete pavement. The thickness design of jointed pavements was derived from performance equations developed from the AASHO Road Test predicting the future serviceability as a function of equivalent 18-kip single-axle load applications. These methods usually have resulted

in thicknesses less than that for jointed concrete pavement. Reported correlations were also made based on deflections comparisons (*8*) made in Texas, but they were not as conclusive. The 1986 AASHTO Design Guide describes thickness design for jointed and continuously reinforced concrete pavements by the same performance equations, meaning no reduction in CRC thickness. These equations consider the traffic level, concrete strength, modulus of support (K value), load transfer, terminal serviceability index, and design reliability. Load transfer is characterized by a load transfer coefficient (J), which is recommended in terms of the shoulder type. Tied concrete shoulders allow for lower J factors, which leads to less thickness. The J factor ranges from 2.9 to 3.2 for an asphalt shoulder to 2.3 to 2.9 for a tied concrete shoulder. Justification for the J factor has been somewhat subjective in past design guides (*9,10*) and still is to a certain extent, inasmuch as it is based on experience and mechanistic stress analysis (*3*). The applicability of equations and relationships describing the performance of jointed concrete pavements to CRC pavements has never been verified. Many state thickness standards have established 8 in. as a minimum CRC pavement thickness. However, the trend has been toward greater CRC pavement thicknesses since reports have been favorable of 10-in. CRC pavements under heavy traffic loads (*11*). Current design practice in which yielding pavement thicknesses are too thin has been under suspicion (*12*).

Several early failures have been attributed to excessive deflections under heavy loads, suggesting that greater thicknesses will improve performance. A move toward greater design thicknesses for CRC pavements is likely to be beneficial for performance. It appears, however, that the recommended increase in thickness is arbitrarily determined in the most recent version of the AASHTO Design Guide, i.e., there appears to be no well-defined, rational method to determine the thickness of CRC pavement. Since punchouts are the primary structural type of distress in CRC pavements, there is a need to understand punchout distress mechanisms and how they relate to thickness design and pavement performance to establish a basis for mechanistic thickness design. Arguments for increased CRC design thicknesses are difficult to justify unless punchout-related mechanisms are incorporated into the design procedure. Given the uncertain performance of CRC pavement, there is little doubt that thickness design must address more directly the variables that influence punchout performance (*12*).

Recently developed mechanistic analysis (*13–15*) models have established markedly different types of structural behavior between jointed and CRC pavements. Consequently, consideration for load and support conditions different from those of the AASHO Road Test in mechanistic terms extends beyond the design procedure of a simple thickness ratio (*10*). This problem is particularly evident in the consideration of stresses and strains leading to the development of punchout distress in CRC pavements. Since it is not reasonable to determine CRC design thickness based on jointed concrete behavior, a constant thickness ratio may not provide adequate reliability against the development of premature punchout distress. Based on a review (*16*) of the nature of and factors leading to punchout distress, a brief discussion and analysis of the failure modes associated with the punchout process in CRC pavements are presented.

BASIC FAILURE MODES LEADING TO PUNCHOUT DISTRESS

Four failure modes, relating to punchout distress based on the results of an in-depth field study (*16*), are proposed as fundamental thickness design considerations for CRC pavements. The analysis of the failure modes is based a priori on uniform support conditions. This analysis requires the use of a non- or low-erodible subbase. The failure modes are illustrated in Figure 1 in typical developmental sequence. Mode I failure is fracturing because of reinforcing bar pullout from the surrounding concrete. Fracturing of this nature has been noted in concrete pullout tests (*17,18*) and develops in the concrete at a steel stress range of 14 to 18 ksi. Field measurements of steel strains at the crack face indicate that this range of stress is frequently exceeded in the colder months of the year. Cyclic bond stresses in the concrete induced from environmental factors can result in a crack growth process, noted in the field study (*16*), around the reinforcing bar, effectively destroying the load transfer capability of the bar as a void develops. Additionally, a loss of bond stiffness (*19*) and pavement bending stiffness occurs. Bearing failure or rebar looseness can also lead to a void around the reinforcement and can have a detrimental effect on the pavement performance similar to the pullout fracture. Pullout failure may be difficult to avoid since the threshold stress is frequently exceeded. Therefore, the load transfer contribution of the reinforcing bar should be ignored.

Mode II, spalling of the transverse crack, is a function of the pavement stiffness. Because of the above assumption about the development of rebar voids, the pavement stiffness is significantly reduced. A certain amount of support loss can be allowed because results from the field study indicate that good performing CRC pavements have experienced some loss of edge support. As suggested in one study, there may be a reduction in pavement stiffness at the cracks because of gradual joint deterioration and declining load transfer efficiency (*20*). These conditions provide adequate justification to determine spall-related stresses based on a reduced pavement stiffness. The pavement stiffness cycles between high and low, mostly as a function of the temperature and the concomitant opening and closing of the cracks. The reduction in stiffness behavior, which occurs on a daily basis, can be assumed to predominate during the winter season. Reduced pavement stiffness is not only a function of the crack width (*21*) but also of the position of the reinforcing steel (*22*). Therefore, spall-related stresses can be determined as a function of the pavement stiffness, design crack width, steel percentage, and the position of the reinforcement in the slab. The narrower the transverse cracks the stiffer the overall pavement system, which in turn lowers the spall-related stresses. This mode of failure is a visual sign of progressive punchout development.

Failure mode III, shown in Figure 1, is a loss of load transfer along transverse cracks. Since the bar is assumed to provide no load transfer, the load transfer of the crack is solely a function of the crack width. Given a constant crack width, the load transfer will decrease under repetitive loading. The resulting load transfer efficiency is based on test results by the Portland Cement Association (PCA) (*5*) for 1 million load applications, which are interpreted as 1 million coverages.

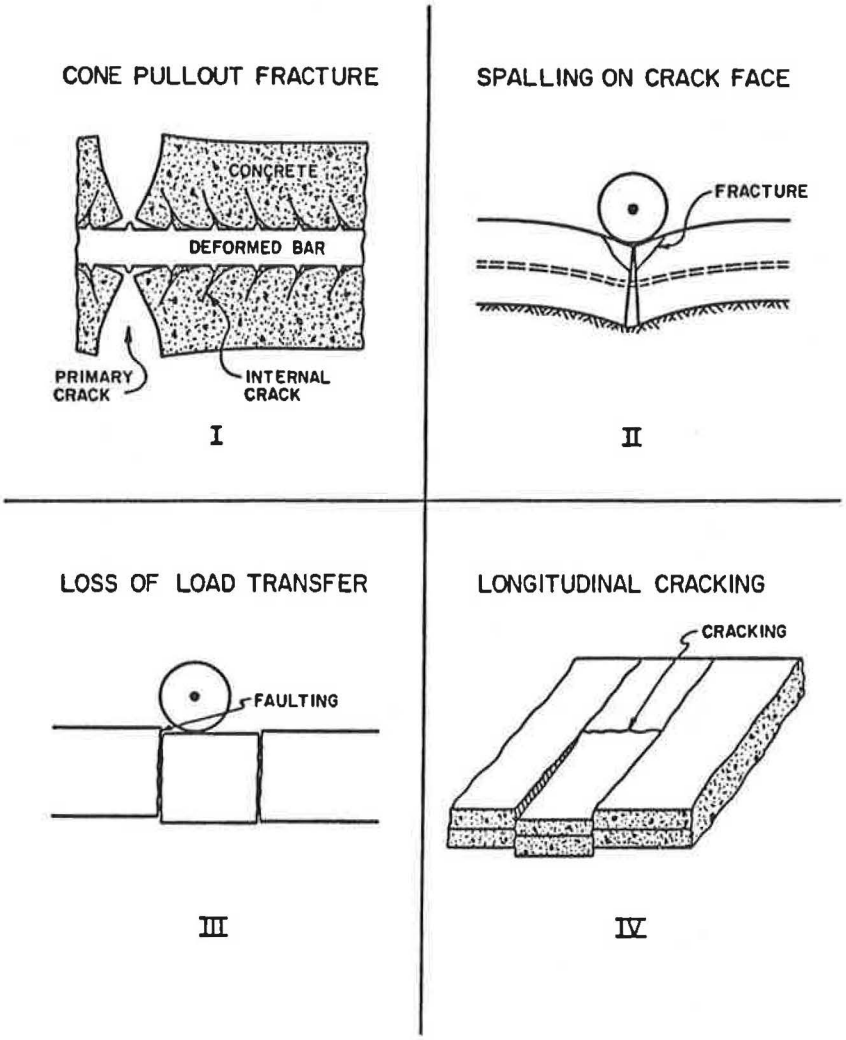

FIGURE 1 Failure modes related to punchout distress in CRC pavement.

The final mode of failure, mode IV, is related to bending stresses in the transverse direction. These stresses typically are not significant in CRC pavement so long as there is a high load transfer across the cracks (before spalling) or the crack spacing is greater than 4 ft. Transverse bending stresses should be considered in most instances since the crack spacing distribution in CRC pavement typically ranges below 4 ft. The load transfer has been noted to decrease significantly with spalling (type 2) in CRC pavements with thicknesses between 8 and 10 in. The transverse bending stresses should be increased in response to the change in load transfer.

SHEAR AND LOAD TRANSFER MECHANISM

As suggested in the description of mode I failure, a reduction in pavement stiffness may result from either pullout failure or bearing failure around the steel, both of which have been observed in field studies. The alternative to the development of excessive bar looseness is cone pullout fracture, which, if it occurs, will be the dominant cause for loss of pavement stiffness. In either case, the load transfer capability of the steel is lost and the load transfer consequently becomes dependent on the crack width and the aggregate interlock. Colley and Humphrey (*5*) of the PCA developed laboratory test data investigating the effect of crack width caused by aggregate interlock on load transfer characteristics in concrete pavements. This study was conducted using an instrumented test slab shown in Figure 2 subjected to a repetitive 9-kip load. The joint in the test slab was an induced crack from a metal strip 1 in. in height placed at the pavement bottom and top. During the repetitive loading, measurements of joint opening and slab deflections on the loaded and unloaded slab were made at regular intervals. The loading sequence across the joint was similar to a continuous application of truck loads traveling approximately 30 mph. Test results in the form of joint effectiveness (E_j), joint opening, and loading cycles for a 7- and a 9-in. slab thickness using a 6-in. gravel subbase are shown in Figure 3*a* and *b*. Joint effectiveness is similar to load transfer efficiency in that if the deflections on the loaded and unloaded slabs are equal then the joint effectiveness is 100 percent. [Note: the load transfer efficiency (LTE) is the unloaded deflection divided by the loaded deflection, in percent.]

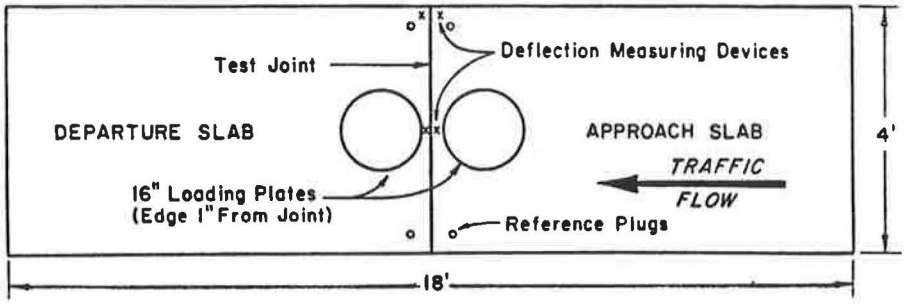

FIGURE 2 Plan of PCA test slab and instrumentation (*5*).

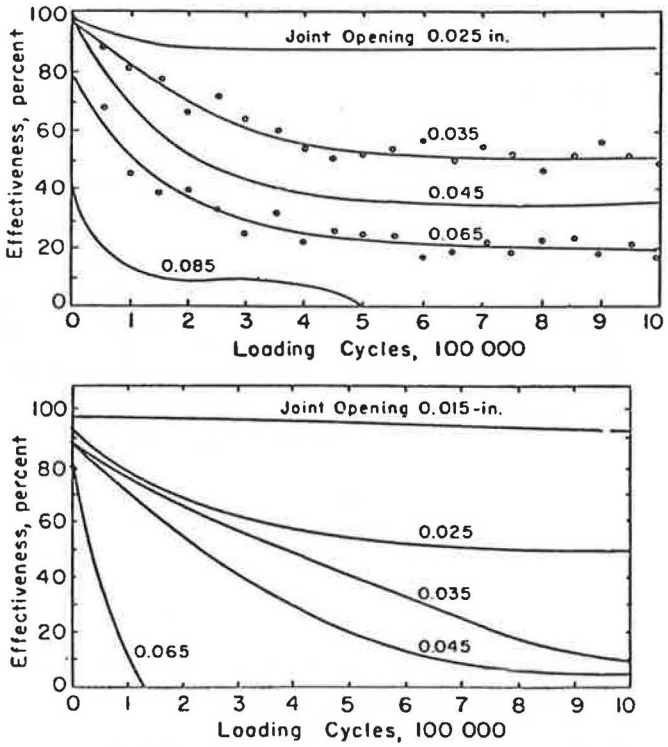

FIGURE 3 Influence of joint opening on effectiveness: (*top*) 9-in. concrete slab, 6-in. gravel subbase (*5*); (*bottom*) 7-in. concrete slab, 6-in. gravel subbase (*5*).

The results indicate that the joint effectiveness tends to level off after about 700,000 to 800,000 load applications. The level of joint effectiveness at 1 million applications may provide a useful basis relating joint or crack width to an ultimate joint effectiveness for design purposes. Figure 4 shows the change in the final joint effectiveness with the joint opening for the 7- and 9-in. thicknesses. Some results were also obtained for other subbase types and are shown in Figure 4, which indicate that foundation strength can improve the load transfer performance. The results from the 7- and 9-in. thicknesses are linearly extended to include other thicknesses. The joint effectiveness from the linear extensions was converted into load transfer efficiency and replotted in Figure 5. Further laboratory tests and field studies should be conducted to validate the extrapolations made from the PCA test data.

To extend the results of the PCA load tests to other load conditions and pavement configurations, load or shear stresses caused by the aggregate interlock must be determined for the test conditions. Using the load results directly is not reasonable since the laboratory loading conditions are different from those in actual CRC pavement. This difference is mostly because of the width of the test specimen, load position, and the height of the roughened interface where the aggregate interlock functioned. All of these factors can be accounted for in the slab analysis model ILLI-SLAB (*13*). This model allows determination of the load transferred by the aggregate interlock at each node along the transverse crack. Modeling the test slab with the ILLI-SLAB program yielded load stresses on the joint face for the test thicknesses plus the range of thicknesses in which the load transfer data had been extended. These results are shown in Figure 6.

Shear stresses can be found from other slab configurations, such as CRC pavement with closely spaced cracking (Figure 7), and related to the test slab conditions. A comparison of

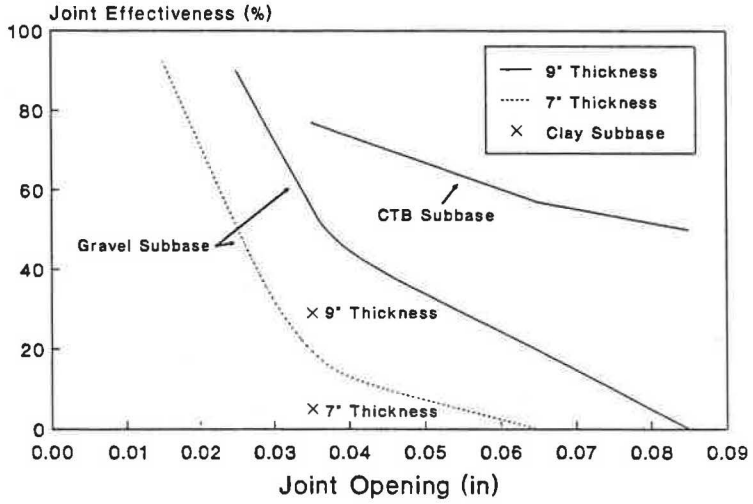

FIGURE 4 Joint effectiveness and joint opening relationship for 1 million load applications.

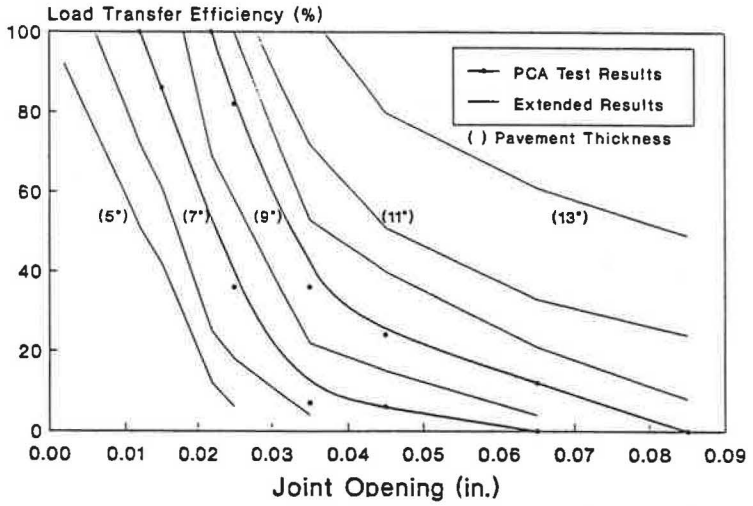

FIGURE 5 Load transfer efficiency and joint opening relationship for thicknesses 5 to 13 in.

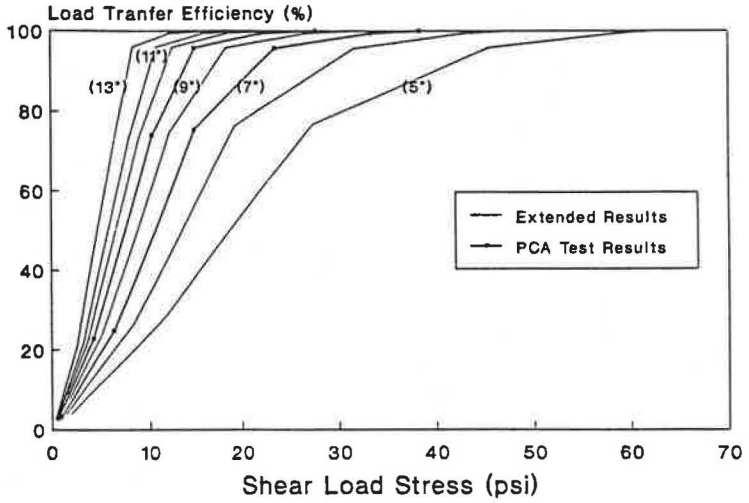

FIGURE 6 Computed load stress for PCA load transfer test results.

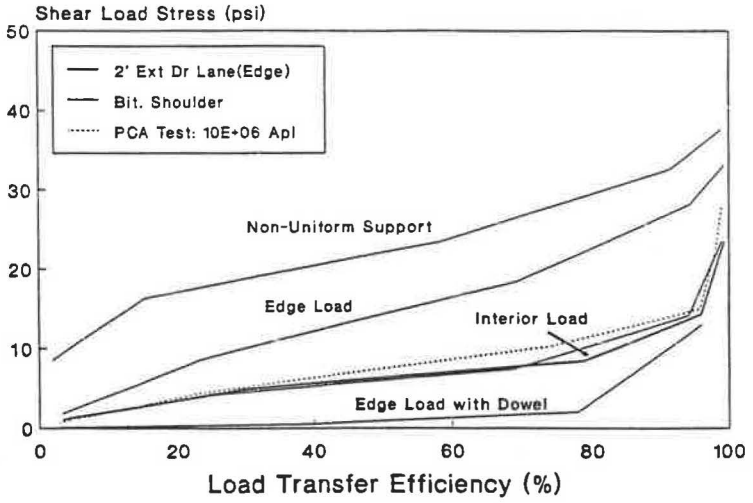

FIGURE 7 Shear load for various load conditions.

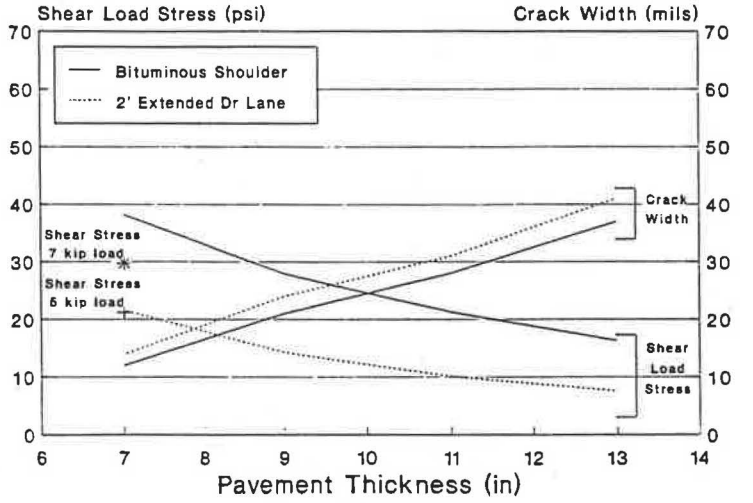

FIGURE 8 Effect of pavement thickness on shear load stress and required crack width (9-kip edge load).

a bituminous shoulder and a 2-ft extended driving lane is made in Figure 7 with the PCA test slab. An edge load position for the bituminous shoulder is adjacent to the outer pavement edge where an edge load position for the extended driving lane is 2 ft from the outer pavement edge. Greater shear stresses occur with a bituminous shoulder condition. The edge loading of a bituminous shoulder with non-uniform support represents the most severe loading conditions for shear stresses, as would be expected. The non-uniform support condition (see Figure 13) extends across the lane under the loaded slab in the ILLI-SLAB model. The loading condition for a 2-ft extended driving lane is not as severe as the loading conditions for the PCA test slab, whereas a bituminous shoulder load condition with the rebar contributing to the load transfer further lowers the shear stress. However, the latter difference is not as pronounced with LTEs greater than 90 percent. Little difference in shear stress is noted between an interior load position (inner wheel path) and the edge load position with the extended driving lane. Similar results were found between a 10-foot tied concrete shoulder and the extended driving lane.

Figure 6 indicates the LTE for a given thickness and load stress information that is entered into Figure 5 to determine the required joint opening (or crack width in the case of CRC pavements) to maintain the given level of LTE for 1 million coverages. Using Figures 6 and 5, in that order, the corresponding limiting crack widths are found and illustrated in Figure 8. This figure draws a comparison of edge loading between a bituminous shoulder and a 2-ft extended driving lane, with change in slab thickness at approximately a 95 percent LTE. This figure describes a fundamental relationship between required or limiting crack width and pavement thickness in terms of load transfer applicable to CRC thickness design.

SPALLING ON THE TRANSVERSE CRACK

Spalling in CRC pavements has been shown to be related to the loss of bending stiffness at the transverse crack (*16*). Discussions and results indicated that the reduction in bending

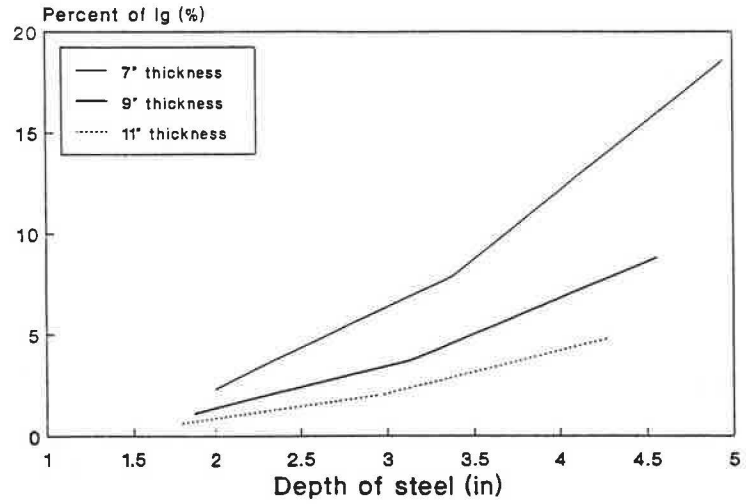

FIGURE 9 Pavement stiffness (I_{crk}) based on percentage reduction of gross moment of inertia (I_g).

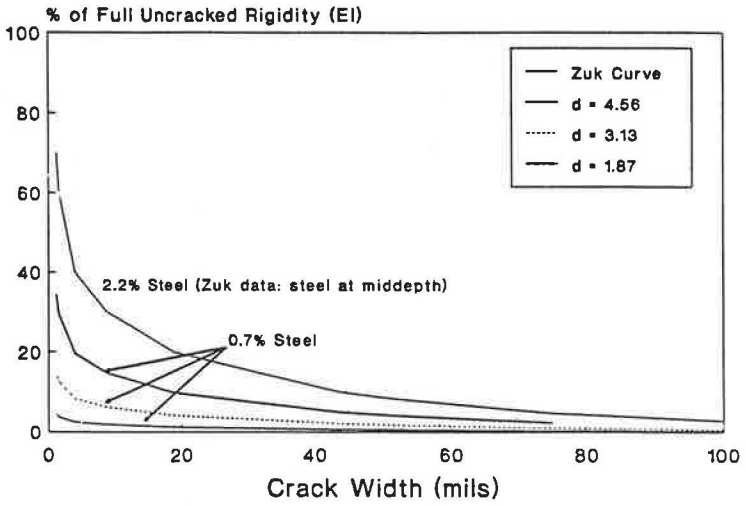

FIGURE 10 Reduction in bending stiffness as a function of crack width (depth of steel noted).

stiffness was cyclic in nature and dependent on the overall pavement temperature. Effective stiffness determined from NDT results indicated that a reduction in pavement bending stiffness of 90 percent was not uncommon. On this basis, spall stress can be determined using equations derived from elastic analysis of a crack section presented for the reduced moment of inertia (I_{crk}):

$$I_{crk} = b(kd)^3/3 + Na_s(d - kd)^2$$

$$= (kd)^3/3 + ntp(d - kd)^2 \text{ (per width } b)$$

where

b = unit width,
kd = distance to the neutral bending axis of the transformed section,
n = modular ratio [steel modulus (E_s)/concrete modulus (E_c)],
d = depth of steel,
t = pavement thickness, and
p = percent of steel [steel area (A_s)/concrete area (A_c)].

The reduced bending stiffness is found from a ratio of the cracked moment of inertia to the uncracked moment of inertia (Figure 9).

Zuk's (*21*) laboratory results for a cracked section shown in Figure 10 provide a relationship between the bending stiffness and the crack width for a cracked section. This relationship is extended to other cracked sections on the basis of the cracked moment of inertia, which is a function of the percent and position of the reinforcement. The percent reinforcement in the test specimens used by Zuk was 2.2 percent. The cracked moment of inertia for the test specimens was 17.9 percent of the gross moment of inertia (I_g). The same analysis can be applied to different thicknesses of CRC pavement shown in Figure 9 for 0.7 percent steel with various depths to the centroid of the reinforcement. Using the ratio between the per-

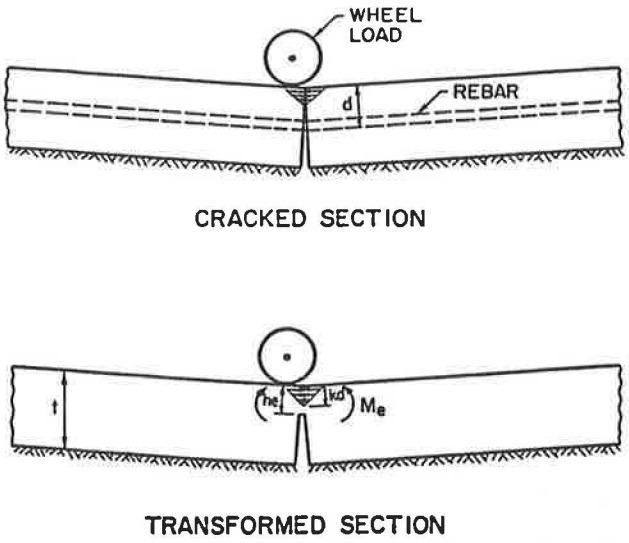

FIGURE 11 Transformation of cracked CRC pavement section.

cent reduction in the I_g for the CRC pavement sections to the percent reduction in I_g of the Zuk test specimens, a bending stiffness and crack width relationship can be developed for CRC pavement shown in Figure 10. In this figure, a comparison between the bending stiffness of a Zuk test specimen and a 9-in. cracked CRC section with 0.7 percent steel placed at various depths is shown. A crack width/stiffness relationship is defined as a function of the depth of steel.

The spall stresses may be found from the compressive and shear stress that develop on the transverse crack face while under load. Shear stresses, which have been discussed previously, and compressive stresses found independently and superimposed on the crack face can be one method of finding the spalling stress. The compressive stresses can be determined using ILLI-SLAB to model a transformed section of CRC pavement. The transformed section is the equivalent of a cracked section with steel reinforcement that has homogeneous material properties and provides the same bending stiffness as the cracked section (Figure 11). The cracked moment of inertia is used to determine the depth (h_e) of the transformed section as $h_e = \sqrt[3]{(12I_{crk})}$ (per unit width). A comparison between the depth to steel (d), depth to the neutral axis (kd), and the equivalent depth (h_e) indicates that the equivalent depth is greater than kd but less than d. The equation for k is found in terms of the depth to the centroid of the steel.

$$k = \{[pn(pn + 2r)]^{1/2} - np\}/r$$

where r is the ratio of the depth to the centroid of the steel (d) to the pavement thickness (t).

The equivalent depth (Figure 11) is input into ILLI-SLAB as the depth of the elements comprising a special case transverse crack. Load transfer by aggregate interlock is normally modeled in the ILLI-SLAB program by a spring element with 1 degree of freedom with displacement in the vertical direction at each node (*13*). The special case transverse crack is represented with reduced depth elements to model the change in bending stiffness that occurs at the crack. Modeling the transverse crack in this manner allows compressive stresses (σ_{ex}) and the bending moment (M_e) to be determined for the equivalent section as

$$M_e = (h_e)^2\sigma_{ex}/6$$

The compressive stress (σ_{cx}) of the cracked section is based on the equivalent bending moment (Figure 12):

$$M_e = Cjd = Tjd$$

$$= \sigma_{cx}kd(d - kd/3)/2$$

$$\sigma_{cx} = 6M_e/[kd^2(3 - k)]$$

The compressive stress is a function of the depth of the reinforcement (d) below the pavement surface, as shown in Figure 13. Compressive stresses for supported and unsupported conditions are included in the figure. In an unsupported condition, the pavement is only partially supported across the width of the lane shown in the figure. This condition is represented in ILLI-SLAB by a reduced K value under the loaded slab. The depth of steel is extended to the bottom of the pavement section, which represents the stresses, which are small, in an uncracked section. The compressive stresses approach this condition for high radius of relative stiffness (l_k) values. (Note: $l_k = [Eh^3/[12\ (1 - \mu)^2k]\}^{1/2}$, where E, h, and μ are the modulus of elasticity, pavement thickness, and Poisson's ratio, respectively.) The compressive stresses are much greater in the region of low l_k values. The compressive stresses are a function of the depth of steel in this region.

The finite element method (FEM) was again employed to develop spall-related stresses from a combined loading of compressive and shear stresses. The FEM mesh with the superimposed loading is shown in Figure 14 in which a 6-in. section of pavement was modeled using a linear, plane strain element. A boundary condition of zero displacement was used on the opposite boundary. The FEM results were consistent as long as the model section of pavement was 6 in. or greater. The maximum tensile stress normally occurs near the neutral bending axis on the crack face. Field results indicated that severe spalling is approximately 2 to 3 in. in depth. Spalling can begin closer to the pavement surface for unsupported conditions since the shear stress may not act over the full pavement thickness. Shear stresses were limited to the pavement above the steel for the unsupported conditions, whereas shear stresses were applied over the full pavement depth for the supported conditions. The support conditions have a sig-

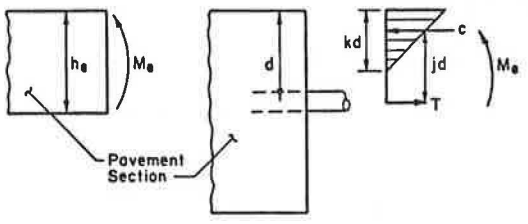

FIGURE 12 Bending moment in equivalent and cracked sections.

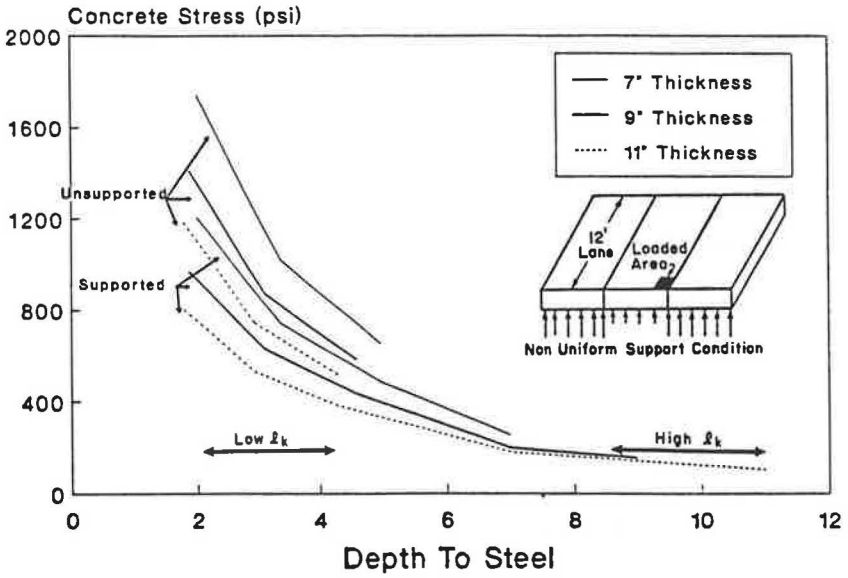

FIGURE 13 Compressive stress for a bituminous shoulder of a cracked section based on ILLI-SLAB analysis.

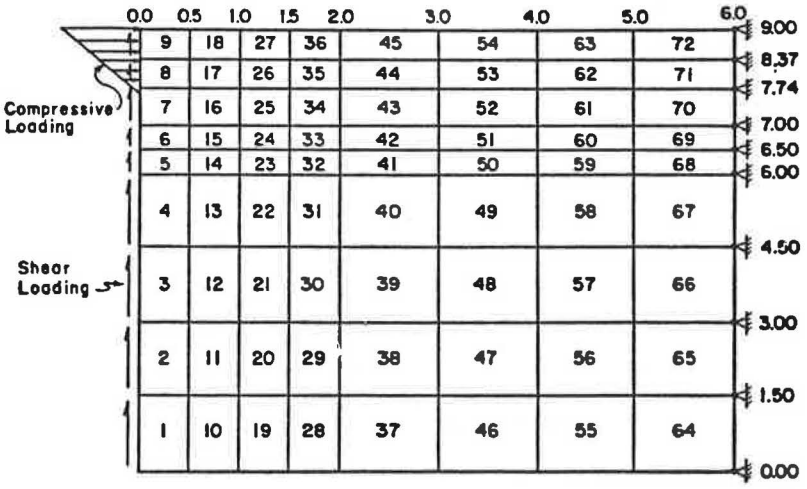

FIGURE 14 Nodal and loading layout for FEM modeling. (Element numbers are shown; nodal coordinates are in inches.)

nificant effect on the spalling stresses. The modeling of unsupported loading conditions tends to verify the field observations. The maximum tensile stresses are shown in Figure 15 as a function of the depth to steel and the support condition. The extended driving lane and the 10-ft tied shoulder reduce spalling stresses approximately 30 percent.

Figures 10 and 15 indicate that the crack width and the depth of steel have an influence on the pavement stiffness and consequently will also influence the spall stresses. Figure 16*a* illustrates the relationship between spall stress and pavement stiffness (caused by the effect of depth of steel). This information can be combined with information from Figure 10 to draw a relationship between crack width and spall stress for a given depth of steel shown in Figure 16*b*. The change in spall stresses is on the order of 50 to 60 psi between the range of crack widths of 10 to 40 mils (1 mil = 10^{-3} in.). Crack widths below 10 mils correspond to low spall stresses. This value corresponds to conditions of high pavement stiffness, as measured by l_k values at transverse cracks approximately 30 in. and greater, which may exist roughly 25 percent of the time.

TRANSVERSE BENDING STRESSES

The formation of longitudinal cracking by lateral stresses caused by wheel load has been thoroughly reviewed by others (*11*). Crack spacing and load transfer have been shown to significantly affect the lateral stresses. Transverse bending stresses (σ_a), illustrated in Figure 17*a*, are low at high values of LTE. Based on ILLI-SLAB results, the effect of support conditions are shown for a 2-ft crack spacing in Figure 17*b*. These stresses are significant below an LTE of 70 percent but increase at a

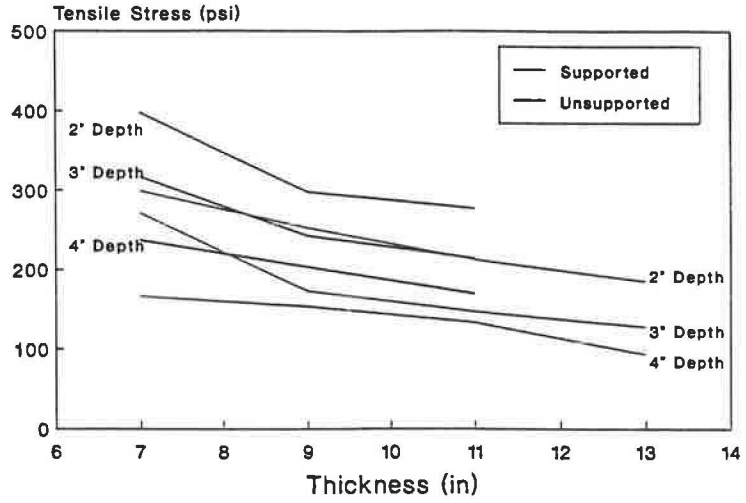

FIGURE 15 Maximum tensile spall stresses for bituminous shoulder.

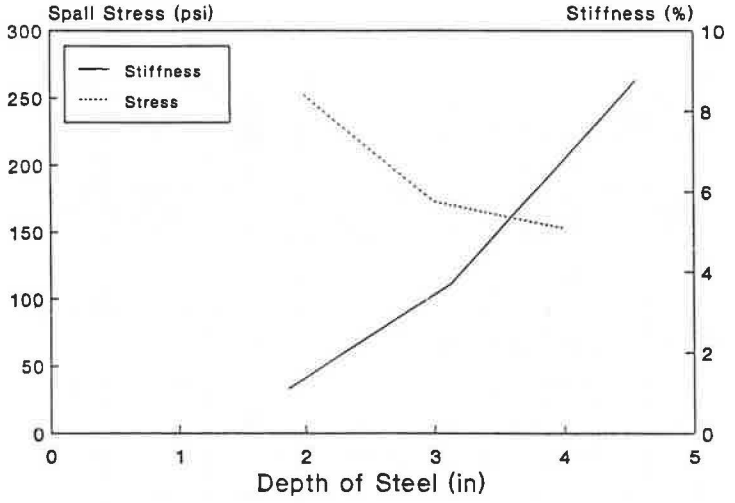

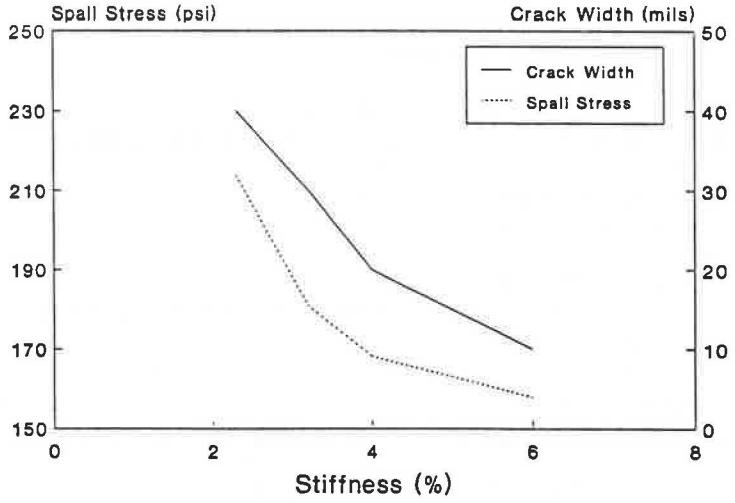

FIGURE 16 (*Top*) Spall stress/stiffness relationship for 9-in. CRC pavement with 0.7 percent steel. (*Bottom*) Spall stress/crack width relationship for 9-in. CRC pavement with 0.7 percent steel (d = 3.1 in.).

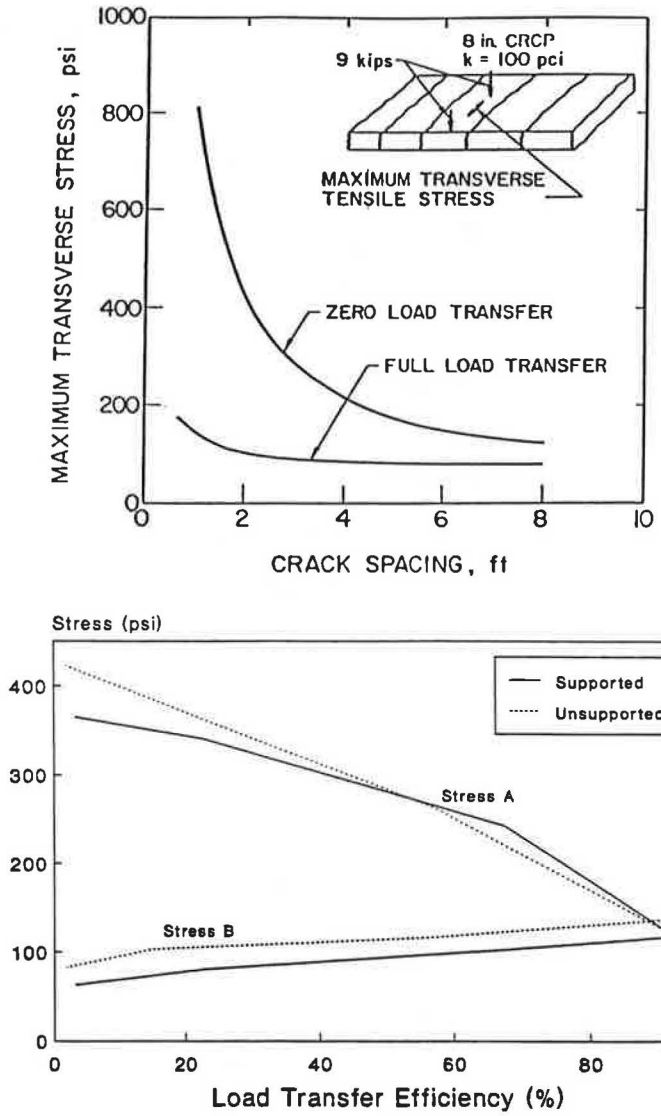

FIGURE 17 (*Top*) **Effect of load transfer across transverse cracks and crack spacing on maximum transverse tensile stress in CRC pavement (*1*).** (*Bottom*) **Transverse and longitudinal bending stresses for 9-in. CRC pavement as a function of LTE (2-ft crack spacing).**

uniform rate below 90 percent LTE. In comparison, the longitudinal bending stresses (σ_b) are relatively low and normally of no concern. According to these results, loss of load transfer has a more significant effect on the bending stresses than does loss of support. The loss of load transfer must develop before longitudinal cracking stresses develop. This point reemphasizes the importance of the spalling mechanism discussed previously in a thickness design procedure.

Figure 18 illustrates a comparison between σ_a and σ_b and provides some basis for selection of optimal crack spacing. The σ_b stress drops with decreasing crack spacing as long as the load transfer remains high. In the case of spalling and loss of load transfer, a crack spacing between 3 and 4 ft is desired. This cracking interval is selected because if the LTE remains high then either of the stresses within that range is not excessive. However, if the LTE becomes low then the stresses corresponding to the high load transfer condition will not be exceeded. Crack spacing outside of this range will cause higher stresses in either case of LTE, leading to a shorter fatigue life. The crack spacing range of 3 to 4 ft provides a balance between the maximum stresses σ_a and σ_b, causing the stresses to be somewhat independent of the load transfer. Spall stresses can have a significant influence on the thickness design for a 2-ft crack spacing but would have less of an impact for a 4-ft crack spacing. Deflection and subgrade stresses are not a problem unless the cracking spacing drops below 3 ft. A balanced condition between stresses σ_a and σ_b results in the case of a 2-ft extended driving lane or a 10-ft tied shoulder for a crack spacing range between 5 and 6 ft. The stresses are much lower than those for the bituminous shoulder case in the 3- to 4-ft range. The stresses in the 3- to 4-ft range for the 2-ft extended shoulder case are approximately 5 to 6 percent lower than the stresses for the bituminous shoulder case in the same range.

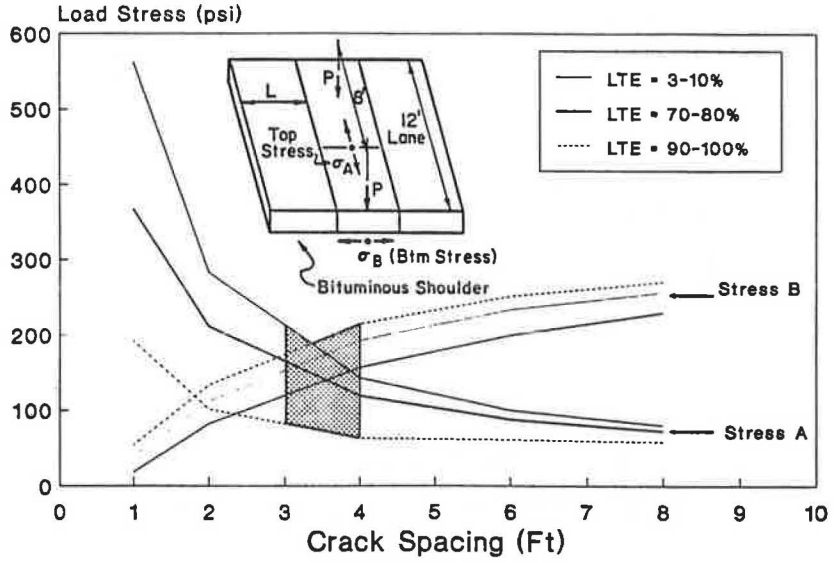

FIGURE 18 Comparison of σ_a and σ_b with crack spacing for a 10-in. pavement thickness.

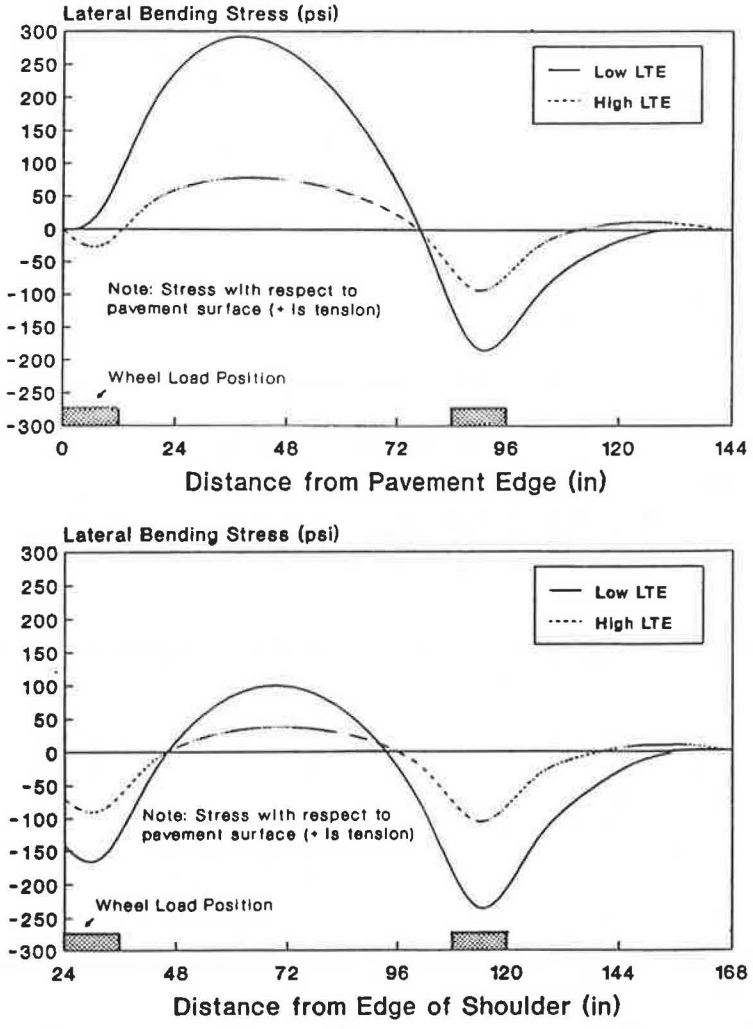

FIGURE 19 Comparison between shoulder types of stress distribution for 9-in. pavement (2-ft crack spacing): (*top*) bituminous shoulder; (*bottom*) 2-ft extended driving lane.

The location of the maximum bending stress is between the wheel load positions approximately 30 in. from the pavement edge for a bituminous shoulder type. The maximum stress location of the 2-ft extended driving lane changes to the inner load position. The stress distribution for these two shoulder types is illustrated in Figure 19 for a 9-in. CRC pavement and for two levels of load transfer. The load behavior for a 10-ft tied shoulder is similar to that for a 2-ft extended driving lane, except that the maximum stresses with a 10-ft tied shoulder are 20 to 30 psi lower.

SUMMARY

Current thickness design procedures inadequately address punchout distress and mechanisms related to it. CRC pavement behavior is different from jointed concrete behavior, and thickness design should not be based on jointed concrete thickness design methods. Design methods that allow for subbase erosion should be based on failure mechanisms leading to punchout distress. CRC pavement performance has indicated that a small amount of erosion can be tolerated, but good design practice should require low or nonerodible subbases. Subbase design is critical to CRC pavement performance since loss of support leading to loss of load transfer has been identified as the primary cause of punchout distress. An optimum crack spacing between 3 and 4 ft is desirable since the maximum longitudinal and transverse bending stresses are minimized in terms of load transfer within this cracking range. Maintaining high load transfer is critical to good CRC pavement performance, particularly outside of this cracking interval, and is highly dependent on the crack width.

Basic failure modes leading to punchout distress were proposed based on a field study and literature surveys of CRC pavement performance. Failure mechanisms were suggested and analyzed in terms of crack widths, pavement stiffness, and load transfer. Although the analysis in some instances extended beyond the limits of the original test data, a useful method was established in which to consider such data and a basis was provided for conducting further testing.

ACKNOWLEDGMENT

This paper is based on the results of a cooperative study between the Illinois Department of Transportation (DOT) and the University of Illinois sponsored by the Division of Highways of the Illinois DOT and FHWA.

REFERENCES

1. W. E. Chastain, Sr., J. A. Beanblossom, and W. E. Chastain, Jr. AASHO Road Test Equations Applied to the Design of Portland Cement Concrete Pavements in Illinois. In *Highway Research Record 90*, HRB, National Research Council, Washington, D.C., Oct. 1965, pp. 26–42.
2. J. S. Dhamrait and R. K. Taylor. *Behavior of Experimental CRC Pavements in Illinois*. Physical Research No. 82. Illinois Department of Transportation, March 1979.
3. "*AASHTO Interim Guide for the Design of Pavement Structures*. AASHTO Committee on Design, AASHTO, Washington, D.C., 1986.
4. *Design of Continuously Reinforced Concrete for Highways*. Associated Reinforcing Bar Producers—CRSI, Chicago, Ill., 1981.
5. B. E. Colley and H. A. Humphrey. *Aggregate Interlock at Joints in Concrete Pavements*. HRB, National Research Council, Washington, D.C., 1967.
6. M. Won and B. F. McCullough. *Research Report 472-2, Texas SDHPT: Evaluation of Proposed Texas SDHPT Design Standards for CRCP*. The Center for Transportation Research, University of Texas, Austin, Dec. 1987.
7. B. F. McCullough, J. C. M. Ma, and C. S. Noble. *Research Report 177-17: Limiting Criteria for The Design of CRCP*. The Center for Transportation Research, University of Texas, Austin, Aug. 1979.
8. J. M. Gregory, A. E. Burks, and V. A. Pink. *Continuously Reinforced Concrete Pavements: A Report of the Study Group*. TRRL Laboratory Report 612. U.K. Transport and Road Research Laboratory, Crowthorne, Berkshire, England, 1974.
9. J. M. Gregory. Continuously Reinforced Concrete Pavements. *Proc. Institution of Civil Engineers*, Part 1, May 1984, 76, pp. 449–472.
10. K. W. Heinrichs, M.-J. Liu, M. I. Darter, S. H. Carpenter, and A. M. Ioannides. *Rigid Pavement Analysis and Design*. Department of Civil Engineering, University of Illinois, Urbana-Champaign, Oct. 1987.
11. S. A. La Coursiere, M. I. Darter, and S. A. Smiley. Performance of Continuously Reinforced Concrete Pavement in Illinois. *Civil Engineering Studies, Transportation Engineering* Series No. 10. University of Illinois, Urbana-Champaign, 1978.
12. *NCHRP Synthesis of Highway Practice 60: Failure and Repair of Continuously Reinforced Concrete Pavement*. TRB, National Research Council, Washington, D.C., July 1979.
13. A. M. Tabatabaie and E. J. Barenberg. Finite-Element Analysis of Jointed or Cracked Concrete Pavements. In *Highway Research Record 671*, HRB, National Research Council, Washington, D.C., 1978.
14. J. Ma, and B. F. McCullough. *Research Report 177-9: CRCP-2, An Improved Computer Program for the Analysis of Continuously Reinforced Concrete Pavements*. The Center for Transportation Research, University of Texas, Austin, August 1977.
15. R. P. Palmer, M. Olsen, and R. L. Lytton. *Research Report 371-2F: TTICRCP—A Mechanistic Model for the Prediction of Stresses, Strains, and Displacements in Continuously Reinforced Concrete Pavements*. Texas Transportation Institute, Texas A&M University, College Station, August 1987.
16. D. G. Zollinger. *Investigation of Punchout Distress of Continuously Reinforced Concrete Pavements*. Ph.D. thesis. University of Illinois, Urbana-Champaign, 1989.
17. D. H. Jiang, S. P. Shah, and A. T. Andonian. Study of the Transfer of Tensile Forces by Bond. *ACI Journal*, Proceedings Vol. 81, No. 3, May–June 1984, pp. 251–259.
18. Y. Goto. Cracks Formed in Concrete Around Deformed Tension Bars. *ACI Journal*, Proceedings Vol. 68, No. 4, April 1971, pp. 244–251.
19. R. M. Mains. Measurement of the Distribution of Tensile Stresses Along Reinforcing Bars. *ACI Journal*, Proceedings Vol. 48, Nov. 1951, pp. 225–252.
20. T. Krauthammer and K. L. Western. Joint Shear Transfer Effects on Pavement Behavior. *Journal of Transportation Engineering*, ASCE, Vol. 114, No. 5, Sept. 1988, pp. 501–529.
21. W. Zuk. Analysis of Special Problems in Continuously Reinforced Concrete Pavements. *Bulletin 214*, HRB, National Research Council, Washington, D.C., 1959.
22. A. Abou-Ayyash and W. R. Hudson. *Report 56-22: Analysis of Bending Stiffness Variation at Cracks in Continuous Pavements*. Center for Highway Research, University of Texas, Austin, August 1975.

Publication of this paper sponsored by Committee on Rigid Pavement Design.

Prestressed Concrete Pavement: Instrumentation, Behavior, and Analysis of Horizontal Movements

ELLIOTT DAVID MANDEL, NED H. BURNS, AND B. FRANK MCCULLOUGH

The long-term work plan for the initial design phase of the McLennan County prestressed concrete pavement (PCP) overlay consisted of the determination of variables that are relevant to design, the development of models and design procedures, and the study of the effect of environmental factors on PCP slabs. The evaluation of the performance of PCP, with specific observation of horizontal slab displacements caused by changes in temperature, is discussed. The behavior of the PCP is characterized by the results of a field data analysis. The instrumentation of the PCP slabs is described, graphs of measured displacements of the slabs for daily temperature cycles are presented, and a regression analysis of the slab movements is discussed. Finally, conclusions and recommendations based on the instrumentation program and data analysis are outlined.

Prestressed concrete pavement (PCP) takes advantage of the high compressive strength of concrete to prevent or decrease tensile stresses during service. When a permanent horizontal compressive stress is introduced to a pavement slab during construction, its capacity to withstand traffic and environmental loads is increased. This compression of concrete slabs results in a potentially cost-efficient alternative to traditional pavements or pavement overlays.

This paper addresses applications of pavement theory by reporting the analysis of data collected from in situ PCP slabs on Interstate 35 in Texas. Initial performance of the PCP has been reported previously (*1*,*2*), and recent performance has been reported in detail (*3*,*4*). The data are used to characterize the behavior of the slabs caused by environmental loads and to calibrate a model that predicts the behavior of PCP. The results of this study are offered as input to an ongoing process of understanding PCP for the purpose of refining the design process for its wider implementation.

GENERAL BEHAVIOR

All concrete pavements are subject to constant fluctuations in temperature because of daily and seasonal thermal cycles. These temperature changes cause individual pavement slabs to undergo two types of movements: volumetric and curling. Motion that is subjected to restraint at boundaries or gravity loads causes stress to develop in the concrete. The magnitudes of displacement and stress determine the behavior and ultimate serviceability of a pavement.

Volumetric Movement

Since PCP slabs are much longer than they are wide or thick, longitudinal expansion and contraction are the most significant volumetric movements. Thermal expansion and contraction of pavement are restrained by frictional forces imparted by the subbase onto the bottom surface of a slab. When it expands, the slab is subjected to compressive stresses caused by the frictional resistance of the subbase. Similarly, when a slab contracts it is subjected to tensile stresses. Because the inherent material properties of plain concrete provide high compressive strength but low tensile strength, contraction of a slab dictates whether it will crack from a tensile stress that exceeds its tensile capacity. For slab movements that are symmetrical with respect to the longitudinal centerline, a long slab experiences a higher magnitude of tensile stress on contraction than a short slab because the stress accumulates from the ends of a slab to the middle. The amount of stress accumulation also depends on the frictional characteristics of the subbase; a smooth interface between the slab and the subbase provides less resistance than a rough one, resulting in an increase in magnitude of longitudinal movement and a decrease in tensile stress. In PCP, the slabs are precompressed so that they can have longer lengths without suffering damage from tensile stresses. Figure 1 illustrates the effect of subbase frictional restraint on the tensile stress in a pavement slab and the combined effect of friction and precompression on slab stresses.

Curling Movement

Temperature gradients across the thickness of the pavement resulting from a time-lag effect of heat transfer from the top surface to lower regions in the slabs cause curling movements. When the ambient temperature increases, the top region of a slab experiences a more rapid increase in temperature than the bottom region. This effect causes the top region to undergo

E. D. Mandel, DeLeuw, Cather & Company, Washington, D.C. 20005. N. H. Burns, Department of Civil Engineering, The University of Texas at Austin, Austin, Tex. 78712. B. F. McCullough, Center for Transportation Research, The University of Texas at Austin, Austin, Tex. 78705.

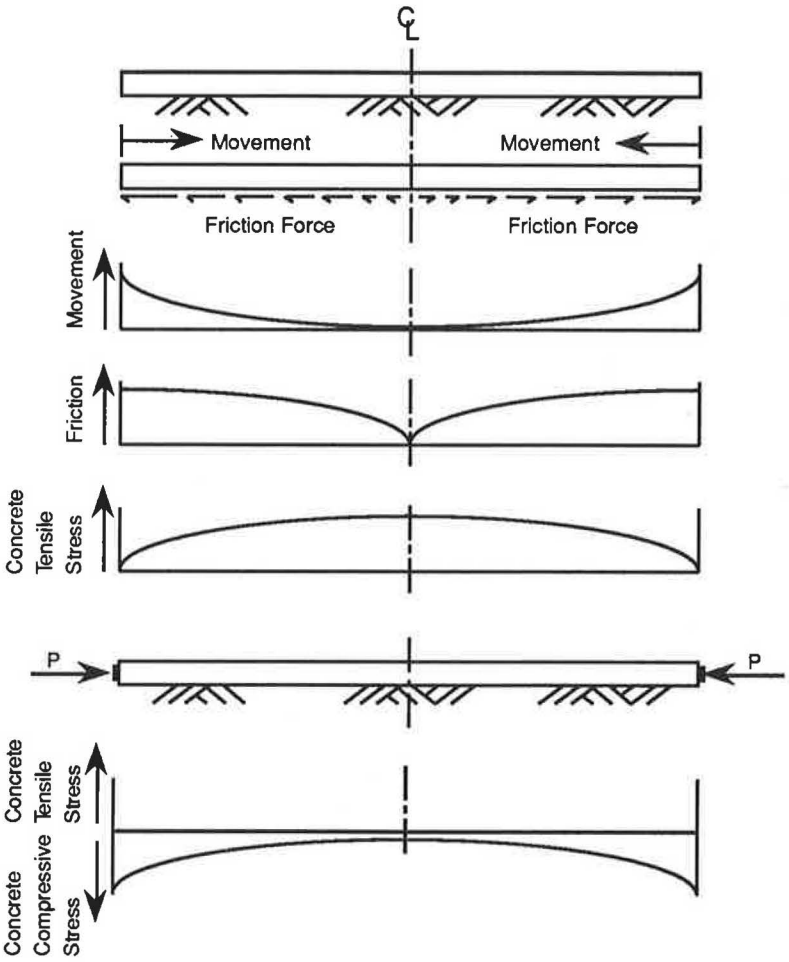

FIGURE 1 Effect of subbase frictional restraint on stress in a concrete slab for a temperature decrease and the additional effect of precompression by force *P*.

a more rapid volumetric increase than the bottom region. Similarly, when the ambient temperature decreases, the top region experiences a more rapid volumetric decrease than the bottom region. The differential in volumetric deformation through the thickness of the pavement causes the slabs to curl vertically. This movement of the slabs fluctuates constantly as the temperature gradient across the thickness of the slab changes, reversing the direction of induced curling movement. For long pavement slabs, curling movements can be large, causing significant tensile stress in the concrete. In addition, large curling movements can cause the slab to pull away from the subbase; if enough separation occurs, repetitive traffic loads can cause pumping of material from beneath the slab, resulting in large voids under the pavement.

PREVIOUS RESEARCH

The current study on the behavior of PCP is an extension of previous research conducted at The University of Texas at Austin from 1984 to 1987. A series of conceptual and experimental investigations into the design and implementation of PCP were carried out during that time. These studies examined several separate aspects of PCP, including the application of special prestressing techniques, the evaluation of projected in situ parameters, and the formulation of design procedures. The research provided information required for the design, construction, and early-life instrumentation of a 1-mile experimental prototype section of a PCP overlay located in central Texas (*1*,*2*,*5*–*9*).

OBJECTIVES AND SCOPE

Field work performed on the McLennan County, Texas, PCP overlay from July 1988 to February 1989 is described, as well as analytical work performed subsequently. The collection and analysis of horizontal movement data are covered, as well as instrumentation details. Although curling movement data are available, the results will be reported elsewhere.

LAYOUT OF THE PCP

The experimental prototype section of PCP in McLennan County is located on Interstate 35 southbound, about 15 mi north of Waco. The section is 1 mi long and contains a total of 32 prestressed slabs. The slabs consist of a PCP overlay 6

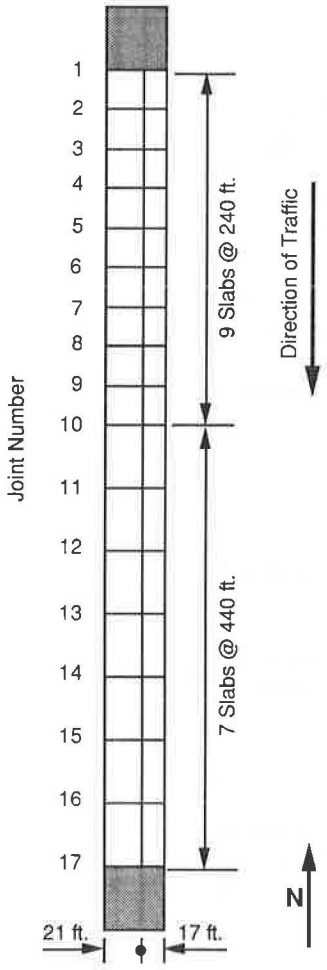

FIGURE 2 Layout plan of the McLennan County PCP experimental section.

in. thick over an existing 11-in. jointed concrete pavement (JCP) with an intermediate 3-in. ACP stress-reducing course. The pavement is 38 ft wide and consists of two 12-ft lanes, a 10-ft outside shoulder, and a 4-ft inside shoulder. It has the following dimensions in plan:

- 9 slabs at 240 ft by 21 ft
- 7 slabs at 440 ft by 21 ft
- 9 slabs at 240 ft by 17 ft
- 7 slabs at 440 ft by 17 ft

A layout plan, including the joint numbering system of the entire experimental section, is shown in Figure 2.

PREVIOUS INSTRUMENTATION

An instrumentation program was carried out during the early life of the McLennan County overlay (*2*). Measurements taken at that time were intended to provide a verification of predicted values of concrete stress and slab movements caused by both prestressing and daily temperature cycles. The measurement program included

1. Determination of daily fluctuations in ambient temperature, concrete temperature at middepth of the pavement slabs, and the temperature gradient over the thickness of the pavement slabs;
2. Measurement of horizontal and vertical slab movements and joint widths;
3. Measurement of tendon elongations during stressing operations;
4. Measurement of concrete strain in the slabs; and
5. Determination of concrete strength and modulus of elasticity at early ages.

CURRENT INSTRUMENTATION

A second instrumentation program for the McLennan County PCP (covered herein) was carried out to monitor movements of the slabs after changes in the material properties of the concrete had stabilized and after shrinkage and creep effects essentially were complete. Information collected in this instrumentation program was used to characterize the long-term behavior of the PCP.

Field Visits

Work performed at the McLennan County PCP site included site surveys, preliminary measurements, installation of instrumentation equipment, and data collection. Data collection took place from July 1988 to February 1989. During that time six field visits were made. The field visits took place under varying conditions of moisture and ambient temperature—three during hot and dry conditions, one during mild and dry conditions, and two during cold and wet conditions. Table 1 outlines the five data collection field visits and an additional trip. The duration of all data collection periods was 24 hr, with the exception of the sixth field visit, which lasted 48 hr.

The array of weather conditions covers the maximum range of temperatures that occurred at the site. It is difficult to evaluate whether the wet moisture conditions can be considered as the extreme conditions; 1988 was a drought year with almost no precipitation from July to December. The conditions described as "wet" in Table 1 were moist from rain that occurred 1 to 2 days before data collection.

Instrumentation Set-Up

Concrete "dead-man" anchors were used to support dial gauges and linear voltage-distance transducers (LVDTs). The anchors consisted of typical 6-in. by 12-in. concrete cylinders with embedded threaded inserts that receive ⅞-in. threaded dowels. Two inserts were installed in case one failed to function. Rubber stoppers protected the inserts when they were not in use. The anchors were inserted into the soil, leveled, and secured into place with concrete, about 18 in. from the west edge of the slabs. Then, for each field visit, a vertical steel dowel with a threaded end was screwed into each anchor, and horizontal dowels were secured and attached to the verticals with 90-degree dowel clamps. Dial gauges or LVDTs were then secured to the horizontals. This set-up allowed for the

TABLE 1 DATA COLLECTION FIELD VISITS

Field Visit	Date	Maximum Ambient Temperature	Minimum Ambient Temperature	Weather Condition
2	July 26, 1988	107.13°F	74.80°F	Hot, Dry
3	August 6, 1988	104.00	75.85	Hot, Dry
4	August 26, 1988	107.87	71.28	Hot, Dry
5	November 5, 1988	84.00	41.72	Mild, Dry
6	January 21, 1989	64.22	27.39	Cold, Wet
7	February 9, 1989	62.87	30.90	Cold, Wet

temporary fabrication of instrumentation supports at the work site and for their removal after data collection was completed for each field visit.

To give the dial gauge and LVDT plunger-pins a positive reaction-stop, the slabs were equipped with receptacles. For horizontal movements, steel angles (3 in. by 3 in. by ⅜ in.) were bolted onto inserts that were drilled and epoxied onto the edges of the slabs. For curling movements, plastic receptacles were used to provide a smooth and level surface. Each receptacle consisted of a 3-in. by ⅜ in. by ¾ in. polyvinyl-chloride pipe that was epoxied to the top surface of a slab and filled with hot (liquid) sulfur mortar. When the liquid cooled and solidified, a flat and level surface resulted. A smooth surface was created by epoxying a 1½ in. by 1½ in. by ¼ in. plastic square to the top of the sulfur.

Temperatures were measured using thermocouples. Six thermocouples were drilled and grouted into the PCP to measure concrete temperature. Two thermocouples were located at each of three depths—1 in., 3 in. (middepth), and 5 in. The middle thermocouples were used for correlation with horizontal movements, and the top and bottom thermocouples were used for correlation with curling movements. Ambient temperature was measured by placing a thermocouple in the shade.

Measurement

The number of locations on the slabs that could be instrumented simultaneously was limited by the availability of dial gauges. Figure 3 shows a plan view of the instrumented slabs. Instrumentation locations labeled with "/3" or "/6", respectively, indicate third or sixth points along the slab length. During the first three field visits data were collected from joint locations only so that joint displacement data could be based on the largest possible sample. For the remainder of the field visits, displacement data were collected at locations along slab lengths to characterize the displacements of entire

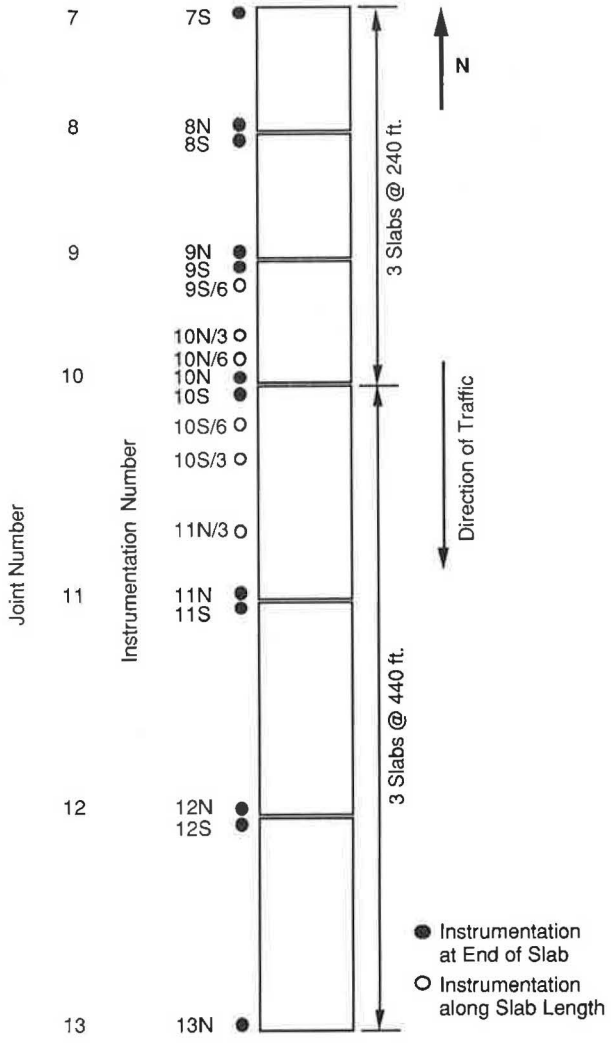

FIGURE 3 Instrumented slabs and instrumentation locations.

slabs. The instrumentation set-up allowed for the measurement of horizontal and vertical slab movements with respect to an arbitrary datum. Displacements measured from the first data reading at each location for each field visit.

Prevention of Error

Several methods for avoiding error in final versions of data were employed. These methods include prevention of interference, redundant readings, and internal checking of data. Interference was prevented in two ways: steel dowels were encased in foam insulation to prevent error caused by uneven heating from the sun, and temporary masonry walls were constructed to prevent error created by wind gusts from traffic. Redundancy of data readings included two slab temperature readings at each of the three depths—1 in., 3 in., and 5 in.—and at Joint 10, horizontal slab movements were measured with both dial gauges and LVDTs. The measurements of horizontal slab movements could be internally checked because the sum of the movements measured by dial gauges or LVDTs at the ends should add up to the change in joint opening measured with dial calipers.

DATA ANALYSIS

This section describes the treatment of the field data collected at the McLennan County PCP. The data include measurements of horizontal and vertical slab displacements, joint widths, ambient temperatures, and concrete temperatures at three depths in the pavement. Only the analysis of horizontal displacements and their corresponding concrete temperatures at middepth in the slabs is included in this paper. Hankins et al. (*3*) included a complete listing and graphic presentation of all data.

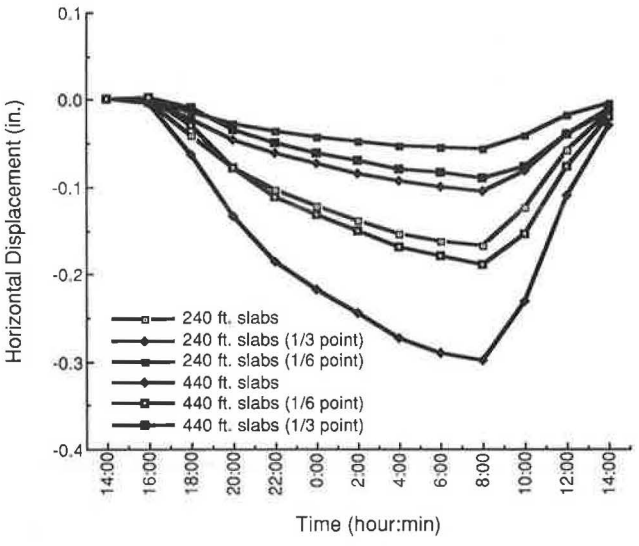

FIGURE 4 Average horizontal slab displacements at various times during a 24-hr observation cycle for field visit 5. Data for both slab lengths and at intermediate points are shown.

DATA REDUCTION

To effectively use the data collected in the field, a data reduction process was designed and performed. The purpose was to transform field data into numbers that could be used to characterize the behavior of the PCP in a concise manner. The process included

1. Normalizing displacement data to a common axis;
2. "Smoothing" erroneous data by using a redundant reading, or by backcalculating from a closure measurement;
3. Organizing the data by field visit, slab type, and type of instrumentation location; and
4. Performing a statistical reduction of the data.

Figure 4 is a typical graph of the horizontal displacement versus time obtained from the reduction process. This graph is for field visit 5 and covers both slab lengths and intermediate points. The complete set of data may be found in Hankins et al. (*3*).

BEHAVIOR ANALYSIS

The design of a PCP involves the evaluation of two major aspects of the horizontal slab movements: the character of slab activity during temperature changes and the range of joint widths between slabs. The former is of interest because stresses in the slab are a direct function of displacements. The latter affects the placement of slabs (in which the design criteria are meant to avoid extremely wide joint widths and complete closure of the joints). Slab activity also affects the range of joint widths, that is, slabs with more active horizontal movements will cause a larger range of joint widths.

Regression Analysis of Horizontal Displacements

Analysis of slab activity for temperature changes was performed by calculating a series of linear regression equations for horizontal displacements as a function of the slab's middepth temperature. This independent variable provided the best correlation. Figure 5 is a typical graph of slab displacements as a function of decreasing and increasing temperature. Plots for all instrumentation locations are presented in Appendix B as reported by Mandel et al. (*4*). The equations are linear, in which the abscissa (T) is the concrete temperature at middepth of a slab in degrees Fahrenheit, and the ordinate (Y) is the horizontal displacement from the initial data reading for a field visit. Table 2 shows a compilation of the regression equations for all field visits, along with coefficients of determination (R^2).

All R^2 values are high: two-thirds of the equations have values greater than 0.95. The lowest value is 0.854. These data indicate that the linear equations can predict horizontal displacements with a high degree of accuracy. This regression analysis does not indicate, however, whether stresses in the slab can be predicted with a linear model; stresses are a function of the accumulation of frictional forces under a slab, and any nonlinear behavior of the subbase frictional restraint could cause stress magnitudes to vary nonlinearly.

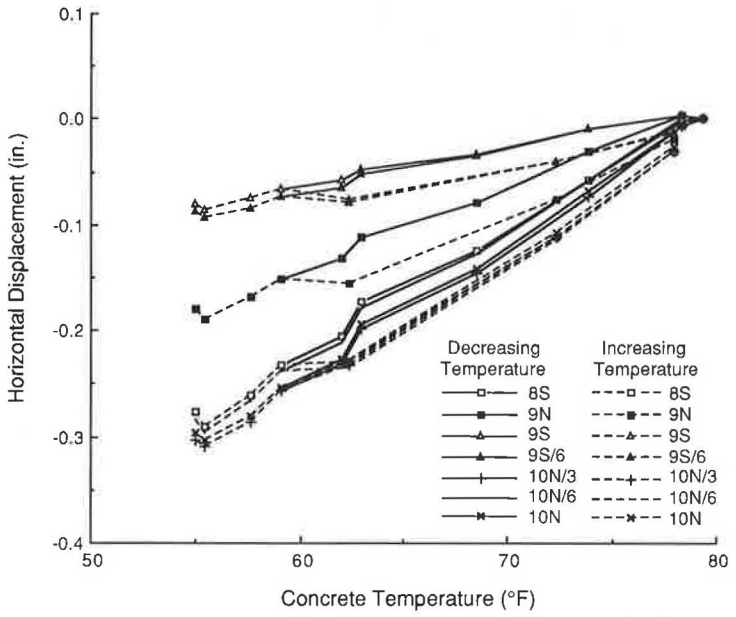

FIGURE 5 Horizontal slab displacements of 440-ft slabs versus change in concrete temperature for field visit 5.

As expected, the slopes in the equations increase for the longer slabs. The ratio of slab lengths between the 440-ft and the 240-ft slabs is 1.835, and the ratio between the average values of the slopes in the equations for the slabs is 2.024, 10.31 percent higher. This suggests that the increase in horizontal activity with increased slab length is not linear.

The slopes follow logical trends for the various measurement locations. The average slopes for displacements at the joints are 5.890×10^{-3} and 1.193×10^{-2} in./°F for the 240-ft and 440-ft slabs, respectively. At the sixth points, the average slopes are 3.883×10^{-3} and 6.977×10^{-3} in./°F, 65.93 percent and 58.48 percent of the slopes at the joints. At the third points, the average slopes are 1.990×10^{-3} and 3.237×10^{-3} in./°F, 33.78 percent and 27.13 percent of the slopes at the joints, and 51.25 percent and 46.40 percent of the slopes at the sixth points. The horizontal activity varies approximately linearly with respect to the geometry of the slabs. In addition, it appears that for both 240- and 440-ft lengths, almost the entire slab is moving. Figure 6 shows a graph of the slopes of the regression equations as a function of the distance from the centerlines of the slabs.

The regression equations do not show a strong trend for various moisture levels. Field visits 6 and 7 took place under moist conditions; the 440-ft slabs have slightly smaller slopes for these visits, and there is no definitive trend for the 240-ft slabs. One explanation for there not being large differences for field visits 6 and 7 is that the slabs might not have been completely saturated, and therefore expansion and contraction characteristics of the slabs would not have changed enough to show up in the data. Another explanation is that the horizontal activity is not very sensitive to changes in moisture levels. The reason for this would be that the regression equations relate horizontal movements to the concrete temperature at middepth of the slabs. The moisture level might affect the lag time between changes in ambient temperature and changes in concrete temperature, but the expansion and contraction characteristics of the slab would not necessarily change appreciably.

The data reveal that horizontal displacements, although behaving almost perfectly linearly in most instances, show a small amount of nonlinearity in others. The displacements for the 440-ft slabs during field visits 5 and 7 clearly exhibit nonlinear variation of displacements with respect to concrete temperature. The nonlinearity of the displacements observed in these two visits is probably because of either changes in the rate of heating of the concrete (caused by differences in the rate of heat absorption by the concrete, which is caused by differences in atmospheric filtering of radiation) or a pronounced effect of hysteresis (energy-absorbing capacity) in the force-displacement behavior of the subbase frictional restraint. It is not possible to draw an exact conclusion for the cause of this effect, but previous research has indicated that the nonlinear behavior of the subbase friction should be considered in the analysis of horizontal displacements of rigid pavement slabs (*1*).

Analysis of Joint Widths

The determination of an initial joint width for construction of PCP depends on the following factors:

- The projected amount of creep and shrinkage that will occur during the early life of the pavement,
- The projected amount of elastic shortening a slab will undergo during stressing operations,
- The width requirements for inserting a protective neoprene seal into the joint, and
- The expected range of temperatures and subsequent horizontal displacements that the slabs will experience throughout their service lives.

TABLE 2 REGRESSION EQUATIONS FOR HORIZONTAL DISPLACEMENTS

Field Visit	Measurement Location	Regression Equation	Coefficient of Partial Determination
2	240-foot slab (joint)	$Y=(5.374 \times 10^{-3}) T - 0.586$	$R^2=0.854$
	440-foot slab (joint)	$Y=(1.281 \times 10^{-2}) T - 1.422$	$R^2=0.951$
3	240-foot slab (joint)	$Y=(5.148 \times 10^{-3}) T - 0.558$	$R^2=0.884$
	440-foot slab (joint)	$Y=(1.212 \times 10^{-2}) T - 1.323$	$R^2=0.970$
4	240-foot slab (joint)	$Y=(6.076 \times 10^{-3}) T - 0.653$	$R^2=0.931$
	440-foot slab (joint)	$Y=(1.270 \times 10^{-2}) T - 1.371$	$R^2=0.854$
5	240-foot slab (joint)	$Y=(6.792 \times 10^{-3}) T - 0.542$	$R^2=0.991$
	240-foot slab (sixth point)	$Y=(4.206 \times 10^{-3}) T - 0.335$	$R^2=0.982$
	240-foot slab (third point)	$Y=(2.344 \times 10^{-3}) T - 0.186$	$R^2=0.993$
	440-foot slab (joint)	$Y=(1.217 \times 10^{-2}) T - 0.970$	$R^2=0.983$
	440-foot slab (sixth point)	$Y=(7.697 \times 10^{-3}) T - 0.611$	$R^2=0.970$
	440-foot slab (third point)	$Y=(3.717 \times 10^{-3}) T - 0.295$	$R^2=0.932$
6	240-foot slab (joint)	$Y=(6.089 \times 10^{-3}) T - 0.358$	$R^2=0.991$
	240-foot slab (sixth point)	$Y=(3.738 \times 10^{-3}) T - 0.219$	$R^2=0.971$
	240-foot slab (third point)	$Y=(1.887 \times 10^{-3}) T - 0.112$	$R^2=0.988$
	440-foot slab (joint)	$Y=(1.106 \times 10^{-2}) T - 0.649$	$R^2=0.980$
	440-foot slab (sixth point)	$Y=(6.948 \times 10^{-3}) T - 0.402$	$R^2=0.964$
	440-foot slab (third point)	$Y=(3.138 \times 10^{-3}) T - 0.182$	$R^2=0.920$
7	240-foot slab (joint)	$Y=(5.864 \times 10^{-3}) T - 0.542$	$R^2=0.985$
	240-foot slab (sixth point)	$Y=(3.706 \times 10^{-3}) T - 0.335$	$R^2=0.966$
	240-foot slab (third point)	$Y=(1.738 \times 10^{-3}) T - 0.186$	$R^2=0.984$
	440-foot slab (joint)	$Y=(1.074 \times 10^{-2}) T - 0.970$	$R^2=0.981$
	440-foot slab (sixth point)	$Y=(6.287 \times 10^{-3}) T - 0.611$	$R^2=0.947$
	440-foot slab (third point)	$Y=(2.855 \times 10^{-3}) T - 0.295$	$R^2=0.904$

For the current study, a sample range of maximum and minimum joint widths was determined; Figure 7 summarizes the results. These maximums and minimums represent a range of ambient temperatures from 17.6°F to 107.13°F.

The joint widths were measured at scribe marks on the joint hardware so that the readings could be compared consistently. The joint edges are not perfectly parallel, so the reported maximum and minimum widths are not necessarily the absolute maximum and minimum widths for the entire length of a joint. In fact, several of the joints between 240-ft slabs were observed to be completely closed during hot weather measurements. Joints between 440-ft slabs never completely closed.

Regression equations were calculated for the joint width data. Figures 8 and 9 show graphs of the joint width data for the two slab lengths along with the corresponding regression equations.

Seasonal Slab Operation

Overall seasonal behavior of horizontal movements of the slabs is a function of daily temperature cycles superimposed over seasonal temperature cycles. This superimposition causes slabs to operate, on a daily basis, at various seasonal datum values. During the summer season, the joint widths are small, and horizontal displacements occur over a range of small joint widths. Similarly, during the winter season, horizontal displacements occur over a wide range of joint widths.

CONSISTENCY AND ERROR ANALYSIS

Consistency Analysis

The consistency of horizontal displacements gives an indication of how reliable the measurements are. High consistency

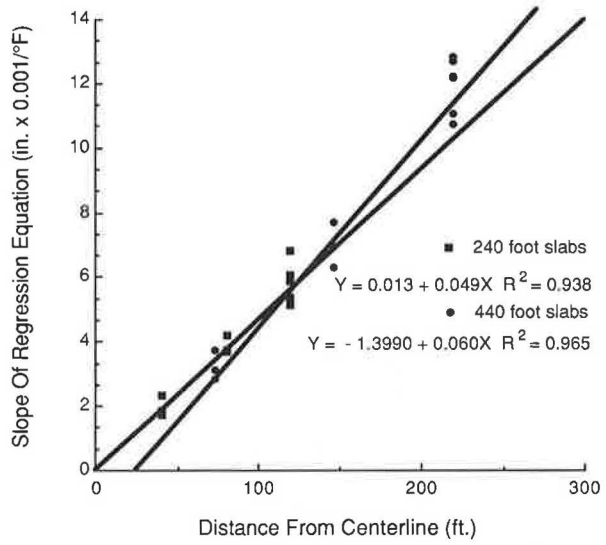

FIGURE 6 Slopes of the regression equations in Table 2 as a function of distance from slab centerline.

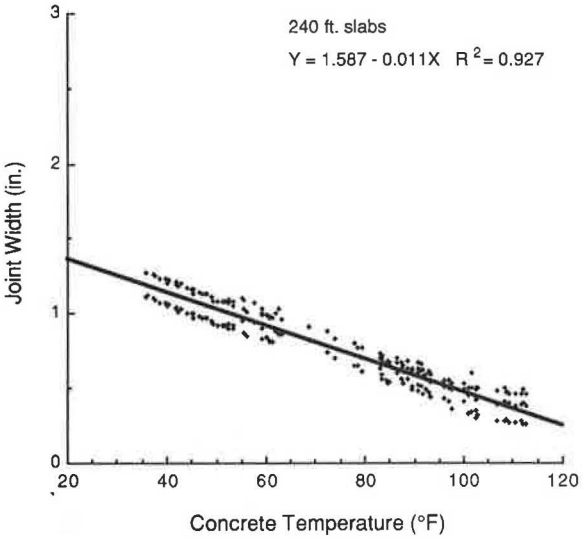

FIGURE 8 Regression equation for joint widths between 240-ft slabs.

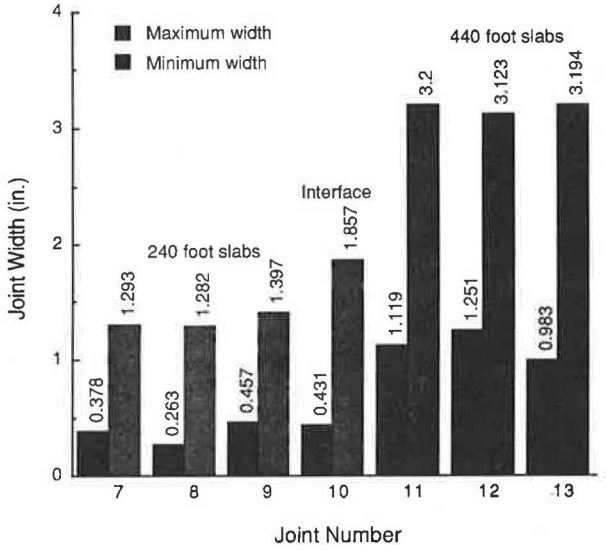

FIGURE 7 Maximum and minimum joint widths for all field visits.

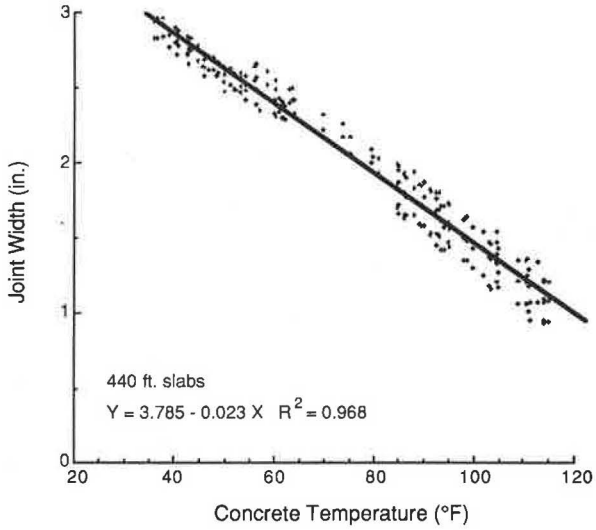

FIGURE 9 Regression equation for joint widths between 440-ft slabs.

in the data would indicate a high degree of reliability in analysis and recommendations, whereas wide scatter in the data would indicate that any analysis of the data, or any recommendation based on the data, would not be as well founded.

The PCP slabs were keyed and dowelled to the subbase at their centerlines so that the middle section of the slabs would not shift from horizontal movements. Therefore, the slabs were expected to expand and contract symmetrically about their centerlines. Consistency analysis of horizontal displacement data was performed by comparing the maximum change in horizontal movement divided by the corresponding change in concrete temperature for all instrumentation locations and all field visits. Figure 10 shows plots of these values for slab displacements at joints by instrumentation location for all field visits.

Inspection of Figure 10 shows that consistency of slab movements per degree of temperature is generally high. The legend codes refer to instrumentation locations shown in Figure 3. Location 10N shows the most activity of the 240-ft slabs for the first three field visits, and 9S shows the least. Location 11N generally shows the most activity for the 440-ft slabs. The magnitude of daily slab activity for a particular change in temperature depends on many factors, including the amount of radiant solar heat that penetrates the atmosphere, coefficient of thermal expansion of the concrete, thermal transmissivity of the concrete, moisture levels, and local deviations in subbase frictional restraint. It is not possible, with the given data, to pinpoint the reasons for more or less slab activity at a particular location or for a particular field visit.

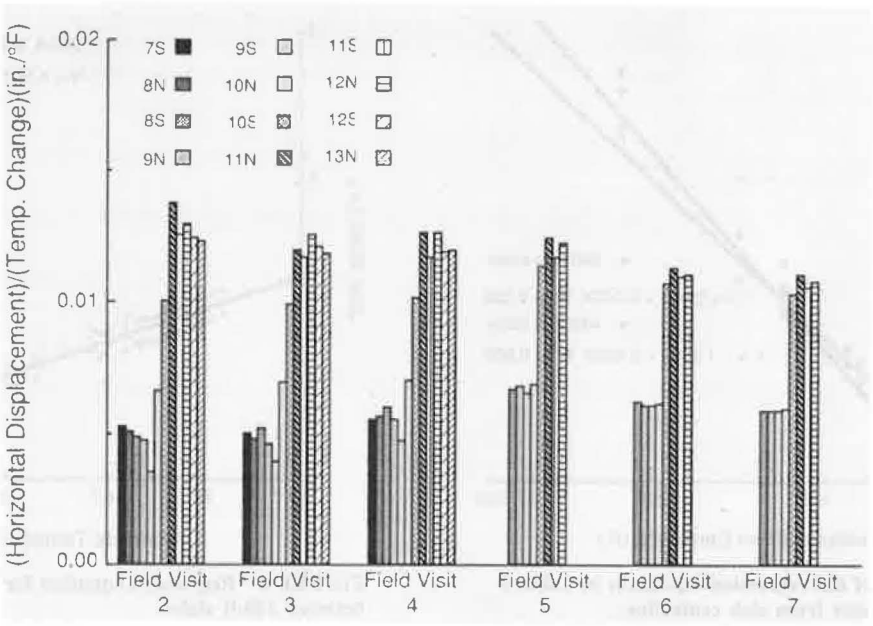

FIGURE 10 Consistency of horizontal slab displacements per degree of change in concrete temperature for all joint locations.

Error Analysis

Error in horizontal measurements can be checked for internal closure. The sum of the displacements of slabs at a joint should be equal to the change in joint width. Therefore, a closure check was made by comparing the maximum horizontal slab displacement at each joint for a field visit with the corresponding change in joint width.

As a final check, the values of the sum of horizontal displacements and the change in joint width were plotted in Figure 11. A regression equation was calculated (shown on the graph); it shows that the slope of the regression line is 0.98, that the Y-intercept is small, and that the coefficient of partial determination, R^2, is 0.99. A value of 1.0 for the slope and the R^2 value would indicate a perfect closure for all measurements; thus, overall the error in measurement is small.

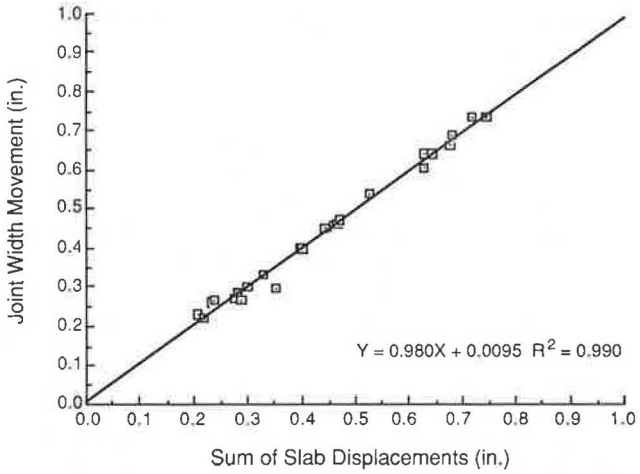

FIGURE 11 Regression equation relating sum of slab displacements and corresponding joint width movements for all joints and all field visits.

SUMMARY

Slab movements are significant. Measurements indicate that entire slabs are moving (Figure 6). Resulting maximum joint widths range from about 1.5 in. to 3 in. Additionally, slab movements correlate well with concrete temperatures at mid-depth of the slabs. The techniques used for measuring slab movements work well. This success is indicated by small cross-check errors.

This study investigated slab movements that occur after shrinkage and creep of the concrete have already occurred. The regression equations that result from these movements are basically the same for all data samples. Regression equations for the 240-ft slabs have flatter slopes than those for the 440-ft slabs. When the slab temperature rises above about 107°F, joints between 240-ft slabs may close, as was observed from the data.

General design equations for predicting slab movements have been developed. The equations are derived by using slopes of regression equations for 440-ft slabs (Figure 6). For McLennan County, PCP joint movements can be predicted by

$$\Delta X_{j-T} = \Delta X_0 + (-2.8 + 0.06\,L)\,(T_i - T_0)$$

where

ΔX_{j-T} = net joint width at any temperature (T_i), in.;
ΔX_0 = joint width at reference temperature, in.;
L = slab length, ft;
T_0 = reference concrete temperature, °F; and
T_i = concrete temperature at time i.

For any portland cement concrete pavement placed on a polyethylene sheet the general equation is

$$\Delta X_{j-T} = \Delta X_0 + (-257 + 11L)\,\alpha_c(T_i - T_0)$$

where α_c is the thermal coefficient of expansion of concrete, in./in./°F.

CONCLUSIONS AND RECOMMENDATIONS

This section outlines the final conclusions and recommendations of this study organized into the categories of instrumentation and data analysis.

Instrumentation

The instrumentation program for this study was highly successful. The collected data indicated trends that were directly parallel with expected results. The outcome of the instrumentation program justifies the following conclusions:

- The method of using buried anchors to support instrumentation worked well. The supports were extremely stable and therefore provided a reliable foundation for the equipment.
- The method of measuring displacements by both the dial gauges and LVDTs gave consistent and identical results. The 2-hr period between measurement readings was frequent enough to characterize movements but still allowed enough time to gather a large amount of data.
- The method of measuring temperatures using thermocouples gave accurate and consistent temperatures.

The following recommendations result from experiences that were encountered either during data collection or as a result of analysis that depends on instrumentation. They are offered as guidelines for any instrumentation program that is designed to measure phenomena similar to those in the program for this study:

1. Although exact effects of moisture levels on magnitudes of displacement were not qualified in this study, future instrumentation programs that investigate environmental effects on pavement should consider the importance of measuring the moisture level at various depths in the concrete.
2. The construction program for experimental protypes should include a major consideration of subsequent determination of material properties. A large sample of material specimens (cylinders, material-test beams, etc.) should be made at the time of construction so that material properties for long-term investigations can be determined directly.

DATA ANALYSIS

The analysis of slab displacements for each slab length for a field visit allowed for the direct comparison of slab behavior for various seasonal conditions. The use of regression equations to characterize slab movements was helpful in comparing the behavior of all slabs for all instrumentation locations. Furthermore, the error analysis indicated that measurements were correct and quite accurate. The following points outline specific conclusions from the analysis of horizontal displacements:

1. The regression analysis of horizontal slab movements shows that displacements can be described by a linear equation. The slopes of the equations vary at close to a linear rate for displacements measured at the joints, the sixth points, and the third points. These data indicate that almost the entire slab moves on a daily basis.
2. Average slopes of the regression equations can be used to predict slab movements as a function of temperature. For the 240-ft slabs, the average rate of movement was 5.89×10^{-3} in./°F. For the 440-ft slabs, the average rate of movement was 1.193×10^{-3} in./°F.
3. The analysis did not show a strong trend for various moisture conditions. This may have been because the slabs were not completely saturated.
4. Maximum and minimum measured joint widths were 1.397 in. and 0.263 in. for the 240-ft slabs and 3.20 in. and 0.983 in. for the 440-ft slabs.
5. Overall seasonal behavior of the slabs indicates that daily fluctuations occur constantly, whereas the seasonal data for the movements change.
6. The consistency of slab movements for the entire study is quite high. Standard deviations of movements per degree change in temperature are 0.646×10^{-3} and 0.621×10^{-3} in./°F for the 240- and 440-ft slabs, respectively.
7. Field observation revealed that some joints were completely closed for prolonged ambient temperatures in excess of about 100°F (no damage to the slabs or joint hardware occurred).

The following recommendations result from the analysis of horizontal movements, as well as field observations:

1. Apparently, less shortening of the slabs occurred during the early life of the 240-ft slabs than was initially expected. Since maximum measurements of joint widths for the 240-ft slabs were 1.397 in., well within serviceability limits (about 3.5 in.), there is a wide margin of safety against excessive joint widths. An initial joint width of 0.5 in. for a 240-ft slab (otherwise constructed under similar conditions) would prevent the joints from completely closing.
2. The joints for the 440-ft slabs always remained within serviceable limits. These joints were also set closed at the time of construction. No change is recommended for the initial setting of joints for these slabs.

REFERENCES

1. A. Mendoza-Diaz, N. H. Burns, and B. F. McCullough. *Behavior of Long Prestressed Pavement Slabs and Design Methodology*. Research Report 401-3. Center for Transportation Research, The University of Texas, Austin, September 1986.
2. J. R. Maffei, N. H. Burns, and B. F. McCullough. *Instrumentation and Behavior of Prestressed Concrete Pavements*. Research Report 401-4. Center for Transportation Research, The University of Texas, Austin, November 1986.
3. K. Hankins, E. D. Mandel, N. H. Burns, and B. F. McCullough. *Performance Test on a Prestressed Concrete Pavement—Presentation of Data*. Research Report 556-1. Center for Transportation Research, The University of Texas, Austin, 1989.
4. E. D. Mandel, B. F. McCullough, and N. H. Burns. *Prestressed Concrete Pavement: Instrumentation, In-situ Behavior and Analysis*. Research Report 556-2. Center for Transportation Research, The University of Texas, Austin, 1989.

5. S. J. O'Brien, N. H. Burns, and B. F. McCullough. *Very Early Post-Tensioning of Prestressed Concrete Pavements*. Research Report 401-1. Center for Transportation Research, The University of Texas, Austin, June 1985.
6. N. D. Cable, N. H. Burns, and B. F. McCullough. *New Concepts in Prestressed Concrete Pavement*. Research Report 401-2. Center for Transportation Research, The University of Texas, Austin, December 1985.
7. W. S. Chia, B. F. McCullough, and N. H. Burns. *Field Evaluation of Subbase Friction Characteristics*. Research Report 401-5. Center for Transportation Research, The University of Texas, Austin, September 1986.
8. B. W. Dunn, N. H. Burns, and B. F. McCullough. *Friction Losses in Unbound Post-Tensioning Tendons*. Research Report 401-6. Center for Transportation Research, The University of Texas, Austin, November 1986.
9. W. S. Chia, N. H. Burns, and B. F. McCullough. *Effect of Prestress on the Fatigue Life of Concrete*. Research Report 401-7. Center for Transportation Research, The University of Texas, Austin, November 1986.

Publication of this paper sponsored by Committee on Rigid Pavement Design.

Control of Faulting Through Joint Load Transfer Design

ANASTASIOS M. IOANNIDES, YING-HAUR LEE, AND MICHAEL I. DARTER

The development of mechanistic empirical algorithms for more realistic estimates of anticipated faulting in concrete pavements is described and evaluated. Earlier theoretical investigations are considered, interpreted through more recent finite element results, and calibrated using an extensive data base of field observations. A factor influencing faulting is the dowel-concrete bearing stress, for which an improved method of determination is presented. A procedure is outlined for assessing the need for dowels in both plain and reinforced jointed concrete pavements, also resulting in an estimate of the required bar diameter so that significant faulting is prevented. Application of the procedure is facilitated through use of program PFAULT, which can be implemented on a personal computer.

In the last several years, significant deterioration has been observed in many jointed plain or reinforced concrete pavements (JPCP or JRCP), even though most had been designed in accordance with conventional codes of practice. The major types of distress exhibited are usually faulting, spalling, and corner cracking. Lockup of joints is also fairly frequent and causes the opening of nearby transverse cracks with subsequent deterioration. Joint repair procedures are costly and have contributed to a large proportion of rehabilitation contracts. These observations call for a re-examination of accepted joint design methodologies in light of recent theoretical, analytical, and empirical data.

In the design and construction of doweled or undoweled joints for portland cement concrete (PCC) pavements, a disparity exists among the practices adopted by agencies in the 50 states, as well as among those reported from foreign countries. The main reasons for this are the following:

1. The state of the art with respect to the theoretical treatment of the pertinent problems is still fairly elementary and strictly applicable only to highly idealized conditions;
2. Climatic and geotechnical considerations vary widely from state to state and from country to country;
3. The number, frequency, magnitude, and geometry of applied traffic loadings are considerably different in each locality, whereas concepts used to reduce mixed traffic to a design traffic number are often theoretically unfounded and sometimes fundamentally flawed;
4. As a corollary of 1–3 above, a large degree of empiricism derived from local experience enters the design and construction approaches of each agency.

Department of Civil Engineering, University of Illinois at Urbana-Champaign, 205 N. Mathews Ave., Urbana, Ill. 61801.

This paper reports on some aspects of a broader FHWA study whose main objectives included the development of design guidelines for the prevention of faulting through the proper use of doweled joints in PCC pavements. The approach used to achieve this goal was mechanistic in nature, calibrated with empirical inputs stemming from an extensive data base of field observations. A major factor was the bearing stress developing at the dowel-concrete interface, for which a new method of determination is proposed. In addition, by using nonlinear multiple regression techniques, algorithms were developed for estimating transverse joint faulting, as a function of a wide range of pavement system parameters. A mechanistic evaluation of these statistical formulae has identified several limitations of the current state of the art, and has led to the formulation of pertinent recommendations for future research.

ANALYTICAL METHODS FOR DOWELED JOINTS

The first rational procedure for the design of doweled joints in concrete pavements was presented by Westergaard in 1928 (*1*). This crude but ingenious method enabled engineers to base on theoretical principles such decisions as those pertaining to the number and spacing of dowels to be used. The analytical treatment assumed that a point load was applied midway between two dowels and that the deflected shape of the loaded side of the joint coincided at all points with the basin formed by the unloaded slab. Thus, all dowels were assumed to be perfectly rigid. The background for this method consisted entirely of Westergaard's earlier analytical studies of the one-slab problem (*2*). Nonetheless, two important new conclusions were reached:

1. Only the two, or at most four, dowels nearest to the load need be considered as active, since the contribution of more remote bars is negligible; and
2. Dowels are effective in reducing the bending stress developed in the loaded slab only if they are spaced closely enough (at less than 2 ft apart).

These two issues remained the prominent foci of the debate that followed in the next several decades, even to the present day.

The Arlington tests (*3*) provided the first documented opportunity for a field study of dowel performance. Their results corroborated Westergaard's conclusions, suggesting that a dowel spacing of closer than 2 ft may be necessary. As

indicated by theory, using larger bars at a closer spacing will increase the stiffness of the dowels, thus enhancing their effectiveness in load transfer. This type of spacing should be done judiciously, however, since it may also cause a detrimental increase of restraint to longitudinal warping or curling. Thus, dowels that are too stiff may cause more distress in the pavement slab than would result from their complete omission (*4*).

In their independent investigations of the stress condition existing in and around the dowel bars, Grinter (*5*) and Bradbury (*6*) made reference to Westergaard's single-slab edge loading solution. Their analytical treatments, however, dispensed with Westergaard's original restrictive assumptions and were instead based on a method presented by Timoshenko and Lessels (*7*), which considers the dowel as an infinite beam encased in an elastic medium. This approach is sensitive to a parameter that has been difficult to determine with any degree of accuracy, namely, the modulus of dowel support (K). Despite early warnings that such calculations "should be taken as significant qualitatively rather than quantitatively" (*8*), the Timoshenko procedure had been used exclusively in related studies until the introduction of the finite element method (FEM) in the 1970s.

Credit for the prominence of the Timoshenko analysis is generally given to the theoretical and experimental expositions by Friberg published in the late 1930s (*9,10*). This investigator presented a set of design equations for evaluating dowel deflections, moments, and stresses, provided the shear force transferred by the dowel could be determined (*10*). Thus, the concrete bearing stress (σ_b) arising under the dowel bar (responsible for spalling distress and dowel looseness) is given by the formula

$$\sigma_b = K\Delta_0 \tag{1}$$

where K is the modulus of dowel support (FL^{-3}) and Δ_0 is the deflection of the dowel with respect to the concrete at the face of the joint (L). Note that the primary dimensions are abbreviated herein as L for length, F for force, and, later, Θ for temperature. Deflection, Δ_0, may be evaluated from

$$\Delta_o = \frac{P_i}{4\beta^3 E_d I_d}(2 + \beta\omega) \tag{2}$$

where

P_i = shear force acting on any particular dowel, transferred across the joint (F);
ω = width of joint opening (L);
E_d = modulus of elasticity of the dowel bar (FL^{-2}); and
I_d = moment of inertia of dowel bar cross-section (L^4).

For solid round bars,

$$\Delta_0 = \frac{\pi d^4}{64} \tag{3}$$

where d is the dowel bar diameter (L) and β is the relative stiffness of the dowel-concrete system (L^{-1}),

$$\Delta_0 = \left(\frac{Kd}{4E_dI_d}\right)^{1/4} \tag{4}$$

In deriving these equations, use was made once again of Westergaard's early theoretical works (*2*), leading Friberg to conclude that dowels at distances greater than an "effective length" (e) of 1.8 times the radius of relative stiffness of the slab-foundation system (l) from the point of application of the external load were inactive and did not influence the moment at the load point. Recall that l is defined as

$$l = \left(\frac{Eh^3}{12(1 - \mu^2)k}\right)^{1/4} \tag{5}$$

where

E = slab modulus of elasticity (FL^{-2});
μ = slab Poisson's ratio;
h = slab thickness (L); and
k = modulus of subgrade reaction (FL^{-3}).

Friberg (*10*) was also the first investigator to suggest that the load transferred by each dowel could be reasonably assumed to decrease linearly with distance from the point of loading. Friberg's additional assumption of a value of 1,000,000 psi/in. for the modulus of dowel support (K) for all pavement systems elicited considerable discussion. Thus, Grinter postulated that K ranged between 300,000 and 1,500,000 psi/in. but also anticipated a "maximum variation of a hundred-fold" in the value of this parameter (*11*). Less attention was paid to Friberg's assertion of an effective length of $1.8l$, despite the fact that this would not be in accordance with Westergaard's own conclusions (*1*). For a typical l-value of 36 in. and dowel spacing of 2 ft, Westergaard's assumption that only the two dowels closest to the load are active would correspond to an effective length of only $1.0l$. Data presented by Sutherland (*12*) also supported a shorter effective length.

A potential for a real breakthrough in analytical methods for doweled joints was created in the late 1970s with the introduction of the FEM. Although the capabilities of this versatile numerical tool are far from exhausted even to this day, several important observations have already been made. Tabatabaie et al. (*13,14*) were among the first to present a finite element model of the doweled joint; they concluded that "only the dowels within a distance $1.0l$ from the center of the load are effective in transferring the major part of the load." They concurred with Friberg's adoption of a linear approximation to the dowel shear force diagram, but suggested that this should begin with a maximum under the load and diminish to zero at a distance of $1.0l$ from this point.

Finite element studies by Tabatabaie also led to the conclusion that the dowel diameter (d) and concrete modulus of elasticity (E) have a very significant effect on the maximum dowel deflection and concrete bearing stress. Slab thickness (h) and subgrade modulus (k) play a much lesser role. Earlier laboratory investigations by Marcus (*15*) and Teller and Cashell (*16*) had also pointed out the same effects. The following relationship for the critical concrete bearing stress (σ_{bc}) was developed, "based on the result of two- and three-dimensional" finite element analyses (*14*):

$$\sigma_{bc} = \frac{(800 + 0.068\,E)}{d^{4/3}}(1 + 0.355\,\omega)sP\alpha_i \tag{6}$$

where

s = dowel spacing (L);
P = applied wheel load (F); and
α_i = load location coefficient (dimensions unclear), i.e., 0.0091 for edge load, 0.0116 for protected corner load, and 0.0163 for unprotected corner load.

All parameters in this expression employ the kip as the unit of force and the inch as the unit of length, whereas σ_{bc} is expressed in pounds per square inch.

PROPOSED METHOD FOR MAXIMUM BEARING STRESS DETERMINATION

Recent research has provided additional evidence supporting the conclusion reached by Tabatabaie and others that the effective length over which dowels are active in load transfer is considerably shorter than was assumed by Friberg. Joints designed under the assumption that all dowels within $1.8l$ from the applied load are effective have exhibited unacceptable performance (e.g., substantial faulting (*17*)), indicating that a more conservative approach is necessary. Therefore, a comparison was conducted during the present study between Tabatabaie's formula (which assumes an effective length of $1.0l$) and Friberg's original equation. This comparison is shown in Figure 1 for a typical PCC pavement section under a single-wheel 9-kip edge load. The pertinent system parameters were as follows: E = 4,000,000 psi; μ = 0.15; h = 10 in.; k = 50 psi/in.; l = 51.1 in.; d = 0.75 in.; s = 12 in.; $K = 1.5 \times 10^6$ psi/in.; $E_d = 29 \times 10^6$ psi; ω = 0.2 in. The assumed percentage of load transferred across the joint ranged from 0 to

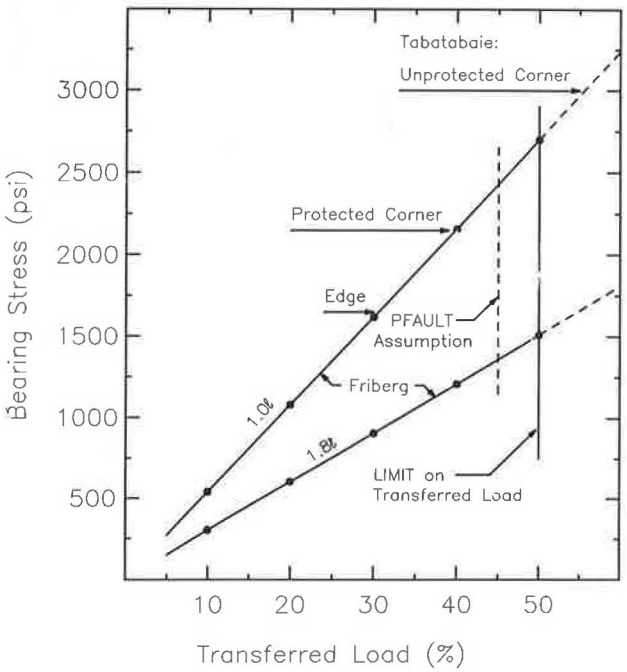

FIGURE 1 Bearing stress formula for a typical PCC pavement section under a single-wheel 9-kip edge load. Data are adapted from Friberg and Tabatabaie (*9,10,13,14*).

the maximum value of 50 percent. The maximum bearing stress, calculated using Friberg's equation on the basis of his linear diminution assumption over an effective length, was $1.8l$. This approach yields a straight line, whose slope is entirely dependent on the assumed effective length. Therefore, decreasing this length to $1.0l$ results in a second straight line, located above the $1.8l$ line and having a steeper slope. Clearly, a more conservative estimate of the maximum bearing stress (i.e., a greater value) is obtained with the shorter assumed effective length.

The actual percentage of load transferred across a doweled joint may be estimated by comparison of Friberg's predictions to the calculated maximum bearing stress according to Tabatabaie et al. (*14*). These percentages are also shown in Figure 1, for the three loading locations considered, i.e. loading at an edge, at a protected corner, and at an unprotected corner. It is apparent that a high assumed percentage of load transferred (close to 50 percent) leads to a conservative estimate of the maximum bearing stress. A value of 45 percent was adopted in this study to account for the possibility of some dowel looseness.

It is interesting to note that both the Friberg and Tabatabaie formulae for the determination of bearing stress can be rewritten as

$$\sigma_b = A(\text{structural}) \times B(\text{load}) \tag{7}$$

The first term, A, is entirely determined by the structural characteristics of the pavement system, whereas the second term, B, quantifies the transferred load. It would be reasonable to expect that at least the A-term should be the same according to the two equations. This, however, is not true, as illustrated by the following calculations for the case considered above:

1. Tabatabaie:

$$A = \frac{(800 + 0.068\ E)}{1000\ d^{4/3}}(1 + 0.355\ \omega)$$

$$= 1.6849 \text{ (units unclear, but should be in.}^{-2}) \tag{8}$$

2. Friberg:

$$A = \frac{K(2 + \beta\omega)}{4\beta^3 E_d I_d}$$

$$= 2.5812 \text{ in.}^{-2} \tag{9}$$

The discrepancy in this case is on the order of 35 percent. Friberg's term is considered superior, however, since it is theoretically based and dimensionally consistent. Note that parameters K and E_d do not enter Tabatabaie's formula. Dowel support was not explicitly prescribed in his three-dimensional finite element analysis, whereas a value of 1,500,000 psi/in. was assumed as "conventional" in his two-dimensional investigations. A value of E_d of 29,000,000 psi was assumed by Tabatabaie.

Turning now to the load B-term in these equations, it is possible to express this as follows:

$$B = P_i = P \times \text{TLE} \times f_d \tag{10}$$

where TLE is the transferred load efficiency, expressing the ratio of the load transferred across the entire length of joint (P_T) to the total applied load (P), that is,

$$\text{TLE} = \frac{P_T}{P} \times 100 \text{ percent} \tag{11}$$

and f_d is a dimensionless distribution factor indicating how much of the total transferred load acts on any given dowel bar (usually on the critical bar), i.e.,

$$f_d = \frac{P_i}{P_T} \times 100 \text{ percent} \tag{12}$$

Note that the distribution factor (f_d) does not depend on the amount of load transferred but is entirely the consequence of the dowel spacing and of the assumptions regarding the effective length and the linear diminution of the dowel shear forces with distance from the applied load. For the case considered in Figure 1, Friberg's linear diminution approach leads to distribution factor values for the critical dowel (f_{dc}), of 13 percent for an effective length of $1.8l$, and 23 percent for $1.0l$. This illustrates once again the conservative nature of the shorter effective length. Tabatabaie, on the other hand, defines the transferred load by any given dowel as:

$$B = P_i = \alpha_i s P \tag{13}$$

In this expression, TLE is not explicitly stated, whereas the load location is accounted for. Note that here both P and P_i are expressed in pounds, and s is expressed in inches, whereas α_i takes the values quoted above. Assuming TLE = 45 percent, Tabatabaie's equation yields the following distribution factors for the critical dowel:

f_{dc} = 24 percent for edge loading,

31 percent for protected corner loading, and

43 percent for unprotected corner loading.

Friberg presumably considered edge loading only, and for this loading condition good agreement is observed. The distribution factor for an unprotected corner is almost twice as large as that for edge loading. This observation is confirmed by results shown in Figure 2, obtained using a recently modified version of finite element computer program ILLI-SLAB (Ioannides and Korovesis from a paper in this Record). The pavement section considered in developing Figure 1 was retained; a contact pressure of 90 psi was assumed. First, a single-wheel load was applied at the edge or at the corner of the slab. Because the broader FHWA study was primarily concerned with 18-kip single axle loading (dual tires), the variation of the distribution factor under such a load (applied at the corner) was also examined. The effective length (e) for both single-wheel loadings (i.e., at the edge and at the unprotected corner) is found to be closer to $1.0l$, instead of to $1.8l$, as concluded by Friberg (*10*). On the other hand, the single-axle (dual-wheel) load at the corner leads to $e \approx 2.0l$, indicating that the effective length is not constant but it is sensitive to the gear configuration.

Referring to the geometry of the transferred load distribution diagram assumed by Friberg, it can be shown that the value of f_{dc} can be determined to a good approximation using, for edge loading,

$$f_{dc} = \frac{s}{e} \tag{14}$$

and for corner loading,

$$f_{dc} = \frac{2s}{e + s} \tag{15}$$

Both Figure 2 and Equations 14 and 15 suggest that for the case of a single-wheel load, the critical distribution factor pertaining to a corner load is almost twice as large as the corresponding edge loading value. Furthermore, under corner loading conditions, a single-wheel leads to responses similar to those obtained using a single-axle (dual-wheel) load, since

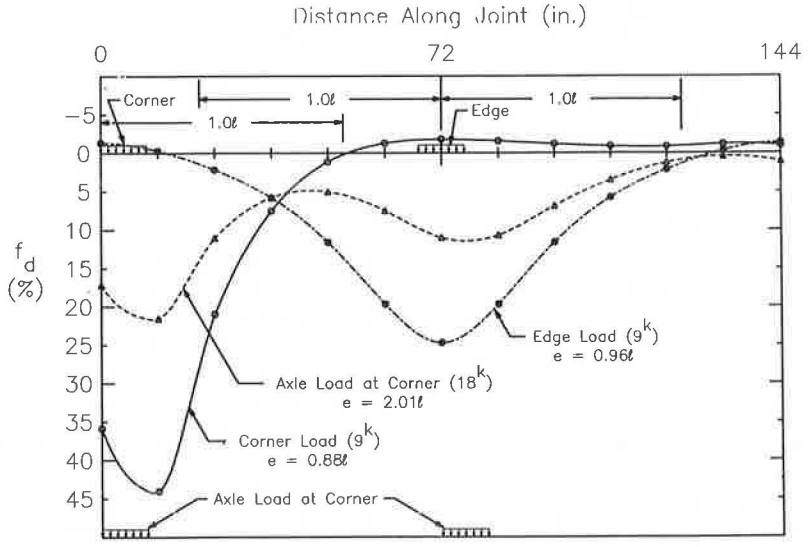

FIGURE 2 Distribution factor (f_d) from ILLI-SLAB.

the product ($f_{dc} \times P$) in Equation 10 is approximately the same in both cases. Consequently, a single wheel applied at the corner can be regarded as the critical (design) loading condition.

Using Equation 15 for f_{dc} in the load B-term, and Friberg's structural A-term, the maximum bearing stress may be determined in a manner that accounts for both the location of the load and the rest of the parameters entering Friberg's theoretical development. Results obtained during this investigation using ILLI-SLAB indicate that TLE is only slightly affected by load location and is generally about 42 ± 1 percent. The assumed value of 45 percent is, therefore, somewhat conservative, as desired.

The proposed bearing stress determination method outlined above has been incorporated into an interactive computer program called PFAULT, prepared for FHWA for the estimation of faulting (*18*). Given below is the formula used in PFAULT to determine the critical bearing stress:

$$\sigma_{bc} = \frac{K(2 + \beta\omega)}{4\beta^3 E_d I_d} \times P \times \text{TLE} \times f_{dc} \qquad (16)$$

in which f_{dc} is determined by using Equation 15, assuming $e = 1.0l$. The dowel spacing is set to 12 in. since the PFAULT data base contained only such sections. As noted above, P = 9,000 lbs, and TLE = 45 percent. The joint width (ω) is calculated by using Equation 17, as described below. The following inputs are tentatively adopted since they had also been assumed in analyzing the field data that provided the data base for PFAULT: K = 1,500,000 psi/in.; $E_d = 29 \times 10^6$ psi.

The sensitivity of the proposed method for determining the maximum bearing stress was investigated for a wide range of d, s, h, and k values (*18*). Dowel diameter (d) clearly emerged as the most important of these variables. The reduction in σ_{bc} with increasing d is particularly dramatic at the smaller dowel diameters ($d \leq 1$ in., say). The sensitivity of σ_{bc} to the rest of the parameters considered is considerably smaller. It follows, therefore, that since the required dowel diameter is greatly affected by the assumed value of modulus of dowel support (K) it is imperative that a good estimate of the latter be obtained before proceeding to a faulting calculation. Unfortunately, no method exists today for this purpose.

CALIBRATION OF MECHANISTIC-EMPIRICAL FAULTING ALGORITHMS

In conventional practice, the amount of transverse joint faulting for PCC pavements is commonly estimated by developing mechanistic-empirical algorithms by using a data base containing in-service pavement data. Accordingly, the NCHRP Project 1-19 (COPES) data base (*17*) was employed in the calibration of PFAULT. Nonlinear multiple regression techniques from the SPSS software package (*19*) were applied in describing the variation of measured faulting with respect to three mechanistic parameters—concrete dowel bearing stress, joint opening, and corner deflection. This can contribute toward more realistic and accurate estimates of anticipated transverse joint faulting, in both doweled and undoweled pavements. Guidelines for dowel design may also be formulated on the basis of such a mechanistic-empirical approach.

Estimating Faulting in Doweled Pavements

The COPES data base (*17*) contains information from doweled pavement sections from the following four states: Illinois, Louisiana, Minnesota, and Nebraska. Both JPCP and JRCP are included. In addition, 12 sections of JRCP from the experiment at Rothsay, Minnesota, were incorporated into the PFAULT data base. These were designed with 27-ft joint spacing over granular, asphalt, and cement-treated bases.

The maximum concrete bearing stress was computed using the new proposed method of calculation. As indicated by Equation 16, this involves the joint width (ω), which is known to be a highly variable parameter (*20*). The mean value of the joint opening caused by temperature and moisture changes in the slab is computed in PFAULT using the following expression:

$$\omega = C\dot{L}\,(0.5\alpha\Delta T + \varepsilon_s) \qquad (17)$$

where

- α = thermal coefficient of contraction of concrete (Θ^{-1}) (e.g., 5.0×10^{-6} ε/°F);
- ε_s = drying shrinkage coefficient of concrete (approximately $0.5 - 2.5 \times 10^{-4}$ ε, specified as 1.5×10^{-4} ε in PFAULT);
- L = transverse joint spacing (L);
- ΔT = temperature range (Θ), i.e., maximum mean daily air temperature in July minus minimum mean daily air temperature in January; and
- C = dimensionless empirical adjustment factor caused by slab-base frictional restraint (PFAULT assumes that C = 0.65 for stabilized base, and C = 0.80 for granular base).

Equation 17 is a modification of a regression equation, based on "limited field data," presented by Darter (*21*) to provide an approximate estimate of ω "despite the many complexities involved." Introduction of the factor of 0.5 in Equation 17 aims at reflecting a more realistic average condition of joint opening. The faulting algorithm established in this manner for doweled pavements is as follows:

$$\text{FAULT} = \text{ESAL}^{0.5377}\,(2.2073 + 0.002171\,\sigma_{bc}^{0.4918} + 0.0003292\,L^{1.0793} - 2.1397\,k^{0.01305}) \qquad (18)$$

Statistics: R^2 = 0.53; SEE = 0.05 in.; n = 280.

In this formula, ESAL denotes the cumulative 18-kip equivalent single-axle load applications (in millions), σ_{bc} is expressed in pounds per square inch, and L in feet. The effective modulus of subgrade reaction (k) is provided in pounds per square inch per inch, whereas FAULT is expressed in inches. Several climatic variables (e.g., precipitation and freezing index) were also introduced into the regression analysis, but they did not show any statistical significance. A plot of observed versus estimated faulting is presented in Figure 3.

Among the four parameters used for estimating FAULT, a sensitivity analysis showed that σ_{bc} and L are the most significant. Adjusting the joint spacing, slab thickness, and

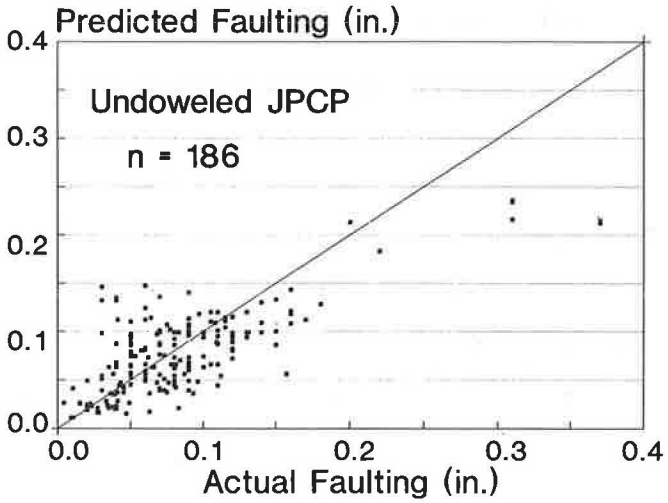

FIGURE 3 Predicted versus actual faulting: nationwide model for undoweled pavements (PFAULT version 1.2).

subgrade support to keep the ratio of L/l below 6, for instance, may therefore help in fault control in JPCP (*22*).

The expression in Equation 18 is primarily a descriptive tool whose predictive capability is not high. This is especially true when a small number of particular sections are considered. As with all statistical algorithms, however, agreement between observed and estimated responses may be expected to increase as the number of test cases considered increases. A review of similar statistically based tools, such as PDMAP, COLD, and PMARP, indicated that reliability problems are widespread, particularly when these are applied to geographical regions other than those included in the original data base (*23,24*). Therefore, the following major deficiencies of the faulting algorithm in Equation 18 must be kept in mind by prospective PFAULT users:

1. Because of the limited number of climatic zones in the data base, climatic variables did not appear significant enough to warrant their explicit inclusion in the formula derived.
2. A variety of other situations existed, in which the range of some of the variables was not sufficient (e.g., permeable base type, subgrade type, edge support, and subdrainage).
3. The possible interactions between individual factors entering the algorithm are ignored.
4. The formula involves the ESAL concept, which is urgently in need of reconsideration (*25*).
5. A number of the implicit assumptions made during the development of this statistical algorithm and its application in PFAULT have been mere intelligent and educated guesses.

In examining the PFAULT data base, deficiencies in the state of the art have dictated choices that may or may not apply to any one situation. In order of their importance, such selections include a universal value of the modulus of dowel support ($K = 1.5 \times 10^6$ psi/in.); a constant value of the radius of the applied load ($a = 5.64$ in.); an empirical-statistical method for calculating joint width (Equation 17); and fixed values for the effective length ($e = 1.0l$) and transferred load efficiency (TLE = 45 percent). The method employed in the determination of the subgrade modulus k was also arbitrary and inconsistent. This method was often based on correlations with soil classification groups or other soil properties, whereas on other occasions it was determined by application of elastic theory. The procedure followed involved increasing k when a treated base was used, as recommended by the Portland Cement Association. This may be a conventional approach, but it has severe limitations as revealed by finite element investigations (*26*), especially for unbonded slab/base interfaces. Use of Equation 18 in cases involving undue extrapolation beyond the data range used in its generation is, therefore, to be avoided. This is particularly true for open-graded drainable bases.

As a result of the limitations noted, the R^2 value of the algorithm in Equation 18 is rather low. Previous attempts at deriving similar algorithms were also fraught with similar weaknesses (*18,21*). It may be expected that substantial progress in the state of the art in mechanistic analysis methods would allow the elimination of the sources of the deficiencies outlined above. In the meantime, a much simpler predictive algorithm proposed by Snyder (*27*) appears promising. This algorithm involves a single independent variable, namely load transfer efficiency in terms of deflection (LTE_δ, defined as the ratio of the deflections on the unloaded and loaded sides of a joint), and displays a considerably higher R^2 value. Snyder's proposal is as follows:

$$FAULT = 23.37 - 0.1288\ LTE_\delta + 141{,}900\ LTE_\delta^{-3.807} \quad (19)$$

Statistics: $R^2 = 0.691$; $SEE = 0.057$ in.; $n = 140$.

In this expression, FAULT is expressed in hundredths of an inch, and LTE_δ is expressed in percent. Note that this relationship is linear, since the third term is negligible for LTE_δ values in excess of 20 percent. A significant improvement of Snyder's model can result if the endurance of LTE_δ over time is investigated and incorporated into the proposed faulting algorithm.

Estimating Faulting in Undoweled Pavements

Prevention of faulting in undoweled pavements relies on effective load transfer through aggregate interlock. The degree and long-term endurance of load transfer by aggregate interlock is affected by the size of joint opening, slab support, thickness of slab, coarseness, angularity and hardness of concrete aggregates, and number of applied load repetitions (Ioannides and Korovesis from a paper in this Record). The slab corner deflection (δ_c) may provide a useful indicator of ensuing deterioration of load transfer efficiency by aggregate interlock and of impending distress because of pumping and faulting (*17*). According to Westergaard (*2*), this deflection is given by

$$\delta_c = \frac{P}{kl^2}\left[1.1 - 0.88\left(\frac{\sqrt{2}\,a}{l}\right)\right] \quad (20)$$

in which a denotes the radius of the applied load (L). A refined expressio ı for δ_c (based on finite element results) was

presented by Ioannides et al. (*28*). PFAULT assumes that a = 5.64 in., which for P = 9,000 lb corresponds to a contact pressure of 90 psi. Furthermore, erodibility factors for the base and subbase materials (ERODF) are introduced. These are similar to the loss of support coefficients recommended by AASHTO (*29*), as follows:

1. Granular material: ERODF = 2.5;
2. Asphalt-treated base: ERODF = 2.0;
3. Cement-treated base (without granular subbase): ERODF = 1.5;
4. Cement-treated base (with granular subbase): ERODF = 1.0; and
5. Lean concrete: ERODF = 0.5.

Regrettably, no permeable base courses were included in the PFAULT data base, even though these are expected to have a major effect on reducing faulting.

The nonlinear regression technique referred to above for doweled pavements was employed in a similar fashion for undoweled pavements. Only plain concrete pavement sections were available in the NCHRP 1-19 data base for undoweled pavements (*17*). The data base included pavement sections from the following states: Georgia, Illinois, Louisiana, Utah, and California. Two extra sections from New Jersey and Michigan were also added. The data base was expanded by 24 additional sections from California, which included the following conditions: half-joint spacing (7.8 ft), thicker slab (11.4 in.), and lean concrete base (effective k-value = 591 psi/in.). Furthermore, 12 sections from the experiment at Rothsay, Minn., were also incorporated. These sections had 27-ft joint spacing over granular-, asphalt-, and cement-treated bases. The resulting nationwide algorithm for estimating faulting in undoweled pavements is given as follows:

$$\begin{aligned} FAULT = ESAL^{0.3157}[&0.4531 + 0.3367\,\omega^{0.3322} \\ &- 0.5376(100\,\sigma_c)^{-0.008437} \\ &+ 0.0009092\,FI^{0.5998} + 0.004654\,ERODF \\ &- 0.03608\,EDGESUP \\ &- 0.01087\,SOILCRS \\ &- 0.009467\,DRAIN] \end{aligned} \quad (21)$$

Statistics: R^2 = 0.55; SEE = 0.03 in.; n = 186.

In this formula

FI = mean air-freezing index in °F days;
EDGESUP = numerical indicator of type of edge support, e.g., 0, if no edge support exists and 1, if edge beam/tied concrete shoulder exists;
SOILCRS = numerical indicator of AASHTO subgrade soil classification, e.g., 0, if A-4 to A-7 and 1, if A-1 to A-3; and
DRAIN = numerical indicator of drainage provided, e.g., 0, if no edge subdrains exist and 1, if edge subdrains exist.

Note that in Equation 21, the mean transverse joint opening (ω) and the Westergaard corner deflection (δ_c) are expressed in inches. Figure 4 shows a plot of observed versus estimated faulting for this formula. A sensitivity study revealed that the effects of ω, ERODF, and EDGESUP are the most pronounced (*18*).

The comments made above with respect to the nature of statistical algorithms and the limitations of Equation 18 apply here as well. Although the effect of some climatic variables is included in this case, caution is still warranted in the application of the resulting algorithm. Unwarranted extrapolation beyond the data range from which Equation 21 was generated is to be avoided, as always. Nonetheless, this mechanistic-empirical tool may be useful in long-term performance evaluations and design applications within the range of data.

The interactive computer program PFAULT, mentioned above, incorporates both faulting algorithms developed in this study, i.e., Equations 18 and 21. The program is available in an IBM-PC compatible version with pertinent documentation. An input guide is included in the report by Heinrichs et al. (*18*).

GUIDELINES FOR THE USE OF DOWELS

Mechanistic-empirical algorithms for estimating faulting can be used in assessing the need for dowel bars and determining the required diameter for pavements similar to those included in the data base used in their development. The application of the PFAULT formulae in this manner is described below.

Jointed Reinforced Concrete Pavements

Dowels are always recommended for JRCP caused by longer joint spacing and expected wider joint opening. The required dowel diameter may be determined using PFAULT, if a threshold faulting level is selected. According to the NCHRP 1-19 data base (*17*), joint faulting in rough pavements [present serviceability index (PSI) ≤ 3.0] was about 0.26 in. In view of the weakness of the correlation in Equation 18, a design faulting magnitude of approximately 0.13 in. is suggested, subject to further verification.

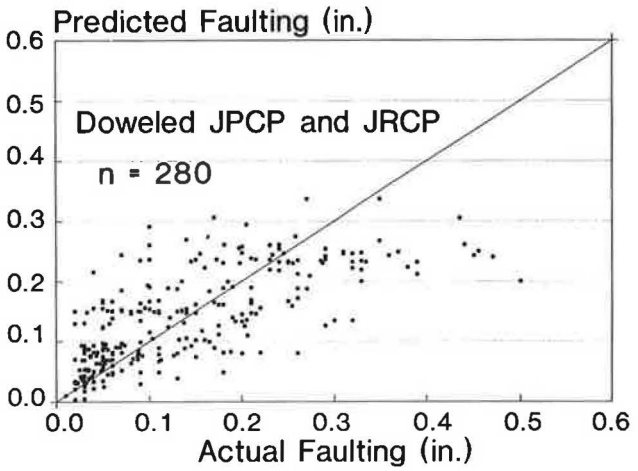

FIGURE 4 Predicted versus actual faulting: nationwide model for doweled pavements (PFAULT version 1.2).

Jointed Plain Concrete Pavements

Dowels often are omitted in the design of JPCP, and aggregate interlock is relied on for load transfer. Aggregate interlock alone often is inadequate, and many such pavements develop serious pumping and faulting. The need for dowels may be assessed by using PFAULT. Referring again to the NCHRP Project 1-19 data base (*17*), JPCP offered a rough ride and exhibited faulting of about 0.13 in. A threshold value of about 0.07 in. may be appropriate for design purposes, subject to further verification. If faulting is excessive, the required dowel diameter may be determined as outlined above for JRCP.

CONCLUSIONS

This paper presents some of the findings of a study conducted for the FHWA, to provide a synthesis of the current state of the art with respect to PCC pavement design, incorporating the results of recent pertinent investigations (*18*). In particular, design guidelines are outlined for assessing the need for load transfer at transverse joints, so that significant faulting is prevented. The proposed procedure can be used in determining whether dowels are needed and in selecting their appropriate size. Theoretical considerations and interpretation of an extensive field data base have led to the development of descriptive mechanistic-empirical algorithms for estimating the expected transverse joint faulting in both plain and doweled concrete pavements. Within the constraints imposed by their statistical nature, the application of these tools is facilitated by the user friendly micro-computer program PFAULT. At the heart of this procedure is a new method for calculating the maximum bearing stress developing at the dowel-concrete interface, which couples earlier theoretical investigations with more recent results from finite element studies.

ACKNOWLEDGMENTS

The investigations for this paper were supported in part by a grant from FHWA, U.S. Department of Transportation. The Project Manager was Stephen Forster. The authors also acknowledge the contributions of K. W. Heinrichs and M.-J. Liu, formerly graduate research assistants at the University of Illinois, in the statistical analyses performed.

REFERENCES

1. H. M. Westergaard. Spacing of Dowels. *HRB Proc.*, Vol. 8, 1928, pp. 154–158.
2. H. M. Westergaard, Computation of Stresses in Concrete Roads. *HRB Proc.*, Vol. 5, 1925, pp. 90–112.
3. L. W. Teller and E. C. Sutherland. The Structural Design of Concrete Pavements, Part 4. *Public Roads*, Vol. 17, No. 8, Oct. 1936, pp. 175–192.
4. E. F. Kelley. Application of the Results of Research to the Structural Design of Concrete Pavements. *Public Roads*, Vol. 20, No. 5, July 1939, pp. 83–104.
5. L. E. Grinter. Design of Reinforced Concrete Road Slab. *Bulletin No. 39*, Texas Engineering Experiment Station, 1931.
6. R. D. Bradbury. Design of Joints in Concrete Pavements. *HRB Proc.*, Vol. 12, 1932, pp. 105–141.
7. S. Timoshenko and J. M. Lessels. *Applied Elasticity*. Westinghouse Technical Night School Press, 1925.
8. L. E. Grinter. Discussion: Effect of Dowel-Bar Misalignment Across Concrete Pavement Joints, by A. R. Smith and S. W. Benham. *Transactions*, ASCE, Vol. 103, 1938, pp. 1145–1162.
9. B. F. Friberg. Load and Deflection Characteristics of Dowels in Transverse Joints of Concrete Pavements. *HRB Proc.*, Vol. 18, Part 1, 1938, pp. 140–154.
10. B. F. Friberg. Design of Dowels in Transverse Joints of Concrete Pavements. *Transactions*, ASCE, Vol. 105, 1940, pp. 1076–1095.
11. L. E. Grinter. Discussion: Design of Dowels in Transverse Joints of Concrete Pavements, by B. F. Friberg. *Transactions*, ASCE, Vol. 105, 1940, pp. 1096–1116.
12. E. C. Sutherland. Discussion: Design of Load Transfer Joints in Concrete Pavements, by J. W. Kushing and W. O. Fremont. In *HRB Proc.*, Vol. 20, 1940, pp. 494–497.
13. A. M. Tabatabaie. *Structural Analysis of Concrete Pavement Joints*. Ph.D. thesis. University of Illinois, Urbana, 1978.
14. A. M. Tabatabaie, E. J. Barenberg, and R. E. Smith. *Longitudinal Joint Systems in Slip-Formed Rigid Pavements*. Report FAA-RD-79-4, Vol. 2. FAA, U.S. Department of Transportation, 1979.
15. H. Marcus. Load Carrying Capacity of Dowels at Transverse Pavement Joints. *Journal of the American Concrete Institute*, Vol. 23, No. 2, Oct. 1951 (Proceedings Vol. 48), pp. 169–184.
16. L. W. Teller and H. D. Cashell. Performance of Dowels Under Repetitive Loading. *Public Roads*, Vol. 30, No. 1, April 1958, pp. 1–24.
17. M. I. Darter, J. M. Becker, M. B. Snyder, and R. E. Smith. *NCHRP Report 277:* Concrete Pavement Evaluation System (COPES). TRB, National Research Council, Washington, D.C., 1985.
18. K. W. Heinrichs, M. J. Liu, M. I. Darter, S. H. Carpenter, and A. M. Ioannides. *Rigid Pavements Analysis and Design*. Report FHWA-RD-88-068. University of Illinois, Urbana, Dec. 1988.
19. N. H. Nie, C. H. Hull, J. G. Jenkins, K. Steinbrenner, and C. H. Bent. *Statistical Package for the Social Sciences*, 2nd ed. McGraw-Hill, Inc., New York, 1975.
20. M. I. Darter and W. B. Isakson. Thermal Expansion and Contraction of Concrete Pavements in Utah. *Interim Report*, Project 915, Utah Department of Transportation, 1970.
21. M. I. Darter. *Design of Zero-Maintenance Plain Jointed Pavement, Vol. I—Development of Design Procedures*. Final Report FHWA-RD-77-111. FHWA, U.S. Department of Transportation, June 1977.
22. A. M. Ioannides and R. A. Salsilli-Murua. *Slab Length, Slab Width and Widened Lanes Effects in Rigid Pavements*. FHWA, U.S. Department of Transportation; University of Illinois, Urbana, Dec. 1988.
23. National Cooperative Highway Research Program. *Quarterly Progress Report on Project 1-26: January 1–March 31, 1988*. University of Illinois, Urbana.
24. National Cooperative Highway Research Program. *Quarterly Progress Report on Project 1-26: April 1–June 30, 1988*. University of Illinois, Urbana.
25. A. M. Ioannides and R. Salsilli-Murua. Temperature Curling in Rigid Pavements: An Application of Dimensional Analysis. In *Transportation Research Record 1227*, TRB, National Research Council, Washington, D.C., 1989, pp. 1–11.
26. M. Duval and A. M. Ioannides. *Evaluation of the Portland Cement Association Improved Subgrade Modulus Values*. University of Illinois, Urbana, Dec. 1985.
27. M. B. Snyder. *Dowel Load Transfer Systems for Full-Depth Repairs of Jointed Portland Cement Concrete Pavements*. Ph.D. thesis. University of Illinois, Urbana, 1989.
28. A. M. Ioannides, M. R. Thompson, and E. J. Barenberg. Westergaard Solutions Reconsidered. In *Transportation Research Record 1043*, TRB, National Research Council, Washington, D.C., 1985, pp. 13–23.
29. *AASHTO Guide for Design of Pavement Structures*. American Association of State Highway and Transportation Officials. Washington, D.C., 1986.

Publication of this paper sponsored by Committee on Rigid Pavement Design.

Effect of Lane Widening on Lateral Distribution of Truck Wheels

RAHIM F. BENEKOHAL, KATHLEEN T. HALL, AND HARLAN W. MILLER

Past field studies of lateral distribution of trucks on highway pavements are limited in their relevance to current design practices and truck size limits. In particular, little information is available on the effect of widened concrete slabs on lateral distribution of trucks. The Illinois Department of Transportation has constructed test sections of "widened-lane" pavements with 18-in. and 20-in. slab extensions on I-57. Truck wheel placements on these test sections were compared with those observed on nearby conventional 12-ft pavement slabs in a recent study conducted at the University of Illinois. Continuous filming of truck wheel positions was performed with an 8-mm camera mounted on bridges over the highway. Wheel positions were determined to within approximately 0.5-in. precision by scaling distances measured on the films to known dimensions on the pavements. The mean placement of the wheels of over 900 trucks observed on the control sections was about 22 in. from the slab edge. About 2.5 percent of the wheels passed within 6 in. of the slab edge. On the widened-lane sections, the mean placement of truck wheels was about 2 in. closer to the lane edge (marked by the paint stripe) but still 38 to 40 in. away from the slab edge. No slab edge loadings were observed among more than 1,300 observations of truck wheel placements on the widened-lane pavement sections. The results suggest that lane widening is likely to be a cost-effective design improvement for concrete highway pavements that otherwise would be vulnerable to transverse fatigue cracking as a predominant mode of failure.

STATEMENT OF THE PROBLEM

Structural damage to concrete highway pavements is caused primarily by truck loads applied at the outer slab edge. Field observations of concrete highway pavement performance (*1*) have confirmed the findings of many analytical studies that have identified the outer edge as the critical location for fatigue damage accumulation. The major structural distresses observed nationwide are transverse cracking and corner breaks on jointed pavements and punchouts on continuously reinforced pavements, all of which are fatigue failures produced by edge loadings. Load-related longitudinal cracking is far less prevalent on highway pavements than on airfield pavements.

The importance of fatigue cracking to the performance of concrete pavements has prompted a two-pronged effort by researchers to study truck edge loads. Analytical studies employing plate theory (Westergaard's equation) (*2*,*3*), influence charts (*4*), and, more recently, finite element programs (*5*,*6*) have concentrated on quantifying the magnitude of the stress under an edge load and the reduction of this stress with increasing distance of the load from the edge. These and other studies have encouraged design modifications to reduce edge stresses, including increased slab thickness, reduced transverse joint spacing, tied concrete shoulders, and widened lanes, paved a foot or more wider than the standard 12-ft traffic lane width (*7*–*10*). Field studies, meanwhile, have attempted to observe the lateral wander of truck wheels around their mean wheelpath location and to quantify the portion of truck loadings that truly may be considered edge loads (*11*–*19*). These field studies have been conducted by using a variety of data collection methods on various types of roads and have addressed a variety of concerns (not only pavement thickness design but also vehicle operations and roadway geometry). Unfortunately, those field studies that are the oldest and least relevant to current roadway designs and truck characteristics persist in being the most influential to many concrete pavement design procedures and state design policies. In addition, very little field information is available to assess the effect of widened lanes on lateral distribution of truck traffic.

The Illinois Department of Transportation (DOT) has constructed an experimental pavement section with a widened lane design on Interstate 57. The University of Illinois recently conducted a field study and analysis of lateral distribution of truck traffic on the widened-lane pavement sections and on nearby sections of standard designs. The findings of this study are reported in this paper.

SUMMARY OF PAST FIELD STUDIES

Before World War II, when most roads in the United States had traffic lanes less than 12 ft wide, the Bureau of Public Roads studied the effect of roadway width on vehicle operations. Based on observations of some 95,000 vehicles at 47 sites in 10 states, Taragin reported in 1945 (*11*) that vehicle encroachment onto shoulders was much greater for lane widths of 11 ft or less than for 12-ft widths. Largely on the basis of these findings, the 12-ft lane width became the norm in postwar roadway construction and remains so today. Relationships among lane width, vehicle placement, and pavement distress on two-lane highways in Texas were studied by Scrivner in 1955 (*12*). Further research on lateral placement of vehicles on two-lane rural highways with and without paved shoulders was reported in 1957 by the Texas Highway Department (*13*).

Taragin's 1958 study (*14*) on lateral placement of trucks on two-lane and four-lane divided highways drew on data for nearly 20,000 trucks collected at 119 sites in 17 states between

R. F. Benekohal and K. T. Hall, Department of Civil Engineering, University of Illinois at Urbana-Champaign, Urbana, Ill. 61801. H. W. Miller, Region 10, FHWA, 708 Southwest 3rd Ave., Portland, Oreg. 97204.

1948 and 1956. For two-lane highways with 12-ft lanes, lateral displacements from the outer edge of truck dual wheels to the edge of the pavement were reported to have means of 26.4 in. and 10.8 in. for pavements with unpaved and paved shoulders, respectively. Similar results were obtained for 10-ft and 11-ft lanes, leading Taragin to conclude that paved shoulders that clearly contrasted the traffic lane in appearance increased the effective width of each lane by a foot or more.

The mean displacement on four-lane divided highways with unpaved shoulders was 33.6 in.; no data for four-lane divided highways with paved shoulders were reported. If paved shoulders were assumed to have the same effect on four-lane highways as on two-lane highways (i.e., an outward shift of about 15 in.), a mean displacement of 18 in. could be inferred from Taragin's study.

The early Texas and Bureau of Public Roads studies relied on point sampling of vehicle placements by taking measurements directly from the pavement surface. In a 1972 study of the effect of intercity buses on nearby passenger cars, Weir and Sihilling described a system for continuous photographic monitoring of vehicles using cameras mounted inside buses (*15*). Although conducted for purposes unrelated to pavement design, this study introduced following moving vehicles as a means for observing their positions in traffic lanes. Data for Emery's 1975 lateral displacement study for the Georgia DOT (*16*) were collected by observers in passenger cars who followed trucks for 10 mi at a time and visually estimated the trucks' wheel positions every 10 seconds. The mean lateral displacement of the truck wheels from the lane edge was reported as 17.6 in.

Canner and Hale's 1980 study for the Minnesota DOT (*19*) was the first to compare truck positions on pavements with widened slabs or tied concrete shoulders with those on conventional 12-ft-wide slabs with bituminous shoulders. Canner and Hale used the same data collection method as Emery: following trucks for 10 mi and estimating their positions every 10 seconds. Truck positions were recorded and reported in 8-in. intervals, a level of precision felt by the researchers to be coarse, but sufficient for the purposes of the study. The mean lateral displacements computed from the information reported for the sections included in the Minnesota study are shown in Table 1.

The tied concrete shoulder apparently caused trucks to shift their positions 3 to 4 in. closer to the lane edge than to the bituminous shoulders, even though the concrete shoulder had rumble strips. Slab widening apparently caused an even greater shift (about 10 in.) toward the lane edge. Rumble strips on one of the widened slab sections did not appear to significantly affect this shift.

TABLE 1 MEAN LATERAL DISPLACEMENTS FROM MINNESOTA STUDY (*19*)

Section	Lane (ft)	Slab (ft)	Shoulder	Rumble strip	Mean (in.)
I-90	12	12	AC	No	26
I-94	12	12	AC	No	27
I-35	12	12	AC	No	26
TH 169	12	12	AC	No	26
I-90	12	12	PCC	Yes	23
I-94	12	15	AC	No	16
TH 52	12	15	AC	Yes	17

NOTE: All displacements are measured from the lane edge (paint stripe). Means computed to whole inch; measurement accuracy about ±4 in.

Time-lapse photography was used by Miller and Stewart in 1982 (*17*) to monitor traffic on lanes of various widths in Toronto. They found this technique to be superior to other methods of collecting lateral distribution data. Lee et al. returned to the truck-following method in a 1983 study of truck positions on Texas highways (*18*). Trucks were monitored by using a video camera mounted in a van, and measurements were made by displaying the videotape on a 19-in. monitor. Of the sources of error encountered in this procedure, among the more serious was image distortion caused by curvature of the monitor screen, for which some compensation was attempted. No mean lateral displacement was reported in the study.

Statistical analysis of the data collected in these past studies has been limited in nearly all cases to presenting histograms of the data, calculating the mean wheel location, and reporting the percentage of vehicles encroaching on the shoulder. However, it is commonly assumed in concrete pavement thickness design that lateral placement of truck wheels is approximately normally and symmetrically distributed about the mean location. This assumption permits calculation of the percentage of truck passes constituting edge loads using normal distribution z-tables. Although this assumption may be valid for aircraft wheels distributed about the centerline of a wide runway or taxiway, there is less reason to believe that it is valid for highway traffic. For example, Emery's data were shown in a 1976 study by Darter to be approximately normal, whereas Taragin's data were not (*20*). The median (50th percentile) value of Taragin's data for two-lane highways with paved shoulders is approximately 18 in., in contrast to the reported mean value of 10.8 in. This type of discrepancy suggests that lateral distributions of highway traffic may be significantly asymmetric, which raises the question of whether it is appropriate to use normal distribution tables to compute edge loadings.

LEGISLATION AFFECTING TRUCK WIDTHS

Previous studies on lateral distribution of trucks must also be viewed in light of legal truck widths in force at the time the data were collected. Width limits were controlled by individual states' regulations between 1913 and 1956, with 96 in. (8 ft) being the maximum in nearly all states. The first federal truck size and weight limits were contained in the Federal-Aid Highway Act of 1956, which set 96 in. as the truck width limit on all interstate highways (with a grandfather clause allowing wider limits already set by a few states to stand) (*21*). The 96-in. limit remained in effect until 1983, when the Surface Transportation Assistance Act of 1982 took effect, increasing the limit to 102 in. (8.5 ft). Only one of the above studies was published after that time, and it is likely that data for that study were collected before the law changed and trucks with wider wheel spacings were on the road.

LATERAL DISTRIBUTION ON WIDENED LANES

Another concern associated with applying the findings of past lateral distribution studies to future pavement designs is the

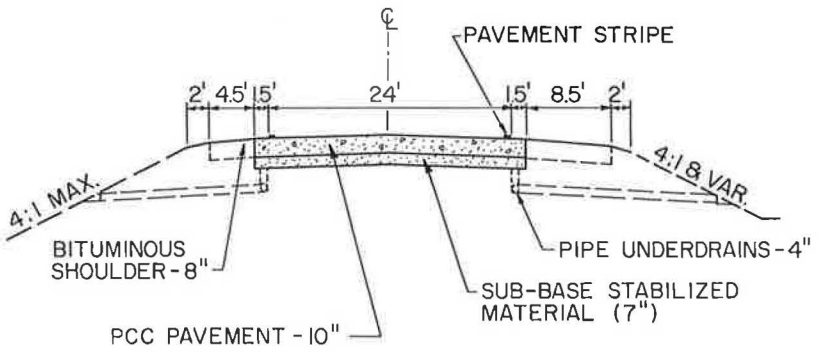

FIGURE 1 Typical cross-section of widened-lane pavement on I-57 near Effingham, Ill.

scarcity of data for pavements with widened lanes or tied concrete shoulders. Some researchers have suggested that widened lanes and concrete shoulders do not provide the strong visual delineation of the shoulder from the traffic lane, which bituminous shoulders provide, and thus do not discourage shoulder encroachment as effectively as bituminous shoulders. Colley et al. (*9*) state that "it is highly improbable that a painted white stripe located 406 mm (16 in.) from the pavement edge will prevent encroachment." The Minnesota DOT's study (*19*) seems to support this assertion; however, the crude measurement method employed in this study casts doubt on the significance of any differences observed.

FIELD DATA COLLECTION

Widened Lane and Conventional Pavement Sections

In 1987, the Illinois DOT constructed a 4.1-mi section of widened-lane pavement on Interstate 57 north of Effingham in east central Illinois. The original 10-in. jointed reinforced concrete pavement (JRCP), which was built in 1964, was recycled and reconstructed as a 10-in continuously reinforced concrete pavement (CRCP) with a 7-in. cement-stabilized subbase and longitudinal edge drains. Figure 1 shows a typical cross-section detail from the widened-lane pavement. The traffic lanes are striped 12 ft wide, but the design calls for the slab to be paved 18 in. wider on each side. Measurements taken during this study showed the pavement to be 18 in. wider in the southbound direction, but 20 in. wider in the northbound direction. A typical cross-section for a conventional Illinois interstate pavement is shown in Figure 2 for comparison. Eight control sections (northbound and southbound) were selected at four sites on I-57 in Champaign, Douglas, and Coles counties. The control sections, as well as the widened-lane sections, had little or no horizontal curvature.

Field Data Collection and Data Reduction

The lateral distribution data collected for this study were obtained by using an 8-mm camera mounted on bridges over the highway. A variety of camera positions and angles were tried in an effort to identify the set-up that gave the best view of truck wheels in the outer lane and allowed measurement of their positions to the greatest degree of precision. Two-inch-square holes spaced 2 in. apart were cut in a cardboard template 2 ft long, which was used to paint marks on the pavement. The template was placed perpendicular to the outer lane edge stripe and the pavement was marked 60, 120, and 200 ft downstream from the bridge. The positions of truck wheels passing over the paint marking could be determined with a precision of less than 1 in. at the 120-ft and 200-ft locations. Better precision (0.5 in. or better) was obtained at

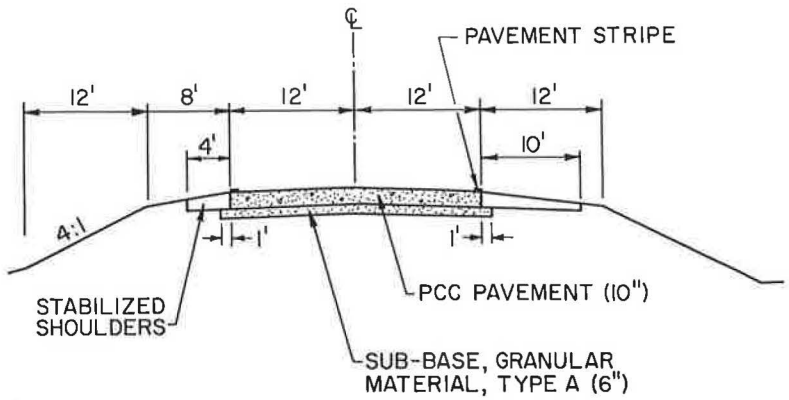

FIGURE 2 Typical cross-section of control sections on I-57 between Champaign and Effingham, Ill.

the 60-ft location, so a camera angle directed at the pavement 60 ft from the bridge was selected for use at all of the test sites.

The position of the camera on the bridge was also selected after much trial and error, at positions ranging from one aligned with the paint stripe to one several yards farther away from the paint stripe. The camera position that provided the best view of truck wheels passing over the template without significant visual distortion was one above the outer edge of the outer shoulder, 10 ft from the paint stripe. This location resulted in a camera position at a slight angle from the traffic lane as well as at a downward angle to the roadway. To check for distortion and the possible need for a correction factor, a scale striped in 2-in. increments was placed across the lane, and actual distances on the scale were compared to distances measured on film. From this comparison it was determined that lateral distortion was not significant.

A variety of filming methods were tested before a satisfactory one was identified. Continuous filming of all traffic on the highway was tried first and consumed a lot of camera film. Next the camera was operated with its automatic timer feature active and an operator-controlled trigger, so that as a truck approached the operator could start the camera and take a series of time-lapse images of the truck. Even at the fastest shutter speed available, however, truck wheels were not always filmed at the spot on the pavement at which the camera was aimed. The most satisfactory method eventually proved to be having the operator watch for an approaching truck and trigger the camera to film continuously for the several seconds during which the truck passed under the bridge and through the camera's field of view.

Data collection was not performed on days when, in the operator's judgment, a significant cross-wind was present that might influence truck positions. Only tractor-semitrailers were filmed; no data were collected for single-unit trucks or passenger cars. Using the methods described, a total of 1,304 trucks were filmed on the two widened-lane sections and 912 trucks were filmed on the control sections. The trucks' positions were determined by projecting the movie films onto a screen and measuring the distance from the side of the outer wheel to the edge of the pavement. The distances measured on the films were scaled to actual distances by constant factors determined from the actual measured widths and filmed widths of the paint stripe and the widened slabs.

STATISTICAL ANALYSIS

Normality of Control Section Data

The lateral distribution data collected on the control sections are summarized in Table 2. In most cases, the data did not appear to be normally distributed. Examples of this are shown in Figure 3 using data from control sections 1 and 5. In each case, the actual data frequencies are indicated by bars, and the theoretical frequency of a normal distribution with the same mean and variance is indicated by a curve. Most of section 1's actual frequencies to the left of the mean are less than the theoretical frequency, whereas most of the actual frequencies to the right of the mean exceed the theoretical frequency. The mean of these data is 20.09 in., whereas the median is about 18 in. Section 1 exhibited the most pronounced skew; among the other control sections, the median was skewed an inch or less from the mean. No consistent leftward or rightward skew was observed among the eight control sections.

Normality should not be judged only by skewness, however. The mean of the data for control section 5 (24.34 in.) is very close to the median (24 inches). Nonetheless, the distribution does not appear to be normal. Actual frequencies exceed theoretical frequencies on both sides of the mean and fall short of theoretical frequencies in the vicinity of the mean.

To examine the normality of the control section distributions, chi-square (χ^2) tests were performed on each of the eight data sets. The computed χ^2 values and the theoretical

TABLE 2 SUMMARY OF LATERAL DISTRIBUTIONS MEASURED ON CONTROL SECTIONS OF I-57 IN ILLINOIS

Section	Number	Mean	Std Dev	Location
1	146	20.087	8.479	I-57 SB Champaign Cty Rd 25
2	84	25.716	6.854	I-57 NB Douglas Cty Rd 1250 N
3	48	24.422	7.382	I-57 NB Douglas Cty Rd 600 N
4	136	18.411	8.226	I-57 NB Champaign Cty Rd 25
5	118	24.345	8.259	I-57 SB Coles Cty Locust Rd
6	64	24.071	7.893	I-57 NB Coles Cty Locust Rd
7	146	24.844	8.239	I-57 SB Douglas Cty Rd 600 N
8	170	22.682	8.204	I-57 SB Douglas Cty Rd 1250 N
Total	912	22.659	8.396	

Notes: Mean displacements are distances from the slab edge, in inches.

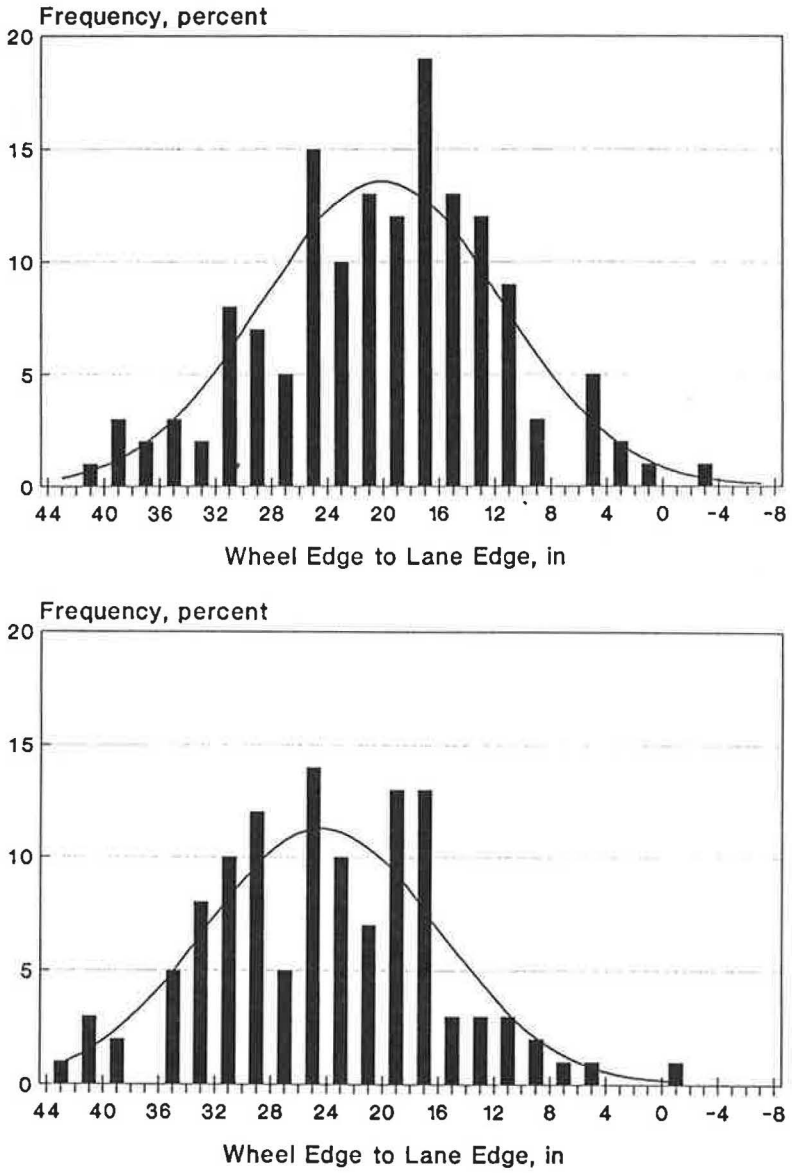

FIGURE 3 Actual versus theoretical distribution of wheel positions for control sections 1 (*top*) and 5 (*bottom*).

values at a significance level of $\alpha = 5$ percent are shown in Table 3. For seven of the eight data sets, the computed values exceed the theoretical values, implying that those seven data sets exhibit a significant departure from a normal distribution. The observed significance level of each test, also reported in Table 3, showed that five of the eight data sets would be judged not normal even at a significance level of $\alpha = 1$ percent.

Equality of Variances on Control Sections

Any significant differences among the means of the eight control sections can be identified by an analysis of variance, provided that the data sets meet the assumptions required for use of the *F*-statistic. Ideally, the data sets compared should be independent and normally distributed and have a common

TABLE 3 RESULTS OF CHI-SQUARE TESTS FOR GOODNESS OF FIT OF CONTROL SECTION DATA TO NORMAL DISTRIBUTION

Section	χ^2_{calc}	K	$\chi^2_{K-3,\alpha=5\%}$	Observed Significance
1	23.08	14	19.67	98
2	18.84	10	14.07	>99
3	18.28	6	7.81	>99
4	22.91	14	19.67	98
5	24.00	13	18.31	>99
6	27.97	8	11.07	>99
7	26.54	15	21.03	>99
8	20.67	15	21.03	93

NOTE: The null hypothesis H_0 that the data are normally distributed $N(\mu,\sigma^2)$ is rejected with 95 percent confidence if the calculated value χ^2_{calc} exceeds the theoretical value $\chi^2_{K-3,\alpha=5\%}$, where K is the number of intervals and α is the level of significance. The observed significance level corresponds to the level at which χ^2_{calc} equals the theoretical value of $\chi^2_{K-3,\alpha=5\%}$.

TABLE 4 TEST FOR HOMOGENEITY OF VARIANCE OF CONTROL SECTIONS

Given: J sample variances $s_1^2, s_2^2, \ldots s_j^2$, of relatively large (> 25) samples $n_1, n_2, \ldots n_j$ from populations with possibly different means and variances, all unknown

Null hypothesis H_o: $\sigma_1^2 = \sigma_2^2 = \ldots = \sigma_j^2$
Alternate hypothesis H_a: at least two σ_i^2 are unequal

Let: Y_{ij} = i^{th} observation in j^{th} sample
$\bar{Y}_j$ = j^{th} sample mean

$$G = \Sigma (n_j - 1) \left[\ln s_j^2 - \frac{\Sigma (n_j - 1) \ln s_j^2}{\Sigma (n_j - 1)} \right]^2 / k^2$$

$$k = 2 + [1 - (1 / \bar{n})] m$$
$$\bar{n} = (\Sigma n_j) / J$$

$$m = \frac{(\Sigma n_j) \Sigma \Sigma (Y_{ij} - \bar{Y}_j)^4}{[\Sigma \Sigma (Y_{ij} - \bar{Y}_j)^2]^2} - 3$$

If H_o is true and all n_j are reasonably large, G has approximately a χ^2 distribution with J-1 degrees of freedom. A formal test of H_o at a significance level α is:

Reject H_o if $G > \chi^2_{\alpha,J-1}$

Do not reject H_o if $G \leq \chi^2_{\alpha,J-1}$

For the 8 control section data sets:

See Table 1 for observations and sample variance of each data set.

$\bar{m} = 0.092$
$\bar{n} = 912 / 8 = 114$
$k = 2 + [1 - (1 / 114)] 0.092 = 2.0912$
$k^2 = 4.373$
$G = 2.92$
$\chi^2 = 14.07$

$2.92 \leq 14.07$

Therefore do not reject H_o, assume variances are homogeneous.

variance. Although the control section distributions already have been shown to be nonnormal, an analysis of variance from a previous study (*22*) still may be used to compare their means, provided that their variances are homogeneous:

> If the number of observations in each group is reasonably large, inferences made about means assuming normality remain valid for nonnormal populations, all other things being equal. . . In particular, the F test is essentially unaffected if the underlying populations are all of the same form.

To ensure that the data sets are of the same form, a test of the equality of their variances can and should be conducted. Unfortunately, the most commonly used tests for comparing variances are severely affected by nonnormality. One test for homogeneity of variance that applies to large samples and is insensitive to departures from normality is given by Layard (*23*). Applied to the eight sets of control section data, Layard's test confirms that the variances are homogeneous, as shown in Table 4. The *F*-statistic is therefore appropriate for use in comparing the means of the data sets.

Comparison of Control Section Mean Displacements

The results of the analysis of variance, given in Table 5, confirm that significant differences do exist among the eight control section means at a significance level of $\alpha = 5$ percent.

The seven degrees of freedom provided by the eight data sets permit up to seven specific comparisons to further investigate differences in the control section means. However, only five comparisons were judged to be of interest. It should be noted that since they are not independent (all being related by the mean square error), these comparisons cannot be tested individually at a particular significance level α and all be simultaneously considered valid at that same level of α. The five individual comparisons were therefore made at a significance level of $\alpha = 1$ percent, so that their simultaneous confidence level is $(1 - \alpha)^5 = (0.99)^5 = 0.951$ = approximately 95 percent.

One of the comparisons made was between the pair of sections 1 and 4 and the remaining six sections, since these two means (20.1 and 18.4 in.) are noticeably less than those

TABLE 5 ANALYSIS OF VARIANCE OF CONTROL SECTIONS

Source	Degrees Freedom	Sum of Squared Errors	Mean Square Error	F calc	F theor
Total	911	64,156			
Trtmnt	7	5,515	788	12.14	2.01
(1)	1	4,647	4,647	71.63	6.63
(2)	1	198	198	3.05	6.63
(3)	1	1,225	1,225	18.88	6.63
(4)	1	564	564	8.69	6.63
(5)	1	523	523	8.06	6.63
Error	904	58,631	64.86		

Notes: Some significant difference among the eight treatment means is indicated by F_{calc} (12.14) greater than $F_{0.05,7,\infty}$ (2.01).

Significant comparisons are indicated by F_{calc} (see table) greater than $F_{0.01,1,\infty}$ (6.63). These comparisons are made individually with 99 percent confidence; their simultaneous confidence level is $(0.99)^5$ = 95 percent.

Comparisons:

(1) { 1, 4 } versus { 2, 3, 5, 6, 7, 8 }
(2) { 1 } versus { 4 }
(3) { 8 } versus { 1, 4 }
(4) { 8 } versus { 2, 3, 5, 6, 7 }
(5) { 2 } versus { 8 }

of the other six sections. Table 5 shows that these two sections are significantly different from the other control sections.

The mean of section 8 (22.7) is about 2 in. greater than that of section 1, but about 2 in. less than those of the remaining five sections. As Table 5 shows in two comparisons, the difference in means between section 8 and these two groups is significant.

At two of the four bridge locations, the means of the data measured in opposite directions appeared to be noticeably different. As noted above, the means of sections 1 and 4 (southbound and northbound at Champaign County Road 25) differ by 1.5 in. The means of sections 2 and 8 (northbound and southbound at Douglas County Road 1250 N) differ by a full 3 in. As Table 5 shows in two comparisons, the difference between the means of 1 and 4 was not statistically significant, whereas the difference between the means of 2 and 8 was significant. At the two other locations used in the study, the difference in means by direction was so slight (0.4 in. between sections 3 and 7, 0.2 in. between sections 5 and 6) that comparisons did not seem warranted.

The analysis of variance tests only for significant differences in means and does not compare entire distributions. The cumulative percent frequency distributions for the eight control sections shown in Figure 4 illustrate the notable difference between sections 1 and 4 and the remaining six sections, but does not make obvious the differences found among the other sections. The points at which the curves cross the 50 percentile line in Figure 4 correspond to the *median* values of the distributions, and not the *mean* values.

Lateral Distributions on Widened-Lane Sections

A summary of the data collected on the widened-lane sections is given in Table 6. Five rolls of film were shot on each test section, each roll on a different day. A total of 691 trucks were observed on the southbound section, which is widened 18 in., and 613 trucks were observed on the northbound section, which is widened 20 in. The mean displacements reported in Table 6 are measured from the edge of the slab and can be converted to displacements from the lane edge by subtracting 18 and 20 in., respectively. When this is done, the values for the two sections appear similar. Mean displacements from the lane edge range from 17.0 to 23.2 in. on the southbound section, with an overall mean of 20.09 in., and mean displacements range from 18.3 to 21.5 in. on the northbound section, with an overall mean of 20.55 in.

Of the 691 trucks observed on the southbound section, the smallest measured distance from the slab edge was 10.9 in., a 7.1-in. encroachment over the lane edge stripe but still well outside the range in which it could be considered an edge loading. On the northbound section, the smallest measured wheel distance from the slab edge among 613 observations was 17.1 in., an encroachment of 2.9 in. over the lane edge stripe.

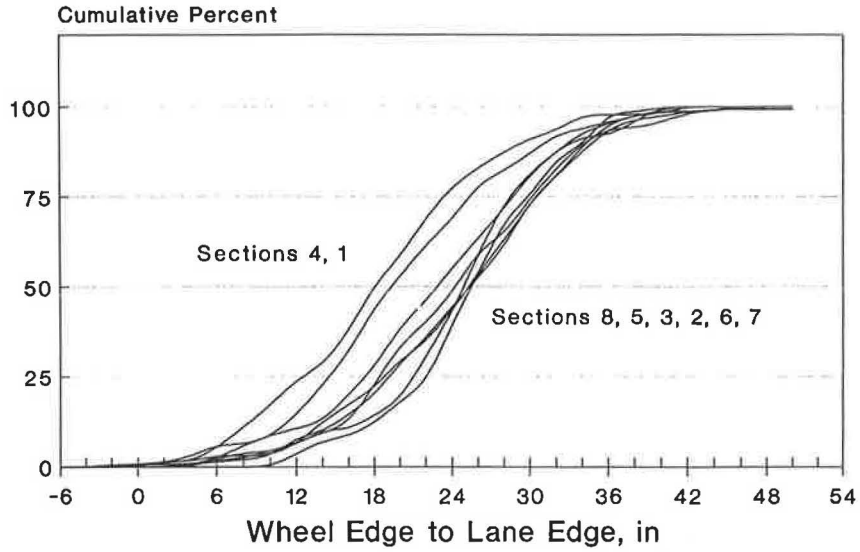

FIGURE 4 Cumulative percent frequency distributions for control sections.

Widened-Lane Lateral Distributions Compared by Direction

The variances of the northbound and southbound widened-lane lateral distributions were confirmed to be homogeneous by using Layard's test. The similarity in the means (20.55 and 20.09 in.) suggests, and an analysis of variance confirms, that no significant difference exists between the distributions observed in the two directions.

CONCLUSIONS AND RECOMMENDATIONS

The findings of past field studies on lateral distribution of trucks on conventional 12-ft lanes should be examined carefully and applied with caution. All of the past field studies on lateral distribution were conducted before enactment of legislation permitting 8.5-ft truck widths, and some were conducted using approximate data collection methods. The method employed for this study, filming truck wheels on the pavement at fixed spots, was felt to provide sufficiently accurate and precise measurements.

The mean lateral displacement of truck wheels from the pavement edge on conventional 12-ft-wide lanes ranged from 18.4 in. and 25.7 in. on eight pavement sections, with an overall mean of 22.7 in. However, significant differences were observed among the mean displacements, despite the pavement sections being of the same geometric design, all located on the same interstate highway, and all within 70 mi of each other. Variance in lateral distribution, however, was consistent among all of the control sections.

Using a mean and standard deviation for lateral distribution of trucks, and assuming the distribution to be normal, a pavement designer can compute the percentage of truck loads in any desired interval of the distribution as the area under the normal curve within this interval. Although conditions will vary depending on the specific design features of the pavement, as a rule of thumb only loads within about 6 inches of the slab edge will produce significantly high stresses at the slab edge. For the eight control sections in this study, the percentage of loads within 6 in. of the slab edge ranged from less than 1 to about 7.5 percent, with an overall average of about 2.5 percent. The designer should keep in mind that whatever quantity for percent edge loads is computed in this fashion may be somewhat overconservative or underconservative if the assumption of a normal distribution is not valid.

The findings of this study clearly show that the paint stripe, and not the slab edge, is the more influential factor in truck wheel placement on widened-lane pavements. The mean lateral distance from the lane edge was only about 2 in. less on 18-in. and 20-in. widened pavement sections than on control sections. With respect to both mean and variance, no statistically significant differences in lateral distributions were detected for the 18-in. and 20-in. widened-lane pavement sections.

Among more than 1,300 observations of truck wheel placements on widened-lane pavement sections, the smallest measured from the slab edge was 10.9 in. There were, in other words, no edge loadings observed among some 1,300 total loadings. The practical significance of this to structural design of concrete pavements is noteworthy: lane widening is likely to be a cost-effective design improvement for pavements whose probable mode of failure will be accumulated fatigue damage manifested by slab cracking. For pavements likely to fail in other ways (e.g., joint deterioration or D-cracking), other design improvements should be investigated.

The trends observed in this study may be fairly typical, but the actual statistics are specific to the sites studied and should not be applied to design of pavements at other sites without great caution. Research into the effects of pavement conditions, shoulder conditions, weather conditions, traffic volume, and other factors on lateral distribution of trucks is strongly encouraged. Meanwhile, pavement designers should view with skepticism any reported national average for truck wheel positions and verify assumed distributions with field observations whenever possible. The methodology used in this study for field data collection is suggested as reasonable for other studies.

TABLE 6 SUMMARY OF LATERAL DISTRIBUTIONS MEASURED ON WIDENED-LANE TEST SECTIONS ON I-57 IN ILLINOIS

18-INCH WIDENED-LANE SECTION:

Film Roll	Number	Mean	Std Dev	Location
1	129	34.978	8.671	I-57 SB Effingham Cty mp 165
2	131	38.528	7.398	(same)
3	127	41.229	9.520	(same)
4	195	38.235	9.071	(same)
5	109	37.336	9.840	(same)
Total	691	38.091	9.077	

20-INCH WIDENED-LANE SECTION:

Film Roll	Number	Mean	Std Dev	Location
1	107	41.376	9.244	I-57 NB Effingham Cty mp 165
2	127	41.466	9.312	(same)
3	145	41.486	9.707	(same)
4	126	38.342	8.590	(same)
5	108	39.949	8.242	(same)
Total	613	40.546	9.375	

Note: All mean displacements are expressed as distance from the side of the wheel to the edge of the concrete slab, in inches. Subtract 18 inches and 20 inches respectively to obtain mean displacement from the lane edge.

ACKNOWLEDGMENTS

The authors gratefully acknowledge Ernest J. Barenberg for initiating this study, the Kent Research Assistantship Program for providing financial support for this study, and Illinois DOT District 7 Engineer Maurice R. Topel and Distrist 7 Design Engineer Darrell J. Fuesting for their technical assistance.

REFERENCES

1. M. I. Darter and E. J. Barenberg. *Zero-Maintenance Pavement: Results of Field Studies on the Performance Requirements and Capabilities of Conventional Pavement Systems*. Report FHWA-RD-76-105. University of Illinois, Urbana-Champaign, 1976.
2. H. M. Westergaard. New Formulas for Stresses in Concrete Pavements of Airfields. *Transactions*, ASCE, Vol. 113, 1948, pp. 425–444.
3. A. M. Ioannides, M. R. Thompson, and E. J. Barenberg. The Westergaard Solutions Reconsidered. In *Transportation Research Record 1043*, TRB, National Research Council, Washington, D.C., 1985.
4. G. Pickett and G. K. Ray. Influence Charts for Concrete Pavements. *Transactions*, ASCE, Vol. 116, 1951, pp. 49–73.
5. H. H. Huang and X. J. Deng. Finite Element Analysis of Jointed Concrete Pavements. *Journal of Transportation Engineering*, ASCE, Vol. 109, No. 5, Sept. 1983, pp. 689–705.
6. A. M. Ioannides. Finite Element Analysis of Slabs on Grade for a Variety of Loading and Support Conditions. *Proc., 3rd International Conference on Concrete Pavement Design and Rehabilitation*, Purdue University, W. Lafayette, Ind., 1985.
7. K. W. Heinrichs, M. J. Liu, M. I. Darter, S. H. Carpenter, and A. M. Ioannides. *Rigid Pavement Analysis and Design*. Report FHWA/RD-88/068. University of Illinois, Urbana-Champaign, 1988.
8. A. M. Ioannides and R. A. Salsilli-Murua. *Slab Length, Slab Width, and Widened Lane Effects in Rigid Pavements*. Field Evaluation of Newly Developed Rigid Pavement Design Features. University of Illinois, Urbana-Champaign, 1988.
9. B. E. Colley, C. G. Ball, and P. Arriyavat. Evaluation of Concrete Pavements with Tied Shoulders or Widened Lanes. In *Transportation Research Record 666*, TRB, National Research Council, Washington, D.C., 1978, pp. 39–51.
10. J. S. Sawan and M. I. Darter. Structural Evaluation of PCC Shoulders. In *Transportation Research Record 666*, TRB, National Research Council, Washington, D.C., 1978.

11. A. Taragin. Effect of Roadway Width on Vehicle Operations. *Public Roads*, Vol. 24, No. 6, 1945.
12. F. H. Scrivner. *Effect of Lane Width on Traffic Behavior for Two-Lane Highways*. Texas Highway Department Research Project No. 5, Austin, 1955.
13. *Vehicle Speed and Placement Survey on Two-Lane Rural Highways*. Texas Highway Department, Austin, 1957.
14. A. Taragin. Lateral Placements of Trucks on Two-Lane Highways and Four-Lane Divided Highways. *Public Roads*, Vol. 30, No. 3, 1958, pp. 71–75.
15. D. H. Weir and C. S. Sihilling. *Measures of Lateral Placement of Passenger Cars and Other Vehicles in Proximity to Intercity Buses on Two-Lane and Multi-Lane Highways*. Federal Highway Administration, Environmental Design and Control Division, 1972.
16. D. K. Emery, Jr. A Preliminary Report on the Transverse Lane Displacement for Design Trucks on Rural Freeways. Presented at American Society of Civil Engineers Pavement Design Specialty Conference, Atlanta, Ga., 1975.
17. E. J. Miller and G. N. Stewart. Vehicle Lateral Placements on Urban Roads. *Journal of Transportation Engineering*, ASCE, Vol. 108, No. 5, 1982.
18. C. E. Lee, P. R. Shankar, and B. Izadmehr. *Lateral Placement of Trucks in Highway Lanes*. Report FHWA/TX-84/33-310-1F. University of Texas, Austin, 1983.
19. R. M. Canner and J. Hale, Jr. *Vehicle Shoulder Encroachment and Lateral Placement Study*. Report FHWA/MN-80/6. FHWA, Minnesota Department of Transportation, St. Paul, 1980.
20. M. I. Darter. *Design of Zero-Maintenance Plain Jointed Concrete Pavement, Volume 1, Development of Design Procedures*. Report FHWA-RD-77-111. University of Illinois, Urbana-Champaign, 1976.
21. *Special Report 211: Twin Trailer Trucks*. TRB, National Research Council, Washington, D.C., 1986.
22. R. B. Miller and D. W. Wichern. *Intermediate Business Statistics: Analysis of Variance, Regression, and Time Series*. Holt, Rinehart and Winston, New York, 1977.
23. M. W. J. Layard. Robust Large Sample Tests for Homogeneity of Variance. *Journal of the American Statistical Association*, Vol. 68, 1973, p. 195.

Publication of this paper sponsored by Committee on Rigid Pavement Design.

Validation of Concrete Pavement Responses Using Instrumented Pavements

ERNEST J. BARENBERG AND DAN G. ZOLLINGER

Mechanistic based pavement design procedures require validated mathematical models and calibrated transfer functions. The transfer functions can be calibrated only by observing the performance of pavements over time. The mathematical models can be calibrated by comparing the fundamental pavement responses to load and climate with the responses predicted by mathematical models. Two instrumented pavement sections are described that were constructed in Illinois to validate the mathematical models used in the development of a mechanistic based pavement design procedure for jointed concrete pavements. The type and location of gauges and the material properties and testing procedures used are detailed. Typical results and the significance of results with respect to the analysis models used and the design procedure developed using the models are presented. Effects of bonding between the slab and the lean concrete subbase and the implications of tied portland cement concrete shoulders are demonstrated. Effects of temperature changes are shown to be a major factor in the responses of the pavements.

Over the past several years, the University of Illinois, under the sponsorship of the Illinois Department of Transportation, has developed mechanistic based procedures for jointed and continuously reinforced concrete pavements. Validation of the design procedure was one of the tasks included in the study, which included short- and long-term validation. The long-term validation involves a comparison of the actual pavement performance over a number of years versus the predicted performance. Short-term validation involved a comparison of actual pavement responses with responses predicted using the mechanistic models in the design procedure.

During the summer of 1986, as a part of the short-term validation, a number of jointed and continuously reinforced concrete (CRC) pavement test sections were instrumented at two locations in Illinois. Gauges were installed in 5 sections of CRC pavements and 22 sections of jointed pavements. A total of 16 different pavement sections were instrumented, with 11 of the jointed sections replicated. The instrumented sections included three slab thicknesses of the jointed and two of the CRC pavements, with four different joint spacings in the jointed pavements. Instrumented sections of both jointed and CRC sections had varying drainage characteristics.

Strains in the pavement sections were recorded at specified intervals starting as soon as possible after the concrete had initially hardened. After the concrete had reached its design strength, but before the pavements were opened to traffic, the pavements were loaded with static and moving loads by using a truck with an 18-kip single axle load. The data were first collected in the memory of a Compaq portable computer with 640K memory, quickly reviewed for potential errors, and then transferred to floppy disks.

Currently there are over 100 floppy disks (360K capacity) filled with data, and more are being collected. These data are being analyzed and evaluated as time permits. As a check on the recording equipment, strains in the concrete and steel under static loading were also read using an SR-4 strain indicator type N.

Preliminary evaluation of the data indicates that the analysis models used in developing the design procedure accurately predict the strains caused by load in the concrete pavement. Strains caused by temperature and moisture changes in the concrete are also significant in the performance of these pavements. These results indicate that both the relative and absolute strains caused by temperature and moisture changes in the pavement were, on the average, greater than expected. Interpretation of these data is very difficult because the pavements with the greatest thermal and shrinkage strains probably have the least restraint and hence the least stress, whereas those with the least strain probably have the greatest restraint and hence the greatest stress.

Details of the instrumentation installed in the pavements are described and the type of data available from the instrumentation package is presented. Procedures used to analyze the data and examples and implications of the findings to date are discussed.

PROJECT DESCRIPTION

Two instrumented demonstration projects were designed and constructed for validation of proposed design procedures for jointed plain concrete (JPC), jointed reinforced concrete (JRC), and CRC pavements in the state of Illinois. Demonstration project FA 409 was constructed near Carlyle, Ill., approximately 20 mi south of I-70 on US-50, and demonstration project FA 401 was constructed near Freeport, Ill., approximately 40 mi west of Rockford, Ill. on US-20. Layout of these projects along with details regarding joint layout, pavement thicknesses, pavement type, and drainage conditions at the project sites are shown in Figures 1 and 2 and are reported elsewhere (*1*). The strain gauges were installed during the construction phase to monitor the effects of wheel load and temperature-induced strains. Table 1 summarizes the instrumented slabs at each project site.

E. J. Barenberg, Department of Civil Engineering, University of Illinois, Urbana-Champaign, Urbana, Ill. 61801. D. G. Zollinger, Department of Civil Engineering and Texas Transportation Institute, Texas A&M University, College Station, Tex. 77843.

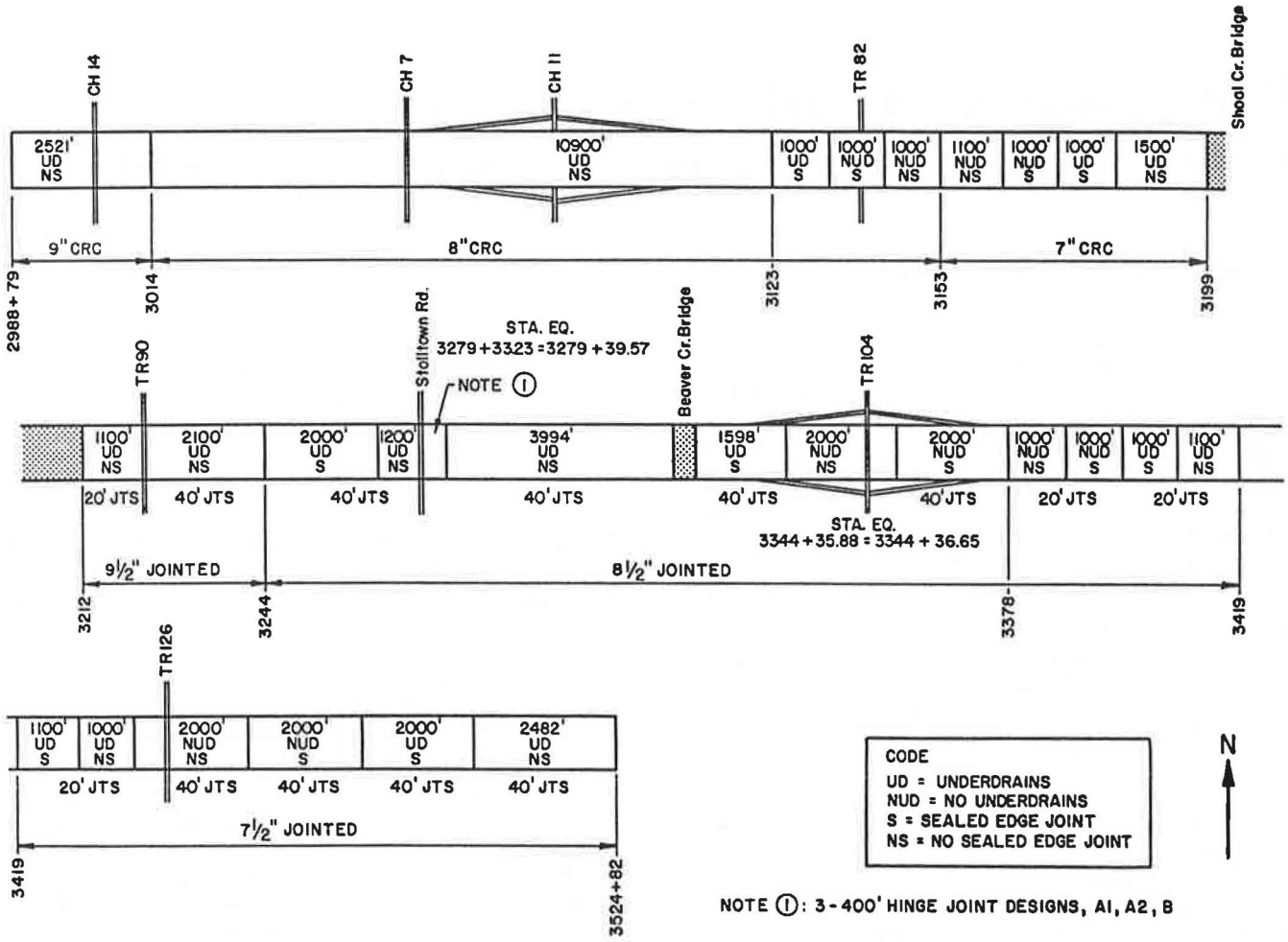

FIGURE 1 Carlyle, Illinois, demonstration project layout.

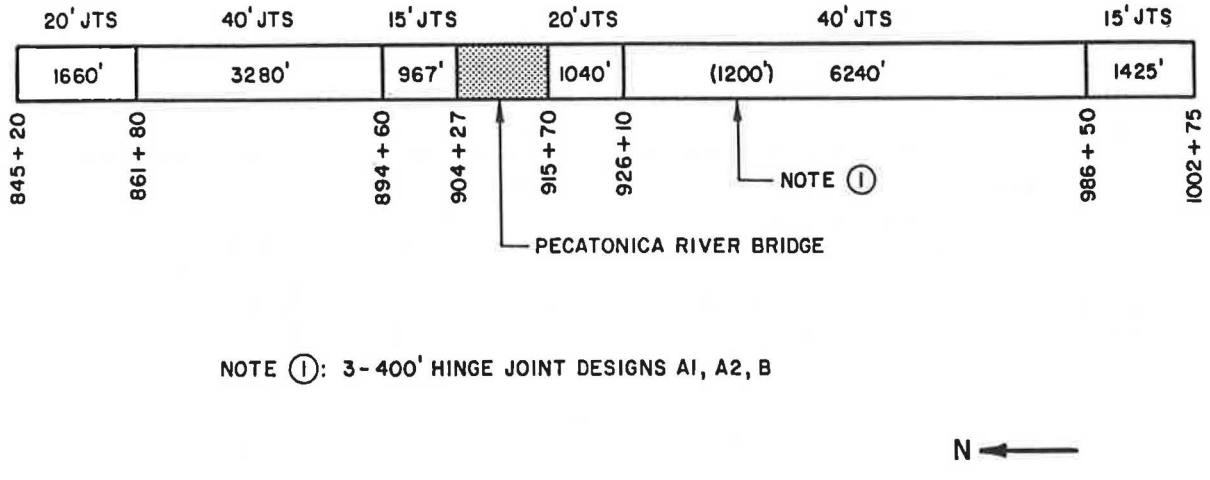

FIGURE 2 Freeport, Illinois, demonstration project layout.

TABLE 1 SUMMARY OF GAUGES IN JOINTED PAVEMENTS

Location	Station	Joint Spacing	Thickness	# of Gauges	Joint Type	Ref Fig
Carlyle	3216+08	20′	9-1/1"	5	dowel	4
	3218+68			5	"	4
	3226+08	40′		12	"	6
	3229+88			12	"	6
	3264+91	20′(A1)	8-1/2"	13	hinge	7
	3266+91			13	"	7
	3273+31	13′-4"(B)		13	"	5
	3274+91			13	"	5
	3432+06	20′	7-1/2"	5	dowel	4
	3439+06			5	"	4
	3485+66	40′		12	"	6
	3505+66			12	"	
Freeport	846+91	20′	10"	5	dowel	4
	875+46	40′		12	"	6
	896+05	15′		5	"	8
	970+10	20′		5	"	4
	927+30	20′(A1)		13	hinge	7
	292+70			13	"	7
	935+30	13′-4"(B)		13	"	5
	935+30			13	"	5
	985+27	40′		12	dowel	6
	999+87	15′		5	"	8

STRAIN GAUGE LAYOUT AND SLAB INSTRUMENTATION

Polyester-encapsulated wire-type electrical resistance gauges, Series "PM," manufactured by Tokyo Sokki Kenkyujo (PML-120 and PML-60 obtained through Texas Measurements, Inc.), were placed in the concrete. The wire-type strain gauge and lead wires were hermetically sealed between polyester resin plates, and the entire gauge was coated with a gritty substance to promote bonding to concrete.

To eliminate localized effects, the gauge length was chosen to span several aggregate particles. Since the maximum particle size in the portland cement concrete (PCC) was 1.5 in., a gauge length of 4.75 in. was selected.

The electrical conducting wires used in the strain gauges undergo a change in resistivity with changes in temperature. Another temperature effect is caused by the gauge being bonded to a test material (concrete) that has a different coefficient of thermal expansion than the resin gauge material. Therefore, a temperature compensation gauge or "dummy" gauge was installed in parallel with each active gauge. To maintain them in an "unstrained" condition, dummy gauges were placed in a polyvinylchloride (PVC) tubing, which was then sealed to prevent intrusion of the concrete, and the entire tube was cast into the pavement slab adjacent to the active gauges. This scheme worked well for measuring the load strains but was not as satisfactory for evaluating the temperature-related strains.

A typical instrumented jointed slab layout indicating the locations of the active gauges is shown in Figure 3. Other

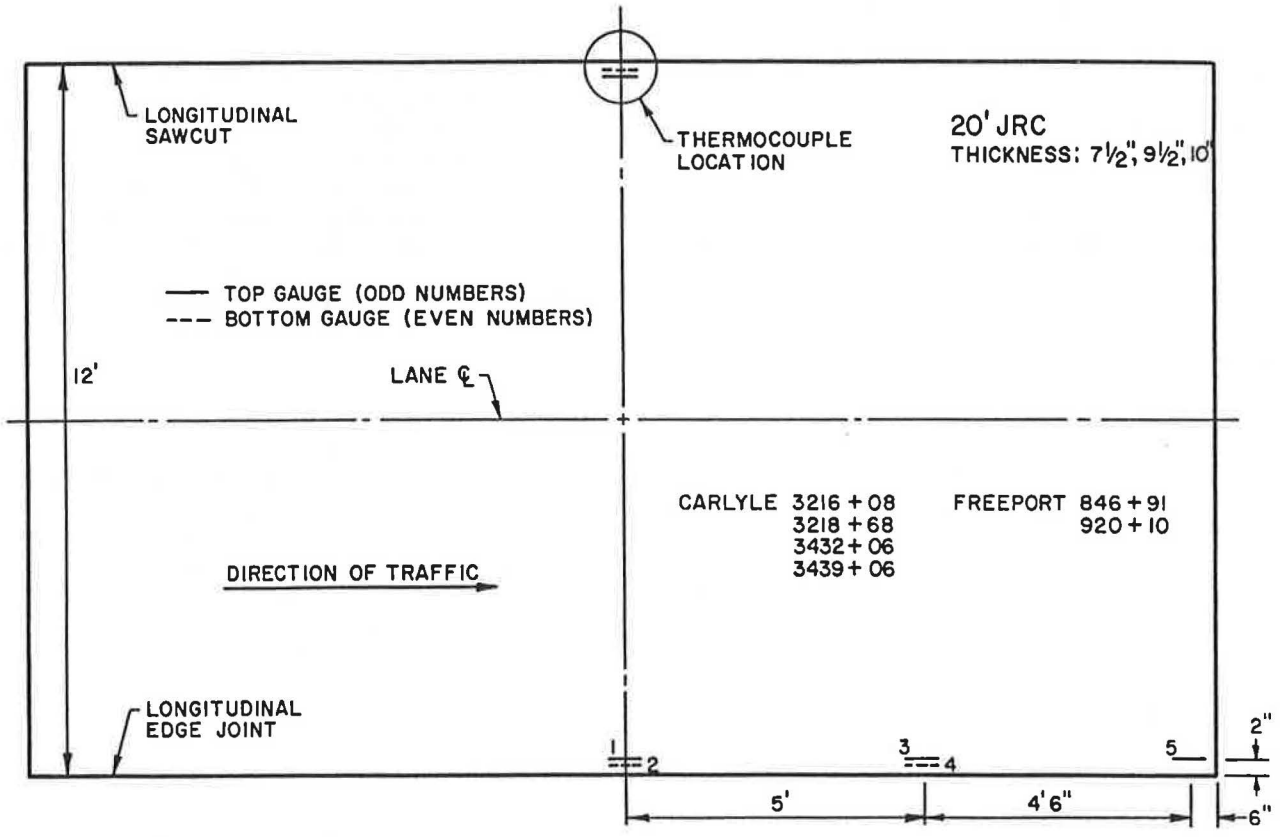

FIGURE 3 Instrumented slab layout.

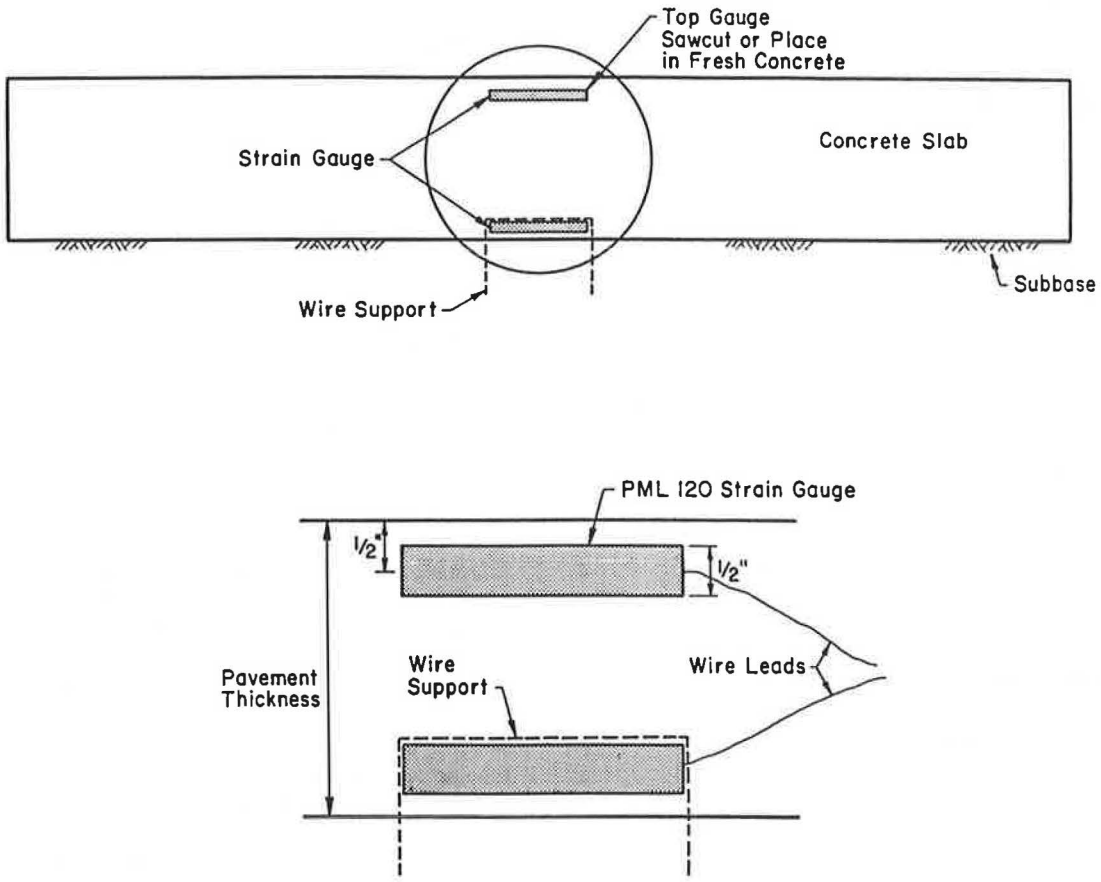

FIGURE 4 Strain gauge pavement installation.

similar joint spacing and gauge layout configurations were also included in the project instrumentation (*1*) but are not shown here. The gauges were strategically placed to measure the maximum strain caused by a wheel load placed at or near the pavement edge and the strain caused by slab curling. Gauges were generally placed in pairs along selected transverse and longitudinal joints with one gauge at the slab top and the other near the bottom. Gauges at the slab corners were reference gauges, so only the top gauge was installed at these locations.

Encapsulated gauges were also installed in several CRC pavements, but these are reported here only briefly for reference. The measured strains in the CRC pavements are reported elsewhere (*2*). Basically, the gauges in the CRC pavements were positioned to measure transverse and longitudinal strains in the concrete midway between the transverse cracks. Gauge installation procedures for the CRC pavements were essentially the same as those for the jointed pavements, except that all top gauges were installed using the saw-and-grout method discussed later. Strain gauges were also installed on several longitudinal steel bars in the CRC pavements. The gauges on the reinforcing bars were positioned so that strain gradients along a bar segment near and adjacent to transverse cracks could be established.

After the roadway had been graded and trimmed, but before the subbase (lean concrete) was placed, a 4-ft-deep trench was cut from beyond the outer edge of the shoulder to approximately the wheel path in the paving lane. A PVC conduit was installed in this trench, and lead wires from the dummy gauges and the gauges placed at the bottom of the pavement were routed through the conduit. Grooves were cut in the top of the subbase to run the lead wires from the individual gauges to the conduit inlet box. The lead wires were carefully marked to indicate the gauge and location and were run to an outlet box attached to a 4-by-4 post beyond the outer edge of the shoulder.

Accurate location of the gauges was considered to be essential if meaningful data were to be collected. As soon as the lean concrete subbase had cured, the proposed locations of the bottom gauges were marked on the subbase surface. A support system consisting of a thin metal rod bent into the shape of a U was installed in two holes drilled into the subbase, as shown in Figure 4. The gauges were then attached to the supports. Installation of the top gauges is discussed later.

During the paving operations, the contractor was requested to slow the paving speed and reduce the concrete head as the paver approached the instrumented sites. Approximately 5 min before the paver reached the instrumented site, plastic concrete was placed directly over and around each gauge to prevent movement of the gauges and tearing of the lead wires. This procedure appeared successful as no gauges were lost because of the paving operations.

An acceptable procedure for supporting the top gauges in the concrete was not found, so the gauges were installed in the concrete after the finishing operations were complete. Three different procedures were used for this installation.

The first method for installing the top gauges was to saw a groove in the hardened concrete and then to bond the gauges in place by using a sand cement grout. This procedure was effective but did not provide immediate readings of the strains. There was also some concern about the long-term effectiveness of the grout, which is essential for transferring the strains from the concrete to the gauges. All of the top gauges in the CRC pavements were installed in this manner.

A second method involved placing a wood plug in the fresh concrete at the approximate gauge location. As soon as the concrete had taken on a set, the plug was removed and the gauge was placed in the void. Again, the gauge was grouted into place by using a sand cement grout. Because it permitted earlier readings of the strains, this method was judged superior to the first method. The main problem with this approach was the concern about the long-term effectiveness of the grout.

The third procedure involved working the gauge into the fresh concrete and carefully compacting the fresh concrete around the gauge. The lead wires were also worked into a groove in the fresh concrete, which was cut with a trowel. This method alleviated the concerns over the grout effectiveness and permitted immediate readings of the strains. However, accurate placement (both alignment and depth) was more difficult to achieve with this procedure. With some practice, this would be the recommended procedure for any future installations.

STRAIN RECORDING

Strains are measured as voltage changes in the strain meters within the system. These voltage changes are then amplified, processed, displayed, and stored. For every gauge and every reading there must be a zero value and a calibration reading. Calibration readings were recorded with strain readings.

For static loading, the strains were read using a portable strain meter, and the data were recorded manually. For the dynamic loading, the readings were recorded on a recorder, capable of recording 10 channels of data simultaneously. These readings were recorded on tape and then transferred to floppy disks and read directly into a spread sheet using Lotus 1-2-3.

One of the most difficult tasks in collecting this type of data is to minimize unwanted electrical noise. Much of the noise comes from such sources as electrical high-tension wires near by, automobile ignition sparks, radio signals, and other sources. High-quality lead wires, connectors, and mating plugs were used to keep the noise to a minimum. However, the first attempt at recording the strains under dynamic loading still produced significant noise problems. Through careful grounding of the equipment and installation of high-frequency filters a significant amount of the noise was eliminated for the subsequent tests.

THERMOCOUPLES

Temperature changes in the concrete and temperature gradients through the slab can significantly affect the measured responses of PCC pavements. Thermocouples were installed near the top and bottom of several slabs within the test site. The thermocouples were installed near the pavement edge in CRC pavements and near a corner in the jointed pavements. The thermocouples were installed by fastening them to a polyester tube at the desired heights and fastening the tube to reinforcing bars in the pavements.

During the load testing procedures, the thermocouples were read directly with a potentiometer or a digital thermometer. For longer-term readings, that is, readings taken over 24-hr or longer periods, the temperature data were recorded on a multichannel, battery-powered portable recording system. The recording device was programmed to sample the data at preselected intervals throughout the test period. The device had a memory of 64K and, when the device was filled, the data were transferred directly to floppy disks using a portable IBM-compatible computer system.

MATERIALS

Subgrade Soils

Soils at the test site near Carlyle in southern Illinois were mainly glacial till, overlain with a relatively thin layer of wind-deposited loess. The soil types ranged from silt loam to clays, with the predominant soil type a silty clay.

The soil at the test site near Freeport in northern Illinois was also glacial till and was classified as a silt loam with an AASHTO classification of A-4(8), with poor drainage characteristics. Soil support at this site was non-uniform, because there were a number of rock outcroppings within the test site.

Plate load tests were conducted at each site after the final grading but before placing the subbase. The tests were run at random locations throughout the project sites. The k values obtained from the plate load tests for both sites are given in Table 2.

Falling weight deflectomer (FWD) tests were run on the top of the subgrade to obtain dynamic k values. A 30-in.-diameter plate was placed on the subgrade, and the FWD test was run on top of the plate. Dynamic tests were run only at the Carlyle site. These results are also shown in Table 2 along with a ratio of the dynamic to the static k values. The average ratio of dynamic to static k is 1.30, with a standard error of 0.26.

Subbase

The subbase for both projects was lean concrete with a compressive strength of approximately 2,500 psi after 1 year of service. In Illinois this material is commonly referred to as "econocrete." The econocrete was placed with a concrete paver to a depth of 4 in. and finished with a float, and a coat of liquid curing compound was applied. The specifications called for the subbase to cure for 7 days before placing the concrete.

Concrete

Concrete used in both test projects met the Illinois Department of Transportation (IDOT) standards for paving class concrete. The IDOT standards call for a mix with a 14-day strength of 650 psi, when tested in flexure under center point loading.

TABLE 2 SUMMARY OF PLATE LOAD TEST RESULTS

	Project 409 Carlyle, IL			Project 401 Freeport, IL
	Static k psi	Dynamic k psi	Ratio Dynamic k/Static k	psi
	116	120	1.03	529
	119	202	1.70	412
	50	145	2.90	360
	174	194	1.12	527
	86	128	1.49	248
	210	129	0.64	282
	143	119	0.83	312
	169	124	0.73	345
Avg.	133	145	1.30	377
std dev	51	34	.74	105

Sufficient beam specimens were cast from the concrete used in the instrumented slabs so that 14-, 28-, and 90-day strengths could be determined. The beams tested to measure the 28- and 90-day strengths were stored on the project sites. The beams were wrapped in plastic sheets to prevent drying, buried in a pit alongside the pavement, and covered with moist sand. Thus, the beams were cured until testing under conditions comparable to the concrete in the pavement. Maturity meters were also installed at project sites to monitor the concrete strength development before loading and testing.

Table 3 shows a summary of the 28-day concrete properties for the Carlyle project. The effective modulus of rupture under third point loading was 713 psi, with a compressive strength of 5,332 psi. The modulus of elasticity measured during compressive testing was 4.16 × 10 psi. The variability in the concrete properties was very low, with the coefficient of variation under 10 percent for both the compression and flexure test results.

TABLE 3 28-DAY CONCRETE FLEXURAL AND COMPRESSIVE STRENGTH AT CARLYLE, ILL.

Station	Flexural Strength Center Point*	Third Point**	Compressive Strength*	E x 10⁶
3216+12	989	840	6084	4.43
3229+87	802	682	4651	3.88
3262+50	856	728	5736	4.32
3275+00	840	714	--	--
3352+50	-	-	5335	4.16
3395+00	-	-	5229	4.12
3432+50	750	638	--	--
3505+00	827	703	4994	4.03
3510+00	806	685	--	--
Average	838	713	5332	4.16
STD DEV	74	63	502	.20
Coef of Var (%)	8.8	8.8	9.4	5.72

* Measured Value
** Calculated Value at 85% of Center Point Load

TYPICAL TEST RESULTS

Pavements at both sites were tested under both static and moving truck axle loads. The primary load system was a single-axle truck with 18 kips on the rear axle. Initial tests on the pavements at Carlyle were during July 1986, approximately 30 days after placing the concrete for the mainline pavement slabs, and before the tied concrete shoulders were added. These same pavements were retested during the summer of 1986, after the shoulders had been added and the pavements had been open to traffic. Pavements at the Freeport site were tested initially during the fall of 1986, both with and without tied shoulders similar to the tests at Carlyle.

Pavements at both sites have subsequently been tested under similar loading conditions, in both the summer of 1987 and the late spring of 1988. In all, a total of over one hundred 360K capacity floppy disks have been filled with data. Since most of the gauges installed are still active and in good working order, it is anticipated that subsequent testing will be done on these sites.

Since the primary focus of the testing for this project was to validate the ILLI-SLAB model to predict pavement response to load, sufficient data were reduced as soon as possible to verify this for several different pavement configurations and loading conditions. Examples of results obtained are presented herein. However, much of the data have not yet been reduced, and work is continuing on this phase of the study. More complete results will be presented in the literature over the next few years.

Jointed Concrete Pavements

Figure 5 shows some typical comparisons obtained between the calculated and measured strains in jointed concrete pavements. The maximum strains were recorded by gauges installed near the edge of the slab at a point midway between transverse joints (gauges 1 and 2, Figure 3), with a static wheel load placed directly over the gauge. Variation in strains at the midslab position (gauges 1 and 2) as the load was moved away from the gauge location is also shown in Figure 5. The appar-

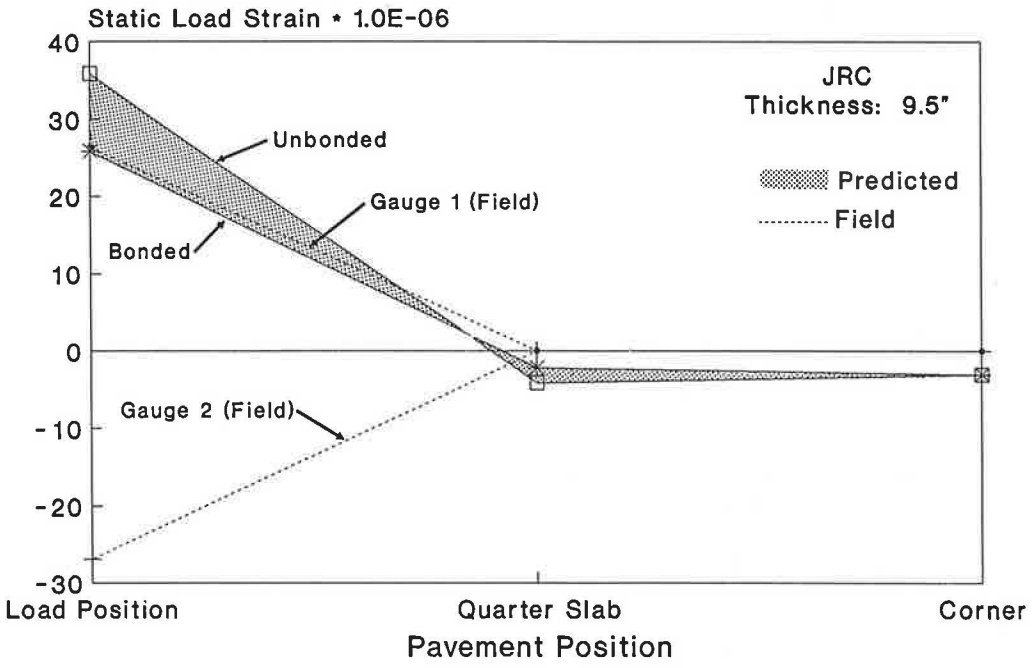

FIGURE 5 Typical results from measured strains under load from Illinois HPR projects 401 and 409.

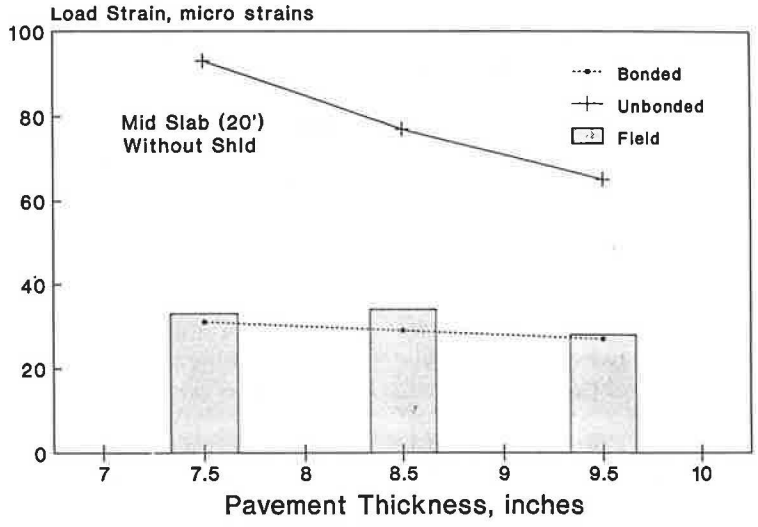

FIGURE 6 Load strain at midslab without tied PCC shoulder [18-kip single-axle load (SAL)].

ent "mirror image" strains (+ and −) are from gauges at the top and bottom of the slab.

One of the more interesting aspects of these data is the effect of bond between the slab and the subbase. The theoretical results are shown for both the bonded and unbonded conditions based on ILLI-SLAB analyses (*3*). The measured strains suggest that there was significant bonding between the slab and subbase when these tests were conducted. Tests conducted in the late spring of 1988 indicate that this bond may be breaking down.

Since the gauges away from the immediate loaded area show small strains, the remainder of the data presented herein for the jointed pavements is from midslab gauges only.

Figure 6 shows measured and calculated strains from a series of slabs 7.5, 8.0, and 9.5 in. thick. In these data the measured strains are in good agreement with the calculated values for the bonded condition, but the calculated strains for the unbonded condition are significantly greater than those for the bonded condition.

Figure 7 shows the effect of speed on the measured strains in the pavements. Again, the measured and theoretical results for the bonded case are in good agreement, but the theoretical results for the unbonded condition are significantly higher.

The effects of tied PCC shoulders on the strains in the jointed pavements are shown in Figure 8. The trends with regard to speed and bonding to the subbase are the same as those shown for the slabs without shoulders (Figures 6 and 7). The results clearly show the benefits of tied shoulders in reducing edge strains in jointed PCC pavements.

TABLE 4 THERMAL GRADIENT DURATION PERIODS

Location	Station	Thickness	Season	Thermal Gradient Positive	Negative	Zero
Carlyle	3432+06	7-1/2"	Summer 86	28%	47%	25%
			Fall 86	10%	71%	19%
			Winter 86	5%	78%	17%
			Spring 87	46%	27%	27%
			Average	22%	56%	22%
	3218+68	9-1/2"	Summer 86	36%	57%	7%
			Fall 86	9%	84%	7%
			Winter 86	8%	67%	25%
			Spring 87	52%	40%	8%
			Average	26%	62%	12%
Freeport	937+30	10"	Summer 86			
			Fall 86	12%	26%	62%
			Winter 86	18%	35%	47%
			Spring 87	25%	43%	32%
			Average	18%	35%	47%
		Overall Average		22%	51%	27%

Temperature Strains

Temperature gradients were recorded for both the jointed and CRC pavements. Figure 9 shows the gradients in a jointed pavement for the winter of 1986 and the spring of 1987, along with the gradients and percent time assigned for the gradients in the design procedure for jointed concrete pavements. Table 4 gives a summary for the gradients at various times for both sites.

Results from measured strains caused by curl are somewhat more difficult to interpret. If, for example, a slab is fully restrained, and if the thermal expansion of the gauge and the concrete are the same, then there should be no measured strains in the slab caused by curl. Conversely, if a slab is completely unrestrained, then the measured strains caused by curl should be equal to the thermal strain differential between the top and bottom of the slab, but there would be no curl stress. The actual situation is somewhere between these two extremes; the only way to get an estimate of the curl strains is to have one gauge located in a position where one would not expect any curl restraint, and to evaluate the difference between the restrained and unrestrained gauge readings.

Using the strain difference technique, the strains in a typical jointed concrete at Carlyle were determined and are shown in Figure 10. The measured strains show good agreement with the theoretical strains for curl in these pavements. The theoretical strains were determined by using an algorithm developed from a series of runs with the ILLI-SLAB program, with the weight of the slab as the restraint.

SUMMARY

Instrumented pavement sections are a powerful tool for validating mathematical models used to predict the basic response of pavements. Throughout this paper the results, both measured and calculated, have been given as strains. Strains are a basic pavement response that can be measured, as compared with stresses, which are fictitious values that can be calculated only if a value is assumed for the E of the material being tested. Measured strains are real physical properties and can be considered basic pavement responses.

Results obtained from these tests indicate that the models used in the pavement analysis provide an accurate response of the pavement to both load and environmental conditions, provided the appropriate conditions are used in the analyses. Bonding of the slab to the subbase can, for example, have a significant impact on the results. For design, one can always assume the worst condition, and, if the other condition happens, there is a greater factor of safety in the design. When evaluating the accuracy of the models, however, it is vital that one know the true condition of the pavement, or, as shown in the paper, some of the results will be different than is expected.

Results from the instrumented pavements verify that climatic conditions have a profound effect on the behavior of PCC pavements. For jointed PCC pavements the combined curl and warping strains can be as large or larger than the anticipated load strains.

For CRC pavements, the total changes from the temperature at which the slab was cast have a profound impact on

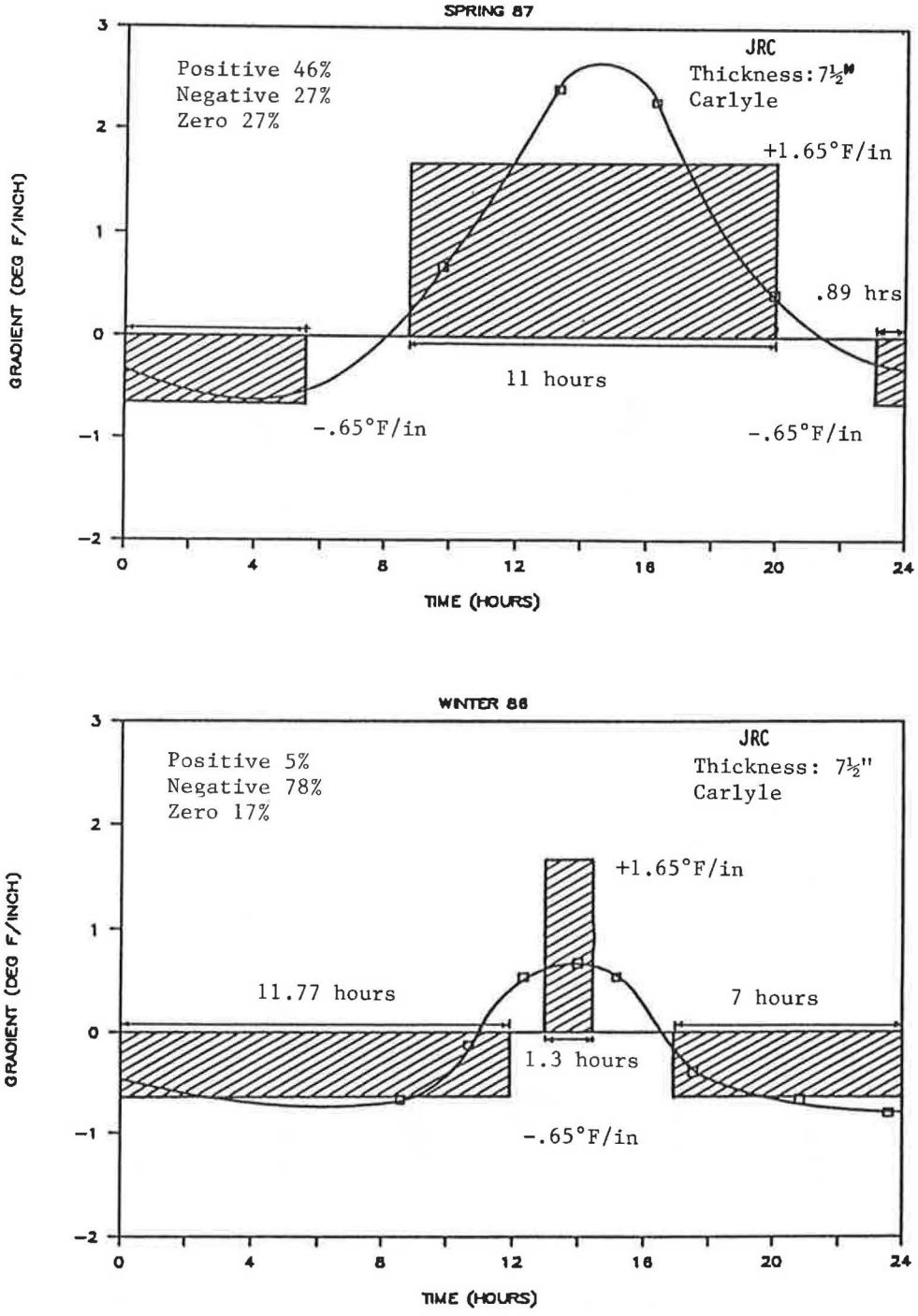

FIGURE 9 Seasonal pavement temperature gradients with equivalent time versus gradient diagrams (spring 1987 and winter 1986).

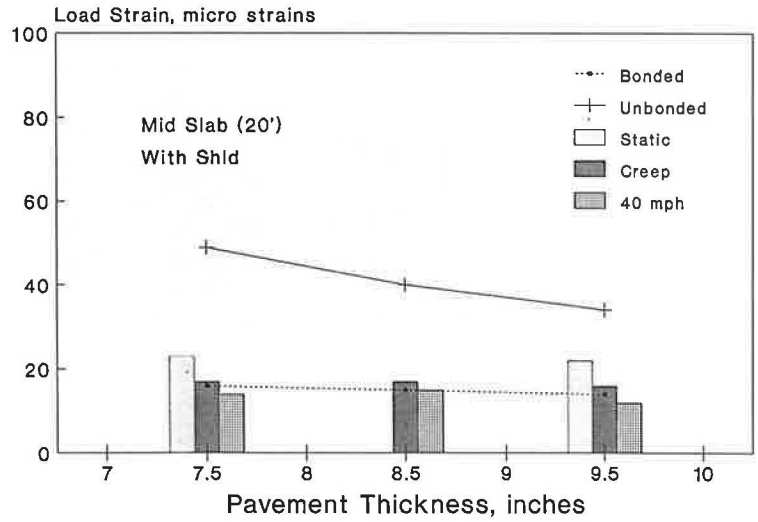

FIGURE 7 Load strain at midslab with tied PCC shoulder (18-kip SAL).

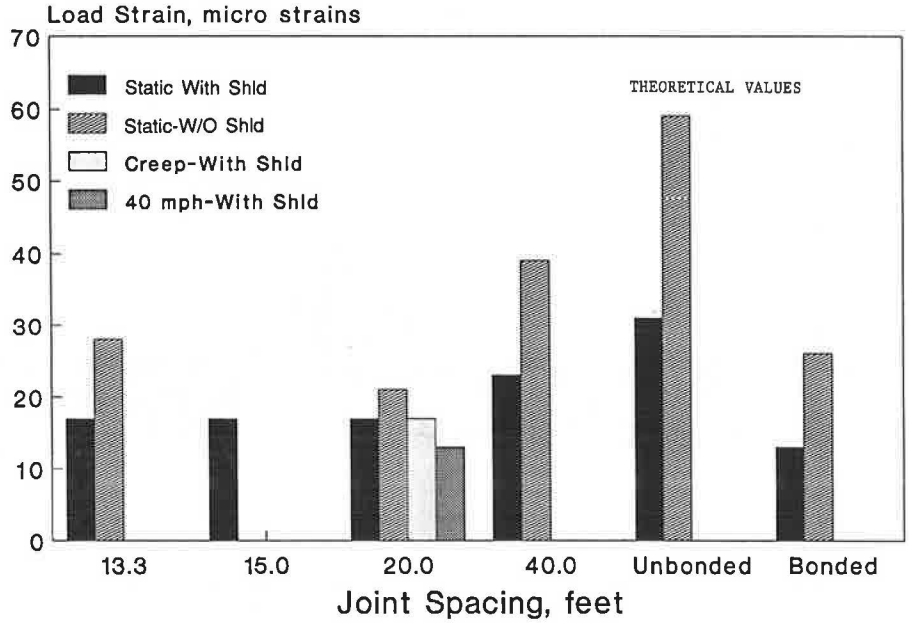

FIGURE 8 Comparison of load-induced strain at various joint spacings (static and dynamic strains).

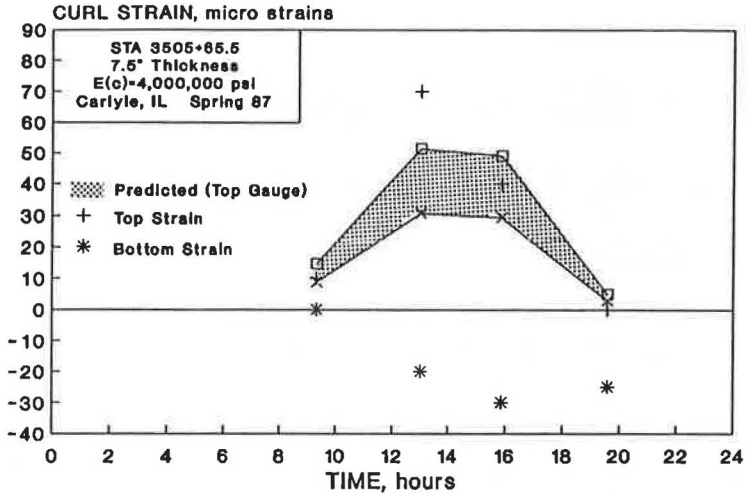

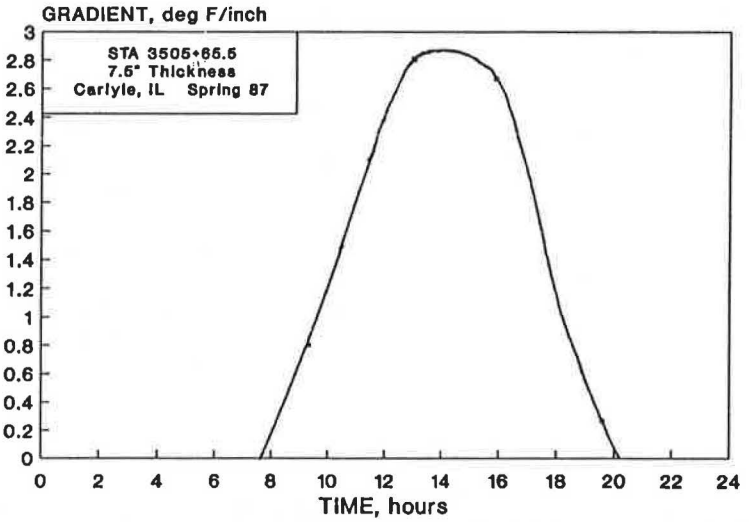

FIGURE 10 Comparison of measured and theoretical curl strains.

the strains in both the steel and the concrete. Thus, it appears that climatic conditions at the time of construction are major factors in the behavior and performance of CRC pavements.

REFERENCES

1. D. G. Zollinger and E. J. Barenberg. *Background for Development of Mechanistic Based Design Procedure for Jointed Concrete Pavements.* Civil Engineering Studies, Transportation Engineering Series 56, Illinois Cooperative Highway Research Program Series 224, University of Illinois, Urbana-Champaign, May 1989.
2. D. G. Zollinger and E. J. Barenberg. *Continuously Reinforced Pavements: Punchouts and Other Distresses and Implications for Design.* Civil Engineering Studies, Transportation Engineering Series 59, Illinois Cooperative Highway Research Program Series 227. University of Illinois, Urbana-Champaign, March 1990.
3. A. M. Tabatabaie and E. J. Barenberg. Finite-Element Analysis of Jointed or Cracked Concrete Pavements. In *Transportation Research Record 671*, TRB, National Research Council, Washington, D.C., 1978, pp. 11–19.

Publication of this paper sponsored by Committee on Rigid Pavement Design.

Evaluation of the Subbase Drag Formula by Considering Realistic Subbase Friction Values

MEHMET M. KUNT AND B. FRANK MCCULLOUGH

A modification of the reinforcement formula that considers the realistic frictional characteristics of subbase types is presented. The objective of this study is not to abandon the current formula but to arrive at a better formula, one that considers the field observations. Rational reinforcement design is important because the amount of reinforcement affects the restraint on the movement of a pavement section, or slab, and the long-term performance. This study was the result of a need to revise the reinforcement formula based on the subbase drag theory. The reinforcement formula was modified in accordance with the experimental results obtained concerning subbase frictional resistance. The modification was necessary to include the actual characteristics of subbase friction in the reinforcement design formula for both continuously and jointed reinforced concrete pavements. The new formula reflects the experimental results concerning subbase friction. It represents the actual components of frictional resistance at the interface: adhesion, bearing, and shear. The implementation of information from this study will result in more rational reinforcement design. The formula calculates the steel requirement for the middle of the slab; in other words, the calculated value is the maximum requirement, and the locations between the free end and the middle of the slab will require less reinforcement. Further experimental study is necessary to calibrate the new formula.

In the revised 1985 AASHTO Guide for Design of Pavement Structures (*1*), the friction factor is used to develop a nomograph for estimating the required steel percentage for both continuously reinforced concrete pavement (CRCP) and jointed reinforced concrete pavement (JRCP) for transverse and longitudinal reinforcement, respectively. As mentioned in this guide, this parameter corresponds to the coefficient of friction. For various subbase materials, the recommended and currently used friction factor varies from 0.9, for natural subgrade, to 1.8, for stabilized subbases. With the use of this factor it is assumed that the amount of subbase frictional force is directly proportional to the weight of the slab.

The first studies involving frictional resistance measurement started as early as 1924. The main objective of those experiments was to observe the relationship between the friction value and the subbase type. The observed values were obtained before the use of stabilized subbases. According to the results of recent research performed at the Center for Transportation Research of The University of Texas at Austin (*2,3*), the frictional resistance is primarily a function of the subbase type and the magnitude of resistance is independent of slab thickness. Thus, all the JRC pavements laid over cement-stabilized subbases experienced excessive cracks, regardless of the thickness of the slab.

Center for Transportation Research, The University of Texas at Austin, Austin, Tex. 78705.

OBJECTIVE

The primary objective of this study was to demonstrate the limitations of subgrade drag theory by considering new data. The next objective was to rederive the subgrade drag equation to more precisely reflect the subbase frictional analysis observed in the field. New findings on frictional restraint at the interface of the slab and subbase required a revision of the subbase friction concept. A formula was developed for the design of both CRCP transverse reinforcement and JRCP longitudinal reinforcement (*1*). The derivation of the present formula is based on the classical friction concept. In other words, the resultant friction force is mainly a function of slab weight, not of the frictional characteristics of the subbase. In reality, the frictional resistance consists of three components: adhesion, bearing, and shear at the interface (*2*). For each subbase type, the relative effect of each component is different. That is why the failure plane for unbounded subbase occurs at the interface, whereas for bounded subbase, it occurs within the subbase.

LIMITATIONS OF THE CURRENT FORMULA

The steel requirement is mainly dependent on the thickness of the slab, not the subbase type, because the assumed friction factors are more or less the same for various subbase types. This is one of the limitations of the current reinforcement formula that was observed when it was compared with the results of a previous study (*2*). From experience it can be concluded that there is a significant difference in applied frictional resistance among the various subbase types. A slab on a cement-stabilized subbase experiences more cracks than one on an asphalt-stabilized subbase.

DERIVATION

The derivation of the reinforcement formula is the result of equating the force in steel at the middle of the slab, assuming that a crack has formed at that location, to the developed frictional force. Although the current formula is based on the same equilibrium, it lacks the representation of the actual

subbase frictional characteristics. Among the subbase types, only untreated clay fits the classical friction pattern. The purpose of this paper is to explain the reason for the modification of the nomograph (and the formula of the nomograph) by using the recent findings reported elsewhere (*2,3*).

The current formula is

$$P_{sold} = \frac{L\mu}{2f_s} \times 100 \tag{1}$$

where

P_{sold} = percent steel required by using the old formula,
μ = friction factor,
L = length of the slab (ft), and
f_s = maximum allowable stress of steel (psi).

The derivation of this formula is given later, but a modification is necessary, because the subbase is the major parameter for the resulting frictional resistance. The current approach in the AASHTO guide assumes that the magnitude of frictional resistance is independent of the subbase type.

The friction factor values for certain subbase materials are included in Table 1. Table 1 also shows the push-off test results for the same subbase types from Project 459 (*2,3*).

The equilibrium condition of the slab after the first crack formation (approximately $L/2$ from the free end) is illustrated in Figure 1. The resultant friction force should be balanced with the load in steel. The equilibrium is formed as

$$P = P_F$$

where

P = force carried by the steel for a unit width of slab (lb) and
P_F = frictional force applied to the unit width of slab (lb).

The frictional force, simply, equals the contact area of one-half of the slab times the frictional resistance:

$$P_F = \frac{L}{2} \tau_F B$$

where

τ_F = frictional resistance (psi) and
B = width of the pavement (ft).

TABLE 1 SUBBASE FRICTION VALUES

Subbase Type	μ-Value from Guide	μ-Value[a] Measured	Frictional Resistance (psi)
Cement-Treated granular base	1.8	52.3	15.40
Flexible Subbase	1.5	5.0	3.37
Asphalt-stabilized granular base	1.8	3.8	2.20
Lime-treated clay	1.8	2.9	1.70
Untreated clay	0.9	1.9	1.10

[a]Based on 1st cycle of push-off tests

Converting the units of L and B from feet to inches, to be compatible with the rest of the equation, results in

$$P = \frac{144\ L\ \tau_F\ B}{2} \tag{2}$$

where

P = the load of the longitudinal steel (lb),
τ_F = the frictional resistance (psi),
L = length of the slab (ft), and
B = width of the slab (ft).

We know that

$$P = A_s f_s \tag{3}$$

where

A_s = area of the longitudinal steel (in.^{2}) and
f_s = maximum allowable stress of the longitudinal steel (psi).

By definition, percent of steel is the ratio of steel area to the concrete area, i.e.,

$$P_s = \frac{A_s}{A_c} \times 100 \tag{4}$$

or

$$A_s = \frac{P_s A_c}{100}$$

Since

$$A_c = 12\ D\ B$$

then

$$A_s = \frac{12\ P_s\ D\ B}{100} \tag{5}$$

If Equation 5 is inserted into Equation 3 and Equation 3 is equated to Equation 2, the following equation is obtained:

$$\frac{P_{snew} D\ 12\ B\ f_s}{100} = \frac{144\ L\ \tau_F\ B}{2} \tag{6}$$

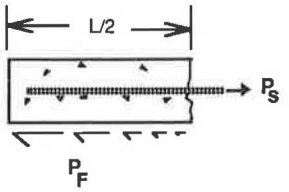

FIGURE 1 Equilibrium of forces after the first crack occurs.

where

P_{snew} = percent steel required by using the new formula.

Rewriting Equation 6 in terms of P_{snew},

$$P_{snew} = \frac{7200\ L\ \tau_F\ B}{12\ D\ Bf_s}$$

The width of the slab (B) is assumed to be the unit width, and it is automatically dropped from the formula. All the dimensions were converted to pound-inch units. After conversion, the P_{snew} formula becomes

$$P_{snew} = \frac{600\ L\ \tau_F}{Df_s} \tag{7}$$

RESULTS

P_{snew} and P_{sold} for various subbase materials are compared in Figures 2 and 3. The data for these plots are given in Table

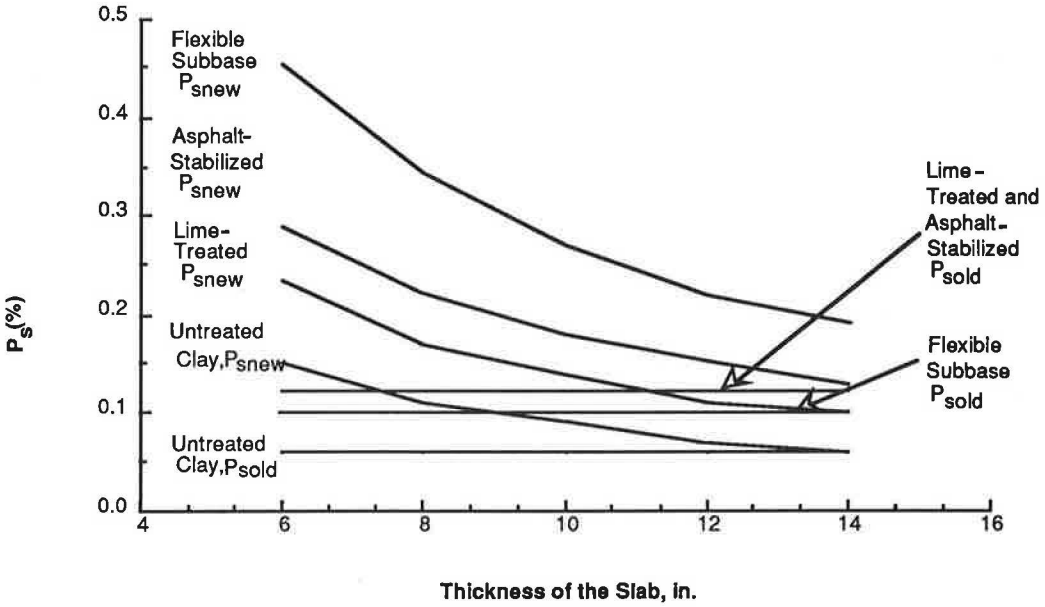

FIGURE 2 Steel percentage requirement of four different subbase materials, by using P_{snew} and P_{sold}.

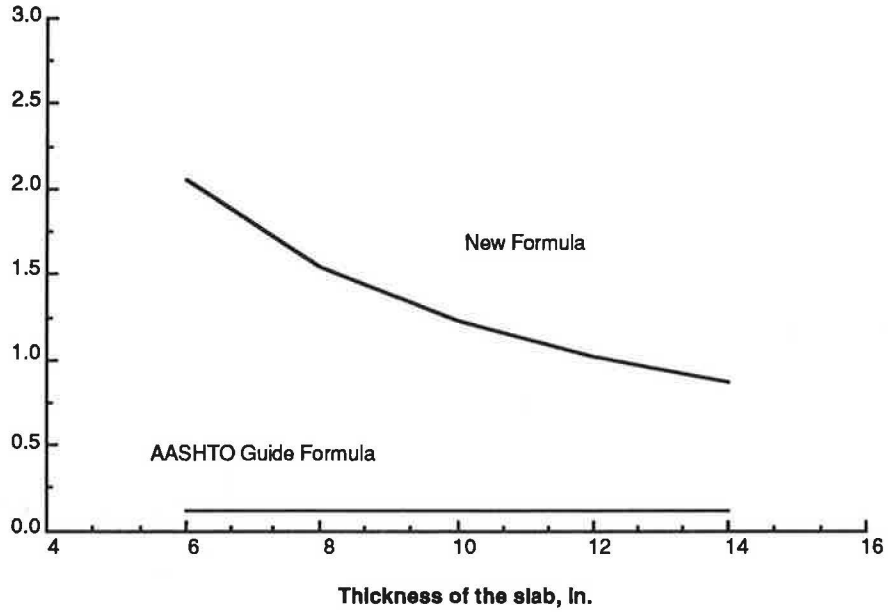

FIGURE 3 Steel percentage requirement of cement-treated base, by using P_{snew} and P_{sold}.

TABLE 2 DATA SHEET FOR P_{snew} VERSUS P_{sold} (f_s = 65,000 PSI)

Subbase Type	Length of Slab	μ	τ	D_{equiv}	P_{sold}[a] (%)	P_{snew} D=6	D=8	D=10	D=12	D=14
Untreated	25	0.90	1.10	14.70	0.020	0.060	0.046	0.036	0.030	0.026
Clay	60				0.060	0.145	0.112	0.088	0.073	0.063
	80				0.080	0.194	0.150	0.117	0.097	0.084
	100				0.100	0.242	0.187	0.146	0.121	0.104
Asphalt-	25	1.80	2.20	14.70	0.050	0.121	0.094	0.073	0.060	0.052
Stabilized	60				0.119	0.290	0.224	0.176	0.146	0.125
	80				0.158	0.387	0.299	0.234	0.194	0.167
	100				0.198	0.484	0.374	0.293	0.242	0.209
Flexible	25	1.50	3.37	26.96	0.041	0.185	0.143	0.112	0.093	0.080
Subbase	60				0.099	0.445	0.344	0.269	0.222	0.192
	80				0.132	0.593	0.458	0.358	0.296	0.256
	100				0.165	0.741	0.573	0.448	0.371	0.320
Lime-	25	1.80	1.72	11.50	0.050	0.095	0.073	0.057	0.047	0.041
Treated	60				0.120	0.227	0.175	0.140	0.113	0.098
	80				0.160	0.307	0.234	0.183	0.151	0.131
	100				0.198	0.378	0.292	0.229	0.189	0.163
Cement-	25	1.80	15.35	102.30	0.050	0.844	0.652	0.510	0.422	0.364
Stabilized	60				0.119	2.026	1.566	1.225	1.013	0.875
	80				0.158	2.702	2.087	1.633	1.350	1.167
	100				0.198	3.377	2.610	2.041	1.688	1.458

[a] Percent reinforcement predicted by using the old formula.

2. As can be observed, P_{snew} is higher than P_{sold} for all the materials (for all the thicknesses), except for the slab on lime-treated base (LTB). For slab on LTB, P_{sold} becomes higher than P_{snew} if the slab thickness is 12 in. or higher. The old formula does not vary with thickness, whereas the new one does (Figure 4).

DISCUSSION OF RESULTS

As can be observed in Figures 2 and 3, P_{sold} becomes larger than P_{snew} when the thickness is greater than a certain value. A close examination of the steel percentage formula is necessary to see whether the old and new reinforcement formula can be combined.

Assume that we have a certain kind of subbase with a given frictional characteristic (i.e., that τ and μ are known). Then let us equate Equation 1 to Equation 7:

$$P_{sold} = P_{snew} \tag{8}$$

If we use the right-hand sides of both of the equations, Equation 8 becomes

$$\frac{L\mu}{2f_s} \times 100 = \frac{6L\,\tau_F}{Df_s} \times 100 \tag{9}$$

Rewriting Equation 9 in terms of D, and calling the thickness D_{equiv}, gives

$$D_{equiv} = 12\,\frac{\tau_F}{\mu} \tag{10}$$

which creates an equation for calculating the equivalent thickness. Any thickness less than D_{equiv}, the thickness calculated from Equation 10, for the given subbase types will create a higher P_{snew}, whereas greater thicknesses will create the opposite case, $P_{sold} > P_{snew}$, as illustrated in Figures 2 and 3.

In the derivation of the new steel percentage formula, frictional resistance was assumed to be constant throughout the length of the slab. The maximum frictional resistance occurs at the free end of the slab and then gradually decreases to zero at the center of the slab. In other words, assuming the maximum friction for the complete length of the slab will result in higher reinforcement values. Therefore, in reality, the representative frictional resistance should be less than that used in the derivation. However this requires an extensive use of the computer program for both material and environmental conditions. If an average frictional resistance, calculated by using the computer program, is used in the formula, it will be variable even for the same subbase type. This is mainly because of the dependency of frictional resistance on the slab movement. Therefore, the use of the above assump-

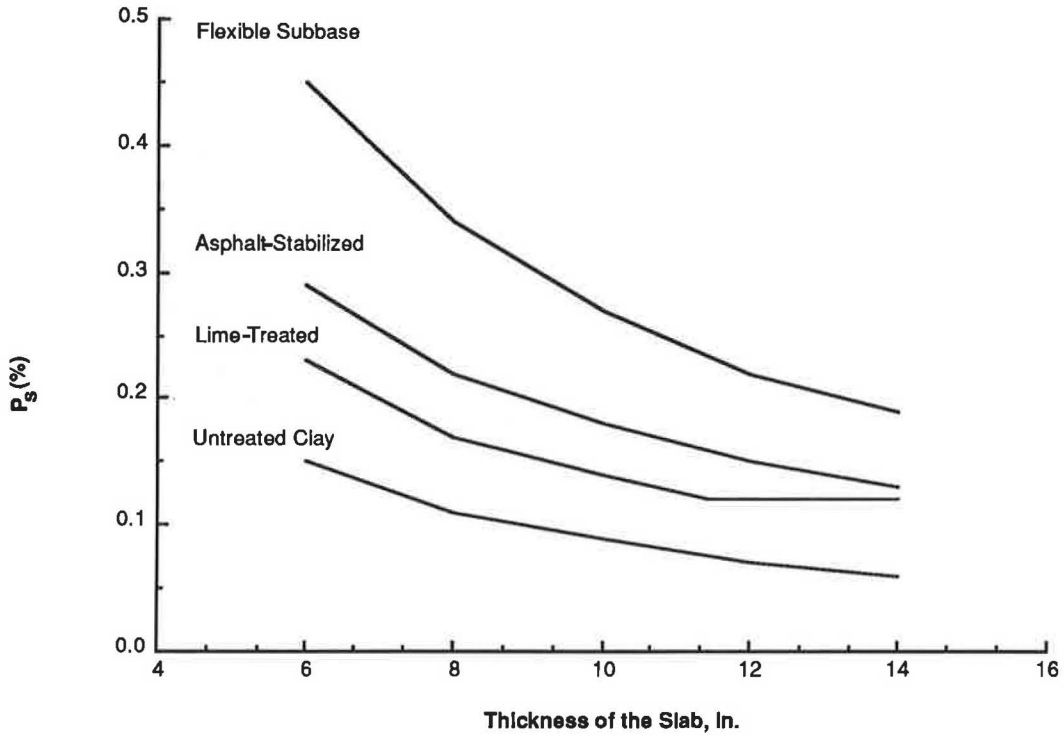

FIGURE 4 Combination of AASHTO P_s formula with the new P_s formula.

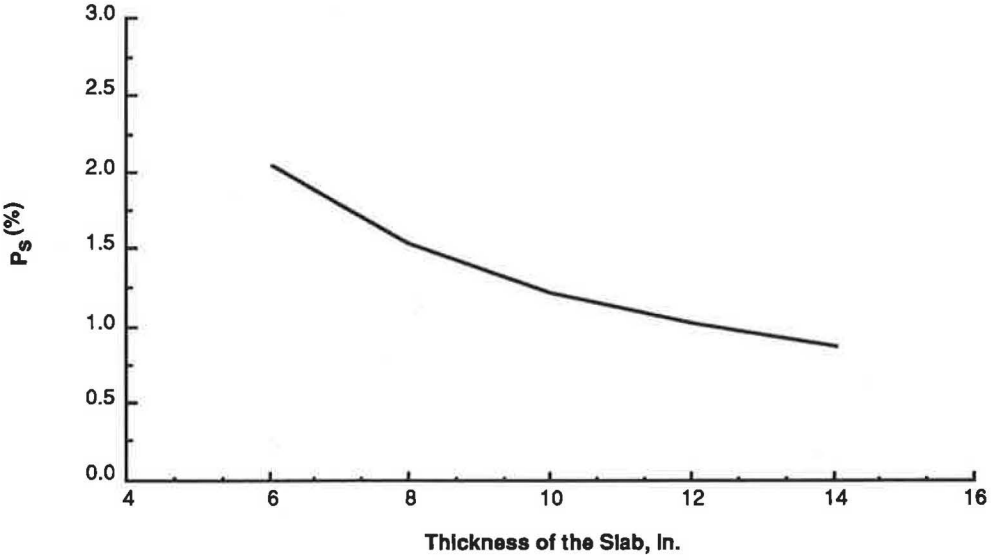

FIGURE 5 Combination of AASHTO P_s formula with the new P_s formula for cement-treated base.

tion is accepted as long as the formula is used as a guideline for the reinforcement design. Another important point is the high steel percentage requirement of the slab laid on cement-stabilized subbase (Figure 5). A solution to this problem is to use a bond breaker, which is, in fact, the asphalt-stabilized subbase illustrated in Figure 4. The use of a bond breaker will lower the steel percentage requirement considerably.

CONCLUSIONS

1. Previous subgrade drag theory is incorrect, because, instead of representing the frictional characteristics of the subbase, the friction factor, which resulted in a friction force, is merely a function of the slab thickness.
2. The rederived formula represents much better than the previous formula the actual frictional resistance of a range of available subbase types.
3. The use of the new formula yields an approximate result. The variation of friction along the slab length requires use of a program for calculating the friction force and, in turn, increasing the accuracy of the required steel percentage.
4. The P_{snew} formula is inadequate for D for thicknesses larger than D_{equiv}. The equivalent thickness is a function of the friction coefficient and the frictional resistance.

RECOMMENDATIONS

1. An interactive algorithm should be developed (like the one in the JRCP computer program) to calculate the actual frictional resistance corresponding to the slab movement. The current formula will be used until the interactive program is available.
2. The use of the P_{snew} formula yields higher tensile stresses in concrete because of the amount of restraint to relative movement, for $D < D_{equiv}$, so the use of P_{snew} will increase the number of cracks. This development requires further study to observe the effect on long-term pavement performance.
3. The combined P_{sold} and P_{snew} (Figures 4 and 5) for various thicknesses will not be a good substitute for the AASHTO Guide equation (Equation 1). Especially for cement stabilized subbases, it is not economically feasible to use up to 2 percent steel reinforcement to keep the cracks tighter. The high expense can be avoided by using a bond breaker to lower the subbase frictional resistance to a reasonable value.
4. A reasonable frictional resistance value, one that is lower than the maximum one, should be selected for the subbase type under consideration. In other words, the magnitude of frictional resistance is a function of slab movement. It varies from maximum at the free end to zero at the middle of the slab. Therefore, the maximum frictional resistance used in the formula is always higher than it should be.

REFERENCES

1. *Guide for Design of Pavement Structures.* AASHTO, Washington, D.C., 1986.
2. J. W. Wesevich, B. F. McCullough, and N. H. Burns. *Stabilized Subbase Friction Study for Concrete Pavements.* Research Report 459-1. Center for Transportation Research, The University of Texas at Austin, April 1987.
3. A. J. Wimsatt, B. F. McCullough, and N. H. Burns. *Methods of Analyzing and Factors Influencing Frictional Effects of Subbases.* Research Report 459-2F. Center for Transportation Research, The University of Texas at Austin, November 1987.

Publication of this paper sponsored by Committee on Rigid Pavement Design.

Field Performance and Evaluation of Thin Bonded Overlays

DAVID G. PESHKIN AND AMY L. MUELLER

Bonded concrete overlays of jointed concrete pavements currently are not used widely for pavement rehabilitation. As part of a major FHWA research project, between 1987 and 1988 an extensive performance evaluation of 16 different bonded overlay designs at 10 locations in 6 states was carried out. The projects were located in three different environmental zones and involved a variety of low- to high-volume pavements. The overlays ranged in age from 3 to 11 years at the time of the surveys. The field performance surveys consisted of the following elements: a comprehensive field survey to identify, measure, and map pavement surface distresses; a debonding survey; the measurement of roughness and a panel present serviceability rating; deflection testing with a falling weight deflectometer; and a materials testing and sampling program. Historical traffic data were collected to estimate the accumulated 18-kip equivalent single axle loads (ESALs) on the pavement before and after the overlay was placed. Environmental data were also collected to describe the nature of the environmental forces to which the various sections were subjected. Previous research projects or state reports were reviewed to characterize the construction conditions and the preoverlay condition of the pavements. The results of the field survey are presented for each pavement section based on all of the major measured parameters. Overall, it was found that bonded concrete overlays showed mixed success. Some of the projects appeared to be nearing failure, based on the accumulation of surficial distresses and the apparent widespread debonding that was observed. In general, it was found that debonding was a cause for concern on many of the projects.

Portland cement concrete (PCC) pavements constitute a large percentage of pavements that are designed to carry high volumes of heavy traffic. When designed, constructed, and maintained properly, PCC pavements can be expected to provide a long service life. Many factors, however, contribute to the accelerated deterioration of pavements, including construction deficiencies, design loadings in excess of those forecasted, materials problems, and unanticipated changes in traffic patterns. It is not surprising, therefore, that there exists a good deal of interest in the rehabilitation of PCC pavements. Of the major rehabilitation approaches—resurfacing, recycling, restoration, and reconstruction—resurfacing (or overlays) is one of the most commonly performed methods of restoring rideability and improving structural capacity.

The most frequently constructed type of overlay is made of asphalt concrete (AC). An AC overlay can be placed fairly rapidly, at a very competitive cost, and with little shutdown time of the facility. However, there are two major problems associated with AC overlays: reflection cracking and rutting. These problems contribute to a shorter service life than is desired in many cases for a rehabilitation strategy on high-volume, heavily loaded pavements. Also, a fairly thick AC overlay is required to improve the structural capacity of the pavement.

An intriguing alternative to the construction of an AC overlay is the use of PCC as an overlay material. A bonded PCC overlay holds the promise of an extended service life, increased structural capacity, and lower life cycle costs, compared with other overlay techniques. Although the initial cost of a bonded PCC overlay may be higher than those of an AC overlay, the benefit of longer life and reduced maintenance costs suggest that bonded overlays can be a viable resurfacing alternative.

The research presented in this report was performed as part of the second phase of a two-phase study for the FHWA, entitled Performance/Rehabilitation of Rigid Pavements. Phase I of this project is devoted to a performance evaluation of selected PCC pavements, with the goal of improving the inputs to new pavement design. The second phase of the project examines the rehabilitation of jointed concrete pavements. One of the goals of Phase II is to evaluate the performance of selected projects, including previously reviewed projects, perform additional testing and/or analysis to verify and/or improve recommended design and construction procedures, and to develop improved design and construction procedures for this technique. The evaluation and performance of the bonded overlay projects selected for this study are presented in this paper.

Bonded overlays currently are not widely used for pavement rehabilitation, except in Iowa, so there are not many candidate sections available for study. A total of 16 different bonded overlay designs at 10 locations in 6 states (covering 3 climatic zones) were evaluated for this project during surveys conducted between 1987 and 1988. All of the overlay projects were constructed since 1976; the age of the original pavement varied considerably. An attempt was made to include sections on interstates or pavements subjected to heavy traffic. Most of the sections that are discussed here are also included in an earlier rehabilitation study performed for the FHWA and in other summary evaluations performed by the FHWA (*1*,*2*). The data from the 1985–1986 FHWA surveys, where available, are presented for comparison with the more recent data. Table 1 presents the pavement sections that were included in this study.

DATA COLLECTION

Field surveys were conducted by using procedures similar to those in use for the Strategic Highway Research Program (SHRP) Long-Term Pavement Performance (LTPP) project.

ERES Consultants, Inc., 1401 Regency Dr. East, Savoy, Ill. 61874.

TABLE 1 BONDED OVERLAY SECTIONS INCLUDED IN STUDY

Project	Route	Location	Original Construction Date	Overlay Construction Date
NY 6	I-81	Syracuse, NY	1957	1981
IA 1	I-80	Grinnell, IA	1964	1984
IA 2	I-80	Avoca, IA	1966	1979
IA 3	C 17	Clayton County, IA	1968	1977
IA 4	SR 12	Sioux City, IA	1954	1978
IA 5	US 20	Waterloo, IA	1958	1976
CA 13	I-80	Truckee, CA	1964	1984
SD 1	SR 38A	Sioux Falls, SD	1950	1985
WY 1	I-25	Douglas, WY	1969	1983
LA 1	US 61	Baton Rouge, LA	1959	1981

A detailed distress survey was performed using LTPP guidelines. Debonding, a failure mode of major concern with this rehabilitation method, was estimated using a combination of "sounding" the pavement and limited coring. For the sounding, the survey crew consisted of two people, one to tap the pavement using a 4-lb hammer, and the other to record whether the sound represented a bonded or debonded layer. A debonded area was said to be present if the pavement gave off a hollow sound, or one of "low frequency." When a debonded area was located, its extent was identified by pounding with the hammer and establishing a contour of the debonded area on the pavement surface. It must be stressed that the debonding estimated for these sections is the result of limited testing using a partially subjective technique. To accurately characterize the extent of debonding it would be necessary to survey a larger area of the project with a laboratory-tested method.

Pavement surface roughness was collected for all of the sections with the aid of a Mays Ride Meter. The survey crew also gave a subjective rating of the rideability of each pavement section, in the form of an average present serviceability rating (PSR). The roughness and PSR data that are presented here represent a very small sample size, and no clear relationship exists between the two values. Deflection testing was performed with the use of a Dynatest Model 8002 falling weight deflectometer (FWD).

Coring and boring were performed at each project location. The retrieved cores were subjected to a visual inspection and a verification of thickness. The bond between the overlay and the existing pavement was tested by applying a shearing force on the monolithic core using a specially constructed apparatus and a compression testing device. Data compiled by the states and submitted to FHWA on truck types and axle load distributions (W-4 tables) were used to calculate truck factors by state and to calculate the number of 18-kip equivalent single axle loads (ESALs) applied to each section. This information was used to estimate the number of ESALs carried by the pavement before the overlay construction and the number of ESALs that had been applied since placement of the overlay.

INTERSTATE 81—SYRACUSE, N.Y. (NY 6)

The first project location was on I-81, near Syracuse, N.Y. The original pavement was constructed in 1957 as a 9-in. doweled, jointed reinforced concrete pavement (JRCP) with 43-ft joint spacing, placed on a 12-in. aggregate base. The original JRCP pavement displayed extensive longitudinal and transverse crack deterioration. This deterioration most likely was a result of the use in the original concrete of coarse aggregate susceptible to freeze-thaw deterioration. Freeze-thaw cycling caused pop-outs in the pavement surface and disintegration beneath the surface similar to D-cracking. The areas that showed the most deterioration were those surface areas exposed to water and areas in which water could be held and trapped, such as the pavement edges and joint faces. Many of the deteriorated areas had been repaired with asphalt patches.

Pavement blowups had occurred during the life of this pavement. In 1972, doweled, full-depth repairs were placed at as many transverse joints as funding permitted. In 1980, many of these repairs were showing deterioration also. Slab cracking was also present on this section, particularly over existing culverts. Before placement of the bonded overlay in 1981, it is estimated that the outer lane of this pavement had sustained 3,350,000 18-kip ESAL applications, the middle lane, 1,260,000 ESAL applications, and the inner lane, 350,000 ESAL applications.

Overlay

In 1981, a 3-in. bonded PCC overlay was constructed following extensive surface preparation. The deteriorated concrete (at almost all of the transverse joints) was milled to a depth of 3 in. The milling generally extended about 2 ft on either side of the joint. About 90 percent of the length of the longitudinal joints required the same milling. These depressed areas were paved over at the same time as the overlay was placed. Pressure relief joints were placed at blowup locations and at either end of northbound and southbound mainline structures over NY-31. Wire mesh was placed over areas of existing cracking where it was felt that the existing mesh was no longer functioning. The surface of the rest of the pavement was milled to a depth between 0.25 and 0.50 in. The pavement was then sandblasted to remove any remaining loose material or contaminants. A cement-sand grout spread by hand and broomed onto the pavement was placed shortly ahead of the paver. Temperatures at the time of placement ranged from about 50°F to nearly 90°F.

TABLE 2 INTERSTATE 81 (SYRACUSE, N.Y.) PERFORMANCE DATA

	1985 FHWA SURVEY	FIELD SURVEY 1987		
	OUTER LANE	OUTER LANE	LANE # 2	LANE # 3
Average PSR	N/A	3.2	N/A	N/A
Mays Roughness, IN/MI	N/A	135	N/A	N/A
Transverse Faulting, IN	0.05	0.07	N/A	0.11
Transverse Cracks/MI L	231	152	300	76
M	5	20	5	0
H	0	0	0	0
Long. Crk., LIN FT/MI L	0	20	0	0
M	0	0	0	0
H	0	0	0	0
% Joints Spalled	0	0	0	0
ESAL's on Overlay (millions)	1.10	2.36	1.01	0.26

% Joint Corners Debonded	95
% Area of Wheelpath Debonded	0
% Total Area Debonded	3

Immediately after paving, the plastic concrete was scored with a straight edge and an edging tool directly over the transverse joints, using previously marked guide locations. Within 5 to 6 hours after placement of the concrete overlay, the transverse joints were sawed to a depth of 5 in. This depth compensated for the additional thickness of the overlay at the transverse joints from the additional milling performed there. The longitudinal joint between lanes was sawed to a depth of 2 in. The transverse joints were sealed with a preformed compression sealant.

Performance of the Overlay

Since construction of the overlay in 1981, this pavement has experienced 2,360,000 ESALs in the outer lane—over 70 percent of the total estimated traffic carried on the original pavement from 1957 through 1981. As an examination of Table 2 shows, there is some cracking and faulting present. There is more transverse cracking in the second lane. The ride is fairly rough, indicating that some problems are developing. Almost all of the corners tested showed debonding. The average size of the debonded area at each corner was about 2 ft^2.

A center slab core showed that the PCC overlay appeared to be completely bonded to the existing slab. A core was also retrieved from a slab corner. Good bond existed between the overlay and the original slab, but the core was not recovered in one piece, having disintegrated from the level of the original slab reinforcement and below.

The overall performance of this section, surveyed 6 years after construction, is not very good. It is very likely that there was too much deterioration present on the original pavement to warrant the construction of a bonded overlay.

INTERSTATE 80—GRINNELL, IOWA (IA 1)

The next project location was on I-80 in central Iowa, near Grinnell. The original pavement was constructed in 1964 as a 10-in. doweled JRCP on a 4-in. aggregate base. The transverse joint spacing was 76.5 ft. Before construction of the overlay, it is estimated that the outer lane had sustained 11,800,000 ESALs and the inner lane, 2,230,000 ESALs.

Overlay

In 1984, a 4-in.-thick, bonded concrete overlay was constructed on this pavement. By then, the original pavement exhibited extensive distress: there were 110 broken interior corners noted in the construction plans. Before construction of the overlay, however, extensive full-depth repairs were placed; 458 areas were noted as being already in place and the construction of an additional 260 patches was required, again according to the plans. Epoxy-coated tie bars were placed on chairs above full-depth concrete repair joints that did not constitute a pavement joint before placement of the overlay. Longitudinal subdrains with transverse outlets were added to the project. At areas of broken interior corners, a depressed area of 4 in. was to be created by milling.

The initial surface preparation consisted of milling to a depth of 0.25 in., except at the locations where 4 in. was specified. The final preparation of the surface consisted of sandblasting. A cement-water grout was sprayed on the cleaned surface just before the application of the overlay. The transverse joints were sawed the full depth of the overlay and sealed with joint sealant material and backer rope. Joints at full depth patches were not sawed. The longitudinal joint was sawed to a depth of 1.5 in.

TABLE 3 INTERSTATE 80 (GRINNELL, IOWA) PERFORMANCE DATA

	1985 FHWA SURVEY	FIELD SURVEY 1988	
	OUTER LANE	OUTER LANE	LANE # 2
Average PSR	N/A	4.2	4.2
Mays Roughness, IN/MI	N/A	69	44
Transverse Faulting, IN	0.05	0.02	N/A
Transverse Cracks/MI L	222	210	225
M	11	0*	0
H	0	0	0
Long. Crk., LIN FT/MI L	21	0	0
M	0	0	0
H	0	0	0
% Joints Spalled	0	4.8	6.7
ESAL's on Overlay (millions)	1.87	6.31	1.41

* Several cracks were sealed and counted as low severity

% Joint Corners Debonded	22.2
% Debonded Crack Corners	27.1
% Area of Wheelpath Debonded	0
% Total Area Debonded	5.8

Performance of the Pavement Section

The results of the field survey from this section are found in Table 3. Table 3 shows that after 4 years of service and 6,310,000 ESALs, the pavement was still performing satisfactorily. The amount of traffic carried by the overlay in 4 years was over 50 percent of the total traffic carried by the original pavement in 20 years. Bonding survey results are also summarized. Debonding was occurring at both joints and cracks, although none was noted in the wheelpaths.

Cores were retrieved from the pavement at a center slab and corner location. The center slab core was in excellent condition, with no distresses noted. The core from the corner, however, was not recovered intact. Extensive horizontal cracking passed through the aggregate and the mortar, starting about 3 in. below the surface of the original slab. Several inches of the bottom of the core were disintegrated. The bond shear strength between the concrete layers, as measured at the corner, was 714 psi. A value of 200 psi is considered the minimum necessary for good performance.

After 3 years of heavy traffic, the only distresses noted were transverse cracking and some joint spalling. A comparison between the results of a 1985 survey and those of the 1988 survey showed no indication of progressive deterioration. However, many of the transverse cracks were of medium severity when surveyed in 1985. These cracks were routed and sealed in 1986, thereby reducing further deterioration of the cracks. The estimated amount of debonding suggests that further deterioration of this section may occur.

INTERSTATE 80—AVOCA, IOWA (IA 2)

The next project was located in west central Iowa, on I-80 near Avoca. The original pavement, constructed in 1966, consisted of a short section of 10-in. doweled JRCP on a 4-in. aggregate subbase, with 76.5 ft transverse joint spacing. It exhibited D-cracking at the transverse and longitudinal joints before construction of the overlay. This probably consisted of low to medium severity D-cracking at most of the joints. Before construction of the overlay, it is estimated that the pavement had sustained 5,410,000 ESALs in the outer lane and 810,000 ESALs in the inner lane.

Overlay

In 1979 a 3-in. bonded overlay was constructed on this pavement. Approximately 400 yd^2 of partial depth repairs and 153 yd^2 of full-depth repairs were specified for severely deteriorated areas before placement of the overlay. The continuity of the steel was not maintained in these patches. Pressure relief joints were constructed on an average of every 800 ft. These joints were sawed in the overlay approximately 4 in. wide within 24 hours and sealed with a preformed urethane foam.

The pavement was milled to a depth of 0.25 in. before resurfacing. In areas where there was deteriorated D-cracked pavement the milling extended to a depth of 1 in. Final surface preparation consisted of sandblasting and airblasting. Before placement of the overlay, longitudinal edge drains were installed. Transverse outlets were placed at 1,000-ft intervals. The grout used to bond the overlay consisted of a cement and sand mixture. No longitudinal joint was sawed, but the transverse joint was sawed the full depth of the overlay.

Performance of the Pavement Section

Results of the distress survey are found in Table 4. The table shows some deterioration, with 0.1 in. of faulting and dete-

TABLE 4 INTERSTATE 80 (AVOCA, IOWA) PERFORMANCE DATA

	1985 FHWA SURVEY	FIELD SURVEY 1988	
	OUTER LANE	OUTER LANE	LANE # 2
Average PSR	N/A	N/A	3.7
Mays Roughness, IN/MI	N/A	N/A	173
Transverse Faulting, IN	0.06	0.1	N/A
Transverse Cracks/MI L	164	211	162
M	26	6*	0
H	0	0	0
Long. Crk., LIN FT/MI L	53	0	0
M	0	5280**	0
H	0	0	0
% Joints Spalled	0	25	23.1
ESAL's on Overlay (millions)	4.82	7.93	1.39

* Centerline joint not sawed.

** Sealing may have changed M. sev. cracks to L. sev.

% Joint Corners Debonded	30
% Debonded Crack Corners	11.4
% Area of Wheelpath Debonded	0
% Total Area Debonded	1.7

riorated transverse cracks in the outer lane. There was also a large amount of transverse joint spalling present. Apparent debonding was present at both joint and crack corners, although it was more prevalent at joint corners. At the time of the survey, the overlay had carried approximately 7.9 million ESALs in the outer lane and 1.4 million ESALs in the inner lane, which is approximately 50 percent more than the original pavement had carried.

The center slab core was in good condition with no distresses noted. The core retrieved from the slab corner showed good bonding, but the original slab was totally deteriorated, with extensive cracking and disintegration. The slab appeared to have had a bituminous subsealing, because asphaltic material had infiltrated cracks at the bottom of the slab. The shear test performed on the center slab core showed a bond of 756 psi.

This bonded overlay has performed fairly well in light of the loads it has carried. It was placed over a pavement that probably showed distress at every transverse joint. Although the overlay does not exhibit D-cracking at the joints, there were a large number of spalled joints and transverse cracks. Deteriorated cracks and transverse joints are showing signs of debonding.

COUNTY ROUTE C-17—CLAYTON COUNTY, IOWA (IA 3)

Another experimental project was located in east central Iowa, near the Mississippi River. The original pavement, constructed in 1968, was a two-lane, 22-ft-wide and 6-in.-thick JPCP, with 40-ft joint spacing. It was constructed on a granular surfaced, secondary roadway that had been shaped to the required cross-section. The existing pavement had experienced 350,000 ESALs in the eastbound direction and 150,000 ESALs in the westbound direction before placement of the overlay.

Overlay

The original pavement was badly cracked, and numerous patches were placed before construction of the overlay. Also, the sections that were thicker and reinforced were constructed over areas of the pavement that were more severely deteriorated, thus skewing the performance results somewhat. A total of seven different sections, designated IA 3-1 through 3-7, were evaluated. These included variations in the following: overlay thickness; surface preparation; concrete water reducing admixtures; reinforcement; and sawing of joints. The full range of variables in this 1.3-mi-long project is described in previously published reports (*1*,*3*).

The grout used was a mix of cement and sand and was spread using brooms and squeegees. The overlay was reinforced with No. 4 reinforcing bars placed on 30-in. centers in 3-, 4-, and 5-in.-thick sections. Transverse joints were marked with nails and resawed following paving. These were cut to a depth of 1.5 in., with the exception of the 2-in.-thick slab, which had a 1-in. sawcut. A longitudinal joint was sawed only on 300 ft of the project, as an experimental feature.

Performance of the Pavement Sections

The field survey results are presented in Table 5. This 10-year-old project displayed significant distress over most of its length. It is estimated that at the time of the field survey, the eastbound lane had experienced 1.0 million ESALs and the westbound lane had experienced 0.4 million ESALs. The results of the bonding survey are also shown in Table 5. Debonding appeared to be widespread on all of the sections, especially at cracks, but also at most of the transverse joints. The section with the least overall debonding was the 2-in. overlay. The 3-in. and 5-in. overlays had the most debonding.

Pavement cores were retrieved from five sections. All of these cores showed the pavement to be in good condition,

TABLE 5 COUNTY ROAD 17 (CLAYTON COUNTY, IOWA) PERFORMANCE DATA

	3 - 1		3 - 2		3 - 3		3 - 4		3 - 5		3 - 6		3 - 7	
	3 in OL Sandblast		3 in OL Sandblast Reinforced		5 in OL Milled		5 in OL Milled Reinforced		4 in OL Sandblast		4 in OL Milled Reinforced		2 in OL Sandblast	
	EB	WB	EB	WB	EB	WB	EB	WB	EB	WB	EB	WB	EB	WB
Transverse Faulting, IN	0.07	N/A	0.08	N/A	0.16	N/A	0.11	N/A	0.17	N/A	0.11	N/A	0.06	N/A
Transverse Cracks/MI L	14	14	0	0	132	0	0	66	0	0	0	0	16	4
M	284	185	264	106	330	132	330	132	236	177	462	396	20	24
H	14	28	0	0	0	0	66	66	15	0	264	0	0	0
Long. Crk., LIN FT/MI L	0	0	634	0	0	0	0	0	0	0	0	0	63	0
M	5834	0	4963	0	10098	5280	9834	2574	7065	1755	7920	4554	246	214
H	114	0	0	0	462	0	0	0	15	15	660	0	0	0
% Joints Spalled	66.7	22.2	0	0	0	33.3	0	33.3	54.6	27.3	33.3	0	44.5	27.8
ESAL's on Overlay (millions)	1.03	0.44	1.03	0.44	1.03	0.44	1.03	0.44	1.03	0.44	1.03	0.44	1.03	0.44

% Joint Corners Debonded	100	50	100	N/A	77.8	N/A	92.9
% Crack Corners Debonded	100	100	100	N/A	100	N/A	91.7
% Area of Wheelpath Debonded	0	0	0	N/A	0	N/A	0
% Total Area Debonded	69.6	72.3	77.9	N/A	46.5	N/A	26.2

with no visible deterioration. The average shear strengths obtained from tests run on corner cores ranged from 310 psi to 586 psi.

This is the only project that allows for a comparison between some of the various design variables that influence the performance of a bonded overlay. For example, Table 5 shows that a comparison of sections 3-1 and 3-2 should show the effects of reinforcement, as should a comparison of sections 3-3 and 3-4. Section 3-1, 3-5, and 3-7 can be used to examine the effects of the overlay thickness on performance. However, these apparent effects are confounded by other variables, particularly cracking of the original pavement before the overlay was constructed. Also, it should be noted that sections 3-2, 3-3, 3-4, and 3-6 were short and that the presentation of the observed distresses on a per mile basis has most likely skewed the results; sections 3-1 and 3-7 were much longer. Finally, this pavement receives much more heavy truck traffic in the eastbound lane than in the westbound lane. In general, the distresses were considerably less severe in the westbound lane.

STATE ROUTE 12—SIOUX CITY, IOWA (IA 4)

A bonded overlay project was constructed in the western part of Iowa, on State Route 12 (SR-12) in Sioux City. The original pavement, constructed in 1954, consisted of a 9-in. nondoweled JPCP, with a 20-ft transverse joint spacing. The pavement had sustained approximately 1,660,000 ESALs in the outer lane and 180,000 ESALs in the inner lane before placement of the overlay.

Overlay

In 1978, a 3-in. bonded concrete overlay was constructed on this pavement. The surface preparation consisted of removal of an old AC overlay, followed by milling. Partial depth repairs were also carried out before placement of the overlay. These consisted of milling the pavement at deteriorated areas until sound concrete was reached. A cement-sand grout in a 1:1 ratio was used to bond the overlay to the existing pavement. The joints were sawed directly over existing joints. The transverse joints were sawed through the overlay, and the longitudinal joints were sawed to a depth of 1 in. Because the existing joints were not well aligned, it was sometimes difficult to follow the underlying joint pattern.

Performance of the Pavement Section

The distresses noted during the field survey are shown in Table 6. These distresses are representative of a pavement in fairly good condition, although there is a large amount of longitudinal cracking. The distresses in the inner lane are higher than those in the outer lane. It was estimated that at the time of the survey the outer lane had sustained 1.3 million ESALs and the inner lane had sustained 0.2 million ESALs. This is about the same amount of traffic carried by the original pavement before construction of the overlay. Results from the debonding survey are also presented. Debonding had begun to develop along cracks and joints, and 5.5 percent of the total slab area showed signs of debonding, which may be cause for future concern. These data indicate a progressive deterioration of the overlay, especially in the amount of medium to high severity cracks and faulting.

Cores were retrieved from both center slab and slab corner locations. These cores both were in excellent condition, with no noticeable deterioration. Shear tests performed on the corner core indicated a bond of 537 psi.

This 10-year-old overlay project is performing well. The excessive longitudinal cracking may be caused by the insufficient depth of cut of the longitudinal joint.

US-20—WATERLOO, IOWA (IA 5)

Another bonded concrete overlay section is located in east central Iowa on US-20. The original pavement was constructed in 1958. The pavement consisted of 10 in. of nondoweled JPCP on an aggregate base with a transverse joint spacing of 20 ft. The original 10-in. slab exhibited extensive D-cracking. There was considerable spalling of the transverse joints, especially near the intersection with the longitudinal joints. Some of these areas had been repaired with bituminous patches. Approximately 1,190,000 ESALs had been applied to the outer lane and 95,000 ESALs had been applied to the inner lane before construction of the overlay.

Overlay

In 1976, a 3-in.-thick bonded overlay was placed on this pavement. However, extensive work was completed on the pavement before that construction. Partial depth repairs at the joints consisted of additional milling of approximately 2 in. of the deteriorated pavement, sandblasting, grouting, and fill-

TABLE 6 STATE ROAD 12 (SIOUX CITY, IOWA) PERFORMANCE DATA

	1985 FHWA SURVEY	FIELD SURVEY 1988	
	OUTER LANE	OUTER LANE	LANE # 2
Average PSR	N/A	N/A	2.4
Mays Roughness, IN/MI	N/A	N/A	163
Transverse Faulting, IN	0.04	0.07	N/A
Transverse Cracks/MI L	4	10	5
M	13	55	50
H	0	5	15
Long. Crk., LIN FT/MI L	40	0	0
M	84	100	5260
H	0	0	0
% Joints Spalled	10	4.4	29.6
ESAL's on Overlay (millions)	0.87	1.34	0.15

% Joint Corners Debonded	3.3
% Debonded Crack Corners	8.3
% Area of Wheelpath Debonded	0
% Total Area Debonded	5.5

ing of the patched area with new concrete. This work was performed at 30 joints for the full width of the pavement, and at 5 joints for one-half the width. Also, full depth repairs were constructed at four locations. Finally, 4-in. pressure relief joints were sawed at either end of the project before the placement of the overlay and also were constructed in the overlay.

In preparation for placement of the overlay, the entire top 0.25 in. of the pavement was milled off. This was followed by sandblasting. Just before placement of the overlay, the surface of the pavement was cleaned by airblasting. The grout used was a 1:1 mix of cement and sand, with enough water added to produce a creamy consistency. Existing transverse joints were marked with nails on the shoulder. The resurfacing was then sawed a minimum of 1 in. deep over approximately 20 percent of the existing transverse joints. Of the 38 joints where no partial depth patching was done, 7 were sawed after resurfacing. No centerline joint was sawcut in the pavement overlay. After 2 or 3 months, most of the transverse joints had reflected through the resurfacing.

Performance of the Pavement Section

The results from the field survey are summarized in Table 7 and show that this 12-year-old overlay is in very poor condition. This overlay exhibits extensive cracking and joint spalling and has noticeable transverse joint faulting. The condition of the inner lane is similar to that of the outer lane; it also had signs of D-cracking in the overlay. There were approximately 1.3 million ESALs applied on the overlay in the outer lane and 0.1 million applied in the inner lane. This is about 110 percent of the traffic applied on the original pavement before rehabilitation.

TABLE 7 US-20 (WATERLOO, IOWA) PERFORMANCE DATA

	1985 FHWA SURVEY	FIELD SURVEY 1988	
	OUTER LANE	OUTER LANE	LANE # 2
Average PSR	N/A	2.4	2.6
Mays Roughness, IN/MI	N/A	174	201
Transverse Faulting, IN	0.07	0.12	N/A
Transverse Cracks/MI L	40	198	168
M	216	228	228
H	0	18	6
Long. Crk., LIN FT/MI L	216	601*	222
M	0	5334*	0
H	0	0	0
% Joints Spalled	0	40	50
ESAL's on Overlay (millions)	1.07	1.32	0.11

* Centerline joint not sawed.

% Joint Corners Debonded	83.3
% Debonded Crack Corners	76.9
% Area of Wheelpath Debonded	0
% Total Area Debonded	45.7

The bonding survey results suggest that there is a serious loss of bond developing between the overlay and the original pavement. The debonding is primarily associated with distresses occurring at the joints and cracks, and not in the wheelpath.

Sample cores were obtained from representative slab corner and center slab locations. The center slab core was in good condition, with no noted distresses. The corner core, however, was in poor condition. It had primarily horizontal cracking throughout the aggregate and mortar, extending to within 0.25 in. of the original surface. A shear test performed on the center slab core showed a bond of 706 psi; the shear strength from the corner core was only 160 psi.

As is noted previously, the original pavement was severely distressed by D-cracking at the time of the overlay construction. D-cracking and spalling had evolved into severe joint deterioration, necessitating widespread repair both before placement of the overlay and as preoverlay repair. This pavement is now approaching a failed condition. The original pavement was most likely not a good candidate for the selection of a bonded overlay as the appropriate rehabilitation strategy because of the extensive D-cracking.

INTERSTATE 80—TRUCKEE, CALIF. (CA 13)

The I-80 thin bonded concrete overlay project is located in a mountainous region of central California. The original pavement was constructed in 1964 and consisted of 8 in. of nondoweled JPCP on a 4-in. cement-treated base (CTB) and a 12-in. aggregate subbase. The transverse joint spacing was a random pattern of 12-13-19-18 ft.

The original pavement was exhibiting some random cracking when the overlay was constructed. Also, much of I-80 in this mountainous region had experienced a severe loss of wearing surface in the wheelpaths because of the use of chains on tires during periods of inclement weather. Before the placement of the overlay in 1984, the outer lane of the pavement had experienced approximately 5,900,000 ESALs. The inner lane had experienced approximately 860,000 ESALs.

Overlay

A bonded concrete overlay was constructed on this section in 1984. It was 2 in. thick for a distance of 750 ft and 4 in. thick for 300 ft. Before placement of the overlay, the sealant material in the random cracks was removed by impact hammers. Contraction joints were also cleaned out. The initial surface preparation for the existing concrete pavement consisted of cleaning by shot blasting. The final surface preparation was by airblasting. An epoxy was used as the bonding agent. It was applied to the existing pavement just before the overlay, which was placed within 36 hours of shot blasting. Placement temperatures ranged from 46°F to 86°F. Reinforcement was placed in the overlay in the inner, or second, lane. This reinforcement consisted of both No. 4 rebar and welded wire. There was no reinforcement used in the outer lane.

The transverse joints were sawed directly over the joints in the existing pavement to the full depth of the overlay and sealed with silicone. The two lanes were paved separately, so

no special provisions were made for a longitudinal joint. The specifications required sawing of the transverse joints within 12 hours of paving.

Performance of the Pavement Section

The distresses measured on the pavement section are summarized in Table 8. These indicate a pavement that is performing well, although there are transverse and longitudinal cracks present. It is not known how many of these are reflected cracks. The bonding survey results show that an extraordinarily large area of this pavement appears to be debonded. This debonding does not appear to be restricted to joints or the wheelpath area but covers substantial portions of the entire slab area. An informal survey of this project by Caltrans in 1986 revealed minimal debonding. It is estimated that the overlay had sustained 3.1 million ESALs in the outer lane and 0.5 million ESALs in the inner lane at the time of the survey. This figure is slightly more than 50 percent of the traffic carried by the original pavement until construction of the overlay.

This pavement has good serviceability and no faulting. However, there is a fairly large amount of low-severity transverse and longitudinal cracking that has not yet deteriorated. Given the extent of the debonding, some type of further deterioration is likely. The cause of the apparent debonding may be related to the performance of the epoxy grout or environmental conditions at the time of paving. An earlier bonded overlay (1981) in the same area failed to develop bond, although in that instance a cement grout was used and the debonding occurred almost immediately.

SR-38A—SIOUX FALLS, S.D. (SD 1)

The SR-38A project is located in the extreme southeastern portion of South Dakota, on State Route 38A. The original pavement, constructed in 1950, consisted of 8 in. (203 mm) of nondoweled JPCP on a 6-in. aggregate base. The transverse joint spacing was 15 ft. A survey conducted before construction of the overlay showed that 4 percent of the pavement area required full-depth patching. There were 1,100 linear ft of longitudinal cracking recorded, and 60 percent of the transverse joints were spalled. Corner breaks were also noted, as were transverse cracking, delamination, and large areas of asphalt overlay and patching already in place. Several blowups had occurred on the pavement; these had been repaired either with AC patches or full-depth concrete repairs. The pavement had sustained approximately 1,130,000 ESALs in each direction by the time the overlay was constructed.

TABLE 8 INTERSTATE 80 (TRUCKEE, CALIF.) PERFORMANCE DATA

	FIELD SURVEY 1987	
	OUTER LANE	LANE # 2
Average PSR	4.2	N/A
Mays Roughness, IN/MI	134	N/A
Transverse Faulting, IN	0	N/A
Transverse Cracks/MI L	245	136
M	0	0
H	0	0
Long. Crk., LIN FT/MI L	1002	543
M	0	0
H	0	0
% Joints Spalled	3	1.5
ESAL's on Overlay (millions)	3.09	0.53

% Joint Corners Debonded	75
% Area of Wheelpath Debonded	19
% Total Area Debonded	56.8

Overlay

The 3-in.- and 4-in.-thick, bonded concrete overlay was constructed in 1985. Only the 3-in. section was evaluated for this project. Extensive repairs were performed before placement of the overlay, including 51 full-depth patches and additional partial-depth patching. The partial-depth patches were prepared and then filled as part of the overlay paving operation. Four different methods of reinforcing the longitudinal cracks were tried, including placing tie bars on chairs, placing bent tie bars in predrilled holes on either side of the crack, tying tie bars to reinforcing steel rails running parallel along either side of a crack, and placing the tie bars in sawed slots.

After all of the patching was completed and the undesirable deteriorated material was removed, the pavement was shot-blasted. A cement-water grout, used to bond the overlay, was sprayed onto the surface immediately before application of the overlay. Ambient temperatures during placement ranged from 57°F to 80°F. Three transverse cracks occurred during rapid cooling of the pavement from a severe thunderstorm that produced a cold rain.

The transverse joints were sawcut the full depth of the overlay as soon as possible after placement of the overlay. The cuts were made across a single lane, guided by two sets of reference pins, in an attempt to compensate for the nonuniformity of the joints. The longitudinal joint was specified to be cut within 48 hours of paving, but was actually sawed at the same time as the transverse joints. In addition, seven 4-in.-wide pressure relief joints were constructed along the project.

Soon after the sawing was completed, 20 random transverse cracks, most very short, developed. These cracks were routed and sealed with epoxy. During the first day of paving, a random centerline crack occurred on 720 ft of overlay before sawing of the longitudinal joint. The sawing time was adjusted, but the overlay still developed another 5,100 ft of random centerline cracking. These cracks were also sealed, with the sealant material determined by the crack's location. No delamination of the overlay was detected on the project after construction.

A survey made a year later indicated a small amount of reflection cracking. The only cracks that weren't reflection cracks were located along the boundary of full-depth repairs in the overlay or the next slab.

Performance of the Pavement Section

A field survey was conducted on this pavement in May 1988, after nearly 3 years of service and 0.71 million ESALs in each lane. This is over 60 percent of the traffic carried by the pavement in the 25 years of service before construction of the overlay. The distresses were nominal, consisting of some longitudinal cracking and slight transverse joint spalling. These results are shown in Table 9. A bonding survey was also performed and showed that very little of the pavement was debonded. The only debonded areas consisted of 9 percent of the slab corners tested.

Cores were taken from the slab center and corner. They were both in excellent condition, with no signs of deterioration or distress. The shear strength between the overlay and the pavement, measured from a corner core, was 675 psi—higher than the shear strength obtained from the slab center core.

This bonded overlay is performing very well after 3 years of service and approximately 710,000 ESALs. This good performance is occurring despite the preexisting distresses and the need for widespread preoverlay repairs. It is not known whether the good performance is a result of some design factor or whether the low number of applied ESALs has helped to minimize the presence of deterioration.

INTERSTATE 25—DOUGLAS, WYO. (WY 1)

The Douglas, Wyo., project is located on I-25, in the southeastern corner of the state. The original pavement, constructed in 1969, was an 8-in.-thick nondoweled JPCP on an aggregate base, with a 20-ft transverse joint spacing. When the overlay was constructed, the original pavement was relatively sound, with some transverse and longitudinal cracking and corner breaks evident in limited areas. Minor pumping and faulting were observed throughout the project. Maintenance operations up to the time of the 1983 overlay construction included sporadic joint resealing and maintenance patching with an AC cold mix. It is estimated that the outer lane of the pavement had sustained 1,970,000 ESALs before construction of the bonded overlay. In 1983, many different repairs were carried out on this section. These included subsealing in the outer lane for the entire length of the project with a cement-pozzolan grout, full and partial depth repairs, and joint and crack resealing.

TABLE 9 STATE ROAD 38A (SIOUX FALLS, S.D.) PERFORMANCE DATA

	1985 FHWA SURVEY	FIELD SURVEY 1988	
	EB LANE	EB LANE	WB LANE
Average PSR	N/A	4.2	4
Mays Roughness, IN/MI	N/A	59	72
Transverse Faulting, IN	0.02	0.03	N/A
Transverse Cracks/MI L	0	0	0
M	0	0	0
H	0	0	0
Long. Crk., LIN FT/MI L	0	63	0
M	0	73	250
H	0	0	0
% Joints Spalled	0	1.3	6.3
ESAL's on Overlay (millions)	0.11	0.71	0.71

* Centerline joint not sawed.

% Joint Corners Debonded	9.2
% Area of Wheelpath Debonded	0
% Total Area Debonded	0.1

Overlay

Before placement of the 3-in. overlay, the pavement was milled to a depth of 0.5 in. and then sandblasted. The final surface preparation consisted of airblasting immediately before the application of the bonding agent. The temperature range during the paving period was between 65°F and 86°F. A cement-water mixture was used as the bonding agent, with a maximum water-cement ratio of 0.62. The transverse joints were sawed full depth above the marked joints of the original pavement, except for at several locations. They were then sealed with a silicone sealant before the pavement was opened to traffic. The longitudinal joint was sawed along the middle of the overlay slab, to an initial depth of 2 in. However, the original longitudinal joint was formed with an insert, which may have made it difficult to locate and follow the longitudinal joint.

Performance of the Pavement Section

The pavement was evaluated several times by the Wyoming State Highway Department. Deflection testing performed shortly after construction showed that one area appeared not to have been successfully undersealed and that there were three slabs that appeared not to be bonded. Cores taken less than 1 year after construction showed shear strengths ranging from 223 to 360 psi. One year after construction, there were a few interior corners that had become debonded and broken out. The extent of this problem was considered minimal. A subsequent survey conducted by the state in the spring of 1986 showed extensive deterioration, consisting of fine transverse cracks spaced 6 in. to 9 in. apart over the entire project. There were many areas of the project that were experiencing more severe cracking and several areas that had broken up.

This pavement was next evaluated by the FHWA in 1986. Debonding was noted at the intersection of reflected transverse and longitudinal cracks. There were also about a dozen instances of small corner breaks with associated debonding. Some transverse cracks occurred in relation to missawed joints. There was minor cracking attributable to reflection of underlying cracks or joints. Some of the cracks had developed minor spalling. According to the Wyoming State Highway Department, this cracking had begun to develop during the winter and spring of 1985–1986.

Table 10 presents the results of the 1988 field survey. Overall, the pavement showed significant deterioration, with a large number of medium severity transverse cracks and extensive longitudinal cracking. The distresses are notably higher in the outer lane than in the inner, less traveled lane. There appears to be a debonding problem at over one-half of the

TABLE 10 INTERSTATE 25 (DOUGLAS, WYO.) PERFORMANCE DATA

	1986 FHWA SURVEY	FIELD SURVEY 1988	
	OUTER LANE	OUTER LANE	LANE # 2
Average PSR	N/A	4.2	4
Mays Roughness, IN/MI	N/A	82	113
Transverse Faulting, IN	0.01	0.04	N/A
Transverse Cracks/MI L	21	158	0
M	0	42	0
H	0	0	0
Long. Crk., LIN FT/MI L	42	232	0
M	0	2165	528
H	0	296	11
% Joints Spalled	8.3	23	3.8
ESAL's on Overlay (millions)	1.12	1.90	0.13

* Centerline joint not sawed.

% Joint Corners Debonded	52.9
% Area of Wheelpath Debonded	1
% Total Area Debonded	3.6

corners and in 1 percent of the wheelpath area. This is a large amount of debonding for a 4-year-old project. The loads applied to the overlay at the time of the survey were 1.9 million ESALs in the outer lane and 0.1 million ESALs in the inner lane—over 95 percent of the traffic carried by the original pavement before construction of the overlay. The amount of longitudinal cracking appears to be the most serious problem, as much of it is deteriorated. The transverse cracking could also further deteriorate and develop into excessive roughness.

A joint core was retrieved from a representative slab corner. There was no bond between the existing pavement and the overlay, as the overlay section was totally separated from the underlying pavement.

This project is in fairly good condition in terms of serviceability, with a high PSR, but the debonding observed suggests that further cracking may occur. The original pavement required extensive rehabilitation before the overlay construction, which may be an indication that a bonded overlay might not have been the most appropriate rehabilitation strategy.

SUMMARY AND CONCLUSIONS

The pavement sections investigated in this study represent the majority of the bonded overlays that have been constructed in the United States. The original pavements ranged in age from 9 years to 35 years before overlay. The overlays ranged in age from 3 years to 11 years. The original pavements and the overlays had carried a wide range of traffic levels. In fact, several of the overlays have carried nearly as much or more traffic than the original pavements.

These overlays were constructed by using various surface preparations and bonding agents. Because of the various design factors involved in the design and construction of each overlay, the effect of many of these factors was confounded. Therefore, no strong conclusions regarding surface preparation or bonding agent could be drawn.

It is believed that curing conditions play a large role in the performance of bonded overlays. The ambient conditions at the time of concrete placement have an effect on the curing and bonding of the overlay. Rapid curing is associated with shrinkage cracking and debonding of the overlay, particularly at the corners. Undesirable climatic conditions may also cause rapid drying of the grout, which will not promote a good bond between the overlay and the original surface. Information regarding the curing conditions in this project was unavailable, however, and these conclusions can not be substantiated by the results presented herein.

Sawing of the transverse as well as longitudinal joints soon after placement of the overlay is critical in controlling the deterioration of the joints. Several of the sections exhibited cracking because of inadequate joint sawing or no joint sawing at all. For example, no longitudinal joint was sawed on IA 2, and only 20 percent of the transverse joints were sawed on IA 5. Not surprisingly, these sections exhibited more cracking at higher severity levels than sections whose joints were sawed.

There was a large degree of difference in the amount of preoverlay repair performed. Many of the sections had extensive preoverlay repairs whereas others had very little. The conclusions regarding preoverlay repair are fairly clear. If the existing slab has working cracks, deteriorated joints, or materials problems, and an overlay is placed on the slab, the chances of the overlays performing well are not good. It is believed that working cracks in the existing slab propagate quickly through the overlay. The sections on IA 3 and IA 5 show this type of propagation.

Deteriorated joints resulting from excessive spalling of materials problems result in problems in the overlay. The IA 5 section showed deterioration of the overlay joints caused by inadequate support from the original slab, which exhibited "D" cracking.

Several of the sections exhibited serviceabilities of 3.2 or less. These pavements have failed in terms of their serviceable lives. Closer examination shows that these sections are in poor structural condition as well, typically exhibiting cracking and faulting.

- NY 6—This section had a serviceability rating of 3.2 and showed transverse cracking, faulting, and a large degree of debonding at the corners.
- IA 3—Although it was not possible to determine the serviceability of these sections because of the geometry of the roadway, observations were made regarding their remaining serviceable life. The extensive deterioration of the slabs and the amount of debonding present indicate that the sections are near failure.
- IA 4—The IA 4 section had a serviceability of 2.4, indicating that the pavement was very rough. The section exhibited a large amount of longitudinal cracking and some medium and high severity transverse cracking, as well as some faulting.
- IA 5—The serviceability rating given to the IA 5 section was 2.4. This rating indicates failure of the section in terms of rideability. The section also exhibited extensive transverse cracking, several shattered slabs, a high level of faulting, and longitudinal cracking. All of these indicate a serious structural failure.

Because of inadequate documentation, the condition of the original pavement after full-depth repairs (if performed) and before overlay is unknown. This information would be useful in determining the amount of deterioration in the overlay that may be attributed to deficiencies in the original slab.

Unfortunately, many of the factors that affect the performance of the bonded overlays cannot be compared in this study because they are confounded by the various designs, climates, curing agents, bonding agents, and so on. Also, bonded overlays are typically constructed to either improve the structural capacity of a pavement or correct a surficial defect (*4*). It was not possible to determine whether any of the overlays evaluated for this study were constructed for either of these reasons. Generally, the bonded overlays that were studied had mixed success. However, it is believed that with proper preoverlay repair, thorough cleaning and preparation of the surface, use of a good bonding agent, careful placement and curing of the concrete, and proper joint sawing techniques, many years of benefit can be attained through the placement and use of bonded overlays. Also, the effect of the selection of proper candidate sections for this rehabilitation technique cannot be understated.

ACKNOWLEDGMENTS

This work was performed under an FHWA contract. The authors gratefully acknowledge the assistance of the many state engineers who have helped in all phases of this project, including taking field surveys, collecting data, and responding to the numerous requests for further information. Special thanks are due to the following individuals: Jerry Bergren of the Iowa Department of Transportation (DOT); Dan Johnston of South Dakota DOT; Ken Swedeen of Wyoming DOT; Jim Woodstrom of CALTRANS; Bill Temple of Louisiana Department of Transportation and Development; and Richard Obuchowski of New York State DOT. The assistance of Sue James, who was responsible for much of the data collection and manipulation on this project, is also deeply appreciated. Finally, without the guidance provided by Roger Larson, FHWA Contract Manager, this project would have been lacking.

REFERENCES

1. M. I. Darter and E. J. Barenberg. *Bonded Concrete Overlays: Construction and Performance.* Project 4K07812AQ6. U.S. Army, September 1980.
2. E. J. Felt. Resurfacing and Patching Pavement with Bonded Concrete. *HRB Proc.*, Vol. 35, 1956.
3. M. L. Johnson. *Bonded, Thin-Lift, Non-Reinforced Portland Cement Concrete Resurfacing.* Project HR-191. Iowa Highway Research Board, Ames, June 1980.
4. D. G. Peshkin, A. L. Mueller, K. D. Smith, and M. I. Darter. *Structural Overlay Strategies for Jointed Concrete Pavements, Vol. III—Performance Evaluation and Analysis of Thin Bonded Concrete Overlay.* Report FHWA-RD-89-144. FHWA, U.S. Department of Transportation, July 1989.

Publication of this paper sponsored by Committee on Rigid Pavement Design.

Heavily Loaded Trailers: An Approach to Evaluate Their Interaction with Asphalt Concrete Pavements

JORGE B. SOUSA, JIM MCGHIE, AND BOB SHEPARD

The Permits Department of the California Department of Transportation is often asked to issue permits for the movement of unusual vehicle configurations. It then becomes necessary to evaluate the damage these configurations cause. The shaking table of the Earthquake Engineering Research Center at the Richmond Field Station was used to investigate and compare some aspects of the dynamic behavior of a new super-heavy haul vehicle trailer (JXS), equipped with an hydraulic cylinder-nitrogen suspension, with those of four other, currently used, semitrailer types. Based on the data obtained during the tests conducted on the shaking table improvements on the JXS suspension were made, and it can be concluded that levels of the dynamic component of the loads, induced by the JXS at normal highway operations, are within the same range of magnitude as those produced by the other trailers studied. The results also suggest that the difference in performance between trailers equipped with leaf-spring suspensions and trailers equipped with air bag suspensions is greater than the difference between tridem trailers and tandem trailers equipped with air bags. From a dynamic point of view, the effect of suspension type appears to be more significant than the number of axles.

The purpose of this study was to compare the relative behavior of the JXS super-heavy haul vehicle trailer, equipped with an hydraulic cylinder-nitrogen suspension, with that of four currently used semitrailer types. This heavy trailer is capable of carrying 150,000 lb of payload (as tested), distributed over 32 tires (Figure 1). Three semitrailers and a jeep were used for the comparison. Two semitrailers were equipped with tandem axles (one of the tandem trailers had a leaf-spring suspension and the other an air bag suspension), and the third was equipped with a tridem axle using an air bag suspension. The jeep (auxiliary dolly) was equipped with 2 axles (16-tire group) with a walking beam suspension.

One of the new features of the JXS trailers (design by Trans World Crane, Inc., for Jake's Heavy Lift & Transport International) is the configuration of the suspension and the axle (Figure 2). The JXS (Jake's EXtra Speed) axle, developed for use by the heavy-haul transporter at normal highway speeds, can be positioned at various points on the trailer's frame. Because load equalization would be difficult over many axle points on a long and wide structure, it was decided that a suspension having extensive vertical travel in which each axle steers would be necessary. An hydraulic cylinder-nitrogen suspension system satisfied these requirements. The suspension uses a 6-in.-diameter cylinder with an 18-in. stroke and can steer to ±45 degrees. The nitrogen system used was designed to give the vehicle a stability float similar to, but slightly stiffer than, an automobile coil spring suspension.

The Permits Department of CALTRANS (California Department of Transportation) is often asked to issue permits for the movement of unusual vehicle configurations such as the JXS. With the increasing number of these vehicles, it becomes necessary to evaluate the damage they cause. One way to complete this evaluation would be to use the mechanistic design for pavement sections. This method allows comparisons of the relative performance of sections under the influence of these various types of trailers, providing that time histories of the loads applied are known.

The shaking table of the Earthquake Engineering Research Center (EERC) at the University of California Richmond Field Station (RFS) was used to investigate some aspects of the dynamic behavior of trailers. By individually exciting a set of dual tires with known amplitudes and frequencies and simultaneously reading the loads under each set of dual tires, it is possible to determine the frequency response function of the vehicles for the frequency range tested. It is also possible to generate time histories of loads under various types of excitation.

Using the frequency response function of the trailer and the profile of typical highway roads, it is possible to determine the power spectral density of the loads actually applied by each tire. As part of this study, the RPL (Reduction of Pavement Life Index) of each of the trailers was also determined (under specific conditions speed and pavement roughness, i.e., amplitude and frequency of excitation).

TESTING PROGRAM

Equipment and Instrumentation

The principal intent of this research was to compare the performance of various suspension systems and to determine the effects of the suspension and trailer designs on pavement performance. For this reason, eight load cells were used to directly measure the loads applied by each set of dual tires. Wooden blocks were placed beneath the other tires to keep the trailer level.

J. B. Sousa, Richmond Field Station, Building 40, University of California at Berkeley, Berkeley, Calif. 94720. J. McGhie, Trans World Crane, Inc., 3600 Kennebec Drive, Eagan, Minn. 55122. B. Shepard, Division of Transportation Operations, State of California Department of Transportation, 112 N St., Sacramento, Calif. 95814.

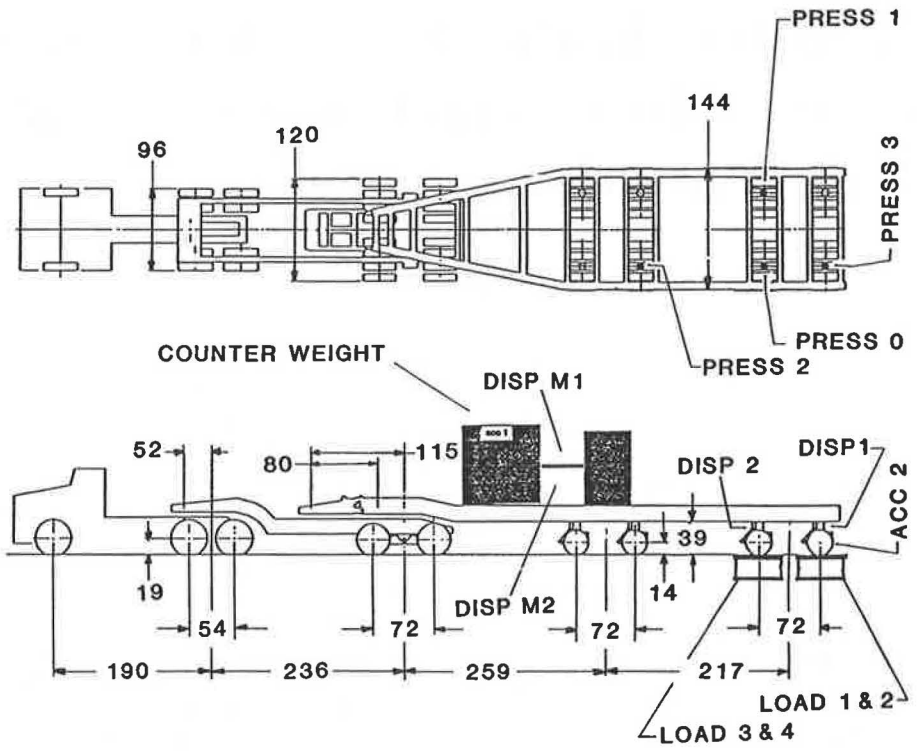

FIGURE 1 JXS trailer on a 9-axle configuration with location of the transducers.

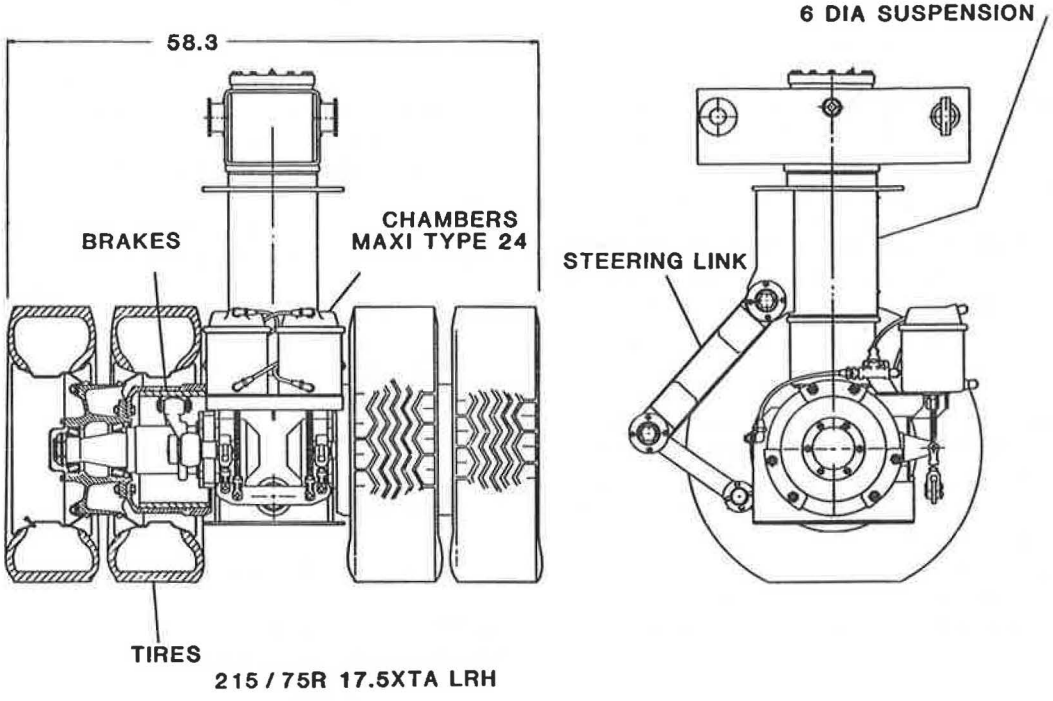

FIGURE 2 JXS axle and piston diagrams.

A beam was fabricated and attached to the shaking table so that the axial movement of the table could be transmitted to a specified set of dual tires (Figure 3). This beam contains two parts. One acts as a major cantilever beam extending out from the shaking table. This cantilever was physically attached to the table by four 60 TF prestressed rods positioned 3 ft apart. The other part is a movable L-shaped cantilever. One side attaches to the major cantilever beam, and the other side contains a load cell (load 1) on top of which a set of dual tires can be placed. A potentiometer (disp b) was placed between this L-shaped piece and the ground floor to measure the actual input displacements to the set of dual tires (this reading should be equal to the vertical displacements of the shaking table plus the deflection of the beams).

An accelerometer was positioned on the top central position of the heaviest counter weights used to ballast the trailers (acc 1). Another accelerometer positioned near the end of the axle being excited by the L-shaped cantilever beam recorded the acceleration.

On the JXS, four pressure transducers were used to record the pressures in the pistons (press0, press1, press2, and press3). Figure 1 diagrams the location of the transducers. Additionally, every piston was instrumented with a potentiometer to record the displacements (disp 1 through disp 8) and two additional accelerometers were positioned at each end of the trailer to help identify modal frequencies. During the tests on conventional trailers the number of channels was reduced.

Testing Sequence

Several tests were performed on each trailer. To determine the frequency response function (*1,2*) of a trailer it is necessary to excite it with known sinusoidal amplitudes and frequencies and monitor its response. Several frequency response functions can be obtained for a single vehicle. Essentially these functions can be perceived as black boxes. From one end known frequencies and amplitudes are input, and from the other end the responses are measured.

In this study the inputs were the amplitudes and frequencies of the displacements applied to a selected set of dual tires. The monitored responses essentially represent the time variation of the loads under the tires and the time variation of the vertical accelerations of the counter weight(s) placed on the trailers. The frequency response function of the load under the set of dual tires being excited was determined for each trailer. Several other frequency response functions can also be derived from the data obtained.

The experimental work was subdivided into testing sequences. A detailed description of the test sequences has been presented previously (*3*). Generally each sequence of tests contained at least one test with a random input with a white noise acceleration (the amplitude of the acceleration is the same at all frequencies) within the frequency range of interest (0 to 20 Hz) and a series of tests composed of sinusoidal inputs between 0.8 and 20 Hz. During each sequence all characteristics of the trailer being tested remained the same. During these sequences about 40 Mbytes of data were collected. In this paper only selected aspects of the data analysis are presented.

DATA ANALYSIS

Determination of the JXS Piston's Friction

During the initial stages of testing, the piston exhibited slip/stick behavior under sinusoidal input; in other tests, it did not exhibit any displacement. This irregularity was attributed to piston friction caused by the bearing or the seals, or both. To determine the magnitude of the friction forces, data were interpreted from tests in which the piston moved. To minimize errors caused by inertia forces, a low-frequency test (1.5 Hz) was selected for analysis.

Figure 4 displays the time variation of the force applied to the piston, the piston displacement, and the pressure variation in the piston. From the displacement trace the slip/stick pattern can be observed. The variation in the oil pressure, caused by the sudden movement of the piston, can be identified in the pressure trace. The force variation indicated variations of approximately ± 1.0 kip.

Studying the data that were gathered between 0.48 sec and 0.75 sec confirms that the piston did not move while the force was steadily increasing (roughly between -0.8 klb and 1.0 klb). The piston did not move until enough force was present to break the frictional forces.

For this case it can be assumed that

$$\text{Force}_{(\text{friction})} = \text{Pressure}_{(\text{piston})} * \text{Area}_{(\text{piston})} - \text{Force}_{(\text{tires})}$$

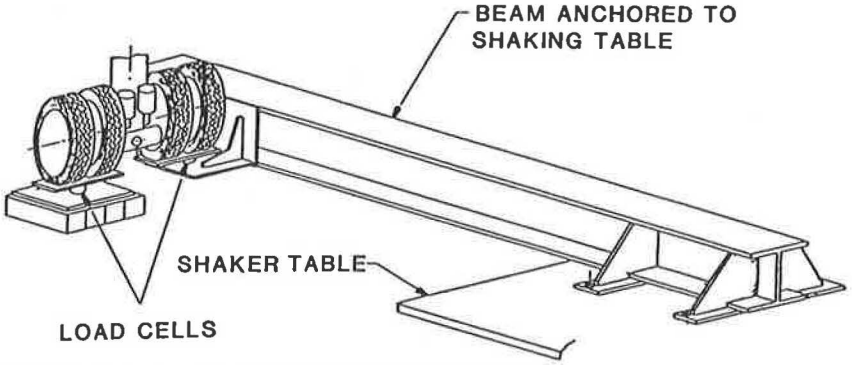

FIGURE 3 Schematic representation of the I-beam extending from the shaking table to transmit excitation to a set of dual tires.

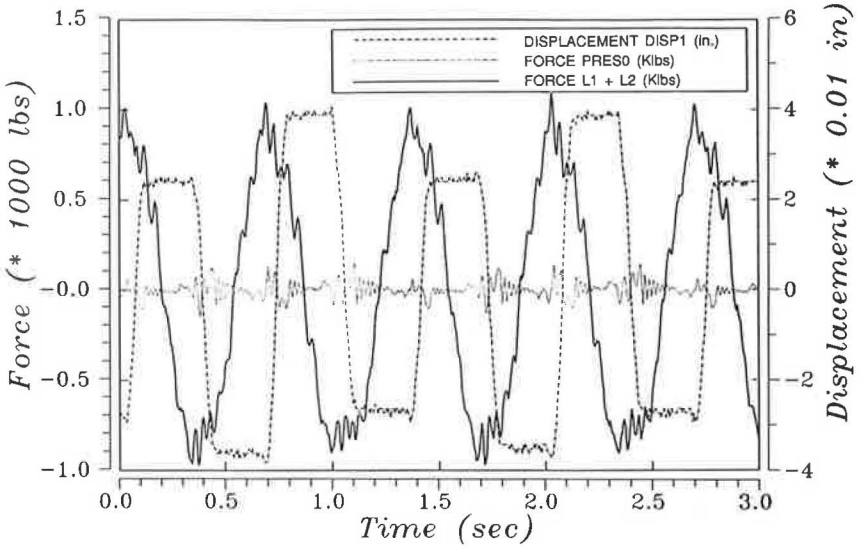

FIGURE 4 Time variation of displacements, pressure, and forces for PISTON I at 1.5 Hz.

Figure 5 plots the time variation of the friction force for this case (identified as the trace of Piston I). The figure indicates that the frictional forces can be as high as 2 klb.

Based on this finding, the piston (Piston I) was replaced by another (Piston II) in which the bearing and seals were machined to higher tolerances and lubricated. Figure 6 graphs the time variation of force displacements and pressure for Piston II under the same conditions as for Piston I. The slip/stick behavior is still present, but the force necessary to break static friction is now of a lower magnitude.

Figure 5 compares the variation of the frictional forces with time, for both pistons. The magnitude of the friction forces in Piston II was reduced to about 600 lb. The magnitude of the force caused by pressure variation is quite small, accounting for only about 200 to 300 lb of the load. The predominant frequency present in the traces is 24 Hz, probably because of the oil column resonance in the hydraulic lines.

Effects of Piston Friction

Dynamic Effects

The effects of friction can be both beneficial and detrimental to vehicle performance. Figure 7 shows the frequency contents of the acceleration for the counter-weights placed on the JXS system. For each frequency the graph indicates the amplitude of the accelerations caused by a random input on the left rear piston.

The trace, represented by a solid line, was obtained with Piston I. It is clear that there are two predominant frequencies, one at 2 Hz and the other at 7.5 Hz. A few additional peaks can be identified at 6.5, 9, 11, and 24 Hz.

For Piston II the trace is quite different. The peak at 2 Hz is still present; however, the peak at 7.5 Hz no longer exists. Peaks at 5.0, 6.5, and 11.0 Hz are now noticeable. The response

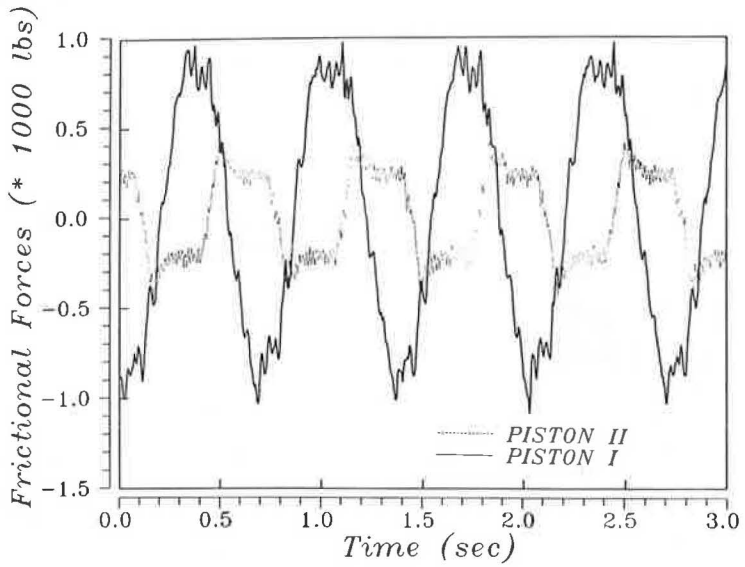

FIGURE 5 Time variation of frictional forces for PISTON I and PISTON II.

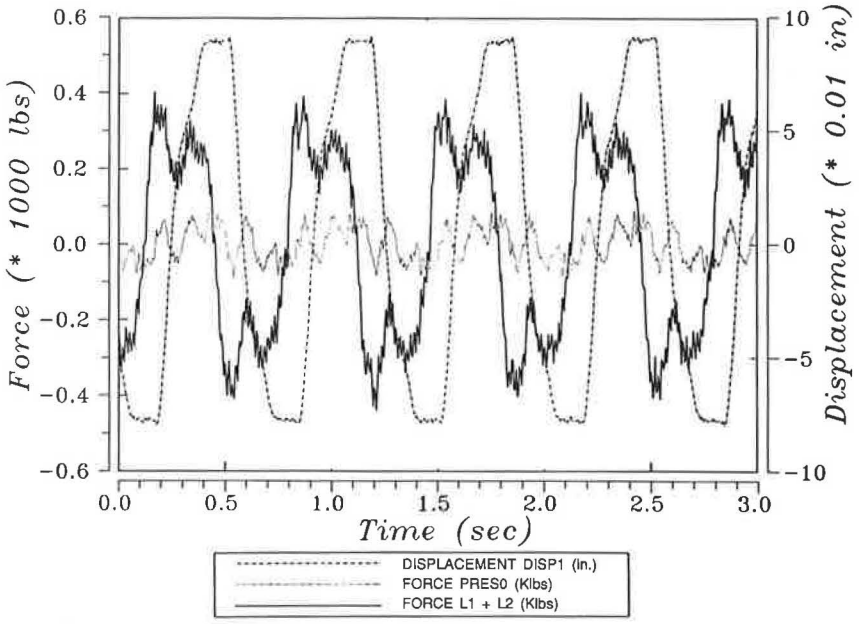

FIGURE 6 Time variation of displacements, pressure, and forces for PISTON II at 1.5 Hz.

of the vehicle, except for the decrease in performance at 11.0 Hz, is improving by offering a "softer" ride.

Static Effects

Before the tests were executed at RFS, the tractor/trailer combination stopped at scales during the trip from Las Vegas to Richmond. Table 1 shows the values of the weight obtained from each axle. These values show that the air bag and the walking beam suspensions provided a good load axle distribution. However, the JXS exhibits axle load differences as high as 5,580 lb.

During the tests the friction for Piston I was measured at 2,000 lb. Therefore, the maximum load difference between the two axles can be as high as 8,000 lb (2 pistons × 2 axles × 2,000) (note that each axle on the scale encompasses two JXS axles or two pistons). These values are of the same order of magnitude as the values recorded by the scales.

Based on the results obtained from the shaking table, all pistons on the JXS where modified, and a series of static tests were later performed by CALTRANS in Las Vegas, Nev., to investigate if load distribution characteristics had improved. Column 3 shows typical results obtained by driving the JXS on to the load cells. Significant improvement has been achieved by reducing the piston's friction levels.

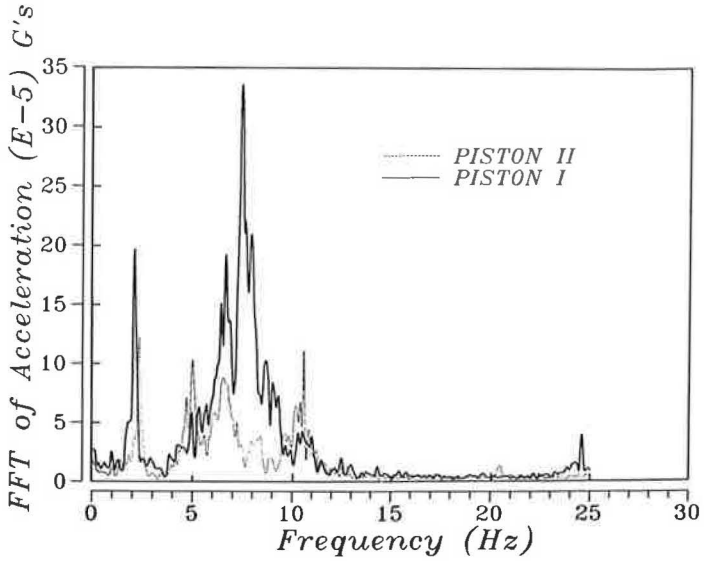

FIGURE 7 Comparison of the accelerations on counter weight for PISTONS I and II.

TABLE 1 AXLE WEIGHTS OBTAINED AT WEIGH STATIONS

	(1) SCALES A (10E3 LBS)	(2) SCALES B (10E3 LBS)	(3) NEW PISTONS (Load Cells) (10E3 LBS)	(4) REMARKS
AXLE 1	17.0	17.16		FRONT AXLE
AXLE 2	20.2	21.08		
AXLE 3	20.3	20.08		AIR BAGS
AXLE 4	22.4	22.66		
AXLE 5	21.6	21.92		WALKING
AXLE 6	23.4	23.78	30.20	
AXLE 7	26.7	27.02	30.46	
AXLE 8	29.2	28.90	30.02	JXS
AXLE 9	28.3	29.36	29.30	

Investigation of Nonlinearities in Vehicle Response

Three levels of random displacements were provided to the JXS trailer at the rear left piston. Figure 8 diagrams the time history of the displacements measured with the potentiometer disp b (located between the L-shaped piece and the ground floor). It can be observed that the three traces are of similar shape, differing only by the amplitude (600, 500, and 100).

During these tests the acceleration of the counter weight was recorded. The fast fourier transform (FFT) of this acceleration was divided by the FFT of the input displacements (Figure 9). If the trailers had linear response the three traces would be superimposed.

Although the trace displayed reaches up to 30 Hz, the most meaningful fraction is between 0 and 12.0 Hz. Beyond this range the noise levels are of the same magnitude as those of the components, thus affecting the interpretation.

These results indicate that a typical frequency response analysis of truck behavior cannot be performed in this study because this type of analysis assumes a linear response for the structure being studied. However, this approach could be implemented to evaluate suspension and vehicle behavior if input levels in laboratory studies are within those provided by normal highway operations. Unfortunately the amplitude/frequency ranges that could be provided by the shaking table do not cover the full spectrum that can be encountered in rough pavements.

Response of the Trailers to Random Input

One particularly interesting variable is the capability of a trailer to minimize the level of acceleration induced to the payload. Figures 10 through 13 compare the FFT of the vertical acceleration recorded on the counter weights for the various trailers. At the lower frequency ranges the JXS outperforms the other trailers. In the higher frequencies (i.e., 5 to 12 Hz) the walking beam and the air bag 3 exhibit better

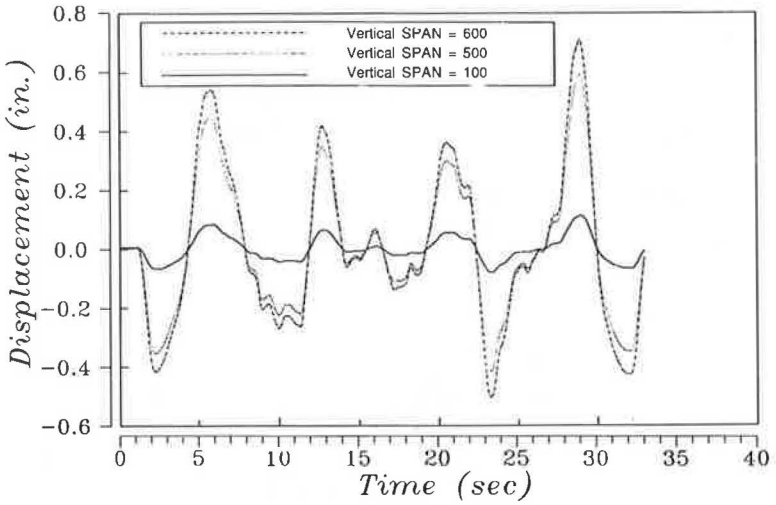

FIGURE 8 Time histories of the input displacement for three different levels of vertical SPAN.

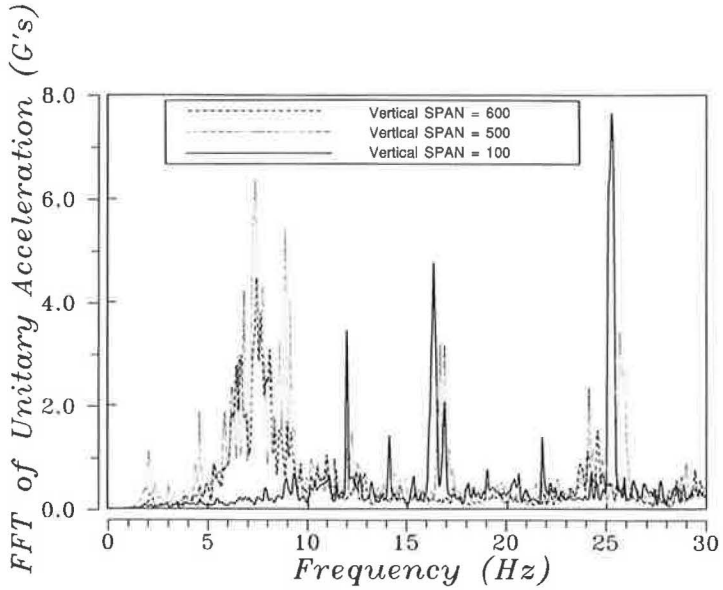

FIGURE 9 FFT of the relative accelerations of the counter weight for the three levels of input displacement.

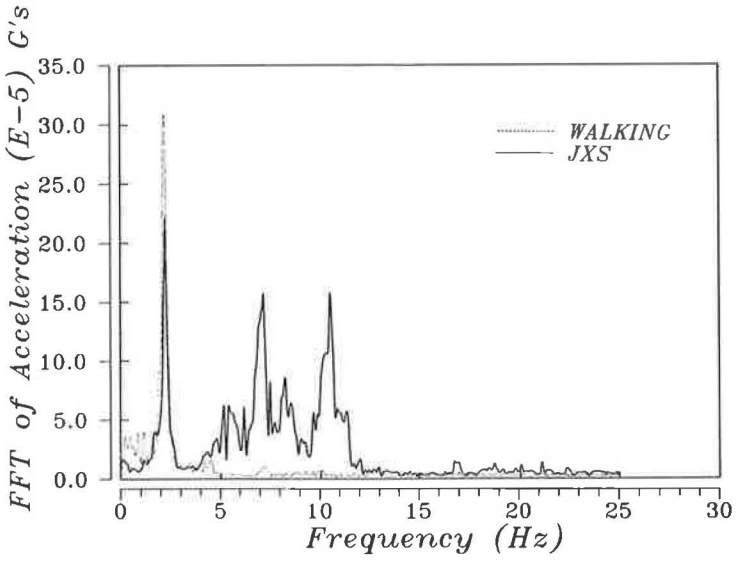

FIGURE 10 Comparison of the accelerations of counter weight between the JXS and the WALKING BEAM.

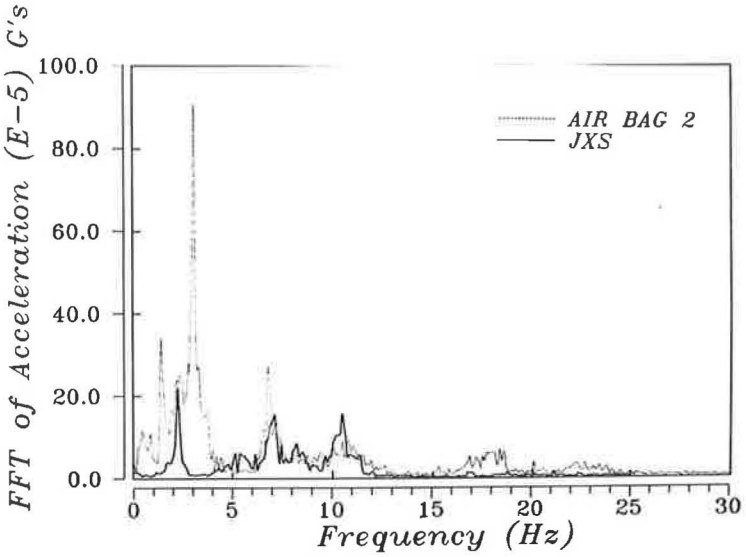

FIGURE 11 Comparison of the accelerations of counter weight between the JXS and the AIR BAG 2.

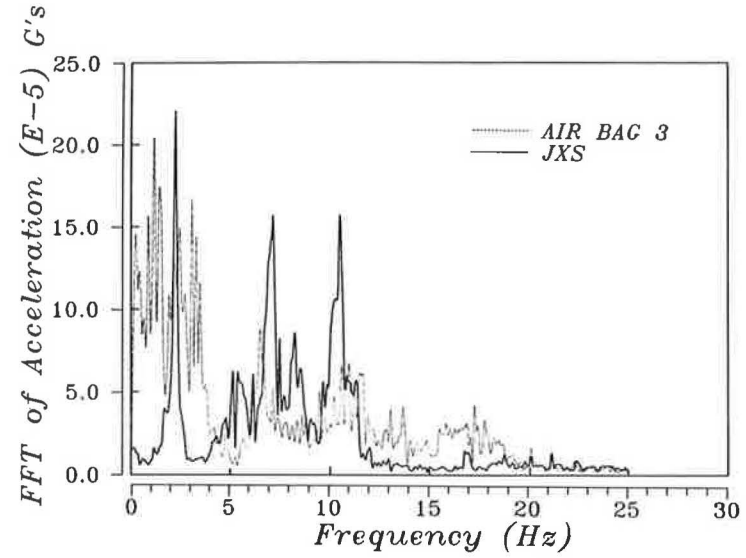

FIGURE 12 Comparison of the accelerations of counter weight between the JXS and the AIR BAG 3.

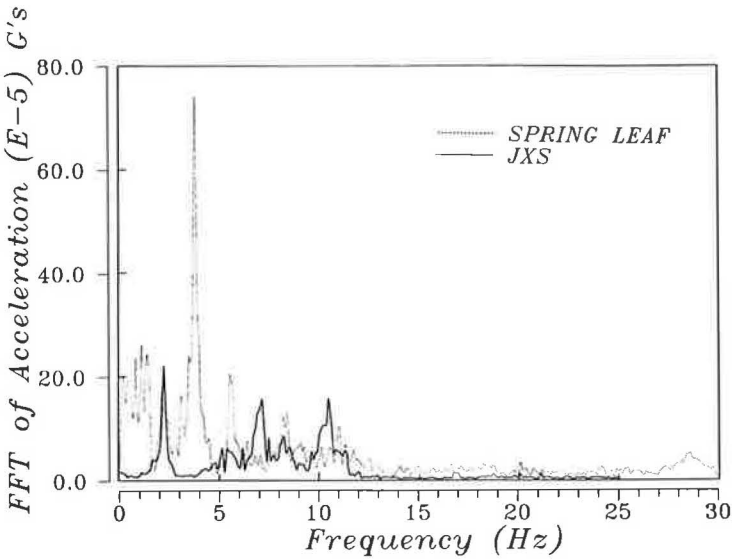

FIGURE 13 Comparison of the accelerations of counter weight between the JXS and the LEAF-SPRING.

performances. The comparison with the walking beam is not quite appropriate because the jeep equipped with the walking beam was of very small dimensions. Resonance frequencies caused by a long frame (such as the JXS or even the other semitrailers) are not present within the frequency range studied. Furthermore, the dimension of the counter weight was such that it almost totally covered the jeep, thus preventing the excitation of any resonance mode in the frame.

The data also suggest that generally the leaf-spring semitrailer exhibits the worst performance.

Determination of the Frequency Response Functions

To evaluate its behavior to dynamic inputs, the behavior of JXS was compared with that of other trailers. For each trailer the same input (displacement of dual right rear tires) was imposed at various frequencies. Figure 14 graphs the input for each of the trailers. The shaking table is unable to provide displacements of high amplitudes at high frequencies; therefore, the amplitude at 1 Hz was 0.25 in. and at 12 Hz was, at most, 0.025 in.

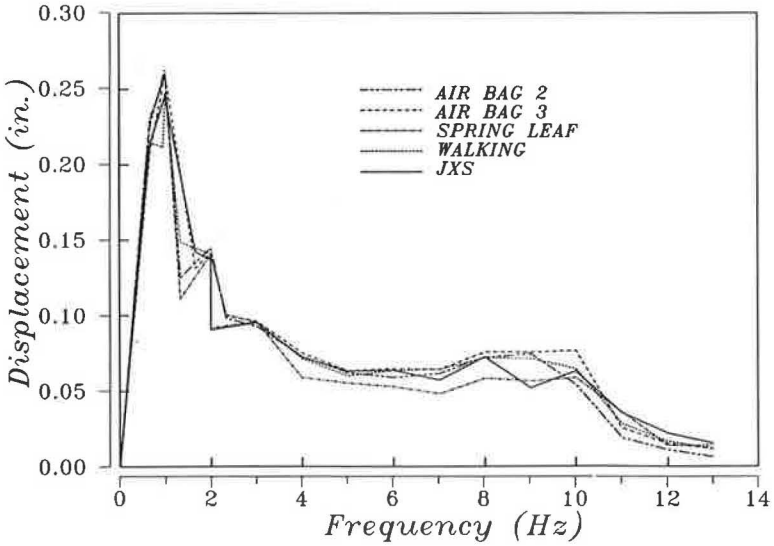

FIGURE 14 Input displacement amplitudes for sinusoidal excitation, applied to the trailers (function of frequency).

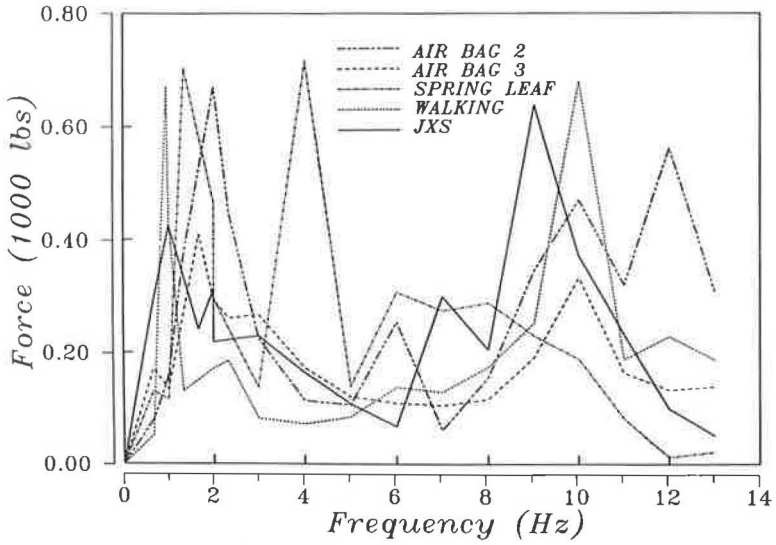

FIGURE 15 Force amplitude obtained from the frequency sweep for load 1 for all trailers.

Figure 15 displays the values obtained for the force ($L1$) (see Figure 1) under the dual right tires for the various trailers.

Two major peaks can be globally identified, one at about 1 to 2 Hz and the other at about 9 to 12 Hz. The first corresponds to the body's predominant mode of vibration and the second to the predominant frequency resonance of the suspension (axle assembly). In the case of JXS, it is possible that in the high frequency range (9 to 12 Hz) flexure and torsional modes might be present.

Figure 16 shows the frequency response function $H[L1/b](w)$ [or force amplitude ($L1$)/Input Displacement Amplitude (b)] (in pounds per inch) so the responses of various trailers can be compared. It is the frequency response function at each frequency of each of the trailers for the load analysis. Essentially these traces indicate the magnitude of the dynamic load that would be produced (if linearity is assumed) by sinusoidal displacement with 1 in. of amplitude imposed at the tires.

These values indicate that the dynamic component of the loads that can be expected for the JXS are within the same order of magnitude as the loads produced by any other trailer. The solid trace presents the peaks at 7 Hz and the other at 9 Hz, indicating the frequencies that are most unfavorable for the JXS. For the lower frequency range, which is most likely to be encountered on normal highway conditions, the JXS mostly offers the same or better load response. It is also noticeable that the airbag 2 exhibits the worst performance

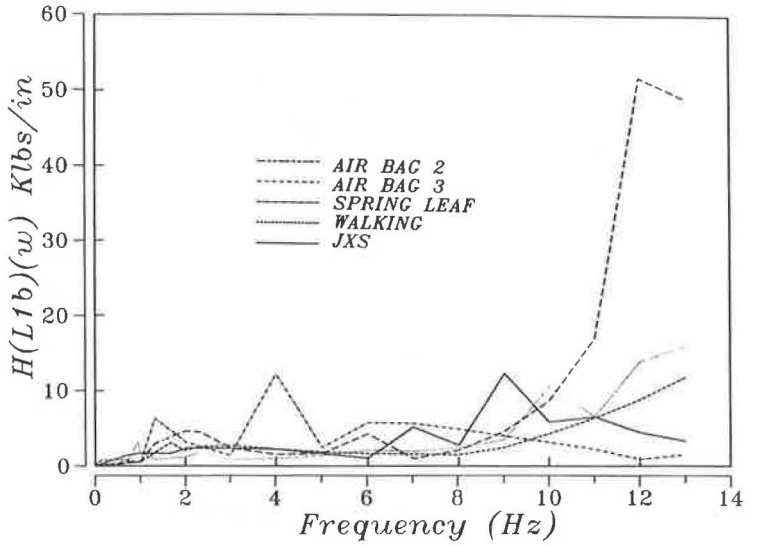

FIGURE 16 Frequency response function of the various trailers.

at about 12 Hz. Although air bags are generally chosen because they offer a softer ride, that does not necessarily imply benign effects to the pavement.

On-the-Road Performance of the JXS

After JXS was laboratory tested, its performance on the highways was investigated so that some of the observations made on the shaking table could be validated.

The following transducers were mounted on the JXS trailer:

- One accelerometer recorded the vertical acceleration of the heaviest counter weight.
- One accelerometer recorded the vertical acceleration of the right rear axle. The accelerometer was positioned at the middle of the axle, just beneath the piston.
- One accelerometer was positioned at the center rear end of the frame to measure vertical acceleration.
- The four pressure transducers used during the testing sequences remained in position. They were used to monitor pressure variations in the piston.
- Eight potentiometers monitored the displacement of the pistons. Unfortunately, data from the transducers cannot be used because the file containing the calibration contents was lost.

The transducers were excited by a very low-noise alternating current (AC) signal conditioner. All data were recorded by an on-board TOSHIBA 3200 portable microcomputer. The 115 AC power supply was provided by a gasoline generator. A line tamer was used to stabilize the current. The data acquisition software permitted the continuous recording of 4.8 sec of data at a rate of 200 conversions per sec per channel with 12-bit accuracy. A Metrabyte DAS16F board performed the analog to digital conversions.

The road test was executed on Tuesday, June 21, 1988, between 6:00 and 7:00 p.m. on Interstate 80 between the Richmond Field Station and the Cordelia scales. At this time traffic was heavy and maintaining speed was difficult. Therefore, the velocity information ascertained with the data is not accurate. For example, during preparation of a file to receive data obtained at speeds of 55 mph on rough pavement, the speed dropped to about 20 mph. Therefore, all data associated with this section are presented with reservations.

There was an attempt to include information in the data files about respective roughness levels and speed. The experts on roughness were the drivers of the trucks. They were asked to characterize roughness levels on a scale of 0 to 5 (0—very smooth, 5—very rough). The speed was read directly from the speedometers of the trucks. From all the various data records only two are analyzed here. One was obtained at approximately 55 mph over a jointed rough PCC pavement section. The other was obtained at about 25 mph over a relatively smooth asphalt pavement.

Figure 17 graphs the FFT of the vertical accelerations of the counter weight. At lower velocities, the accelerations are kept at levels below 0.02 *g* with peaks at 1.5, 2.8, 8.0 and 11.0 Hz, peaks at frequencies close to those identified with the shaking table. Note that these peaks are not expected to agree with those obtained by the shaking table because on the freeway the counter weight is subjected to a multitude of inputs (one for each tire).

At roughly 50 to 60 mph on a rough PCC pavement a very strong peak can be observed. Although the spacing of the joints is the cause of the peak (clearly if the pavement were perfectly smooth no vibrations would be noticeable) the fact that it occurs at 9 Hz is because of the physical characteristics of the JXS. This resonant frequency was also observed during the tests on the shaking table especially when Piston I was present. This could be caused by the friction still present on the other pistons. The cause of the resonance frequency at 9.0 Hz is not because of the presence of friction in the piston; instead it is because of the size, weight, and physical characteristics of the JXS frame. The friction causes the excitation at that frequency by preventing the free movement of the pistons that lock and, therefore, directly transmit the excitations to the frame from the road. If the friction were reduced this peak might not be as high. Figure 7 shows the acceler-

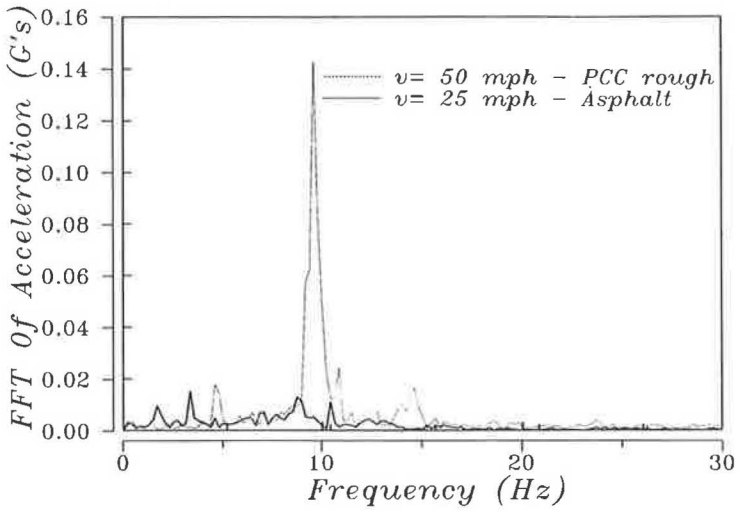

FIGURE 17 FFT of accelerations of the counter weight placed on the JXS for two on-the-road conditions.

TABLE 2 STATIC LOADS UNDER VARIOUS SUSPENSIONS

(1) LOAD (KIP)	(2) AIR BAG2	(3) AIR BAG 3	(4) LEAF-SPRING
L1	4.58	4.55	5.39
L2	4.99	4.23	6.55
L3	3.81	3.91	1.22
L4	4.60	5.13	2.61
L5		4.13	
L6		6.00	
MEAN	4.49	4.65	3.94
VARIANCE	**0.24**	**0.61**	**5.99**

ations of the counter weight recorded during the tests with Piston I and Piston II on the shaking table. The effects of reduced friction are quite noticeable.

Load Distribution Characteristics of the Various Suspensions

Load distribution characteristics can be examined from a static or a dynamic point of view. The first applies, for instance, when a vehicle slowly goes over a curb with a set of dual tires and stays there. The other is applicable for a moving vehicle going over, for example, a pothole or a step fault on a PCC pavement. This analysis was performed only with the data obtained from the semitrailers equipped with air bags and leaf-spring suspension as they are standard configurations.

Table 2 displays the static component of the load for the various vehicles. These are the mean values of the static load recorded for an input sinusoidal excitation at 1 Hz. The static values for other frequencies were also investigated with similar values of variance and mean. It is clear that the leaf-spring suspension has the poorest static load distribution characteristics. (Note: the load cells were placed under the tires by individually raising each axle with a jack.)

To investigate the sharing capabilities of a suspension in a dynamic environment an approach similar to that described in On-the-Road Performance was followed.

The dynamic load ratio was defined as

$$\mathrm{DLR}(w) = \sum_{i=1}^{i=N} \mathrm{Amp}_{(i,w)} \Big/ \sum_{i=1}^{i=N} \mathrm{Sta}_{(i,w)} \qquad (1)$$

where

i = a dual set of tires;
N = the number of sets of dual tires on the suspension;
$\mathrm{Amp}_{(i,w)}$ = amplitude of the dynamic component of the load applied by dual set of tires i at frequency w; and
$\mathrm{Sta}_{(i,w)}$ = the mean value of the load (static component) applied by the set of dual tires i.

Essentially the sum of the dynamic components of all the loads applied by the tires is divided by the sum of the static components of the same loads. A DLR of 0.30, for instance, indicates that the magnitude of all the dynamic loads was 30 percent of the static loads. This value implies that the loads transmitted to the pavement can be as high as 130 percent of the static load and as low as 70 percent.

Generally a good suspension will minimize the DLR, whereas a bad suspension will induce higher dynamic components of the load on all tires, thus causing a higher value for the DLR.

Two factors can contribute to a high DLR: (a) the suspension is such that it causes high components of dynamic load, and (b) the suspension does not provide a good equalization of the load among the tires. It is difficult to identify which of those two factors plays a more important role in a high DLR. Figure 18 graphs the variation of the DLR with frequency for the various vehicles. The leaf-spring suspension clearly presents the worst performance. The DLR for this suspension is higher at almost all frequencies. The air bag 2 performs relatively well, except at 2 Hz, where the roll mode of resonance induces high dynamic loads, imposing very poor load distribution, and at 12 Hz at the natural frequency of the axles.

Comparing the shape of the curves in Figure 18 with those in Figure 16, it is apparent that the dynamic components on the set of tires not being excited contribute strongly to a high DLR for the leaf-spring. This value can be caused by poor load distribution capabilities.

The DLR depends on the frequency of the load (for sinusoidal inputs) as observed in Figure 18. If the DLR were computed only at 6 Hz, for example, the $\mathrm{DLR}_{\mathrm{airbag3}}$ would be higher than the $\mathrm{DLR}_{\mathrm{airbag2}}$; however, at 10 Hz the order is reversed. These data imply that if suspensions or trailers are compared based on ratios of this type, obtained from their responses when traveling at a given speed on a given pavement profile, the conclusions cannot be extrapolated to other speeds or other pavement profiles or even to other payload levels.

PAVEMENT PERFORMANCE CONSIDERATIONS

For specific pavement types, it is important to decide which modes of distress contribute to pavement deterioration and, therefore, to a reduction in pavement serviceability. For asphalt pavements, the major modes of distress directly associated with load are fatigue, cracking, and rutting. For portland concrete cement pavements, step faulting at the joints (in undoweled pavements) and fatigue cracking appear to be the major causes of loss in serviceability because of traffic loadings.

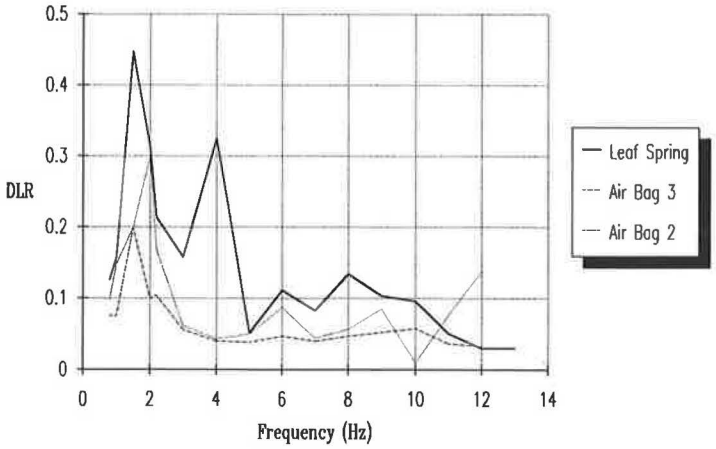

FIGURE 18 Variation of DLR with frequency for three semitrailers.

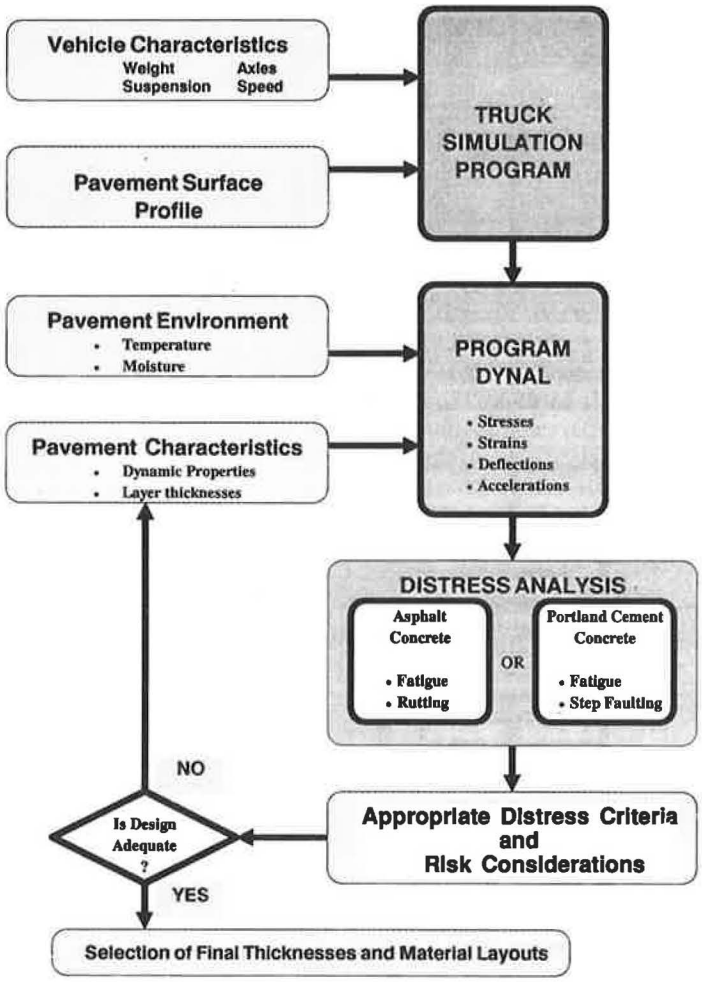

FIGURE 19 Diagram for analysis of a pavement section.

As seen in Figure 19, analysis of a specific pavement section involves determining if the section under consideration will be able to sustain the anticipated loading; if not, a new section must be selected and checked.

To illustrate the process, consider fatigue analysis. Results of studying the fatigue response of asphalt concrete indicate that the following expression is a reasonable damage determinant (*4*).

$$\log N_f = 15.947 - 3.291 * \log(E_t/10^{-6}) - 0.854 * \log (S_{mix}/10^3) \quad (2)$$

where

N_f = number of load applications to 10 percent cracking,
E_t = tensile strain (resulting from load) repeatedly applied, and
S_{mix} = dynamic stiffness modulus of the asphalt bound layer.

The program ELSYM (*5*) can be used to ascertain strains resulting from anticipated static loads. According to the above expression, for a particular strain level there is a number of load repetitions (N) that can be sustained before cracking takes place. Since there will be a range in loads and thus in strains, the cumulative effects of the various strain levels must be considered. This can be done by using the linear summation of cycle ratios cumulative damage hypothesis:

$$\sum_{i=1}^{n} (n_i/N_i) = 1 \quad (3)$$

where

n_i = actual number of load repetitions at strain level i, and
N_i = allowable number of load repetitions at strain level i (from Equation 2).

When the linear sum of cycle ratios reaches unity in this expression, the pavement is no longer considered serviceable and rehabilitation is required.

The objective of the design process is to find a suitable combination of materials and layer thickness that permit the anticipated loads to be carried for a prescribed period of time.

As seen from the above discussion and from the illustration (Figure 19), there are essentially four steps in the process for defining representative interactions between a vehicle (truck) and the pavement. They are

1. Definition of vehicle characteristics through direct measurements of response, e.g., through the use of the shaking table, a simulator like that developed by PACCAR (*6*), or by means of computer analysis using truck simulation programs such as RIDE (*6*) or DYMOL (*7*).
2. Definition of representative pavement profiles.
3. Definition of the pavement response to the loads generated from items 1 and 2.
4. Definition of adequate distress analyses and distress criteria for representative pavement materials.

Comparative analysis can be performed by keeping some of the variables constant and varying others. Two such comparative analyses were undertaken to evaluate the relative behavior of the trailers tested. They are as follows:

1. Mechanistic quasi-static analysis—considered the relative effect of the various levels of strain caused by the various trailers, assuming no dynamic effects, that is, truck loads were assumed to be applied on an infinitely smooth pavement surface.
2. Determination of the RPL index for each trailer (*8*)—looked separately at the dynamic effects of the suspension on pavement damage (life) for the same time history of input displacement.

Mechanistic Quasi-Static Analysis

To investigate the relative effects of the loading level and spacing between loads (tires) on pavement performance, a typical asphalt concrete pavement section was selected (see Table 3). The 12-in.-thick asphalt layer was subdivided into two layers so that different temperature could be simulated.

The computer program ELSYM was used to determine the maximum tensile strain on the bottom asphalt layer for the loads imposed by each of the trailers. The columns of Table 4 display the intermediate steps (columns 1 through 7) and final result (column 8) of this analysis.

TABLE 3 PAVEMENT SECTION USED FOR ANALYSIS

(1) LAYER	(2) PROPERTIES
Asphalt Concrete	H = 6 in. ν = .15 E = 800 000 PSI
Asphalt Concrete	H = 6 in. ν = .10 E = 1 200 000 PSI
Base	H = 6 in. ν = .35 E = 10 000 PSI
Subgrade	ν = .35 E = 5 000 PSI

TABLE 4 DETERMINATION OF THE TOTAL WEIGHT (lb) TRANSPORTED BY EACH TRAILER DURING A PAVEMENT LIFE

(1) TRAILER	(2) # Tires Susp.	(3) Load (lbs) (E+03)	(4) MAX Strain (E-04)	(5) # rep. Failure (E+06)	(6) #rep/ pass (E+06)	(7) # passes	(8) lbs transp./ pavement life (3)*(7)(E+9)
Single	4	18	.649	22.557	1	22.6	**406**
Tandem	8	34	.574	33.791	2	16.9	**574**
Tridem	12	42	.510	49.861	3	16.6	**698**
Walking beam	16	60	.780	12.317	2	6.2	**370**
JXS-12	16	60	.683	19.067	2	9.53	**572**
JXS-14	16	60	.641	23.497	2	11.75	**705**

The data for column 5 were obtained by introducing the values of column 4 into the formula (formula 1). This value represents the number of times that an axle of the trailer could pass over that pavement section. The estimated number of passes of a trailer (column 7) was obtained simply by dividing that number by the number of axles (column 6), given that the maximum strain occurred under that axle.

Most analyses stop at this stage, and trailers or suspensions are compared based on the number of repetitions to failure on a particular pavement. According to this approach, the trailer equipped with a single axle would be recommended for yielding the maximum number of repetitions ($N = 22.6 \times 10^6$). However, the main purpose of a road is not to withstand repetitions but to provide the means by which a payload can be transported from point A to point B. Therefore, an alternative method for comparing trailers is to compute the amount of payload they could carry over the life of a pavement. This value can be obtained by multiplying the number of passes the pavement can withstand by the total load carried with each pass (column 7).

It is now clear that a JXS-14 (14 ft overall width) would be capable of carrying more load over the life of the pavement section studied than any other trailer. In fact, it could carry twice that carried by a trailer equipped with a single axle. The jeep equipped with the axle walking beam (16-tire group) appears to be the least effective with only 370×10^9 lb carried versus 704×10^9 lb for the JXS-14.

These values are specific for the pavement section studied. The results presented are only relative to the California Department of Transportation permit program and may not be the same for other states. For a complete evaluation of the relative performance of the trailers several other pavement sections should be investigated under different conditions (i.e., temperature and moisture content) and also for PCC pavements. Such studies were beyond the scope of this project.

Determination of the RPL Index for Each Trailer

This section investigates the effects of the dynamic loads generated by each of the trailers on pavement performance. Determining the relative damage effects of the five types of trailers could be completed in three steps:

1. Determination of the time histories of the tensile strain at the bottom of a representative pavement structure using dynamic material properties. The strains can be computed using a new computer code, SAPSI (*9*), developed by Chen and Lysmer. This code simulates the dynamic response of layered systems to dynamic surface loads and incorporates the variation of the material properties with loading frequency.

2. Determination of pavement life expectancy using generally accepted fatigue criteria. For each of the trailer types, the number of load applications to failure can be computed. The linear summation of cycle ratio cumulative damage hypothesis (Miner's Hypothesis) can be used to assess the relative damage imposed at each level of strain.

3. For purposes of comparison, a reduction of pavement life index (RPL) can be developed for each trailer type. Each RPL value represents the percentage of pavement life consumed solely by the dynamic effects imposed by one type of trailer (*8*). The definition of the RPL is as follows:

$$RPL(\text{trailer}) = 1 - N_F(\text{trailer})/N_F(\text{static}) \quad (4)$$

where

$N_F(\text{static})$ = number of load applications to failure computed by current quasi-static methods and
$N_F(\text{trailer})$ = number of load repetitions to failure (taking into consideration the dynamic effects of the suspension).

During this analysis it must be assumed that the dynamic loads produced by the trailer on a rough surface are a random phenomenon. Consequently, any particular point on the pavement may be subjected to the full spectrum of loads that a given truck might apply. In essence, any single point in the wheel path is likely to sustain the same level of loading as any other point. In addition, it has been shown (*9*) that velocity effects of a moving load (velocity 0) on a layered structure can be assumed negligible for velocities up to 70 mph.

Chen showed (*9*) that it is not necessary to take into consideration the inertia effects of the pavement when determining the time histories of the strains caused by dynamic loads. This permits the use of a simpler static linear elastic layered program like ELSYM instead of the use of SAPSI. Stresses, strains, and deflections can be calculated by the quasi-static procedure described previously.

The approximate time history of the response (stress, strain, deflection) of the pavement can be obtained by multiplying the response to a unit static load by the intensity of the load at each time step. It is important, however, to use the actual dynamic load history and material properties associated with the specific loading conditions to conduct this simplified analysis.

Given that this is just a comparative study between trailers, the material properties of the pavement can also be assumed. However, to determine the RPL for the various trailers, the time histories of the loads produced by the random excitation applied by the shaking table were used, specifically, the load produced by the tandem tires being directly excited (L1).

For this comparative analysis, because of the variance in number of wheels, axles, and axle and wheel spacing, it must be assumed that a pavement section is specially designed for each of the trailers so that the maximum static strain applied to the bottom layer of the individual pavement section would be the same in each of the sections. Since uniform static strain can now be assumed, it is possible to determine the dynamic effect of each trailer type. To specifically focus on a comparison of the dynamic behavior of the various trailers, it was assumed that they would all cause the same static strain, 0.0001.

Since the strain is proportional to the load, time variations of the load would produce proportional time variations of the strain. With this in mind it can be concluded that L_1 (t) (the time history of the loads in L_1) can be converted to $e_1(t)$ (the time history of the tensile strain on the bottom of the asphalt layer for this trailer) by

$$e_1(t) = 0.0001 * L_1(t)/\text{mean } (L_1(t)) \quad (5)$$

Therefore, during the 33 sec of strain, time histories at 200 sample/sec, 6,600 digitized strain levels were obtained.

The attainable number of repetitions to failure was computed using the fatigue law discussed in Mechanistic Quasi-Static Analysis. The RPL values obtained for the various trailers are as follows:

Trailer	*RPL (%)*
Quasi-static	0.0
JXS (Piston II)	0.73
Walking beam	0.76
Spring-leaf	1.11
Air Bag 3	0.92
Air Bag 2	0.77

With these assumptions in mind it is clear that if there were no dynamic effects, all trailers traveling in their own pavement section would each yield the same pavement life. This pavement life would be the quasi-static life. However, the time variation of the strains causes various levels of pavement life consumption with each pass. The most "benign" is the JXS (0.73) followed by the walking beam. The most destructive is the spring-leaf (1.11).

For normal highway operation, RPL values can be as high as 40 percent on very rough pavements and at higher traveling speeds (*8*). The values obtained in this analysis varied between 0.73 for a JXS and 1.11 for the trailer equipped with the leaf-spring suspension. These significantly lower numbers are because the random (white noise) displacement under the set of dual tires was not sufficiently high to simulate that type of highway operation. Furthermore, only one set of tires was excited. On normal highway operations all tires are simultaneously excited. Because of these two factors, the relative difference of RPL values obtained for the various suspensions and axle configurations can be considered significant, indicating different levels of performance. It is expected that larger RPL values and larger differences would be obtained if a high-speed test over a rough pavement were simulated. The relative difference may, however, be different because of nonlinearities in suspension behavior.

CONCLUSIONS AND RECOMMENDATIONS

From these studies the following conclusions can be made:

1. Because of nonlinearities in vehicle response, the frequency response functions must be determined within the amplitude range that is expected to be encountered in normal highway operations.
2. From tests conducted on the JXS trailer it was determined that the pistons had a 2,000-lb friction level. After modifications, a new piston was mounted and tested and a friction level of 600 lb was ascertained. The shaking table proved effective in these determinations.
3. From data obtained during the tests conducted on the shaking table it can be concluded that levels of the dynamic component of the loads induced by the JXS at normal highway operations are within the same range of magnitude as those produced by the other trailers studied.
4. In most analyses, comparisons of trailer or truck performance are based on the number of repetitions to failure that can be applied to a particular pavement section. According to this approach, the trailer equipped with a single axle would be recommended for yielding the maximum number of repetitions ($N = 22.6\,E + 6$). However, the main purpose of a road is not to withstand repetitions but to provide the means by which a payload can be transported from point A to point B. Therefore, an alternative method for comparing trailers is to compute the amount of payload they could carry over the life of a pavement. This value can be computed by multiplying the number of passes the pavement can withstand by the total load carried with each pass.

By applying this currently adopted methodology it is clear that a JXS-14 is capable of carrying more load over the life of the pavement section considered than any other trailer studied. In fact, it could carry about twice that carried by a semitrailer equipped with a single axle.

5. It is apparent that the semitrailer equipped with the leaf-spring suspension induces the highest dynamic components of the loads [highest RPL, DLR(w) and generally higher $H[L_1/b](w)$] and also exhibits the worst load distribution characteristics.

Both air bag suspensions exhibit a similar overall dynamic behavior. Whereas the RPL value for the tridem was worse than that of the tandem, the DLR(w) and the $H[L1/b](w)$ of the tridem were generally better than those of the tandem.

The relative difference of values suggests that the difference of performance between trailers equipped with leaf-spring suspensions and trailers equipped with air bag suspensions is greater than the difference between tridem trailers and tandem trailers equipped with air bags. From a dynamic point of view the effect of suspension type appears to be more significant than the number of axles.

6. A road test, despite its limited scope, indicated that the JXS operated at velocities of up to 60 mph with a maximum recorded vertical acceleration on the counter weight, over a rough portland cement concrete pavement section, of 0.15 *g* at a predominant frequency of 9 Hz. This value is expected to improve if the friction is significantly reduced in all pistons.

These conclusions enhanced the need of discussion and research in the following areas:

1. The determination of the frequency response function of trailers and trucks appears to be an effective tool for predicting trailer behavior. Tests should be conducted with a frequency sweep of at least a 0.1-Hz interval and with amplitudes varying within the range of values expected from highway operations. Road roughness data should be collected to make this possible.
2. On-the-road comparisons of the behavior of trucks and trailers should be made over pavement sections with various levels of roughness. Such tests should be performed to identify levels of roughness above which excessive damage is caused by the dynamic component of the loads. Furthermore "typical" sections of highway should be identified and surveyed to provide data for theoretical comparisons of trailers, suspensions, and axle configuration.
3. Further studies should be conducted to compare measured behavior (from item 2) to model predictions of stresses, strains, and deflections on pavements. A highly reliable model should be useful to evaluate new suspensions, load limits, and tire/axle configurations on pavements.
4. Use of the concept of "pounds carried per pavement life" could have major implications in the design, size, and characteristics of trucks and trailers and in the trucking industry overall.

REFERENCES

1. N. C. Nigan. *Introduction to Random Vibrations*. MIT Press, Cambridge, Mass., 1983.
2. M. W. Sayers. *Dynamic Terrain Inputs to Predict Structural Integrity of Ground Vehicles*. UMTRI-88-16. University of Michigan, Ann Arbor, April 1988.
3. J. B. Sousa. *Dynamic Response of Heavily Loaded Truck Trailers*. Report to CALTRANS, California Department of Transportation, Sacramento, December 1988.
4. F. N. Finn, C. Saraf, R. Kulkarni, K. Nair, W. Smith, and A. Abdullah. The Use of Distress Prediction Subsystems for the Design of Pavement Structures, Vol. 1. *Proc., 4th International Conference on the Structural Design of Asphalt Pavements*, University of Michigan, Ann Arbor, August 1977, pp. 3–38.
5. C. L. Monismith, F. N. Finn, G. Ahlborn, and N. Markevich. *A General Analytically Based Approach to the Design of Asphalt Concrete Pavements*. University of Michigan, Ann Arbor, 1987, pp. 344–365.
6. G. Hu. Simulation of Heavy Truck Ride Using a Desktop Computer. SAE Technical Paper Series 871557. Presented at the Future Transportation Technology Conference and Exposition, Seattle, Wash., August 1987.
7. C. E. Lee. Concepts of Weight-in-Motion. Presented to the National Weight-in-Motion Conference, Denver, Colo., July 1983.
8. J. B. Sousa, L. Lysmer, S. S. Chen, and C. L. Monismith. Dynamic Loads: Effects on the Performance of Asphalt Concrete Pavements. Presented at 67th Annual Meeting of the Transportation Research Board, Washington, D.C., January 1988.
9. S. S. Chen. *The Response of Multi-Layered Systems to Dynamic Surface Loads*. Ph.D. dissertation. University of California, Berkeley, June 1987.

Publication of this paper sponsored by Committee on Flexible Pavement Design.

Overlay Design Method for Flexible Pavements in Arizona

MICHAEL S. MAMLOUK, JOHN P. ZANIEWSKI, WILLIAM N. HOUSTON, AND SANDRA L. HOUSTON

A rational overlay design method for flexible pavements in Arizona, which includes roughness, fatigue, and plastic deformation models, has been developed. The roughness model is based on an analysis of the change in roughness because of overlay and the rate of change in roughness after overlay for typical Arizona roads. The fatigue model uses a shift factor to adjust existing fatigue criteria for the rate of crack development of pavements in the state. The plastic deformation model ensures that the overlay is thick enough so that expected traffic loads will not induce significant plastic deformations in underlying layers. The three design models are incorporated into a microcomputer program for computing the optimum overlay thickness, estimating the remaining life of an existing pavement, evaluating the life of a user-specified overlay, and performing economic analyses. Twenty in-service pavement sites were selected from Arizona highways covering various geographical and environmental regions, soil types, pavement conditions, and traffic volumes. Nondestructive tests were performed on these sites using the falling weight deflectometer at several stress levels, as well as Dynaflect tests. The layer elastic moduli were back calculated and adjusted for temperature. Asphalt concrete cores and undisturbed subgrade samples were collected and tested in the lab for modulus and other properties. The overlay design procedure has been verified with typical pavement sections in the state. Although the procedure in its current form applies to conditions in Arizona primarily, the design concepts can be used with conditions in other states.

For a variety of reasons, the number of new highway construction projects is steadily decreasing. As a consequence, a higher percentage of highway agency resources is being devoted to upgrading and maintaining existing highways. Thus, overlay design has moved into the forefront of pavement engineering.

The primary goal in overlay design is to provide a pavement that can withstand the applied traffic loads, throughout the design life, without failure, such as excessive cracking, rutting, or loss in serviceability. Fundamental engineering decisions include assessing which sections of highway require overlaying and how much overlay is needed. Mechanistically based design methods should be developed to close the gap between theory and practice and to upgrade the performance of the existing highway system.

The most commonly used overlay design approaches are (a) engineering judgment, (b) standard thickness, (c) empirical, and (d) mechanistic or mechanistic-empirical (*1*). Mechanistic approaches are preferred over others since they characterize the response of the pavement to a load based on basic parameters such as strains or stresses. On the other hand, failure is normally defined by specific mechanisms such as fatigue cracking or rutting, or both. Currently, no completely mechanistically based overlay design method exists. All mechanistically based methods depend in part on empirical relations between pavement parameters and the number of load applications the pavement can support before failure.

A number of overlay design methods for flexible pavements are available (*2–6*). Although these methods cover a wide variety of design concepts and applications, they may not be completely applicable to the conditions in Arizona. The main purpose of this study was to develop a mechanistic-empirical method of overlay design for flexible pavements that could be used by the highway personnel of the Arizona Department of Transportation (ADOT) with a high degree of confidence. In this study, the available overlay design methods were reviewed including a method that was developed by ADOT (*7*). It was decided that sufficient new data were available and could be collected to develop a new procedure tailored to the conditions in Arizona.

The overlay design method presented in this study was developed by the Center for Advanced Research in Transportation (CART) at Arizona State University. The design method was named CODA, which stands for CART Overlay Design for Arizona.

DATA COLLECTION

Currently, the existing highway network in Arizona is approximately 6,000 miles, including Interstate highways, U.S. routes, and state roads. The majority of this network is paved with asphalt. More than 50 percent of these roads are in excellent to good condition, whereas about 25 percent are in poor condition. In this study the data collection process can be divided into three groups: (a) data base search; (b) deflection measurement; and (c) sample collection and laboratory testing, as discussed in the following paragraphs.

Data Base Search

The Arizona Department of Transportation has an efficient, computerized pavement management system (PMS) file that includes various pavement data dating back to 1972. For each milepost of the highway network in the state, and for each year, data such as Maysmeter roughness, cracking, and friction number are available. Rutting data are available for

Department of Civil Engineering and Center for Advanced Research in Transportation, Arizona State University, Tempe, Ariz. 85287.

Interstate highways starting in 1986. Traffic data include average daily traffic, 18-kip equivalent single axle load (ESAL) in the current year, and the average annual traffic growth for the last 10 years. Other data are also available, such as the number of lanes, lane width, and shoulder width.

In addition to the PMS file, a pavement construction history file is available. The construction history file includes layer thicknesses, material types, and year of construction of each layer of the pavement network. These data are stored by construction project.

Deflection Measurement

Although a deflection data file is available in the ADOT computer data base, the available data were incomplete and taken at various dates and for various conditions. Therefore, falling weight deflectometer (FWD) tests were performed at 20 selected sites distributed throughout the state with good historical records. The criteria for the site selection include

1. availability of traffic data,
2. availability of material properties,
3. overlay history of the site,
4. current pavement condition,
5. geographical location, and
6. materials in the pavement structure.

Because one objective of the evaluation of the pavement sites was to permit the evaluation or development of performance models for overlaid pavements, factor 3 was very important. The most desirable pavement site would be one that had been overlaid one time with an overlay near the end of its service life. Sites that meet these criteria would provide direct data on the service life of overlaid pavements in Arizona.

The search process showed that it was not possible to identify 20 sites that completely met the criteria. Therefore, the selection was aimed at satisfying most of the criteria. The selected sites were uniformly distributed throughout the state and covered various climatic zones, as shown in Figure 1. The sites also covered a wide range of traffic volume, roughness, cracking, rutting, and friction number. The material types and layer thicknesses at the test sites are given in Table 1.

For the purpose of this study, FWD testing was performed in the outside wheel track at each site. Ten stations at 10-ft intervals were tested at each site starting at the milepost and proceeding in the direction of traffic. The pavement surface temperature was measured during the test to allow for temperature corrections in the computed modulus values for the asphalt bound layers. The FWD was operated at three load levels (6, 9, and 12 kip) at stations 1, 5, and 10 at each site, whereas a 9-kip load was used at the other stations. In addition to FWD, some sites were also tested using the Dynaflect for comparison and for the possible correlation between FWD results and those from previously gathered Dynaflect data. As expected, the FWD and the Dynaflect results were not well correlated. For the remainder of the study the FWD data were used in the development of the overlay design procedure, because the FWD can represent truck loads more accurately than can the Dynaflect. FWD tests were also conducted at a few locations using 6-, 9-, 12-, 15-, 18-, and 21-kip load

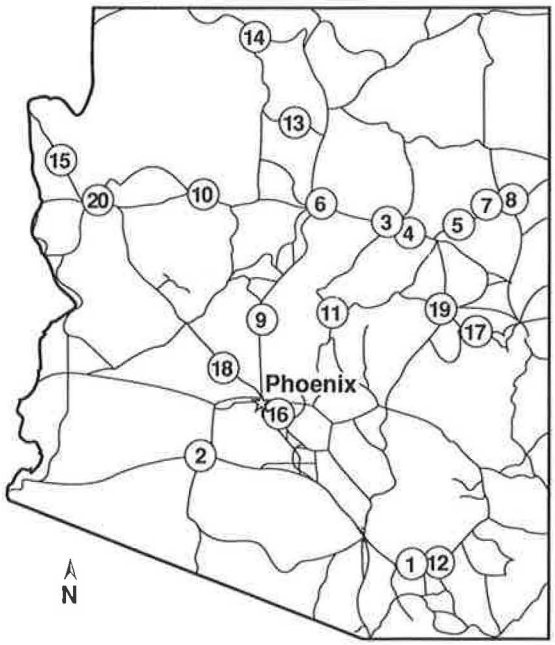

FIGURE 1 Selected test sites in Arizona.

TABLE 1 MATERIAL TYPES AND LAYER THICKNESSES AT THE TEST SITES

Site	AC Thickness (in.)	Base Material	Base Thickness (in.)	Subbase Material	Subbase Thickness (in.)	AASHTO Subgrade Classification
1	8.5	AB	3	SM	12	A-2-4 (0)
2	6	AB	3	SM	6	A-4 (2)
3	12.5	BTB	3	SM	6	A-4 (3)
4	12.5	BTB	3	SM	6	A-2-4 (0)
5	12.5	BTB	3	SM	6	A-2-4 (0)
6	12	AB	6	SM	10	-
7	7.5	CTB	6	SM	6	A-2-4 (0)
8	11	CTB	6	SM	6	A-4 (5)
9	6	AB	2	Sm	17	A-7-b (7)
10	6.5	AB	6	SM	22	-
11	3.5	BS	2	-	-	A-4 (1)
12	6.5	AB	6	SM	15	A-1-b (11)
13	4	BS	3	AB	3	-
14	9	BS	4	AB	4	A-7-b (11)
15	6.5	BS	3	AB	6	A-1-b (0)
16	4.5	BS	2	SM	9	A-2-4 (0)
17	3	BS	2	SM	6	-
18	4	AB	4	SM	15	A-1-b (0)
19	7	AB	3	SM	6	A-4 (2)
20	9.5	AB	4	SM	15	A-1-a (0)

Note AC = Asphalt Conrete
AB = Aggregate Base
BTB = Bituminous Treated Base
CTB = Cement Treated Base
BS = Bituminous Treated Surface
SM = Select Material

levels for the purpose of development of the plastic deformation models.

In addition to deflection measurements, cone penetration tests (CPT) were performed at all 20 sites to investigate the homogeneity of the subgrade material and to measure the depth to bedrock, if any. The CPT provided some understanding of the layering system within the subgrade. However, the test has proven to be impractical for design purposes, primarily because of the high cost and the lack of a precise relationship between CPT and modulus. Therefore, the CPT test results were not used in the development of the overlay design procedure. The analysis of the CPT data is discussed elsewhere (*8*).

Sample Collection and Laboratory Testing

At each of the 20 sites, cores were taken from asphalt concrete layer and the stabilized base layer if available. Disturbed samples were also taken from untreated base and subbase materials as well as from subgrade materials. Undisturbed samples were also collected from subgrade materials using Shelby tubes. During the sampling process, material types and layer thicknesses were recorded, to a depth of about 25 ft, unless bedrock was encountered at a shallower depth.

Asphalt concrete cores were trimmed and tested in the laboratory to determine their diametral resilient modulus according to ASTM D4123 test procedure. The test was performed at temperatures of 41°F, 77°F, and 104°F. Several cores from each site were tested.

The undisturbed subgrade samples were tested in the laboratory using the triaxial resilient modulus test. The test followed the AASHTO T274 test procedure with some modifications (*8*). At least one sample was tested from each site. In addition to resilient modulus testing, sieve analysis and Atterberg limits were performed on subgrade materials. Sieve analysis tests were also conducted on untreated base and subbase materials.

BACK CALCULATION OF MODULI AND COMPARISON WITH LABORATORY MODULI

For the development of the overlay design method, the layer moduli were back calculated using an operator-controlled trial-and-error computer procedure rather than one of the available computer back calculation programs. The reasons for this trial-and-error procedure were to allow for better estimation of moduli values and to allow for the use of five layers above the bedrock to model the pavement system. Thus, the pavement system was represented by asphalt concrete layer, base, subbase, 9-in. compacted subgrade layer, and uncompacted subgrade. In this procedure, a set of typical layer moduli and a specific depth to bedrock were assumed, and the Chevron program (*9*) was used to compute the surface deflections. The layer moduli, as well as the depth to bedrock, were then varied based on the fact that deflections remote from the loaded area are primarily governed by the stiffness of deeper layers. This process was repeated until the computed deflections were close to the measured deflections.

The trial-and-error back calculation procedure was used as a research tool only, in an effort to enhance understanding of the problem and to aid in the subsequent simplification. For the purpose of the routine overlay design, the microcomputer program BKCHEVM was developed to provide an automated back calculation procedure (*8*). The BKCHEVM program is based on the CHEVDEF program (*10*), developed by the U.S. Army Corps of Engineers, with some modifications to simplify use and to improve convergence.

The back calculated moduli of both asphalt concrete surface and subgrade materials were compared with laboratory moduli. In general, back calculated and laboratory moduli were not well correlated. A number of factors that might contribute to these differences were considered and verified with the results obtained from cone penetration testing. The detailed results of this comparison are presented elsewhere (*8*). For the purpose of overlay design, it was concluded that the moduli back calculated from FWD testing are more appropriate for the design process than those obtained from laboratory testing (*8*).

DEVELOPMENT OF OVERLAY DESIGN METHODOLOGY

The majority of roads in Arizona are built with asphalt. These roads vary from heavily traveled Interstate highways to sparsely traveled secondary roads. The state covers a large area from hot desert to snowy highland. Subgrade material type also varies from one part of the state to another, whereas moisture conditions vary depending on the location and season.

Based on the experience of ADOT personnel and the available pavement management data base, the primary mode of failure for flexible pavements in Arizona is roughness. In fact, about 80 percent of overlaid pavements in the state were overlaid because of excessive roughness, about 15 percent because of excessive cracking, and about 5 percent because of rutting. Therefore, three separate design criteria were developed in this study for roughness, fatigue cracking, and plastic deformation as a part of CODA method.

Figure 2 shows the flow of calculations required to meet the problem constraints. A general set of input data is required to define the parameters of the problem. The analyst can then select one or more of four options: overlay design, remaining life of an existing pavement, life of a user-specified overlay, or economic analysis. If the user selects the overlay design option, the roughness, fatigue, and plastic deformation models are used to obtain the required overlay thickness. If the user selects the remaining life option, the program uses both roughness and fatigue models to evaluate the remaining life. If the user selects a specific overlay thickness, the program determines its life based on both roughness and fatigue models. Finally, the user has the option of performing an economic analysis to determine the equivalent uniform annual cost of four rehabilitation strategies: overlay only, mill plus overlay, mill and recycle plus overlay, and reconstruction. The development of the roughness, fatigue, and plastic deformation models are described in the following sections.

Roughness Model

Roughness is the single measure of pavement performance or condition that correlates with the highway user's opinion of

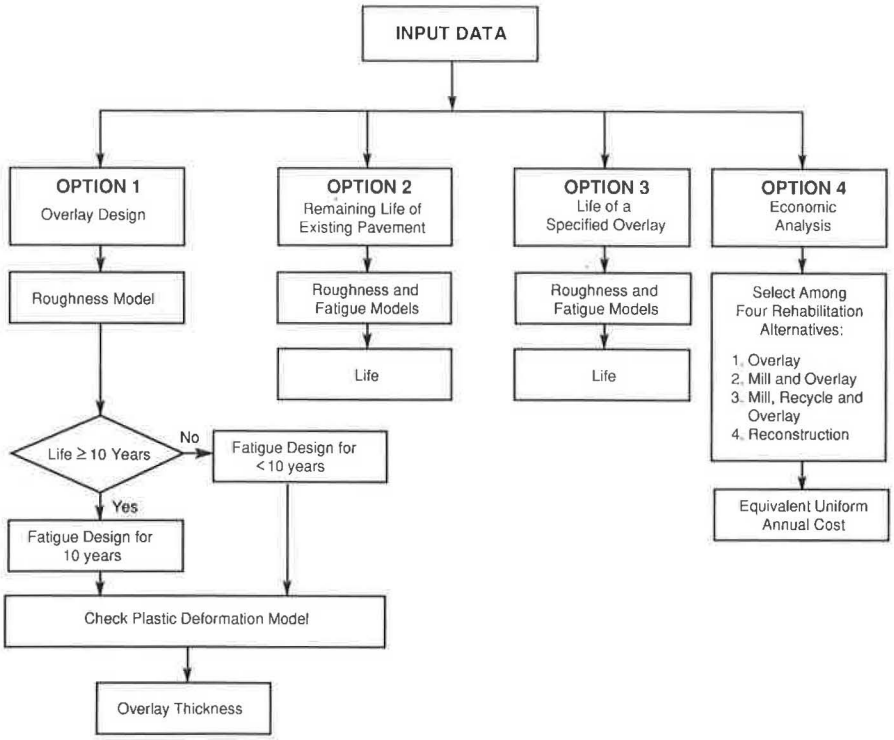

FIGURE 2 Flow chart of the overlay design procedure.

the quality of the pavement. Roughness criteria are a major factor in the project selection process used in ADOT's pavement management system. Thus, a roughness model is an important component in the overlay design process.

Roughness is generally defined as random variations in the longitudinal profile of the pavement surface. The development of random variations in the profile depends on such factors as traffic loads, environment, soil support, and construction variations. The number of variables, and their interactions, that contribute to the development of roughness are too numerous to permit rigorous mathematical modeling. Hence, empirical methods are used for the development of roughness models. Fortunately, the ADOT pavement management data base provides an extensive source of data for the development of roughness performance models. All ADOT roughness data are measured by using the Maysmeter device. A correlation model is available to convert from Maysmeter roughness reading to present serviceability rating (7).

In an overlay design method, two forms of roughness models are required: the change in roughness of the pavement caused by overlay and the rate of roughness development as a function of either time or traffic.

For the development of roughness performance models, the ADOT microcomputer PMS data base was queried to identify all overlay projects constructed since 1960. The projects selected for the analyses had "conventional" overlays, i.e., an asphalt concrete layer placed directly on an existing pavement surface. Other rehabilitation options such as milling, recycling, and asphalt-rubber membranes, were excluded from the data base analyzed during this project.

The data were separated into homogeneous overlay projects. A homogeneous overlay project is defined as having a constant project number, route number, direction, and overlay thickness. The data fields were then averaged across each milepost included in each project. Thus, the roughness data used for statistical analyses consisted of the average for the project for each year. Data for Interstate, state, and U.S. routes were analyzed separately.

Change in Roughness Caused by Overlay

Included in the analysis of the change of roughness are all overlay projects performed since 1972. The initial roughness after an overlay is modeled as the roughness before the overlay minus the reduction in roughness caused by the overlay. The data were analyzed by using various statistical models. The level of roughness after overlay and the change in roughness caused by the overlay were used as dependent variables. The roughness before overlay, thickness of overlay, and type of surfacing layer were used as independent variables.

A multiple regression analysis was performed to define equations for the change in roughness. Only routes with roughness of more than 100 in. per mile before overlay were included in the regression analysis. The smooth pavements were removed from the analysis to avoid placing an artificial limit on the change in roughness that could be obtained with an overlay. For each highway type, there was a strong relationship between the change in roughness and the roughness before overlay.

The reduction in roughness caused by overlays versus the roughness before overlay is shown in Figure 3 for Interstate highways. There is a definite trend between the change in roughness and the roughness before overlay. This trend is expected simply because there is a greater opportunity to improve the roughness of rough roads than to improve the roughness of smooth roads. It is interesting to note from this graph that several routes with relatively low roughness were overlaid. Similar trends were also obtained for U.S. and state routes.

An indicator variable was used to determine if the construction project included an asphalt concrete friction course, ACFC. All Interstate projects had ACFC layers, so this factor could not be evaluated for Interstates. ACFC layers were used on about one-third of both U.S. and state routes. The regression equations for change in roughness are

$$\Delta R = -61.76 + 0.940R_b \qquad R^2 = 0.86 \qquad (1)$$

$$\Delta R = -78.82 + 0.900R_b + 0.104KR_b \qquad R^2 = 0.88 \qquad (2)$$

$$\Delta R = -97.12 + 0.938R_b + 0.153KR_b \qquad R^2 = 0.89 \qquad (3)$$

for Interstates, U.S. routes, and state routes, respectively, where

ΔR = roughness before overlay − roughness after overlay (in./mi);
R_b = roughness before overlay (in./mi);
K = ACFC indicator;
K = 1 if ACFC was placed; and
K = 0 for no ACFC.

It is interesting to note that the slope of the relationship between the change in roughness and the roughness before overlay is almost identical across the three highway types.

The change in roughness versus overlay thickness is shown in Figure 4 for Interstate highways. This figure does not show any identifiable correlation between overlay thickness and the change in roughness caused by the overlay. Again, similar trends were obtained for U.S. and state routes.

Rate of Change in Roughness

For each project a regression analysis was performed between roughness and time to find the rate of increase of roughness (inches per year) after an overlay. For projects overlaid before 1972, the rate was calculated using the data between 1972 and 1987 because no roughness data before 1972 were available. A linear model was used for the change of roughness versus time. Nonlinear models were tested, but they led to improved correlation. The slope of the relationship between roughness and time was used to define the rate of change in roughness. Figure 5 shows a typical relationship between roughness and years since overlay for Interstate highways. U.S. and state routes provided similar trends.

For most projects, there was a strong correlation between roughness and time. The average changes in roughness per year in inches per mile, as measured with the Maysmeter, are 6.7 for Interstates, 5.1 for U.S. routes, and 5.8 for state highways.

The independent variables available in the data base were the regional factor, ESAL, structural number, and the overlay thickness. Graphs of the rate of change of roughness (inches per year) and the above variables for Interstates, U.S. routes, and state routes were analyzed but did not show any specific trends. A multiple regression analysis was performed for each class of highway taking the rate of increase of roughness as the dependent variable and the regional factor, ESAL, struc-

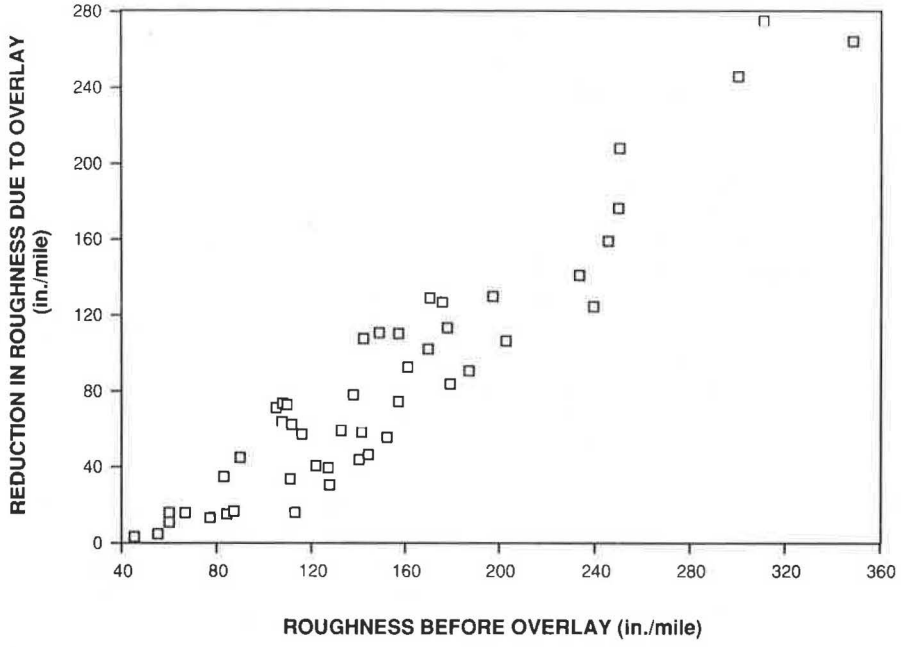

FIGURE 3 Reduction in roughness caused by overlay versus roughness before for Interstate highways.

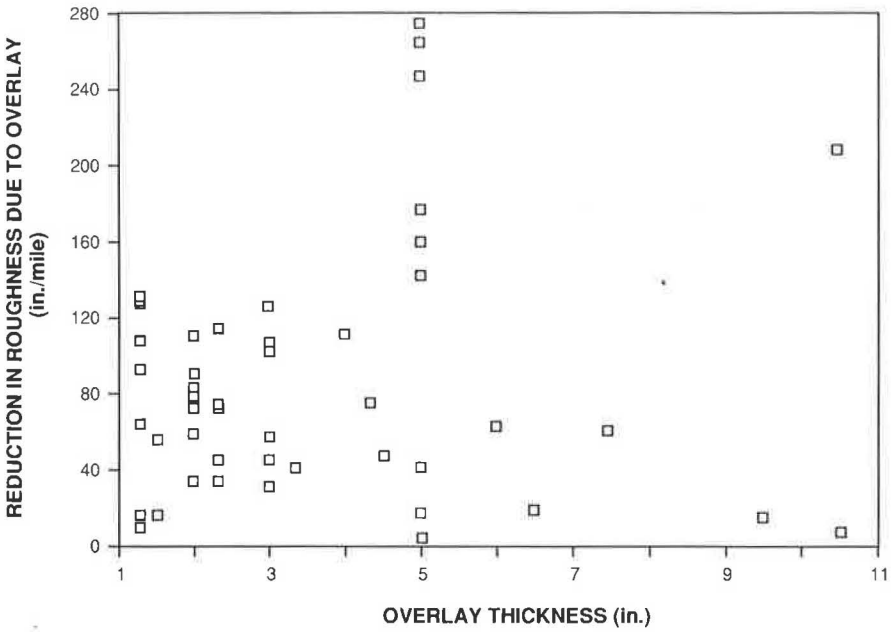

FIGURE 4 Reduction in roughness caused by overlay versus overlay thickness for Interstate highways.

tural number, and overlay thickness as independent variables. Forward stepwise regression analyses were performed but no correlations were detected.

Since none of the independent variables was correlated with the rate of change in roughness, models could not be developed for predicting the increase in roughness as a function of pavement design variables. Hence, the average rate of change in roughness for each highway type can be used for estimating the performance of overlays.

Overlay Life

The conceptual model used to develop the roughness model is shown in Figure 6. The life of an overlay may be estimated by

$$N = (R_L - R_b + \Delta R)/C \tag{4}$$

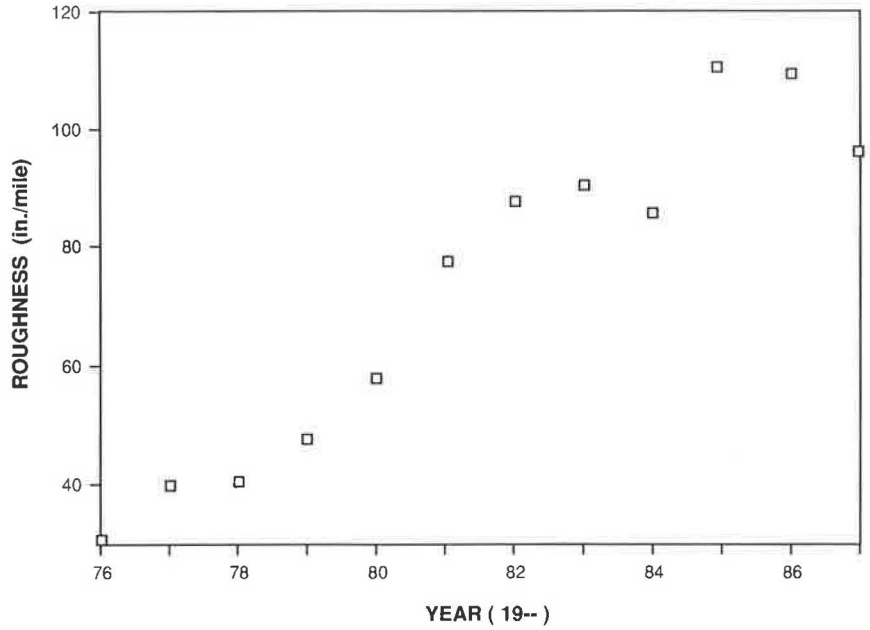

FIGURE 5 Typical rate of change of roughness versus time for an Interstate overlay project.

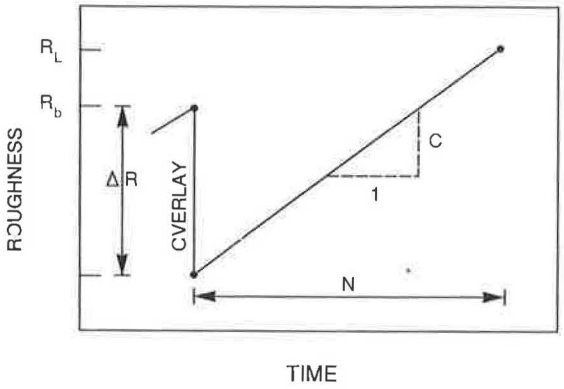

FIGURE 6 Conceptual model for roughness.

where

N = life of overlay until roughness failure in years;
R_L = limiting criteria for roughness (in./mi);
R_b = roughness before overlay (in./mi);
ΔR = predicted change in roughness caused by overlay (in./mi); and
C = rate of change in roughness per year.

The roughness of the section to be overlaid (R_b) is determined by direct measurement with the Maysmeter. Alternatively, R_b may be determined from the ADOT PMS data base. The change in roughness (ΔR) is estimated with Equation 1, 2, or 3 for Interstate, U.S., or state routes, respectively. The roughness level corresponding to the failure of the overlay is designated by R_L. Using relationships previously developed by ADOT, R_L would equal 260 for a present serviceability rating (PSR) of 2.5, and 190 for a PSR of 3.0 (*7*). The selection of an R_L value is a policy decision by ADOT and is in line with the procedures used in the department's pavement management system. The value of R_L can be selected as a function of highway type.

Since Equation 4 is not a function of overlay thickness, it cannot be used to determine the thickness requirements directly. In other words, previous experience with Arizona highways indicates that any practical overlay thickness will support approximately the same number of load applications before reaching the roughness failure condition. Since the normal overlay design life in Arizona is 10 years, Equation 4 can be used to check if a 10-year life is feasible. If the roughness equation results in an overlay life of 10 years or more, the roughness model is satisfied and the overlay is later designed for a 10-year life using the fatigue model. On the other hand, if the roughness equation results in a predicted overlay life of less than 10 years, this shorter life is used as the fatigue life for the fatigue deformation model unless milling or another special treatment is used.

Fatigue Model

The evaluation of fatigue life for asphalt concrete pavements is complex and has been the subject of study by a number of researchers for many years (*11*). The form of the fatigue relations in common use is derived from a logarithmic relation between strain and the number of load cycles to fatigue failure. The relations between the logarithm of strain and the logarithm of load cycles are considered to be linear for asphalt concrete, which results in the following general equation:

$$N_i = K_1 \left(\frac{1}{\varepsilon_i}\right)^{K_2} \tag{5}$$

where

N_i = number of load cycles at strain level i until fatigue failure,
ε_i = calculated tensile strain at the bottom of asphalt layer, and
K_1, K_2 = empirical material constants.

A very important problem with this form of fatigue life characterization is the extreme sensitivity of the equation to small variations in K_2. A number of fatigue models have been developed in previous studies, as shown in Figure 7 (*11*). The slopes (K_2) of these logarithmic functions shown in Figure 7 range between 2.70 and 5.51, with an average value of 3.84.

Model Development

The fatigue model developed in this study is based on data obtained from the 20 selected sites and the fatigue models previously developed by other researchers (Figure 7). Using the 20 Arizona sites, the first step was to compute the cumulative ESALs in the design lane that were applied on the first AC layer, the first overlay (if any), the second overlay (if any), and so on.

Because each site has environmental conditions different from those of other sites, the ESAL data had to be normalized. The regional factor that is currently used by ADOT was selected as an adjustment factor to account for the difference in environmental conditions among various sites (*12*). It was further assumed that the regional factor changes the effect of traffic loads in a linear manner.

Another adjustment that had to be considered was because of the tensile strain at the bottom of the AC layer caused by standard wheel load changes when the pavement is overlaid. In other words, changing the pavement cross-section changes the strain level that the pavement is exposed to when the same load is applied at the pavement surface. Therefore, the ESAL applications had to be adjusted to a single strain level for each site.

For the original pavement, the critical strain for fatigue is at the bottom of the AC layer and when an overlay is placed, the critical strain is still at the bottom of the original AC layer (as long as there is no cracking); however the strain is reduced because of the overlay. In this case Equation 5 becomes

$$N_1 = K_1 \left(\frac{1}{\varepsilon_1}\right)^{K_2} \tag{6}$$

$$N_2 = K_1 \left(\frac{1}{\varepsilon_2}\right)^{K_2} \tag{7}$$

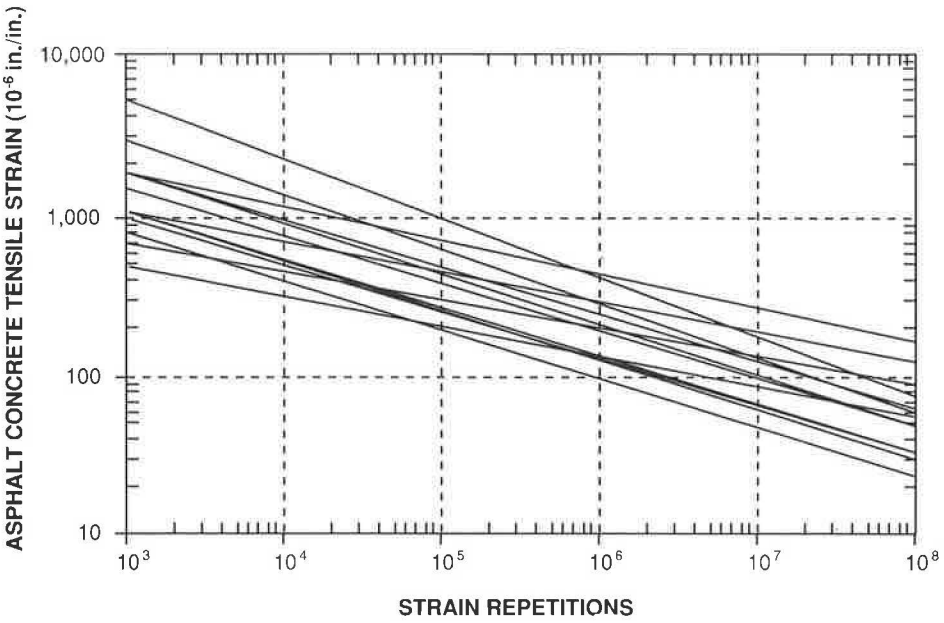

FIGURE 7 Some fatigue relations obtained by other researchers (*11*).

From Equations 6 and 7,

$$\frac{N_1}{N_2} = \left(\frac{\varepsilon_2}{\varepsilon_1}\right)^{K_2} \tag{8}$$

where ε_1 and ε_2 are the strains at the bottom of the original AC before and after overlay, respectively. Thus, the ESAL after overlay has to be adjusted according to Equation 8, then added to the ESAL before overlay to calculate the total ESAL that is matching the tensile strain before overlay (reference strain). The K_2 value was taken as 3.84, which is the average of K_2 values of existing fatigue functions (*11*). If the old AC layer is cracked, the ESAL before overlay cannot be added to the ESAL after overlay and the periods before and after overlay have to be treated separately. In this study the AC layer was considered to be cracked if cracking was 10 percent or more. It was also assumed that cracking is caused only by fatigue.

The tensile strain was calculated by using the Chevron computer program (*9*) for a standard dual-tire load of 9,000 lb and a tire pressure of 100 psi. The back calculated layer moduli previously obtained and adjusted to a standard temperature of 70°F were used. No adjustment was used for tire pressure since the tire pressure in Arizona has not changed significantly in recent years, with an average value in the high 90s and an 80th percentile of slightly more than 100 psi (*13*). In addition, the FHWA study (*14*) showed that the strain at the bottom of the AC layer is not largely affected by minor changes in tire pressure.

The total adjusted cumulative ESAL was plotted versus the reference tensile strain using a log-log scale as shown in Figure 8. A straight line (fatigue function) was selected close to the upper boundary of the band of previous fatigue functions (*11*) with a slope of 3.84. This selected fatigue line lies above most of the uncracked pavement sections, which indicates that uncracked sections have some remaining life. A few uncracked sections lie above the fatigue line, and several cracked sections lie below the line, which indicate some discrepancies. These discrepancies are, however, considered acceptable. The equation of the selected fatigue function is

$$N = 9.33 \times 10^{-7} \left(\frac{1}{\varepsilon_{AC}}\right)^{3.84} \tag{9}$$

where

N = theoretical number of ESAL repetitions until fatigue failure, and
ε_{AC} = tensile strain at the bottom of the AC layer.

Equation 9 is valid for various conditions such as various regions and temperatures because these conditions were normalized to standard conditions. Therefore, if the tensile strain at the bottom of the AC layer is known under these standard conditions, the number of ESAL repetitions until fatigue failure can be computed.

Use of the Fatigue Model

To use the fatigue model, a multilayer elastic program such as Chevron can be used to compute the tensile strain at the bottom of the AC layer caused by a 9,000-lb dual-tire load. The layer moduli can be obtained from the FWD back calculation as discussed earlier.

In many cases the pavement is overlaid before it is significantly cracked. Therefore, the remaining fatigue life of the existing pavement has to be considered and added to the overlay life. This calculation can be accomplished by using the concept of cumulative damage (Minor's law) (*15*). Thus, the optimum overlay thickness is the one that satisfies the following equation.

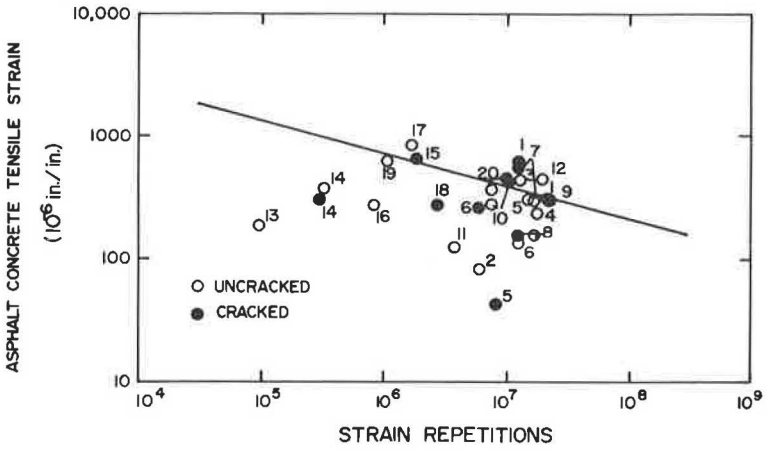

FIGURE 8 Asphalt concrete tensile strain versus strain repetitions for the 20 test sites.

$$\frac{n_1}{N_1} + \frac{n_2}{N_2} = 1$$

$$n_2 = N_2\left(1 - \frac{n_1}{N_1}\right) \tag{10}$$

where

n_1 = actual cumulative ESAL in the design lane before overlay,
N_1 = allowable cumulative ESAL in the design lane before overlay,
n_2 = actual cumulative ESAL in the design lane after overlay, and
N_2 = allowable cumulative ESAL in the design lane after overlay.

To reach this optimum overlay thickness, trial thicknesses can be used and the corresponding cumulative ESALs for each overlay can be computed. A polynomial equation is then fitted to compute the optimum overlay thickness that matches the expected ESAL.

If the existing pavement has been previously overlaid more than once and cracking has not reached 10 percent, the cumulative fatigue is added for each AC thickness. In all cases, the tensile strain is computed at the bottom of the original AC layer.

On the other hand, if the old pavement (before overlay) is cracked (10 percent or more), it is assumed that the old AC layer will not contribute to the cumulative fatigue life after overlay. Therefore, the tensile strain is computed at the bottom of the overlay, and the modulus of the original asphalt surface is assumed to be 40,000 psi.

Plastic Deformation Model

Damage to a pavement structure can arise through a variety of mechanisms, including plastic deformations in the layers of the structure. The ultimate result of these deformations may be cracking, rutting, or simply the development of excessive roughness. However, the initial cause being considered in this part of the design process is plastic or permanent deformations.

This design model deals only with plastic deformations in layers below the AC surface layer. It is assumed that plastic deformations in the overlay layer will be reduced or prevented by improvements in mix design and construction techniques.

In the plastic deformation model, attention is devoted to the plastic strains that are permanent, i.e., not recoverable. However, permanent deformations are much more troublesome to measure in the field than total deformations (elastic and plastic). It has therefore been assumed that the onset of significant plastic deformation corresponds to the onset of nonlinear load deflection response. In other words, as long as the load deflection curve is linear, it is assumed that the plastic deformations are negligible.

Two types of nonlinearity may arise: strain hardening or strain softening. Strain-hardening nonlinearity is believed not to represent a problem to plastic deformation. Therefore, only strain-softening nonlinearity is considered in this model.

Based on data examined to date, it is believed that most pavement sections under consideration for an overlay have sufficient factor of safety in the structural design that plastic deformations are unlikely to be a source of problem. This part of the design procedure is intended to detect and correct those few cases in which vulnerability to excessive plastic deformations is indicated by the FWD test results. Thus, the objective of this design procedure may be stated as follows. When the pavement gets older, the ability of the pavement surface to spread the load to the underlying layers may be decreased because of cracking or other surface failures. In addition, the pavement might be subjected to heavier traffic loads in the future that have not been applied before. Therefore, the objective of plastic deformation design is to provide sufficient overlay thickness that expected traffic loads will not induce significant plastic deformations in the underlying layers.

The design procedure is based on the assumption that the onset of significant nonlinear response can be measured directly with the FWD test. The load corresponding to the onset of significant nonlinear response is designated F_{NL}. The exact

point at which deviation from linear behavior occurs is difficult to select. Therefore, F_{NL} has been defined as the load at which the load deformation curve deviates 10 percent, measured horizontally, from the straight-line extension of the early portion of the curve, as shown in Figure 9.

The detailed step-by-step procedure for the plastic deformation overlay design is as follows.

1. Input existing pavement structure geometry, moduli from back calculation analyses, and highway type (Interstate, U. S., or state).
2. Input FWD data for loads from 6 kip to 15 kip or more. Use 6- 12-kip data to establish the straight line (least-squares fit) and check the higher loads for deviation from the straight line at each sensor.
3. If none of the loads shows 10 percent or more deviation, report that F_{NL} is greater than the maximum FWD applied load and bypass plastic deformation design. If one or more loads show deviation $\geq$10 percent, proceed to step 4.
4. Use linear interpolation to find the load corresponding to 10 percent deviation (F_{NL}).
5. In comparing the stress states, several different stresses at various points in the underlying layers were considered. The maximum octahedral shear stress, $(\tau_{oct})_{max}$, in the subgrade was chosen because it reflects all the components of the stress tensor (*16*). Therefore, use Chevron program with F_{NL} applied to the FWD plate to calculate the maximum τ_{oct} that occurs in the subgrade.
6. Determine the design load (F_{des}), which is the load on a dual wheel that can be used in checking the adequacy of a trial overlay design thickness. The value of F_{des} is chosen so that the probability of an actual dual wheel load exceeding this value is very small. The degree of conservatism in this part of the design can be controlled through the choice of this probability. A sample of axle loads obtained from Arizona highways showed that the selected probabilities were 0.00001, 0.00008, and 0.00008 for Interstate, U.S., and state highways, respectively. These probabilities resulted in an expected number of dual wheel load values exceeding F_{des} of about seven in 1 year.
7. Use Chevron program with F_{des} applied to a dual wheel and calculate the maximum τ_{oct} in the subgrade.

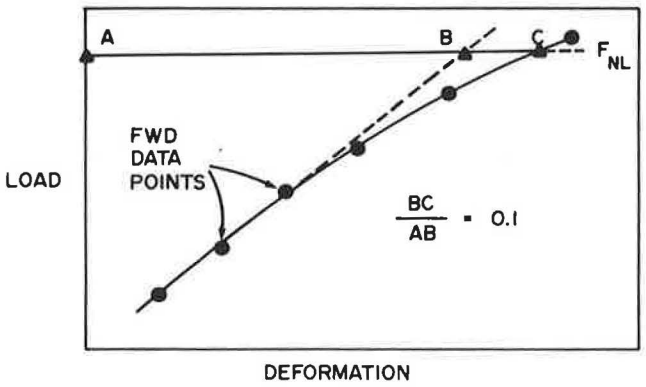

FIGURE 9 Nonlinearity of underlying layers and definition of onset of significant nonlinear response.

8. If τ_{oct} caused by F_{des} is less than or equal to τ_{oct} caused by F_{NL}, report this fact and bypass plastic deformation design. If not, proceed to step 9.
9. With the overlay obtained from fatigue analysis in place, use Chevron program with F_{des} applied to a dual wheel and calculate τ_{oct} in the subgrade.
10. If τ_{oct} in step 9 is less than or equal to τ because of F_{NL}, the pavement is safe against plastic deformation with the overlay. If τ_{oct} in step 9 is more than τ_{oct} caused by F_{NL}, proceed to step 11.
11. Increment the thickness of the overlay in steps until τ_{oct} caused by F_{des} is equal to τ_{oct} caused by F_{NL}.

The preceding step-by-step procedure, including computation of τ_{oct}, has been programmed in the CODA program. The needed parameters have been fixed and the entire plastic deformation design procedure has been automated. The user is required only to input the data indicated in steps 1 and 2. Of course, modifications to the "fixed values" can be made readily to the program if desired. Users who desire to use the plastic deformation model independent of the fatigue analysis should proceed to step 11 after step 8.

It should be noted that the plastic deformation model deserves to be called mechanistic because it addresses permanent deformations, a particular mechanism of damage. Even though some plastic deformation occurs with every load application, the intent of this procedure is to keep the plastic deformations small. This intention corresponds to an attempt to maintain the deformations almost entirely within the elastic range. An extension of this method to include an estimate of the "expected life" of a pavement structure, with respect to plastic deformation, is theoretically possible. However, the art and science of predicting plastic deformations is not sufficiently well developed to justify this extension at the present time.

Complete Overlay Design

The three models—roughness, fatigue, and plastic deformation—were incorporated in the overlay microcomputer program CODA. The traffic load requirement in this method of overlay design is the cumulative 18-kip ESAL in the design lane during the design period. Some existing pavement condition parameters are also needed, such as Maysmeter roughness reading and cracking. Pavement layer thicknesses, material type, previous overlays, if any, and years of construction are also needed.

Since both fatigue and plastic deformation models require the knowledge of pavement and subgrade layer moduli, the first step in the procedure is to run the FWD test on the pavement section under consideration. The fatigue model requires performing the FWD test at a load level of 9,000 lb only, whereas the plastic deformation model (if used) requires running the FWD test at several load levels as discussed earlier.

The FWD deflection data at a 9,000-lb load level are further used to back calculate the pavement and subgrade layer moduli. Since the modulus of the AC layer is significantly affected by temperature, a subroutine was developed in the CODA program to adjust the AC modulus to a standard temperature of 70°F based on the AASHTO guide (*6*).

In addition to overlay design, other features have been incorporated in the CODA program, such as the ability to compute the remaining life of an existing pavement, the life of a user-specified overlay, and economic analysis.

The CODA method of design has been verified with typical pavement sections in Arizona. Although the long-term field performance has not been evaluated, preliminary evaluations indicate that the results are reasonable. A computer workstation has been developed to automate the design process, extract the required data from the data base files directly, and allow a user-friendly procedure.

Although the CODA procedure in its current form applies to Arizona conditions only, the design concepts can be used with other conditions. For example, the rate of change of roughness, the rate of crack development, and axle load distributions can be changed to match the conditions in other states.

SUMMARY AND CONCLUSIONS

In this study a rational overlay design method for flexible pavements in Arizona has been developed. The method combines mechanistic approaches and historical performance of pavements in the state. Three models were developed for design: roughness, fatigue, and plastic deformation. The roughness model is based on the trend of the Maysmeter roughness data of overlaid pavements in the state. The fatigue model considers the fatigue experience of pavements in the state as well as fatigue criteria developed by others. The plastic deformation model ensures that the expected traffic loads will not induce significant plastic deformations in the underlying layers.

The development of the method involved coring and sample collection, laboratory testing, statistical analyses, and computer programming. Twenty in-service pavement sites were selected from Arizona highways covering various geographical and environmental regions, soil types, pavement conditions, and traffic volumes. FWD and Dynaflect tests were performed and the layer moduli were back calculated. In addition, resilient moduli were also evaluated in the laboratory. The back calculated and laboratory moduli were compared and found to be not well correlated. It was concluded that the back calculated moduli from the FWD are more representative of field conditions than of laboratory moduli. Application of the design method CODA requires FWD data but no sample collection or laboratory testing.

The overlay design method developed in this study was incorporated in a user-friendly microcomputer program. The method was verified on typical pavement sections and found to provide reasonable results. Although the method is based on data obtained from Arizona, the design concepts can be applied to conditions in other states.

ACKNOWLEDGMENTS

The authors would like to thank the Arizona Department of Transportation (ADOT) and FHWA for the financial support of this research project. Special thanks go to ADOT personnel, especially J. Delton, J. Eisenberg, F. McCullagh, L. Scofield, and G. Way, for their valuable input and assistance during the course of the project. Thanks are also extended to the Center for Advanced Research in Transportation and the Department of Civil Engineering at Arizona State University for making their facilities available to the authors. R. Perera and T. Anderson, graduate assistants at Arizona State University, performed much of the analysis and program development reported in this paper.

REFERENCES

1. R. E. Smith, M. I. Darter, and R. L. Lytton. Mechanistic Overlay Design Procedures Available to the Design Engineer. In *Transportation Research Record 1060*, TRB, National Research Council, Washington, D.C., 1986.
2. C. L. Monismith and F. N. Finn. Overlay Design—A Synthesis of Methods. *Association of Asphalt Paving Technologists*, Vol. 53, 1984.
3. R. L. Lytton and R. E. Smith. Use of NDT in the Design of Overlays for Flexible Pavements. In *Transportation Research Record 1007*, TRB, National Research Council, Washington, D.C., 1985.
4. R. E. Smith, R. P. Palmieri, M. I. Darter, and R. L. Lytton. *Pavement Overlay Design Procedures and Assumptions, Vol. I, II, and III.* Report FHWA/RD-85/006-008. Federal Highway Administration, U.S. Department of Transportation, October 1984.
5. M. R. Thompson. *Concepts for Developing a Nondestructive Based Asphalt Concrete Overlay Thickness Design Procedure.* Illinois Department of Transportation, Department of Civil Engineering, University of Illinois, Urbana-Champaign, 1982.
6. *AASHTO Guide for Design of Pavement Structures.* AASHTO, Washington, D.C., 1986.
7. G. B. Way, J. F. Eisenberg, J. P. Delton, and J. E. Lawson. Structural Overlay Design for Arizona. *Association of Asphalt Paving Technologists*, Vol. 53, 1984.
8. M. S. Mamlouk, W. N. Houston, S. L. Houston, and J. P. Zaniewski. *Rational Characterization of Pavement Structures Using Deflection Analysis.* Vol. 1. Final Report, Arizona Department of Transportation, Phoenix, December 1988.
9. J. Michelow. *Analysis of Stresses and Displacements in an N-Layered Elastic System Under a Load Uniformly Distributed on a Circular Area.* California Research Corporation, Richmond, Calif., Sept. 1963.
10. A. J. Bush. *Nondestructive Testing for Light Aircraft Pavements.* Phase II, U.S. Army Engineer Waterways Experiment Station, Geotechnical Laboratory, Vicksburg, Miss., Nov. 1980.
11. J. B. Rauhut and T. W. Kennedy. Characterizing Fatigue Life for Asphalt Concrete Pavements. In *Transportation Research Record 888*, TRB, National Research Council, Washington, D.C., 1982.
12. *Preliminary Engineering and Design Manual.* Report ADOTM-XII-TWO-C. Arizona Department of Transportation, Phoenix, Jan. 1985.
13. R. A. Jimenez. *Structural Design of Asphalt Pavements.* Arizona Transportation and Traffic Institute, University of Arizona, Tucson, Nov. 1975.
14. R. Bonaquist, C. Churilla, and D. Freund. Effect of Load, Tire Pressure Type on Flexible Pavement Response. Presented at 67th Annual Meeting of the Transportation Research Board, Washington, D.C., 1988.
15. M. A. Minor. Cumulative Damage in Fatigue. *Transactions of the American Society of Mechanical Engineers*, Vol. 67, 1945.
16. J. C. Jaeger. *Elasticity, Fracture and Flow*, 2nd ed. Wiley, New York, 1962.

Publication of this paper sponsored by Committee on Flexible Pavement Design.

MICH-PAVE: A Nonlinear Finite Element Program for Analysis of Flexible Pavements

RONALD S. HARICHANDRAN, MING-SHAN YEH, AND GILBERT Y. BALADI

A nonlinear mechanistic finite element program called MICH-PAVE has been developed for use on personal computers to aid in the analysis and design of flexible pavements. The program has three major features. First, it utilizes a newly developed flexible boundary concept for pavement analysis. Second, it uses performance models for the prediction of fatigue life and rut depth, utilizing results of the mechanistic analysis (stresses, strains, and other pavement variables). Third, it is "user-friendly." The program was developed for the Michigan Department of Transportation and is in the public domain. The methodology used, and the features of the program, are described.

More and more in recent years pavement design is being based on mechanistic analysis. The migration from empirical methods to mechanistic analysis has been facilitated by the availability of relatively inexpensive microcomputers that can be used in daily practice. Early computer programs for mechanistic analysis (such as CHEV5L, BISAR, ELSYM5, etc.) modeled pavements as being composed of linear elastic layers and computed deflections, stresses, and strains within a pavement arising from a wheel load. In these programs each pavement layer is assumed to extend infinitely in the horizontal directions, allowing the three-dimensional problem to be reduced to an axisymmetric two-dimensional problem. Because of the linear elastic assumption, multiple wheel loads can be analyzed by superposing the results from single wheel loads.

The main drawbacks of these linear elastic layer programs are that

- They cannot model the nonlinear resilient behavior of granular and cohesive soils;
- They normally assume weightless pavement material;
- They may yield tensile stresses in granular material, which cannot physically occur; and
- They do not account for "locked-in" stresses from compaction during construction.

To overcome these shortcomings, nonlinear analysis programs based on the finite element method have been developed (e.g., ILLI-PAVE). However, because of the large memory and computational effort requirements, these programs primarily have been implemented on mainframe computers. Further, the interaction of the user and these programs, in terms of data input and interpretation of the output, is not "friendly," making their use in daily practice undesirable.

For most state highway agencies, a "user-friendly" flexible pavement program that can be used for the design or rehabilitation of flexible pavements in daily practice is desired. This program should consider all the major factors affecting the design or rehabilitation of pavements. To achieve this, a research study was sponsored by Michigan Department of Transportation (MDOT). The main goal of this research was to review existing analysis and design methods and then to develop a user-friendly nonlinear finite element program that can be used on personal computers in daily practice. Since current personal computers have limited memory capacities, the traditional finite element method, which requires a large amount of memory, cannot be suitably implemented on them unless accuracy is sacrificed. To overcome this shortcoming, Harichandran and Yeh (*1*) proposed a new technique of placing a relatively shallow finite element mesh on a flexible boundary. This technique substantially reduces the memory and computational requirements of the nonlinear finite element method without sacrificing accuracy. In this research, this technique is implemented with user-friendly input and output features, to develop a nonlinear finite element program for the analysis and design of flexible pavements. The program has been named MICH-PAVE.

MATERIAL NONLINEARITY

There are many nonlinear material models that may be used in mechanistic analysis. Four suitable models—the hyperbolic, the resilient modulus, the shear and volumetric stress-strain (also called the contour model), and the third-order hyperelastic models—were reviewed (*2–7*). Of these, the resilient modulus model was chosen as the most suitable at the present time. This choice is based on the applicability of the model to repeated loading patterns experienced by pavements, and on the relative ease of determining the model parameters by state highway agencies. The resilient modulus model characterizes the resilient stress-strain properties of soils through a stress-dependent modulus and a constant Poisson ratio.

For granular soils, the resilient modulus is characterized as

$$M_r = K_1\theta^{K_2} \quad (1)$$

R. S. Harichandran and G. Y. Baladi, Department of Civil and Environmental Engineering, Michigan State University, East Lansing, Mich. 48824. M-S. Yeh, Engineering Office of Taipei Railway Underground Project, 3 Pei-Ping West Road, 3rd Floor, Taipei, Taiwan 100, Republic of China.

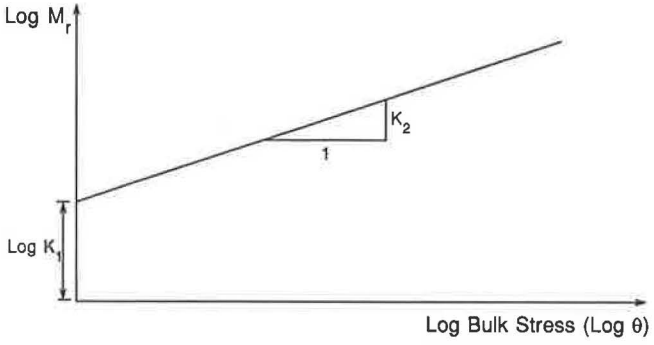

FIGURE 1 Resilient modulus model for granular material.

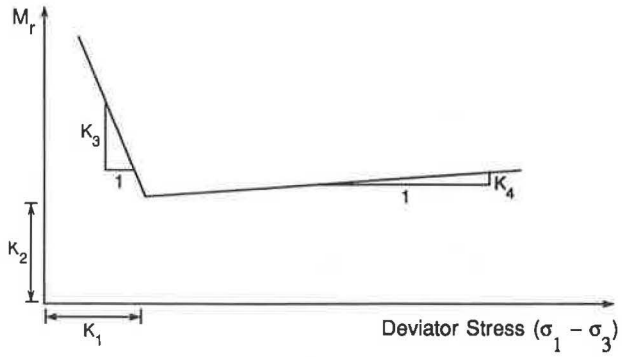

FIGURE 2 Resilient modulus model for cohesive material.

where M_r = resilient modulus (psi), $\theta = \sigma_1 + \sigma_2 + \sigma_3$ = bulk stress (psi), and K_1 and K_2 are material constants. This relationship is illustrated in Figure 1.

For cohesive soils, the resilient modulus is expressed through the bilinear relationship

$$M_r = \begin{cases} K_2 + K_3[K_1 - (\sigma_1 - \sigma_3)] & \text{for } K_1 > (\sigma_1 - \sigma_3) \\ K_2 + K_4[(\sigma_1 - \sigma_3) - K_1] & \text{for } K_1 \leq (\sigma_1 - \sigma_3) \end{cases} \quad (2)$$

where $(\sigma_1 - \sigma_3)$ = deviator stress (psi), and K_1, K_2, K_3, and K_4 are material constants. This relationship is illustrated in Figure 2.

If the finite element method is used with only the resilient modulus model, it will converge extremely slowly. Therefore, Raad and Figueroa (*8*) applied the resilient modulus model with the Mohr-Coulomb failure criterion. The Mohr-Coulomb failure criterion is used to modify the principal stresses of each element in the granular layers and roadbed soil after each iteration so as not to exceed the Mohr-Coulomb failure envelope. Thompson (*9*) used this algorithm in the ILLI-PAVE program. A similar algorithm was developed for MICH-PAVE.

FEATURES OF THE MICH-PAVE PROGRAM

The MICH-PAVE program is capable (depending on the user's choice) of performing either linear or nonlinear finite element analysis of flexible pavements. It assumes axisymmetric loading conditions arising from a single circular wheel load on pavement layers of infinite horizontal extent. The various features of the program are described in this section. Technical details and results from various sensitivity analyses can be found elsewhere (*10,11*).

Mesh Generation and Flexible Boundary

The finite element method needs to satisfy some basic requirements for the mesh, such as the location of the side and bottom boundaries, the size and shape of the elements, and the distribution of the elements in the various regions. To establish criteria for locating the boundaries in a finite element mesh, Duncan et al. (*12*) showed comparisons between displacements and stresses computed using the finite element method and those computed using elastic half-space and layered system analysis.

For an elastic half-space subjected to a uniform circular load, displacements and stresses computed by the finite element method compare well with those determined from the Boussinesq solution, when

- the bottom boundary in the finite element mesh is fixed at a depth of about 18 radii of the loaded area; and
- the vertical side boundary is located at a distance of about 12 radii from the center and constrained from moving radially.

For a three-layered system, a reasonable comparison between the two procedures can be obtained if the bottom boundary in the finite element mesh is moved to a depth of about 50 radii, while maintaining the side boundary at 12 radii.

Previous experience has shown that stresses based on quadrilateral elements will be accurate provided that the length-to-width ratio for the elements does not exceed five to one. Furthermore, smaller elements should be used close to the loaded area, and progressively larger elements may be used in the regions away from the loaded region.

Based on the above considerations and experience, the following mesh generation rules were used. In the radial direction, a mesh with a total width of 10 radii was divided into four zones. The first zone, between 0 and 1 radius, is equally divided into four elements; the second zone, between 1 radius and 3 radii, is equally divided into four elements; the third zone, between 3 radii and 6 radii, is equally divided into three elements; and the fourth zone, between 6 radii and 10 radii, is equally divided into two elements. The MICH-PAVE program will automatically generate the default values of the finite element mesh along the radial and vertical direction. A typical mesh is shown in Figure 3.

In the MICH-PAVE program, a flexible boundary is used instead of a fixed bottom boundary. Therefore, a mesh that is 50 radii deep is not required. Normally when a mesh depth of about 10 radii is used, sufficiently accurate results will be obtained. In general, if the flexible boundary is located too close to the top of the roadbed soil, the displacements may still be accurate, but the stresses may not be. If the boundary is placed too deep, the primary advantages of using the flexible boundary are lost. The flexible boundary is usually placed

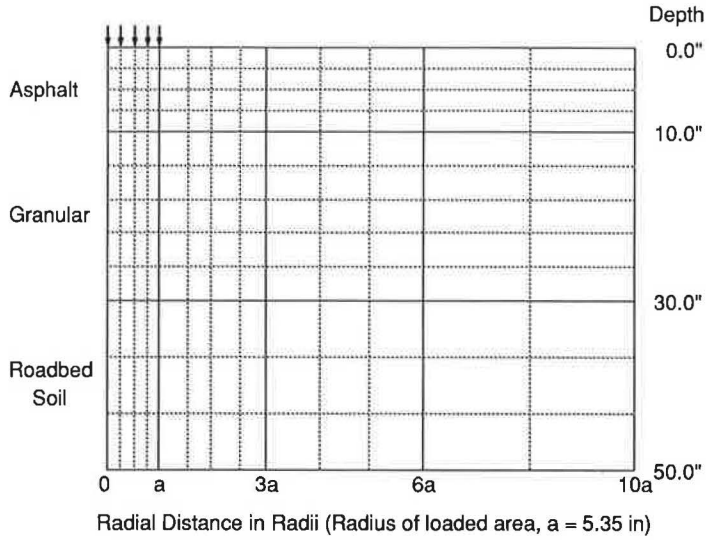

FIGURE 3 Typical finite element mesh.

at about 12 in. below the upper surface of the roadbed soil, or at a depth of 50 in., whichever is greater. In the MICH-PAVE program, the depth at which the flexible boundary is placed is specified by the user, by inputting the depth of the roadbed soil to which stress and strain calculations are required. If the boundary is placed at a depth of less than about 50 in., then the stresses still will be accurate, but the vertical deflections may be overestimated.

Modulus of Half-Space Below Flexible Boundary

The half-space below the flexible boundary is assumed to be homogeneous and linear elastic. The boundary is therefore always placed within the last layer (roadbed soil). Although the modulus of the roadbed soil below the boundary may in reality be stress dependent and vary from one location to another, in most pavement sections the stresses from wheel loads are substantially diminished at the level of the roadbed soil. Thus, the use of a constant modulus below the boundary has a negligible effect on the stresses and displacements above the boundary. In MICH-PAVE, the modulus used for the half-space below the boundary is the average moduli of the finite elements immediately above the boundary. To avoid undesirable "edge effects," the elements closest to the right vertical boundary are not used in computing this average.

Gravity and Lateral Stresses

The MICH-PAVE program includes the effect of gravity and lateral stresses arising from the weight of the materials. At any location within the pavement, the vertical gravity stress (σ_g) is computed as the accumulation of the layer thicknesses multiplied by the appropriate unit weights.

The lateral stress (σ_h) is calculated from the coefficient of earth pressure at rest (K_0) and vertical gravity stress, as

$$\sigma_h = K_0 \sigma_g \tag{3}$$

where

$K_0 = 1 - \sin \phi$ for cohesionless soil and gravel;
$K_0 = 1 - 0.95 \sin \phi$ for cohesive soil; and
ϕ = angle of internal friction.

To approximately account for "locked-in" stresses caused by compaction, the user can input a value for K_0 higher than the coefficient of earth pressure at rest.

Iterative Solution and Convergence Criterion

MICH-PAVE performs nonlinear analysis by the following steps:

1. Initially, the wheel load at the surface is assumed to spread over a 2:1 region (i.e., the radius of the loaded area is assumed to increase by 1 in. for every 2 in. of depth). The stresses arising from this assumed distribution of the wheel load are combined with gravity stresses, to compute the initial resilient moduli for each of the finite elements in granular and cohesive materials.
2. A linear analysis is performed, and a more accurate stress distribution is computed.
3. For those elements that exceed the Mohr-Coulomb failure criterion, the computed stresses are adjusted according to the procedure outlined by Raad and Figueroa (*8*).
4. A new value of the resilient modulus is computed for each element based on the latest stresses.
5. Convergence in the resilient moduli is checked by computing the relative error, $\varepsilon = \Sigma (M_{r,i} - M_{r,i-1})^2 / \Sigma M_{r,i-1}^2$, where $M_{r,i}$ are the current resilient moduli, $M_{r,i-1}$ are the previous resilient moduli, and the summations are taken over all nonlinear elements.
6. Steps 2 through 5 are repeated until the relative error ε is less than 0.001.

7. Displacements, strains, and stresses are then computed at all specified locations, and the fatigue life and rut depth of the pavement are estimated.

Interpolation and Extrapolation of Stresses and Strains at Layer Boundaries

For a pavement section in which various layers are fully bonded (i.e., when no slip occurs at layer boundaries), quantities such as the vertical and shear stresses and the radial and tangential strains should be continuous across layer interfaces. However, because of the low-order interpolation functions chosen in the finite element approach, these quantities are not continuous across element boundaries. Thus, if these quantities are estimated by finite element approach at two adjacent points across an interface, the results will show an apparent discontinuity that is an artifact arising from the error in the finite element method. This result is undesirable and can be overcome by using linear interpolation to estimate these quantities at an interface from those at the middle of the adjacent elements. For example, if σ_1 is the stress at the center of an element immediately above the interface and σ_2 is the stress at the center of an element immediately below the interface, then the stress at the interface obtained by linear interpolation is

$$\sigma = \sigma_1 + \frac{\sigma_2 - \sigma_1}{z_2 - z_1}(z - z_1) \tag{4}$$

where z_1 and z_2 are the depths of the points at which σ_1 and σ_2 are evaluated, and z is the depth of the interface.

Since the finite element approach gives accurate estimates of stresses and strains at the center of elements, but can yield significant error at element edges, even those stresses and strains at the interfaces that are discontinuous across the interface can be in significant error. For quantities such as the radial and tangential stresses that are discontinuous across an interface, it is possible to estimate their values at one side of the interface by linear extrapolation of the values at the center of two elements on that side of the interface. For example, if σ_1 and σ_2 are stresses at the center of two consecutive elements below (or above) an interface, then the linearly extrapolated stress at the lower (or upper) side of the interface is also given by Equation 4, where z_1 and z_2 are the depths of the points at which σ_1 and σ_2 are estimated, and z is the depth of the interface.

Finally, based on prior knowledge of the solution (vertical and shear stresses must be zero at the surface, except for the vertical stress below the wheel load, which must be identical to the tire pressure), the surface stresses are arbitrarily set to their proper values in MICH-PAVE.

The improvement in accuracy obtained through interpolation and extrapolation is illustrated by considering a typical pavement section for linear analysis using the MICH-PAVE and CHEV5L programs. (Results from CHEV5L are accurate for linear analysis and are used as the benchmarks.) In this example, a wheel load of 9,000 lb and a tire pressure of 100 psi were used, with material having the following material properties: Layer 1—AC, E = 300,000 psi, ν = 0.4; thickness = 8 in.; Layer 2—Base, E = 20,000 psi, ν = 0.38, thickness = 12 in.; and Layer 3—Roadbed soil, E = 8,000 psi, ν = 0.45, semi-infinite depth.

A comparison of stresses computed by CHEV5L, and by MICH-PAVE before and after extrapolation, are given in Table 1. Since the materials are assumed to be weightless, gravity stresses are neglected in both programs. Similar comparisons for stresses computed before and after interpolation, and adjustment of surface stresses, are given in Table 2. The plus and minus symbols used for depth indicate points just above and below interfaces. It is clear that interpolation and extrapolation improve the accuracy of these stresses. Similar improvements are obtained for strains.

Equivalent Resilient Moduli for Linear Analysis

In some cases it may be desirable to compare the results of nonlinear finite element analysis with those from a linear analysis or those of elastic layer programs such as CHEV5L, or to utilize the speed or multiple-wheel load capabilities of existing linear analysis programs. In such cases it would be desirable to input to the linear program an equivalent resilient modulus for each layer that reflects the true stress-dependent variation of the modulus within the layer. The equivalent moduli can be estimated from a nonlinear finite element analysis, using the various resilient moduli in each finite element.

MICH-PAVE computes an equivalent resilient modulus for each pavement layer that is obtained as the average of the moduli of the finite elements in the layer that lie within an assumed 2:1 load distribution zone, as shown in Figure 4. The average moduli of those elements within the regions ABGH, BCFG and CDEF are taken as the equivalent moduli for layers 1, 2 and 3, respectively.

TABLE 1 COMPARISON OF RADIAL AND TANGENTIAL STRESSES AT 67 IN. FROM THE CENTER OF THE LOADED AREA

Depth	Radial stress (psi)			Tangential stress (psi)		
(in)	Before	After	CHEV5L	Before	After	CHEV5L
0	-199.02	-167.91	-172.8	-199.02	-167.91	-173.0
8(+)	124.65	106.31	111.6	124.65	106.31	111.9
8(-)	1.84	0.35	0.22	1.84	0.35	0.24
20(+)	2.53	2.49	3.52	2.53	2.49	3.53
20(-)	-0.66	-0.47	-0.23	-0.66	-0.47	-0.23

TABLE 2 COMPARISON OF VERTICAL AND SHEAR STRESSES AT 67 IN. FROM THE CENTER OF THE LOADED AREA

Depth	Vertical stress (psi)			Shear stress (psi)		
(in)	Before	After	CHEV5L	Before	After	CHEV5L
0	143.57	100.0	99.7	2.62	0.0	0.0
8(+)	0.0	12.70	12.25	3.29	2.69	0.55
8(-)	9.15	12.70	12.25	0.65	2.69	0.55
20(+)	3.03	3.10	3.36	0.12	0.11	0.07
20(-)	1.61	3.10	3.36	0.07	0.11	0.07

The use of equivalent resilient moduli obtained through nonlinear analysis utilizing the MICH-PAVE program, in a linear program (CHEV5L), is investigated through typical examples.

Tables 3 and 4 show the material properties of a 12-in. full-depth asphalt concrete (AC) section, and a three-layer section with 3 in. of AC and 12 in. of granular material on roadbed soil (RS). The material properties shown in the tables, including the modulus, Poisson ratio (ν), lateral earth pressure coefficient (K_0), material constants (K_1, K_2, K_3, and K_4) and density have been obtained previously (*5*). A cohesion of 6.45 psi and an angle of friction of 0 degrees were used for the roadbed soil in the full-depth section. For the three-layer section, c = 0 psi and ϕ = 45 degrees were used for the granular material and c = 6.45 psi and ϕ = 0 degrees were used for the roadbed soil. For the granular material and roadbed soil, the equivalent resilient moduli are also shown in the tables. In the MICH-PAVE analysis, the flexible boundary was placed beneath the roadbed soil, at depths of 52 in. and 60 in. for the full-depth asphalt and three-layer sections, respectively.

The sections were analyzed for a wheel load of 9,000 lb and a tire pressure of 100 psi. Figures 5 and 6 show comparisons of surface deflections for nonlinear analysis using MICH-PAVE, and the linear analysis using CHEV5L with the equivalent moduli. Figures 7 and 8 show comparisons of the vertical and radial stresses at 0.5 in. from the center of the loaded area. Deflections and stresses computed by the nonlinear finite element program ILLI-PAVE are also shown in these figures.

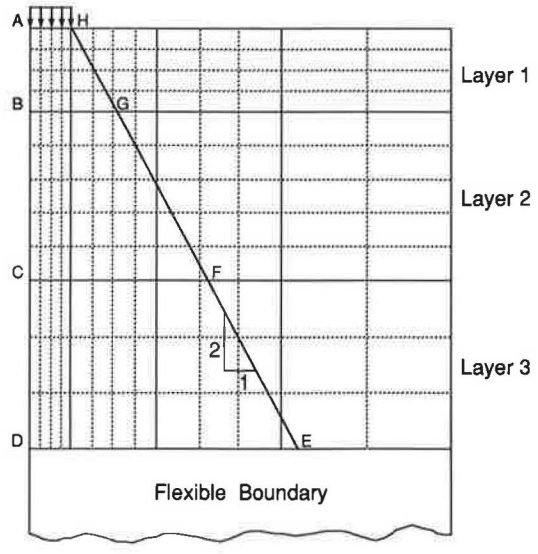

FIGURE 4 Elements used to compute equivalent resilient moduli.

The results indicate that the use of equivalent resilient moduli obtained from nonlinear analysis, in a subsequent linear analysis, gives reasonably similar displacements. Notable differences are obtained in the stresses, because the linear analysis using CHEV5L neglects the weight of the material. In particular, linear analysis can give tensile stresses in granular soils.

The stresses computed using MICH-PAVE and ILLI-PAVE are almost identical. However, ILLI-PAVE tends to give lower surface deflections than MICH-PAVE. Linear analysis, for which accurate results can be obtained through CHEV5L, has shown that displacements obtained by using a flexible boundary (as in MICH-PAVE) are slightly greater and more accurate than those obtained by using a deep fixed boundary (as in ILLI-PAVE) (*10,11*). Using a deep finite element mesh tends to produce a "stiffening" effect, resulting in smaller displacements.

For the three-layer pavement, the variation of modulus within the granular layer and roadbed soil is shown in Table 5 for the first eight elements from the left boundary. The depth and radial distance to the middle of the elements are tabulated. The finite element mesh was similar to that shown in Figure 3, except that the thicknesses of the layers are as given in Table 4. It is apparent that the modulus decreases with depth and radial distance within the granular layer. This is because the bulk stress (θ) decreases with depth and radial distance; hence, according to Equation 1, the resilient modulus follows the same pattern. Within the roadbed soil, however, the modulus increases with depth and radial distance. This increase is because the deviatoric stress ($\sigma_1 - \sigma_3$) decreases with distance away from the wheel load; hence, according to Equation 2, the modulus must also do the same. In MICH-PAVE, the modulus of the half-space below the flexible boundary is taken to be the average modulus of the elements immediately above the boundary. Care must be taken in MICH-PAVE to use a thickness for the roadbed soil that is sufficiently deep; otherwise the modulus of the half-space below the flexible boundary may turn out to be too small, yielding large displacements. It is recommended that the depth from the pavement surface to the flexible boundary (which is determined by the user inputs of layer thicknesses including that of the roadbed soil) be about 50 in. Larger depths have no appreciable effect on displacements.

TABLE 3 MATERIAL PROPERTIES FOR THE FULL-DEPTH AC SECTION

Layer Type	Thickness (inches)	Modulus (psi)	ν	K_0	K_1	K_2	K_3	K_3	Density (pcf)
AC	12	500,000	.4	.67					150
RS	40	8,753*	.45	.82	6.2	3021	1110	-178	115

* Equivalent resilient modulus

TABLE 4 MATERIAL PROPERTIES FOR THREE-LAYER SECTION

Layer Type	Thickness (inches)	Modulus (psi)	ν	K_0	K_1	K_2	K_3	K_3	Density (pcf)
AC	3	500,000	.4	.67					150
Granular	12	22,543*	.38	.60	5,000	.5			140
RS	45	7,435*	.45	.82	6.2	3021	1110	-178	115

* Equivalent resilient moduli

Fatigue and Rut-Depth Predictions

Results from the nonlinear mechanistic analysis, together with other parameters, are used as input to two performance models (fatigue life and rut depth) derived on the basis of field data (*13*), to predict the fatigue life and rut depth of flexible pavements. The models relate the fatigue life and rut depth to the number of equivalent 18-kip single-axle loads, surface deflection, moduli and thicknesses of the layers, percent air voids in the asphalt, tensile strain at the bottom of the asphalt layer, average compressive strain in the asphalt layer, kinematic viscosity of the asphalt binder, and average annual air temperature. Fatigue life and rut depth are useful design parameters on which to base the selection of a suitable pavement section.

User-Friendly Features

MICH-PAVE is designed with menus, data-entry forms, and on-screen plots, to facilitate easy input of data and interpretation of results. It also has extensive error-trapping features. Menus facilitate the selection of various stages of a typical pavement analysis, such as the specification of new data, modification of existing data, analysis, plotting of results, and subtasks within these. The spreadsheet-like data-entry forms allow input data to be entered or edited easily with no format requirements. When possible, suitable data for typical pavements are suggested on the screen. New or changed data are immediately checked for errors, and the user is prompted for corrections. Output from the analysis, such as stresses, strains, and displacements at specified locations, is saved in a file and may also be plotted on the screen. These features make the program easy to use in daily practice.

The program has been structured and optimized for speed, within the memory limitations of present personal computers (640 KB RAM). The total analysis time for typical three- and four-layer pavements is about 2 and 3.5 minutes, respectively, on an IBM AT-compatible computer with an 80287 math coprocessor.

PROGRAM AVAILABILITY

The MICH-PAVE program is in the public domain and may be obtained on request from Larry Heinig, Michigan Department of Transportation, Division of Testing and Research, P.O. Box 30049, Lansing, Mich. 48909. A user's manual is also available (*14*).

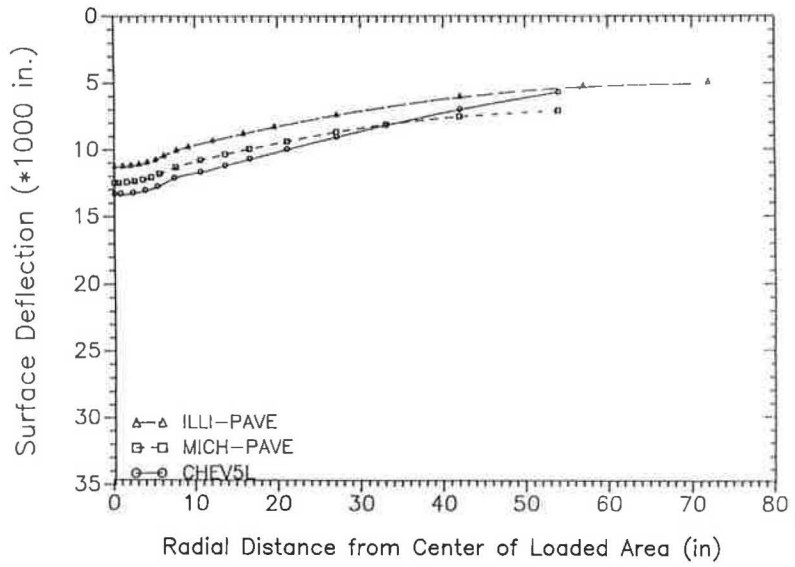

FIGURE 5 Comparison of surface deflection (12-in. full-depth AC).

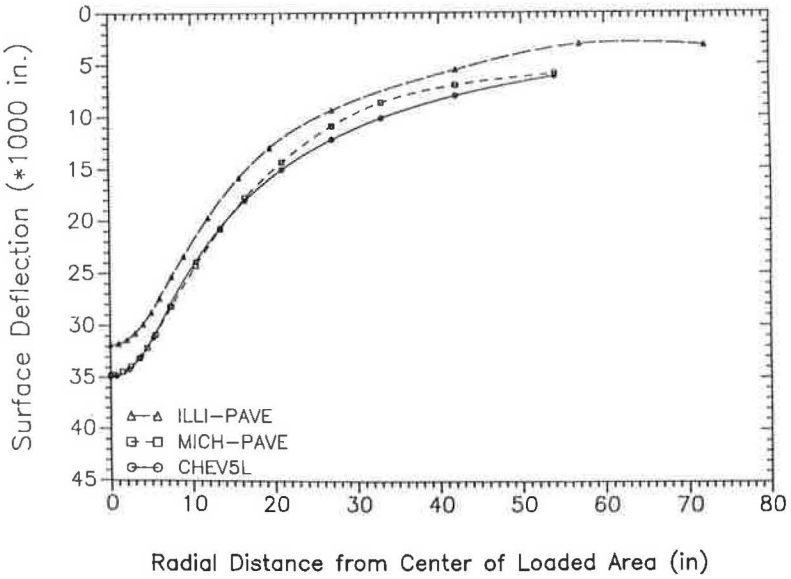

FIGURE 6 Comparison of surface deflection (3-in. AC and 12-in. base).

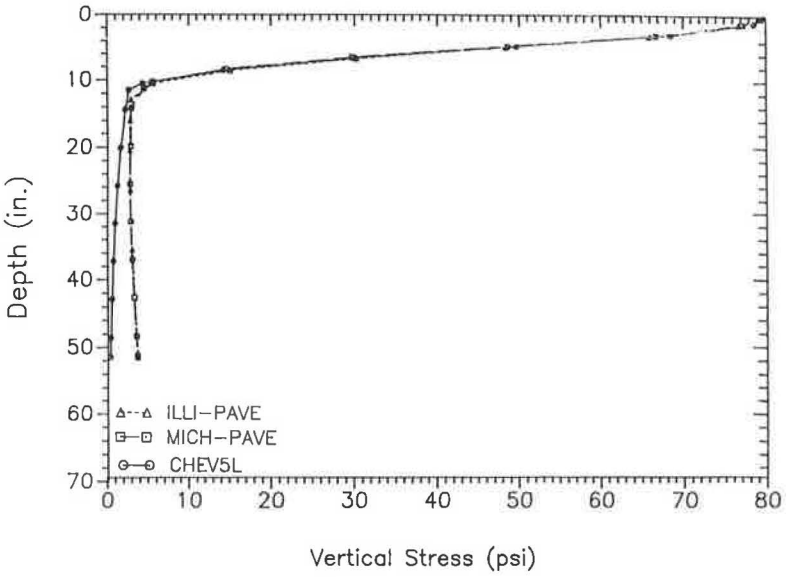

FIGURE 7 Comparison of vertical stress (12-in. full-depth AC).

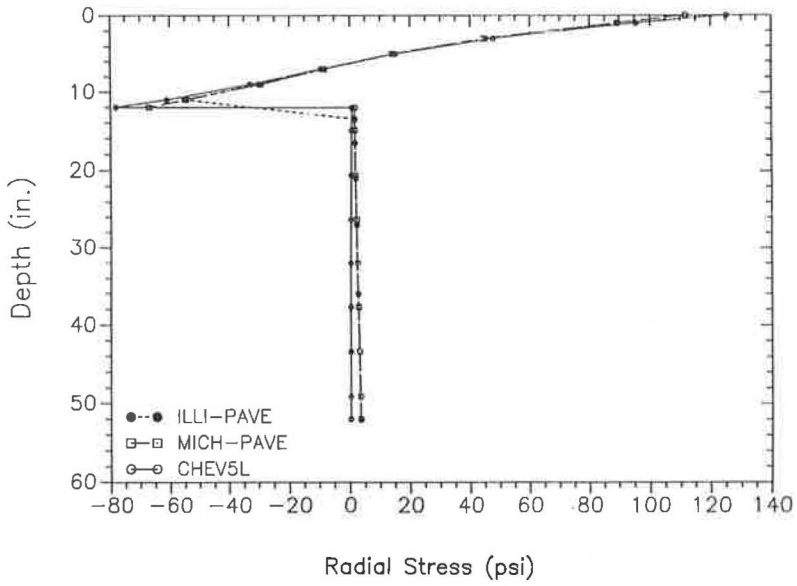

FIGURE 8 Comparison of radial stress (12-in. full-depth AC).

TABLE 5 VARIATION OF MODULUS (PSI) IN GRANULAR AND ROADBED SOIL LAYERS

Layer	Depth (in.)	Radial Distance from Center of Wheel Load (inches)							
		0.67	2.01	3.35	4.68	6.69	9.37	12.04	14.72
Gran.	4.2	36,800	35,400	32,200	27,800	22,100	15,300	12,000	10,300
	6.6	31,600	30,500	28,600	26,100	20,400	16,000	12,700	10,900
	9.0	25,800	25,200	24,200	22,700	20,300	15,500	13,200	11,500
	11.4	21,400	21,100	20,600	19,700	18,500	16,100	13,000	11,900
	13.8	18,200	18,100	17,800	17,400	16,800	15,500	14,000	12,100
RS	22.5	5,640	5,660	5,690	5,750	5,860	6,040	6,290	6,580
	37.5	7,340	7,350	7,360	7,380	7,430	7,520	7,630	7,750
	52.5	8,250	8,250	8,260	8,260	8,270	8,300	8,340	8,380

CONCLUSIONS

The features and methodology used by a state-of-the-art nonlinear finite element program for the analysis of flexible pavements, MICH-PAVE, are described. The analysis accounts for material nonlinearity, the unbound nature of granular soils, and "locked-in" lateral stresses arising from compaction. By utilizing a flexible bottom boundary in the finite element model, the memory and computational effort required by nonlinear analysis are drastically reduced, allowing the program to be used on personal computers. The program is designed to be user friendly, making it suitable for use in daily practice.

Results from the MICH-PAVE program have been compared with those from CHEV5L and ILLI-PAVE. For linear analysis, MICH-PAVE and CHEV5L give similar strains and displacements. The stresses computed by MICH-PAVE, however, account for the weight of pavement materials that are neglected by CHEV5L. For nonlinear analysis, MICH-PAVE and ILLI-PAVE give very similar stresses, but displacements computed by ILLI-PAVE are smaller than those computed by MICH-PAVE. It is believed that the use of a flexible boundary in MICH-PAVE alleviates the "stiffening" effect that results when a deep finite element mesh with a fixed boundary is used.

A method of obtaining a constant equivalent modulus for a pavement layer with a stress-dependent resilient modulus is outlined. The equivalent modulus, estimated from the results of nonlinear analysis, may be used with linear analysis programs to yield surface deflections that would be similar to those computed by nonlinear analysis.

Results of the mechanistic analysis are used as input to two pavement performance models developed using field data. The models employ computed stresses and strains, as well as the average annual temperature and the kinematic viscosity and air voids of the asphalt binder.

ACKNOWLEDGMENTS

The authors would like to express their gratitude to Michigan Department of Transportation (MDOT) for providing the financial support. The contribution of MDOT personnel, and the suggestions made by participants of the 4-week NHI course held at Michigan State University in February 1989, are greatly appreciated.

REFERENCES

1. R. S. Harichandran and M-S. Yeh. Flexible Boundary in Finite Element Analysis of Pavements. In *Transportation Research Record 1207*, TRB, National Research Council, Washington, D.C., 1988, pp. 50–60.
2. J. M. Duncan and C. Y. Chang. Nonlinear Analysis of Stress and Strain in Soils. *Journal of Soil Mechanics and Foundations*, ASCE, 1970, pp. 1629–1653.
3. W. F. Chen and A. F. Saleeb. *Constitute Equations for Engineering Materials*. John Wiley and Sons, Inc., New York, 1982, pp. 516–525.
4. S. F. Brown and J. W. Pappin. Analysis of Pavements with Granular Bases. In *Transportation Research Record 810*, TRB, National Research Council, Washington, D.C., 1981, pp. 17–23.
5. E. J. Yoder and M. W. Witczak. *Principles of Pavement Design*, John Wiley and Sons, Inc., New York, 1975.
6. H. J. Haynes and E. J. Yoder. Effects of Repeated Loading on Gravel and Crushed Stone Base Course Materials Used in the AASHO Road Test. *Highway Research Record 39*, TRB, National Research Council, Washington, D.C., 1963, pp. 82–96.
7. H. B. Seed, C. K. Chan, and C. E. Lee. Resilience Characteristics of Subgrade Soils and Their Relation to Fatigue Failures in Asphalt Pavements. *Proc., 1st International Conference on the Structural Design of Asphalt Pavements*, Ann Arbor, Mich., 1962, pp. 77–113.
8. L. Raad and J. L. Figueroa. Load Response of Transportation Support System. *Journal of Transportation Engineering*, ASCE, Vol. 106, 1980, pp. 111–128.
9. M. R. Thompson. ILLI-PAVE, User's Manual. Transportation Facilities Group, Department of Civil Engineering, University of Illinois, Urbana-Champaign, 1986.
10. M. S. Yeh. *Nonlinear Finite Element Analysis and Design of Flexible Pavements*. Ph.D. dissertation. Michigan State University, East Lansing, 1989.
11. R. S. Harichandran, G. Y. Baladi, and M-S. Yeh. *Development of a Computer Program for Design of Pavement Systems Consisting of Layers of Bound and Unbound Materials*. Report FHWA-MI-RD-89-02. Michigan Department of Transportation, Lansing, 1989.
12. J. M. Duncan, C. L. Monismith, and E. L. Wilson. Finite Element Analysis of Pavements. In *Highway Research Record 228*, TRB, National Research Council, Washington, D.C., 1968, pp. 18–33.
13. G. Baladi. Fatigue Life and Permanent Deformation Characteristics of Asphalt Concrete Mixes. *Transportation Research Record 1227*, TRB, National Research Council, Washington, D.C., 1989.
14. R. S. Harichandran, G. Y. Baladi, and M-S. Yeh. *MICH-PAVE User's Manual*. Report FHWA-MI-RD-89-03. Michigan Department of Transportation, Lansing, 1989.

Publication of this paper sponsored by Committee on Flexible Pavement Design.

Extension of Load Equivalency Factors for Various Pavement Conditions

JACOB UZAN AND ARIEH SIDESS

Analyses of the AASHO Road Test results to derive load equivalency factors (LEFs) as a function of pavement condition (present serviceability index [PSI]) were performed. The results of the analyses show that the LEFs are strongly dependent on the pavement condition, i.e., LEF values increase as the initial PSI decreases. This result may affect the analyses of legal load limits and special movement of heavy trucks. To adapt the above results to multiple loads, a framework based on limiting the strain at the top of the subgrade and various strain criteria for various PSI of the pavement were developed and are presented. A modification to the common Miner's law for damage accumulation was calibrated for tandem axle loads and suggested for use with multiple wheel axles. The use of the proposed framework is illustrated for single, tandem, and multiple axle loads. The results showed that the LEFs of all load configurations are dependent on the condition of the pavement.

State officials who have the responsibility for considering and changing the legal load limits are continuously faced with requests for increasing loads on a specific truck or for allowing heavier loads on new trucks. Based on economic analyses, these requests seem legitimate, in Israel, but there is a strong feeling that the formal result is misleading. The analyses are usually conducted using AASHO Road Test load equivalency factors (LEFs) obtained from newly constructed pavements, but the network on which these loads are applied is not new. In fact, in Israel the network is in rather bad condition, with an average pavement condition index lower than 50. Therefore, the validity of these analyses using AASHO LEFs is questionable. Increasing the LEFs reduces the optimal load to be allowed on the truck.

Highway agencies are also often asked to issue special permits to allow special tractors and trailers to haul very large and heavy machinery for power plants or structural components for bridges. To minimize the damage to pavements and bridges, these tractors and trailers are equipped with numerous axles and tires. Greer (*1*) and Terrel and Mahoney (*2*) analyzed pavements and evaluated their structural capacity to support trailer units with 192 wheels (12 axles with 16 wheels per axle). Kilareski (*3*) presented a study of the potential pavement damage caused by heavily loaded units with four and five axles. The approach to the problem of heavy loads and requests for increasing legal loads is straightforward. Analyses of stresses or strains that develop under these loads can be conducted to evaluate the number of allowable repetitions for the specific loading configuration (*4–6*). Alternatively, the pavement method currently used by the state can be used or adapted to design the road upgrading required to permit the movement of heavy loads (*1*).

In the case studies reported in the literature (*1,2*), although testing programs and analyses were conducted for the specific haul routes, the authors did not consider directly the pavement condition as a variable. If the effect of load magnitude on pavement performance depends on the condition of the pavement, it would imply that various LEFs correspond to various pavement conditions (for the same pavement structure). Such dependence could be attributed to the dynamic effect induced by roughness, resulting in relatively heavier loads as the pavement condition deteriorates, or to nonlinearity in the damage accumulation (Miner's law).

This paper presents a derivation of LEFs based on AASHO Road Test results. The analyses show clearly that LEFs are influenced by the pavement condition, i.e., on the serviceability index at the time of application of the load. A framework is presented to adapt the derivation of LEFs to accommodate heavier loads and a larger number of wheels than in the AASHO Road Test. It is based on computation of vertical strain at the top of the subgrade and calibration with AASHO Road Test results. An illustration of the approach is presented using several load magnitudes and wheel configurations.

DERIVATION OF LOAD EQUIVALENCY FACTORS USING AASHO ROAD TEST RESULTS

The derivation is based on the well-known definition of LEF and AASHO Road Test performance equations:

$$F_j = W_e/W_j \tag{1}$$

where

F_j = LEF for load L_j,
W_j = number of repetitions for load L_j, and
W_e = Equivalent number of repetitions of a reference load L_e (usually taken as 18 kip).

$$W_k = \zeta_k \, 10^{G/\beta_k} \tag{2a}$$

$$\zeta_k = \frac{10^{5.93} \, (SN + 1)^{9.36} \, L_2^{4.33}}{(L_1 + L_2)^{4.79}} \tag{2b}$$

$$G = \log \frac{4.2 - p_t}{4.2 - 1.5} \tag{2c}$$

J. Uzan, Department of Civil Engineering, Transportation Research Institute, TECHNION, Israel Institute of Technology, Haifa, Israel. A. Sidess, YARIV-Civil Engineering and Surveying, 1 Remez St., Givataim 53242, Israel.

$$\beta_k = 0.40 + \frac{0.081\,(L_1 + L_2)^{3.23}}{(SN + 1)^{5.19}\,L_2^{3.23}} \qquad (2d)$$

where

$SN = a_1d_1 + a_2d_2 + a_3d_3$,
L_1 = axle load, in kip,
L_2 = 1 for a single axle, 2 for a tandem axle,
SN = structural number,
p_t = terminal serviceability number,
a_1,a_2,a_3 = layer coefficients,
d_1,d_2,d_3 = layer thicknesses, in in., and
k = index (may be either e or j).

The well-known AASHO LEFs are obtained from the above equations for various terminal serviceability indices (p_t). These factors are related to the pavement damage that begins at a unique initial pavement serviceability index (PSI) of about 4.2 (average of all initial serviceability indices in the AASHO Road Test). If the load equivalency is influenced by the pavement condition, then the usual LEFs are average values for the service life of the pavement, from the time of its construction with an initial PSI of about 4.2 to the time it reaches its terminal PSI. To deal with various initial conditions, the LEF should be redefined as

$$F_j(p_i \rightarrow p_t) = W_e(p_i \rightarrow p_t) \,/\, W_j(p_i \rightarrow p_t) \qquad (3)$$

where p_i is the initial serviceability index and $p_i \rightarrow p_t$ denotes pavement condition deterioration from p_i to p_t. When p_i = 4.2, Equation 3 simplifies Equation 1 corresponding to the usual definition of LEF. When p_i is a value other than 4.2, the number of repetitions should be computed from the performance equations (Equation 2) as follows:

$$W_k(p_i \rightarrow p_t) = W_k(4.2 \rightarrow p_t) - W_k(4.2 \rightarrow p_i) \qquad (4)$$

where k may be either j or e.

Figure 1 shows the components of Equation 4 using the performance curve. When referring to an initial serviceability index (p_i) lower than 4.2, it is assumed that this lower p_i is because of deterioration from past traffic and not because of bad construction. Results of computations of LEFs for four

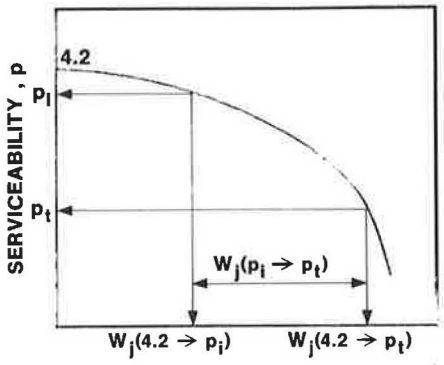

FIGURE 1 Schematic representation of load repetition increment on performance curve.

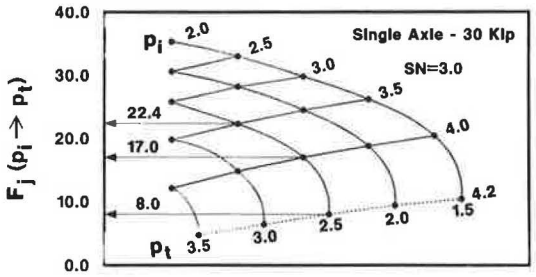

FIGURE 2 Load equivalency factors for 30-kip single axle load as function of PSI.

different load magnitudes and configurations (SN = 3 and various p_i and p_t's) are shown in Figures 2 through 5. The dotted lines in the diagrams correspond to the usual LEFs with p_i = 4.2. From these figures, it is possible to get F_j for any p_i and any p_t. For example, from Figure 2 one can get $F_j(4.0 \rightarrow 2.5)$ = 17.0 as compared with $F_j(4.2 \rightarrow 2.5)$ = 8.0 or $F_j(3.5 \rightarrow 2.5)$ = 22.4. F_j values for lower p_t (for example $F_j[2.0 \rightarrow 1.5]$ = 35.3) are very large compared with the value of 10.4 obtained previously. This example emphasizes the importance of pavement condition on LEFs. It seems that F_j is influenced slightly by the structural number, moderately by the terminal serviceability, load magnitude, and configuration, and highly by the initial serviceability. The results of the AASHO Road Test support the hypothesis that LEFs depend on the initial serviceability.

EXTENSION OF THE LOAD EQUIVALENCY FACTOR TO MULTIPLE WHEEL LOADS

The approach for computing LEFs from AASHO performance equations is restricted to the single and double axle loads that traveled on the test sections. To extend the approach to various axle configurations, a semirational (semiempirical) framework is suggested. This framework is less restrictive than the empirical one. It consists of

1. Stress-strain computation and material characterization;
2. Calibration of a failure criteria using all the available test results; and
3. Validation and implementation of the framework to the unusual loads.

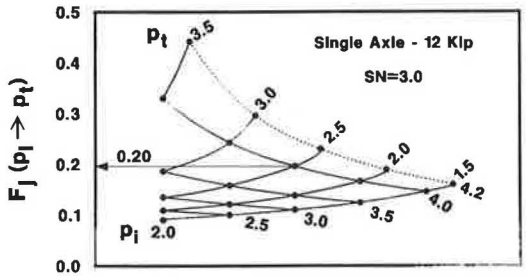

FIGURE 3 Load equivalency factors for 12-kip single axle load as function of PSI.

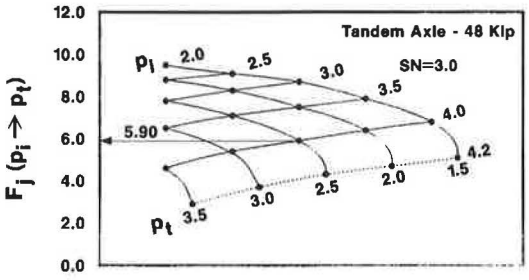

FIGURE 4 Load equivalency factors for 48-kip tandem axle load as function of PSI.

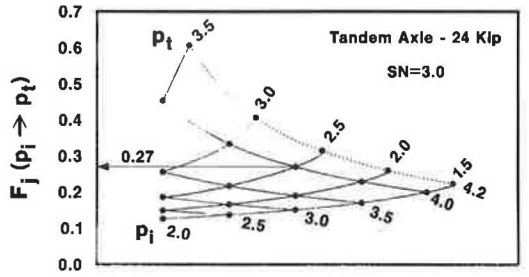

FIGURE 5 Load equivalency factors for 24-kip tandem axle load as function of PSI.

Unless nonlinear material characterization is used, the stress level induced by the unusual loads should not exceed (or should exceed only slightly) the stress level that developed in the test. For simplicity, the proposed framework is based on the linear elastic theory. It could be upgraded by including nonlinear material characterization and analyses.

Development of the Framework

The steps for developing the semirational framework are as follows:

1. *Pavements*—Seven pavement sections of the AASHO Road Test are chosen for analyses (Table 1). The ranges of the layer thicknesses and structural numbers embrace a wide variety of pavements serving from light to heavy traffic loads.
2. *Loads*—All five single axle loads (6, 12, 18, 22.4, and 30 kip) that traveled in the test sections are included in the calibration analyses. In this case, each axle is equipped with two dual wheels on each side; the distance between dual wheels is 14 in., and the contact pressure is 70 psi.
3. *Material properties*—The moduli of elasticity of the subgrade and the asphalt concrete are assumed constant and equal to 5,700 psi (corresponding to a CBR value of 3–4) and 450,000 psi, respectively. The modulus of elasticity of the granular subbase and base material is assumed to depend on both the layer thickness and modulus of the underlying layer. The equations used are those of the USACE granular material characterization for roads (see Smith and Witczak [7]).

$$E_{sub} = E_{sg} (1 + 1.5 H_{sub}/20.0) \quad (5a)$$

$$E_b = E_{sub} (1 + H_b/6.0) \quad (5b)$$

where

E_b, E_{sub}, and E_{sg} = the base, subbase, and subgrade layer moduli, respectively, and
H_b and H_{sub} = the base and subbase layer thicknesses, in in.

4. *Analyses*—Vertical strain at the top of the subgrade is computed for all seven pavement sections, applying all five loads. The computations are made using a microcomputer program for the linear elastic multilayer system (*8*).
5. *Strain criteria*—The number of load applications is computed using Equation 2 for the above-mentioned pavement sections and loads, at three different serviceability indices p_t of 1.5, 2.5, and 3.5. The relationships between the number of load repetitions and computed vertical strain are shown in Figure 6. Various strain criteria are obtained for the various terminal serviceabilities. In addition, when the number of load repetitions is lower than 20,000, the relationship between vertical strain and load repetitions is independent of p_t and begins to curve. By using the number of load repetitions computed from Equation 2 rather than the actual number of load applications, the scatter in Figure 6 is reduced substantially. This reduction is because most of the randomness of the number of load applications is eliminated or filtered out in the regression of Equation 2. The lines in Figure 6 are represented by the following equations (for more than 20,000 load applications):

$$\varepsilon_v = 5.00 \times 10^{-2} W_j^{-0.36} \quad (6a)$$

$$\varepsilon_v = 1.99 \times 10^{-2} W_j^{-0.261} \quad (6b)$$

$$\varepsilon_v = 1.47 \times 10^{-2} W_j^{-0.228} \quad (6c)$$

for p_t = 3.5, 2.5, and 1.5, respectively, where ε_v is the amount of maximum vertical strain at the top of the subgrade and W_j is the number of load applications causing deterioration of the pavement from p_i = 4.2 to p_t. Only single axle loads are

TABLE 1 DESCRIPTION OF PAVEMENT SECTIONS USED IN THE ANALYSES

Pavement No.	Thickness of (in.)			Structural Number
	Asphalt	Base	Subbase	
1	3	0	8	2.20
2	3	6	4	2.60
3	4	3	8	3.06
4	4	6	12	3.92
5	5	6	12	4.36
6	5	9	12	4.78
7	6	9	12	5.22

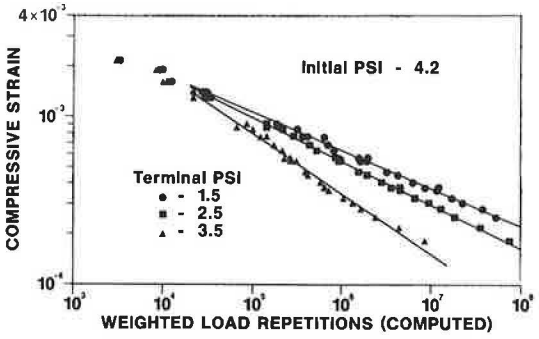

FIGURE 6 Vertical strain at top of subgrade as function of number of load repetitions and PSI for single axles.

used in the development of the above relationships (calibration stage). These relationships are valid only with the material characterization and analyses mentioned above.

The use of the framework for computing LEFs for a single axle is simple: $W_j(4.2 \rightarrow p_t)$ and $W_j(4.2 \rightarrow p_i)$, which are required in Equation 4, may be obtained from Figure 6. For example, to compute the LEF for a pavement with SN = 4.78, 30-kip single axle, $p_i = 3.5$, and $p_t = 2.5$, the following steps are necessary: (a) Compute the vertical strain under the load (under a 30-kip load, one obtains ε_v = 629 microstrains); (b) At this strain level, obtain from Figure 6 or Equation 6 the terms $W_j(4.2 \rightarrow 2.5)$ and $W_j(4.2 \rightarrow 3.5)$. At 629 microstrains, $W_j(4.2 \rightarrow 2.5)$ = 559,600 and $W_j(4.2 \rightarrow 3.5)$ = 190,000; (c) Compute $W_j(3.5 \rightarrow 2.5)$ from Equation 4: 559,600 − 190,000 = 369,600; (d) Repeat steps 1 through 3 with the standard load 18 kip to get $W_e(3.5 \rightarrow 2.5)$ = 3,178,600; (e) Compute the LEF using Equation 3 as 3,178,600/369,600 = 8.6. This value is in good agreement with the value of 9.5, obtained from Equation 2.

Calibration and Verification

The extension of the framework to tandem axles requires some clarification of the rational approach based on cumulative damage. For common pavement thicknesses, the strain distribution shows two clear peaks. These two peaks usually are considered as two separate repetitions, equivalent to dividing by two the number of repetitions obtained from Figure 6. However, this is correct only for thin pavements (or for large spacing between axles of the tandem) when the strain between the axles decreases to zero (full reversal of the strain), or practically to less than 10 percent of the peak strain. For thick pavements (or small spacing between axles of the tandem), the strain distribution may show only one peak. In this case, or practically when the strain between the axles is greater than 90 percent of the peak strain, each pass of the tandem is considered as one application of the peak strain. In reality, the strain between axles (located 60 in. apart) is nearly zero for thin pavements and reaches about half the peak value for commonly thick pavements. This situation calls for a correction of the Miner's damage accumulation law, especially for thick pavements. Such a correction is proposed below based on the AASHO Road Test results for tandem axle loads. For thin pavements, it was found that the strain between axles is near zero, suggesting that no correction is needed. Moreover the computations show that the peak strain under one axle of the tandem is lower than the peak strain under one single axle. The second dual-wheel axle in the tandem induces negative strain at large distances from the load. Such beneficial effect is questionable in flexible pavements because of the presence of highly nonlinear granular material.

To quantify the effect of the tandem axle, the pavement sections listed in Table 1 are analyzed under tandem axle loads (two dual wheels on each side of the axles) of 24, 32, 40, and 48 kip. The vertical strain at the top of the subgrade is computed under these loads, and the number of tandem axle load repetitions is obtained using the AASHO Road Test performance equations (Equation 2). The results are presented in Figure 7, superimposed on the strain criteria of the single axle. The dotted lines represent the strain criteria for tandem axles. It is seen that each pass of the tandem is equivalent to 1.6 passes of a single axle, except in the low range of number of repetitions in which each pass of the tandem is equivalent to about two passes of the single axle.

In view of the above, the following procedure for the analysis of tandem axles is suggested. The maximum strain and the strain between axles of the tandem are evaluated. When the strain between the axles is less than 10 percent of the maximum strain, the tandem axle is considered as two separate applications of the peak strain. When the strain between axles is greater than 90 percent of the maximum strain, the tandem axle pass is considered as only one application of the peak strain. In addition, when the peak strain computed with two dual wheels (on one side of the tandem axle) under or near one axle is smaller than the peak strain computed with one dual wheel (on one side of the single axle), the tandem axle pass is considered as two separate applications of one single axle. In other words, the peak strain obtained for one axle of the tandem, without the "beneficial effect" of the second axle is used to get W_j from Figure 6, and this number is divided by two. When the peak strain, computed with two dual wheels under or near one axle, is equal to or larger than the peak strain computed with one dual wheel (and the strain between the axles is greater than 10 percent and smaller than 90 percent of the peak strain), the tandem axle pass is considered as 1.6 applications. In other words, the peak strain under the two dual wheels is used to get W_j from Figure 6,

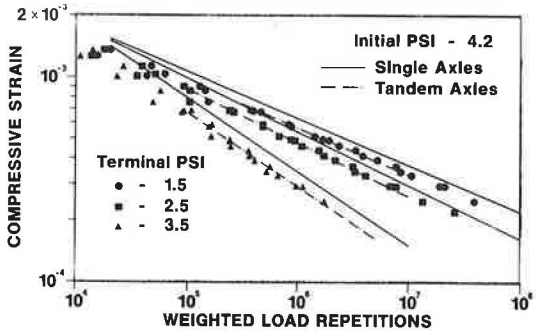

FIGURE 7 Vertical strain at top of subgrade as function of number of load repetitions and PSI for tandem axles.

and this number is divided by 1.6. LEF values computed using the above proposed approach are shown in Figure 8 and compared with those computed from AASHO Road Test-based equations (Equation 2). It is seen that the results are dispersed within a maximum deviation of 20 percent and that they agree very well.

ILLUSTRATION OF THE PROPOSED APPROACH TO MULTIPLE WHEEL LOADS

The extension of the proposed approach to multiple wheel loads is based on the assumption that the "failure" criterion derived for two axles holds also for more than two axles. In the case of multiple axle loads, calibration factors of 0.8 for leading axles and 0.6 for internal axles are suggested. These factors are found as follows. (a) The symmetric strain distribution under a tandem axle that corresponds to 1.6 repetitions of a single axle can be separated into two incomplete cycles (see Figure 9). Because a tandem axle is composed of two leading axles, each axle induces 0.8 (1.6/2) of the damage caused by a single axle. Therefore a calibration factor of 0.8 corresponds to each leading axle. (b) The strain distribution under a tandem axle can be viewed as composed of one complete cycle and one incomplete cycle in the central portion between peaks of the strain distribution (see Figure 10). This central part contributes 0.6 (1.6–1.0) of the damage caused by a tandem axle. Hence a calibration factor of 0.6 is suggested for each internal axle. At this time, no test results exist for calibrating the above factors. However, the above procedure is similar to the Curvature Method presented by Treybig (*5*).

The proposed procedure for computing W_j for multiple axle loads is summarized as follows. When the peak strain computed with all dual-wheels of the n − axles is smaller than the peak strain computed with only one dual-wheel, the multiple axle pass is considered as n separate applications of one single axle. The peak strain obtained for one axle (without the "beneficial effect" of the other axles) is used to get W_j from Figure 6, and this number is divided by n. When the peak strain computed with n dual wheels is equal to or larger than the peak strain computed with one dual wheel, then W corresponding to each peak strain is obtained from Figure 6. These numbers are divided by either 0.8 or 0.6, depending

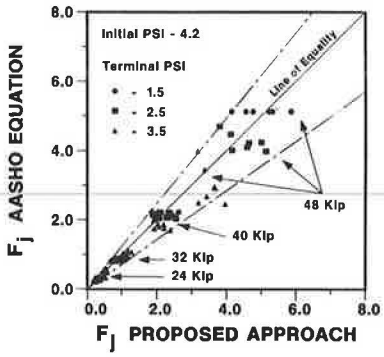

FIGURE 8 Comparison of LEFs obtained using the proposed procedure and AASHO equations for 24, 32, 40, and 48-kip tandem axle loads.

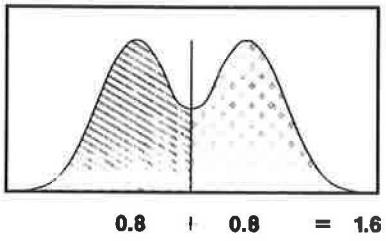

FIGURE 9 Separation of strain distribution of a tandem into two incomplete cycles.

on the position of the peak in the strain distribution. Then an average number of applications is computed on the basis of equal damage.

Tables 2 through 4 summarize results of computation for a very heavy tandem axle (79.2 kip), a four-axle load (with 8.5 kip per wheel) described by Kilareski (*3*), and 24-wheel trailer (with 13.86 kip per wheel), respectively. The 24-wheel configuration, which is composed of six axles with four wheels 36 to 40 in. apart, is different from the other configurations that have dual wheels (two close wheels on each side of the axle). In the cases of heavy loads, only pavements with a structural number larger than 3.5 are considered. The results of the heavy tandem (Table 2) are also shown in Figure 11 and compared with those obtained using Equation 2 (extrapolation of the AASHO Road Test results). It is seen that in all cases, the LEF values increase as the initial serviceability decreases. The LEF values at p_i of 2.5 are about twice as large as the usual LEF values at p_i of 4.2. The effect of pavement conditions under heavy loads on LEF values is similar to, but milder than, the effect obtained with loads that traveled in the AASHO Road Test.

SUMMARY AND CONCLUSIONS

The decision whether or not to change the legal load limits and to issue special permits for extra heavy loads is based on several factors and an economic analysis that considers all costs and benefits that are affected by such a change in legal load limits or special movements. For evaluation of construction and maintenance costs, the use of LEFs is well established. These factors are related to newly constructed pavements, whereas any change in the legal limits takes place at a given pavement condition of the network. The paper presents analyses of the AASHO Road Test results and derives LEFs as function of the pavement condition (PSI). The results of the analyses show that the LEFs are strongly affected by

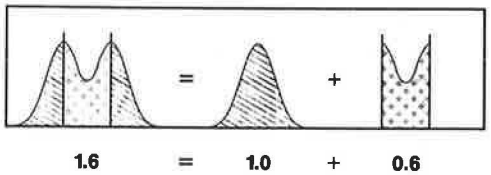

FIGURE 10 Separation of strain distribution of a tandem into one complete cycle and one incomplete cycle.

TABLE 2 RESULTS OF LEF COMPUTATIONS FOR 79.2-KIP TANDEM AXLE

	Initial Serviceability					
	4.2			3.5		2.5
Terminal Serviceability	3.5	2.5	1.5	2.5	1.5	1.5
SN=3.92	15.5	33.8	50.6	65.4	84.0	107.2
SN=4.36	15.9	35.1	52.8	56.9	74.9	94.9
SN=4.78	13.6	30.6	46.7	44.2	59.8	75.2
SN=5.22	14.3	33.0	50.8	44.9	61.9	77.3

TABLE 3 RESULTS OF LEF COMPUTATIONS FOR FOUR-AXLE LOAD

	Initial Serviceability					
	4.2			3.5		2.5
Terminal Serviceability	3.5	2.5	1.5	2.5	1.5	1.5
SN=3.92	22.7	43.9	61.7	71.0	88.4	108.4
SN=4.36	22.8	44.3	62.4	63.3	80.1	97.4
SN=4.78	18.1	37.1	53.6	49.7	65.0	79.2
SN=5.22	20.3	43.4	64.3	56.4	75.8	92.6

TABLE 4 RESULTS OF LEF COMPUTATIONS FOR 24 WHEELS

	Initial Serviceability					
	4.2			3.5		2.5
Terminal Serviceability	3.5	2.5	1.5	2.5	1.5	1.5
SN=3.92	19.4	35.5	48.4	53.6	65.6	79.0
SN=4.36	22.4	43.1	60.4	61.1	77.2	93.6
SN=4.78	29.3	62.6	92.6	86.5	114.9	141.9
SN=5.22	35.5	81.7	125.7	110.9	152.8	190.7

the pavement condition, i.e., LEF values increase as the PSI decreases.

A framework for extending the above results to multiple loads is proposed. This framework is based on computation of the strain at the top of the subgrade and strain criteria for various PSI of the pavement. The use of the framework for single axles is illustrated. For tandem axles, it is shown that the damage accumulation should be modified to take into account the longitudinal strain profile. Finally, heavy loads and multiple wheel load configurations are analyzed and LEFs are computed. The results show that the dependence of LEF on pavement conditions is similar to and milder for multiple wheels than for single and tandem axles.

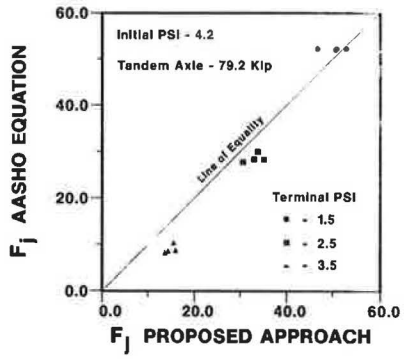

FIGURE 11 Comparison of LEFs obtained using the proposed procedure and AASHO equations for the 79.2-kip tandem axle load.

REFERENCES

1. W. C. Greer. Pavement Design for a 3.5-Million-Pound Vehicle. In *Transportation Research Record 875*, TRB, National Research Council, Washington, D.C., 1982, pp. 32–38.
2. R. L. Terrel and J. P. Mahoney. Pavement Analysis for Heavy Hauls in Washington State. In *Transportation Research Record 949*, TRB, National Research Council, Washington, D.C., 1983, pp. 20–31.
3. W. P. Kilareski. Heavy Vehicle Evaluation for Overload Permits. In *Transportation Research Record 1227*, TRB, National Research Council, Washington, D.C., 1989, pp. 194–204.
4. J. Uzan and G. Wiseman. Allowable Load on Multiple Axle Trucks. In *Transportation Research Record 725*, TRB, National Research Council, Washington, D.C., 1979, pp. 31–36.
5. J. H. Treybig. Equivalency Factor Development for Multiple Axle Configurations. In *Transportation Research Record 949*, TRB, National Research Council, Washington, D.C., 1983, pp. 32–44.
6. F. H. Southgate and R. C. Deen. *Effects of Load Distributions and Axle and Tire Configuration*. Proc., 6th International Conference on Structural Design of Asphalt Pavements, University of Michigan, Ann Arbor, Vol. 1, 1987, pp. 82–93.
7. B. E. Smith and M. W. Witczak. Equivalent Granular Base Moduli: Prediction. *Transportation Engineering Journal*, ASCE, Vol. 107, No. TE6, 1981, pp. 635–652.
8. J. Uzan. The Influence of the Interface Condition on Stress Distribution in a Layered System. In *Transportation Research Record 616*, TRB, National Research Council, Washington, D.C., 1976, pp. 71–73.

Publication of this paper sponsored by Committee on Flexible Pavement Design.

Influence of Axle Group Spacing on Pavement Damage

J. J. HAJEK AND A. C. AGARWAL

Current pavement design guides do not consider the effects of axle spacings. However, in many jurisdictions, higher loads on dual and triple axles are allowed for higher axle spacings. This practice is examined from a pavement viewpoint to ensure that dual or triple axles do not cause disproportionately greater damage than single axles. Damage effects of dual and triple axles on flexible pavements were evaluated as a function of axle spacing. The evaluation was based both on measured and calculated pavement responses to axle loads. Load equivalency factors are significantly influenced by pavement response parameters and by summation methods used for their derivation. The results display significant influence of the axle spacing on pavement damage. This indication should be taken into account when determining legal load limits on the axles. The AASHTO Guide appears to underestimate the damaging effect of dual and triple axles in comparison with single axles.

The extent to which structural pavement damage is caused by heavy vehicles depends on several loading characteristics, including axle loads, axle group configuration and spacing, load contact pressure, and dynamic loading effects, and on their interactions. This paper addresses the effect of one of these load characteristics—axle group configuration and spacing. Based on a recent literature survey, the effect of axle spacing on pavement damage has not been systematically examined before.

Many jurisdictions, for example the province of Ontario, regulate permissible axle group weights according to axle group spacing, whereas others, such as France and Sweden, do not (*1*). In Ontario, the Highway Traffic Act (*2*) prescribes the permissible load limit for a dual axle (also known as tandem) and a triple axle (also known as tridem), which varies according to axle spacing. Axle spacing is defined as the distance between the two individual axles in a dual axle and between the first and the third axles in a triple axle. The variation in permissible loads with the axle spacing traditionally has been based on the load-carrying capacity of the bridge components. The permissible load on a single axle, however, is based on pavement considerations.

The AASHTO Pavement Design Guide (*3*) distinguishes between the damaging effects of dual and triple axle combinations, but assumes that these combinations have the same damaging effects regardless of the axle spacing within the combination. Considering flexible pavements, a tandem axle carrying 8,160 kg (18,000 lb or, technically, 80 kN) on each axle has the AASHTO load equivalency factor of 1.38 regardless of the actual spacing between the two axles. However, if the spacing between the axles exceeds an unspecified distance so that the two axles can be considered to be independent, the corresponding AASHTO load equivalency factor is 2.00.

In 1988, a random survey of 2,089 trucks was conducted at 16 Ontario locations. The data show that the truck axle spacing ranges from about 1.0 m to 10.0 m (3.2 ft to 32 ft) and that its frequency distribution depends on truck type. An example of the survey data for two truck types—trucks with four axles or less and trucks with seven axles or more—is given in Figure 1. Because of data limitations, the frequency distribution of axle spacing in Figure 1 is plotted regardless of axle group type. Thus, a 2-m axle spacing may refer to a dual axle spacing, a two axle group spacing with no automatic load equalization, or the distance between two consecutive axles in a three or four axle group.

The distribution in Figure 1 appears to be bimodal with a dividing line at about 2.0 to 2.5 m. According to the Ontario Highway Traffic Act (*2*), consecutive axles that are not articulated from a common attachment, or that are not designed to automatically equalize the load between the axles, are considered to be single axles if their spacing exceeds (a) 2.5 m in the case of three or four consecutive axles or, (b) 2.0 m in the case of two consecutive axles. Because the maximum allowable weight for a single axle (with dual tires) is always larger than that for an individual axle that is a part of an axle group, the axle group spacing in the range of 2.0 to 2.5 m is avoided.

The objectives of this study were (a) to evaluate the influence of axle spacing on damage caused to flexible pavements, and (b) to determine maximum weights on dual and triple axles that would cause the same damage, axle per axle, as that caused by a single axle with the maximum legal load. The original motivation for this study was the need to develop a procedure for quantifying the damaging effect of various heavy load configurations using the measured pavement responses (surface deflections and asphalt concrete strains) obtained on our experimental testing facility (*4*).

The study is based on measured pavement response data obtained during the course of a Road and Transportation Association of Canada (RTAC) study (*5,6*) and on calculated pavement responses using the elastic layer theory. In both cases, data were obtained for a large variety of axle loads and configurations.

QUANTIFICATION OF DAMAGING EFFECTS FOR VARIOUS AXLE LOADS

The effect of heavy loads on pavement structural damage, such as fatigue (alligator) cracking and rutting, has been tra-

Research and Development Branch, Ministry of Transportation of Ontario, Downsview, Ontario, Canada M3M 1J8.

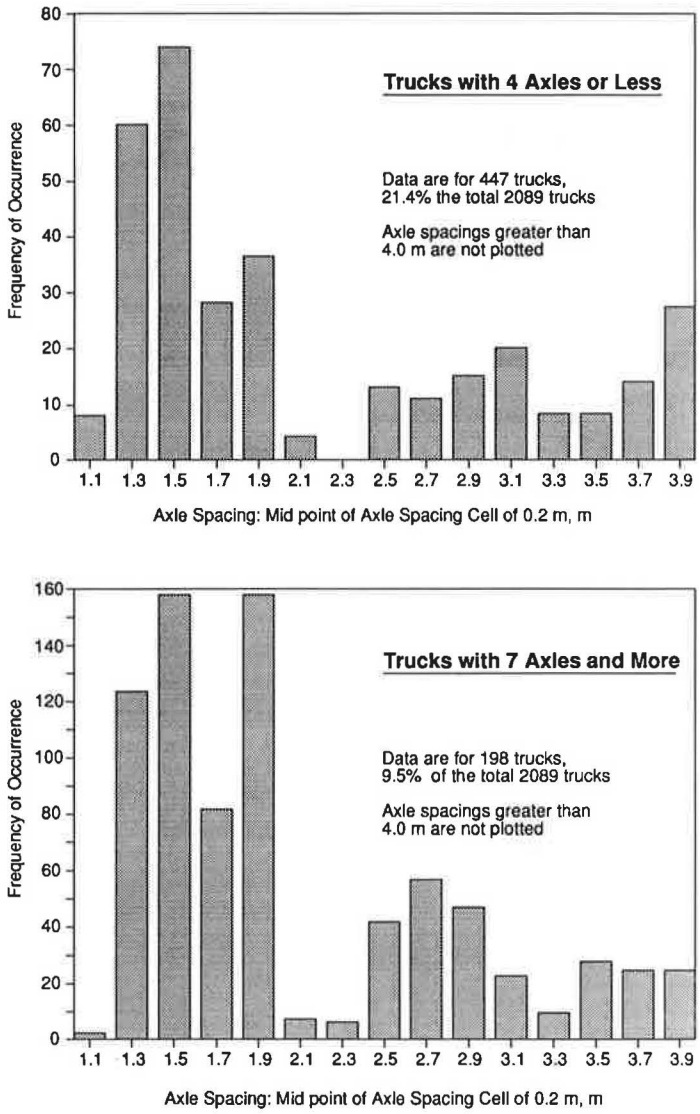

FIGURE 1 Frequency distribution of axle spacing for two truck types.

ditionally expressed using the concept of load equivalency factors (LEFs). For convenience, the LEFs have been related to a standard axle load defined as a single axle with dual tires carrying 8,160 kg (18,000 lb). The damaging effect of other axle loads is expressed in terms of the standard axle load as equivalent single axle load (ESAL) using the load equivalency factors. LEFs can be obtained in two basic ways: by a field experiment or by an analytical evaluation of pavement responses to individual loads. The latter way was used in this study.

LEFs Obtained by Field Experiments

A number of axle loads of a given magnitude and type required to cause a certain level of pavement deterioration (N_i) are determined in the field and are compared to the number of ESALs required to cause the same amount of pavement deterioration on the identical pavement structure N_{ESAL}:

$$LEF = \frac{N_{ESAL}}{N_i} \tag{1}$$

The resulting LEFs depend on the definition of pavement deterioration and its level, and on the type and strength of the pavement structure. Thus, for the same N_i, there may be various LEFs for various pavement types, thicknesses, subgrades, and pavement distresses. The best-known example of a field experiment is the AASHO Road Test of the early 1960s (*7*). The Test encompassed a number of various pavement structures, but on a uniform subgrade. The LEFs were mainly related to pavement damage in terms of roughness, which is directly related to the way the pavement serves the traveling public. This approach to obtaining load equivalency factors is extremely expensive and time consuming.

LEFs Obtained by Analytical Evaluation of Pavement Responses to Individual Loads

Measured or calculated pavement responses to individual load configurations are used to calculate LEFs by assuming the following general relationship:

$$LEF_r = \left(\frac{R_i}{R_{ESAL}}\right)^n \quad (2)$$

where

LEF_r = load equivalency factor based on pavement response r,
R_i = pavement response r to the load of a defined magnitude, and type designated as i,
R_{ESAL} = pavement response r to one ESAL, and
n = exponent to ensure that LEF (from Equation 1) is equal to LEF_r (from Equation 2) for pavement response r.

This approach, used in this study, requires the identification of pavement responses, such as strains and stresses, that cause specific pavement structural distresses. These distresses should be related to pavement deterioration, which affects the way pavements serve the traveling public. As a corollary, it is assumed that increased strains and stresses in the pavement structure increase pavement distresses (and reduce the pavement serviceability). Furthermore, this approach is faced with two main complications. First, load equivalency factors depend on the type and severity of pavement distresses, of which there are many possible combinations. Second, according to Equation 2, it is assumed that the pavement response to an axle group load, which can be rather complex, can be characterized and summarized by one number. However, in the absence of a universally accepted computational procedure to summarize pavement responses in terms of one encompassing number, the use of various computational procedures may yield different results.

Response Parameters Used

The load equivalency factors used by an agency should be based on the pavement distress or distresses that trigger the local need for pavement rehabilitation. For example, Hallin et al. (*8*) developed LEFs for Washington state based on fatigue cracking because "cracking is the principal form of asphalt pavement distress in Washington state." A statistical examination of Ontario pavement distress data (*9*) reveals that practically all 15 routinely evaluated pavement surface distresses occur at the critical levels of severity and density requiring rehabilitation and that fatigue cracking is not a predominant distress. The 15 distresses include raveling, flushing, rutting, distortion, and various types of cracking, such as pavement edge, transverse, and alligator. For this reason, the following three basic pavement responses, linked previously to the formation of pavement distress, have been used in this study:

1. *Pavement surface deflection*. This response has been linked to pavement deterioration, measured mainly in terms of roughness. Several pavement distresses, such as cracking, distortion, and rutting, can contribute to pavement roughness.
2. *Interfacial strain*. Strain at the bottom of the asphalt concrete layer that has been related to fatigue (alligator) cracking.
3. *Vertical strain on the top of the subgrade*. This response has been related both to rutting in the pavement structure and to pavement deterioration.

A typical history of these three responses for a flexible pavement subjected to a moving dual axle load is shown in Figure 2.

Summation of Pavement Responses to Axle Loads

The comparison of damage caused by various loads requires quantification and summation of pavement response curves (Figure 2) resulting from the passage of these loads. Two approaches can be used: discrete summation methods or integration methods. Discrete methods use only discrete values at the peaks and valleys of the response curve, whereas integration methods attempt to use the whole response curve. The two summation methods are illustrated in Figure 3 using pavement response curves obtained for single and dual axles. Also shown in Figure 3 are three various dual axle response curves (Cases a through c), which will be discussed later.

Discrete Methods

Three discrete methods used in this study—RTAC, University of Waterloo, and Peak—are schematically shown in Figure 4. LEFs were calculated by summing peak to valley responses using a modified Equation 2 as follows:

$$LEF_{r,m} = \frac{\sum_{i=1}^{p} (ri)^n}{(R_{ESAL})^n} \quad (3)$$

where

$LEF_{r,m}$ = load equivalency factor to pavement response r and method m.

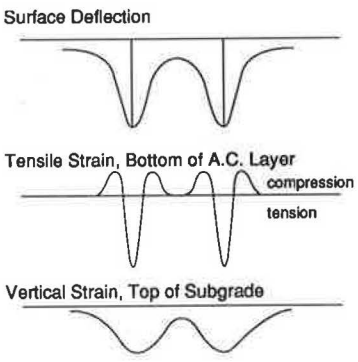

FIGURE 2 Typical response of a flexible pavement to a moving dual-axle load.

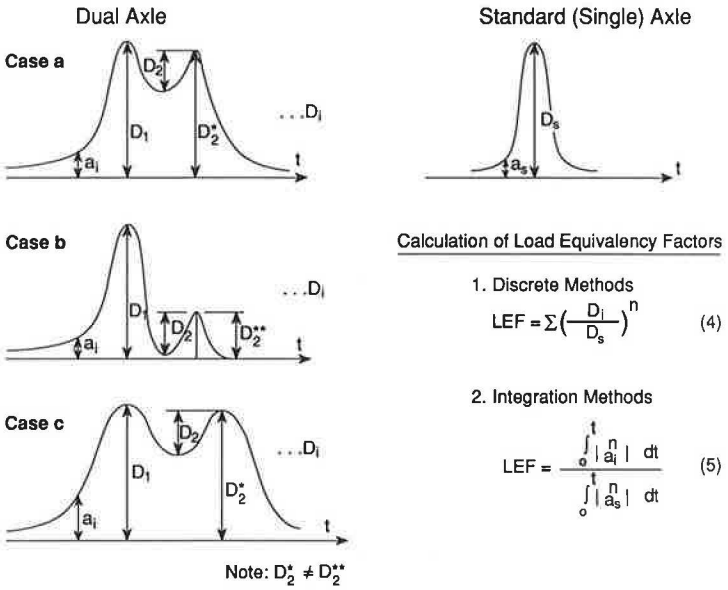

FIGURE 3 Discrete and integration methods for calculation of load equivalency factors.

r_i = discrete pavement response for load cycle i identified by method m.
n = as defined before, adapted to be 3.8. This value was also used in the RTAC study (*5,6*) (both for surface deflections and interfacial strains) and is based on an extensive review by Christison (*6*).
p = number of load cycles (axles).

The exponent n can vary for various pavement response parameters and depends on the procedures used to obtain it. For example, it is well recognized that n derived from laboratory fatigue tests of asphalt concrete mixes depends on the mix composition, the testing conditions, and the definition of failure (*10*).

RTAC Method

The RTAC method was originally used for the analysis of measured pavement responses as part of the Canadian Vehicle Weights and Dimensions Study (*5,6*). For surface deflections (and in this study also for strains on the top of the subgrade), the peak under the lead (first) axle was extracted first, followed by the trough to peak differences in the response curve for the subsequent axles (Figure 4). For interfacial strains, only the peak tensile strains measured from the rest (zero) position were used.

University of Waterloo Method

The University of Waterloo method was developed by Hutchinson et al. (*11*) for isolating and counting pavement surface deflection cycles. In this study, it was also used for the summation of subgrade strains. The method follows an ASTM Standard Practice (*12*), which recommends that the highest peak and lowest valley be used first, followed by the second largest cycle, and so on, until all peak counts are used (Figure 4).

Peak Method

For surface deflections and subgrade strains, the peak method uses the total response under each axle from the rest position. For interfacial strains, the peak method uses the peak to trough rises and falls in the strain history (Figure 4), a procedure that is identical to that recommended by ASTM Standard Practice for Cycle Counting in Fatigue Analysis (*12*); for this reason, the peak method appears to be an improvement over the RTAC method.

Regarding surface deflections, proponents of this method (*13*) argue that even though the surface deflections between two subsequent axles do not reach a rest position, the asphalt concrete layer at this location reverses its curvature (tensile strain to compressive strain [Figure 2]) so that the inclusion of the total deflection best models the overall pavement response.

Another argument in support of this method may be advanced by considering how various response curves, such as those shown for Cases a and b in Figure 3, are accounted for by the peak method. In Case a, the peak axle responses D_1 and D_2^* are nearly equal, whereas in Case b the two peaks differ considerably (D_1 versus D_2^{**}). Case c has the same peaks as Case a, but the duration of the load is longer. All three cases have the same trough D_2. The peak method uses responses D_1 and D_2^* (or D_2^{**} for Case b) and thus distinguishes between the damaging effects of the two Cases a and b, whereas the other two methods, RTAC and Waterloo, do not (they are based on responses D_1 and D_2).

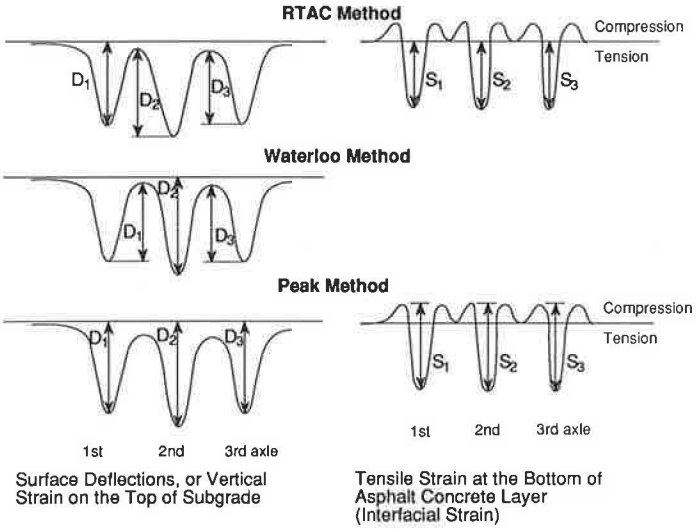

FIGURE 4 Discrete methods used to calculate the effect of multiple-axle groups.

Integration Methods

Flexible pavements respond to loads as visco-elastic systems with resulting permanent and elastic strains. The permanent strains are influenced by both the amount and the duration of load. Integration methods take both spatial and temporal variability of the load into account by integrating the response curve expressed as a function of time or distance. Referring to Figure 3, integration methods distinguish between the response curves of not only Cases a and b, but also between Cases a and c, which have similar peaks but different load duration. The formula developed in this study for calculating LEFs by integration is shown in Figure 3, Equation 5. Conceptually, it resembles the formulation used by Govind and Walton (*14*). The exponent n for this method was also set at 3.8 to enable a direct comparison with discrete methods. There is no precedent in the literature for the value of n.

The integration methods include influence of the rate of loading on pavement damage and eliminate ambiguity in defining the peaks and valleys required for discrete methods. However, the validity of integration methods has not been proven.

MEASURED AND CALCULATED PAVEMENT RESPONSES

Measured Pavement Responses

Measured pavement responses used in this study were taken from the Canadian Vehicle Weights and Dimensions Study (*5*). This 1985 study provides a large set of measured pavement responses in terms of surface deflections and interfacial strains obtained at 14 sites for a variety of loading conditions. The results based on these measurements are referred to in this study as RTAC measurements.

Calculated Pavement Responses

Computational Method

The flexible pavement was modeled as an idealized elastic layered system, and its responses to loads were calculated by the ELSYM5 computer program (*15*). The use of the elastic layer theory to obtain load equivalency factors has been successfully used before (*8,16,17*).

Pavement Structure

Calculations were done for the thin and thick flexible pavement structures shown in Figure 5. The thin section has a structural number (SN) of 3.0 and represents a low-volume road; the thick section has an SN of 5.7 and represents a typical structure for a high-volume facility. The average SN for the 14 sections used in the RTAC study was 5.0.

Pavement Loadings

Analyses were done for single-, dual-, and triple-axle groups. All axles had dual tires spaced about 350 mm (14 in.) apart. The tire footprints were assumed to be circular with a pressure of 690 kPa (100 psi). Axle loads on individual axles ranged from 5,450 kg (12,000 lb) to 11,800 kg (26,000 lb). As the load increased, the tire contact area increased because the tire pressure was held constant. A similar loading arrangement was used by Kilareski (*17*).

Location of Maximum Deflections and Strains

When comparing pavement response to various axle loads, it is important to use the maximum responses in all cases as a

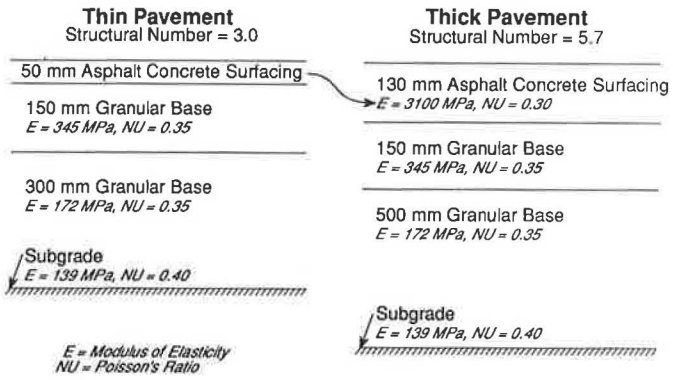

FIGURE 5 Flexible pavement structures used in analysis.

common denominator. Analysis shows that the maximum responses for deflection and strains occur on the line at the midpoint between the dual tires, regardless of axle spacing. The responses along this line were calculated to identify all relevant features of the response curve required for analysis.

RESULTS

Effect of Axle Spacing on Pavement Damage

Load equivalency factors are plotted as a function of axle spacing for double and triple axles in Figures 6 and 7, respectively. For easier comparisons, the axle loading in Figures 6 and 7 is kept constant at a standard design load of 8,160 kg (18,000 lb) per individual axle. The results are briefly interpreted in the following sections.

Summation of Pavement Responses to Axle Loads

Summation methods (methods used to quantify and summarize pavement response curves) have a large influence on LEFs, notably on LEFs based on surface deflections and subgrade strains. In general, the peak method yields the highest LEFs, followed by the Waterloo method and finally by the RTAC method. The LEFs obtained by the integration method are shown only for dual axle and surfaces deflections. Although the integration method appears to be conceptually sound, the selection of the exponent n in Equation 5 (Figure 3) is arbitrary. Based on the available information and data, it is not possible to unequivocally recommend any particular summation method; however, the peak method appears to be the best candidate. As will be shown later, the summation methods have a decisive influence on the LEFs.

Measured Versus Calculated Pavement Responses

It appears that the summation methods have a larger influence on the resulting LEFs than on whether the original pavement responses (on which the methods operate) were measured or calculated. For example, considering LEFs for dual axles based on surface deflections (top of Figure 6), the results can be grouped according to the summation method used instead of whether the pavement responses were measured or calculated. Regarding the quantification of pavement damage caused by various load configurations, future efforts should be directed toward a better understanding of the influence of various pavement response parameters and the summation methods. This approach appears to be a much more fruitful endeavor than the fine tuning of procedures for measuring or calculating pavement responses to loads.

Pavement Response Parameters

Overall, regardless of the summation method used, LEFs based on deflections are larger than those based on strains (interfacial and subgrade) and decrease with increasing axle spacing. The LEFs based on interfacial strains and calculated by the RTAC method increase (rather than decrease) with larger axle spacing. The same also roughly applies to subgrade strains processed by the RTAC method. This phenomenon can be explained by noting that when axles are close together, the compressive strain in asphalt concrete caused by one axle can offset a part of the tensile strain caused by an adjacent axle, effectively reducing the net tensile pavement strain. Because the RTAC method does not work with the total strain cycle (it excludes compressive strain from the calculation of LEFs), but still uses the reduced tensile strain, the RTAC LEFs for interfacial strains can decrease with axle spacing.

Axle Spacing

For thick pavements, axle spacing has a significant influence on LEFs, particularly for those determined for surface deflections and vertical strains using the peak method. As expected, for large axle spacings, all LEFs (for 8,160-kg loads) tend to approach 2.0 for dual axles and 3.0 for triple axles, regardless of response parameters or summation method used.

Pavement Structure

The influence of axle spacing on LEFs decreases with the decrease of pavement structural strength. Thin, structurally weak pavements do not distribute axle loads effectively. Con-

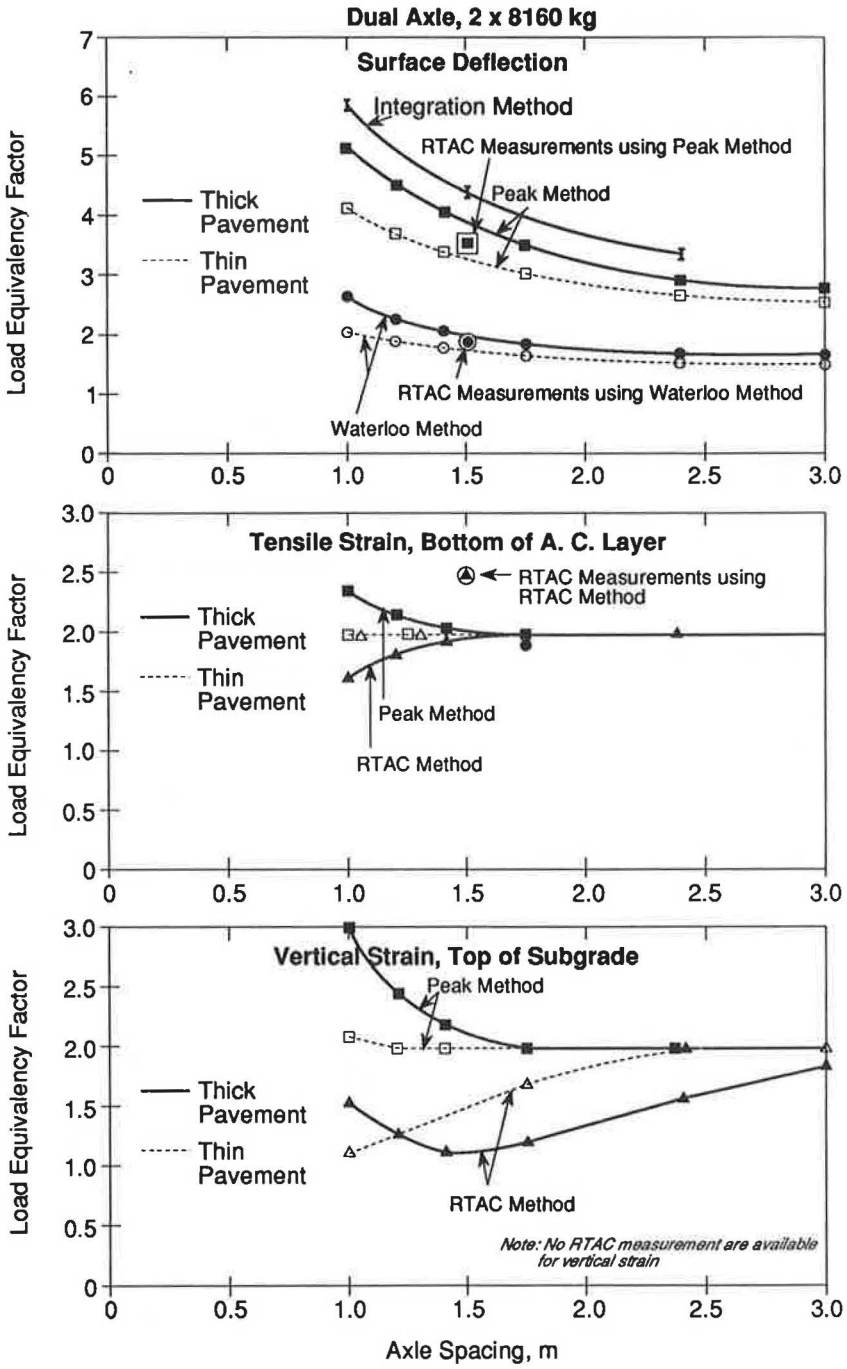

FIGURE 6 Influence of axle spacing on load equivalency factor for dual axles.

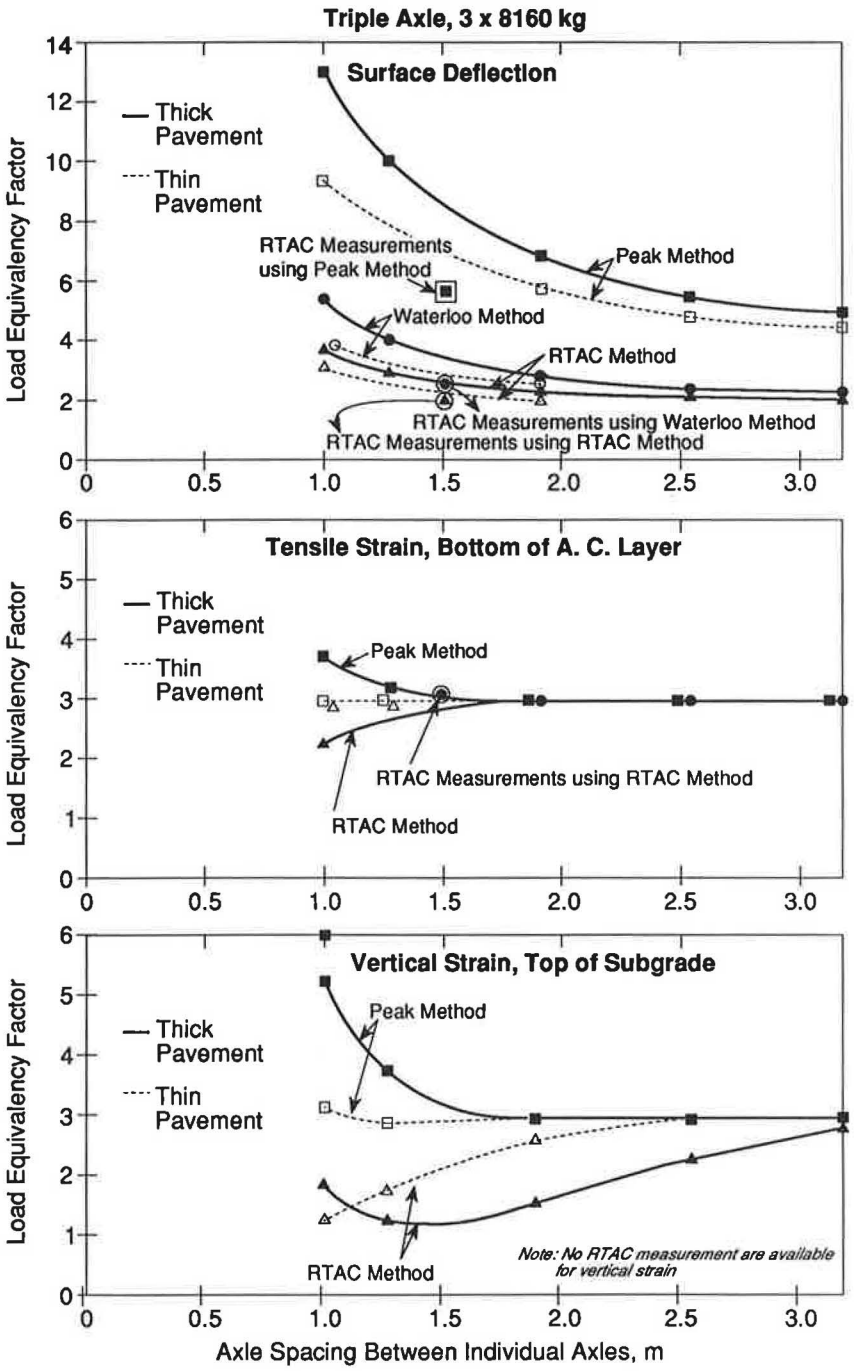

FIGURE 7 Influence of axle spacing on load equivalency factor for triple axles.

TABLE 1 AASHTO LOAD EQUIVALENCY FACTORS FOR TANDEM (DUAL) AND TRIPLE AXLES (*3*)

Axle Type	Zero Spacing (only one axle)	Typical Axle Spacing[1)]	Large Spacing[1)] (independent axles)
Tandem	13.9	1.38	2.0
Triple	above 53	1.66	3.0

Note: The actual spacing is not defined.

Conditions: Flexible pavement, SN = 5, p_t = 2.5,
Load on each individual axle is 8 160 kg (18 000 lb).

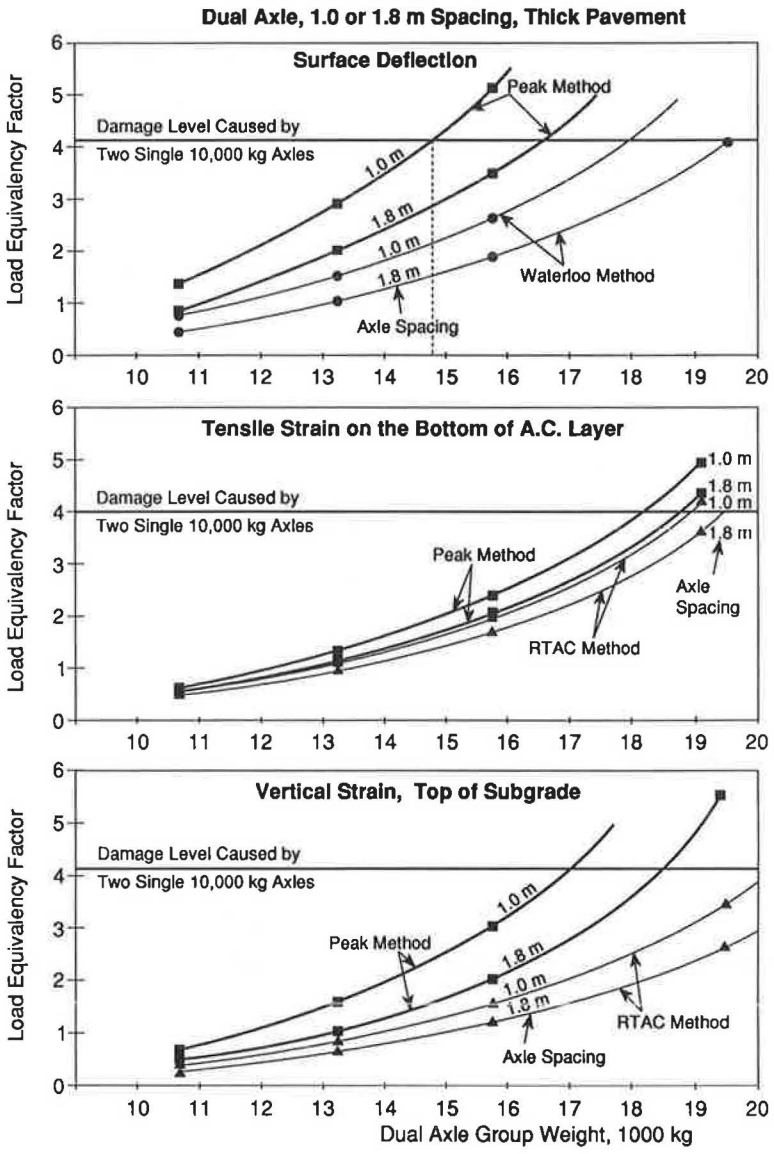

FIGURE 8 Comparison of damage caused by two single axles versus one double-axle group (thick pavement).

sequently, their responses are governed mainly by individual axles and not by the whole axle group. For example, regardless of axle spacing or the summation method used, LEFs for dual axles based on interfacial strains are equal to 2.0.

Comparison with AASHTO Factors

Typical LEFs recommended by the AASHTO Guide (*3*) for dual and triple axles are given in Table 1. The AASHTO LEFs do not change with axle group spacing. Also shown in Table 1 are LEFs for zero spacing and for spacing large enough so that axles can be considered to act independently. This spacing is not defined by the AASHTO Guide. For example, a triple axle with the weight of 8,160 kg (18,000 lb) on each of its three axles has an LEF of 1.66 regardless of axle spacing. When the spacing between the three axles exceeds an unspecified distance, the LEF jumps to 3.0. If, at the other extreme, all three axles are concentrated in one position, the LEF exceeds 53. Considering that the spacing between the consecutive axles can be variable (Figure 1), particularly for axle groups that do not equalize loadings, the results suggest that the AASHTO LEFs would benefit from including the influence of axle spacing.

Damage Comparisons

The maximum allowable axle weight for single axles with dual tires in Ontario is 10,000 kg (22,046 lb). This axle weight represents 2.0 to 2.1 LEFs, depending on the pavement response and pavement structure. The value of 2.0 or 2.1 does not

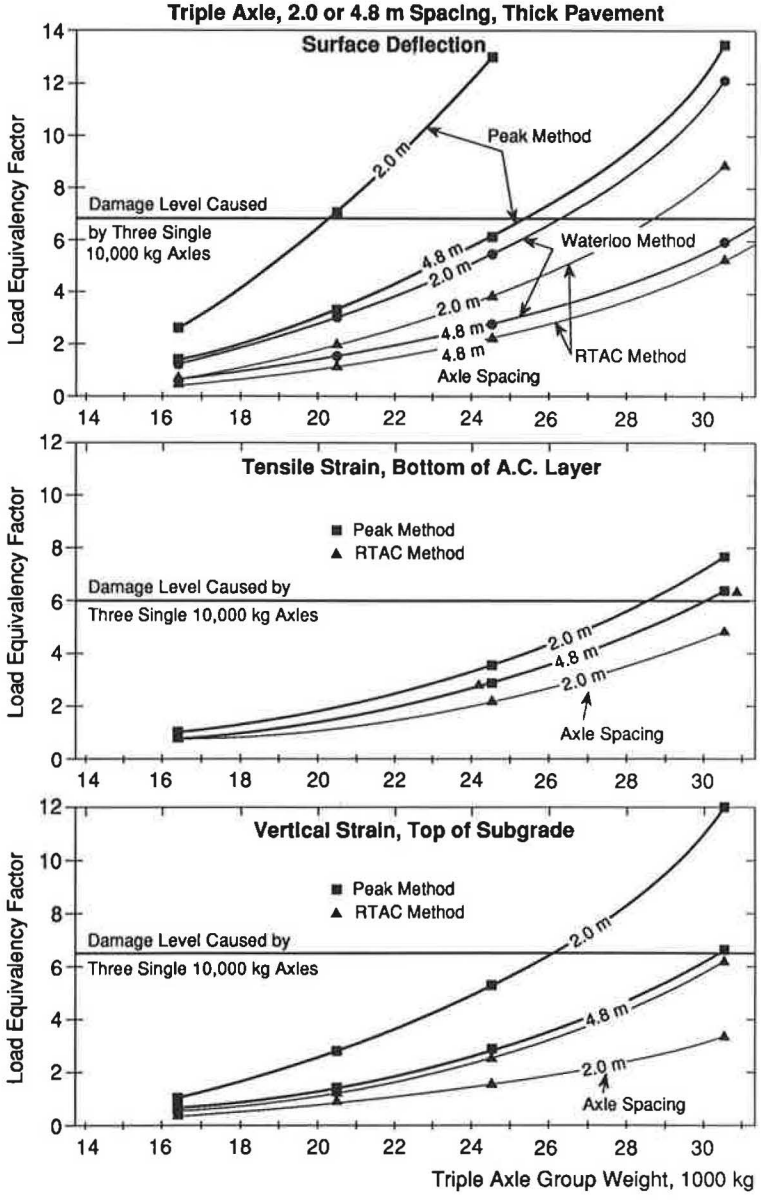

FIGURE 9 Comparison of damage caused by three single axles versus one triple-axle group (thick pavement).

depend on the (discrete) summation methods used because the single axles have only one peak value and the LEF can be calculated directly from Equation 2. The corresponding AASHTO LEF is 2.18 (*3*) (for p_t = 2.5, and SN = 5.0).

If the single axle can be allowed to have a maximum of 2.0 LEFs, then, based on the principle that any axle can cause identical damage, a dual axle can be allowed to have 4.0 LEFs and a triple axle can be allowed to have 6.0 LEFs. Based on this principle, what are the maximum weights for dual and triple axles causing the same pavement damage (per individual axle) as the single axle weighing 10,000 kg? How do these weights compare with legislative limits? These questions are addressed in this section.

Figures 8 and 9 show the influence of axle spacing and axle group weights on LEFs for dual and triple axles. The results are shown only for the thick pavement because they are more representative. Figures 8 and 9 are derived from calculations similar to those used for Figures 6 and 7, respectively. Also shown in the two figures are horizontal lines indicating LEFs (damage levels) for a corresponding number of single axles. For example, considering the results obtained for dual axle and surface deflections (top of Figure 8), based on the peak method and 1.0-m axle spacing, the total dual axle group weight, having the same LEF (causing the same damage) as two single axles with the maximum allowable weight (i.e., 4.20), is about 14,900 kg.

The results of Figures 8 and 9 are summarized in Table 2 together with the AASHTO data (*3*) and the Ontario allowable limits (*2*). The following two basic observations can be made, based on Table 2:

1. Ontario permissible weights for dual and triple axles are lower than those established by any computational scenario with the exception of the deflection-based peak method. The greatest difference (3,400 kg) exists for triple axles with the largest spacing (4.8 m). Ontario regulations allow 28,600 kg, whereas the deflection-based peak method would allow only 25,200 kg.
2. The AASHTO-based weights are higher than the weights based on deflections and interfacial strains regardless of the summation method used. They are roughly similar to the allowable weights based on a subgrade strain response, evaluated by the RTAC method. Overall, it appears that the AASHTO Guide may underestimate the damaging effects of dual and triple axles in comparison with single axles.

CONCLUSIONS AND RECOMMENDATIONS

1. Load equivalency factors are significantly influenced by (a) pavement response parameters (deflection, strains) on which they are based and (b) summation methods used for their calculation. There is a need for a better understanding of the influence of various pavement response parameters and summation methods on the quantification of pavement damage caused by multiple axle-loads.
2. Contrary to the inference based on pavement design guides, axle spacings have a significant effect on pavement damage, which should be accounted for in determining the permissible load limits on dual and triple-axle units.
3. Permissible weights on dual and triple axles in Ontario are generally lower than those determined by the various computational methods used to analyze pavement damage. The peak method, however, gives up to 12 percent lower permissible weights for larger axle spacings than are allowed by Ontario legal limits.
4. It appears that within the practical range of axle spacings, pavement damage can be significantly reduced by increasing axle spacings.

TABLE 2 EQUIVALENT DAMAGE LOADS FOR DUAL AND TRIPLE AXLES[1]

How Determined	Dual Axle, Spacing 1.0 m	Dual Axle, Spacing 1.8 m	Triple Axle, Spacing 2.0 m	Triple Axle, Spacing 4.8 m
Deflections				
Peak Method	14 900	16 700	20 300	25 200
Waterloo Method	18 000	19 600	26 200	28 300
Strains, A.C.				
Peak Method	18 300	18 900	28 300	29 900
RTAC Method	19 000	19 700	32 100	29 900
Strains, Subgrade				
Peak Method	17 100	18 600	26 100	30 100
RTAC Method	20 600	22 000	31 000	35 500
AASHTO[2)]	21 600	21 600	34 300	34 300
Ontario Weight Limits[3)]	15 400	19 100	19 500	28 600

The numbers represent the total weight of dual (or triple) axles in kg that causes the same amount of damage as 2 (or 3) single axles with a maximum allowable weight of 10 000 kg.

Notes: 1) (Thick) flexible pavement, SN = 5.7, See Figure 5
2) Source: Reference 3, SN = 5.7, p_t = 2.5, LEF = 4.2 for dual axle or 6.3 for triple axle.
3) Source: Reference 2

ACKNOWLEDGMENT

The authors would like to express their appreciation to J. Polenek, engineering student, University of Waterloo, who assisted with the computer analysis.

REFERENCES

1. OECD Scientific Experts Group. *Heavy Trucks, Climate and Pavement Damage*. OECD 75775, Organization for Economic Cooperation and Development, 1986, pp. D-6–D-8.
2. *Vehicle Dimensions and Weight Limits in Ontario*. Ministry of Transportation, Compliance Branch, Downsview, Ontario, Canada, 1986.
3. *AASHTO Guide for Design of Pavement Structures—1986*. American Association of State Highway and Transportation Officials, Washington, D.C., 1986.
4. G. M. Stott, J. J. Hajek, and W. A. Phang. *Highway 7N Pavement Response and Vehicle Damage Experiment: Construction, Instrumentation, and Monitoring*. Report PAV-88-01. Ministry of Transportation, Ontario, Canada, 1988.
5. J. T. Christison. *Vehicle Weights and Dimensions Study, Volume 8: Pavement Response to Heavy Vehicle Test Program, Part 1—Data Summary Report*. Roads and Transportation Association of Canada, Ottawa, Ontario, July 1986.
6. J. T. Christison. *Vehicle Weights and Dimensions Study, Volume 9: Pavement Response to Heavy Vehicle Test Program, Part 2—Load Equivalency Factors*. Roads and Transportation Association of Canada, Ottawa, Ontario, July 1986.
7. *Special Report 61E: AASHO Road Test: Report 5—Pavement Research*. HRB, National Research Council, Washington, D.C., 1962.
8. J. P. Hallin, J. Sharma, and J. P. Mahoney. Development of Rigid and Flexible Pavement Load Equivalency Factors for Various Widths of Single Tires. In *Transportation Research Record 949*, TRB, National Research Council, Washington, D.C., 1983, pp. 4-B.
9. J. J. Hajek and W. A. Phang. Moving from Subjective to Objective Evaluation of Pavement Performance. *Proc., 1986 RTAC Conference*, Toronto, Ontario, Canada, September 1986.
10. J. A. Deacon. Load Equivalency in Flexible Pavements. Proc., *Association of Asphalt Paving Technologists*, University of Minnesota, Minneapolis, 1969, Vol. 38, pp. 465–496.
11. B. G. Hutchinson, R. C. G. Haas, P. Meyer, K. Hadipour and T. Papagiannakis. Equivalencies of Different Axle Load Groups. Proc., *2nd North American Conference on Managing Pavements*, Toronto, Ontario, Canada, November 1987.
12. *ASTM Standard E 1049-85, 1986 Annual Book of ASTM Standards*, Vol. 03.01, ASTM, 1986, pp. 764–772.
13. A. Prakash and A. C. Agarwal. *Tri-Axle Study: Proposed Methodology to Study Effect on Pavements*. Internal Report, Ministry of Transportation, Ontario, Canada, 1988.
14. S. Govind and C. M. Walton. A Fatigue Model to Assess Pavement Damage. Presented at 69th Meeting of the Annual Transportation Research Board, Washington, D.C., 1988.
15. *ELSYM5*. Report FHWA-RD-85. FHWA, U.S. Department of Transportation, 1985.
16. H. J. Treybig. Equivalency Factor Development for Multiple Axle Configurations. In *Transportation Research Record 949*, TRB, National Research Council, Washington, D.C., 1983, pp. 32–44.
17. W. P. Kilareski. Heavy Vehicle Evaluation for Overload Permits. In *Transportation Research Record 1227*, TRB, National Research Council, Washington, D.C., 1989, pp. 194–204.

Publication of this paper sponsored by Committee on Flexible Pavement Design.

Fatigue Damage Properties of Asphaltic Concrete Pavements

KUO-HUNG TSENG AND ROBERT L. LYTTON

The development of material property relations for the two fatigue damage properties, K_1 and K_2, which can be used to predict the fatigue life of asphaltic concrete pavements, is described. The fatigue damage properties developed are based on the theory of fracture mechanics along with regression analysis on published beam fatigue data and, thus, can take into account crack initiation, propagation, and material properties that are not accounted for with the conventional strain-based fatigue equation. The approach provides more insight into how these fatigue damage properties reflect the fatigue behavior of asphaltic concrete pavement while producing acceptable estimates of field fatigue life. Derivations have shown that the fatigue damage property K_1 is dependent on the asphalt mixture and pavement properties, such as the parameters of the Paris crack growth law, elastic stiffness, and thickness of the asphaltic concrete layer and that the fatigue damage property K_2 varies with the initial asphalt cement properties, such as asphalt content, viscosity, penetration, and temperature. Two significant functions of the fatigue damage properties developed are (a) the prediction of fatigue life allows for the application of loading with single or dual tires on single, tandem, or triple axles, and (b) they provide for the calculation of load equivalence factors for fatigue life as affected by multiple-axle loads. A shift factor that can be used to adjust the laboratory (or calculated) fatigue damage properties to that measured in the field is also described. This factor takes into account healing and residual stresses between applications of traffic loads that are responsible for the difference in fatigue life between laboratory test results and those measured in the field.

FATIGUE DAMAGE PROPERTIES OF ASPHALTIC CONCRETE PAVEMENTS

The evaluation of fatigue cracking caused by repeated loads is important in the design and prediction of the service life of flexible pavements. The procedure conventionally used for predicting fatigue life is based on the "phenomenological approach," in which, commonly, the fatigue life is measured by laboratory testing with a third-point flexural load applied on a beam under controlled stress or strain conditions at a given temperature and frequency. The fatigue results thus obtained from laboratory tests are expressed as a power law relation between the tensile strain (ε) in the bottom of the beam and the number of load applications to failure N_f. The relation is given by

$$N_f = K_1 (1/\varepsilon)^{K_2} \quad (1)$$

K-H. Tseng, Texas Transportation Institute, Texas A&M University Systems, College Station, Tex. 77843. R. L. Lytton, Civil Engineering Department, Texas A&M University, College Station, Tex. 77843.

where K_1 and K_2 are the phenomenological regression constants. Once K_1 and K_2 are obtained from laboratory tests, the fatigue life of asphaltic concrete pavements can be estimated from Equation 1. A number of laboratory studies (*1*,*2*) have shown that these constants are affected by material properties such as mixture stiffness, air voids, asphalt content, viscosity of asphalt cement, and gradation of the aggregate; by the dimensions of the test sample; and by environmental conditions, such as the temperature during the tests. This information indicates that a more profound understanding is needed of how these two constants, K_1 and K_2, depend on the fatigue behavior and material properties of an asphaltic concrete mix.

The objective of this paper is to present the development of the fatigue damage properties of asphaltic concrete pavements by applying the theory of fracture mechanics to the results of laboratory beam fatigue tests. The prediction of fatigue life based on the fatigue damage properties that are developed also allows for the application of loading with single or dual tires on single, tandem, or triple axles. This development, subsequently, provides for the calculation of load equivalence factors for fatigue life as affected by multiple-axle loads. Along with the fatigue damage properties, a shift factor is described that takes into account the effects of healing and residual stress between applications of traffic loads and can be used to adjust the laboratory (or calculated) fatigue damage properties to that observed in the field.

The complete procedures for predicting fatigue life based on the fatigue damage properties have been included in the FEPASS (*F*inite *E*lement *P*erformance *A*nalysis *S*tructural *S*ubsystem) computer program (*3*), which is a revised version of ILLI-PAVE (*4*). The FEPASS program also has the ability to predict the rutting and loss of serviceability index of in-service payments, taking into account realistic distributions of tire contact pressure, both vertical and horizontal, and has the ability to provide various amounts of resistance to slip between layers. This paper is organized to present a better understanding of fatigue characterization of asphaltic concrete pavements. Other applications of the FEPASS program are presented elsewhere (*3*).

DEVELOPMENT OF RELATION BETWEEN FATIGUE EQUATION AND CRACK GROWTH LAW

Utilizing Paris' crack growth law (*5*), the number of load cycles (N_f) can be expressed as

$$N_f = \int_{C_0}^{C_f} \frac{da}{A(\Delta K)^n} \tag{2}$$

where C_0 is initial crack length, C_f is final crack length, A and n are the fracture parameters, and ΔK is the difference of the stress intensity factor that occurs at the tip of the crack during the passage of a load. In addition to the fracture parameters in Paris' equation, the stress intensity factor caused by the loading conditions and initial crack tip geometry are also required to develop equations that model pavement fatigue life. A finite element computer program is used to evaluate stress intensity factors induced within both the laboratory fatigue beam and the asphaltic concrete layer in pavements. The program, which was originally developed for plane stress or plane strain analysis by Desai and Abel (*6*) was subsequently modified by Jayawickrama (*7*) to allow for the use of the energy release method for evaluating stress intensity factors. The stress intensity factors are then computed for various crack-tip positions. The computed data for an elastic beam fatigue test are reduced to nondimensional form as shown in Figure 1 and are represented by the expression

$$\frac{K}{d^{1/2}\sigma} = r\left(\frac{c}{d}\right)^q \tag{3}$$

where

σ = maximum stress at extreme fiber of the beam ($= E\varepsilon$),
E = the elastic stiffness of the fatigue beam corresponding to the loading frequency and temperature,
ε = the tensile strain at the extreme fiber of the beam,
c = crack length,
d = depth of the beam, and
r and q = regression constants; $r = 4.397$, $q = 1.180$.

A laboratory method that measures the fracture properties and the strain energy release rate directly is presently in use (*8*). This method, which is known as the J-integral method, is applicable to all materials, regardless of their constitutive equations. There are no mechanistic methods available to calculate the J-integral strain energy release rate for pavements in the field, however; thus laboratory methods—although they are applicable to all materials—must remain confined to laboratory applications for the moment, and the linear elastic fracture mechanics method presented here is the only laboratory method for which a mechanistic pavement model is currently available for field applications.

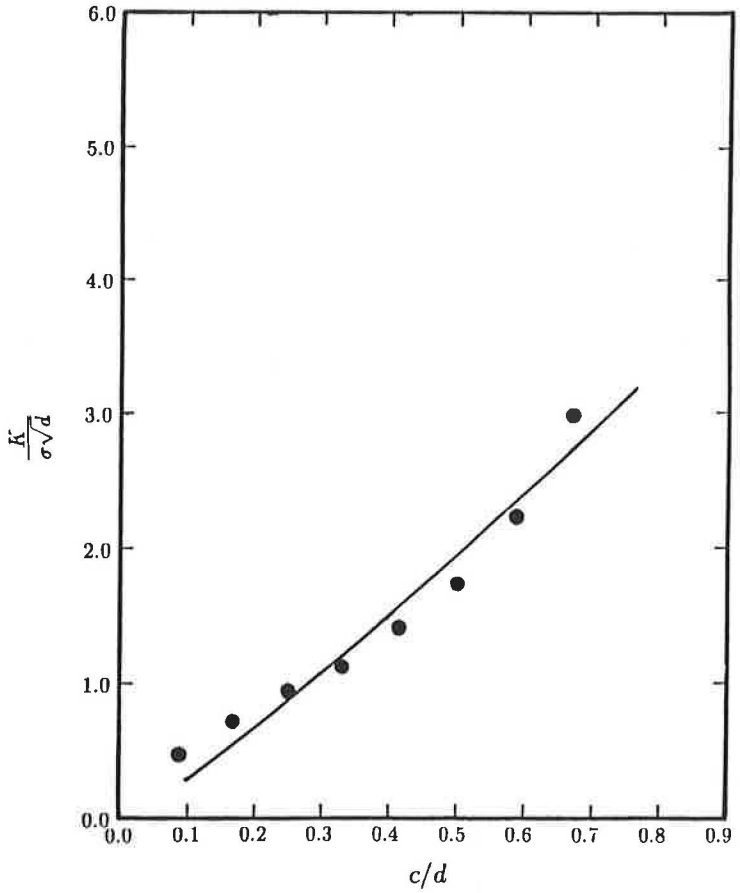

FIGURE 1 Determination of stress intensity factor for various crack-tip positions.

Substituting the stress intensity factor from Equation 3 into Equation 2, the fatigue life (N_f) becomes

$$N_f = \frac{d^{1-\frac{n}{2}}\left[1 - \left(\frac{C_0}{d}\right)^{1-nq}\right]}{A\,(1 - nq)\,(Er)^n}\left(\frac{1}{\varepsilon}\right)^n \tag{4}$$

The initial crack length (C_0) is estimated to be the radius of the largest aggregate particle. This estimation is based on laboratory observations. The fracture coefficients A and n are determined from laboratory tests as the intercept and slope, respectively, on a log-log plot of stress intensity factor (K) versus the rate of crack growth (da/dN). Equation 4 is identical to Equation 1, which is used to describe the fatigue characterization based on the controlled-strain mode in the laboratory. Therefore, the fatigue damage properties (K_1 and K_2) of the fatigue equation can be calculated from

$$K_1 = \frac{d^{1-\frac{n}{2}}\left[1 - \left(\frac{C_0}{d}\right)^{1-nq}\right]}{A\,(1 - nq)\,(Er)^n} \tag{5}$$

and

$$K_2 = n \tag{6}$$

It is apparent from Equation 5 that log K_1 depends in a complex way on K_2 (or n). The empirical observation of a "linear relation" of the two variables is thus shown to be theoretically incorrect, although a plot of log K_1 versus n using Equation 5 normally produces a nearly linear relation. This points up the value of having a theory: the relation in Equation 5 could not have been discovered by using regression analysis.

In addition to the A and n values obtained from laboratory tests, a theoretical equation of crack growth derived by Schapery (*9*) also can be used to calculate these two parameters. Experimental studies (*10*) on asphaltic concrete mixes to verify Schapery's equation have shown that the value of n is evaluated by the following relationship, which is derived from theory:

$$n = 2/m \tag{7}$$

where m is the slope of the tensile creep compliance curve obtained from laboratory creep tests. However, the value of m in this paper is determined alternatively from the straight-line portion of the log-log plot on the mix stiffness versus loading time at the test temperature. A computerized version of the McLeod nomograph (*11*) has been developed by Jayawickrama et al. (*12*) to calculate the values of m and n when creep compliance and other material properties are not available. This program requires input information of (a) penetration at 77°F, (b) viscosity at 275°F or at 140°F, (c) service temperature, (d) asphalt content, and (e) air void content. Alternatively, the same m and n may be calculated using the Van der Poel nomograph (*13–15*) if the ring-and-ball softening point and penetration are available.

Theoretically, based on Schapery's equation, the value of A can be calculated from those variables such as creep compliance, Poisson's ratio, fracture energy, tensile strength, shape of the loading stress pulse, and other factors. The calculation of A by means of Schapery's equation is complicated by the fact that not all of the variables that are required to calculate the value of A in the equation were measured in previously published beam fatigue tests. Data from a total of 32 published beam fatigue tests were collected from three different sources (*16–18*) and are shown in Table 1. A regression equation for estimating A was developed from the data that were available.

In Equation 5, the parameter A can be rearranged as

$$A = \frac{d^{1-\frac{n}{2}}\left[1 - \left(\frac{C_0}{d}\right)^{1-nq}\right]}{K_1(1 - nq)(Er)^n} \tag{8}$$

The value of n and E in Equation 8 are the actual observed K_2, and observed elastic stiffness, respectively, and each value of A is then back calculated from the available 32 beam fatigue test results. The regression analysis is made by using the parameter A as the dependent variable and the observed K_2, observed elastic stiffness, loading frequency, and specimen size as the independent variables. It is found that the value of A is best explained in terms of the exponent K_2 and the elastic stiffness of the mix. The regression equation for A is then developed:

$$\log A = 7.0889 - 2.4755\,K_2 - 2.1163 \log E \qquad R^2 = 0.86 \tag{9}$$

Thus, to use Equation 9 for the estimation of A, the flexural elastic stiffness (E) is calculated from the McLeod-Van der Poel routine (*11,13*), and K_2 is equal to n, which is calculated from $2/m$. The value of m is also calculated with the McLeod-Van der Poel routine. Once the value of A is estimated and m is obtained, the fatigue damage properties (K_1 and K_2) can be evaluated by using Equations 5 and 6.

COMPARISONS OF CALCULATED AND EXPERIMENTAL K_1 AND K_2 AND ELASTIC STIFFNESS

As described previously, it has been shown that the exponent (K_2) of the fatigue relation and the exponent (n) of the crack growth law are equal to each other. Also shown is that the constant K_1 of the fatigue relation is an explicit function of several material properties, including the exponent of the crack growth law and the size of specimen. It is of interest whether these conclusions agree with the experimental results.

The computation of the slope m of the available 32 laboratory data is carried out by using a computerized version of the Van der Poel nomograph (*13*) and modified by Heukelom and Klomp (*14*). This program was originally developed by DeBats (*15*) and is named PONOS. It has been modified to calculate the information that is necessary to determine the fatigue parameters of a mix, such as the values of m and n. Because the data of Kallas and Puzinauskas do not have the ring-and-ball softening point information that is required in the PONOS program, an alternative computerized version of McLeod's nomograph is used to calculate these fatigue param-

TABLE 1 FATIGUE TESTING DATA

Data Source	Mix Type	Asphalt Content	Viscosity at 140 °F	Penetration at 77 °F	R&B Softening Pt.	Air Void	Temp °F	Freq Hz	Max. Size	Stiffness ksi	K_1	K_2
Epps	British 594	7.9		21	140	5.38	68.0	1.67	0.375	570	6.11×10^{-6}	3.383
		6.0		36	125	5.71	68.0	1.67	0.375	228	3.20×10^{-5}	2.485
		6.0		30	129	5.71	68.0	1.67	0.375	273	8.91×10^{-7}	2.952
		6.0		37	127	4.49	68.0	1.67	0.438	288	2.87×10^{-6}	2.832
		6.0		35	129	4.80	68.0	1.67	0.438	318	1.12×10^{-7}	3.260
		6.2		26	132	6.72	68.0	1.67	0.438	298	1.34×10^{-7}	3.222
		5.9		35	129	7.70	68.0	1.67	0.750	154	2.12×10^{-6}	3.602
		6.0		48	55	5.50	68.0	1.67	0.750	576	1.10×10^{-10}	4.170
		5.9		57	53	8.60	68.0	1.67	0.500	368	1.60×10^{-4}	2.350
		5.9		41	58	8.10	68.0	1.67	0.500	335	1.73×10^{-5}	2.713
		5.9		25	63	5.60	68.0	1.67	0.500	303	8.23×10^{-9}	3.671
		5.9		38	56	5.30	68.0	1.67	0.500	477	7.51×10^{-6}	2.794
		4.9		38	56	8.00	68.0	1.67	0.625	340	1.09×10^{-7}	3.220
		4.9		26	61	8.40	68.0	1.67	0.625	390	1.26×10^{-5}	2.662
		4.9		28	57	7.60	68.0	1.67	0.625	499	4.56×10^{-5}	2.500
		4.9		28	56	6.50	68.0	1.67	0.625	497	1.60×10^{-6}	2.893
		4.9		32	59	8.20	68.0	1.67	0.625	362	2.21×10^{-6}	2.856
		4.9		28	56	7.00	68.0	1.67	0.625	500	8.52×10^{-9}	2.698
		4.9		30	57	7.60	68.0	1.67	0.625	430	3.58×10^{-6}	2.798
		4.9		20	70	4.20	68.0	1.67	0.750	274	9.67×10^{-7}	2.970
Santucci	AC	6.0		18	71	5.30	77.0	1.67	0.375	616	1.43×10^{-10}	4.182
		6.0		13	70	5.50	77.0	1.67	0.375	377	3.18×10^{-9}	3.931
		6.0		8.5	66	6.00	77.0	1.67	0.375	866	9.51×10^{-9}	3.678
		6.0		21	66	5.50	77.0	1.67	0.375	1175	3.36×10^{-8}	3.226
		6.0		30	59	3.90	77.0	1.67	0.375	758	9.49×10^{-11}	4.27
		6.0		26	66	4.50	77.0	1.67	0.375	422	4.90×10^{-9}	3.875
Kallas	AC Surface	5.6	2840	57		5.10	70.0	2.0	0.500	195	2.73×10^{-7}	3.26
		5.7	1760	84		4.10	70.0	2.0	0.500	153	1.37×10^{-6}	3.27
		5.2	1220	90		8.60	70.0	2.0	0.500	179	6.52×10^{-5}	2.50
		6.0	2670	84		3.40	55.0	2.0	0.500	469	2.32×10^{-9}	3.99
		6.0	2670	84		3.40	70.0	2.0	0.500	192	4.00×10^{-6}	3.08
		6.0	2670	84		3.40	85.0	2.0	0.500	90.0	1.40×10^{-6}	3.45

eters. Figure 2 shows the correspondence between the K_2 values obtained from the available fatigue data and the K_2 values calculated by means of these two computer programs. As can be observed, the agreement between prediction and experiment is reasonable in general.

The moduli obtained from beam fatigue tests are referred to as the flexural elastic stiffness. It is necessary to know whether the stiffness calculated from the McLeod-Van der Poel computer program will result in acceptable agreement with the measured flexural elastic stiffness. A comparison of the calculated elastic stiffness and those measured flexural elastic stiffnesses is shown in Figure 3. As seen in the figure, the measured and computed stiffness are in reasonable agreement.

Figure 4 shows the difference between the K_1 predicted from Equation 5 and the measured K_1 derived from the beam fatigue test. As can be seen, the predicted values of log K_1 are slightly smaller (more negative) than those log K_1 values produced from the laboratory. Consequently, the fatigue life predicted from Equation 5 and 6 will result in shorter lives than from the fatigue relations based on the beam fatigue test. The reason for this is likely to be the overestimation of the value of A, which is calculated from the regression equation (Equation 9) in terms of the exponent of the crack growth law and the stiffness of the mix only. However, from a theoretical point of view, the value of A also varies with other important factors such as tensile strength, fracture energy of the mix, and others. If an analytical method for computing the J-integral strain energy release rate were available to use in computing the constants in the equation for K_1 (Equation 5), taking into account the actual elasto-plastic viscoelastic constitutive equation of the mixture, the fit in Figure 4 would undoubtedly be better. Table 2 shows the comparisons of the results obtained from the experimental and calculated stiffness (K_1 and K_2).

FATIGUE DAMAGE PROPERTIES CAUSED BY MULTIPLE-AXLE LOADS

The procedures used for calculating the fatigue life of pavements caused by a tandem-axle load are different from those caused by a single-axle load that has been described in the previous section. With a multiple-axle load on a pavement, the radial tensile stress at the bottom of the asphalt layer has multiple peaks instead of just one peak, as with a single-axle load. Thus, the fatigue life of the pavement, in terms of the number of axle loads to failure, is reduced. In Equation 5, the value of K_1 is related to the value of A, which is a function of the wave shape of the loading strain pulse (*9*). A general form of the ratio ξ for a multiple-axle to a single-axle load in A is given as

$$\xi = \frac{\int_0^{\Delta t_m} \omega_m(t)^n \, dt}{\int_0^{\Delta t_s} \omega_s(t)^n \, dt} \tag{10}$$

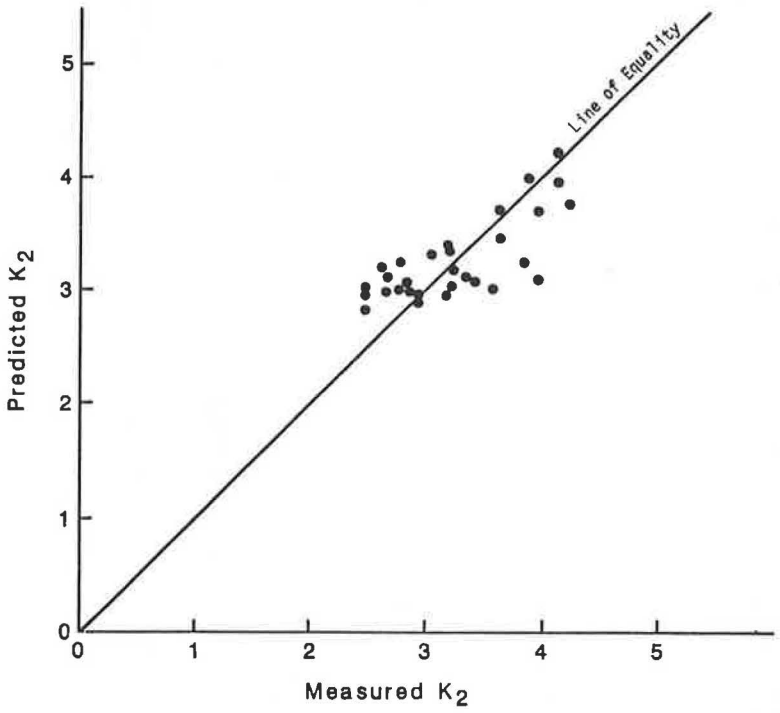

FIGURE 2 Comparison between measured and predicted K_2 values.

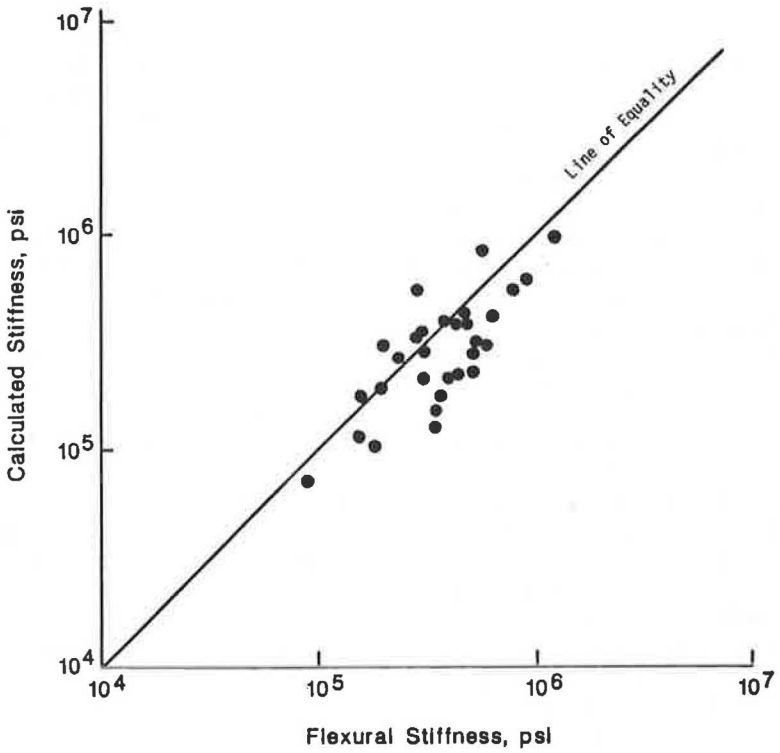

FIGURE 3 Comparison between measured and predicted stiffness.

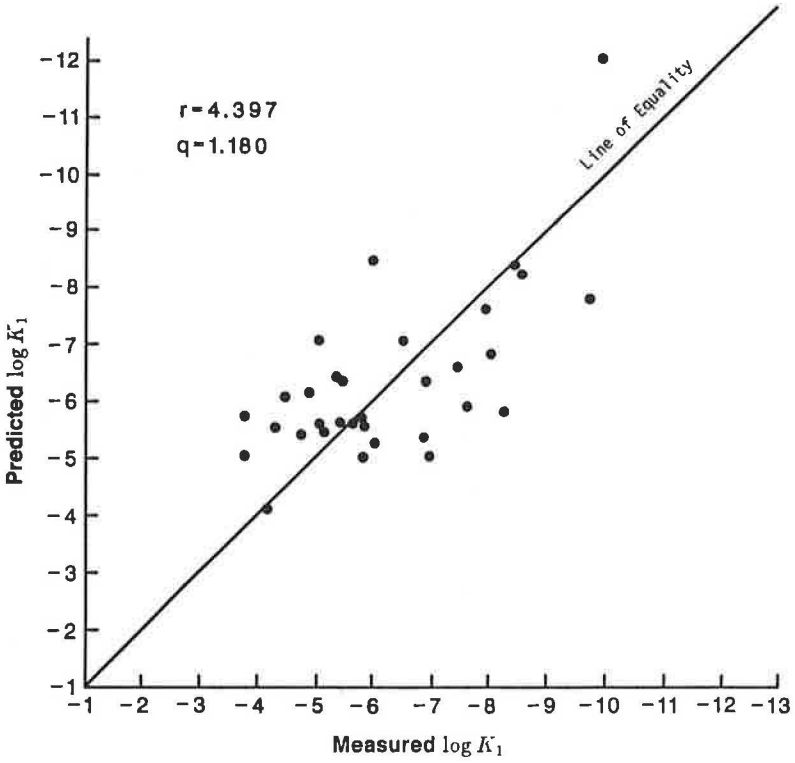

FIGURE 4 Comparison between measured and predicted K_1 values.

where $\omega_m(t)$ is the wave shape of the normalized tensile strain at the bottom of the asphalt concrete layer produced by a multiple-axle load and $\omega_s(t)$ is the wave shape of the normalized tensile strain produced by a single-axle load. Δt_m and Δt_s are the times required for the strain caused by a multiple-axle and a single-axle load, respectively, to build up and diminish. The ratio of these two integrations in Equation 10 is the ratio of the two shaded areas shown in Figure 5, which are the result of raising the normalized wave shaped to the n-power.

The procedure to determine the wave shape of the loading pulse caused by a tandem-axle load, for instance, is first to calculate the tensile strain at the bottom of the asphalt concrete layer. The procedure is done by superposition, adding together the tensile strain caused by the first axle and the overlapping tensile strain caused by the second axle load. The normalized wave shape of the loading pulse is then obtained by dividing the tensile strain from point to point by the peak tensile strain. The loading time (Δ_t) is determined by dividing the distance corresponding to the full range of tensile strain by the vehicle speed. For a single tire on a single axle, the wave shape of the loading pulse is obtained directly from the normalized tensile strain at the bottom of the asphalt concrete layer.

The procedure described above is also applied to calculate the value of the ratio of dual tires on a single axle or multiple axles to a single tire on a single axle. Thus, the expression of the fatigue damage property K_1 for multiple axle loads is given by

$$K_1 = \frac{d^{1-\frac{n}{2}}\left[1 - \left(\frac{C_0}{d}\right)^{1-nq}\right]}{\xi A(1 - nq)(Er)^n} \tag{11}$$

For a specific pavement section and material parameters, the value of the ratio ξ varies with load configuration. To illustrate the calculation of the ratio for the various types of load configuration by using the FEPASS computer program, an example pavement section is used. The thickness of the asphalt concrete layer varies from 1.5 to 6 in., whereas the thickness of the base course is fixed at 8 in. A modulus of 500,000 psi is used for the asphalt concrete; the resilient moduli of the base course and subgrade soils are a function of stress state and are $7{,}000\sigma\theta^{0.35}$ and $27{,}000\sigma_d^{-1.06}$, respectively. All of the calculations are based on a 4,500-lb uniform circular load with 80 psi pressure as representation of the single tire on a standard 18-kip single-axle load. The spacing between dual tires and between axles is assumed to have a value of 12 and 48 in., respectively. The vehicle speed is assumed to be 55 mph.

Table 3 shows the results of calculations of the ratio (ξ) as a function of load configuration, surface layer thickness, and typical values of n. As can be seen in the table, the values of the ratio for single or dual tires on tandem axles are twice those for single or dual tires on a single axle. When the surface thickness is over 4 in., the value of the ratio for dual tires on a single axle or tandem axles to a single tire on a single axle decreases with an increasing magnitude of n. At 4 in. of surface thickness, the value of the ratio for dual tires on a single

TABLE 2 COMPARISONS OF EXPERIMENTAL AND CALCULATED STIFFNESS (K_1 AND K_2)

Data Source	Mix Type	$(E)_{exp}$ ksi	$(E)_{cal}$ ksi	$(K_1)_{exp}$	$(K_1)_{cal}$	$(K_2)_{exp}$	$(K_2)_{cal}$
Epps	British 594	570	301	6.11×10^{-6}	3.39×10^{-8}	3.383	3.143
		228	265	3.20×10^{-5}	8.21×10^{-7}	2.485	2.810
		273	332	8.91×10^{-7}	5.44×10^{-6}	2.952	2.910
		288	339	2.87×10^{-6}	4.29×10^{-7}	2.832	2.980
		318	329	1.12×10^{-7}	4.52×10^{-7}	3.260	3.010
		298	208	1.34×10^{-7}	4.61×10^{-6}	3.222	2.870
		154	113	2.12×10^{-6}	1.30×10^{-6}	3.602	3.030
		576	842	1.10×10^{-10}	8.16×10^{-13}	4.170	4.220
		368	149	1.60×10^{-4}	1.77×10^{-6}	2.350	3.190
		335	127	1.73×10^{-5}	4.01×10^{-6}	2.713	3.120
		303	283	8.23×10^{-9}	1.62×10^{-8}	3.671	3.470
		477	381	7.51×10^{-6}	8.59×10^{-8}	2.794	3.260
		340	149	1.09×10^{-7}	8.80×10^{-6}	3.220	2.950
		390	210	1.26×10^{-5}	6.71×10^{-7}	2.652	3.190
		499	243	4.56×10^{-5}	5.53×10^{-6}	2.500	3.010
		497	314	1.60×10^{-6}	2.01×10^{-6}	2.893	2.960
		362	176	2.21×10^{-6}	2.68×10^{-6}	2.856	3.060
		500	276	8.52×10^{-6}	2.35×10^{-6}	2.698	2.990
		430	219	3.58×10^{-6}	62.48×10^{-6}	2.798	3.030
		274	559	9.67×10^{-7}	3.34×10^{-9}	2.970	3.354
Santucci	AC	616	417	1.43×10^{-10}	1.20×10^{-8}	4.182	3.988
		377	397	3.18×10^{-9}	4.13×10^{-9}	3.931	4.018
		866	613	9.51×10^{-9}	2.56×10^{-8}	3.678	3.785
		1175	978	3.36×10^{-8}	2.60×10^{-7}	3.225	3.369
		758	554	9.49×10^{-11}	3.83×10^{-8}	4.27	3.746
		422	387	4.90×10^{-9}	1.45×10^{-6}	3.875	3.266
Kallas	AC Surface	195	305	2.73×10^{-7}	6.63×10^{-8}	3.25	3.358
		153	179	1.37×10^{-6}	2.71×10^{-6}	3.27	3.177
		179	104	6.52×10^{-5}	8.17×10^{-5}	2.50	2.960
		469	439	2.32×10^{-9}	6.26×10^{-9}	3.99	3.731
		192	190	4.00×10^{-6}	3.77×10^{-7}	3.08	3.332
		90.0	72	1.40×10^{-6}	1.00×10^{-6}	3.45	3.070

axle to a single tire on a single axle varies from 1.29 to 1.14 when the magnitude of n is varied from 2 to 5. This value also implies that the fatigue life of pavements resulting from dual tires on a single-axle load may have a range of 0.78 to 0.88 times smaller than that resulting from a single tire on a single-axle load when an asphalt concrete mix exhibits the properties of n from 2 to 5. The dual tires each carry the same load as the single tire. And by these figures, the passage of a single tire carrying 4,500 lb is equivalent to 0.78 to 0.88 passes of dual tires on a single axle carrying 9,000 lb. Because the latter is the benchmark 18-kip single-axle load, the load equivalent factor in fatigue for a 9-kip single-axle, single-tire load is between 0.78 and 0.88 for a 4-in.-thick asphalt surface layer. Table 4 contains the results of all of these calculations of the 18-kip equivalent single-axle loads in fatigue as a function of load configurations, surface layer thickness, and the values of n.

SHIFT FACTOR

The fatigue life of pavements determined from laboratory fatigue tests generally is lower than that observed in the field. The reason that the equation fails to predict pavement fatigue is because of the following major differences between the field and laboratory loading conditions:

1. In the field, there is a rest period between load applications that allows the pavement material to relax. Laboratory loading is applied rapidly with no rest period between applications.
2. In the field, compressive (or tensile) residual stresses can remain on the bottom of the surface layer after the passage of each load and hence "prestress" the layer so that the tensile stresses that occur when the next heavy load passes cause much less (or much more) fatigue damage, depending on whether the asphalt layer accumulates more (or less) residual stress than the base course layer beneath it. In the field, these residual stresses relax with time; with a sufficient waiting period between loads, no residual stress will remain. In the laboratory, residual stresses also build up in fatigue samples. After several cycles, tension acts on one face during loading and the same magnitude of tension acts on the other face during the rest period between load pulses, as shown in Figure 6.

Thus, the residual stress history of asphaltic mixes in the laboratory is greatly different than that in the field.

Yandell and Lytton (*19,20*) in their study of the residual stress in a pavement have found that, because of residual compressive or tensile strain, the tensile stress resulting from a wheel load application is approximately between 80 and 120 percent of the strain resulting from the preceding wheel load application. During the rest period between load passes, two

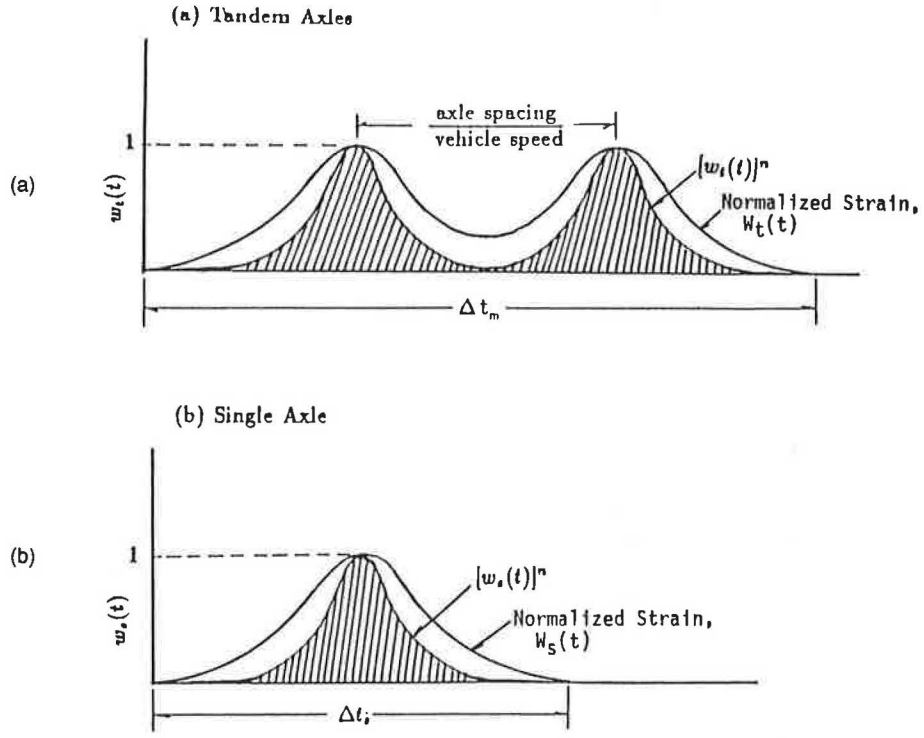

FIGURE 5 Wave shape of loading pulse produced by (a) tandem axles and (b) single-axle load.

TABLE 3 VALUES OF RATIO (ξ) FOR VARIOUS LEVELS OF AXLE CONFIGURATIONS, SURFACE THICKNESS, AND n

$n=\frac{2}{m}$	Surface Thickness (inches)	Ratio, ξ					
		Single Axle		Tandem Axles		Triple Axles	
		Single Tire	Dual Tires	Single Tire	Dual Tires	Single Tire	Dual Tires
2		1.00	1.00	2.00	2.00	3.00	3.00
3	1.5	1.00	1.00	2.00	2.00	3.00	3.00
4		1.00	1.00	2.00	2.00	3.00	3.00
5		1.00	1.00	2.00	2.00	3.00	3.00
2		1.00	1.00	2.00	2.00	3.00	3.00
3	2.0	1.00	1.00	2.00	2.00	3.00	3.00
4		1.00	1.00	2.00	2.00	3.00	3.00
5		1.00	1.00	2.00	2.00	3.00	3.00
2		1.00	1.00	2.00	2.00	3.00	3.00
3	2.5	1.00	1.00	2.00	2.00	3.00	3.00
4		1.00	1.00	2.00	2.00	3.00	3.00
5		1.00	1.00	2.00	2.00	3.00	3.00
2		1.00	1.00	2.00	2.00	3.00	3.00
3	3.0	1.00	1.00	2.00	2.00	3.00	3.00
4		1.00	1.00	2.00	2.00	3.00	3.00
5		1.00	1.00	2.00	2.00	3.00	3.00
2		1.00	1.00	2.00	2.00	3.00	3.00
3	3.5	1.00	1.00	2.00	2.00	3.00	3.00
4		1.00	1.00	2.00	2.00	3.00	3.00
5		1.00	1.00	2.00	2.00	3.00	3.00
2		1.00	1.29	2.00	2.58	3.00	3.87
3	4.0	1.00	1.22	2.00	2.44	3.00	3.66
4		1.00	1.17	2.00	2.34	3.00	3.51
5		1.00	1.14	2.00	2.28	3.00	3.42
2		1.00	1.43	2.00	2.86	3.00	4.29
3	5.0	1.00	1.35	2.00	2.70	3.00	4.05
4		1.00	1.28	2.00	2.56	3.00	3.84
5		1.00	1.22	2.00	2.44	3.00	3.66
2		1.00	2.18	2.00	4.36	3.00	6.54
3	6.0	1.00	2.15	2.00	4.30	3.00	6.45
4		1.00	2.12	2.00	4.24	3.00	6.36
5		1.00	2.07	2.00	4.14	3.00	6.21

TABLE 4 VALUES OF LOAD EQUIVALENT FACTORS FOR VARIOUS LEVELS OF AXLE CONFIGURATIONS, SURFACE THICKNESS, AND n

$n=\frac{2}{m}$	Surface Thickness (inches)	18-kip Equivalent Single Axle Load in Fatigue					
		Single Axle		Tandem Axles		Triple Axles	
		Single Tire 9 kips	Dual Tires 18 kips	Single Tire† 18 kips	Dual Tires‡ 36 kips	Single Tire† 27 kips	Dual Tires‡ 54 kips
2	1.5	1.00	1.00	2.00	2.00	3.00	3.00
3		1.00	1.00	2.00	2.00	3.00	3.00
4		1.00	1.00	2.00	2.00	3.00	3.00
5		1.00	1.00	2.00	2.00	3.00	3.00
2	2.0	1.00	1.00	2.00	2.00	3.00	3.00
3		1.00	1.00	2.00	2.00	3.00	3.00
4		1.00	1.00	2.00	2.00	3.00	3.00
5		1.00	1.00	2.00	2.00	3.00	3.00
2	2.5	1.00	1.00	2.00	2.00	3.00	3.00
3		1.00	1.00	2.00	2.00	3.00	3.00
4		1.00	1.00	2.00	2.00	3.00	3.00
5		1.00	1.00	2.00	2.00	3.00	3.00
2	3.0	1.00	1.00	2.00	2.00	3.00	3.00
3		1.00	1.00	2.00	2.00	3.00	3.00
4		1.00	1.00	2.00	2.00	3.00	3.00
5		1.00	1.00	2.00	2.00	3.00	3.00
2	3.5	1.00	1.00	2.00	2.00	3.00	3.00
3		1.00	1.00	2.00	2.00	3.00	3.00
4		1.00	1.00	2.00	2.00	3.00	3.00
5		1.00	1.00	2.00	2.00	3.00	3.00
2	4.0	0.78	1.00	1.55	2.00	2.34	3.00
3		0.82	1.00	1.64	2.00	2.46	3.00
4		0.85	1.00	1.71	2.00	2.55	3.00
5		0.88	1.00	1.75	2.00	2.64	3.00
2	5.0	0.70	1.00	1.40	2.00	2.10	3.00
3		0.74	1.00	1.48	2.00	2.22	3.00
4		0.78	1.00	1.56	2.00	2.34	3.00
5		0.82	1.00	1.64	2.00	2.46	3.00
2	6.0	0.46	1.00	0.92	2.00	1.38	3.00
3		0.47	1.00	0.93	2.00	1.41	3.00
4		0.47	1.00	0.94	2.00	1.41	3.00
5		0.48	1.00	0.97	2.00	1.34	3.00

† 9 kips each axle
‡ 18 kips each axle

recovery processes may be taking place. In one process, the material relaxes and loses some of its residual stress, thus increasing or decreasing the tensile stress level applied by the next load application. In the other process, the microcracks in the material beyond the visible cracks are allowed to heal partly because of the viscoelastic recovery of the asphalt cement and partly because of the reformation of bond forces in the material after the removal of the applied load. These two effects together will result in increasing the fatigue life of pavements subjected to the traffic loads (*8*).

Based on the findings as described above, Lytton (class notes, 1983) presented an analytical technique that may be used to estimate a shift factor between laboratory and field fatigue life, as shown in Figure 7. The shift factor consists of two components and is given by

$$SF = (SF_r)(SF_h) \tag{12}$$

where

SF_r = the shift factor caused by residual stresses, and
SF_h = the shift factor caused by healing during rest periods.

Shift Factor Caused by Residual Stress

During a rest period, the residual stress (σ_r) relaxes because of the relaxation of the material and is given by

$$\sigma_r(t) = E(t)\varepsilon_r\rho_0 \tag{13}$$

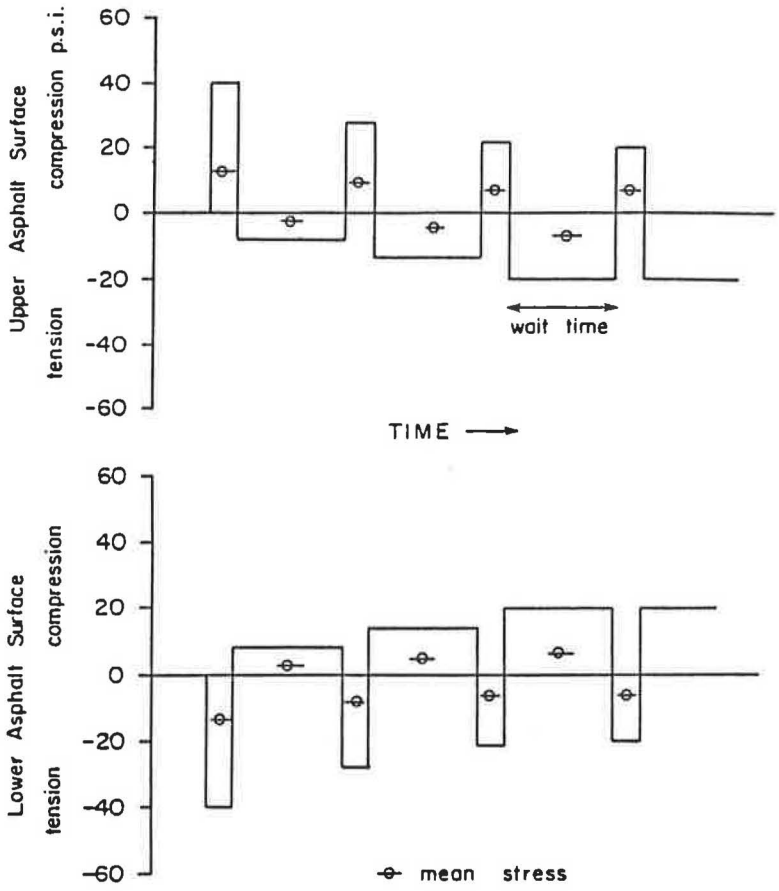

FIGURE 6 Residual stress built up during the fatigue beam test (*15*).

where

ρ_0 = the percent of total strain remaining in the pavement as residual strain immediately after the passage of the load,
ε = total tensile strain, and
$E(t)$ = elastic stiffness at time t.

In this equation, $E(t)$ is a function of time given by

$$E(t) = E_0 t^{-m} \tag{14}$$

where E_0 is the initial elastic stiffness and m is the exponential relaxation rate, which varies between about 0.2 to 0.8 (*21*).

With time, the effective residual strain is equal to residual stress divided by the initial elastic modulus E_0. Thus, the actual tensile strain at the bottom of the asphaltic concrete is given by

$$\varepsilon_t - \varepsilon_r = \varepsilon_t [1 \pm \rho_0 t^{-m}] \tag{15}$$

Thus, the shift factor caused by residual stress can be estimated by

$$SF_r = \frac{N_{fc}}{N_{fa}} = \left(\frac{1}{1 \pm \rho_0 t^{-m}}\right)^{k2l} \tag{16}$$

where, as shown in Figure 7, N_{fa} is the number of cycles to failure for the total tensile strain, N_{fc} is the number of load cycles to failure for the tensile strain altered by the residual stress, and K_{2l} is the value of K_2 determined from the laboratory.

Shift Factor Caused By Rest Periods

To develop the shift factor (SF_h) caused by the effect of rest periods, data from the overlay tester are used. The overlay tester is a fatigue testing machine developed at the Texas Transportation Institute (*10*). The machine was originally designed to model displacement caused by thermal stresses in asphalt pavements resulting from cyclic changes in the ambient temperature. Because of its versatility and repeatability, the overlay tester has made itself a regular part of the laboratory investigation of fatigue characteristics.

Balbissi (*22*), in his study of fatigue characteristics based on laboratory overlay tester tests for Sulflex, revealed that the healing of the material after the rest period produces an increase in the force required to open the crack to the constant displacement level used in the overlay test. This results in an energy increase (Δu_i) as assessed by the area of the load-crack opening loop as shown conceptually in Figure 8. He also found that two empirical relations can be derived from the results

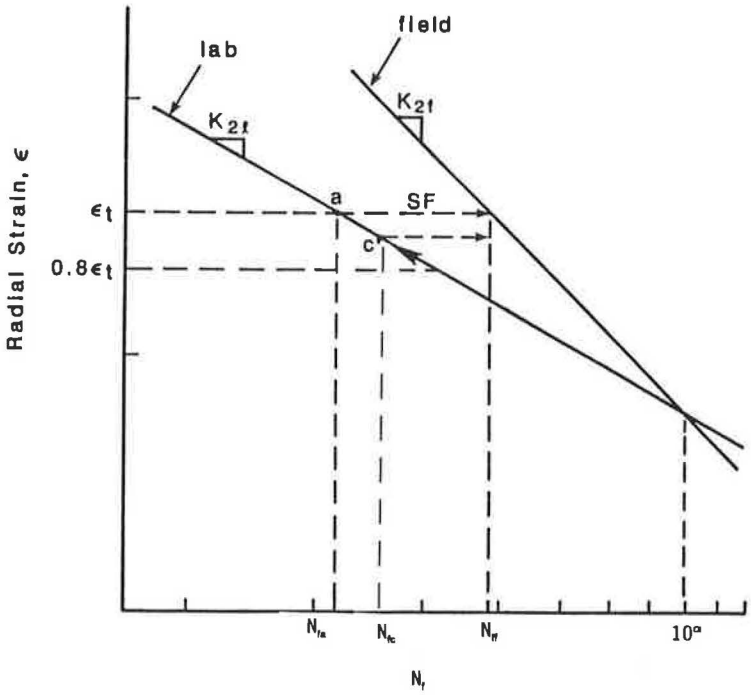

FIGURE 7 Schematic illustration of shift factor.

of the overlay tester tests to evaluate the shift factor for Sulflex caused by the effect of the rest period. These two relations are given as follows:

$$\frac{\Delta u_i}{\Delta u_0} = \left(\frac{t_i}{t_0}\right)^h \tag{17}$$

and

$$\frac{N_f - N_0}{n_{ri}} = \frac{\Delta N_f}{n_{ri}} = m_0\left(\frac{\Delta u_i}{\Delta u_0}\right) \tag{18}$$

where

t_i = the time length of a load pulse with rest periods,
t_0 = the time length of a load pulse without rest periods,
N_f = number of cycles to failure with rest period (t_i),
N_0 = number of cycles to failure without rest period,
n_{ri} = number of rest periods of length (t_i),
Δu_i = change of fracture energy with rest period (t_i),
Δu_0 = change of fracture energy without rest period, and
m_0 and h = regression constants.

Thus, combining Equations 17 and 18, the shift factor (SF_h) can be expressed by

$$SF_h = \frac{N_f}{N_0} = 1 + \frac{n_r m_0}{N_0}\left(\frac{t_i}{t_0}\right)^h \tag{19}$$

This equation indicates an increasing shift factor, caused by healing, as the number of rest periods is increased. In pavements with more frequent traffic, such as passenger vehicles, the rest period is very short and the shift factor should be small; the less frequent vehicles should have a large shift factor.

Based on Balbissi's study, similar relations for asphaltic concrete are assumed in this study. The data obtained from overlay tester tests on asphaltic concrete are summarized in Table 5. According to Equation 19, the regression constant h is equal to 0.427 from the data given. Because there is lack of information on the number of cycles to failure without a rest period (N_0) from the given data, the regression constant (m) cannot be obtained from Equation 18. However, it is assumed that the shift factor caused by the rest period is equal to 13, which is based on the study by Finn et al. (*23*) on Loop 6, section 315 of the AASHO Road Test. The load applications on this section were about 280,000 from November 1958 to September 1959. From this, t_i values can be calculated and t_i is approximately 103 seconds. The t_0 value is equal to 0.025 seconds based on a 30-kip single-axle load vehicle with a velocity of 35 mph. From this information in conjunction with the known regression constant h, the value of m_0 is back calculated from Equation 19. A shift factor (SF_h) of the following form is then developed based on the above-mentioned assumptions and also on the limited available overlay tester data.

$$SF_h = 1 + 5.923 \times 10^{-6} n_{ri}\, t_i^{0.427} \tag{20}$$

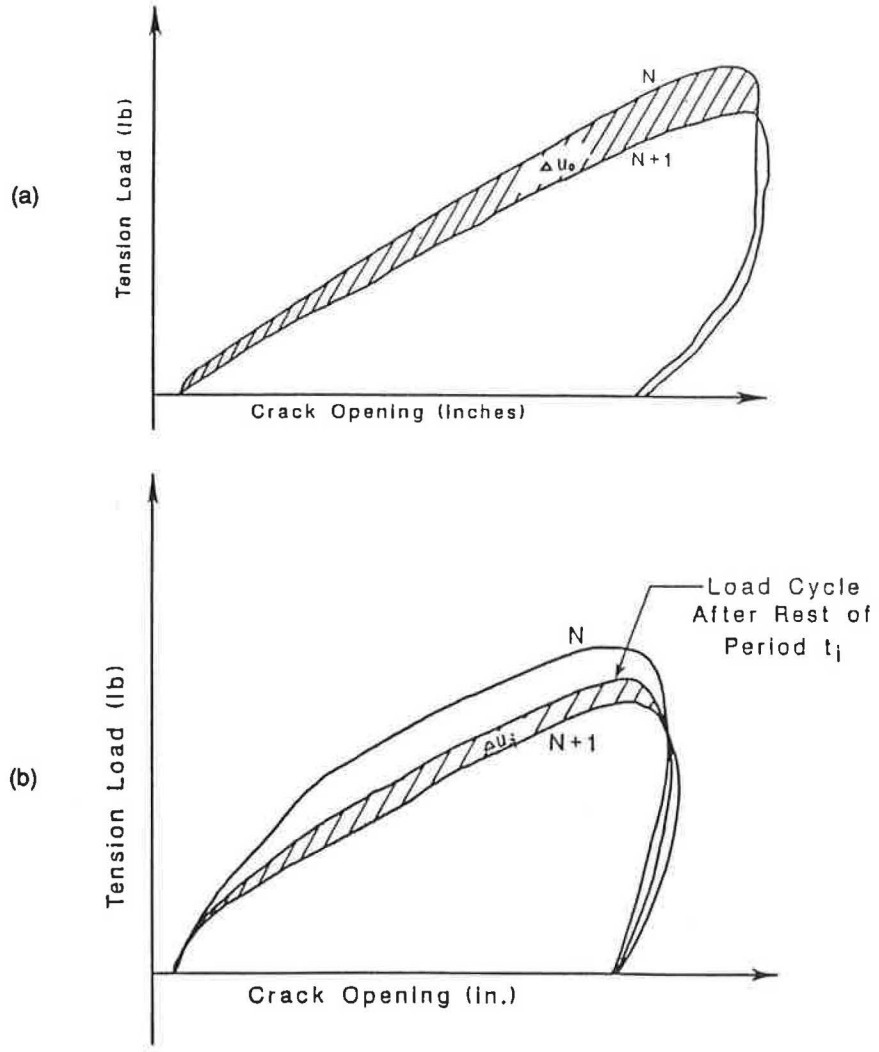

FIGURE 8 Change of fracture energy (a) without rest period and (b) with rest period in the overlay test.

Combining the two shift factor proportions together yields:

$$SF = \left(\frac{1}{1 \pm \rho_0 t^{-m}}\right)^{K_{2l}} \left[1 + 5.923 \times 10^{-6} n_{r_i} (t_i)^{0.427}\right] \quad (21)$$

With the shift factor (SF) known, the values of K_{1f} and K_{2f} (field values of K_1 and K_2) can be calculated from the geometry relation of Figure 7 and are given by

$$K_{2f} = K_{2l} - \frac{\log SF}{\log \varepsilon_t - \left(\frac{\log K_{1l} - \alpha}{K_{2l}}\right)} \quad (22)$$

and

$$K_{1f} = (K_{1l})^{\left(\frac{K_{2f}}{K_{2l}}\right)} (10^{\alpha})^{\left(\frac{K_{2l} - K_{2f}}{K_{2l}}\right)} \quad (23)$$

where

K_{1l} and K_{2l} = laboratory values of K_1 and K_2,
ε_t = maximum tensile strain at the bottom of the asphalt concrete layer, and
α = value at the intersection of the field and laboratory fatigue relations. An estimated value of this constant is 7 to 8, assuming a no-rest condition for the strain level corresponding to passenger traffic.

The use of these equations to predict the fatigue life of flexible pavements in the field has been completed with excellent results for the 12 selected AASHO Road Test sections and for the 8 pavement sections in Florida (*24*). A detailed description of these results and a comparison with observed fatigue lives are discussed in a previous report (*3*) and require more space than is available in this paper. It is sufficient to note that the above formulation works well in predicting the fatigue service life of pavements. An example of these pre-

TABLE 5 SUMMARY OF OVERLAY TEST DATA WITH REST PERIOD

Sample Number	Δu_i	Δu_o	t_i, sec	$\Delta u_i/\Delta u_o$	t_i/t_o
C2034	9.997	29.24	600	0.342	60
	9.837	15.33	1,800	0.642	180
	6.964	13.27	1,200	0.525	120
	8.109	10.82	3,000	0.749	300
	4.303	9.99	300	0.431	30
	5.713	6.25	2,400	0.914	240
C2035	9.166	16.93	600	0.541	60
	10.185	12.13	3,000	0.840	300
	8.329	13.40	1,200	0.622	120
	7.833	10.68	2,400	0.733	240
	5.546	9.75	600	0.569	60
	5.889	9.36	1,800	0.629	180
	1.236	9.36	600	0.132	60

t_o = 10 sec.

dictions is shown in Figure 9, in which a residual stress factor (ρ_0) of −0.20 was used in calculating the shift factor.

CONCLUSIONS

A complete development of the fatigue damage properties for predicting the fatigue life of asphaltic concrete pavements has been presented in this paper. The equations of fatigue damage properties are derived from the theory of fracture mechanics, which models both the beam fatigue testing in the laboratory and crack growth through pavement surface layers in the field. These properties take into account crack initiation, propagation, and material properties and are believed to be a better expression of the fracture process than the phenomenological approach used in fatigue predictions in the past. The principal conclusions based on the development presented in this paper are as follows:

1. The fatigue damage property K_1 of the controlled-strain based fatigue equation is dependent on the properties such as n, A, stiffness, specimen size, and the initial crack size.
2. Based on the relations inferred from Equation 5, the fatigue damage property K_1 increases with increasing asphaltic concrete thickness for brittle mixes with $n > 2$, but increases with thinner layers for ductile mixes with $n < 2$. The K_1 property increases as the maximum size of aggregates in the mix decreases. In other words, an asphalt concrete mix containing a larger maximum size of aggregate will have a shorter life. These relations were not investigated in the experiments analyzed in this paper because none of the experiments used fracture mechanics as a basis for the experimentation. One of the purposes of theory is to propose new relations that can be tested by further experimentation. Because of the obvious success of the theory in other regards, these inferred relations are obvious candidates for the next round of experimentation.
3. The fatigue damage property K_2 of the controlled-strain based fatigue equation and the exponent n of the crack growth law are equal to each other.

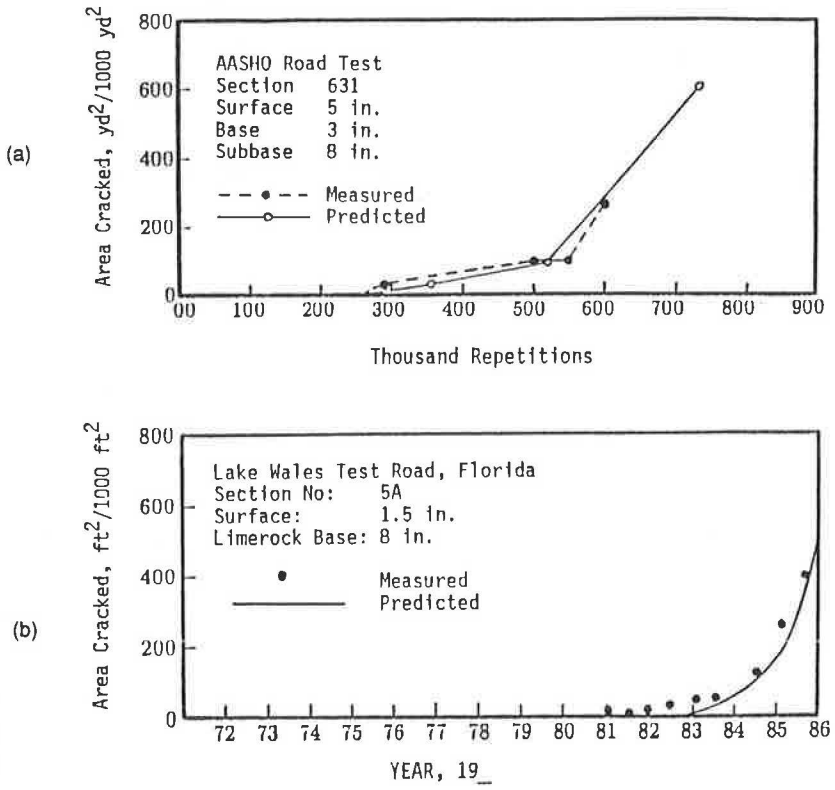

FIGURE 9 Comparison between predicted and measured area cracked in (a) AASHO Road Test section and (b) Florida pavement section.

4. The fatigue damage property K_2 varies with the initial asphalt cement properties, such as asphalt content, viscosity, penetration, and temperature.

5. The fatigue predictions also allow the loading to be applied with single or dual tires on a single axle, tandem axles, or triple axles, and for fatigue load equivalence factors to be calculated.

6. The application of the fatigue damage properties developed can be used to calculate the load equivalence factors that take into account the fatigue life of asphaltic concrete pavements caused by a single-axle load or a multiple-axle load.

7. The known shift factor between the laboratory and field fatigue life is attributable to the effects of healing during the rest period between load applications and residual stresses during the load applications.

REFERENCES

1. C. L. Monismith. Flexibility Characteristics of Asphaltic Paving Mixtures. *Proc., Association of Asphalt Paving Technologists*, Vol. 27, 1958.
2. J. A. Deacon and C. L. Monismith. Laboratory Flexural-Fatigue Testing of Asphalt Concrete with Emphasis on Compound-Loading Tests. In *Highway Research Record 158*, HRB, National Research Council, Washington, D.C., 1967, pp. 1–31.
3. K. H. Tseng. *A Finite Element Method for the Performance Analysis of Flexible Pavements*. Ph.D. dissertation. Texas A&M University, College Station, 1988.
4. *ILLI-PAVE—A Finite Element Program for the Analysis of Pavements*. Construction Engineering Laboratory and the Transportation Facilities group, Department of Civil Engineering, University of Illinois, Urbana, May 1982.
5. P. C. Paris and F. Erdogan. A Critical Analysis of Crack Propagation Laws. *Transactions of the American Society of Molecular Engineering, Journal of Basic Engineering*, Series D, 85, No. 3, 1963.
6. C. S. Desai and J. F. Abel. *Introduction to the Finite Element Method*. Van Nostrand Reinhold, New York, 1972.
7. P. W. Jayawickrama. *Methodology for Predicting Asphalt Concrete Overlay Life Against Reflection Cracking*. M.S. thesis. Texas A&M University, College Station, 1985.
8. Y. K. Kim and D. N. Little. Evaluation of Healing in Asphalt Concrete by Means of the Theory of Nonlinear Viscoelasticity. In *Transportation Research Record 1228*, TRB, National Research Council, Washington, D.C., 1989, pp. 198–210.
9. R. A. Schapery. *A Theory of Crack Growth in Visco-Elastic Media*. Report NM 2764-73-1. Mechanics and Materials Research Center, Texas A&M University, College Station, 1973.
10. F. P. Germann and R. L. Lytton. *Methodology for Predicting the Reflection Cracking Life of Asphalt Concrete Overlays*. Report TTI-2-8-75-207-5, Texas A&M University, College Station, March 1979.
11. N. W. McLeod. Asphalt Cements: Pen-Vis Number and Its Application to Moduli Stiffness. *Journal of Testing and Evaluation*, Vol. 4, No. 4, 1976.
12. P. W. Jayawickrama, R. E. Smith, R. L. Lytton, and M. R. Tirado. *Development of Asphalt Concrete Overlay Design Equations. Vol. I—Development of Design Procedures*. Final Report FHWA/RD-86. FHWA, U.S. Department of Transportation, 1987.
13. C. Van der Poel. A General System Describing the Viscoelastic Properties of Bitumens and Its Relation to Routine Test Data. *Journal of Applied Chemistry and Biotechnology*, Vol. 4, Part 5, May 1954, pp. 221–236.
14. W. Heukelom and A. J. G. Klomp. Road Design and Dynamic Loading. *Proc., Association of Asphalt Paving Technologists*, Dallas, Tex., Vol. 33, 1964.
15. F. T. DeBats. *External Report for the Computer Programs PONOS and POEL*. Amsr0008-72, January 1972.
16. J. A. Epps and C. L. Monismith. Influence of Mixture Variables on Flexural Fatigue Properties of Asphalt Concrete. *Proc., Association of Asphalt Paving Technologists*, Vol. 38, 1969, pp. 432–464.
17. B. F. Kallas and V. P. Puzinauskas. *Flexure Fatigue Tests on Asphalt Paving Mixtures. Fatigue of Compacted Bituminous Aggregate Mixtures*. ASTM Special Technical Publication 508. American Society for Testing and Materials, Philadelphia, 1972, pp. 47–65.
18. L. E. Santucci and R. J. Schmidt. The Effect of Asphalt Properties on the Fatigue Resistance of Asphalt Paving Mixtures. *Proc., Association of Asphalt Paving Technologists*, Vol. 38, 1969, pp. 65–97.
19. W. O. Yandell and R. L. Lytton. *Residual Stresses Due to Travelling Loads and Reflection Cracking*. Report FHWA/TX-79-207-6. Texas Transportation Institute and Texas Department of Highways and Public Transportation, College Station, June 1979.
20. W. O. Yandell and R. L. Lytton. *The Effect of Residual Stress and Strain Build-Up in a Flexible Pavement by Repeated Rolling of a Tire*. Report RF4087-1. Texas Transportation Institute, College Station; American Trucking Associations, Alexandria, Va., Oct. 1979.
21. A. A. A. Molenaar. *Structural Performance and Design of Flexible Pavements and Asphalt Concrete Overlays*. Ph.D. thesis. Delft University of Technology, Delft, The Netherlands, 1983.
22. A. H. Balbissi. *A Comparative Analysis of the Fracture and Fatigue Properties of Asphalt Concrete and Sulphlex*. Ph.D. thesis. Texas A&M University, College Station, 1983.
23. F. Finn, C. Saraf, R. Kulkarni, K. Nair, W. Smith, and A. Abdullah. The Use of Distress Prediction Subsystems for the Design of Pavement Structures. *Proc., 4th International Conference on Structural Design of Asphalt Pavements*, University of Michigan, Ann Arbor, Vol. 1, 1977, pp. 3–38.
24. J. Sharma, L. L. Smith, and B. E. Ruth. Implementation and Verification Flexible Pavement Design Methodology. *Proc., 4th International Conference on Structural Design of Asphalt Pavements*, University of Michigan, Ann Arbor, Vol. 1, 1977, pp. 175–187.

Publication of this paper sponsored by Committee on Flexible Pavement Design.

Assessment of Damage Caused to Pavements by Heavy Trucks in New England

K. Wayne Lee and Wendy L. Peckham

An attempt was made to investigate damage caused to pavements by benchmark (based on federal maximum weight limits for interstate highway systems) and heavy trucks in New England. Because the weigh-in-motion (WIM) data were available from Maine and Rhode Island, this study used WIM data rather than sample or partial data. Two computer programs, HETROM and HETROR, were developed to extract heavy axles or trucks from WIM data for further analysis. Two empirical procedures based on AASHTO Interim and 1986 Design guides were developed. These require two computer programs, HETRIG and HETRNG, respectively, to convert heavy axles to the equivalent 18-kip single-axle loads. After creating the traffic input data, a series of analyses was performed with the aforementioned empirical procedures. In addition, a preliminary analysis was also carried out using mechanistic procedures based on the Asphalt Institute's DAMA and the Federal Highway Administration's VESYS 3A-M programs. There were consistent observations, in all cases, that heavy trucks caused more damage than benchmark trucks. It was also observed that more damage caused by heavy trucks was predicted when there is a higher legal weight limit.

Highway transportation of goods has risen to the top of private sector transportation issues. Innovation in the movement of freight on the highway system promises tremendous productivity advantages but brings with it complex safety and regulatory issues. For example, heavy vehicles, which are being used more frequently, account for a disproportionate share of pavement wear. The size and weight of the vehicle fleet affect the costs associated with building and repairing roads. Research in truck productivity, safety, and road wear will continue to play a significant role in resolving these issues (*1–5*).

This research project investigated one of the issues, i.e., damage caused to pavements on the interstate highway network by benchmark (based on maximum weight limits for an interstate highway system) and heavy trucks. The project was initiated by the New England Surface Transportation Consortium (NETC), Cambridge, Mass. The NETC set their objectives to address the problems of the highway network and to resolve these issues. To achieve these goals, the NETC assigned projects or topics to research teams within the New England region. The pieces of information found in this research will provide a significant link in the objective scheme of NETC. In addition to NETC's primary interest, the consortium would also like to make uniform the five NETC states—Maine, Massachusetts, New Hampshire, Vermont, and Rhode Island—with respect to such factors as weight limits, design methods, and fee issuance (*6,7*). Table 1 shows the limits that currently apply to these states (*8*). This project concurred with this interest by making uniform the weight limits used.

The intent of this project was to provide procedures to assess pavement damage caused by overweight trucks or heavy axles. In doing so, a procedure may be chosen to determine how much damage is occurring on a pavement. The assessment's results can be applied to NETC's goal by providing vital information to plan more adequate pavement designs or issue more appropriate trucking fees, or both. Consequently, the building, repairing, and fee costs more proportionately will reflect the damage.

K. W. Lee, Department of Civil Engineering, The University of Rhode Island, Kingston, R.I. 02881. W. L. Peckham, Design Section, Rhode Island Department of Transportation, Providence, R.I. 02903.

ASSESSMENT OF PAVEMENT DAMAGE CAUSED BY HEAVY TRUCKS

To assess the pavement damage it was necessary to develop procedures to quantify the damage, identify the legal axle loads to be used, select a representative location for the data collection, and formulate input data.

It was found that each NETC state has various combinations of legal load limits, as shown in Table 1. To develop a more uniform procedure for these states, the uniform load limits were set for each axle configuration. These limits were agreed on by the NETC technical committee to follow the current federal load limits.

The representative locations were selected where the weigh-in-motion (WIM) data were available and most recently collected on flexible pavement interstate highways. Two states, Maine and Rhode Island, provided the WIM data to be used.

In addition to the traffic data, the states were also asked to provide the pavement cross-section at the site, properties of subgrade soils, and monthly average air or pavement temperature, or both, on these locations. This project was mainly intended to provide procedures that assess the pavement damage. The project also presents some of the actual effects of heavy trucks on highway pavements. This report could serve as a basis for future studies of this region and related areas.

Data Management

Items for the data management included (a) the site location, (b) pavement structure and truck fleets, (c) the method of

TABLE 1 LEGAL AXLE AND GROSS LOADS BY AGENCY FOR INTERSTATE HIGHWAYS

AGENCY	STATUARY AXLE LIMITS (LB) SINGLE	TANDEM	GROSS VEHICLE WEIGHT (LB) FIVE AXLES	OTHER COMB.	BASIS FOR GROSS WT. LIMIT
MAINE	20,000[a]	34,000	80,000	80,000	SM, BF
MASSACHUSETTS	22,400	36,000	80,000	80,000	SM,BF
NEW HAMPSHIRE	22,400[a]	40,000[b]	80,000	80,000	TB,SM
RHODE ISLAND	22,400	44,000	80,000	80,000	SM,BF
VERMONT	22,400	36,000	80,000	80,000	OT
FEDERAL LIMIT (NETC) (STAA, 1982)	20,000	34,000	80,000		

BF = BRIDGE FORMULA

TB = A TABLE OF ALLOWABLE GROSS VEHICLE WEIGHTS DERIVED FROM THE BRIDGE FORMULA

OT = TABLE OTHER THAN THE BRIDGE TABLE

SM = SPECIFIED MAXIMUM LIMITS

a = 20,000 LB. IF GROSS WEIGHT EXCEEDS 73, 280 LBS

b = 34,000 LB. IF GROSS WEIGHT > 73,280 LBS AND IF AXLES ≤ 8 FT. APART

data collection, and (d) the arrangement of the data collected. The data management was necessary to develop a link from data collection to the analysis process.

Site Location

The data for both states were collected on Interstate 95. The sites were in Yarmouth-Freeport, Maine, and Hopkinton, R.I. The highway in both cases is a four-lane divided highway having two lanes in each direction.

Highway Pavement Structures and Truck Fleets

Route 95 in Maine was opened to traffic in November 1973. The pavement structure consists of a 3-in. asphalt concrete surface course, a 6.5-in. asphalt concrete base course, a 4-in. aggregates base course, a 9-in. aggregates subbase course, and a 16.5-in. selected granular material subgrade (Figure 1). Many of the pavement properties were not supplied; therefore, a majority needed to be estimated. The average air temperature per season is as follows for this area: summer, 66.9°F; fall, 48.4°F; winter, 21.7°F; and spring, 43.1°F. These temperatures are for the year the WIM data were collected.

The original Route 95 interstate in the Hopkinton area of Rhode Island was constructed in 1962. A contract was put out in 1969 for a resurfacing. The original structure consisted of a 3-in. asphalt concrete surface course, a 2.5-in. bituminous macadam penetration course, a 5.5-in. crushed gravel base course, and a 12-in. gravel foundation on the subgrade of a fine brown sand. The resurfacing consisted of a 3-in. asphalt concrete course (Figure 2). Since most of the original construction data were also not available, many of the material properties had to be estimated by using design texts and references (*9–12*). The average air temperature per season is as follows: summer, 72.2°F; fall, 54.4°F; winter, 34.8°F; and spring, 39.4°F. These temperatures are for the year in which the WIM data were collected.

The truck fleet, as mentioned previously, was determined based on the FHWA classifications and legal limits (Table 1).

Data Collection

WIM has several advantages over the conventional static weighing operations. It offers a safe and efficient method for high-volume weighing of trucks (*13*). The WIM technique is also a more precise method to obtain data. Ordinarily, drivers would have to pull off into a weigh station to be statically weighed. Weigh stations are where weight violations are issued most often. Static weighing to obtain research data is conditional because most of the truckers are warned that the weighing is being conducted and opt to either pull off the highway and wait or choose an alternative route to avoid a possible violation. In most cases, when data are being taken using WIM, drivers do not even know they are being weighed. Therefore, a more precise, representative, and accurate group of data can be obtained.

The WIM used for Maine is a semipermanent weight pad, produced by International Road Dynamics, set into the pavement. It consists of two rectangular weighing platforms that rest on a common concrete foundation. They each measure 5 ft, 4 in. by 1 ft, 9 in. by 9 in. deep (1.6 m by 530 mm by 230 mm). Also, it is an associated electronic roadside monitoring system. The platforms are positioned so that there is one in each of the two wheel paths. The loads that are applied to the platforms produce vertical displacement in an oil-filled piston located in the center of the rectangle. These pistons act as load cells. In conjunction with the pistons, inductive loops are used to acquire speed and presence data. The initial installation requires heavy equipment for placement; there-

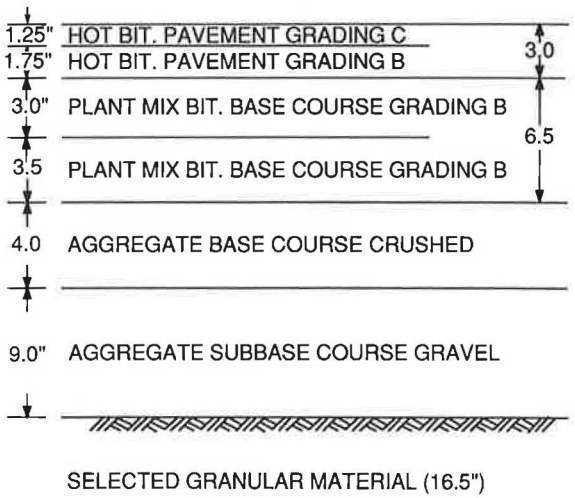

FIGURE 1 Cross-section of pavement structure for the Maine site.

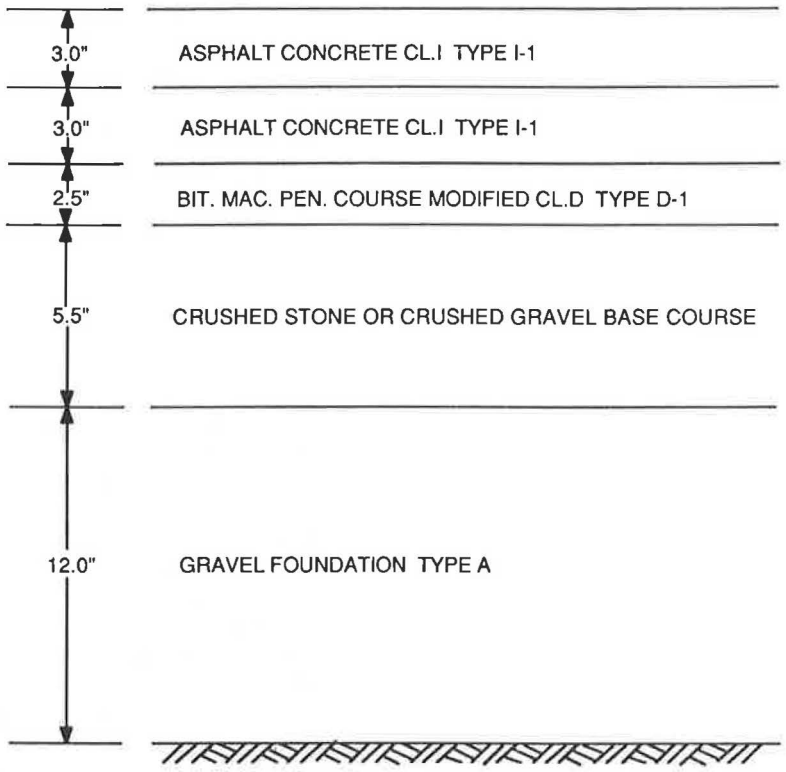

FIGURE 2 Cross-section of pavement structure for the Rhode Island site.

after, it needs only to be programmed and started for data collection. No further set-up or installation is needed.

The WIM used for the data collection in Rhode Island is semipermanent. It is a pad that is adhered to the pavement and left for a period of time, usually 2 days, to collect data (*14*). The pad or weighmat, produced by The Golden River Corporation, uses two inductive loops to acquire speed and presence data. The weighmat is 6 ft wide by 20 in. long and is made of three sheets of steel separated by soft rubber. This set-up acts as a three-plate capacitor. Vertical displacement on the mat produces an increase in capacitance, which is interpreted as a weight via an attached microprocessor-based data collection system. The mat is adhered to the pavement with pop-rivets and bituminous adhesive tape on the edges. It is located in one wheel path of the traffic lane. Its installation takes only 1 hour, but calibration may be required at every installation.

Data Preparation

To utilize available design methods or models, the initial step was the classification of the truck fleet. It was agreed on by the NETC technical committee that the classifications would follow those recommended by the FHWA for uniformity. These configurations are shown in Figure 3.

To work with the heavy trucks, they must be extracted from the original WIM data, which were given to the University of Rhode Island by the two states. Computer programs HETROM and HETROR were developed for this purpose in this study. HETRO stands for Heavy Truck Occurrence. The last characters, M and R, stand for Maine and Rhode Island, respectively. Each one takes its corresponding input data and processes them through comparisons based on the FHWA classifications to sort out the heavy axles. As briefly described above, two different computer programs were developed for the Maine and Rhode Island data sets, since the given format of the WIM data was slightly different. The programs vary through read statements to input the format of a truck occurrence from the data file, and the load unit of the axle weights—kips for Maine and pounds for Rhode Island. The programs first read the data and assign the occurrence to variable names. Each field in a data record has a variable name. The first comparison looks at the truck classification. Then the program sends the data record to the first weight comparison. This comparison depicts whether or not an axle is over the legal limit. The heavy axles are sent to an output file to represent the heavy trucks, and the legal axles are unrecorded. The programs generate output files in a form ready to be used by the empirical methods. The output format can be easily changed depending on its future use.

Procedures To Assess Pavement Damage

The study originally considered utilizing five design methods: the AASHTO Interim Design Guide (*15*); the AASHTO 1986 Design Guide (*16*); the Five Consortium States Design Methods (*10,11*); the Asphalt Institute's DAMA (*17*); and the Federal Highway Administration's VESYS 3A-M (*18*).

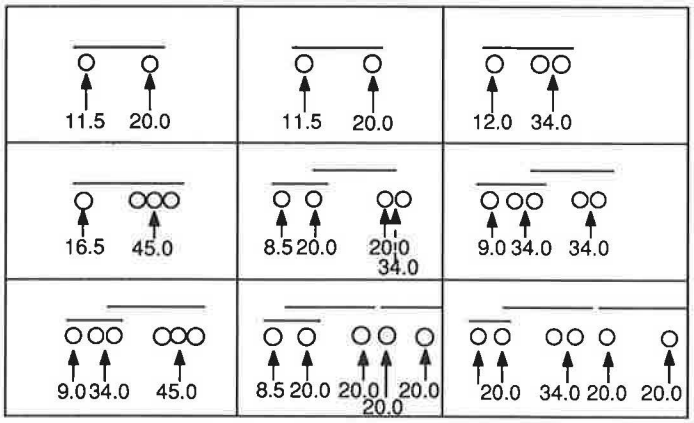

FIGURE 3 Recommended FHWA truck classification and axle loads.

A review of the five states' design methods for flexible pavements indicated that most states use the AASHTO Interim Guide method. The only states with variations to this method are Rhode Island and Massachusetts (*10,11*). Even though there is some uniqueness for these two states in comparison to the others, the end results would be very similar. Thus, no further consideration was given in developing a procedure for NETC states' current methods other than using the same procedure with the AASHTO Interim Guide.

The Procedure Based on AASHTO Interim Design Guide

One of the important concepts used in the AASHTO Road Test in the Equivalent 18-kip single-axle load (ESAL). The ESAL shows the damaging effects of an axle load of any type as expressed as an equivalent number of 18,000-lb single axles. The Guide offers tables to compute equivalency factors for two terminal present serviceability indices (PSI)—2.0 and 2.5. These tables are used for single and tandem axles in the flexible pavement. Because no tridems are used at the road test, two-thirds of the factor for the tandem axles is used to determine the ESAL factors for the tridem axles.

The AASHTO Guide is a semiempirical method that was used in this study to assess pavement damage caused by heavy trucks. It does not, however, take into account the presence of uneven loads between axles or an increase in tire pressure. These issues could be considered better by a mechanistic approach.

After the data are processed through HETROM or HETROR, sorting computer programs, the output is used in the next program based on the AASHTO Interim Design Guide. This computer program, HETRIG, is a modified version of the New Jersey program developed by Barros (*19*). HETRIG stands for the Heavy Truck Impact using the procedure based on the Interim Guide. It was written by utilizing the AASHTO Interim Design Guide method to calculate the accumulated number of ESALs of the heavy axles.

HETRIG computes the corresponding ESAL of each heavy axle according to the traffic equivalence factors provided in the Interim Design Guide charts. An ESAL for each overweight axle is computed and summed for a total ESAL for the truck fleet. In addition to computing ESALs for the heavy trucks, the program also computes ESALs for a fleet of legal weight trucks hauling the same total weight as one of the heavy trucks. The program subtracts all the weight over the acceptable amount for each heavy axle and transfers it to the additional truck. It computes ESALs for the fleet of all legally loaded trucks and no heavy trucks. Consequently, a comparison can be made to see the difference in ESALs between the fleet with and without heavy axles hauling the same amount of freight.

The computed ESALs are also available to be compared with the design ESALs of the highway where the data were collected. Pavements are designed to carry a certain number of loads within a specified amount of time. For instance, if a pavement had a value of 10 million ESALs for a 20-year design life, this would be equivalent to 500,000 ESALs per year. If heavy trucks operating on this pavement have an ESAL of 200,000 annually, then 40 percent of the pavement's serviceability is consumed by this type of traffic yearly.

Tables 2 and 3 indicate that there were 46,956 and 315,042 heavy trucks on the travel lane annually (1988) at the Maine and Rhode Island sites, respectively. For the Maine site, the total occurrence of heavy trucks was originally 78,260 for the combined two lanes. Assuming that 60 percent of the trucks will use the travel lane, the total occurrence of 46,956 was estimated. Then, the total occurrences were converted by the program to cause 227,273 and 1,911,337 ESALs of pavement damage at the Maine and Rhode Island sites, respectively.

Only the state of Maine provided the average daily design ESALs for the Yarmouth-Freeport site as being 1,017, which was converted to the average annual design ESALs of 371,205. For the Rhode Island site, the annual design ESALs were estimated by multiplying 371,205 by the ratio of heavy truck occurrences of two sites (= 315,042/46,956), i.e., 2,490,527. Based on these design ESALs, the losses of pavement life

TABLE 2 ASSESSMENT RESULTS FOR THE MAINE SITE BY A PROCEDURE BASED ON THE AASHTO INTERIM GUIDE

HEAVY AXLES FOR BOTH LANES IN THE YEAR OF 1988

AXLE TYPE	TOTAL OCCURRENCES	TOTAL EXCESS WEIGHT, LBS	AVG EXCESS WEIGHT PER OCCURRENCE,LBS
SINGLE AXLE	120,848	204,282,001	1,690
TANDEM AXLE	5,720	28,379,000	4,961
TRIDEM AXLE	1,560	18,428,800	11,813
TOTAL	128,128	251,089,802	

18-KIP equivalent AXLE LOAD ANALYSIS, ANNUAL DATUM
(ONLY ON THE TRAVEL LANE ASSUMING 60% OCCUPATION)

	TOTAL OCCURRENCES	MODELED GROSS WEIGHT, KIPS	MODELED 18-KIP ESAL	MODELED ESAL % OF DESIGN
HEAVY TRUCKS	46,956	3,596,367	227,273	61.2
LEGALIZED TRUCKS	53,073	3,912,189	194,216	52.2
DIFF-ERENCE	6,117	315,822	-33,057	-9.0

TABLE 3 ASSESSMENT RESULTS FOR THE RHODE ISLAND SITE BY A PROCEDURE BASED ON THE AASHTO INTERIM DESIGN GUIDE

HEAVY AXLES FOR ONE LANE IN THE YEAR OF 1988

AXLE TYPE	TOTAL OCCURRENCES	TOTAL EXCESS WEIGHT, LBS	AVG EXCESS WEIGHT PER OCCURRENCE,LBS
SINGLE AXLE	89,180	319,774,001	3,586
TANDEM AXLE	362,726	2,738,161,792	7,549
TRIDEM AXLE	12,740	269,496,500	21,154
TOTAL	464,646	3,327,432,293	

18-KIP EQUIVALENT AXLE LOAD ANALYSIS, ANNUAL DATUM

	TOTAL OCCURRENCES	MODELED GROSS WEIGHT, KIPS	MODELED 18-KIP ESAL	MODELED ESAL % OF DESIGN
HEAVY TRUCKS	315,042	31,485,010	1,911,337	76.7
LEGALIZED TRUCKS	418,788	34,784,419	1,324,367	53.2
DIFF-ERENCE	103,746	3,299,409	-586,970	-23.5

were computed as 61.2 percent and 77.0 percent for the Maine and Rhode Island sites, respectively. The loss can be interpreted as follows: that for 1 year the corresponding percentage of pavement life was consumed solely by heavy trucks.

Because of the important benefits of transporting cargo by truck, a legal fleet was created so that heavy trucks were eliminated. A legal fleet is defined as trucks only at or under federal limits. It was achieved by adding more trucks to the original heavy truck fleet number. The additional trucks carry the excessive weight taken from the heavy trucks; therefore all trucks are transporting at or under the federal legal load limit. Tables 2 and 3 show that the additional 6,117 and 103,746 trucks would be added to the fleets to carry the excessive weights in Maine and Rhode Island, respectively. Because each additional truck also introduces a tare weight, the pavement is required to carry an additional 315,822 and 3,299,409 pounds over a 1-year period at the Maine and Rhode Island sites, respectively. But even with the additional tare weight load the consumed design ESAL percentage decreased to 52.2 percent and 53.0 percent, respectively. This decrease occurred because each axle group was required to carry less weight; consequently, the total ESALs computed were lower. Therefore, the same amount of cargo can be transported and cause less damage to the pavement.

Tables 2 and 3 also supply the various impact and traffic mix data for the Maine and Rhode Island sites. At the Maine site, the net loss in service life attributable to detected heavy trucks is 61.2 less 52.2, or approximately 9.0 percent, whereas at the Rhode Island site the net loss is 76.7 less 53.2, or approximately 23.5 percent. Whereas the Maine legal limits are the same as the federal limits or the benchmarks (Table 1), the Rhode Island legal limits are higher than the federal limits, especially for the tandem axle. This could explain why there is a greater difference in total heavy ESALs and total legal ESALs for the Rhode Island site. At the Maine site the difference is almost negligible. Also of note is that 94 percent of the overweight trucks observed were single trucks. Consequently, it can be concluded that more damage will occur when the legal limits are higher.

The Procedure Based on 1986 AASHTO Design Guide

The 1986 AASHTO Design Guide is a culmination of the revisions made to the AASHTO Interim Guide. Most steps for the procedure based on the 1986 Design Guide are the same as the one based on the Interim Guide. The inputs needed for this procedure are again the heavy truck data and the design ESAL for the highway pavement. The Interim Guide program treats the tridem axles as 3/2 a tandem axle and computes them using the tandem method, whereas the 1986 Guide computes them separately as tridems using the tridem conditions.

Tables 4 and 5 show the results for the Maine and Rhode Island sites using the procedure based on the 1986 Guide method (HETRNG), respectively. These tables portray the actual number of heavy truck occurrences within a 1-year period and their total weight, ESALs, and percentage of design ESALs.

The computed ESALs for heavy trucks are 228,053 and 1,933,618 for Maine and Rhode Island, respectively. The consumed design ESALs were 61.2 percent and 80.6 percent, respectively. HETRNG also gives the legalized information for the same fleet. With an additional 6,117 and 103,746 trucks, the computed ESAL values were 195,401 and 1,313,268, and the consumed design ESAL percentages were 52.2 percent and 54.8 percent, respectively. Again it is observed that the same cargo can be transported legally causing less damage to the pavement. Again, the difference between heavy and legal

TABLE 4 ASSESSMENT RESULTS FOR THE MAINE SITE BY A PROCEDURE BASED ON THE 1986 AASHTO DESIGN GUIDE

HEAVY AXLES FOR BOTH LANES IN THE YEAR OF 1988

AXLE TYPE	TOTAL OCCURRENCES	TOTAL EXCESS WEIGHT, LBS	AVG EXCESS WEIGHT PER OCCURRENCE,LBS
SINGLE AXLE	120,848	204,282,001	1,690
TANDEM AXLE	5,720	28,379,000	4,961
TRIDEM AXLE	1,560	18,428,800	11,813
TOTAL	128,128	251,089,802	

18-KIP equivalent AXLE LOAD ANALYSIS, ANNUAL DATUM
(ONLY ON THE TRAVEL LANE ASSUMING 60% OCCUPATION)

	TOTAL OCCURRENCES	MODELED GROSS WEIGHT, KIPS	MODELED 18-KIP ESAL	MODELED ESAL % OF DESIGN
HEAVY TRUCKS	46,956	3,596,367	228,053	61.4
LEGALIZED TRUCKS	53,736	3,912,189	195,401	52.6
DIFF-ERENCE	6,117	315,822	-32,652	-8.8

TABLE 5 ASSESSMENT RESULTS FOR THE RHODE ISLAND SITE BY A PROCEDURE BASED ON THE 1986 AASHTO DESIGN GUIDE

HEAVY AXLES FOR ONE LANE IN THE YEAR OF 1988

AXLE TYPE	TOTAL OCCURRENCES	TOTAL EXCESS WEIGHT, LBS	AVG EXCESS WEIGHT PER OCCURRENCE,LBS
SINGLE AXLE	89,180	319,774,001	3,586
TANDEM AXLE	362,726	2,738,161,792	7,549
TRIDEM AXLE	12,740	269,496,500	21,154
TOTAL	464,646	3,327,432,293	

18-KIP EQUIVALENT AXLE LOAD ANALYSIS, ANNUAL DATUM

	TOTAL OCCURRENCES	MODELED GROSS WEIGHT, KIPS	MODELED 18-KIP ESAL	MODELED ESAL % OF DESIGN
HEAVY TRUCKS	315,042	31,485,010	1,933,618	77.6
LEGALIZED TRUCKS	418,788	34,784,419	1,313,268	52.7
DIF-FERENCE	103,746	3,299,409	-620,351	-24.9

ESALs was far greater for Rhode Island than it was for Maine. Tables 2 through 5 relate the occurrence of each axle type and the excessive weight for each group and the fleet. The comparisons indicate that when the same amount of weight is hauled legally, i.e., within the load limits, less damage will be done to the highway pavement. Less damage is done even with the additional tare weight of the extra trucks required to haul the excess weight. For both states, the procedure based on the 1986 Design Guide provides a slightly higher ESAL value than the one based on the Interim Guide.

The Procedure Based on Asphalt Institute's DAMA

The Asphalt Institute computer program, DAMA, was originally developed to analyze a multilayered elastic pavement structure by a cumulative damage technique for a single or dual wheel load system (*20,21*). The program also can be used for design purposes by analyzing several proposed pavement structures. Most pavement structures made of asphalt concrete, emulsified asphalt mixtures, untreated aggregate materials, and subgrade soils can be analyzed with a maximum of five layers.

Only the maximum strain at a given interface is used for the computation of the damage. The fatigue cracking of each stabilized layer and the subgrade deformation distresses are observed on a cumulative monthly basis. The design life and number of load repetitions to failure are summarized for fatigue cracking and deformation, in which the governing layer is also noted for the design situation. Environmental aspects are also considered in DAMA.

The third procedure, or the first mechanistic procedure, utilized the Asphalt Institute's DAMA program to compute the amount of fatigue cracking and permanent deformation caused by the heavy trucks. Tables 6 and 7 show the summary of damage computed, the pavement design life, and the governing layer of the design for the Maine and the Rhode Island sites, respectively. The outputs show the damage or reduction in design life because of heavy trucks. It relates the damage or life reduction in terms of fatigue cracking and deformation (rutting). The layer with more damage cracking governs the design. Because this program does not allow analysis of a pavement structure with two aggregate layers, the structures had to be modified. For both states the two aggregate layers were combined to be analyzed as one base layer. The subbase was converted into the base by lessening the thickness by a ratio of the layer coefficients, i.e., $0.1(12.0)/0.14 = 8.5$ or approximately 9.0 in. Therefore, the subbase layer for Rhode Island was converted into an additional 9 in. of base.

The Procedure Based on FHWA's VESYS 3A-M

The computer program VESYS was originally developed by FHWA in cooperation with the Massachusetts Institute of Technology (MIT). The original mechanistic model, VESYS II-M was based on an application of the viscoelastic theory to the design of pavements. From research findings, the model has been improved continuously, allowing various versions to be made available. This study used VESYS 3A-M, which is the latest version and is based on the elasto-plasticity theory. This model can be used on a wide range of paving materials, axle loads, and environmental conditions. The model predicts the performance of the pavement in terms of PSI as derived from the AASHTO Road Test. The program expresses PSI in the form of cracking, rutting, and roughness variables. To produce these variables, it uses information about the material properties, geometry of the pavement, traffic, and environment.

TABLE 6 ASSESSMENT RESULTS FOR THE MAINE SITE BY A PROCEDURE BASED ON THE ASPHALT INSTITUTE'S DAMA

	ESAL DETERMINED BY THE INTERIM GUIDE		ESAL DETERMINED BY THE 1986 GUIDE	
	HEAVY TRUCKS	LEGALIZED TRUCKS	HEAVY TRUCKS	LEGALIZED TRUCKS
DAMAGE:				
FATIGUE	.1358E-00	.1161E+00	.1363E+00	.1156E+00
DEFORMATION	.4633E-02	.3959E-02	.4649E-02	.3942E-02
DESIGN LIFE:				
FATIGUE	7.4 YRS	8.6 YRS	7.3 YRS	8.7 YRS
DEFORMATION	216 YRS	253 YRS	215 YRS	254 YRS

TABLE 7 ASSESSMENT RESULTS FOR THE RHODE ISLAND SITE BY A PROCEDURE BASED ON THE ASPHALT INSTITUTE'S DAMA

	ESAL DETERMINED BY THE INTERIM GUIDE		ESAL DETERMINED BY THE 1986 GUIDE	
	HEAVY TRUCKS	LEGALIZED TRUCKS	HEAVY TRUCKS	LEGALIZED TRUCKS
DAMAGE:				
FATIGUE	.2680E+00	.1857E+00	.2711E+00	.1841E+00
DEFORMATION	.5429E-01	.3762E-01	.5493E-01	.3731E-01
DESIGN LIFE:				
FATIGUE	3.7 YRS	5.3 YRS	3.6 YRS	5.3 YRS
DEFORMATION	18.4 YRS	26.6 YRS	18.2 YRS	26.8 YRS

The procedure utilizing the VESYS 3A-M program provides a more sophisticated and precise way to determine the damage caused to the pavement by heavy vehicles.

Tables 8 and 9 show the summary of the resulting damage and pavement life for the Maine site and Tables 10 and 11, for the Rhode Island site. Only the ESALs determined by HETRNG are used because the 1986 AASHTO Design Guide is the most current.

Tables 8 through 11 portray the following observations on the damage and pavement life. The values of cracking, rutting, roughness, and PSI are recorded for each of the specified periods of analysis. The values except for PSI appear to increase with an increase in time. This increase is to be expected because an increase in load repetitions causes an increase in damage, which decreases the PSI, which is also expected.

The tables also show values of pavement service life. The value is the time in years at which the pavement reaches its terminal serviceability index. The value of 2.5 is used because it is the value recommended by AASHTO for interstate highways. Tables 8 and 9 show that, for the Maine site, heavy trucks caused a shorter service life than legalized ones. Tables 10 and 11 indicate that, for the Rhode Island site, heavy trucks caused greater damage than legalized trucks. These values were expected because the ESAL values for legalized trucks are lower than those for the heavy ones. The most important observation was that the heavy trucks consistently provided shorter life than the legalized trucks in both cases.

CONCLUSIONS AND RECOMMENDATIONS

The conclusion and recommendations based on the findings of this investigation are summarized below.

Conclusions

1. It was necessary to develop two computer programs, HETROM and HETROR, to extract heavy truck occurrences from the WIM data for the Maine and Rhode Island sites, respectively.
2. Through either the computer program HETRIG or HETRNG the equivalent 18-kip single axle loads (ESALs) for the heavy trucks were computed as an initial step for each procedure developed.
3. Four procedures including the above computer programs

TABLE 8 RESULTS OF VESYS ANALYSIS USING ESAL OF HEAVY TRUCKS BASED ON THE 1986 GUIDE CONVERSION FACTOR FOR THE MAINE SITE

ANALYSIS TIME	DAMAGE INDEX	RUTTING DEPTH	ROUGHNESS	PSI
1.0 YRS	.24599E+00	.17097E+00	.82936E+00	4.38
5.0 YRS	.60222E+01	.36272E+00	.37358E+01	3.22
10.0 YRS	.23844E+02	.50142E+00	.71463E+01	2.60
20.0 YRS	.13641E+03	.75591E+00	.16273E+02	1.51

NOTE: THE PREDICTED SERVICE LIFE IS 11.69

TABLE 9 RESULTS OF VESYS ANALYSIS USING ESAL OF LEGALIZED TRUCKS BASED ON THE 1986 GUIDE CONVERSION FACTOR FOR THE MAINE SITE

ANALYSIS TIME	DAMAGE INDEX	RUTTING DEPTH	ROUGHNESS	PSI
1.0 YRS	.20866E+00	.16447E+00	.76752E+00	4.42
5.0 YRS	.51077E+01	.34892E+00	.34571E+01	3.29
10.0 YRS	.20225E+02	.48236E+00	.66135E+01	2.68
20.0 YRS	.11571E+03	.72718E+00	.15060E+02	1.63

NOTE: THE PREDICTED SERVICE LIFE IS 12.74

TABLE 10 RESULTS OF VESYS ANALYSIS USING ESAL OF HEAVY TRUCKS BASED ON THE 1986 GUIDE CONVERSION FACTOR FOR THE RHODE ISLAND SITE

ANALYSIS TIME	DAMAGE INDEX	RUTTING DEPTH	ROUGHNESS	PSI
1.0 YRS	.26417E+01	.27005E+00	.17169E+01	3.78
5.0 YRS	.64668E+02	.57561E+00	.78058E+01	2.43
10.0 YRS	.25606E+03	.79742E+00	.14995E+02	1.50
20.0 YRS	.14649E+04	.12054E+01	.34329E+02	-0.33

NOTE: THE PREDICTED SERVICEABILITY LIFE IS 4.48

TABLE 11 RESULTS OF VESYS ANALYSIS USING ESAL OF LEGALIZED TRUCKS BASED ON THE 1986 GUIDE CONVERSION FACTOR FOR THE RHODE ISLAND SITE

ANALYSIS TIME	DAMAGE INDEX	RUTTING DEPTH	ROUGHNESS	PSI
1.0 YRS	.17940E+01	.24640E+00	.14292E+01	3.90
5.0 YRS	.43917E+02	.52518E+00	.64980E+01	2.64
10.0 YRS	.17390E+03	.72755E+00	.12483E+02	1.79
20.0 YRS	.99485E+04	.10998E+01	.28577E+02	0.16

NOTE: THE PREDICTED SERVICE LIFE IS 6.18

were developed to assess pavement damages caused by heavy trucks using the following four available pavement design methods or models:

- AASHTO Interim Guide,
- AASHTO 1986 Guide,
- Asphalt Institute's DAMA, and
- FHWA's VESYS 3A-M.

The ratios of expected lives for legalized trucks to heavy trucks are summarized below.

Site	*Interim Guide*	*1986 Guide*	*DAMA*	*VESYS 3A-M*
Maine	.85	.85	.83	.91
R.I.	.69	.68	.69	.72

4. Only traffic variables were considered for the analysis by using procedures based on AASHTO's Guides. There was no significant difference in pavement damage caused by heavy trucks when procedures based on AASHTO Interim and 1986 Design Guides were compared.

5. For (specified) distress analysis, procedures based on mechanistic models (e.g., DAMA and VESYS 3A-M) could be utilized for damage assessment. Because of the lack of availability of input data except traffic, only demonstration analyses were performed with a reasonably estimated input data set.

6. There were consistent observations, in all cases, that heavy trucks caused more damage than benchmark trucks.

7. Finally, more damage from heavy trucks was predicted when there were higher legal weight limits.

Recommendations

1. Although most NETC states are still using the AASHTO Interim Guide primarily for the pavement design, it is highly desirable to use the procedure based on the 1986 AASHTO Design Guide to assess pavement damage caused by heavy trucks.

2. Because of limitations of DAMA (e.g., only one untreated base layer), the procedure based on VESYS 3A-M appears to be more appropriate for the mechanistic analysis.

3. Procedures based on DAMA and VESYS 3A-M require mechanical properties of pavement materials, such as resilient modulus of subgrade soils and fatigue and creep properties of asphaltic materials. Furthermore, VESYS analysis calls for preparing specimens using a California Kneading compactor. For a more accurate analysis, the above properties and equipment should be available in New England.

4. It is recommended that mechanistic methods (e.g., VESYS 3A-M) be used to assess effects caused by the configurations, tire pressure, nonstandard vehicles, and variables other than traffic.

5. Because of the lack of construction records or necessary data for this study (e.g., design ESAL for the Rhode Island site), the absolute values of results need to be validated for the interpretation. It is recommended that all NETC states look into establishing a good, possibly computerized, data base as a subset for the pavement management system for future activities.

ACKNOWLEDGMENTS

The authors wish to thank members of the NETC Truck Management Technical Committee for their cooperation and encouragement in performing this research project. Special appreciation is extended to Rhode Island Department of Transportation and FHWA engineers for their essential continuing support and assistance throughout the program. Finally, we would like to express our thanks to the staff of the Engineering College of the University of Rhode Island who collaborated with us at various stages in preparing this paper.

REFERENCES

1. D. R. Luhr and B. F. McCullough. Structural Analysis of AASHO Road Test Flexible Pavements for Performance Evaluation. In *Transportation Research Record 888*, TRB, National Research Council, Washington, D.C., 1982.
2. C. M. Walton, Chien-Pie Yu, and Paul Ng. Procedure for Assessing Truck Weight Shifts Resulting From Changes in Legal Limits. In *Transportation Research Record 920*, TRB, National Research Council, Washington, D.C., 1983, pp. 19–25.
3. W. C. Arnold. Trial Strategy and Techniques in Enforcing Laws Relating to Truck Weights and Sizes. *NCHRP Research Results Digest 154*, 1986.
4. *Effects of Heavy Vehicle Characteristics on Pavement Response and Performance—Phase II.* Report NCHRP Project 1–25(1), TRB, National Research Council, Washington, D.C., 1987.

5. *Excessive Truck Weight: An Expensive Burden We Can No Longer Support*. Report to the Congress, CED-79-94, United States General Accounting Office, Washington, D.C., 1979.
6. *The Development of a Common Regional System for Issuing Permits for Oversize and Overweight Trucks Engaged in Interstate Travel*. Massachusetts Institute of Technology, Cambridge, May 1986.
7. Agreement to Pursue the Implementation of a Common Set of Procedures for Issuing Permits for Oversize and Overweight Trucks Engaged in Interstate Travel. NETC Policy Committee, Cambridge, Mass., April 28, 1987.
8. R. L. Terrell and C. A. Bell. *NCHRP Synthesis of Highway Practices 131: Effects of Permit and Illegal Overloads on Pavements*. TRB, National Research Council, Washington, D.C., September 1987.
9. E. J. Yoder and M. W. Witczak. *Principals of Pavement Design*, 2nd ed. John Wiley and Sons, Inc., New York, 1975.
10. *Design Procedure for Flexible Layered Pavements*. Rhode Island Department of Transportation, Providence, January 1984.
11. *Pavement Design*. Massachusetts Department of Public Works, Boston.
12. *Standards and Specifications for Road and Bridge Construction*. Rhode Island Department of Transportation, Providence, 1971.
13. W. D. Cunagin. *NCHRP Synthesis of Highway Practice 124: Use of Weigh-In-Motion Systems for Data Collection and Enforcement*. TRB, National Research Council, Washington, D.C., 1986.
14. *Weighing in Motion*. Rhode Island Department of Transportation, Providence, 1988.
15. *AASHTO Interim Guide for Design of Pavement Structures—1981*. American Association of State Highway and Transportation Officials, Washington, D.C., 1981.
16. *AASHTO Guide for Design of Pavement Structures*. American Association of State Highway and Transportation Officials, Washington, D.C., 1986.
17. *Thickness Design—Asphalt Pavements, Highways, and Streets*. Manual Series 1 (MS-1), The Asphalt Institute, College Park, Md., September 1981.
18. W. J. Kenis. *Predictive Design Procedures, VESYS, Users Manual*. FHWA, March 1976.
19. R. T. Barros. Analysis of Pavement Damage Attributable to Overweight Trucks in New Jersey. In *Transportation Research Record 1038*, TRB, National Research Council, Washington, D.C., 1985.
20. *Research and Development of the Asphalt Institute's Thickness Design Manual (MS-1)*, 9th ed., Research Report 82-2, RR-82-2. The Asphalt Institute, College Park, Md., August 1982.
21. *Computer Program DAMA, User's Manual*, Computer Program 1 (CP-1). The Asphalt Institute, College Park, Md., October 1983.

Publication of this paper sponsored by Committee on Flexible Pavement Design.

Effect of Fracture Healing on Laboratory-to-Field Shift Factor

ADLI AL-BALBISSI AND DALLAS N. LITTLE

Laboratory fatigue testing of asphalt concrete can be used to predict field performance. The introduction of a shift factor is necessary to account for the effects of residual stresses and healing that occur in the field but do not occur in the laboratory. In this study the healing mechanism in asphalt concrete is investigated. A theoretical hypothesis for the shift factor and a new approach to characterizing the toughness of paving mixtures based on the *J*-integral concept are also introduced. The shift factor is assumed to consist of the combined effect of a strain recovery component and crack recovery component. The two components can be determined from simple laboratory tests, including stress relaxation, beam fatigue, and the overlay tests. The fracture mechanics approach, the J^*, is based on the path-independent J integral, which can be defined as the energy released per unit area of crack extension. The J^* parameter is adopted to characterize material toughness.

Loss of structural or functional pavement serviceability because of load-related fatigue cracking has long been a major topic of concern to highway engineers. Such failures often occur because of improper prediction of pavement fatigue life or premature failure from crack propagation. It is important, therefore, to understand the mode of fracture initiation and propagation for careful design of highway or airport pavements. Such understanding may lead to a procedure for estimating a shift factor between laboratory and field results that will consider the actual mechanics of fracture. Although such a factor may seem to be of little use to someone dealing with everyday pavement problems, it is of great significance for a more accurate prediction of pavement life and can be of great practical value.

The primary goal of this study is to introduce a practical approach to estimating the shift factor and to investigating and evaluating the effect of rest periods on healing fatigue-caused fractures in asphalt-treated mixtures. It is believed that the effect of healing and residual stresses that occur in the field but not in the laboratory are the major factors that will contribute to more accurate prediction of fatigue performance. In fact, prediction of field performance based on laboratory testing will normally result in miscomputation of the pavement life by a range of 300 to 2,000 percent. Identification of the healing mechanism and quantification of the effects of selected variables will, no doubt, lead to a much improved ability to predict pavement life. It will provide the basis for procedures to increase the life of asphalt structures by maximizing the healing process.

A. H. Al-Balbissi, Civil Engineering Department, Jordan University of Science and Technology, Irbid, Jordan. D. N. Little, Texas A&M University, College Station, Tex. 77843.

Evidence for the existence of a healing mechanism has been provided by several laboratory studies, in addition to that produced by the AASHTO Road Test. The most detailed study has been reported by Routhly and Sterling (*1,2*), with additional evidence being provided by McElvaney and Pell (*3*), Borgin and Fourier (*4*), and Van Dijik (*5*). These studies have attempted to quantify the effect of rest periods and have expressed the result as a ratio of the number of cycles to failure with rest to the number of cycles to failure without rest. The studies mentioned above all indicate that the ratio is greater than one, that is, life measured during cyclic loading that includes rest periods is greater than life under continuous cyclic loading. These studies support the view that asphaltic materials have the capacity to recover from the effects of stress— that is, there is a healing mechanism. Previous studies have also mentioned that the healing process is affected by the rate of loading, stress level, duration of rest periods, and the method used to apply the loads.

METHODOLOGY

Although there is not much literature about healing studies for asphalt cement and asphalt concrete, there is literature about evaluating the healing of polymers. The experimental concept for the evaluation of healing has generally been to select a convenient dimensionless recovery ratio, such as the ratio of fracture stress for the virgin material to fracture stress of the healed material. In many relevant studies the healing process was described as taking place in several stages (*6,7*). Woo and O'Conner (*6*) and Jud et al. (*7*) were able to develop relations for strength, elongation to break, impact energy, and fracture parameters as a function of time, molecular weight, temperature, pressure, and processing conditions. Many of their theoretical predictions were supported by experimental data. These studies provided excellent indications that mechanical means (through the laws of fracture mechanics) can be used to determine the strength change caused by healing. In this study the energy concept is selected as the indicator for material healing. This criterion is adopted because of its engineering significance and its relative ease of measurement.

In addition, the increase in dissipated energy resulting from rest time is adopted to outline a model for the estimation of a shift factor between laboratory and field results.

The testing procedure used in this study employed the overlay tester, which was developed at Texas A&M University, College Station. The overlay tester is a fatigue testing machine designed to model displacements caused by thermal stresses in asphalt pavements resulting from cyclic changes in the

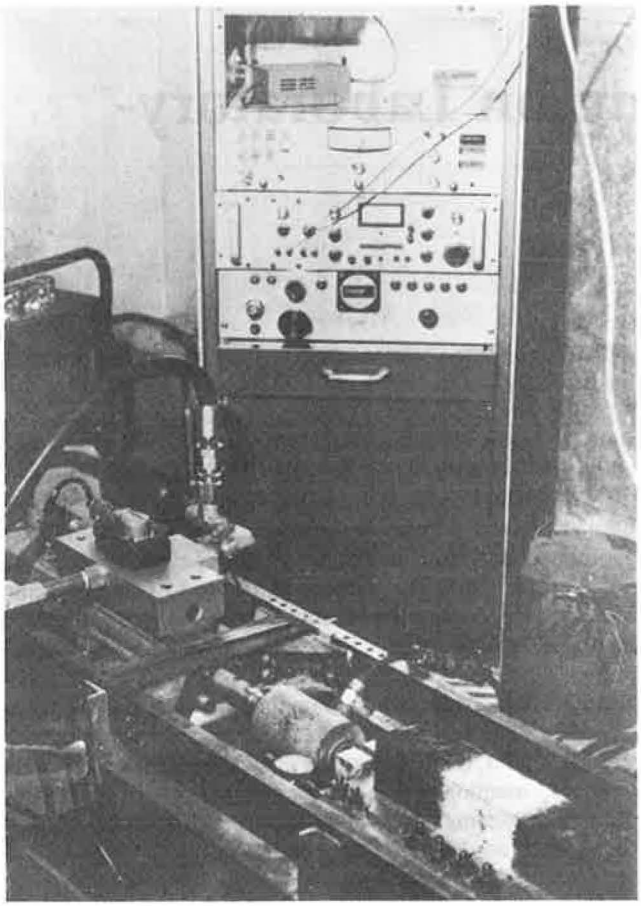

FIGURE 1 Overlay testing device.

ambient temperature. A servohydraulic mechanism controls the rate of loading as well as the crack opening displacement and allows a controlled strain condition to be maintained throughout the test.

Beam samples 3 in. by 3 in. by 15 in. are prepared and then cured in an environmentally controlled room (77°F, 25 percent relative humidity) for a minimum of 3 days. Each sample is glued to a pair of aluminum base plates in an arrangement that simulates the construction of an overlay over a cracked or jointed pavement. Figure 1 shows an illustration of the testing device. Figure 2 shows an illustration of specimen mounting. The overlay tester is calibrated to ensure the desired maximum displacement of 0.04 in. or 0.02 in. A movement of 0.04 in. is approximately equivalent to the displacement experienced by a Portland cement concrete pavement with 15-ft joint or crack spacings as it undergoes a 60°F change in pavement temperature. The actual testing procedure consists of subjecting the overlay samples to an oscillating movement of opening and closing the butt joint of the two base plates. This type of movement causes a crack to form from the bottom of the sample upward through the sample. "Failure" is defined as the condition in which a continuous reflection crack is visible up both sides of the sample and across the entire width of the top of the sample, as observed when the overlay tester is in the "open" position. Under this condition, the load required to open the gap between the

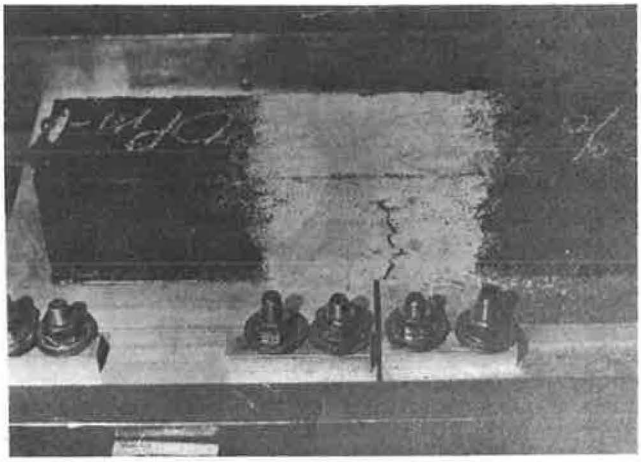

FIGURE 2 Specimen mounted on plates.

sample base plates is caused by the frictional forces that must be overcome to separate the two sample parts.

A loading rate of one cycle per 10 seconds was used throughout the test program. The cyclic motion was maintained except during the rest periods, during which the samples were left in the "closed" position. The load and displacement values were monitored and recorded only during selected cycles of each test. An X-Y recorder was used to plot the applied load versus displacement relationship during the selected cycles. Figure 3 shows an illustration of the X-Y plotter. Figure 4 illustrates the general shapes of typical load versus displacement graphs at various stages during the test.

ANALYTICAL APPROACH

To precisely evaluate the energy associated with fracture fatigue or, more generally, crack propagation, one must select a theoretically sound analytical approach. The science of fracture mechanics offers such an approach. Of course, asphalt cement and, in turn, asphalt concrete is not a linear-elastic material. Consequently, linear-elastic fracture mechanics is not valid. It is safe to assume that the behavior at the crack tip is nonlinear with a relatively large plastic zone preceding the crack tip. Possible methods of analysis include the crack tip opening displacement method (CTOD), *R*-curve analysis, or the *J*-integral method.

Under conditions of plane strain in which the crack tip plastic zone is small, linear elastic analysis is appropriate. For materials and conditions under which the plastic zone becomes larger, it is important that the effective crack length be used to calculate an effective stress intensity factor. However, because the plastic zone itself is a function of the stress intensity factor, an iterative process is necessary to calculate an effective stress intensity factor; as the size of the plastic zone adjustment becomes larger, relative to the crack size, the computation becomes less accurate. Under such conditions a method that permits extension of linear-elastic fracture mechanics into the elastic-plastic region must be used. The *J*-integral is best suited for the analysis of test data in this study. A major advantage of the *J*-integral method is that it does not require a stringent

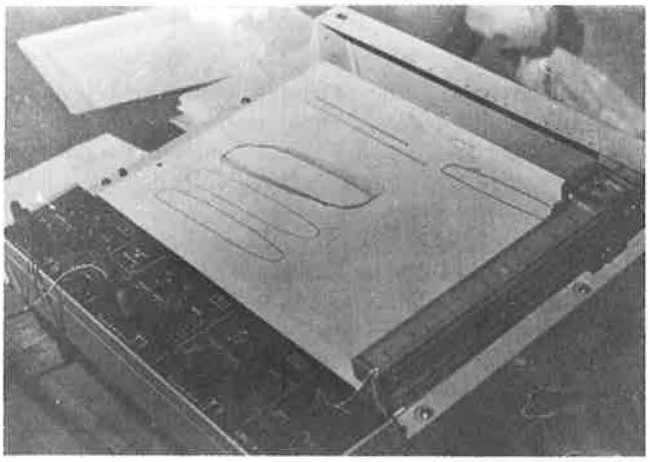

FIGURE 3 X-Y plotter.

specimen size to ensure an acceptable small plastic zone size. The method allows the determination of energy release rate (J_1) using a small specimen. Although pavement materials can be assumed to behave elastically in fracture because of their large size, size limitations of laboratory specimens prevent similar behavior. The large size of pavement constitutes a constraint to the development of a large plastic zone; thus, elastic behavior can be assumed. Conversely, the development of a large plastic zone in laboratory specimens is expected. The usefulness of the *J*-integral analysis is that one can infer information about the behavior of the elastic pavement based on laboratory specimens that may have experienced elastic deformation. The rationale is that the amount of energy released by a specific material per unit area of crack extension will be the same regardless of the size of the specimen. The *J*-integral procedure provides a way to calculate this energy release rate for an elastic material from small specimens that may have some plastic deformation.

The path-independent *J*-integral proposed by Rice (*8*) is a method of characterizing the stress-strain field at the tip of a crack by an integration path taken sufficiently far from the crack tip to be substituted for a path close to the crack tip region. Thus, even though considerable yielding occurs in the vicinity of the crack tip, if the region away from the crack tip can be analyzed, behavior of the crack-tip region can be inferred.

The *J*-integral is defined as the energy released per unit area of crack extension. It may be interpreted as the potential energy difference between two identically loaded bodies having neighboring crack size, or

$$J = -(1/B)\,(dv/da) \tag{1}$$

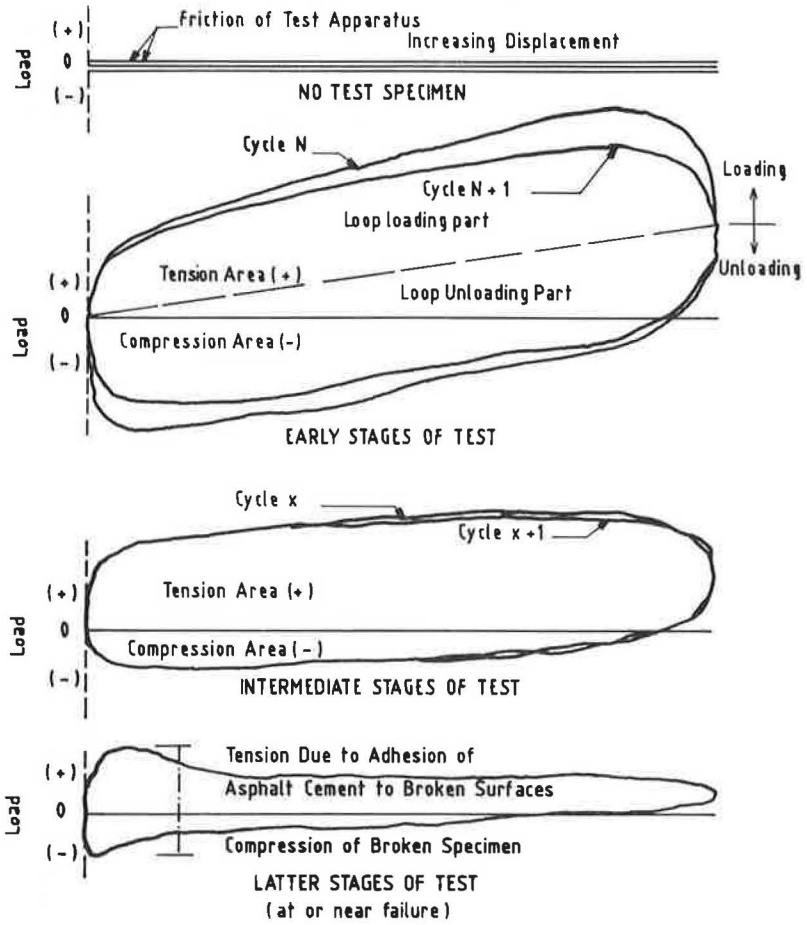

FIGURE 4 Typical recordings of load versus displacement at various stages during an overlay test.

where

V = potential energy,
B = thickness, and
a = crack depth.

This definition is shown schematically in Figure 5. A more detailed discussion of the J-integral is provided elsewhere (*8*).

Path independence of the J-integral has been shown thus far by using only the deformation theory of plasticity, which does not allow for unloading. Therefore, the J-integral fracture criteria must presently be restricted to conditions under which unloading does not occur. In the overlay test, cyclic loading and unloading of the specimen occur, which suggests that the J-integral cannot be used, because the basic definition of the J-integral is the energy released per unit area of crack extension. The difference then in the released energy between the case with unloading and the case without unloading is manifested in the area under the load-displacement curve, i.e., when unloading is considered, the V^* includes all the area enclosed by the load-displacement loop, as illustrated in Figure 4. Therefore, the parameter

$$J^* = (1/B)\ (dv^*/da) \tag{2}$$

where V^* is the energy released, including the unloading area, was adopted for analysis. The total area (V^*) reflects the energy released by the material and includes the effect of unloading. Therefore, the J^* parameter is deemed to be appropriate to characterize material toughness (the name J^* was adopted because it is analogous to the J-integral definition).

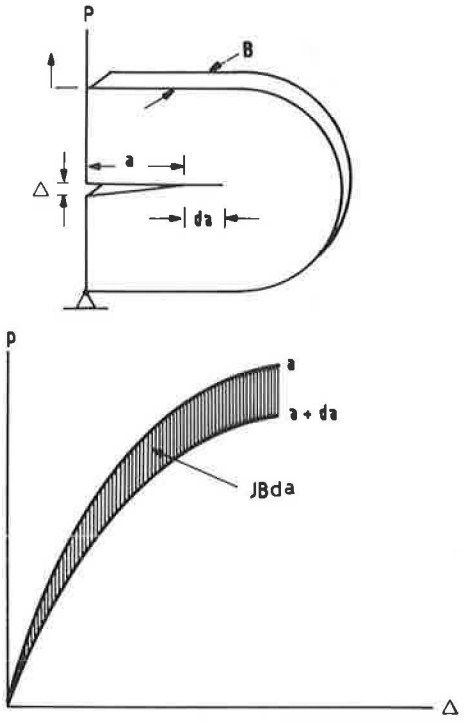

FIGURE 5 Interpretation of J-integral.

STUDY OF EFFECT OF REST PERIODS ON HEALING

The fatigue characteristics of pavement mixes are determined in continuous loading tests. These conditions do not resemble actual loading conditions in the field. Under traffic, the pavement is loaded discontinuously because the passage is interrupted by rest periods.

Preliminary tests of this study indicated that a single rest period had no significant effect on pavement life or fracture characteristics. To obtain a more complete insight into the effect of rest periods on the fatigue life, more tests were performed. A summary of these tests is given in Table 1.

The results of various duration of rest indicate that very long rest periods did not induce significantly greater strain recovery than did shorter rest periods. Several durations were attempted on the same specimen. Test results show that the recovery rate decreased as the test progressed. Generally, test results showed that within a rest period of between 15 and 40 minutes, a considerable proportion of the recovery can be achieved, and longer rest periods of 1 or 2 days do not substantially increase recovery. However, a 40-minute period was not much better (in terms of added energy) to a 15-minute rest period. In addition, a gap of 40 minutes between traffic vehicles in a real application occurs only on highways with very low traffic volume. Fatigue is more a problem in highways with moderate to heavy traffic. Therefore, for these practical purposes, a rest period of 15 minutes was implemented in the remainder of the tests.

Tests with a variable number of rest periods showed a very high correlation between the number of rest periods and fatigue life. The results showed an increase in fatigue life of the specimen by a factor of 2 to 5 when rest periods were introduced. These results were consistent at the two displacement magnitudes examined.

SHIFT FACTOR HYPOTHESIS

The shift factors used to transform the laboratory phenomenological fatigue model into a field "equivalent" have, in the past, been determined empirically. Perhaps the best known version was developed by Finn et al. (*9*) from AASHTO Road Test data.

Yandell and Lytton (*10,11*) conducted a detailed study of the residual stresses in a pavement. They indicated that, because of residual compressive strain, the tensile strain resulting from a wheel load application is equivalent to 80 percent of the strain that resulted from the preceding wheel load application. Furthermore, the authors presented some enlightening hypotheses on how the fatigue shift factor is affected by rest periods and residual stresses. The authors examined these hypotheses through the study of the effect of rest periods on the fatigue life of plasticized sulfur binders used in asphalt-like mixtures. These studies have substantiated their hypotheses.

During a rest period, two recovery processes may take place. In one process the material relaxes and loses some of its residual strain. In the other process the material is given time to heal from its distressed state, during which the size of the plastic zone ahead of a formed crack is reduced. During this time a portion of the crack can be closed because of the

TABLE 1 SUMMARY OF OVERLAY TESTS

Displacement magnitude (in)	With rest periods	Without rest periods
	No. of Specimens	
0.02	4	4
0.04	4	4
	Rest period duration (hr.)	
	1 4 24	
	No. of specimens	
0.02	2 1	1
0.04	2 1	1

	Number of rest periods						
	1-10	11-20	21-30	31-40	41-50	51-60	No. rest
	Number of specimens						
0.04	2	2	2	2	2	2	2

compression resulting from bond forces between the particles of the material after the removal of the applied load. These two effects will result in increasing the expected fatigue life of a specimen.

Considering the fact that a field loading pattern is similar to laboratory loading with rest periods, an analytical approach can be postulated to estimate a shift factor between laboratory and field results. In this approach the shift factor is assumed to consist of two components as follows:

$$SF = (SF_r)\,(SF_h) \tag{3}$$

where

SF_r = the shift caused by residual stresses, and
SF_h = the shift caused by crack healing and plastic zone reduction.

The behavior of the material during the residual strain component (SF_r) is very much analogous to relaxation characteristics and strain recovery characteristics. This behavior permits the assumption of similar decay and recovery patterns. The stress relaxation relationship can be presented in the form

$$E(t)/E_0 = t^{-n} \tag{4}$$

where

$E(t)$ = the elastic modulus at time t,
E_0 = the initial elastic modulus, and
n = the slope of the relaxation curve.

The ratio of the strain at a given time to the initial strain $[P(t)/(P_0)]$ can be fitted to a relationship of the following form:

$$P(t) = 1 - (1 - P_0)t^{-n} \tag{5}$$

To reflect this characteristic pattern on the expected fatigue life, the following relationship is assumed:

$$SF_r = \left\{1/\left[1 - (1 - p_0)t^{-n}\right]\right\}^{k_2} \tag{6}$$

where k_2 is the slope of the beam fatigue laboratory relationship between the number of cycles to failure (N_f) and initial strain.

The shift factor component related to crack healing is estimated on the basis of rest period analysis. These analyses revealed a relationship between added energy and the logarithm of rest duration of the form

$$du = e^{h \log t} \tag{7}$$

where

du = the added energy,
t = time, and
h = constant.

The analysis also revealed a direct relationship between the amount of added energy and the increment in specimen life of the form

$$d\,n_f = a + m\,(du) \tag{8}$$

Combining the last two equations gives

$$d\,n_f = a + m\,(e^{h \log t}) \tag{9}$$

Using the above equation with coefficients developed experimentally, dn_f, and consequently n_f, were computed for various time periods. Furthermore, a relationship between cycles to failure and number of rest periods was developed (Figure 6) from the analysis of rest periods. Using this relationship, the corresponding number of rest periods (n_r) for the computed N_f was determined. The variable $(n_f/n_0 - 1)/n_r$, where n_0 is the fatigue life without rest, was then computed for the various time periods. A relationship of the following form was then fitted to the computed variables:

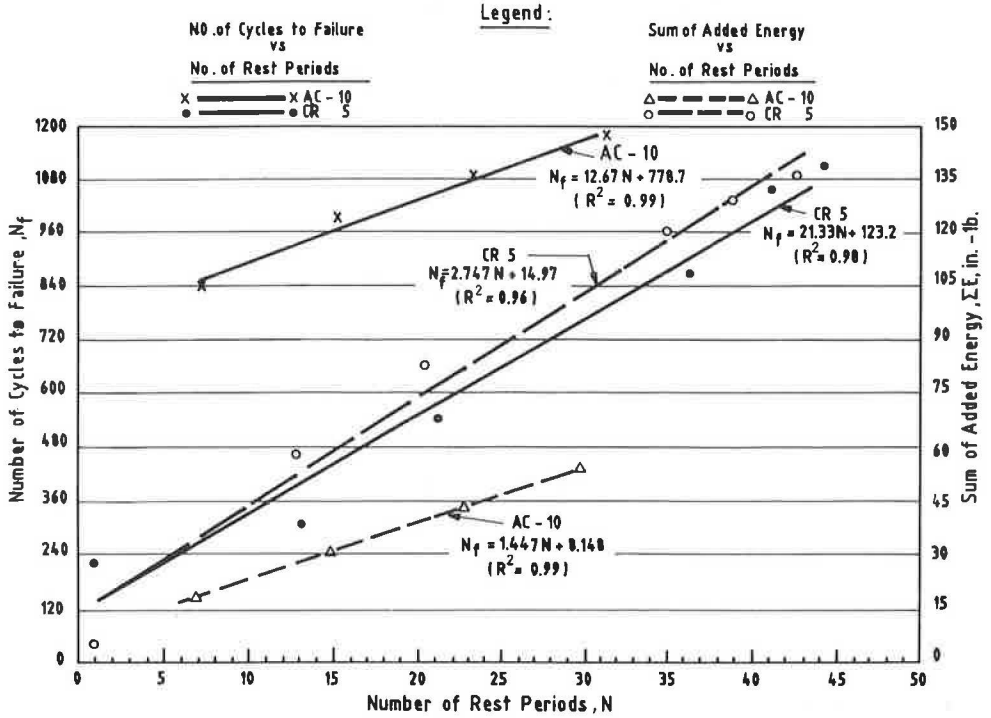

FIGURE 6 Relationships between (a) number of cycles to failure and number of rest periods and (b) sum of added energy and number of rest periods.

$$(N_f/N_0 - 1)/n_r = 5.685 \times 10^{-3}\, e^{1.956(\log t)} \quad (10)$$

which can be reduced to

$$(N_f/N_0) = 1 + 5.685 \times 10^{-3}\, e^{1.956(\log t)} \quad (11)$$

Combining the two shift factor proportions yields

$$SF = \left\{1/\left[1 - (1 - p_0)\, t^{-n}\right]\right\}^{k2} \times \left[1 + 5.685 \times 10^{-3}\, e^{1.956(\log t)} n_r\right] \quad (12)$$

Using a $K_2 = 2.998$ (a typical slope coefficient developed for plasticized sulfur binders in beam fatigue tests) and typical slope values of stress relaxation curves (n) for the same materials, with various numbers of rest periods (n_r), several combinations of SF_r and SF_h were computed and are presented in chart form in Figure 7. The chart can be used to select the two components of the shift factor that correspond to a certain rest time. The total shift factor will be the product of the two components. Asphalt cement (AC-10) is expected to have a higher shift factor because it showed better healing characteristics. Test results indicate a K_2 value of 3.726 for asphalt cement (AC-10). This will result in higher values for SF_r and, consequently, a higher overall shift factor.

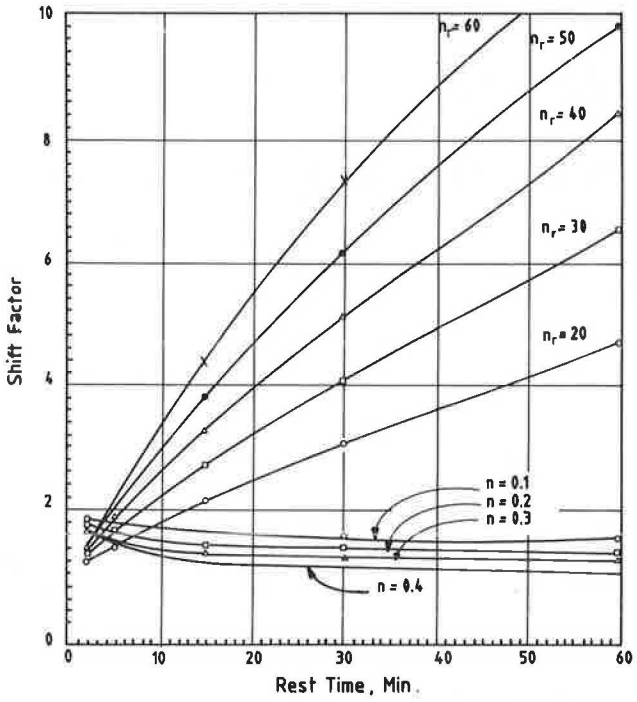

FIGURE 7 Shift factor chart.

TABLE 2 LABORATORY-TO-FIELD SHIFT FACTORS USED FOR ASPHALT CONCRETE AND SULPHLEX

	Shift Factors		
N_{lab}	T = 36°F	T = 68°F	T = 110°F
10^2	18.8	12.9	7.9
10^3	10.5	7.7	5.3
10^4	5.8	4.6	3.5
10^5	3.2	2.8	2.5
10^6	1.8	1.7	1.5
10^7	1.0	1.0	1.0
10^8	0.56	0.60	0.66

All parameters on the righthand side of the shift factor relationship can easily be determined from laboratory tests. Coefficients of the crack healing portion can be determined from overlay tests with rest periods. The n parameter can be determined from a relaxation test and the K_2-parameter can be determined from a simple beam fatigue test. This relationship presents a simple, practical, and convenient means to estimate a shift factor between laboratory and field results.

ANALYSIS OF TEMPERATURE EFFECT

To illustrate the effect of temperature on the shift factor and to demonstrate the field conditions for comparative analysis it was necessary to represent field conditions. The shift factors suggested by Pickett et al. (*12*) (Table 2) were selected for both asphalt concrete and Sulphlex for the following reasons:

1. Utilization of identical shift factors for asphalt and Sulphlex is considered an acceptable approach until field verification indicates that different factors should be used,
2. The rest period analysis points out a similar healing response for Sulphlex CR5 and AC-10 specimens, and
3. Shifting AC-10 laboratory beam fatigue data by means of the Pickett factors yields a realistic failure criterion, which is comparable to that of Finn et al. (*13*) (Figure 8).

The time-temperature shift factors (a_T) for Sulphlex and asphalt mixtures with various aggregates and gradations were then compared and are shown in Figures 9 through 11. The following are apparent from these figures:

1. Shift factors for asphalt concrete and Sulphlex for each mixture evaluated were similar. In fact, the effect of binder on a_T was not statistically significant.

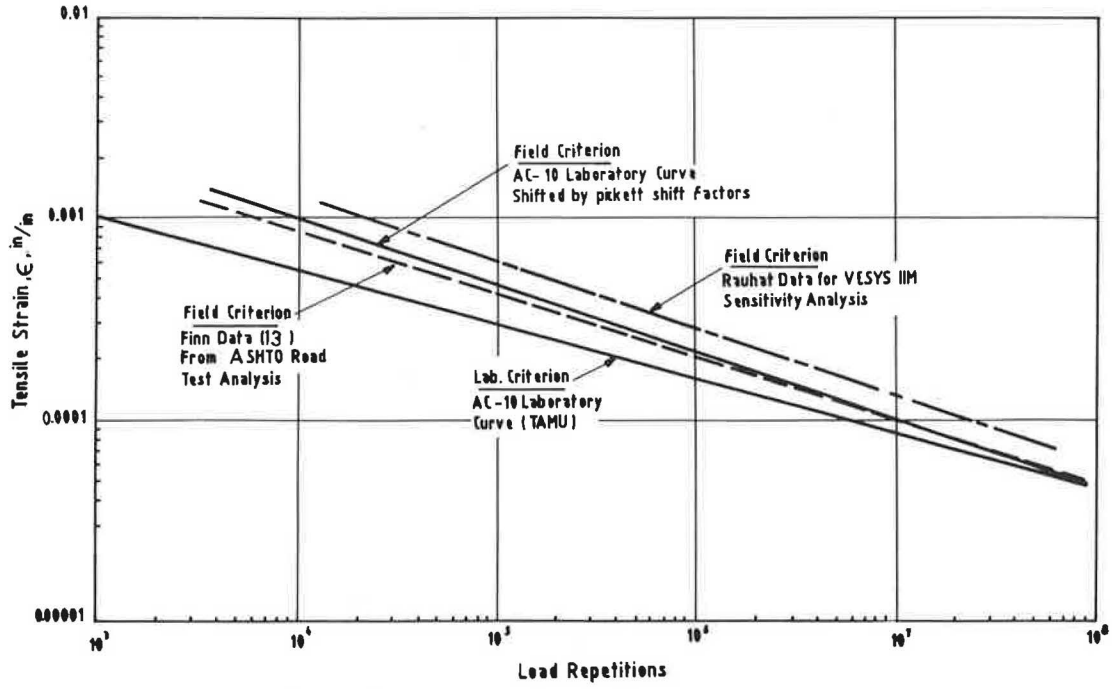

FIGURE 8 Illustration of laboratory-to-field shifts.

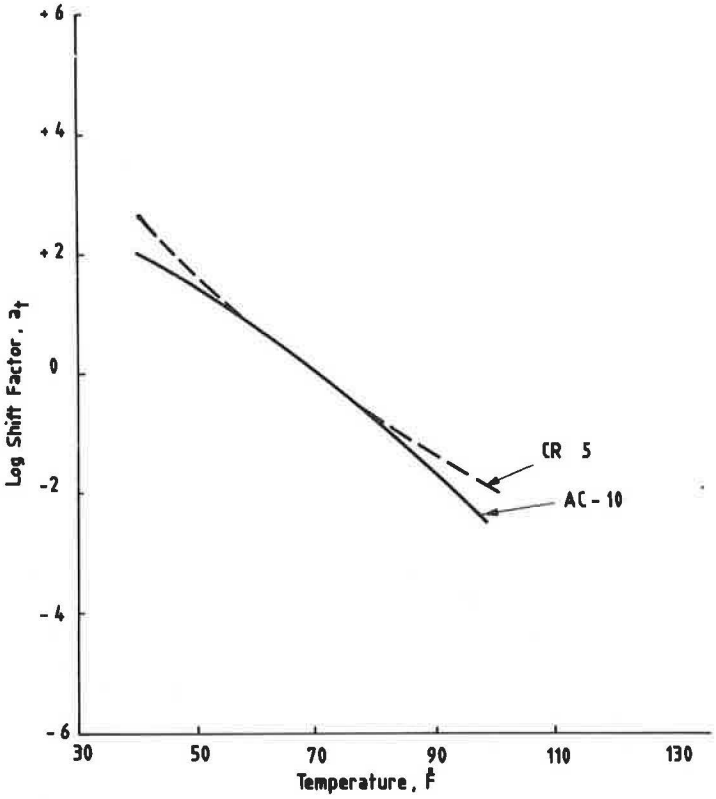

FIGURE 9 Time-temperature shift factor for mixtures with crushed limestone aggregates.

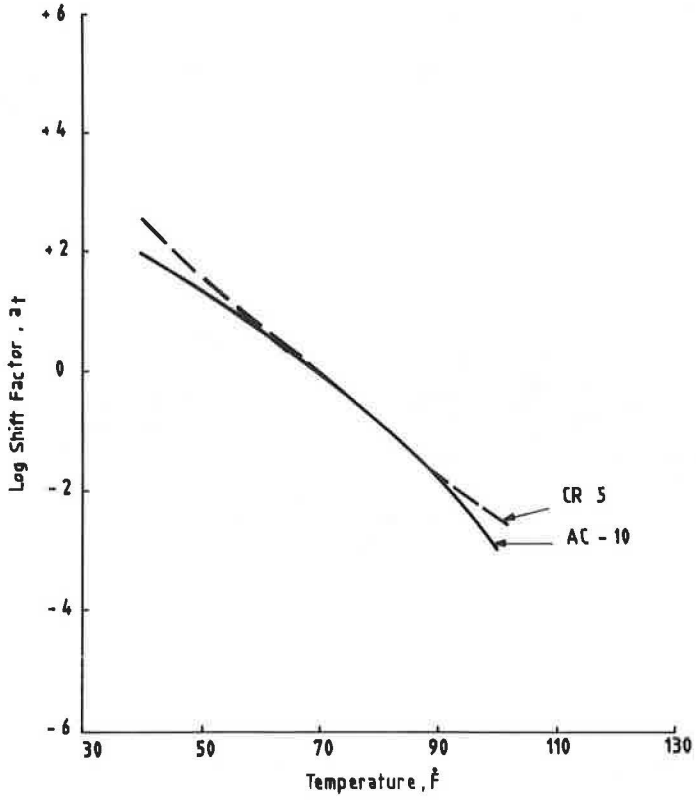

FIGURE 10 Time-temperature shift factor for mixtures with basalt aggregate.

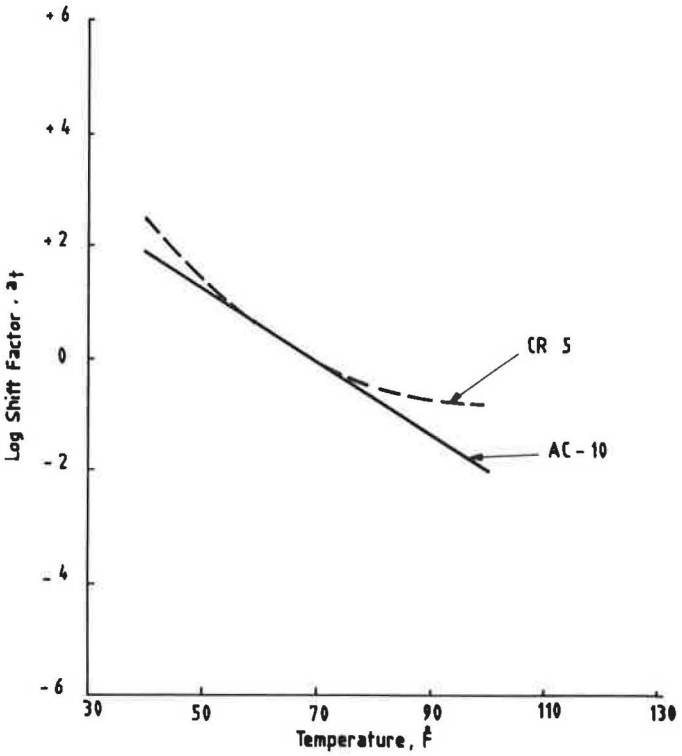

FIGURE 11 Time-temperature shift factor for mixture with river gravel aggregate.

2. Ranges of shift factors between 100°F and 40°F are typical of those found in the literature for asphalt concrete (*12*) and sulfur extended asphalt mixtures.
3. The effect on the shift factor of aggregate type was as great as that of binder type.

Although for practical engineering purposes both Sulphlex and asphalt concrete can be considered linearly viscoelastic, the application of a horizontal shift factor along the log time abscissa to produce a master curve is subjective. The value becomes even more subjective when the shift factor is described in terms of beta. The term beta is defined as the ratio of the change in $\log_{10} a_T$ over a change in temperature or a temperature interval.

$$\text{Beta} = \text{Delta}(\log_{10} a_T)/\text{Delta } T \quad (13)$$

This value assumes a linear relationship between $\log_{10} a_T$ and temperature. As can be seen from Figures 9 through 11, this relationship is not the case. The values of beta are presented in Table 3.

CONCLUSIONS

In this study a new approach to characterizing the fracture behavior of paving mixtures has been introduced. A modified form of the *J*-integral was implemented. The modified form is based on the total area under the load displacement curve that includes the unloading portion instead of just the loading area in the conventional *J*-integral approach. A major advantage to this approach is the ability to extend the analysis into the elastic-plastic region, thus eliminating the requirements for a stringent specimen size to ensure plane strain conditions.

The analysis of rest periods indicated a direct relationship between the number of rest periods and fatigue life. The analysis showed that an increase in fatigue life results from an increase in the number of rest periods. Additionally, the rate of incremental benefit from rest periods diminishes as the duration of the rest period increases (Figure 12). The rate of added energy decreases substantially for rest periods longer than 30 minutes. The recovery trend as a function of time can be described by an exponential function. Material recovery patterns as a function of crack length resemble energy release patterns.

The theoretical basis for a shift factor is presented based on Lytton's hypothesis. The shift factor is assumed to consist of the combined effect of a strain recovery component and crack recovery component. The two components can be determined from simple laboratory tests consisting of stress relaxation, beam fatigue, and overlay tests. Limited rest period testing on AC-10 specimens and CR5 specimens at room temperature reveal that although the fracture propagation life (N_f) is superior for AC-10 specimens compared with that for CR5 specimens, healing properties at 73°F are similar.

TABLE 3 SUMMARY OF BETA VALUES

Binder	Aggregate	Air Voids Content, %	BETA
AC-10	CLS	6-8	0.080
		3-5	0.070
		3-5	0.090
	RG	2-3	0.095
	Basalt	3-5	0.089
CR5	CLS	3-5	0.075
	Basalt	6-8	0.070
	RG	2-3	0.080

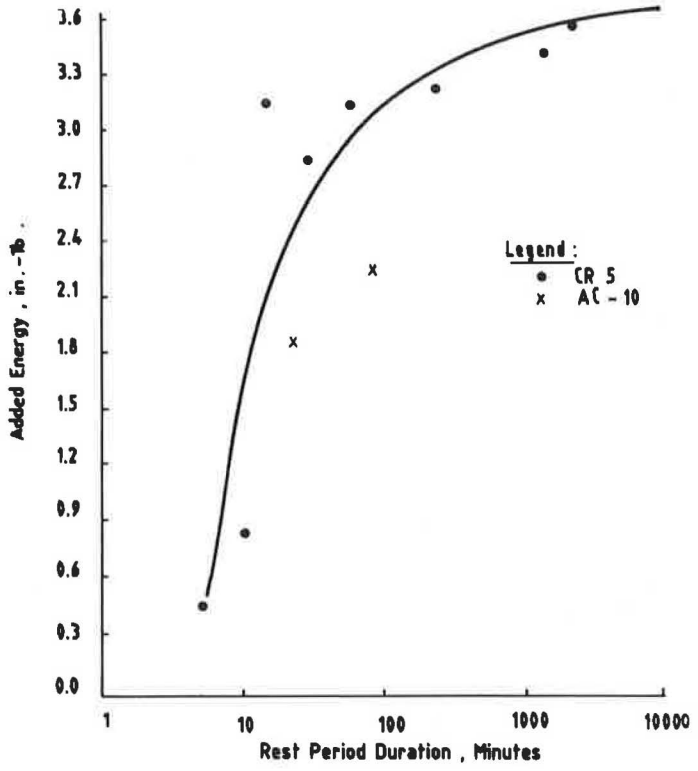

FIGURE 12 Effects of duration of rest period on energy required for crack propagation (specimens were CR5 and crushed limestone).

REFERENCES

1. K. D. Routhly and A. B. Sterling. The Effect of Rest Periods on the Fatigue Performance of a Hot-Rolled Asphalt Under Reversed Axial Loading. *Proc., Association of Asphalt Paving Technologists*, Vol. 39, 1970.
2. K. D. Routhly and A. B. Sterling. *Some Effects of Loading History on the Fatigue Performance of Rolled Asphalt*. Report LR496. Transport and Road Research Laboratory, Crowthorne, Berkshire, England, 1972.
3. J. McElvaney and P. S. Pell. Fatigue Damage of Asphalt: Effect of Rest Periods. *Highways and Road Construction*, Vol. 41, No. 1766, October 1987.
4. P. Borgin and J. B. Fourier. Performability, Fatigue, and Healing Properties of Asphalt Mixes. *Proc., 2nd International Conference on the Structural Design of Asphalt Pavements*, Ann Arbor, Mich., 1967.
5. W. Van Dijik. Practical Fatigue Characteristics of Bituminous Mixes. *Proc., Association of Asphalt Paving Technologists*, Vol. 44, 1975.
6. R. P. Woo and K. M. O'Conner. A Theory of Crack Healing in Polymers. *Journal of Applied Physics*, Vol. 52, No. 10, 1981.
7. K. Jud, H. H. Kausch, and J. G. Williams. Fracture Mechanics Studies of Crack Healing and Welding of Polymers. *Journal of Materials Science*, Vol. 16, No. 1, 1981.
8. J. R. Rice. A Path Independent Integral and the Approximate Analysis of Strain Concentration by Notches and Cracks. *Journal of Applied Mechanics, Transactions*, ASME, Vol. 35, June 1968.
9. Use of Distress Prediction Subsystems for Design of Pavement Structures. *Proc., 4th International Conference on the Structural Design of Asphalt Pavements*, University of Michigan, Ann Arbor, 1977.
10. W. Yandell and R. L. Lytton. *Residual Stresses Due to Travelling Loads and Reflection Cracking*. Report 207-6. Texas Transportation Institute, College Station.
11. W. Yandell and R. L. Lytton. *The Effect of Residual Stress and Strain Build-Up in a Flexible Pavement by Repeated Rolling of A Tire*. Report RF4087-1. Texas Transportation Institute, College Station.
12. *Extension and Replacement of Asphalt Cement by Sulfur*. Report FHWA-RD-78-95. FHWA, U.S. Department of Transportation, March 1978.
13. F. Finn, C. L. Saraf, R. Kulkarni, K. Nair, W. Smith, and A. Abdullah. *NCHRP Report 291: Development of Pavement Structural Subsystems*. TRB, National Research Council, Washington, D.C., 1986.

Publication of this paper sponsored by Committee on Flexible Pavement Design.

Probabilistic Modeling of Flexible Pavements

PHILIPPE L. BOURDEAU

A number of uncertainties and random factors play a role in the deterioration process of pavements under the effect of traffic. A probabilistic approach can make allowance for the stochastic nature of this process and provide a better rationale for the design methods. An extension in this direction of the empirical design method derived from the AASHO road tests for flexible pavements with unbounded granular layers is presented. The probabilistic development addresses two aspects of the problem. First, the reliability assessment of a pavement section is obtained by considering the Shook and Finn design equation as a function of two random variables—the expected number of traffic loads and the California bearing ratio (CBR) of the subgrade soil. The formulation is a second-order, second-moment development of this equation. It requires knowledge of only the means and standard deviations of the random variables. This model compares favorably with a statistical analysis of the AASHO test results. A sensitivity analysis indicates that the CBR variability has a dramatic influence on the pavement reliability. The uncertainty on the expected traffic loads has little effect on the reliability for a large number of axle loads. Hence, the mean value of the expected traffic load is a sufficient estimate of this parameter. Second, an analytical model is formulated for the coefficients of equivalence of the (unbounded) granular materials of the base and subbase courses, using the theory of stochastic stress propagation in particulate media. It is shown that these coefficients are representative of the ability of the granular course to spread the applied load in a diffusion process. They are expressed as functions of the angle of internal friction of the material, and a modified formulation is derived for the equivalent thickness of the pavement.

A number of uncertainties and random factors play a role in the deterioration process of pavements under the effect of traffic. A probabilistic approach can make allowance for the stochastic nature of this process and provide a better rationale for the design methods. This paper presents an extension in this direction of the empirical design method derived from the AASHO road tests for flexible pavements with unbounded granular layers. The Shook and Finn model (*1*), which accounts for the bearing capacity of the subgrade, was used.

The probabilistic development addresses two aspects of the problem:

1. The reliability of a pavement section as a function of the variability of its subgrade bearing capacity and expected traffic load; and
2. The fundamental relationship between the coefficients of equivalence of granular materials of the pavement and their mechanical properties.

School of Civil Engineering, Purdue University, West Lafayette, Ind. 47907.

BACKGROUND

A basic equation resulting from the AASHO road tests (*2*) expressed the decrease of the trafficability index (p) of a given flexible pavement structure as a function of the number of applied loads:

$$p = c_0 - (c_0 - c_1)\cdot(W/\rho)^{\beta} \quad (1)$$

where

c_0 and c_1 = initial and final values of the trafficability index,
W = number of applied equivalent axle loads, and
ρ = maximum capacity of the structure, in number of axle loads.

The empirical coefficients ρ and β in Equation 1 were related to the mechanical properties of the pavement structure through its equivalent thickness, written in the case of a three-layer structure resting on a semiinfinite subgrade as

$$D = a_1 D_1 + a_2 D_2 + a_3 D_3 \quad (2)$$

where D_1, D_2, and D_3 are the respective thicknesses of the asphaltic concrete wearing course, gravel base course, and sandy gravel subbase (Figure 1). The regression coefficients, a_1, a_2, and a_3 are the coefficients of equivalence of the materials. They represent the relative contribution of each material to the overall strength of the structure. This concept of equivalent thickness implies that two structures built with different materials and course thicknesses, but exhibiting identical D values, would have the same rate of decrease of their trafficability. The validity of this statement should, however, be considered in light of the particular conditions under which the tests were performed. These are, for example, related to the climatic context, the available subgrade bearing capacity, the drainage conditions, and the types of structures experimented. This later aspect is particularly noteworthy because the failures observed in the AASHO road tests occurred often by loss of bearing capacity of the subgrade.

It was shown by Skok and Finn (*3*) that a strong correlation exists between the vertical stress on the subgrade calculated according to the elastic multilayer theory and the equivalent thickness found from the empirical model of the AASHO tests. This hypothesis was corroborated by additional parametric studies (*4*,*5*). Therefore, it seems reasonable to consider the propagation of vertical loads in the subgrade as the dominant factor of the observed mechanisms.

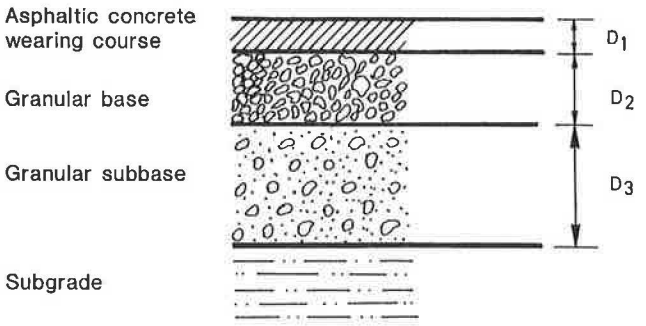

FIGURE 1 Typical four-layer system of flexible pavement tested in AASHO road tests.

RELIABILITY-BASED DESIGN

A measure of the bearing capacity of the subgrade was introduced into the AASHO empirical model by Shook and Finn (*1*), thus enabling the design method to be applied to geotechnical conditions differing from those of the AASHO tests. Their modified model related the necessary equivalent thickness of a pavement structure to the number of equivalent axle loads, and the CBR of the subgrade, as

$$D = f(W,L_1,L_2)\cdot(CBR_0/CBR)^{0.4} \tag{3}$$

In Equation 3, CBR_0 denotes the bearing ratio measured during the AASHO tests, and CBR is the actual bearing ratio of the considered subgrade. The function f resulted from a regression analysis:

$$f = -20.5 + 2.07\ln W + 0.669L_1 + 0.0932L_1L_2 \tag{4}$$

where

L_1 = axle load and
L_2 = 0 for single axle, 1 for double axle.

In the above equations, D should be expressed in inches (1 in. = 25.4 mm) and L_1 in kip (1 kip = 4.448 kN). Equation 4 does not include the safety factor originally applied by Shook and Finn to the number of axle loads.

A major uncertainty involved in the design of pavement structures arises from the assessment of the subgrade bearing capacity because of the large scattering encountered in CBR measurements. It is not unusual to observe coefficients of variation of this parameter (i.e., the ratio of the standard deviation over the mean value) in the range of 20 to 40 percent. For example, according to European road design codes (e.g., as noted by others [*6*]), a roadbed can be considered a homogeneous section even if the coefficient of variation of its bearing ratio is as high as 50 percent. Uncertainty is also involved in predicting the number of traffic loads (W) to be carried by a given road section during its expected life.

Second-Moment Approximation

The framework of a probabilistic model was suggested recently (*7*) to assess the reliability of a road section when the above uncertainties are considered. A comprehensive presentation of this approach is given herein.

The reliability of a pavement section, i.e., the probability of its survival under prescribed operating conditions, is defined as the probability that the equivalent thickness D required at any time during the life of the pavement will be less than the design value D^*. From another standpoint, provided that the CBR is a spatially uncorrelated process in the longitudinal direction, the probability of D exceeding D^* can be interpreted as the fraction of the considered pavement section length that will be unable to carry the expected number of axle loads for the whole lifetime of the pavement.

Seldom are the complete statistical distributions of engineering properties accessible. Fortunately, significant information is contained in the first moment about the origin of a random variable, the mean, and its second moment about the mean, the variance. Considering the necessary equivalent thickness (D) as a function of the two random variables (CBR and W), its mean and variance can be expressed as functions of the means and variances of the random variables. A second-moment representation of D is obtained by expanding Equation 3 into Taylor series truncated after the quadratic terms. A detailed description of this method can be found elsewhere (*8,9*). The following approximations result for the mean and variance of D, respectively:

$$\mu_D = D(\mu_W,\mu_{CBR}) + \frac{1}{2}\frac{\partial^2 D}{\partial W^2}(\mu_W,\mu_{CBR}) \cdot s_W^2 + \frac{1}{2}\frac{\partial^2 D}{\partial CBR^2}(\mu_W,\mu_{CBR}) \cdot s_{CBR}^2 \tag{5}$$

$$s_D^2 = \left(\frac{\partial D}{\partial W}(\mu_W,\mu_{CBR})\right)^2 \cdot s_W^2 + \left(\frac{\partial D}{\partial CBR}(\mu_W,\mu_{CBR})\right)^2 \cdot s_{CBR}^2 \tag{6}$$

where μ and s denote, respectively, the mean and standard deviation of the variables written in subscripts.

Introducing Equation 3 in Equations 5 and 6 gives

$$\mu_D = \frac{1}{(\mu_{CBR})^{0.4}} \cdot (1.531f(\mu_W) - 1.585V_W^2 + 0.429f(\mu_W)\, V_{CBR}^2) \tag{7}$$

$$s_D^2 = \frac{1}{(\mu_{CBR})^{0.8}} \cdot (10.043V_W^2 + 0.374f^2(\mu_W)\, V_{CBR}^2) \tag{8}$$

with

$$f(\mu_W) = -20.5 + 2.07\ln(\mu_W) + 0.669L_1 + 0.0932L_1L_2 \tag{9}$$

where V_{CBR} and V_W are the coefficients of variation of the CBR and number of axle loads, respectively.

Based on the knowledge of only its two first statistical moments, the function D may be modeled as a normal (Gaussian) variate. However, considering that the necessary equivalent thickness can take only finite positive values, the use of

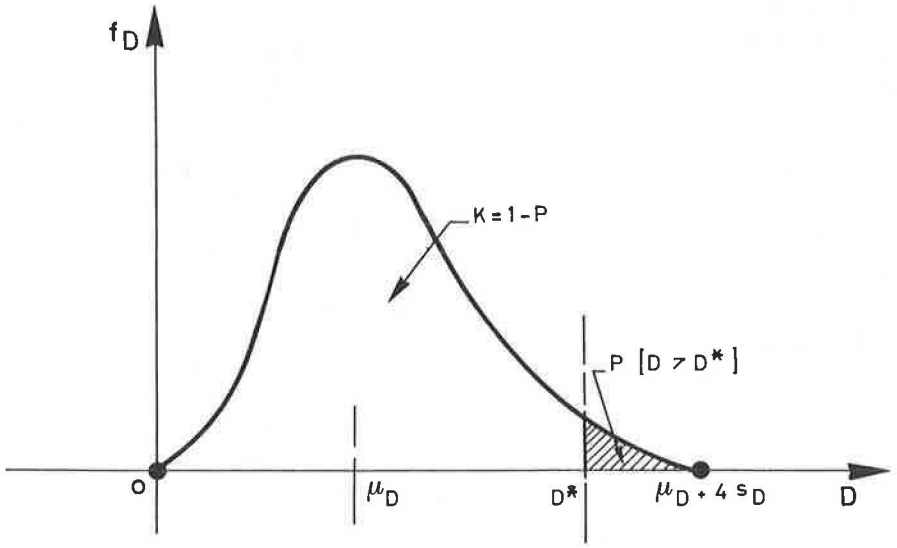

FIGURE 2 Beta distribution model of the necessary equivalent thickness (D) where μ_D is the mean value of D, s_D is the standard deviation of D, D^* is the design value of D for a reliability K, and P is the probability of distress.

the Beta distribution is more appropriate in this case. In effect, the versatility of the Beta distribution function allows for the modeling of bounded random variables. A comprehensive discussion on the engineering application and benefit of this type of distribution function can be found elsewhere (*10*). For the purpose of the reliability computations, the lower and upper bounds of the Beta distribution for D were selected as zero and four times its standard deviation above the mean, respectively. A typical distribution for D is shown in Figure 2 with a sketch of the probability of distress, $P[D > D^*]$. The reliability is given by

$$k = 1 - P[D > D^*] \tag{10}$$

From a design standpoint, the value of the required level of reliability should be selected and, using the distribution of D, the corresponding value of the design equivalent thickness computed. It involves finding the value D^* corresponding to a selected shaded area in Figure 2 (easy-to-use charts or computer software exists to perform this simple operation for the Beta distribution).

Parametric Study

A parametric study was carried out using the proposed model, to investigate the sensitivity of the required thickness for the asphaltic concrete wearing course (D_1) to the variability of the random variables (*CBR* and *W*). The wearing course thickness (D_1) was computed according to Shook and Finn (*1*) as

$$D_1 = \frac{D^* - D_2 - 0.75D_3}{2} \tag{11}$$

where D_2 and D_3 are the base and subbase course thicknesses, respectively.

The data used in the parametric study are summarized in Table 1, and the results are presented in Figure 3*a* and *b*. The thickness needed for the wearing course increases rapidly with the coefficient of variation of the subgrade *CBR* and with the required reliability of the pavement. For example, for a desired reliability level of 95 percent, D_1 must be increased from about 2 in. to more than 3 in. if the coefficient of variation of the *CBR* increases from 20 to 40 percent. On the other hand, the uncertainty on the number of axle loads has practically no influence on the design (horizontal lines of D_1 versus V_W for constant V_{CBR} in Figure 3*b*). This is a conse-

TABLE 1 DATA USED IN THE PARAMETRIC STUDY

Thickness:
D_2 = 5.9 in. (15 cm)
D_3 = 9.8 in. (25 cm)
CBR of Subgrade:
μ_{CBR} = 10
V_{CBR} = 40% when V_W variable
Expected Traffic:
L_1 = 18 kip
L_2 = 0 (single axle)
μ_W = 10^7 axles
V_W = 15% when V_{CBR} variable

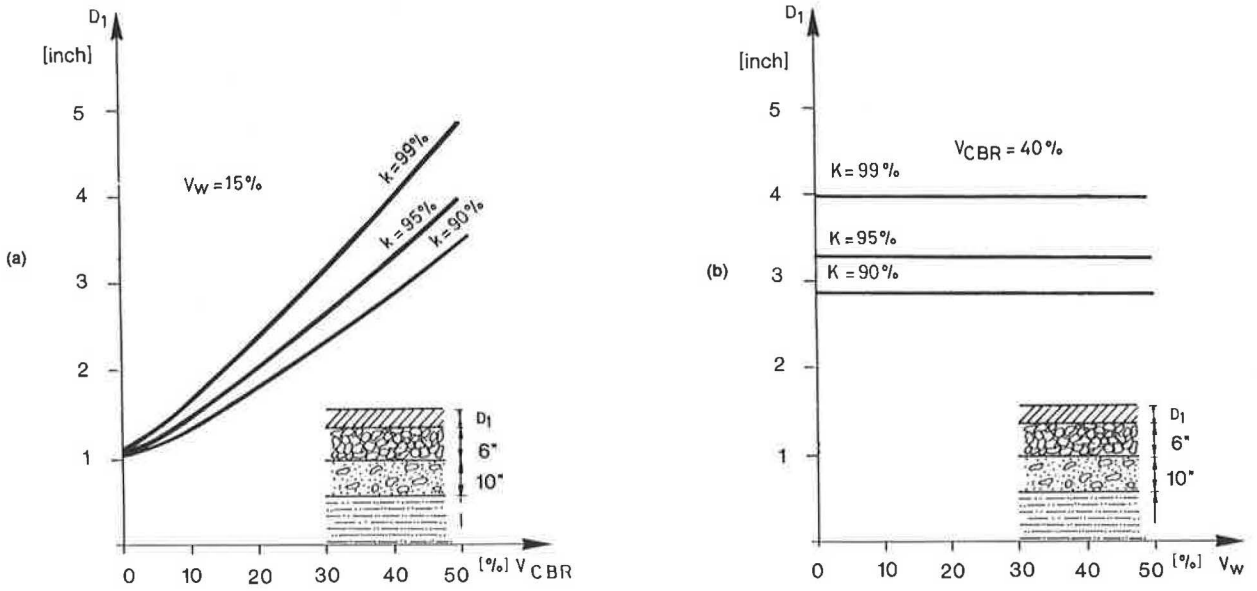

FIGURE 3 Parametric study: influence of the variability of the CBR (*a*) and expected traffic (*b*) on the required thickness (see data in Table 1) where V_{CBR} is the coefficient of variation of the bearing ratio of the subgrade, V_W is the coefficient of variation of the expected traffic loads, and D_1 is the thickness of the wearing course required for a reliability K.

quence of the logarithmic form of Equation 4. Thus, the proposed model may be simplified by representing the expected traffic load (W) in Equations 7 and 8 by its mean value only (μ_W). This simplification leads to the following expressions for the mean and standard deviation of the necessary equivalent thickness:

$$\mu_D = \frac{f(\mu_W)}{(\mu_{CBR})^{0.4}} \cdot (1.531 + 0.429\, V_{CBR}^2) \tag{12}$$

$$s_D = \frac{0.612}{(\mu_{CBR})^{0.4}} \cdot f(\mu_W) \cdot V_{CBR} \tag{13}$$

Application to the AASHO Road Tests

The statistics of the subgrade in situ *CBR* reported for the AASHO road tests indicated a mean value of 2.9 and a coefficient of variation of 35 percent (Figure 4). On this basis, the proposed probabilistic method can be applied to the case of the AASHO tests, using the coefficients of equivalence of the materials recommended by Shook and Finn (*1*), i.e., $a_1 = 2$, $a_2 = 1$, and $a_3 = 0.75$.

The results are summarized in Figure 5 and compared with the experimental data for the range of applied traffic loads. The theoretical curve obtained for a reliability of 95 percent leads to design values of D that are 4 in. larger than the experimental mean values. From their statistical analysis of the test results, Shook and Finn also concluded that to cover the experimental data points with a 95 percent confidence level, the average regression line had to be shifted by an amount of 4 in.

COEFFICIENTS OF EQUIVALENCE FOR THE GRANULAR MATERIALS

In the previous section, it was shown how the reliability of a flexible pavement structure can be evaluated for a given value of its equivalent thickness. In practice, the design of a structure at a given level of reliability requires not only the assessment of its necessary equivalent thickness, but also the determination of the resulting thicknesses for the individual layers. An empirical linear relationship, Equation 2, was derived from the AASHO road tests to relate these quantities to the equivalent thickness. Numerical values fitting the AASHO test data were proposed for the coefficients of equivalence of the materials, such as in Equation 11. However, the use of these empirical values for materials differing from those of the experimented structures is questionable. To date, the coefficients of equivalence have not been related explicitly to the engineering properties of the materials. An analytical model is formulated herein to accomplish this.

Theory of Stochastic Stress Diffusion

The conventional approach to assess the transmission of traffic load through a pavement system is to compute stresses by using the theory of linear elasticity. Such solutions require the assumption of an equivalent continuum. Furthermore, unless anisotropy is explicitly introduced, the elastic solutions are unable to account for the state of compaction of the granular materials and its effect on the distribution of stresses in the pavement layers.

In the present model, the transmission of applied load through the pavement layers is described using the theory of stochastic

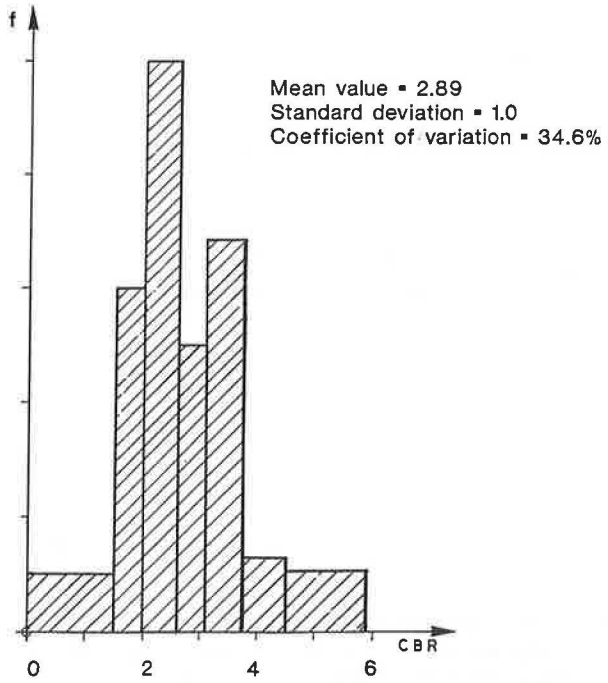

FIGURE 4 Statistics of the subgrade CBR in the AASHO road tests.

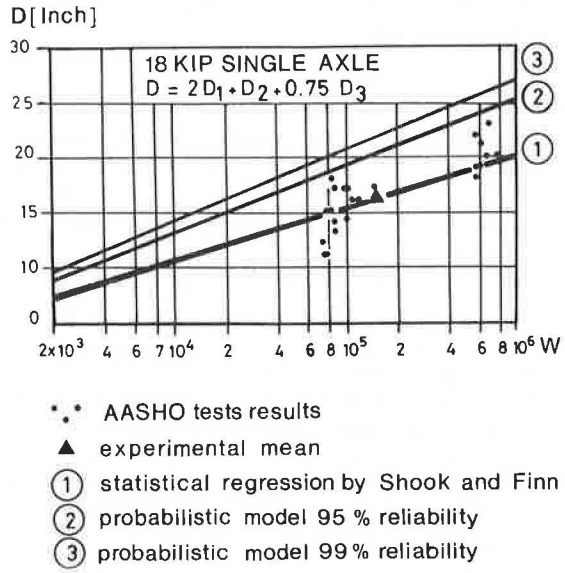

FIGURE 5 Application of the reliability-based model to the AASHO road tests (modified after Shook and Finn [*1*]). *D* is equivalent thickness and *W* is number of applied axle loads.

stress diffusion in particulate media developed by Sergeev (*11*) and Harr (*12*). A detailed formulation of the theory can be found elsewhere (*13*,*14*). Instead of assuming continuity and homogeneity of the medium, its particulate and inherently random nature is recognized, and boundary value problems are solved by using probabilistic arguments. The transmission of applied loads is the result of the propagation of contact forces between particles. This can be modeled as the progression with depth of a vertical force undergoing random lateral fluctuations when proceeding from a particle to its neighbor. For two-dimensional plane strain conditions, this model leads to a diffusion-type equation:

$$\frac{\partial \bar{S}_z}{\partial z} = C \frac{\partial^2 \bar{S}_z}{\partial x^2} \tag{14}$$

where $\bar{S}_z(x,z)$ is the expected vertical stress at a point (defined by the coordinates x and z), and C is the coefficient of diffusion that governs the rate at which the particulate material spreads the applied surface load. The coefficient C can be expressed as

$$C = \nu \cdot z \tag{15}$$

where the coefficient of diffusivity (ν) is a state parameter of the material. From a structural viewpoint, ν is influenced by such factors as stress-induced anisotropy of the granular assembly, intergranular friction properties, and state of compaction of the medium.

For a concentrated surface load (P) the solution of Equation 14 is a bell-shaped Gaussian density function (Figure 6):

$$\frac{\bar{S}_z(x,z)}{P} = \frac{1}{z\sqrt{2\pi\nu}} \exp\left(\frac{-x^2}{2\nu z^2}\right) \tag{16}$$

These results were generalized for distributed applied loads, axisymmetric or tridimensional geometry, and multilayer soil systems (*12*).

Let us consider a system consisting of three courses of particulate material of thicknesses H_1, H_2, and H_3, resting on a semiinfinite subgrade (Figure 7*a*). The expected vertical stress at each interface under the load is denoted by $\bar{S}_{zi}$. By definition, the equivalent thickness $\tilde{H}_1$ of layer 1 is the thickness of material 2, which can be substituted to the thickness H_1 of material 1 without modifying the distribution of vertical stresses in layer 2. In other words, the vertical stress $\bar{S}_{z2}$ in the equivalent structure shown in Figure 7*b* ($\tilde{H}_1$, H_2, H_3) is equal to the stress at the same level in Figure 7*a*. The equivalent thickness of layers 1 and 2, $\tilde{H}_2$ is defined in the same way, as is

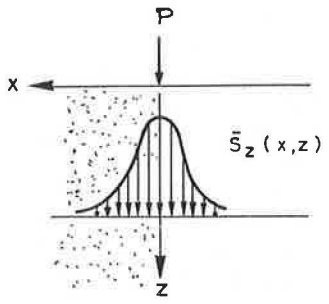

FIGURE 6 Vertical stress distribution in a semi-infinite particulate medium under a concentrated surface load.

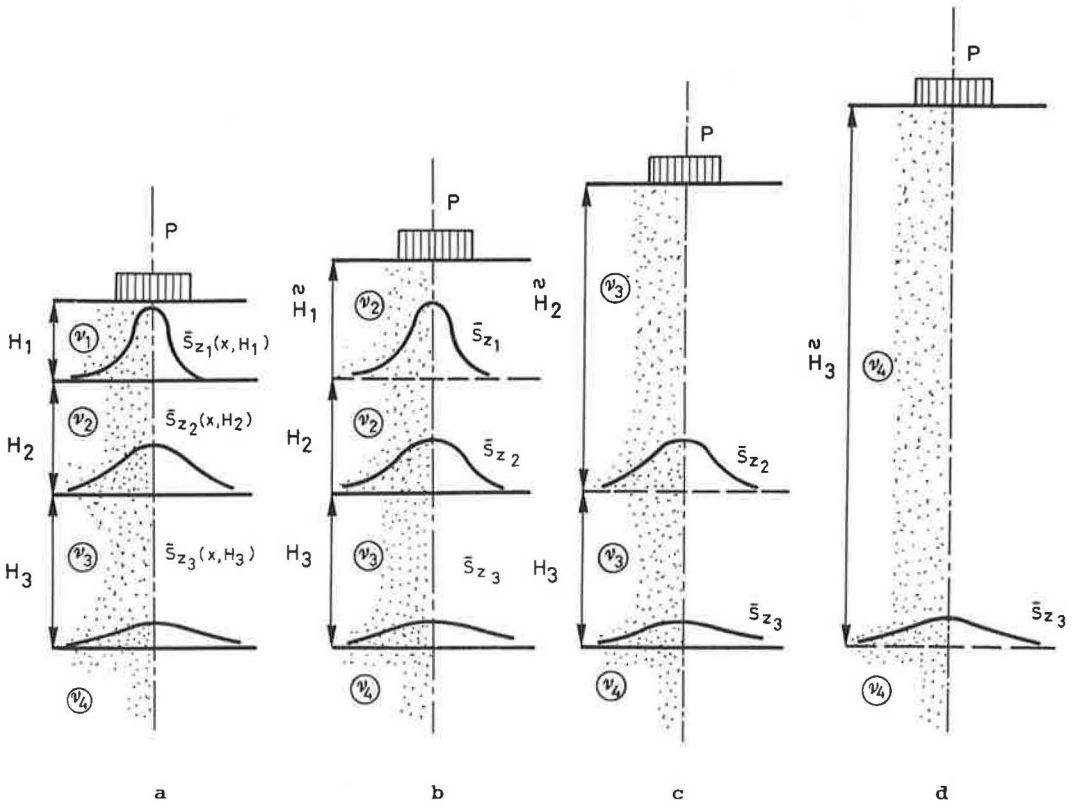

FIGURE 7 Concept of equivalent thickness in a stratified particulate medium where $\bar{S}_{zi}$ is the vertical stress at interface i and ν_i is the coefficient of stress diffusivity in layer i.

also the equivalent thickness of layers 1, 2, and 3 (Figure 7*c* and *d*):

$$\tilde{H}_3 = H_1\sqrt{\frac{\nu_1}{\nu_4}} + H_2\sqrt{\frac{\nu_2}{\nu_4}} + H_3\sqrt{\frac{\nu_3}{\nu_4}} \tag{17}$$

where ν_1, ν_2, ν_3, and ν_4 are the coefficients of stress diffusivity of the layers.

For a system of N layers, a recurrence relationship can be derived (*12*):

$$\tilde{H}_{N-1} = H_1\sqrt{\frac{\nu_1}{\nu_N}} + H_2\sqrt{\frac{\nu_2}{\nu_N}} + \ldots + H_{N-1}\sqrt{\frac{\nu_{N-1}}{\nu_N}} \tag{18}$$

According to this model, $\tilde{H}_3$ represents the thickness of subgrade material that can be substituted for the other courses without modifying the state of vertical stress in the subgrade. Thus, for a given subgrade material characterized by its coefficient of diffusivity (ν_4) systems with the same value of $\tilde{H}_3$ are equivalent from the standpoint of the vertical stress distribution applied to the subgrade. This condition is written:

$$H_1\sqrt{\nu_1} + H_2\sqrt{\nu_2} + H_3\sqrt{\nu_3} = H_3\sqrt{\nu_4} = \text{constant} \tag{19}$$

or, more generally

$$\frac{\sqrt{\nu_1}}{b}\cdot H_1 + \frac{\sqrt{\nu_2}}{b}H_2 + \frac{\sqrt{\nu_3}}{b}H_3 = \text{constant} \tag{20}$$

where b is an arbitrary constant.

Application to a Pavement System

There is conceptual and formal analogy between the equivalent thickness of a pavement and the equivalent thickness defined in the theory of stochastic stress diffusion for a stratified particulate medium. Identifying Equation 20 to Equation 2 leads to

$$D = a_1D_1 + \frac{\sqrt{\nu_2}}{b}D_2 + \frac{\sqrt{\nu_3}}{b}D_3 \tag{21}$$

where

a_1 = empirical coefficient of equivalence related to the asphaltic concrete wearing course;
ν_2 and ν_3 = coefficients of stress diffusivity of the granular base and subbase courses;
D_1, D_2, D_3 = thicknesses of the courses in inches; and
b = constant.

Recalling that the stochastic theory of stress propagation was at first derived for cohesionless particulate materials, the wearing course asphaltic concrete in a flexible pavement does not conform strictly to the hypotheses of the theory in its present state of development. Thus, in Equation 21, the contribution of the wearing course is represented by an empirical coefficient, whereas the analytical solution is applied to the granular material courses.

Conceptually, the coefficient of diffusivity of a cohesionless soil (ν) is related to the coefficient of lateral pressure and is influenced by the stress history and the shear strength of the granular material. For loose, normally consolidated granular soils, it was shown that ν can be approximated by the coefficient of earth pressure at rest (K_0) and thus related to the angle of internal friction of the material (*13*,*14*).

In the present case of a pavement structure with compacted granular materials, the coefficient of stress diffusivity is approximated by the coefficient of passive earth pressure K_p:

$$\nu = tg^2 (45° + \phi'/2) \tag{22}$$

where ϕ' is the effective angle of internal friction. Therefore, D in Equation 21 becomes

$$D = a_1 D_1 + \frac{1}{b} \tan(45° + \phi_2'/2) D_2 + \frac{1}{b} \tan(45° + \phi_3'/2) D_3 \tag{23}$$

Comparison with the AASHO Road Test Results

The granular materials of the AASHO road tests were a crushed gravel for the base course (stabilized base courses are not considered in this study) and a sandy gravel with added fines for the subbase. For a comparison with the proposed model, in absence of published shear test results, the friction angle of these materials is estimated to range between 40 and 45 degrees for the base course, and between 25 and 35 degrees for the subbase.

From Equations 2 and 23, the ratio a_3/a_2 of the equivalence coefficients is

$$a_3/a_2 = \tan\left(45° + \frac{\phi_3'}{2}\right) \Big/ \tan\left(45° + \frac{\phi_2'}{2}\right) \tag{24}$$

As shown in Table 2, theoretical and experimental estimates for this ratio are close. Furthermore, the proposed model is in agreement with the value of a_3/a_2 obtained by Shook and Finn (*1*) for $\phi_2' = 43°$ and $\phi_3' = 30°$ (Figure 8). These values introduced into Equation 23 give a value of 2.3 for the constant b leading to

$$D = 2D_1 + 0.435 \tan(45° + \phi_2'/2)\, D_2 + 0.435 \tan(45° + \phi_3'/2)\, D_3 \tag{25}$$

with D, D_1, D_2, and D_3 in inches. Equation 25 is a generalized form of the Shook and Finn (*1*) expression for the equivalent thickness and can be integrated into the reliability-based model developed in the previous section.

TABLE 2 COEFFICIENTS OF EQUIVALENCE OF THE GRANULAR COURSES a_3/a_2 FOR THE AASHO ROAD TESTS

Computed using the proposed model

ϕ'_2	ϕ'_3	a_3/a_2
40°	25°	0.73
	30°	0.81
	35°	0.90
45°	25°	0.65
	30°	0.72
	35°	0.80

Empirical values from the tests

reference	a_3/a_2
HRB [2] without seasonal ponderation	0.71
Shook and Finn [1]	0.75
HRB [2] with seasonal ponderation	0.79
Painter [15]	0.81

CONCLUSIONS

A probabilistic extension of the empirical method derived from the AASHO road tests for the design of flexible pavements has been proposed. The reliability assessment of a pavement section is obtained by considering the Shook and Finn (*1*) design equation as a function of two random variables, the expected number of traffic loads, and the CBR of the subgrade soil. The formulation is a second-order, second-moment development of this equation, which requires knowledge of only the means and standard deviations of the random variables. The model compares favorably with that from a statistical analysis of the AASHO test results. A sensitivity analysis indicates that the CBR variability has a large influence on the pavement reliability. The uncertainty on the expected traffic loads has little effect on the reliability when a large number of axle loads is considered. Hence, the mean value of the expected traffic load is a sufficient estimate for this parameter.

An analytical model has been formulated for the coefficients of equivalence of the (unbounded) granular materials of the base and subbase courses, using the theory of stochastic stress propagation in particulate media. It is shown that in the context of this theory, these coefficients represent the property of the granular course to spread the applied load in a diffusion process. A modified formulation is derived for the equivalent thickness of the pavement, and the coefficients are simply expressed as function of the angles of internal friction of the materials.

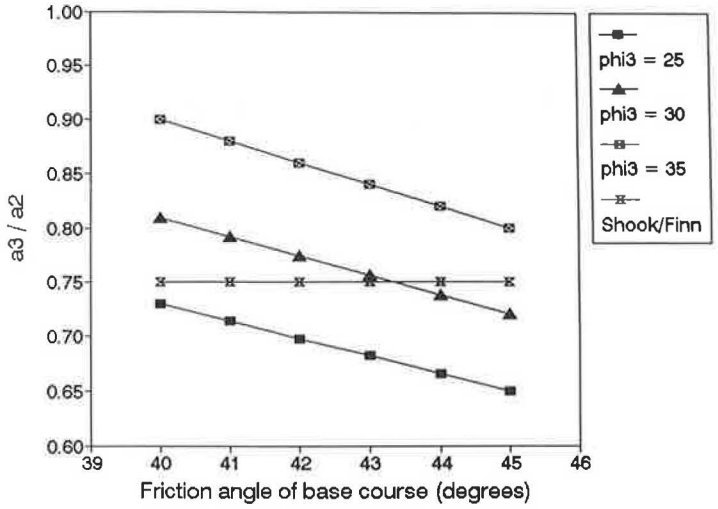

FIGURE 8 Coefficients of equivalence of the granular courses a_3/a_2. Comparison of theoretical and empirical models (see also Table 2).

ACKNOWLEDGMENT

The analytic development reported in this paper was carried out at the Soil Mechanics Laboratory of the Swiss Federal Institute of Technology, Lausanne, Switzerland. The author is indebted to E. Recordon for his support and encouragement. The support provided by Purdue University during the preparation of this paper is also acknowledged.

REFERENCES

1. J. F. Shook and F. N. Finn. Thickness Design Relationships for Asphalt Pavements. *Proc., International Conference on the Structural Design of Asphalt Pavements*, University of Michigan, Ann Arbor, 1962, pp. 52–83.
2. *Special Reports 61-B and 61-E: The AASHO Road Test—Pavement Research*. HRB, National Research Council, Washington, D.C., 1962.
3. E. L. Skok and F. N. Finn. Theoretical Concepts Applied to Asphalt Concrete Pavement Design. *Proc., International Conference on Structural Design of Asphalt Pavements*, University of Michigan, Ann Arbor, 1962, pp. 412–440.
4. P. L. Bourdeau. *Le Concept d'Epaisseur Equivalente dans les Methodes Empiriques de Dimensionnement des Chaussées Souples*. Research Report GX75. Soil Mechanics Laboratory, Swiss Federal Institute of Technology, Lausanne, September 1982.
5. P. L. Bourdeau and E. Recordon. Dimensionnement des Chaussées Souples, Point de Vue Probabiliste. *Annales ITBTP*, No. 420, 1983, pp. 1–15.
6. Association Suisse de Normalisation. *Dimensionnement, Portance et Homogeneité au Niveau de la Forme*. SNV Code 640 317, VSS, Zurich, 1971.
7. P. L. Bourdeau. Probabilistic Design of Flexible Pavements. *Proc., ASCE Specialty Conference on Probabilistic Methods*, Virginia Polytechnic and State University, Blacksburg, May 1988, pp. 124–127.
8. G. T. Hahn and S. S. Shapiro. *Statistical Models in Engineering*. John Wiley and Sons, Inc., New York, 1967.
9. M. E. Harr. Reliability-Based Design in Civil Engineering. McGraw-Hill, New York, 1987.
10. F. Oboni and P. L. Bourdeau. Simplified Use of the Beta Distribution and Sensitivity to the Bound Locations. *Structural Safety*, Vol. 3, 1985, pp. 63–66.
11. I. J. Sergeev. The Application of Probability-Process Equations to the Theory of Stress Distribution in Non-Cohesive Foundation Loads. *Soil Mechanics and Foundation Engineering*, No. 2, 1969, pp. 84–88.
12. M. E. Harr. *Mechanics of Particulate Media. A Probabilistic Approach*. McGraw-Hill, New York, 1977.
13. P. L. Bourdeau. *Analyse Probabiliste des Tassements d'un Massif de Sol Grannulaire*. These de Doctorat des Sciences Techniques, No. 628. Swiss Federal Institute of Technology, Lausanne, 1986.
14. P. L. Bourdeau and M. E. Harr. Stochastic Theory of Settlement in Loose Cohesionless Soils. *Geotechnique*, in press, 1989.
15. L. J. Painter. Analysis of AASHO Road Test Data by the Asphalt Institute. *Proc., International Conference on the Structural Design of Asphalt Pavements*, University of Michigan, Ann Arbor, 1962.

Publication of this paper sponsored by Committee on Flexible Pavement Design.

Computer Simulation of Load Equivalence Factors

W. J. KENIS AND C. M. COBB

AASHTO's load equivalence factors are evaluated with the aid of a computational model for predicting flexible pavement response. First, the VESYS 5 computer program was verified to assure that it could be used to conduct computer road tests. Following this, damage produced by steering axles at the AASHO Road Test was evaluated in an effort to quantify the error in the AASHTO equivalence factors, because steering axles were neglected in the development of these equivalencies. Next, the computer model was used in the conduct of computer road tests with the goal of developing equivalence factors for conditions not present at the AASHO road test site. Finally, exponential relationships relating pavement deflections and strains to load equivalencies based on cracking and rutting were developed.

Traffic volume, vehicle weight, speed, tire pressure, axle spacing, and vehicle suspension are factors that must be considered when studying pavement response. Added to these are environmental conditions that constantly change, inflicting damage to the pavement. Material properties of flexible pavements, for example, are influenced not only by temperature, but also by vehicle speed. Thus, it is tempting for the pavement engineer to make simplifying assumptions in pavement design, reducing the number of variables to those that significantly affect pavement response. One such simplifying assumption involves the concept of the equivalent single axle load (ESAL) and load equivalence factor (LEF). It allows the design engineer to reduce the numerous vehicles traveling on the road to an equivalent number of single axles. The concept was first developed from the AASHO Road Test results and has been in common use since.

Because the data from the AASHO site are limited to the conditions at the site, it is desirable to investigate those factors not studied at the site; because the cost of conducting similar road tests is prohibitive, it becomes economically justifiable to use computational pavement response models. For example, tridem axle configurations, now common on the nation's highways, were not included in the AASHO Road Test traffic. Other factors not studied include axle spacings, vehicle spacings, transverse positions of the vehicles on the pavements, truck speed, and tire pressures. In addition, steering axles were neglected in the development of load equivalence factors (except for vehicles having just two single axles).

This paper includes the results of the following research objectives.

W. J. Kenis, FHWA, HNR 20, 6300 Georgetown Pike, McLean, Va. 22101. C. M. Cobb, Department of Civil Engineering, Louisiana Tech University, Ruston, La. 71272.

- Calibrate the VESYS 5 program to simulate the response measured at the AASHO Road test.
- Evaluate pavement response caused by steering axles in the AASHO Road Test experiments.
- Calculate LEFs based on serviceability and damage.
- Evaluate relationships between primary response LEFs and damage-based LEFs.

EQUIVALENCY CONCEPTS

At the AASHO Road Test site a number of identical thickness designs were used in various loops so that a single design was independently subjected to several different traffic loadings. Ten different vehicle types (Figure 1) were used in the test. Only one vehicle type was used in each lane so that each pavement section was subjected to only one type of loading. The distribution of vehicles was such that axle load applications accumulated at the same rate in all traffic lanes throughout the test period. Except when road conditions were prohibitive because of pavement distress or weather conditions, the vehicles traveled at a constant speed of 35 mph (*1*).

The primary objective of the AASHO Road Test was to establish relationships between pavement performance and design characteristics such as layer thicknesses and loading parameters. The LEFs developed as a result of the AASHO Road Test were calculated from performance equations based on the relationship between the number of load repetitions and the present serviceability of the pavement. A standard single-axle load of 18 kips was adopted. The AASHTO LEF for criteria based on present serviceability index (PSI) is

$$LEF_{PSI} = W_0/W_x|_{PSI} \quad (1)$$

where W_0 is the number of standard single axles to a limiting value of PSI and W_x is the number of any axle (single or tandem) of load x to the same limiting value of PSI. It may also be expressed in terms of the AASHTO performance equation as

$$LEF_{PSI} = \{(Lx + L2)/(18 + 1)\}^{4.79} L_2^{-4.33} g^{(1/\beta 18 - 1/\beta X)} \quad (2)$$

where L_x is the load on any single or tandem axle, β is a function of L_x plus the structural capacity of the pavement, g is a function of the ratio of the serviceability indexes and L_2 = 1,2 the axle code for single or tandem axles, respectively (*2*). With the exception of two-axle trucks, the steering

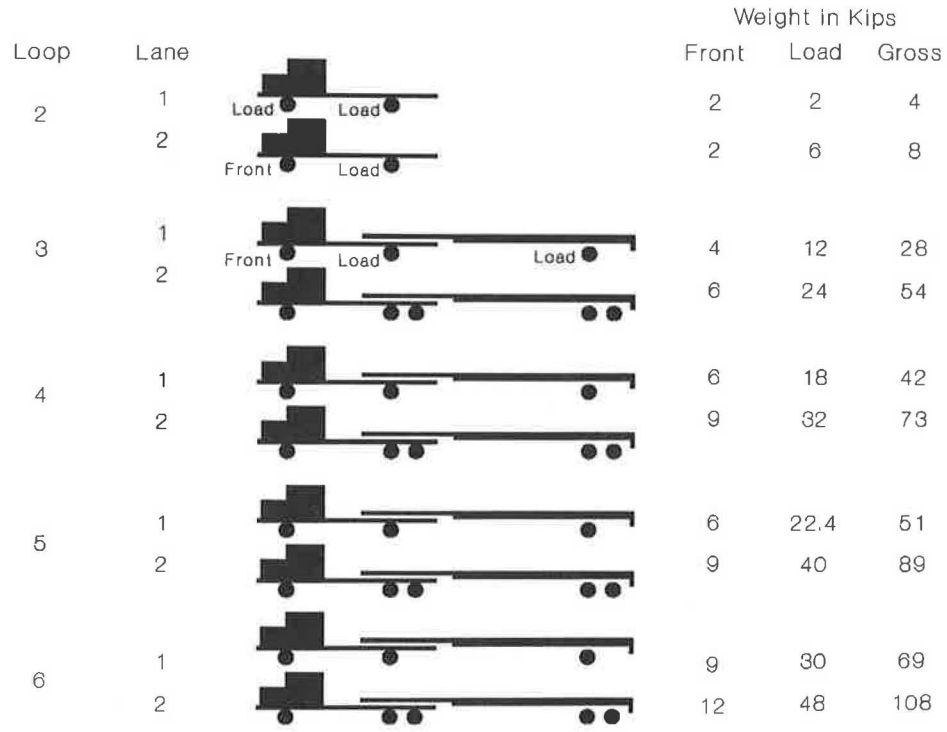

FIGURE 1 AASHO trucks (*1*).

axles of the vehicles were not considered to be load axles and no provision was made in the road test analyses to study the significance of the steering axles on pavement performance. Later, Scala (*3*) suggested that the steering axles at AASHO contributed only about 3 percent of the total damage caused by the test vehicles. However, he also suggested that for some vehicles traveling on today's highways, the steering axle carries a greater portion of the load than those used in the AASHO Road Test and may therefore contribute significantly to the total damage.

Previously, the AASHTO Design Guide included equivalencies for only single-axle loads up to 40 kips and tandem-axle loads to 48 kips. The latest AASHTO Design Guide, published in 1986, includes equivalences for single-axle loads to 50 kips, tandems to 90 kips, and tridems to 90 kips. To obtain these new equivalencies, Equation 2 was used. For tridems, the axle code in Equation 2 was given the value of three. There is some uncertainty as to the validity of extending these equations to generate equivalencies for loads and axles not applied at the road test.

It was observed by Scala (*3*) that the AASHTO equivalence factors expressed by Equation 1 are approximately equal to the fourth power of the ratio of the actual loads:

$$LEF_{PSI} = (L_x/L_0)^4 \tag{3}$$

This relationship is commonly known as the Fourth Power Law where L_0 takes on the standard values 18, 30, and 40.7 for single-tandem and tridem-axle loads.

In addition to present serviceability, other pavement response measures might be used as a basis for determining load equivalence factors. For damage-based criteria (D)

$$LEF_D = W_0/W_x|_D \tag{4}$$

where W_0 and W_x are evaluated at a limiting value of distress rather than PSI, and LEF_D is known as a damage equivalence factor. If one makes certain linearity assumptions on the flexible pavement fatigue cracking damage equation,

$$W|_c = K1(1/e)^{K2} \tag{5}$$

where $K1$ and $K2$ are fatigue material property constants and W is evaluated at some limiting measure of cracking, then on substitution into Equation 4 for the respective loads, the following primary response strain equivalence equation is obtained:

$$LEF_e = (e_x/e_0)^{K2} \tag{6}$$

In this equation, e is the tensile strain (primary response) for the respective loads at the bottom of the AC layer. Similarly, an expression for primary response deflection equivalency may be developed by using the rut depth equation

$$RD = d_x\mu_R W^{\alpha_R} \tag{7}$$

where d_x is pavement maximum surface deflection and μ_R and α_R are pavement system permanent deformation properties. Equation 4 may be used in Equation 7 to yield

$$LEF_d = (d_x/d_0)^{1/\alpha_R} \quad (8)$$

Canadian research regressed rebound deflection (d) against number of load repetitions to limiting PSI (*4*) to obtain

$$LEF_{PSI} = (d_x/d_0)^b \quad (9)$$

where b is the regression coefficient from various field experiments. Because Equations 6, 8, and 9 are functions of strain or deflection, they are called primary response equivalencies. We can solve for the exponent in any of Equations 6, 8, or 9; however, it is more enlightening to develop a general expression

$$Q = \log LEF_j/\log (PR_x/PR_0) \quad (10)$$

where Q is the exponent $1/\alpha_R$, b, or $K2$; PR is the deflection or strain primary response; and j is an identifier for PSI, cracking, or rutting. This expression is awkward when the primary response ratio or the LEF is close to or equal to 1.

One other major concern with the above equivalencies is that of defining d_x or e_x for multiple-axle configurations. For instance, Canada has defined d_x in Figure 2 for multiple axles

$$LEF_d = (d_1/d_0)^{3.8} + \Sigma((d_{i+1} - T_i)/d_0)^{3.8} \quad (11)$$

where

d_i, T_i = peak deflection and trough of axle i for an n axle group,

$(d_{i+1} - T_i)$ = difference in magnitude between the maximum deflection recorded under each succeeding axle and the minimum residual deflection preceding the axle, and

d_0 = pavement surface deflection caused by the standard single-axle dual tire load.

A similar approach is used in VESYS 5. The primary strain or deflection response at any point in the pavement caused by multiple axles is obtained through superposition of the response at that point caused by each axle in the multiple-axle configuration. The proportional amount of peak to valley, as shown in Figure 2, determines the magnitude of the response to be used in the repeated load damage models. For example, for tandem axles the equation would be

$$\text{Response 1} = \max [d_1, d_2]$$

$$\text{Response 2} = \min [d_1, d_2] - T_1 \quad (12)$$

The algorithm generalizes readily to higher multiple-axle groups. This procedure differs from the Canadian method in that it assigns no special treatment to the lead axle in the axle group. Rather, it assumes that the greatest damage is caused by the greatest response, regardless of which axle appears to be producing that response.

VESYS COMPUTATIONAL MODEL

The evolution of the VESYS series of computational pavement models began in the mid-1970s with the development of a prototype version, VESYS 2M, a closed form three-layer viscoelastic model (*5*). Since the development of VESYS 2M, ten other versions have been produced (*6*).

Given parameters that define the pavement, environment, and loading, VESYS can predict the pavement's behavior over time. Initially, layer theory is used to calculate primary response stress, strain, and deflection under a static loading. These values are used along with traffic loading in cumulative damage models to predict cracking, rutting, and roughness. Finally, the present serviceability index is computed.

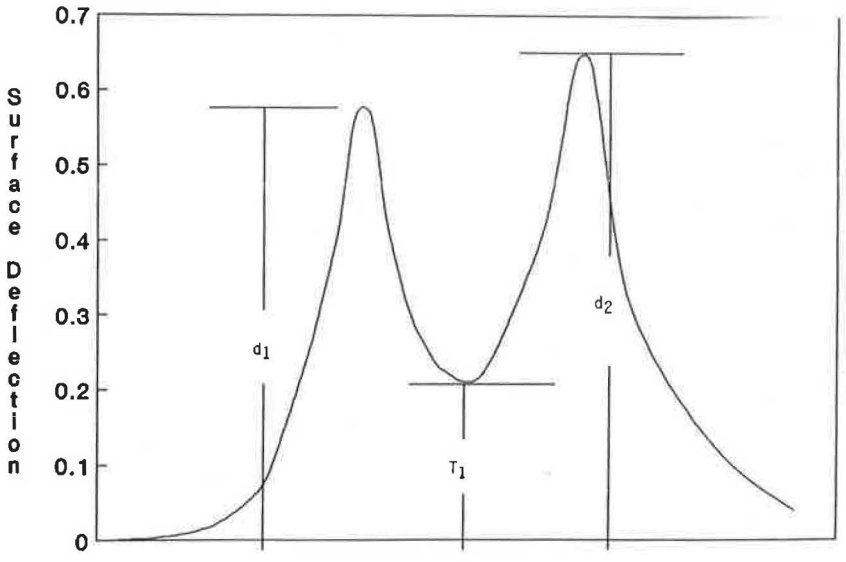

FIGURE 2 Tandem axle.

VESYS 5 has the unique feature of analyzing pavement response caused by single, tandem, or tridem axle loadings. Traffic volumes are specified in AADT (average annual daily traffic) wherein each axle group is considered to be one component of the traffic. The actual vehicle configuration may consist of several axle groups up to three axles. Each group is counted separately in the AADT designation. The user also specifies the number and length of time periods into which the traffic flow over the entire analysis period is divided. The percentage of each axle group composed in the AADT is specified and may be adjusted for seasonal variation (B. Brademeyer, unpublished FHWA data).

VERIFICATION AND CALIBRATION

Any newly developed computational pavement model must first be verified for realistic ranges of environmental, material, and traffic parameters. Once it is verified, the model can be calibrated so that predictions of pavement response are within a desirable degree of accuracy for a specific set of conditions. Calibration may be done either internally or externally (*7*). Internal calibration is carried out by adjusting program inputs (usually material properties). External calibration is achieved by applying a calibration factor to the program output.

Most of the mechanistic models comprising VESYS 5 and used in this study were verified and calibrated for AASHO conditions in previous studies. However, in this study VESYS 5 is further calibrated internally by comparing results of damage predictions with measured values of rutting, cracking, and serviceability from the 16 AASHO Road Test sections shown in Table 1. The sections were selected so that two thickness designs could be analyzed over the entire range of loading configurations for the main loops (3 through 6).

A study conducted by Kenis et al. (*8*) in 1982 developed values for layer stiffness moduli, permanent deformation properties (GNU and ALPHA), and fatigue properties $K1$ and $K2$ for four seasons. These values are shown in Table 2 and were applied to determine inputs for VESYS 5 for use in the calibrations.

The traffic rates applied to VESYS (for the calibrations) were kept identical to the rates applied at the AASHO test site.

Seasonal Data

VESYS 5 has the capability of modeling environmental changes at variable intervals of up to 12 seasons per year. Primary response is generated for each season. Determination of the number and length of seasons was done by analysis of deflection measurements taken at the AASHO Road Test every 2 weeks. These deflections were averaged for the 2-year period and are plotted as shown in Figure 3. The environmental change having the greatest effect on deflections is the spring thaw, beginning around March 18 and ending around May 13. Pavement temperatures for each season were obtained by adding 24°F to the average air temperature for each of five seasons, as suggested by Rauhut and Jordahl (*9*). It was determined from this plot that the conditions at the AASHO Road Test could adequately be modeled with the five seasonal intervals shown.

Layer Stiffness Moduli

Adjustments were made to the stiffness moduli of Table 2 so that they would correspond with the seasons selected for VESYS 5. The final values used for the study are given in Table 3. The surface layer creep compliance curve shown in Figure 4 was used along with the time temperature shift relationship (*8*):

$$a_T = t_T/t_{T0} \tag{13}$$

where

t_{T0} = time corresponding to the compliance at reference temperature T_0,

TABLE 1 MAIN DESIGNS FOR AASHO LOOPS 3 THROUGH 6

AASHO LOOP	Axle Type	Axle Load (pounds)	AASHO Section Number* 4-3-8 Design		4-6-9 Design	
3	Single	12,000	121		139	
	Tandem	24,000		122		140
4	Single	18,000	589		577	
	Tandem	32,000		590		578
5	Single	22,400	481		455	
	Tandem	40,000		482		456
6	Single	30,000	269		303	
	Tandem	48,000		270		304

* Surface-Base-Subbase Thickness, inches

TABLE 2 MATERIAL PROPERTIES USED BY KENIS ET AL. (*14*)

Material Property	Winter	Spring	Summer	Fall
Modulus (KSI)				
Surface	1600	550	140	450
Base	40	30	40	40
Subbase	20	15	20	20
Subgrade	4.5	3	4.5	4.5
Permanent Deform				
Surface				
GNU	0.04	0.078	0.10	0.082
ALPHA	0.60	0.72	0.60	0.71
Base				
GNU		Variable Function of Stress		
ALPHA	0.75	0.75	0.75	0.75
Subbase				
GNU		Variable Function of Stress		
ALPHA	0.75	0.75	0.75	0.75
Subgrade				
GNU	0.04	0.15	0.04	0.04
ALPHA	0.75	0.75	0.75	0.75
Fatigue				
Surface				
K1	1.0E-13	1.8E-12	1.3E-8	3.0E-1
K2	5.10	5.01	4.87	4.99

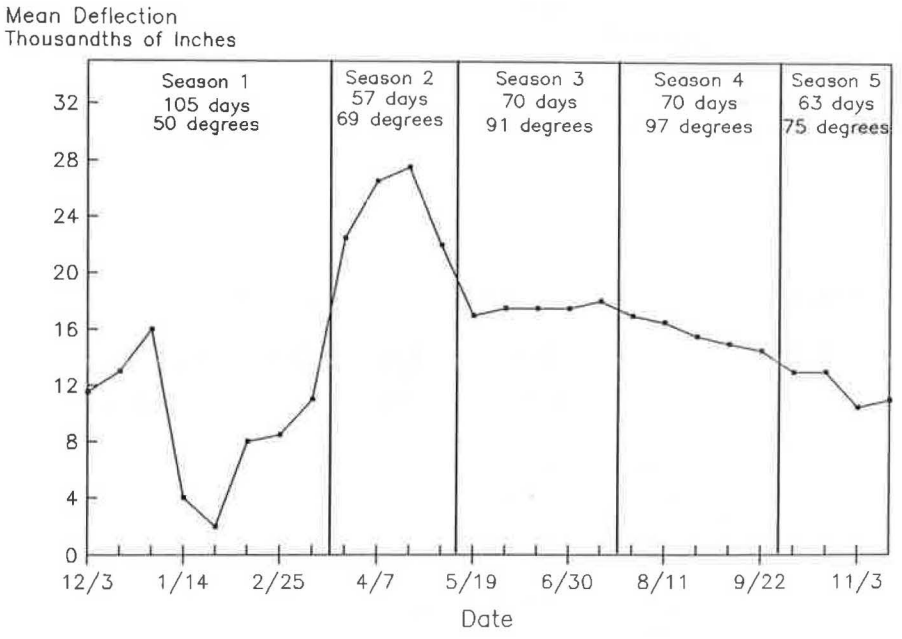

FIGURE 3 AASHO loop 1.

TABLE 3 SEASONAL LAYER MODULI

	Moduli (ksi) for				
	Season 1	Season 2	Season 3	Season 4	Season 5
Surface	1,600	550	170	140	460
Base	42	30	33.5	37	41
Subbase	21	15	16.5	18	21
Subgrade	4.7	3.3	3.8	4.1	4.6

NOTE: Season 1: 105 days, 50°F; season 2: 57 days, 69°F; season 3: 70 days, 91°F; season 4: 70 days, 97°F; and season 5: 63 days, 75°F.

t_T = time corresponding to the same compliance on shifted curve at temperature T, and
a_T = time temperature shift factor = $10^{(T_0 - T)\beta}$

The time t_{T0} on the master creep compliance curve of Figure 4 for any temperature T (with t_T estimated to be 0.03) is obtained by

$$t_{T0} = (0.03)10^{(T-70)\beta} \quad (14)$$

where $\beta = 0.054$ as recommended by Rauhut and Jordahl (*9*). To obtain the surface stiffness moduli, the compliance for each temperature is taken from the master creep compliance curve and inverted.

For the spring season, base and subbase stiffness moduli were obtained from nomographs found previously (*10*). Results from CBR tests (*11*) taken before placement of the pavement at the AASHO Road Test were used to estimate spring subgrade moduli.

For the remaining seasons, base, subbase, and subgrade stiffness moduli were obtained by adjusting the values selected for spring using several different procedures, viz., seasonal multipliers and back calculations using deflection basins measured at the AASHO Road Test (*2*).

Layer Permanent Deformation Properties

The results of repeated load tests conducted by the FHWA on a control mix of asphalt concrete at 40°F, 75°F, and 90°F were used to obtain values of ALPHA and GNU for the surface layer for input to VESYS 5 (*8*). Values of GNU for the base and subbase in the Kenis et al. study (*8*) were established as functions of deviator stress. However, a recent study by Leahy (unpublished FHWA data) showed that deviator stress has little influence on GNU for these layers. Preliminary runs for the current study supported Leahy's conclusion. The ALPHA values for the base and subbase, when varied, were found to have little influence on pavement response for all seasons (*8*).

Data from the AASHO Road Test (*11*) indicate that the moisture content in the subgrade was about 14 percent for the spring and 12 percent for the other seasons. The relationship between GNU and moisture content for the subgrade is plotted in Figure 5. The effect of moisture content on ALPHA for the subgrade has not been established. The initial values from the study by Kenis et al. (*8*) were used to make adjustments through trial and error until reasonably good predictions of rutting were obtained. Table 4 shows final values of GNU and ALPHA used in this study.

Fatigue Properties

Fatigue properties ($K1$ and $K2$) for the surface layer have been established at 70°F to be approximately 2.0×10^{-12} and 5.0, respectively (*9*). Seasonal adjustments to these values were made using adjustment factors given in the VESYS user's manual (*5*). Again, calibration was obtained through trial and error by comparing measured values of cracking with VESYS 5 predictions. Values of $K1$ and $K2$ used for the surface layer in the equivalency analysis are as follows:

	Season 1	*Season 2*	*Season 3*	*Season 4*	*Season 5*
$K1$	6.0×10^{-12}	2.0×10^{-12}	1.0×10^{-10}	1.3×10^{-07}	1.0×10^{-11}
$K2$	5.1	5.01	4.95	4.87	4.99

Calibration Simulations

The examples of pavement response given in Figure 6, are evidence of reasonable predictions of rutting (*a*), cracking (*b*), and serviceability for single and tandem axles (*c*) at AASHO. Inner and outer wheel path damage are evidence of a high

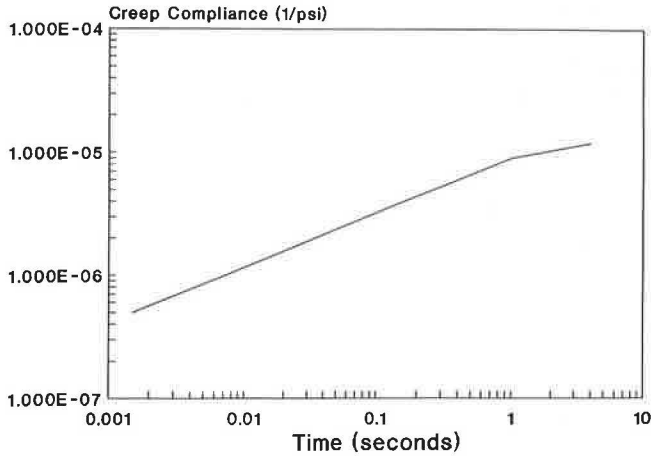

FIGURE 4 Road test surface (*8*).

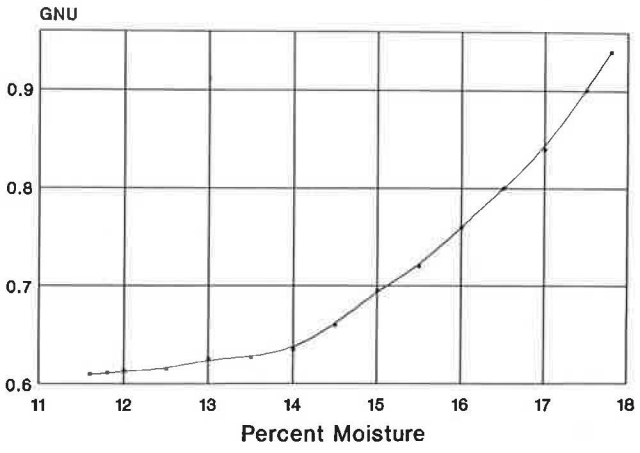

FIGURE 5 Subgrade GNU (*8*).

TABLE 4 SEASONAL LAYER PERMANENT DEFORMATION PROPERTIES

	GNU/ALPHA				
	Season 1	Season 2	Season 3	Season 4	Season 5
Surface	.04 .50	.055 .45	.10 .72	.10 .60	.082 .71
Base	.045 .75	.1 .75	.215 .75	.23 .75	.15 .75
Subbase	.01 .75	.04 .75	.938 .75	.04 .75	.015 .75
Subgrade	.04 .75	.05 .50	.04 .75	.04 .75	.04 .75

degree of variability as indicated in the plots. Considering that the seasonal material properties for all sections are represented by a single value, deviations from measured data are expected. It is interesting to note that the deviations between measured inner and outer wheel path often are greater than deviations between VESYS and any one of the measured values. The results of these simulations establish VESYS as a suitable tool for analysis of the main objectives of this study.

ANALYSIS

To study the main objectives, a single pavement design (corresponding to AASHO sections 121, 122, 269, and 270 of loops 3 and 6) having surface, base, and subbase thicknesses of 4, 3, and 8 in., respectively, was selected. Axle loads and tire pressures used are given in Table 4. They were selected so that the contact radii ranged from 5 to 8 in. (which also corresponds to the range for AASHO vehicles). The AASHO traffic rates were used in VESYS for the steering axle analysis; however, adjustments were made to these rates for the LEF damage and primary response analyses.

Steering Axle Analysis

To study the validity of neglecting steering axles in the development of AASHTO LEFs, each of the four vehicles shown in Figure 1 for loops 3 and 6 was applied in a VESYS 5 simulation both with and without steering axles. Traffic rates identical to those at AASHO were used. An example of the resulting damage predictions is given in Figure 7 for AASHO test section 270. It is obvious from this plot that very little pavement damage was caused by the steering axles in the VESYS simulation. Simulations on the other three vehicles produced identical conclusions. For the four sections analyzed, average steering axle damage was about 2.10 percent for rutting, 0.125 percent for cracking, and 1.31 percent for serviceability. Simulation of the remaining sections at the road test should yield similar results because all of the steering axles supported approximately the same percentage of loading.

Serviceability and Damage-Based Analysis

Initial computer runs made with the AASHO traffic rates for tridem axle configurations resulted in total loss of serviceability early in the simulation, during the first spring thaw. This loss led to equivalencies for very heavy tridem axle loadings that were unexpectedly low. These equivalencies are plotted in Figure 8 and are compared with the AASHTO equivalencies. Thus, traffic rates were lowered so that damage occurred at a stable rate throughout the simulation period, but the relative variability in traffic volume was maintained over the five seasons. Using the adjusted traffic rates, load equivalence factors based on VESYS 5 predictions of rutting, cracking, and serviceability were calculated for comparison with AASHTO LEFs using Equation 1 for serviceability and Equation 4 for rutting and cracking. Terminal levels of ¾ in. for rutting, 50 percent for cracking, and 3.0 for serviceability were used in determining equivalencies. The calculated equivalencies are given in Figures 9 through 12.

Figures 9 and 10 compare AASHTO LEFs to those based on the VESYS 5 predictions of serviceability. In general, the VESYS 5 serviceability LEFs for all axle configurations are closely correlated with AASHTO LEFs. Minor deviations are apparent, suggesting that equivalencies based on VESYS 5 predictions of serviceability increase at a rate slightly lower than do AASHTO equivalencies.

VESYS predictions of damage-based LEFs are plotted in Figures 11 and 12. Tridem equivalence is plotted in Figure 11 for three different damage criteria. The choice of damage criterion appears to have a mixed effect on LEF; however, rutting equivalencies are, in general, lower for all configurations. Rutting LEFs are also plotted in Figure 12 but grouped according to axle configuration instead of damage criterion (for other damage criteria, the plots are similar in shape). Figure 12 suggests the existence of a consistent relationship between equivalencies for multiple-axle configurations.

An interesting phenomenon can be observed from Figures 11 and 12. In the figures it is apparent that a wide range of axle loads have equivalencies based on rutting approximately equal to one. For these axle loads, failure occurred during

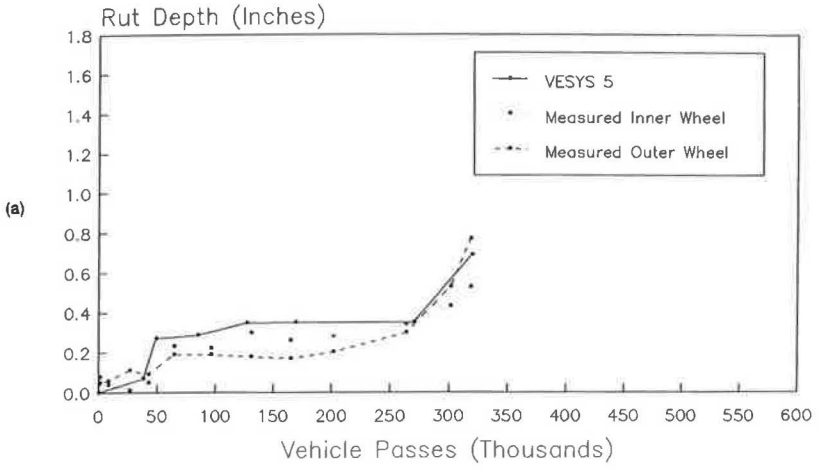

(a)

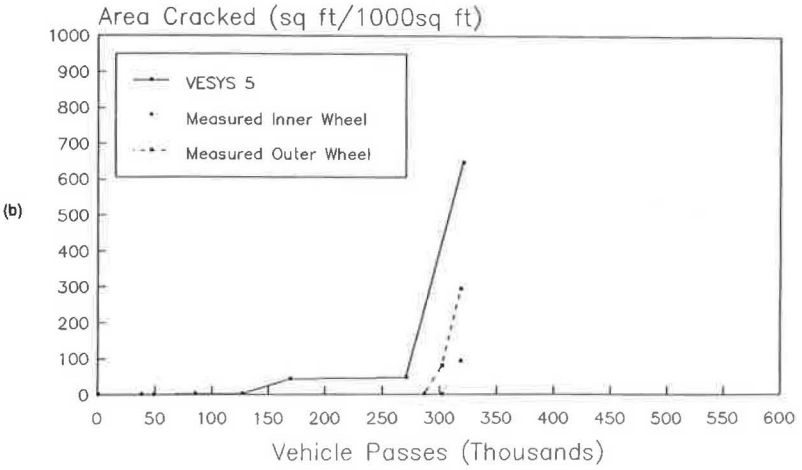

(b)

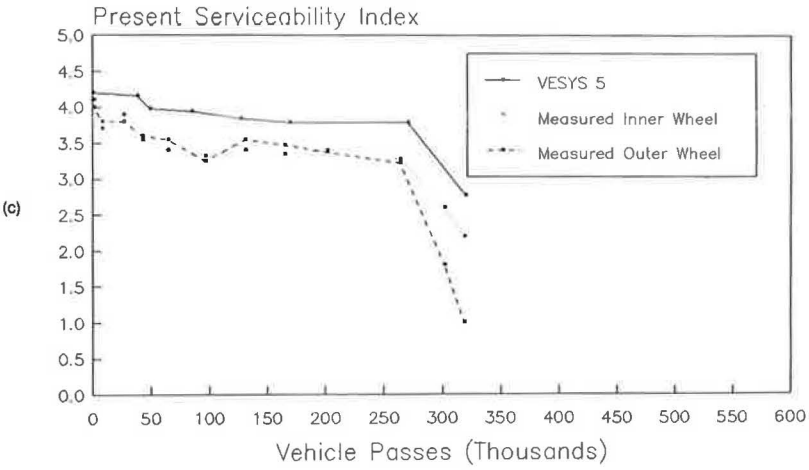

(c)

FIGURE 6 AASHO Section 121, 4-3-8 pavement 12 K single: (*a*) rut depth; (*b*) area cracked; and (*c*) present serviceability index.

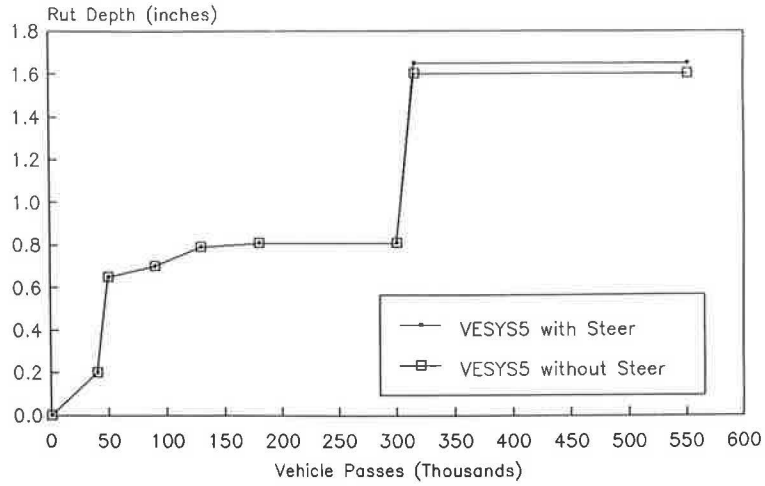

FIGURE 7 AASHO Section 270, 4-3-8 pavement 48 K tandem.

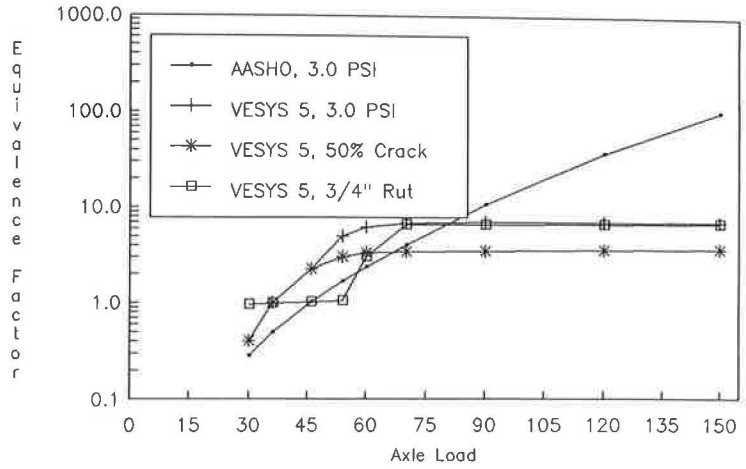

FIGURE 8 Tridem equivalence (AASHO traffic rate).

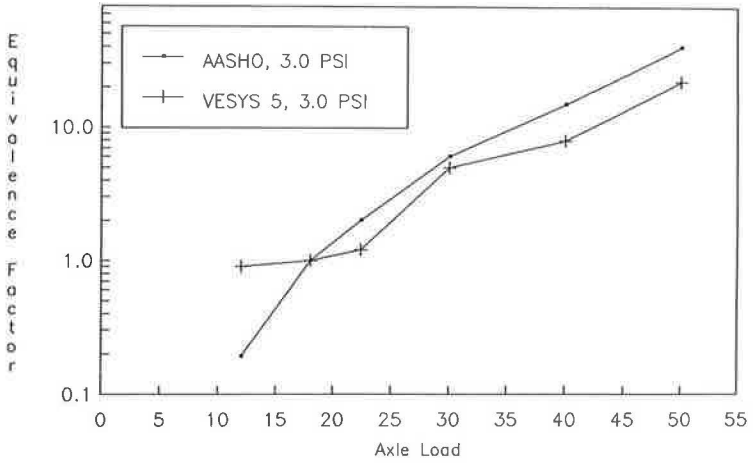

FIGURE 9 Single-axle equivalence (adjusted traffic rate).

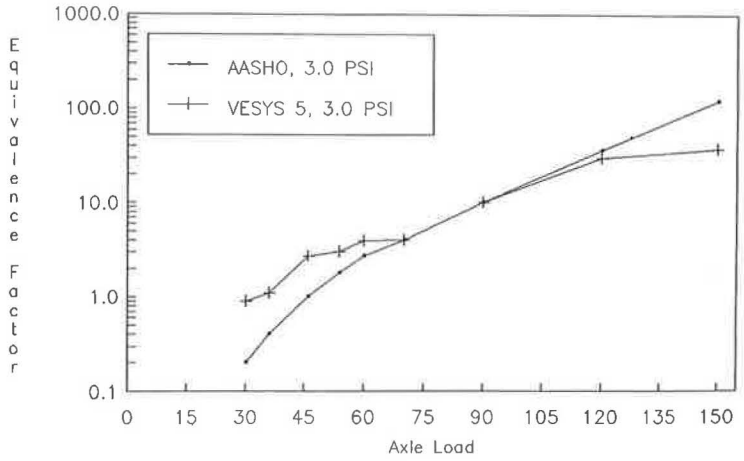

FIGURE 10 Tridem equivalence (adjusted traffic rate).

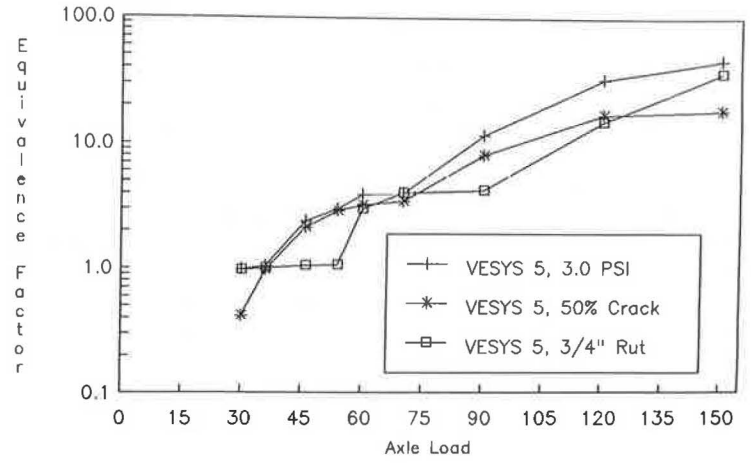

FIGURE 11 Tridem equivalence (adjusted traffic rate). VESYS predictions of damage-based LEFs.

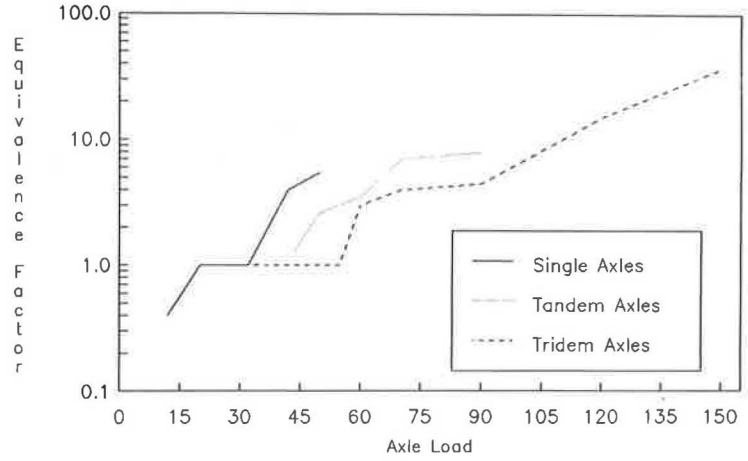

FIGURE 12 VESYS rutting equivalence (adjusted traffic rate).

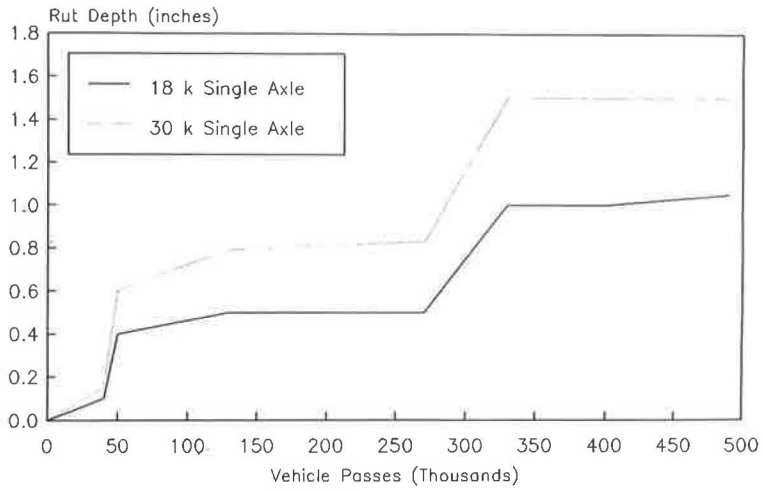

FIGURE 13 VESYS 5 rutting predictions (AASHO traffic rate).

the second spring thaw, as was the case with the 18-kip standard. The existence of this phenomenon is described in Figure 13, which shows VESYS 5 predictions of rutting for the 18-kip standard and for the 30-kip single-axle loads. The sharp increase in rutting to levels above ¾ in. occurs at approximately the same number of repetitions (250,000 to 300,000 vehicle passes) for both loads. The equivalency for the ¾-in. failure level is 1.00, whereas the equivalency for a ½-in. failure level is much higher at approximately 6.00.

These examples illustrate that the season in which failure occurs (also a function of traffic rate) has an important influence on the value of the load equivalence factor. Generally, if failure occurs during the same seasons of the same year for both the standard axle load and the load for which the equivalency is being obtained, the equivalency will be close to one. If failure occurs for one of the axle loads during the following year, the equivalency will be higher for loads greater than the standard and lower for loads smaller than the standard, assuming that traffic rates are not altered. It is important to note that from the four main traffic loops at the road test, 45 percent of the sections were removed from the test before the end of the first spring season. This percentage is broken down by load as follows:

Singles	*Tandems*
12 kip—77%	24 kip—87%
18 kip—50%	32 kip—47%
22.4 k—37%	40 kip—37%
30 kip—17%	48 kip—13%

The above analyses suggest that, had traffic rates been reduced so that all sections lasted throughout the test period, the AASHTO load equivalencies would have been higher for loads greater than the standard and lower for loads smaller than the standard.

Primary Response Analysis

Strain Based—The AASHTO and the cracking LEFs (Figures 9–12) were related to the strain ratios for each of the five seasons and for each of the single-, tandem-, and triple-axle loads (Table 5) using Equation 10. The exponent was then

TABLE 5 AXLE CONFIGURATIONS USED IN LOAD EQUIVALENCE ANALYSIS

Single Axles		Tandem Axles		Tridem Axles	
Load	Tire Pressure	Load	Tire Pressure	Load	Tire Pressure
12 kip	75 psi	24 kip	75 psi	30 kip	75 psi
18 kip	75 psi	32 kip	75 psi	36 kip	75 psi
22.4 kip	75 psi	40 kip	75 psi	46 psi	75 psi
30 kip	75 psi	48 kip	80 psi	54 kip	75 psi
40 kip	75 psi	60 kip	100 psi	60 kip	75 psi
50 kip	80 psi	70 kip	115 psi	70 kip	75 psi
		90 kip	135 psi	90 kip	75 psi
				120 kip	100 psi
				150 kip	135 psi

calculated for all cases. Exponents for tandem-axle cracking LEFs are plotted in Figure 14 (similar trends were observed for single and tridems). Note that the curves tend to infinity when the strain ratios are close to or equal to one. Also, when the LEF in the numerator is identically equal to one, an undefined 0/0 condition exists. Strain ratios close to one occur when the global maximum strain of the axle group approaches that strain produced by the 18k standard single-axle load. Note that the tandem exponent is a positive number at all times. This exponent is positive because the numerator of Equation 10 (log of cracking LEF) is at all times greater than the denominator (log of strain ratios). A similar set of curves (not shown) for tandems was produced using "log of AASHTO LEF" in the numerator. The exponents, although positive numbers, were generally smaller than those based on cracking simply because the AASHO LEFs used were generally smaller than the cracking LEFs.

For singles and tridems the AASHTO LEFs generally were larger (for intermediate loads) than cracking LEFs, and thus the exponents based on AASHTO LEFs were generally larger than those based on cracking LEFs. This analysis suggests that the magnitude, the behavior, and the type of LEF used in the numerator play a significant role in the power law formulation.

Another equally important observation from Figure 14 demonstrates the sensitive nature of the power law formulation, especially for winter and summer conditions. For all axle types and for all formulations (AASHTO or cracking), the exponent at the intermediate load level is higher for the warmer seasons. This higher value is directly attributable to the magnitude of the strain ratios used in Equation 10 (the LEF in the numerator as defined for each load is an average value over all seasons). Thus the strain ratios in the warmer seasons (at intermediate load levels) are significantly smaller than the strain ratios in the colder seasons. This occurrence is a result of using linear elastic layer theory when the contact radius is increased (if contact pressure remains constant) as load is increased. Had contact pressure been increased and contact radius been held constant as load was increased, then the large differences between winter and summer strain ratios would have been negligible. Since contact radius does, in fact, increase with increasing axle load, there is justification for developing seasonal LEFs.

Deflection Based—The exponential relationship between VESYS predictions of deflections and AASHTO LEFs was calculated similarly as for strain analysis. Tridem axle exponents for winter and summer seasons are plotted in Figure 15. Here the exponents are well-behaved, exhibiting values over all load levels between 3.5 and 4; in addition, there is little evidence of any seasonal effects on the exponents. Similar curves were obtained for single and tridems.

When rutting LEFs are used in the numerator of Equation 10, very erratic but not invalid curves are obtained. Tandem exponents are shown plotted in Figure 16. A similar reasoning as applied in the strain ratio analysis is also valid here. When the LEF in the numerator is close to one, the exponent approaches zero. This erratic behavior is solely caused by the environmentally induced stepwise behavior of the rutting LEFs shown in Figure 11. Again this illustrates the major effect that traffic rate and seasonal material property changes have on establishing levels of axle equivalency.

CONCLUSIONS AND RECOMMENDATIONS

- The good agreement between VESYS-5 predictions of rutting, cracking, and PSI with measured values at the AASHO Road Test is justification for using VESYS to conduct extended road tests and analyses. The good agreement also justifies the internal calibration methodology applied for the calibration.
- The steering axles at the AASHO Road Test had virtually no influence on pavement response. Therefore, the fact that they were neglected in the development of the AASHTO load equivalence factor equations is appropriate.
- The relationship between seasonal material properties and traffic rate can significantly influence load equivalence factors. To establish load equivalencies that are representative of the entire range of seasons, traffic rates should be adjusted so that damage occurs at a fairly constant rate throughout the test period. To achieve a more accurate estimation of the

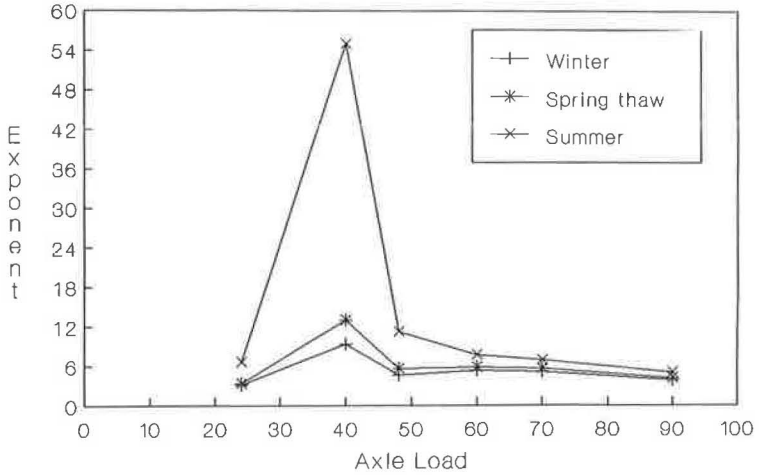

FIGURE 14 Strain-based LEF exponents: tandems (based on cracking LEF).

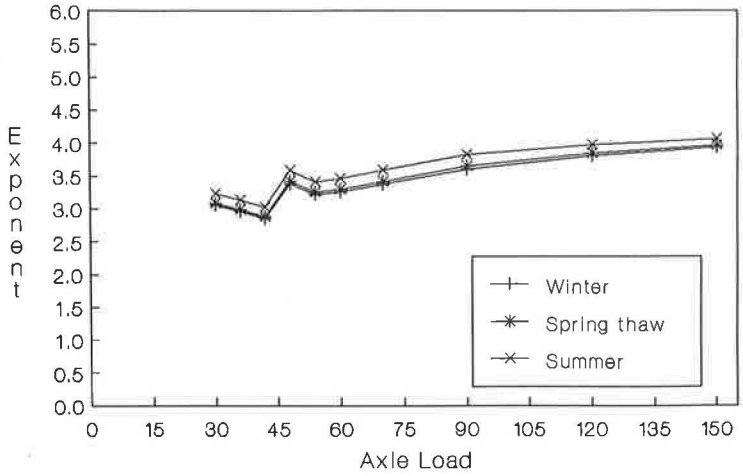

FIGURE 15 Deflect-based LEF exponents: tridems (based on AASHO LEF).

relative damage caused by various vehicle types, seasonal load equivalence factors should be considered. If traffic at the AASHO Road Test had been adjusted so that all sections lasted throughout the test period, the resulting load equivalence factors may have been different. This information is particularly important in light of the fact that the failure rate of sections subjected to lighter loads was considerably higher than the failure rate of sections subjected to heavier loads.

- Ratios of strains and deflections raised to an exponent can be used to determine load equivalence factors. The exponents based on strain vary with season; exponents based on deflection are similar for all seasons. The logarithmic power law expression is sensitive to the type, shape, and magnitude of the LEF used in the numerator.

Further study of the relative damage caused by the various vehicle types should use "computer test road" simulations to verify the

- Feasibility of using entire vehicle equivalencies,
- Effect of traffic rate on the AASHO LEF,
- Feasibility of seasonal load equivalence factors, and
- Feasibility of using primary response as a measure of vehicle damaging effects.

ACKNOWLEDGMENTS

Financial support for C. M. Cobb was provided through the National Highway Institute graduate research fellowship program. The information was condensed and edited from an FHWA unpublished report\M.S. thesis prepared by C. M. Cobb while he was a Louisiana Tech University, Ruston, Graduate Research Fellow at the Turner Fairbank Highway Research Center. Technical support for the study was provided in part by Pavements Division, FHWA, Office of Research, Development and Technology Transfer and Department of Civil Engineering, Louisiana Tech University. Special thanks are extended to Leslie K. Guice of Louisiana Tech University and to Donna Malec for her support in producing this document.

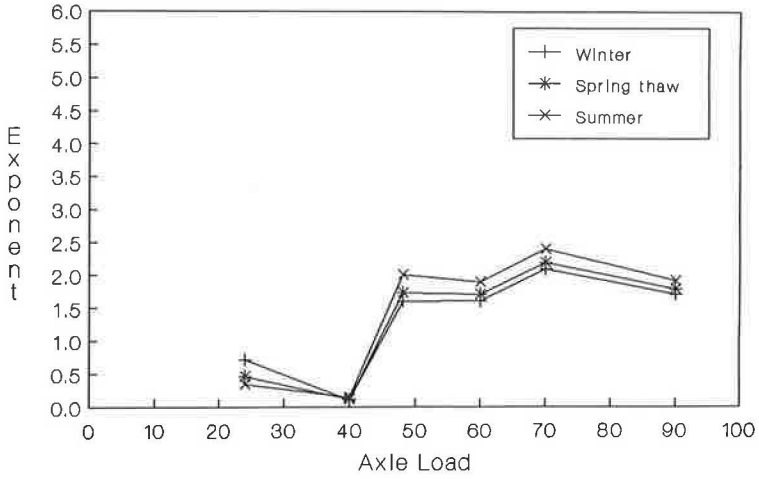

FIGURE 16 Deflect-based LEF exponents: tandems (based on rutting LEF).

REFERENCES

1. *Special Report 61A: The AASHO Road Test, History and Description of Project*. HRB, National Research Council, Washington, D.C., 1961.
2. *Special Report 61E: The AASHO Road Test, Report 5, Pavement Research*. HRB, National Research Council, Washington, D.C., 1962.
3. A. J. Scala. Comparison of the Response of Pavements to Single and Tandem Axle Loads. In *Australian Road Research Board: Proceedings of the 5th Conference*, Canberra, Ware Publishing Pty. Ltd., 1970.
4. J. T. Christison. Vehicle Weights and Dimensions Study, Vol. 8. In *Pavements Response to Heavy Vehicle Test Program, Part 2, Technical Report, Load Equivalency Factors*. Roads and Transportation Association of Canada, July 1986.
5. W. J. Kenis. *Predictive Design Procedures, VESYS Users Manual—An Interim Design Method for Flexible Pavements Using the VESYS Structural Subsystem*. Report FHWA-RD-77-154. FHWA, U.S. Department of Transportation, January 1978.
6. W. J. Kenis. The Rutting Models of VESYS. *Proc., 25th Conference on Paving and Transportation*, The University of New Mexico, Albuquerque, January 1988.
7. M. G. Sharma, W. J. Kenis, and M. Mirdamadi. Evaluation of Mechanical Parameters of In-Service Pavements from Field Data. *Proc., 6th International Conference on the Structural Design of Asphalt Pavements*, Ann Arbor, 1987.
8. W. J. Kenis, J. A. Sherwood, and T. F. McMahon. Verification and Application of the VESYS Structural Subsystem. *Proc., 5th International Conference on the Structural Design of Asphalt Pavements*, University of Michigan, Ann Arbor, and Delft University of Technology, Delft, The Netherlands, Vol. 1, August 1982.
9. J. B. Rauhut and P. R. Jordahl. Effects on Flexible Highways of Increased Legal Weights Using VESYS IIM. Report FHWA-RD-77-116, FHWA, U.S. Department of Transportation, Washington, D.C., January 1978.
10. *NCHRP Report 128: Evaluation of AASHO Interim Guides for Design of Pavement Structures*. HRB, National Research Council, Washington, D.C., 1972.
11. *Special Report 61B: The AASHO Road Test, Report 2, Materials and Construction*. TRB, National Research Council, Washington, D.C., 1962.

Publication of this paper sponsored by Committee on Flexible Pavement Design.

AASHTO Flexible Pavement Design Method: Fact or Fiction?

B. J. Coree and T. D. White

In 1986 AASHTO published the *AASHTO Guide for Design of Pavement Structures*. This new publication incorporates the original development of the Road Test data combined with some extensions applying theoretical and empirical models. A review of this document, the superseded interim guides, technical literature, and the original Road Test reports revealed a number of opportunities for reexamining the Road Test results. These opportunities included an evaluation of the patterns of performance contained in the raw data, an examination of the mathematical formulation of the performance and design equations, and a probabilistic analysis of the Road Test results, treating the layer coefficient as a distributed random variable instead of as a uniquely determined number.

The flexible pavement design method of AASHTO is now well established: the final edition of a series of interim guides was recently (1986) adopted by AASHTO. This document (*1*) adds significant volume and some additional factors to the design process. Specifically, the new AASHTO guide incorporates the original development of the Road Test data with more recent additions relating to subsurface (internal) drainage, materials, reliability, and others.

One interesting observation is that the developments in the new guide appear to accept the original AASHTO formulations as a starting point. Taking this approach ignores the wealth of information contained in the original AASHO Road Test data. New analytical techniques, additional years of experience with pavement performance, and much hard thinking on the results of the Road Test provide an opportunity that was missed in developing the new Guide. In lieu of a fundamental approach, the developments presented in the new Guide that affect the design procedure were evolved by a combination of theoretical and empirical models. The cause and effect of the actual AASHO Road Test performance is not incorporated.

The AASHTO methodology is used by a number of states in some form or another. In many cases, states have modified details of the method to better suit their peculiar circumstances and experience. Other states have made modification only to the various constants in the original formulation. Overall, some of the statistical constants and coefficients originally developed in the analysis of the Road Test results have taken on physical meanings that are not valid.

A recent research project initiated by the Indiana Department of Transportation (INDOT) required the authors to determine the "layer coefficients" for the ten bituminous mixtures currently being specified in Indiana. INDOT uses the original AASHO formulation with their own set of layer coefficients. However, INDOT has recognized that, although the range of mixtures specified represents a vast array of performance characteristics, the assignment of a single-layer coefficient to characterize them is both unrealistic in engineering terms and inefficient in financial benefit.

As part of the preliminary research task, a literature review was undertaken. In the review of the literature, a specific effort was made to establish the definition of layer coefficient and the original method for calculating this parameter. The results of this otherwise simple task initially proved to be highly disturbing. Subsequently, further analysis highlighted some interesting possibilities. This paper is about the findings and conclusions of this preliminary part of the project.

Much of this preliminary research is definitive, although some is still speculative, since the project is ongoing.

LAYER COEFFICIENT

Considerable disagreement is apparent about both the definition and the recommended method of measurement of layer coefficients.

For example, the following statements are from the 1986 AASHTO Guide (*1*):

- "The structural number is an abstract number . . . converted to actual thickness of surfacing, base and subbase, by means of appropriate layer coefficients representing the relative strength of the construction materials."
- "In effect, the layer coefficients are based on the elastic moduli M_R and have been determined based on stress and strain calculations in a multilayered pavement system" (Section 1.2).
- ". . . it is not essential that elastic moduli of these materials are characterized. In general, layer coefficients derived from test roads or satellite sections are preferred" (Section 2.3.3).

At the International Conference on the Structural Design of Asphalt Pavements, Shook and Finn (*2*) stated the following:

"It is believed that the coefficients a_1, a_2, a_3 are functions of the strengths of the various layers involved. At the present time (1962), however, no entirely satisfactory techniques are available for defining or measuring these strength factors."

B. J. Coree, ERES International, Inc., 1401 Regency Drive East, Savoy, Ill. 61874. T. D. White, School of Civil Engineering, Purdue University, West Lafayette, Ind. 47907.

Perusal of existing and current literature reveals that two predominant methods have been adopted for estimating the layer coefficients of bituminous materials: (a) a power law relating the layer coefficient to the resilient modulus (M_R) (e.g., see Figure 2.5 in the AASHTO Guide [*1*]) and (b) based on Odemark's equivalent stiffness hypothesis (*3*), an analogous relationship is used, wherein the one-third power of the ratio of the material modulus to that of a reference material (whose layer coefficient is presumed known) gives the ratio of the unknown layer coefficient to that of the reference material.

Assuming a relationship between strength and the layer coefficient is a surprising extrapolation, since no measure of structural strength or adequacy was included in the data used to calibrate the AASHO model. The only variables used in the AASHO model (*4*) are given in Table 1.

It is readily apparent that none of these variables are measures of strength, although it is conceded that the layer thicknesses may be indirect strength indicators. Further, no cognizance was given to the annual cyclic subgrade strength. Instead, the subgrade strength was assumed to be uniform throughout the Road Test, as was climate.

The AASHO statistical flexible pavement design model was set up to integrate the effects of (a) traffic, (b) pavement (materials and layer thicknesses), and (c) serviceability (or level of distress). These effects were measured either directly or indirectly through the factors in Table 1. The development of the AASHO model is given below. A review of this development shows that the layer coefficient is a secondary parameter, whose significance is as a regression coefficient, or a calibration constant. If any physical significance is attributed to the layer coefficient, the significance should be relative to the resistance to distress, rather than to the structural capacity of the layer material.

AASHO MODEL

Background

The basis of the AASHO model is a decay curve, wherein it is assumed that the condition of a pavement will deteriorate, or decay, with accumulated traffic (this implies a certain element of time). To implement this model, the concept of functional pavement serviceability was developed. This concept resulted in the composite measure known as the present serviceability index, (PSI), which results from a regression equation relating the distress measurements given in Table 1 to an aggregated subjective rating of the adequacy of the pavement by a panel of adjudicators. A scale of 0 to 5 was assigned to the panel rating and subsequent qualitative serviceability index. A serviceability of 5 is the ideal, or perfect, pavement. Pavement serviceability has several important characteristics.

TABLE 1 AASHO ROAD TEST MEASURED VARIABLES

Factor	Variable Description	Variable	Unit
Traffic	No. of axle repetitions	W	No.
	Axle weight	L_1	kip
	Axle type	L_2	1 = single 2 = tandem
Pavement	Surfacing thickness	t_1	in.
	Base thickness	t_2	in.
	Subbase thickness	t_3	in.
Distress	Extent of cracking	C	ft²/1,000 ft²
	Extent of patching	P	ft²/1,000 ft²
	Slope variance (roughness)	SV	
	Rut depth	RD	in.

- Initial serviceability (p_0) is considered to be the serviceability of the freshly constructed, untrafficked pavement. The ideal pavement has to be rare. In fact, newly constructed flexible pavements at the Road Test reflected an average serviceability index value of 4.2.
- Terminal serviceability (p_t) is considered to be that level of serviceability at which the pavement is deemed to be no longer performing its required function. The lower, limiting value of p_t at the Road Test was 1.5.
- Present serviceability (p) is the measured, or estimated, level of serviceability at any time during the life of the pavement. Under normal circumstances then $p_0 > p > p_t$.

Using these definitions, the AASHO model may be stated:

$$\left(\frac{W}{\rho}\right)^{\beta} = \frac{p_0 - p}{p_0 - p_t} \tag{1}$$

where W is the number of axle (18-kip) repetitions that will reduce the serviceability from p_0 to p, ρ represents the number of axle repetitions at terminal serviceability (p_t), and β is a shape factor. Simply stated, the cumulative traffic at any time as a proportion of the traffic capacity of the pavement is represented as a power function of the proportion of usable serviceability consumed.

By a simple mathematical rearrangement, the more familiar form of the AASHO relationship is obtained:

$$\begin{aligned}\log_{10}(W) &= \log_{10}(\rho) + \frac{\log_{10}\left(\frac{p_0 - p}{p_0 - p_t}\right)}{\beta} \\ &= \log_{10}(\rho) + \frac{G}{\beta}\end{aligned} \tag{2}$$

where G represents the logarithm of the serviceability ratio.

Calibration

On each section of the Road Test, the present serviceability (p) and traffic (W) were determined at intervals of 2 weeks throughout the life of the section. The unknown parameters (β and ρ) were obtained by regression analysis. The summarized data used for the original regression analysis is in the form shown in Table 2. In Table 2, the logarithm of traffic is given for serviceabilities of 3.5, 3.0, 2.5, 2.0, and 1.5. These five points then provided the data for the regression used to obtain estimates of β and ρ. It should be noted that on a log-log plot of W versus G, the relationship in Equation 2 is linear.

Having obtained the two parameters (β and ρ) for each section, it was assumed that these parameters were functions of the section design (i.e., thickness) and traffic type. On this basis the following functional relationships were assigned to β and ρ:

$$\rho = A_0 \cdot (D + 1)^{A_1} \cdot (L_1 + L_2)^{A_2} \cdot L_2^{A_3} \quad (3a)$$

$$\beta = 0.4 + B_0 \cdot (D + 1)^{B_1} \cdot (L_1 + L_2)^{B_2} \cdot L_2^{B_3} \quad (3b)$$

In these equations L_1, L_2, and D (where D is the total pavement thickness) were known for each section. The eight unknown constants A_{0-3} and B_{0-3} were obtained by regression analysis. A variant regression was conducted in which the thickness index D was given by $D = a_1 \cdot t_1 + a_2 \cdot t_2 + a_3 \cdot t_3$, such that "these coefficients were permitted to vary so that the three elements of the pavement structure might each enter into the thickness index, (D), with a different weight per unit thickness" (*3*). This linear combination of the layer thicknesses provided a better regression and was retained in the model, with the transformed thickness (thickness index D) becoming better known as the structural number (SN) and the coefficients a_{1-3} as the layer coefficients. The well-known values for the layer coefficients obtained from the Road Test are given in Table 3. As listed, the raw traffic data were referred to as "unweighted," whereas the "weighted" traffic was adjusted in an empirical fashion to attempt to take into account the varying effect of the annual climatic cycle on the subgrade. This technique was the only concession originally given to the effect of climate or variable subgrade support.

Interpretation

The review of the AASHO Road Test analysis showed the layer coefficient to be no more than a regression coefficient with no truly ascribable physical or engineering meaning other than being a form of scaling or normalizing constant. Certainly, no connotation of strength could be assumed since no measurement of strength had been used in its derivation. As a result of this situation, some concern developed about being able to discriminate the strength and performance characteristics of the asphalt mixtures being specified by INDOT. At this stage it was deemed wise to determine the variability (distribution) of the layer coefficients found at the Road Test. The distributions were obtained by using the original equations (3*a* and 3*b*), but solving for the layer coefficients section by section rather than globally. Thus the layer coefficients (a_{1-3}) for each section were determined. Because the materials in each layer were designed to be uniform throughout the Road Test, variation in the value of the layer coefficients was expected to be minimal.

The resulting distributions of the section-by-section calculations are shown in Figure 1. The only adjustment made to these distributions was to constrain the layer coefficients to be non-negative. Such a constraint may be explained on the

TABLE 2 AASHO ROAD TEST: SERVICEABILITY DATA (*4*)

FACTORIAL EXPERIMENT—DESIGN 1
FLEXIBLE PAVEMENT, UNWEIGHTED APPLICATIONS
(Continued)

			INDEX DAY											
			11	22	33	44	55							
			APPLICATIONS THROUGH INDEX DAY - THOUSANDS											
			80	233	445	807	1114							
			SERVICEABILITY TREND LEVEL					LOG APPLICATIONS THROUGH INDEX DAY					STRUCTURE DESIGN			
			3.5	3.0	2.5	2.0	1.5	4.901	5.368	5.648	5.907	6.047				
LOOP	LANE	SECTION	LOG UNWEIGHTED APP. TO SERVICEABILITY LEVEL[a] (x.xxx)					SERVICEABILITY TREND VALUE ON INDEX DAY[aa] (x.x)					D_1	D_2	D_3	SECTION
													(in.)			
3	1	165		4766	4782	4790	4806						2	0	00	165
3	1	125		3204	3397	3531	3633						2	0	04	125
3	1	143	4846	4850	4854	4858	4862						2	0	08	143
3	1	133	4813	4854	4874	4881	4883						2	0	08	133
3	1	113	4774	4783	4798	4806	4813						2	3	00	113
3	1	135	4842	4846	4850	4858	4862						2	3	04	135
3	1	159		4828	4891	4921	4946	23					2	3	08	159
3	1	127	4756	4850	4862	4874	4887						2	6	00	127
3	1	157	4457	4918	4940	4946	4952	32					2	6	04	157
3	1	111	5715	5760	5793	5820	5858	39	37	37			2	6	08	111
3	1	137	4336	4874	4881	4883	4883						3	0	00	137
3	1	163	4893	4914	4931	4934	4940	34					3	0	04	163
3	1	109	4904	4957	4990	4994	4998	35					3	0	08	109
3	1	147	4457	4828	4846	4854	4858						3	3	00	147
3	1	107	4891	4921	4934	4940	4940	31					3	3	04	107
3	1	115		4854	4899	4921	4940	25					3	3	04	115
3	1	129	5035	5179	5703	5741	5748	39	29	27			3	3	08	129
3	1	117	4874	4911	4934	4940	4940	31					3	6	00	117
3	1	131	5280	5664	5756	5762	5769	38	34	30			3	6	04	131
3	1	155	5538	5756	5804	5862		33	36	34	19	16	3	6	08	155
3	1	119	4747	4874	4883	4887	4889						4	0	00	119
3	1	141	4846	4883	4885	4889	4891						4	0	04	141
3	1	153	4889	4931	4990	5022	5036	34					4	0	08	153
3	1	145	4901	4901	4904	4904	4904	35					4	3	00	145
3	1	151	4828	4921	4998	5030	5036	32					4	3	04	141
3	1	121	5056	5732	5765	5779	5786	36	34	33			4	3	08	121
3	1	161	4887	4990	5076	5159	5250	34					4	6	00	161
3	1	149	4870	4994	5030	5035	5035	33					4	6	00	149

TABLE 3 AASHO ROAD TEST LAYER COEFFICIENTS

Traffic	Coefficient[a]		
	a_1	a_2	a_3
Weighted	0.44	0.14	0.11
Unweighted	0.37	0.14	0.10

[a] a_1, Asphaltic concrete, a_2, crushed limestone base, and a_3, sand-gravel base.

basis that regardless of whether strength or serviceability was to be considered, an increasing layer thickness must lead to an increase in the overall strength or serviceability. Consideration of the layer coefficient distributions in Figure 1 caused considerable concern. The degree of variation, particularly in the surfacing (the most closely controlled material), was surprising. In a specific review of the literature, a measure of confirmation was provided by the values given in Table 10 of an earlier TRB report (*4*) in which it was shown that the value of a_1 varied from 0.33 to 0.83 (weighted) and from 0.33 to 0.78 (unweighted).

Considering the degree of control exercised at the Road Test, further research and analysis were essential to resolve the apparently fatal layer coefficient variability represented in Figure 1. The term fatal is emphasized because it seems futile to discriminate the structural quality of various asphalt mixtures when the single asphalt mixture at the Road Test resulted in such great variability. Consequently, after both the methodology and the computations were found to be substantially correct, a copy of the original Road Test data for the flexible pavement sections was obtained from the TRB. This detailed data base provided qualitative improvement in the data being analyzed.

Remarks

In the remainder of this paper, the raw, or unweighted, traffic data will be used, because the weighting function is somewhat arbitrary and would be difficult to transform for application to sites or climes other than Ottawa, Ill.

For reference, the relationships used by AASHO after the final regressions are given for the standard 18-kip single axle (standard axle) configuration:

Weighted:

$$\log_{10}(W) = 9.61 \cdot \log_{10}(SN + 1) - 0.20 + \frac{\log_{10}\left(\frac{4.2 - p}{2.7}\right)}{0.4 + \frac{1{,}096}{(SN + 1)^{5.19}}} \quad (4a)$$

Unweighted:

$$\log_{10}(W) = 8.94 \cdot \log_{10}(SN + 1) + 0.35 + \frac{\log_{10}\left(\frac{4.2 - p}{2.7}\right)}{0.4 + \frac{140{,}155}{(SN + 1)^{8.73}}} \quad (4b)$$

ROAD TEST DATA

The remaining Road Test data held by the TRB is a reduced set of the original data. Many files, folders, and card decks that had not been used have been deleted. The remainder, transferred to computer tape, have been preserved. Of par-

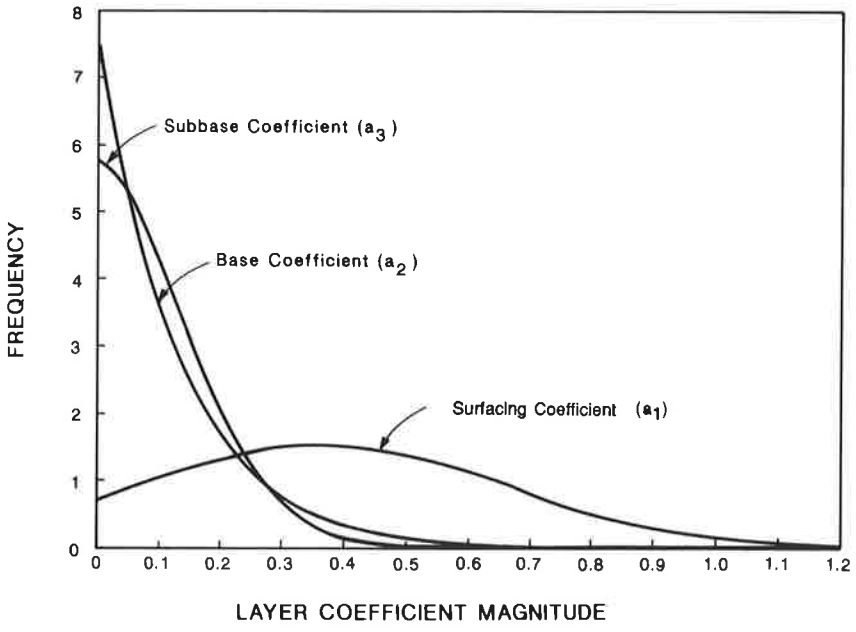

FIGURE 1 AASHO Road Test: layer coefficient distribution.

TABLE 4 RETAINED AASHO ROAD TEST DATA FORMAT

Field #	Description	Field #	Description
1	Loop No.	7,8	Extent of Cracking
2	Lane No.	9,10	Extent of Patching
3	Section No.	11,12	Slope Variance
4	Surfacing Thickness	13,14	Rut Depth
5	Base Thickness	15	PSI
6	Subbase Thickness	16	Accumulated Traffic
		17	AASHO Day

ticular value is that the results from the full factorial experiment have been retained.

The data from the full factorial experiment were reduced to permit easier manipulation, and the data fields given in Table 4 were maintained.

In this file, complete observational data are available for each section for each AASHO day (1 AASHO day = 14 real days). Not only can the PSI (present serviceability index) versus traffic history for each section be reconstructed, but the component parts of the PSI (cracking, patching, slope variance, and rut depth) can be examined. It is not well recognized that the amount of patching at the Road Test was essentially negligible; equally important is that there was no routine maintenance undertaken on the pavement sections such as might be expected on in-service highway pavements.

After the data file was reviewed, all observations were removed for sections after overlay. Data from overlaid sections were not used in the original layer coefficient determination. Subsequently, plots were prepared for PSI versus traffic, PSI versus log (traffic) and PSI versus AASHO day. Examples of these plots are given in Figures 2*a*–*c*. Examination of these figures reveals that the AASHO model provides a very poor predictive model. In addition, both sets of data (observed and predicted) were submitted to analysis through the SPSS statistical package. The "Runs Test" of this statistical package returned a *z*-statistic of 16 (typically a value of less than 2.0 might be expected). Thus, although the overall regression might appear reasonable in terms of the r^2 statistic, the model is otherwise inappropriate. (Although the values of the r^2 statistic pertaining to the Road Test are not easily found in the literature, it is believed that the values are 0.23 for unweighted traffic and 0.49 for weighted traffic.)

A review of Figure 2 reveals that the shapes of the curves are not as would have been expected. Instead of being smoothly downcurving, the data appeared to turn sharply downward at either one or two reasonably well-defined events. This was apparent in both the PSI versus traffic (top) and PSI versus $\log_{10}$ (traffic) (middle) plots, although more pronounced in the former. In the PSI versus AASHO day plot (bottom) the locations of these two critical events were particularly noticeable and were found to correspond very closely with the periods of spring thaw.

Not all sections showed this tendency; however, in those that did not, a downward step was noted occurring at the same times. On the PSI versus AASHO day plots the curves appeared to be generally piecewise linear, i.e., the PSI decreased linearly at one rate and then linearly at a much greater rate. In some cases, this decrease in PSI took the form of a step function, with the original slope being reestablished. These observations are shown schematically in Figure 3. Figure 3 outlines three observed performance patterns:

1. P-A-B (rarely observed except on very thick sections or with very light axle weights): exhibits no significant distress. The slope of the line (rate of decay) is clearly independent of traffic volume (axles per day); it is equally independent of climatic (freeze/thaw) events.
2. P-A-C-D-E: a number of sections showed this pattern, in which a distinct and sudden loss of serviceability was noted (ALC) coinciding with the first spring/thaw. Some of these sections cracked, but the majority survived the first year uncracked. Those sections that survived with a crack failed at the onset of the next winter, whereas the uncracked survivors generally failed during the following freeze/thaw event.
3. P-A-F: a large number of sections exhibited this behavior, failing rapidly and catastrophically during the first freeze/thaw event.

The overall linearity of these plots was particularly puzzling because there had been no suggestion that time was a significant factor, which is implied by this result. In fact, axle repetitions (traffic) were considered the primary forcing variable. A check confirmed that the rate of trafficking (axles per AASHO day) over the period of the Road Test was not constant; however, the changes in trafficking rates did not coincide with the changes of slope in the plots. Table 5 shows that the rate of section failure ($p_t < 1.5$) is not well correlated with traffic but is highly correlated with the season of the year. Thus, time, as measured by the number of spring/thaw events, appears to be of greater significance than was previously suspected.

In extending the piecewise linear hypothesis from the trafficked sections to the untrafficked sections of Loop 1, only three particularly thin sections displayed the same pattern. As a result, it was concluded that the interaction of time and traffic might be significant. The relatively sudden serviceability loss observed during the spring/thaw periods was addressed by examining the component parts of the PSI. The examination revealed that this phenomenon was paralleled by the initial observation of Class 2 (alligator) or Class 3 (granulated) cracking, or both (Figure 4). The full set of

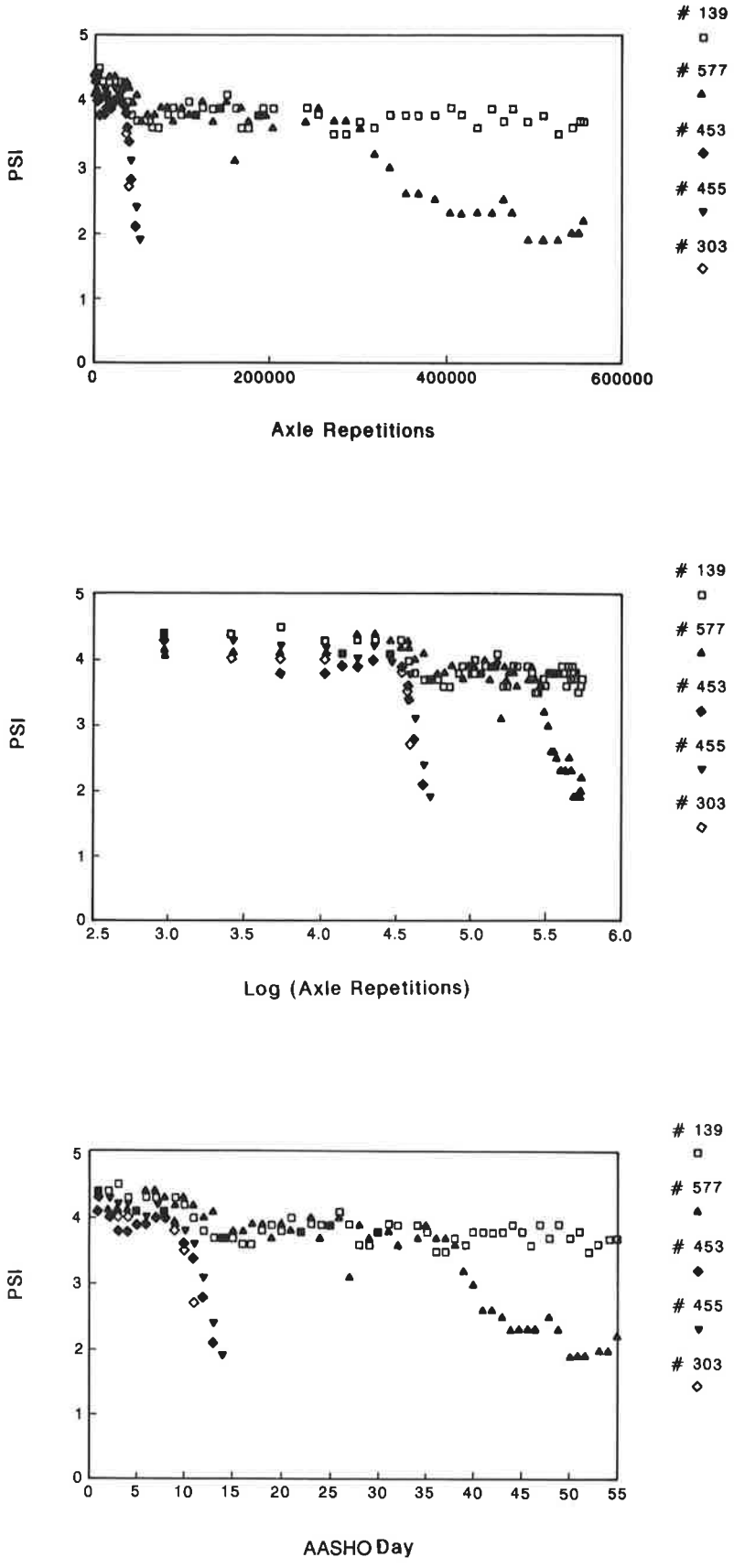

FIGURE 2 AASHO Road Test: serviceability plots: (top) PSI versus traffic; (middle) PSI versus $\log_{10}$ (traffic); and (bottom) AASHO day.

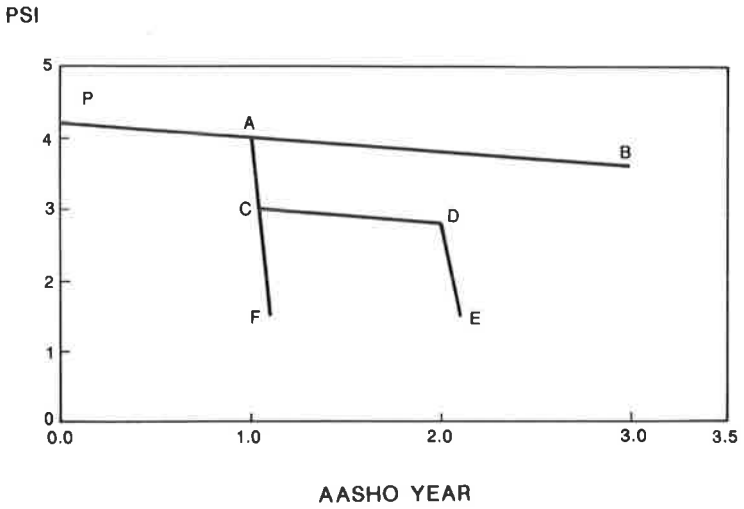

FIGURE 3 AASHO Road Test: performance schematic.

TABLE 5 AASHO ROAD TEST: TRAFFIC AND FAILURE RATES

Season	% Traffic	% Failures
Winter	22	28
Spring	24	60
Summer	30	2
Fall	23	10

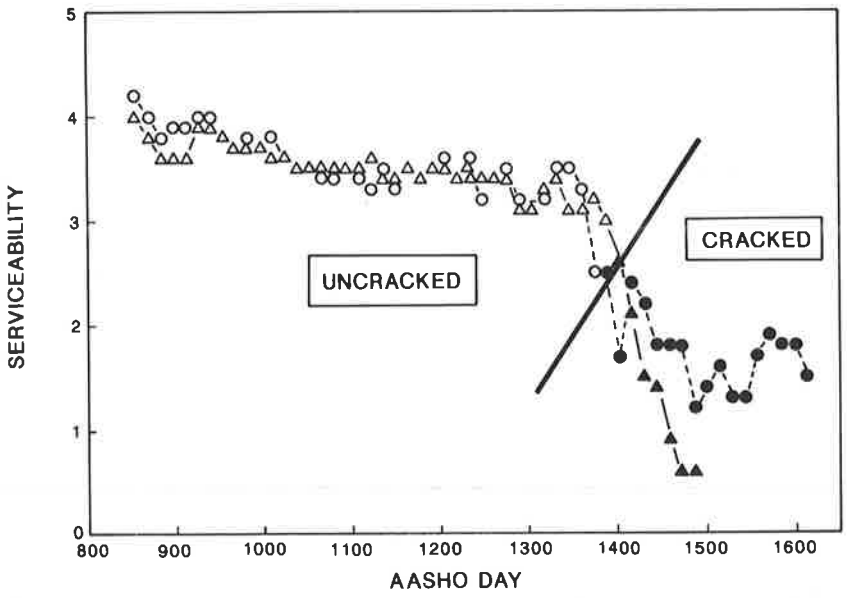

FIGURE 4 AASHO Road Test: effect of cracking on serviceability.

observed data from a number of sections was plotted (Figure 5) (instead of only those at $P = 3.5, 3.0, 2.5, 2.0$, and 1.5 as used in the original AASHO Road Test analysis). This full set of data clearly reflects the piecewise linear relationship contrary to the expectation of Equation 2. The points of intersection of the linear portions of the plots closely match the initial observation of Class 2 or Class 3 cracking, or both. In practical terms, two populations of pavement performance have been observed: (a) integral, uncracked and still-sealed pavement and (b) cracked, disintegrating pavements. Because at the Road Test, most Class 2 or Class 3 cracking was initially observed at, or about, a PSI of 3.0 to 3.5, the final AASHO equations (4a and 4b) are calibrated to failed, or failing, pavements.

CUMULATIVE SUM (CUSUM) PLOTS

If, using the observed data from any section, the cumulative serviceability loss is plotted against AASHO day, a piecewise linear graph will be observed (Figure 6). (In Figure 6 the serviceability loss is given as $(5.0 - p(i))$, and the Cusum as

$$\sum_{i=1}^{t} (5.0 - p(i))$$

where t is the number of AASHO days from the start of trafficking to the point in time considered). In the following analysis, serviceability loss is defined as $(p_0 - p(i))$. Close inspection indicates that the relation rapidly approaches linearity on each leg, i.e., that the data exhibit linearity asymptotically.

If the expected serviceability loss at any time t is represented by a rearrangement of Equation 1, then

$$p_0 - p(i) = \text{Serviceability loss} = (p_0 - p_t) \cdot \left(\frac{W(i)}{\rho}\right)^{\beta} \quad (5)$$

Then, recreating the Cusum plot mathematically:

AASHO Day	*Incremental Loss*	*Accumulated Loss*
1	$(p_0 - p_t) \cdot \left(\frac{W(1)}{\rho}\right)^{\beta}$	$(p_0 - p_t) \cdot \left(\frac{W(1)}{\rho}\right)^{\beta}$
2	$(p_0 - p_t) \cdot \left(\frac{W(2)}{\rho}\right)^{\beta}$	$(p_0 - p_t) \cdot \left(\frac{W(1) + W(2)}{\rho}\right)^{\beta}$
. . .	. . .	. . .
n	$(p_0 - p_t) \cdot \left(\frac{W(n)}{\rho}\right)^{\beta}$	$(p_0 - p_t) \cdot \left(\frac{W(1) + W(2) + \ldots + W(n)}{\rho}\right)^{\beta}$

To approach linearity, Cusum$(n + 1)$ − Cusum(n) must approach a constant value in the limit as n increases. Assuming for simplicity that the traffic rate is constant at w axles per AASHO day (i.e., that $W(n) = n \cdot w$), then

$$\text{Cusum}(n + 1) - \text{Cusum}(n) = (p_0 - p_t) \cdot \left(\frac{w}{\rho}\right)^{\beta} \cdot n^{\beta} \quad (6)$$

If this expression is to be constant, then it may be simplified thus:

$$n^{\beta} = \text{constant} \quad (7)$$

This expression is true only in the limit for all n, as n approaches infinity if β is vanishingly small. For a range of structural number (SN) of 1 to 6, the corresponding range of β in Equation 4b is found to be $0.4 < \beta < 300$. Thus, the piecewise linear relationship observed in Figure 6 cannot be supported by the AASHO model.

The implication of this analysis is that on linear portions ($\beta \approx 0$) of the Cusum plot, traffic (axle weight and repetitions) has no effect, and it is only during those periods when the Cusum is in transition from one linear portion to another ($\beta \neq 0$) that traffic has a significant effect on serviceability.

The mathematics of the Cusum transformation have not been developed sufficiently to permit the derivation of the relationship that gives rise to the observed asymptotically linear Cusum function.

The smoothing effect of the Cusum transformation can clearly be seen in Figure 6 and was used to help identify the critical points (changes of slope) in the behavior of each section.

Figure 7 superimposes the Cusum plots for a number of different sections on the same graph; the axle weight was the same for all of these sections. Although not overly evident, it can be seen that (a) until cracking (a change of slope) separates a section from the main plot, the behavior of all of the sections is essentially the same, (b) in general, the thicker (total pavement thickness) pavements survive the longest before cracking, and (c) within pavements of the same or similar total thickness, those with thicker surfacing t_1 survive longer.

SURVIVAL PROBABILITY

A probabilistic analysis was made in an attempt to quantify, or model, the step function reported above, which was identified as being triggered, or initiated, by a spring/thaw event.

On any given lane of the Road Test (constant axle weight and type) pavements of various composition either failed or survived the first full seasonal cycle of spring/thaw. By trying to relate the elements of structure to the probability of failure

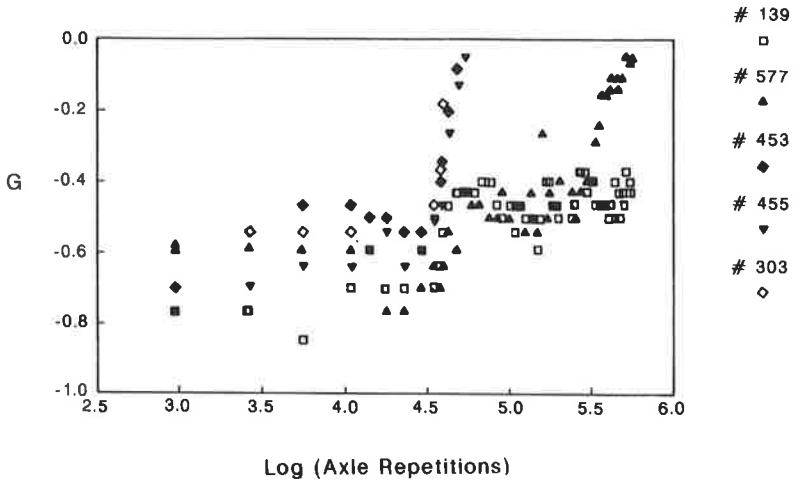

FIGURE 5 AASHO Road Test: section serviceability histories.

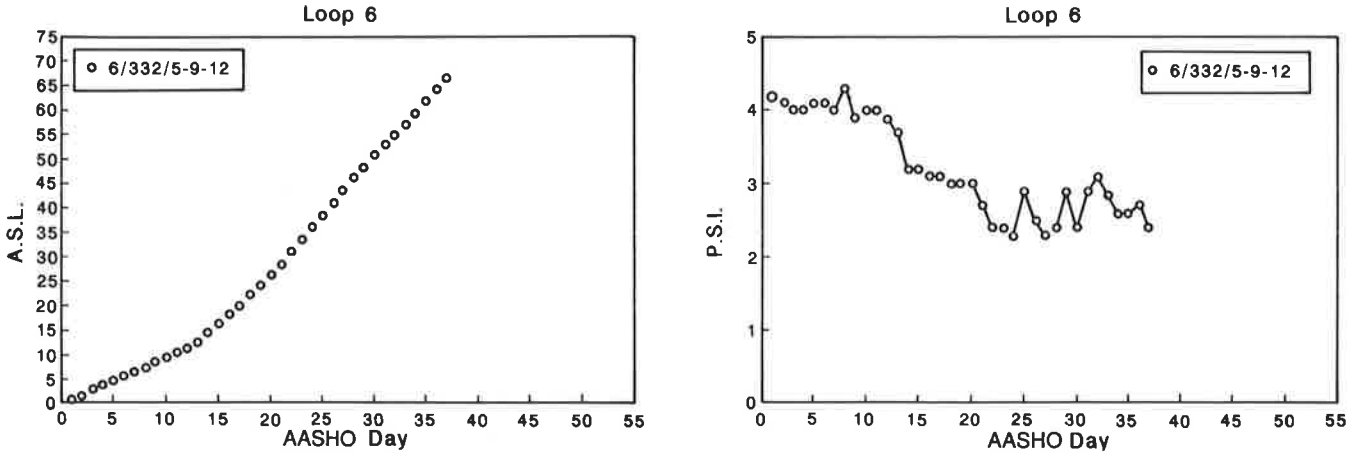

FIGURE 6 AASHO Road Test: accumulated serviceability loss case.

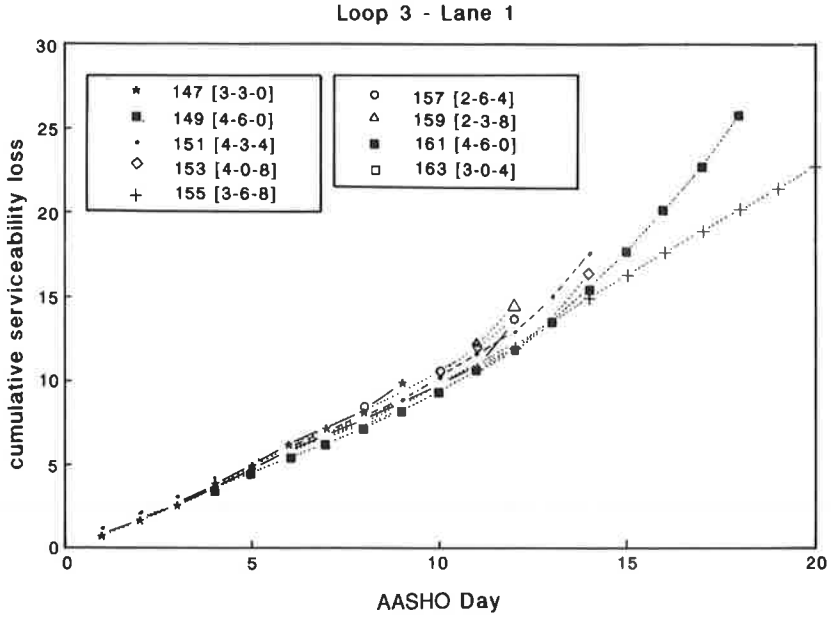

FIGURE 7 AASHO Road Test: ASL plots.

(or survival), certain conclusions could be drawn, i.e., whereas the thicknesses of each individual layer provided a small measure of correlation with the probability of survival, no factor was found to be as significant as the effect of the total physical thickness (surfacing + base + subbase), regardless of the layer thickness combinations.

Although total pavement thickness was particularly significant in this analysis, it is evident that for pavements of the same total thickness, those with thicker surfacing have an enhanced probability of survival. This has been demonstrated by plotting, but the mathematical and statistical analyses are not yet complete.

An example of the first-year survival matrix is given in Figure 8 for Lane 1 of Loop 4 (18-kip single axle), where 1 = survival and 0 = failure (did not survive) (the righthand column under each subbase thickness gives the full pavement thickness for each section). The composite survival regression curves are given in Figure 9 for all the axle weights and types used in the main factorial experiment.

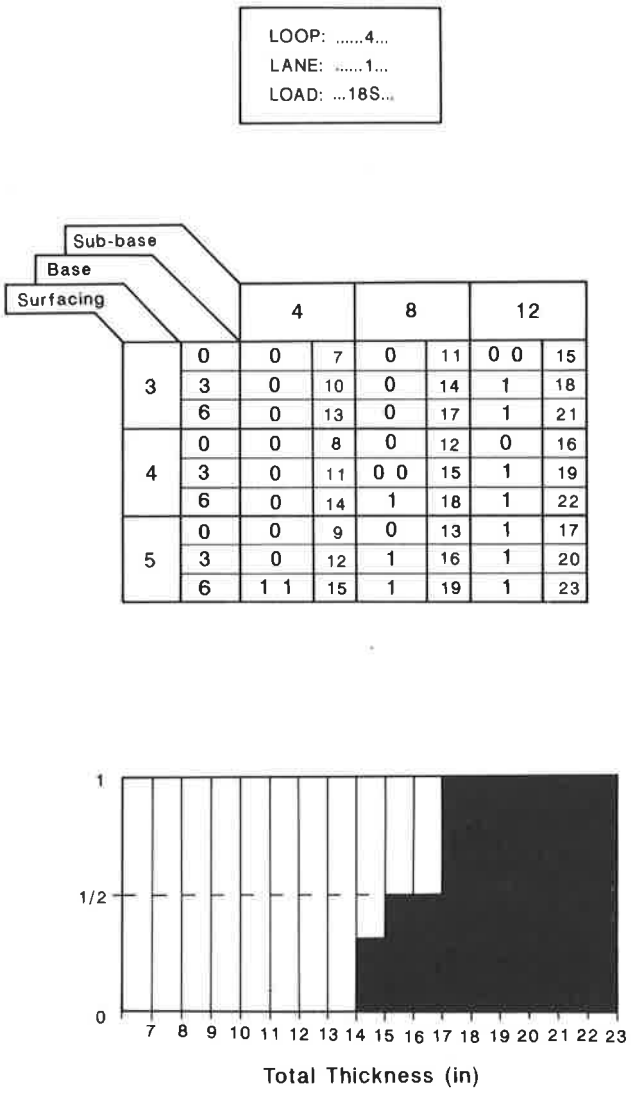

FIGURE 8 AASHO Road Test: one-year survival matrix.

These observations serve to validate the concept of the U.S. Army Corps of Engineers method for frost design, wherein the pavement is first designed from purely structural considerations, and subsequently the total pavement thickness is checked against the anticipated depth of frost penetration.

From the limited data available (two seasonal cycles), the data tend to support the possibility that, among survivors, the probability of survival is Markovian; thus if a pavement has a 0.95 probability of first-year survival, then its 2-year survival probability is 0.95^2, and its n-year survival probability is 0.95^n.

These curves (Figure 9) are of course only applicable to the climatic and subgrade conditions of the Road Test. If the subgrade were free draining, not frost susceptible, or if there were no frost, then it might be reasonable to expect that these curves would translate significantly to the left.

SUMMARY AND CONCLUSIONS

AASHO Model

It has been shown that the AASHO model does not represent the observed behavior of the pavements trafficked at the Road Test. The AASHO model (Equation 1) is biased to more closely represent the behavior of cracked pavement. Within the AASHO model, the layer coefficients are shown to be *secondary regression coefficients* with no direct physical significance. To attribute to them a significance as indicators of strength is spurious. Instead, the layer coefficients are indicators of resistance to serviceability loss.

In the original development of the AASHO model, no cognizance was given to the effect of climate (including its effect on the subgrade support characteristics), i.e., the effect of climate was assumed to be constant from section to section. A tacit assumption was made at the Road Test that all deterioration in pavement serviceability was because of the composite effects of traffic (axle weight and frequency) and pavement structure (materials and layer thicknesses).

However, the present analysis suggests that at Ottawa, Ill., the effect of climate was in fact decisive. The initiating event of all significant deterioration in pavement serviceability was inevitably linked to spring/thaw. The subsequent performance of the trial sections was found to be critically dependent on the observation of Class 2 or Class 3 cracking.

The effect of traffic (frequency) is most difficult to define. However, results of the current analysis indicate that the frequency of loading is critical only during the spring/thaw periods. At other times of the year, the effect of traffic (axle weight) is explicitly clear in the AASHO model (Equation 3a and b); however, the effect of the axle weight is seen to be negligible except in relation to the survival probability, which is significantly affected by the spring/thaw events.

Alternative Analyses

Cusum Analysis

The Cusum analysis outlined in this paper provides a clear method from which the performance of Road Test pavements

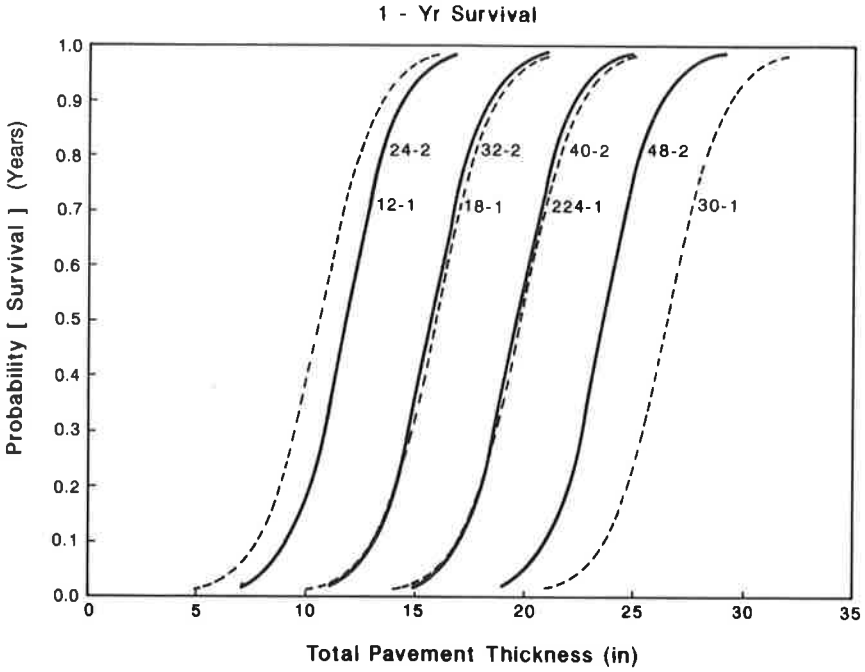

FIGURE 9 AASHO Road Test: survival probability plots.

may be analyzed. The surprising smoothing effect and piecewise linearity lend themselves to the identification of changes in performance. It is anticipated that the study of the Cusum plots and their mathematical basis will provide a more defensible foundation from which to build an alternative pavement performance model.

Probabilistic Analysis

The variability in the factors and parameters associated with pavement design and performance, however well controlled, lends itself readily to a probabilistic analysis. The first analysis presented here clearly demonstrates the power of such an approach.

The new AASHTO Guide (1986) (*1*) advocates the use of reliability concepts. The application of the principles of reliability to empirically derived deterministic formulae (the AASHO model) is fraught with problems during implementation and interpretation. The application of probabilistic methods to pavement design would be better served by a total reanalysis of the Road Test data (and other data bases) from a probabilistic basis; in this fashion the full model (and its submodels) would be internally consistent and far more transportable.

Conclusion

The preliminary results from a study that has highlighted shortcomings in the AASHO model and the interpretation of the Road Test data have been presented. As far as is possible, both observational and mathematical justification for each point raised has been provided.

It is strongly recommended that the AASHO Road Test data be closely scrutinized and reanalyzed in the light of 25 years of hindsight, newer pavement technology tools, and the more recent concepts of probabilistic analysis and reliability. In this way new (and better) models and submodels of pavement behavior and performance may be developed.

ACKNOWLEDGMENTS

The authors wish to acknowledge the patient forbearance of the Indiana Department of Transportation and the FHWA who have tolerated a significant deviation from the original project objective. They also wish to acknowledge and thank Paul Irick and Ron Hudson, both of the original Road Test management team, who listened carefully to the somewhat radical ideas and offered constructive criticism and advice, and who gave the authors the benefit of their individual and collective expertise.

REFERENCES

1. *AASHTO Guide for Design of Pavement Structures*, American Association of State and Highway and Transportation Officials, Washington, D.C., 1986.
2. J. F. Shook and F. N. Finn. Thickness Design Relationships for Asphalt Pavements. *Proc., 1st International Conference on the Structural Design of Asphalt Pavements*, Ann Arbor, Mich., 1962.
3. N. Odemark. Undersökning av elasticitetsegenskaperna hos olika jordarter. Samt teori för berakning av beläggningar enligt elasticitetsteorin. *Statens Vaginstitut meddelande* 77, 1949.
4. *Special Report 61E: The AASHO Road Test: Report 5—Pavement Research*. HRB, National Research Council, Washington, D.C., 1962.

Publication of this paper sponsored by Committee on Flexible Pavement Design.

Thaw Weakening of Pavement Structures in Seasonal Frost Areas

VINCENT C. JANOO AND RICHARD L. BERG

Pavement structures in the northern United States, Canada, Scandinavia, and other seasonal frost areas of the world are subject to freezing in winter and thawing in spring. Most damage to pavements in seasonal frost areas occurs during the spring thaw and, to a lesser extent, during partial thaw periods in winter. To minimize damage, pavement engineers must be able to determine the structural capacity of road and airfield pavements during thawing periods. Four pavement test sections were built in the Frost Effects Research Facility at the U.S. Army Cold Regions Research and Engineering Laboratory in Hanover, N.H., to study the performance of various pavement structures subjected to freeze-thaw cycling. The test sections consisted of asphalt concrete pavement over a clay subgrade, asphalt concrete over crushed gravel on a clay subgrade, asphalt concrete over 178 mm of crushed gravel and 203 mm of clean sand on a clay subgrade, and asphalt concrete over 254 mm of crushed gravel and 127 mm of clean sand on a clay subgrade. Thermocouples were embedded throughout the pavement structure and subgrade, and the pavement structure was subjected to several freeze-thaw cycles. Deflection measurements taken during the thawing periods at four locations in each test section used a Dynatest falling-weight deflectometer (FWD) to validate existing back-calculation procedures for pavements subject to seasonal frost. Soon it became apparent that the back-calculation procedures had difficulties. Another study was initiated to determine if additional information pertaining to freeze-thaw cycling could be obtained from the FWD measurements. The results of the second study are presented.

A pavement evaluation procedure reveals the allowable traffic that a pavement can support for a given loading condition or the allowable load for a given amount of traffic. This allowable traffic is assumed to be applicable at any time of the year, which may be an adequate approximation in non-frost areas. However, seasonal changes in the thermal and moisture regimes of a cold regions pavement structure can greatly affect its (the structure's) bearing capacity and substantially change the allowable traffic loads.

Pavement structures in seasonal frost areas are subjected to freezing in winter, thawing in spring, and intermittent thawing during the winter season. In the winter, the pavement structure modulus increases because of ice bonding of particles in the unbound base and subgrade and in the asphalt layer because of the influence of temperature on the viscosity of the asphalt. During spring thaw, the pavement foundation can become saturated with water from thawing ice lenses, thus reducing the structural adequacy of the base or subgrade, or both. The permeability of the subgrade and existing frozen layers can restrict the drainage of excess water. Therefore, one can expect most damage to occur during the spring thaw period and, to some extent, during the partial winter thaws. Damage to the pavement structure will reveal itself on the surface in the form of fatigue cracking and rutting caused by deformation in the base or subgrade. The length of time a pavement structure is subjected to thaw weakening will vary depending on the frost depth, soil type, degree of saturation, and drainage conditions (*1–5*).

There are several ways to determine pavement strength during thaw. Strength determinations can be made by using destructive methods, such as coring in conjunction with laboratory testing; with the present types of nondestructive testing equipment, for example a falling-weight deflectometer (FWD); or with existing estimated reduction factors (*6–8*). Reduction factors that have been applied in the spring vary from 50 to 85 percent of autumn values. This estimation of strength during thaw periods then allows the appropriate authorities to impose or remove load restrictions to minimize damage to pavements. Using the reduction factors over the entire spring period may be overly conservative on load restrictions.

The U.S. Army Cold Regions Research and Engineering Laboratory (CRREL) is currently developing a nondestructive pavement evaluation procedure for seasonal frost areas using an FWD. Data are lacking on the response of pavements founded on fine-grained subgrade soils subjected to freeze-thaw cycles. To study this effect, test sections were built in the Frost Effects Research Facility (FERF) and subjected to several cycles of freezing and thawing. During the thaw cycles, the pavement response was monitored using the FWD.

This paper describes the test sections, the instrumentation of the pavement sections, and the results of the FWD testing. Further details can be found in a forthcoming CRREL report (*9*).

TEST SECTIONS

Four test sections were constructed in the CRREL Frost Effects Research Facility, which has an interior area of 2,694 m^2 and incorporates 12 test cells (TC) and basins (Figure 1). The test cells in which the pavement structures were built (TC-1–3) are 6.4 m wide, 7.6 m long, and 2.4 m deep. With the exception of TC-1 and TC-2 (Figure 1), all other test cells and basins have concrete floors. TC-1 and TC-2 are founded on a natural till subgrade. The refrigeration system in the FERF can maintain air temperatures in the building between -4°C and 24°C and within a tolerance of ± 3°C. Individual test cells or test basins are generally cooled by placing freezing panels on the surface. A minimum temperature of -35°C maintained within a tolerance of ± 0.8°C is available to the panels.

U.S. Army Cold Regions Research and Engineering Laboratory, 72 Lyme Rd., Hanover, N.H. 03755.

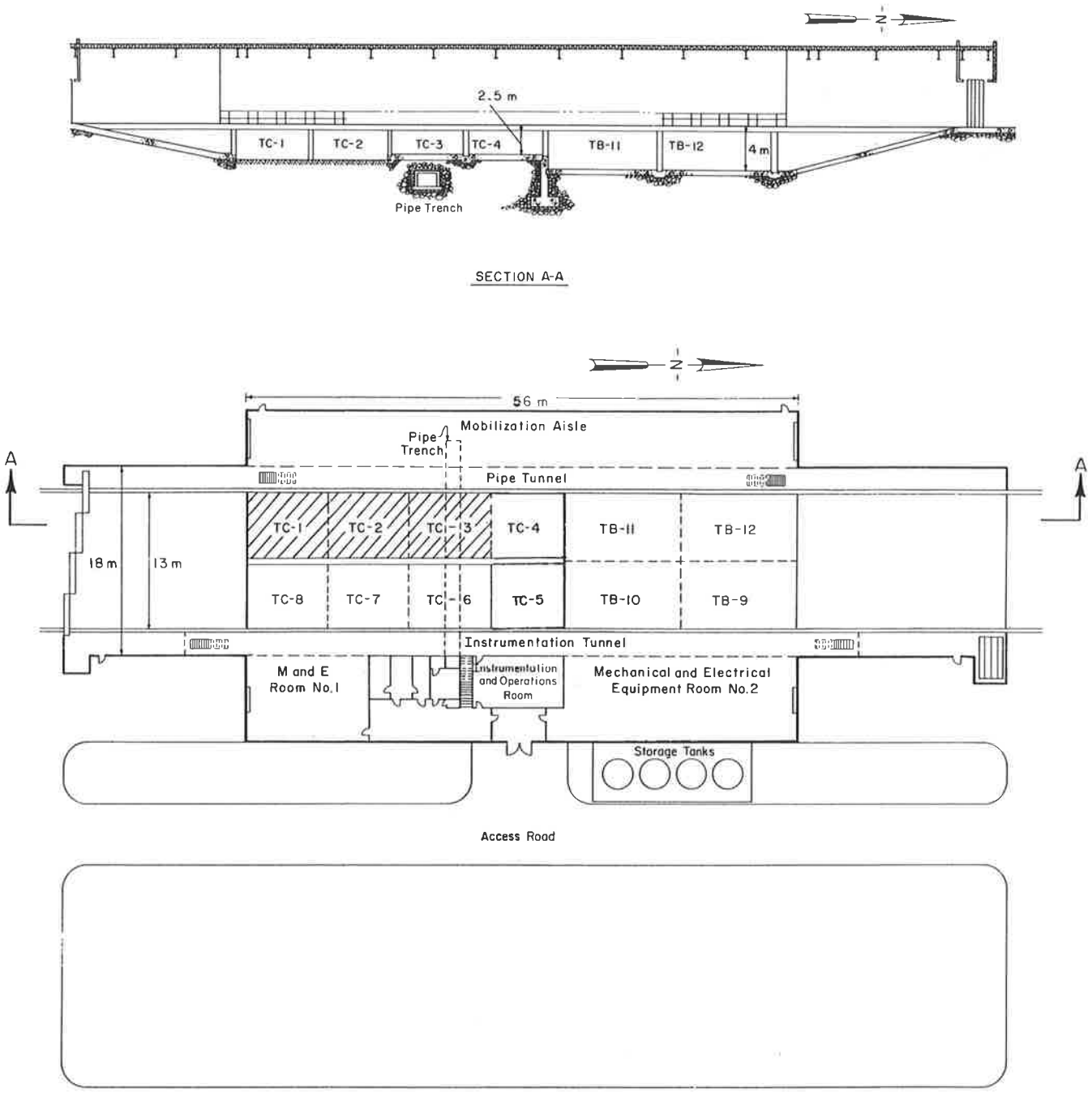

FIGURE 1 Plan and cross-section of Frost Effects Research Facility.

The test sections were 610 cm by 533 cm and 160 cm deep. Test section 1 was extended 150 cm from TC-1 into the ramp area (Figure 1). Cross-sections of the four test sections are shown in Figure 2. Test sections 1 and 2 are full-depth asphalt (152-mm) concrete pavements. The minimum 102 mm of free-draining base, required by the Corps of Engineers in seasonal frost areas, was included in test section 2. Test section 3 was made up of 51-mm asphalt concrete pavement on a 178-mm base course over a 203-mm clean gravel subbase. Test section 4 consisted of a 51-mm asphalt concrete pavement and a 254-mm base course over a 127-mm sandy subbase. A 6.4-mm-thick woven filter fabric was used as a separator between the base and subgrade in TS-2 and between the subbase and subgrade in test sections 3 and 4.

The grain size distribution for subgrade, base, and subbase materials is presented in Figure 3. The subgrade was constructed of clay obtained near the town of Fort Edward in upstate New York. The in situ moisture content of the clay was between 38 and 41 percent. The clay was classified as inorganic and of high plasticity (CH) according to the Unified

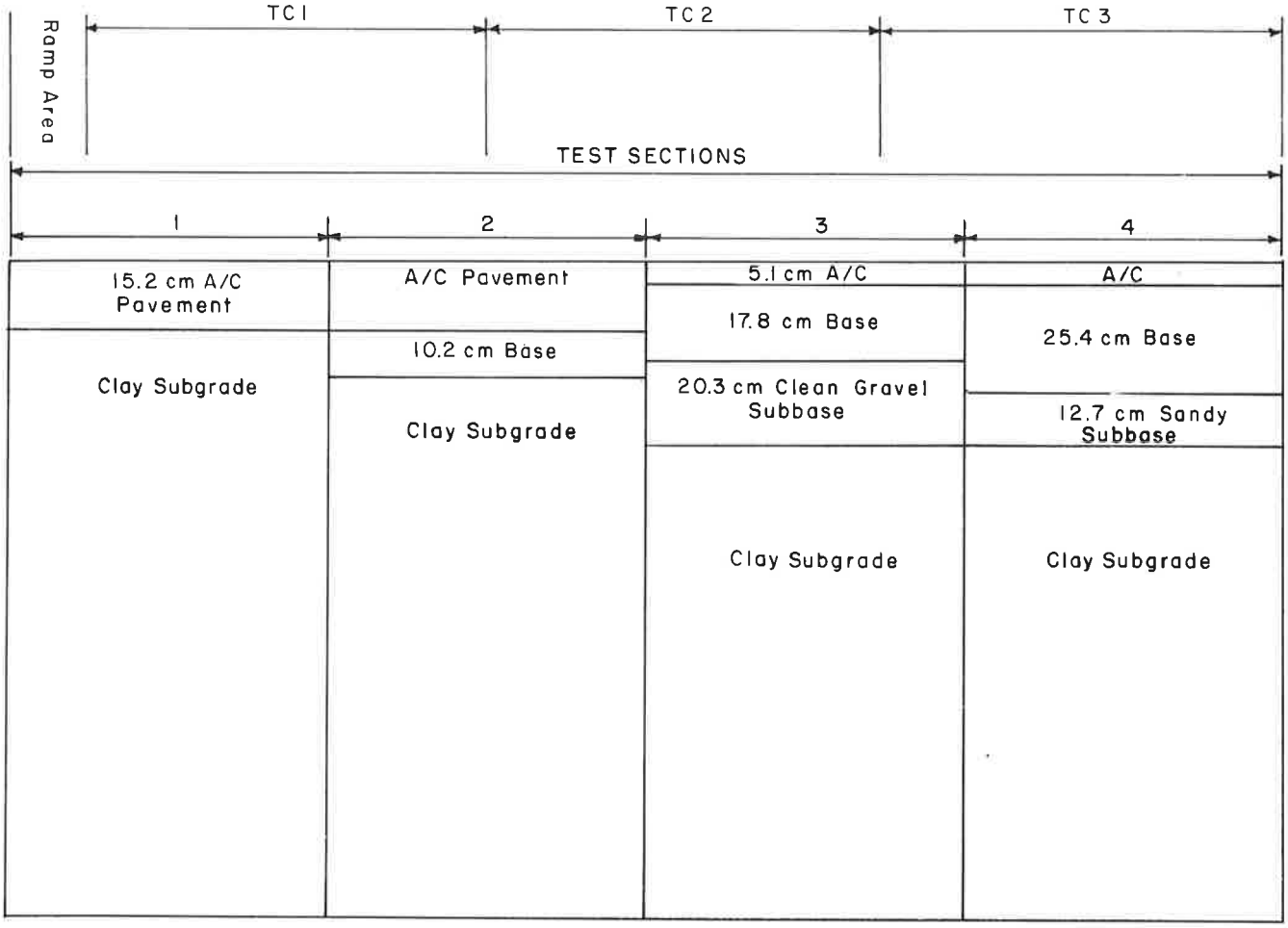

FIGURE 2 Cross-section of test sections.

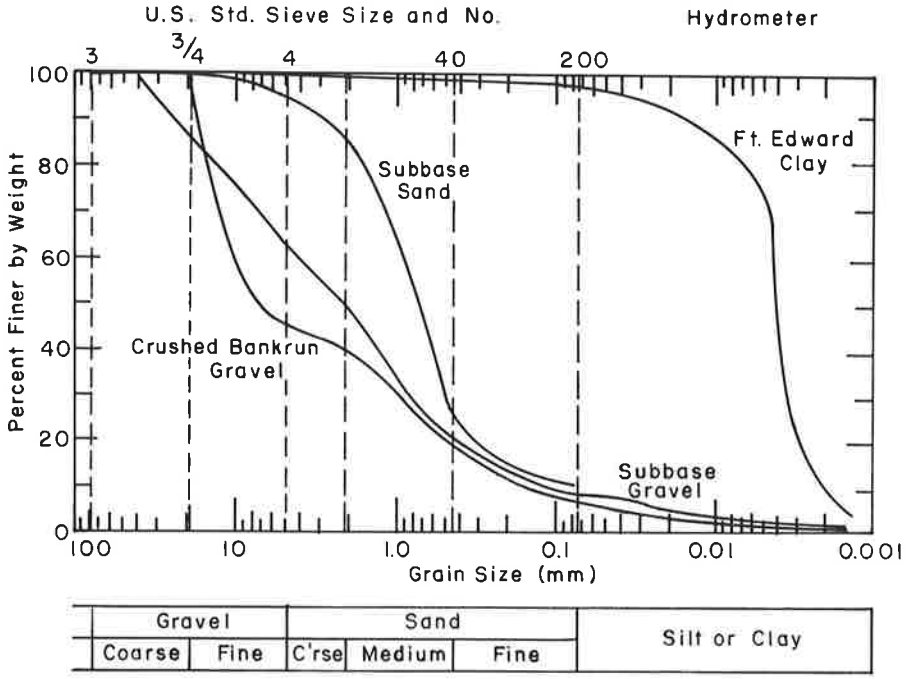

FIGURE 3 Grain-size distribution of test material.

Soil Classification System. Other properties of the clay are presented in Table 1. Based on grain size and Atterberg limit analysis, the clay was classified as an F3 soil with respect to frost susceptibility. From frost-heave laboratory tests, the heave rate was determined to be 0.8 mm per day, which can be considered negligible (*10*).

The base course (Table 1) used in test sections 2, 3, and 4 was crushed bankrun gravel obtained from a gravel pit in West Lebanon, N.H. The material had a coefficient of uniformity (C_u) of 47 and a coefficient of curvature (C_c) of 0.5. The amount of material passing the No. 200 sieve was less than 5 percent. It was classified as a poorly graded gravel with little fines (GP). The final densities of the base course ranged from 2.11 to 2.19 g/cm^3, and water contents ranged from 2.7 to 3.4 percent.

Two subbase materials (Table 1) were used in test sections 3 and 4. In test section 3, the subbase material had a C_u of 30.5 and a C_c of 1.2. The material had more than 50 percent passing the No. 4 sieve and 7 percent passing the No. 200 sieve. It was classified as a gravelly sand with little fines (SW-SC) using the Unified Soil Classification System. The gradation for this material is shown in Figure 3 as "subbase gravel." In test section 4, the subbase material had a C_u of 7 and a C_c of 3.0. The material had more than 90 percent passing the No. 4 sieve and 8 percent passing the No. 200 sieve and was classified as a poorly graded sand with little fines (SP-SC). The gradation of this material is shown in Figure 3 as "subbase sand." The subbase materials were assumed to be compacted at their natural water content of 3.0 percent in test section 3 and 4.4 percent in test section 4.

The asphalt concrete layers in TS-1 and TS-2 consisted of 101 mm of black base and 51 mm of wearing course. The base course was designated as Type B and the wearing course, Type E in the New Hampshire State specifications. The asphalt used for all of the AC layers was an AC 20 (absolute viscosity at 60°C of 2,065 poise; kinematic viscosity at 135°C of 400 cst; penetration at 25°C of 80 dmm; and Penetration Viscosity Number of −0.44. The optimum asphalt content for the base course was 5.25 percent and for the wearing course, 6.4 percent. In TS-3 and TS-4, the AC layer was 51 mm thick, laid in two 25.5-mm lifts. It met all the specifications for the New Hampshire Type E wearing course.

PAVEMENT INSTRUMENTATION

The test sections were instrumented with thermocouples and electrical resistance gauges. The location of these gauges in the test sections is shown in Figure 4. Temperature measurements were made with copper-constantan thermocouples that were placed 152 mm apart in the clay subgrade and 51 mm apart in the subbase, base, and AC layers (with some exceptions). The temperature measurements were taken at a single location in each test section and were assumed to be representative throughout the respective test sections. Determining frost penetration by temperature measurements alone has two disadvantages. First, impurities in the soil/water system tend to depress the freezing point below 0°C. Second, during spring thaw, subsurface temperatures can become nearly isothermal at 0°C.

To overcome this problem, sensors to measure the resistivity of soils during freezing and thawing have been developed at CRREL (*11*). It has been found that water containing small quantities of impurities, such as groundwater, has a typical volumetric resistance of approximately 20 kΩ. Frozen groundwater has a volumetric resistance of from 100 kΩ to several megaohms. A schematic of a resistance probe is shown in Figure 5. The wooden dowel and sensors were placed in a 76-mm-diameter hole to the various depths shown in Figure 5. The holes were then backfilled and compacted in 152-mm lifts using a wooden dowel as a compactor. Measurements were taken every 4 hours, and the data were stored on magnetic tape. Typical temperature and resistance measurements for locating the freezing or thaw depths are shown in Figures 6 and 7.

TESTING PROGRAM

Deflection measurements were obtained using a Dynatest 8000 falling-weight deflectometer at the end of subgrade placement, at the end of construction of the pavements, and during the thawing periods. The test sections were subjected to five freeze-thaw cycles. Traffic was applied during the third and fifth thaw cycles, but the analysis presented in this paper is concerned primarily with the first two freeze-thaw cycles dur-

TABLE 1 PROPERTIES OF CLAY, BASE, AND SUBBASE

	Subgrade	Base	Subbase
Unified Soil Classification System	CH	GP	SW
Specific gravity (G_s)	2.79	2.8	2.8
Liquid limit (LL)	64	-	-
Plastic limit (PL)	28	-	-
Plasticity index (PI)	36	-	-

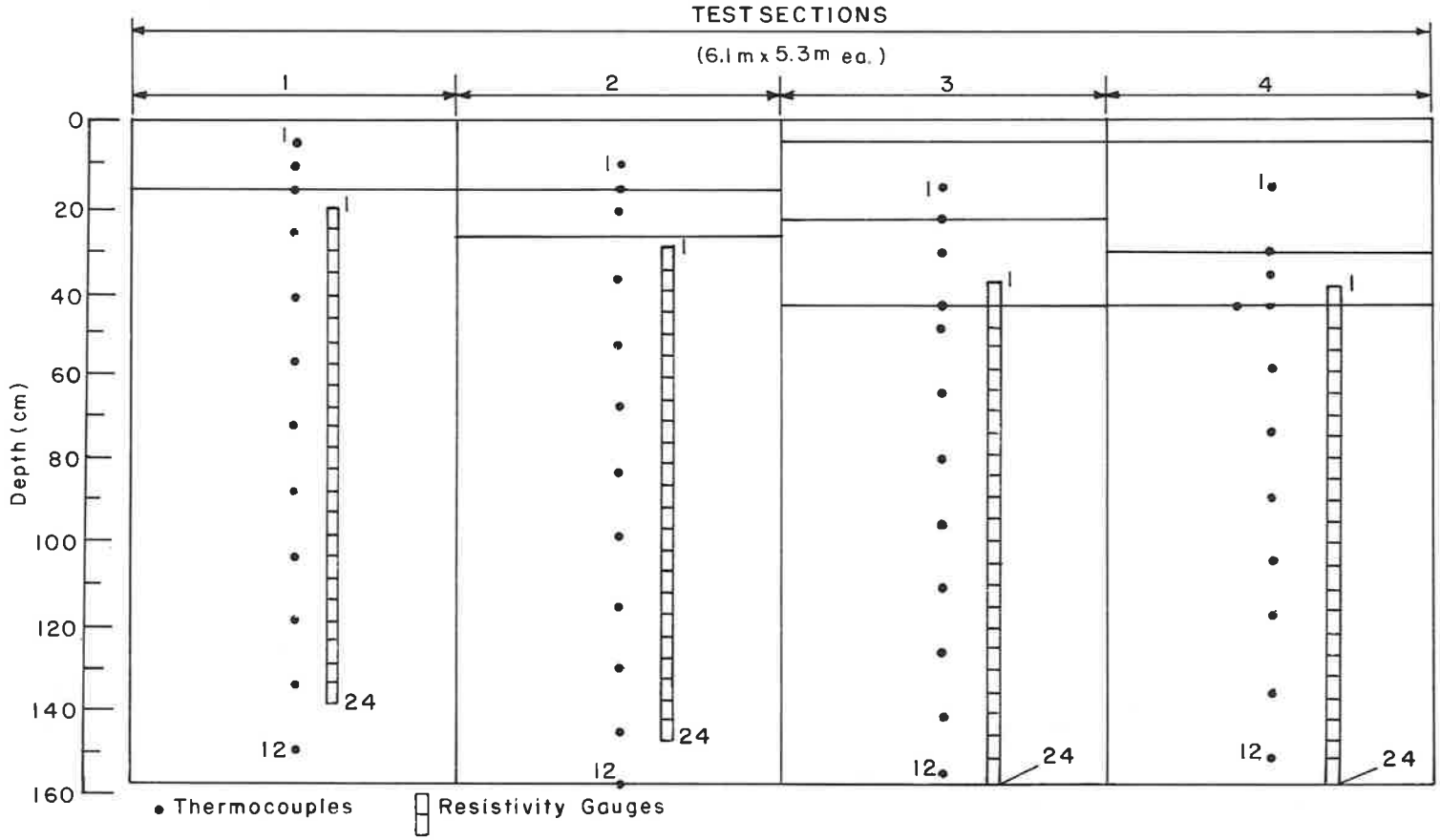

FIGURE 4 Location of thermocouples and resistance gauges in test sections.

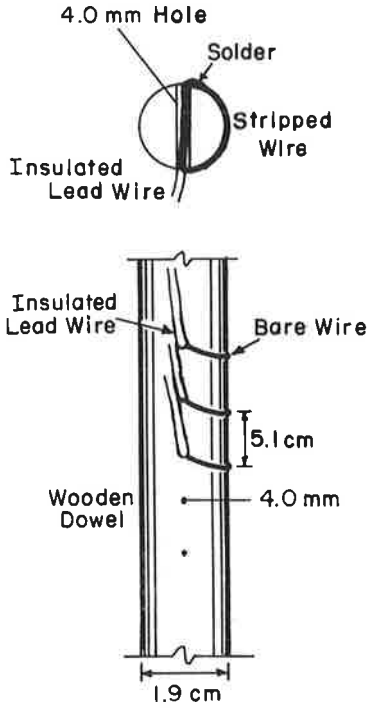

FIGURE 5 Schematic of resistance probe.

ing which the changes in the strength of the pavement structure were caused only by thermal effects.

The test sections were frozen from the top down by placing cooling panels on the surface of the pavements. Freezing was stopped when the frost penetration reached the target depth. This depth was 122 cm for the first cycle and 152.4 cm (the bottom of the test basins) for the second cycle. The freezing rate in the clay subgrade was calculated to be close to 16.5 mm per day during the first freeze cycle and approximately 25.4 mm per day during the second freeze cycle. Berg (*4*) has reported that frost penetration in the field is in the range of 6.4 to 25.4 mm per day. Deflection measurements were taken once a day during the thaw periods at four locations in each test section. Four load levels, composing a set, were used during the thaw cycles: 27, 40, 50, and 67 kN. At each location, each of the load levels was applied twice and two sets of deflection measurements were recorded. The FWD measurements on the pavements were conducted using a 30-cm-diameter plate, with the sensors located at 0, 17.5, 30, 70, 110, 150, and 245 cm.

Thawing of the pavement structure was induced by changes in the ambient building temperature. The temperature during the first two thaw cycles is shown in Figure 8. During the first cycle, the air temperature in the FERF ranged from 15°C to 36°C and during the second thaw cycle it ranged from 4°C to 19°C. The corresponding thaw depths (located by the 0°C isotherm) during the thaw cycles in all test sections are presented in Figures 9 and 10. The average thaw rate during the first thaw cycle was 45 mm per day. During the second thaw cycle, the average thaw rate was 27 mm per day.

ANALYSIS OF FWD DEFLECTION DATA

A representative deflection basin was used to characterize the structural change in the pavement structures during the thaw periods. It was selected with the BASIN program developed at the U.S. Army Corps of Engineers Waterways Experiment Station. The program averages the deflections for a given load (in this case four deflection basins at each load level, because only the second set of deflections from each location was used) and calculates the area of the averaged deflection basin. It then compares the deflection measurements at each location with the averaged values and chooses the input deflection basin that is closest to the averaged basin and area as the representative basin.

We used BASIN to obtain representative 40- and 50-kN-load deflection basins for further analysis. These load levels were of interest to us because one represents current allowable loading conditions (40 kN), and the other (50 kN) could represent high tire pressure loadings, which are more detrimental to thaw-weakened pavements.

Before freezing, FWD measurements were conducted on all the pavement test sections (Figure 11). It can be seen from the figure that the full-depth pavements (TS-1 and TS-2) have lower deflections than their counterparts (TS-3 and TS-4). Based on similar moisture and density measurements in the subgrade in all the test sections (*9*), it was concluded that the difference in the deflection basins in Figure 11 was because the pavement structure was different above the subgrade. Higher deflections from the same applied load signifies a lower modulus, which usually signifies lower shear strength (*12,13*). Based on the above conclusion and on inspection of the deflection basins in Figure 11, one can further conclude that the fourth sensor (70 cm from the center) apparently measured the deflection of the subgrade caused by the applied load. This fourth-sensor deflection was used to characterize the subgrade response during the thaw period as well as to determine the thaw depth. The deflection basins in Figure 11 were also used as reference basins during the thaw cycles.

Typical deflection basins during the first and second thaw cycles for the 40-kN load levels for TS-1 and TS-3 are presented in Figures 12 and 13. The figures clearly show that, as the thaw depth increased, the deflections increased, which, as mentioned previously, can be related to loss of strength of the pavement structure. Similar observations were seen in TS-2 and TS-4. In the second thaw cycle, some recovery was seen (Figure 13). However, in the interest of time, this recovery process was not continued to its conclusion.

Several parameters were studied to characterize pavement response during the thaw period. These parameters were the impulse stiffness modulus (ISM), center deflections, fourth-sensor deflections, and deflection basin areas. The ISM (*14*) is defined as the ratio of the applied FWD load to the corresponding center deflection and is equivalent to the spring constant k in an elastic system. The ISM was found to distinguish various pavement structure types (Figure 14). The full-depth pavement (TS-1 and TS-2) structures show higher ISM values than their TS-3 and TS-4 counterparts. However, the differentiation in ISM in any one pavement structure during thaw is difficult to discern.

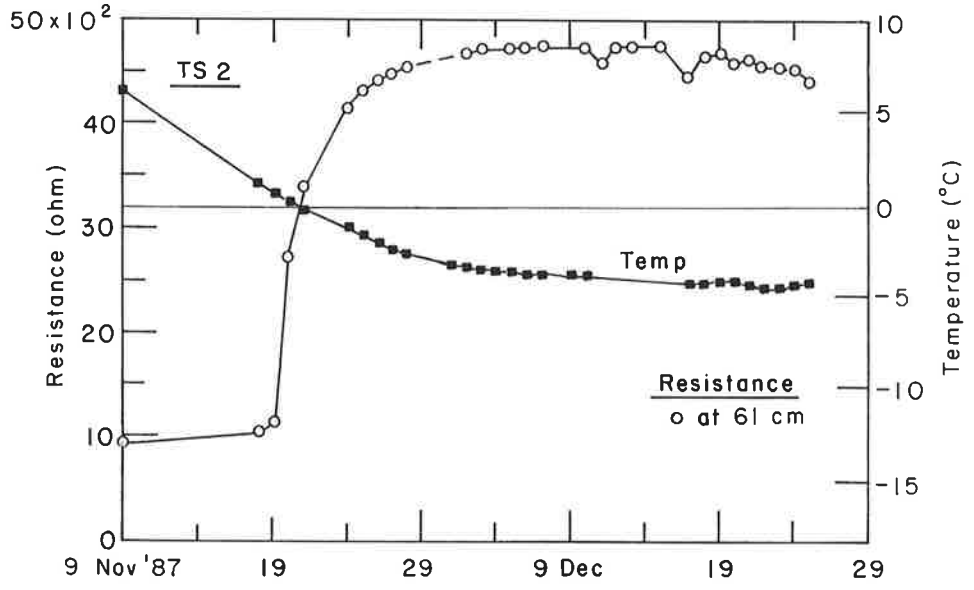

FIGURE 6 Typical temperature resistance measurements for locating freezing front.

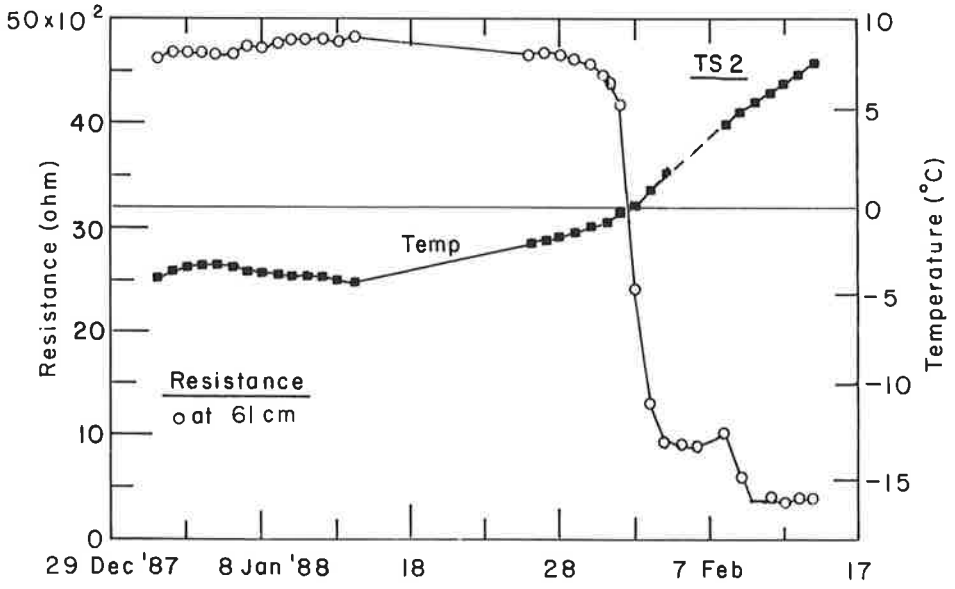

FIGURE 7 Typical temperature resistance measurements for locating thaw depth.

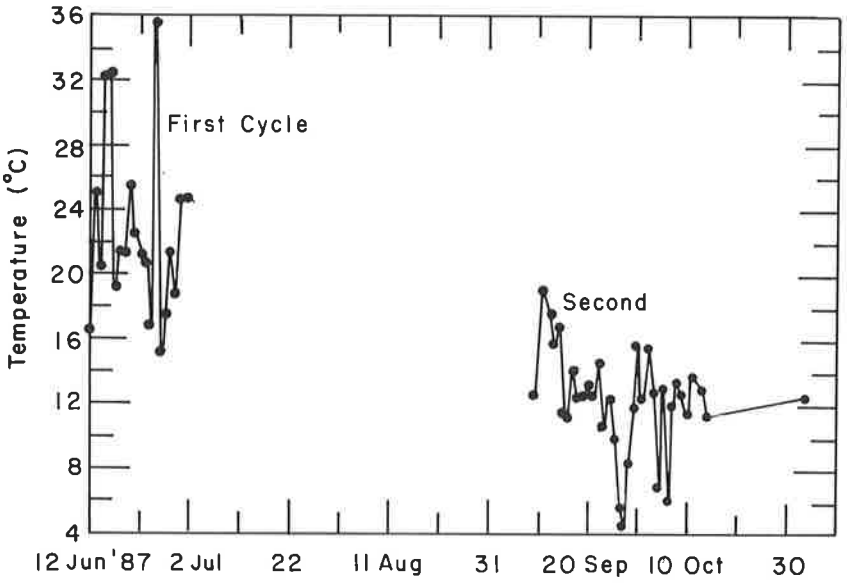

FIGURE 8 Ambient temperature in FERF building during thaw cycles.

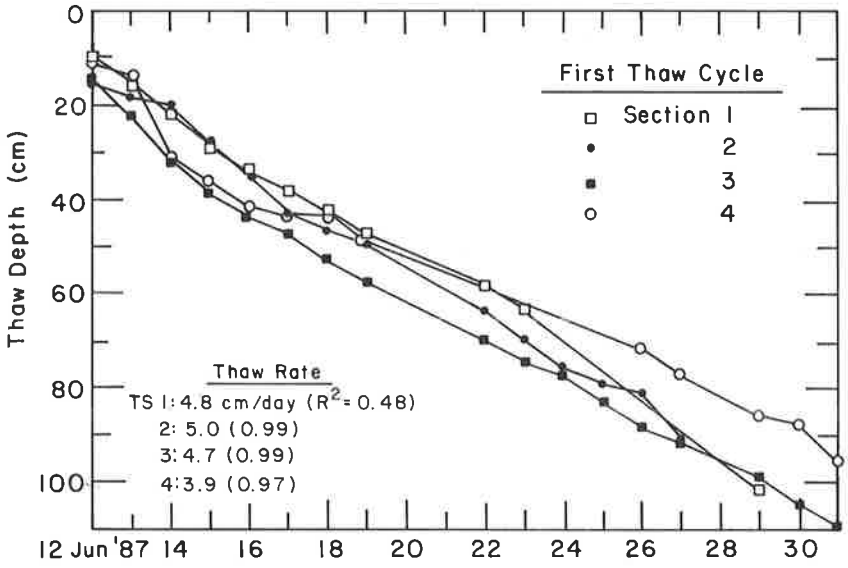

FIGURE 9 Change in thaw depth with time (first cycle).

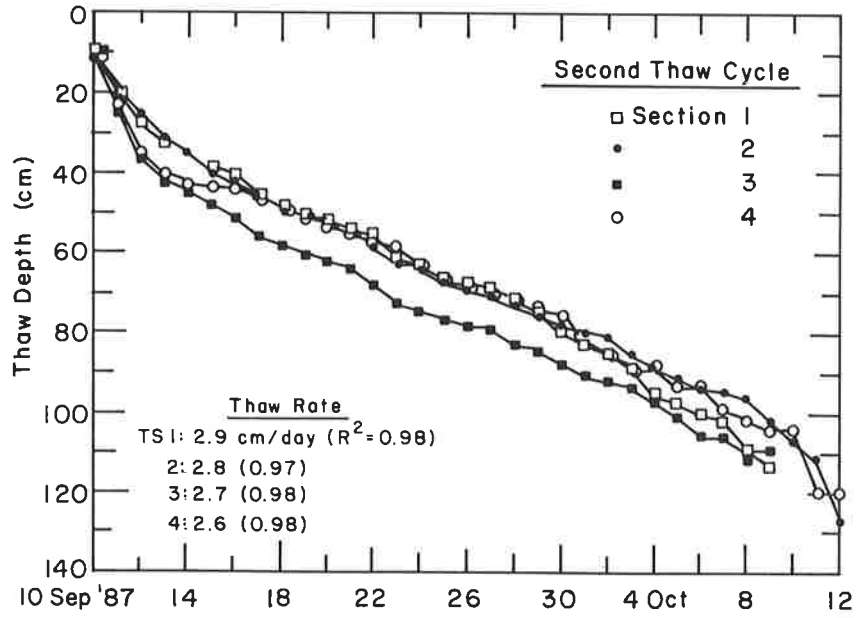

FIGURE 10 Change in thaw depth with time (second cycle).

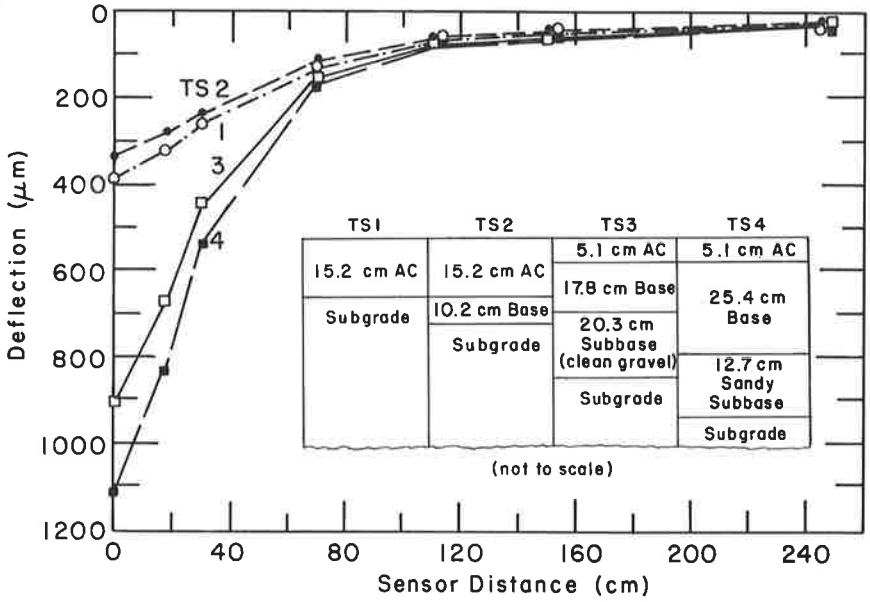

FIGURE 11 Mean deflection basins for all test sections before freezing.

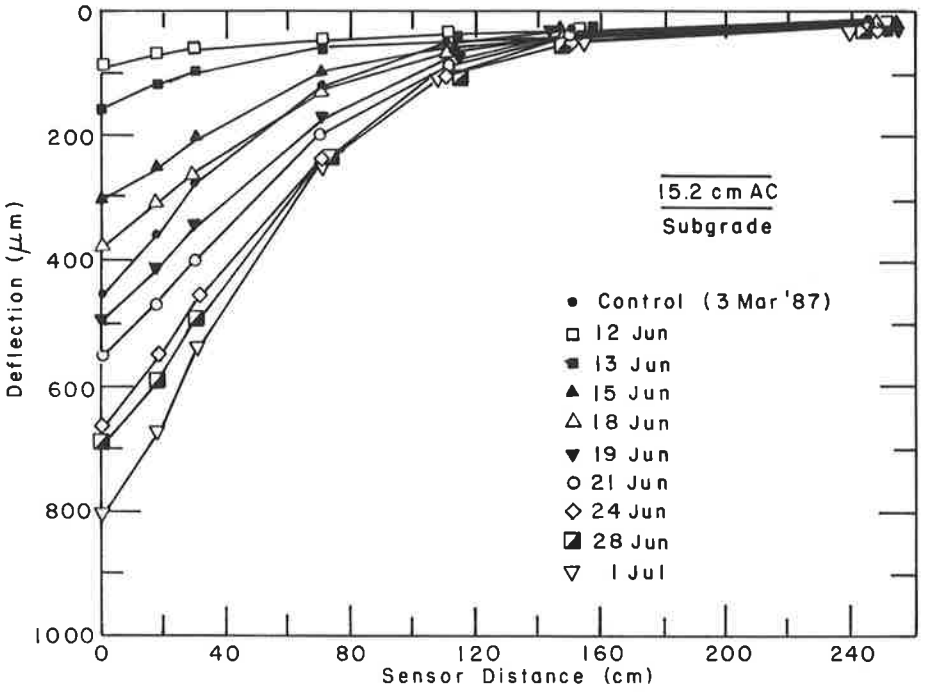

FIGURE 12 Variation of deflection basin area with time in TS-1 (first cycle).

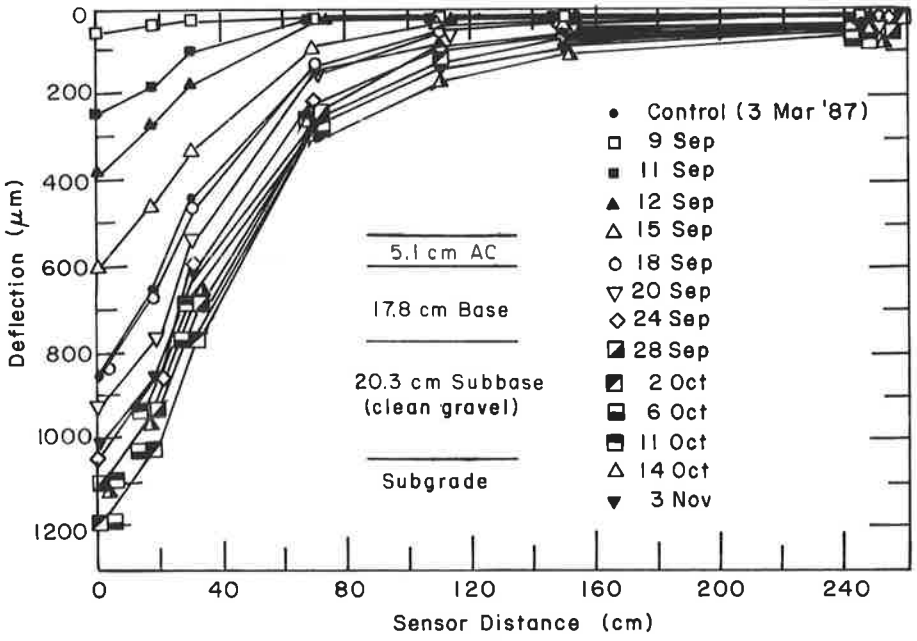

FIGURE 13 Variation of deflection basin area with time in TS-3 (second cycle).

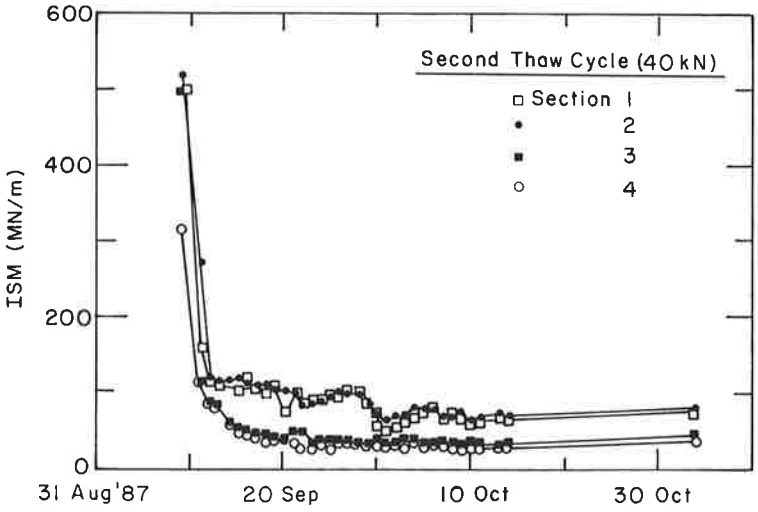

FIGURE 14 Variation of impulse stiffness modulus (ISM) with time (second cycle).

When center deflections are used, it is recommended (*14*) that temperature corrections be applied to the measured deflections or ISMs to account for the deflection of the asphalt concrete pavement at high temperatures. A temperature correction factor based on the ISM values obtained from the test sections was developed. The correction factor (CF) for a thawing pavement structure was determined from

$$CF = \frac{\delta_0 \text{ at } 20°C}{\delta \text{ at other temperatures}}$$

The results are shown in Figure 15. The correlation between the correction factors developed from the test sections and that developed by Bush (*14*) is poor. Similar results were found with TS-1. No attempt was made to determine correction factors for TS-3 and TS-4 because the asphalt concrete thickness was only 51 mm. Bush (*14*) found that for pavement thicknesses less then 76 mm, other factors such as moisture conditions, accuracy of FWD load, and deflections had a greater influence on the measured deflection than did temperature.

It was also found (*9*) that, during the thaw period, approximately 90 percent of the total deflection can be attributed to the deflection of the layers below the asphalt concrete. It was concluded that during winter and spring, and possibly during autumn, correction factors are unnecessary. However, in summer, because of high temperature ranges, correction factors are a critical part of the evaluation procedure.

The other parameters—center deflection, fourth-sensor deflection, and basin areas—showed great promise for use

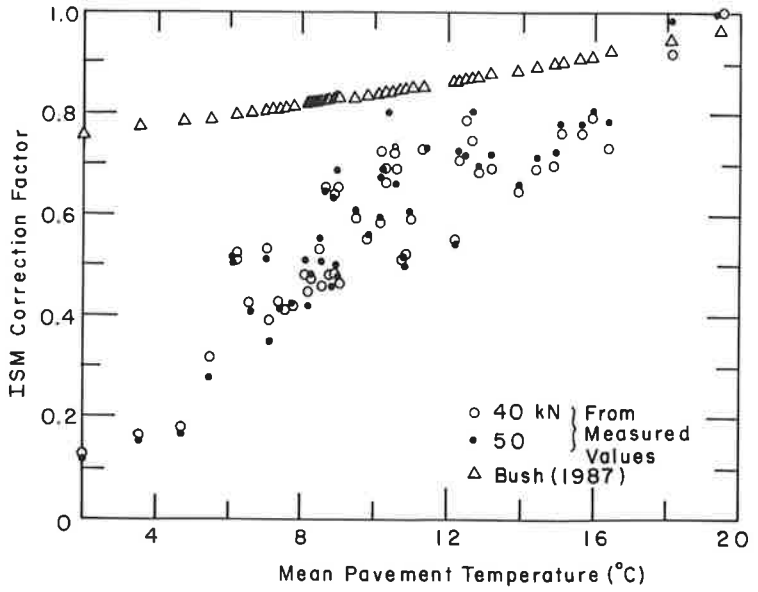

FIGURE 15 Comparison of WES correction factors with correction factors developed from measured deflections.

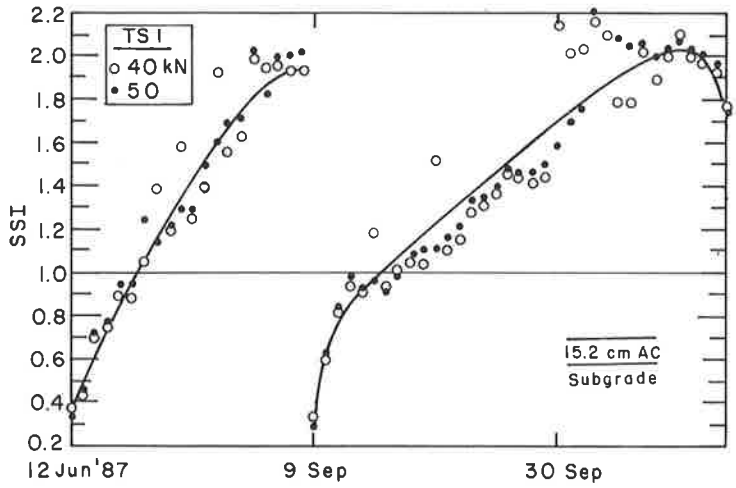

FIGURE 16 Change in the subgrade strength index (SSI) with time in TS-1.

in characterizing pavement response during thaw. However, to be usable all year around, it was decided that the fourth-sensor deflection, which appears to characterize the response of the subgrade only, is the one to use. It is proposed that the ratio of the fourth-sensor deflection during thaw to the same sensor deflection measured before freezing is an indicator of the subgrade strength. This ratio, called the subgrade strength index (SSI) was used to characterize the subgrade strength during thaw. The use of the deflections 70 cm from the center is similar in concept to utilizing the last sensor deflection with the Dynaflect device (placed 124 cm from the center) to characterize the subgrade response.

The variations in SSI with time for TS-1 and TS-3 are shown in Figures 16 and 17. Similar responses were seen in TS-2 and TS-4. The smaller numbers relate to winter conditions and, as thaw progresses, the SSI increases. As seen during the second cycle, this number starts to drop as recovery starts. The data presented in this fashion clearly show the reduction in the subgrade strength (a factor ranging from 2 to 2.2) during thaw. It can also be seen in Figure 17 that the SSI does not change significantly until the thaw depth reaches the bottom of the subbase, i.e., 42 cm from the surface. The results also suggest that in clayey materials recovery from thaw takes time and is not rapid, as suggested by some models.

As mentioned above, the deflection basin areas were studied to characterize the strength of the subgrade during thaw. This concept is similar to that developed by Hoffman and Thompson (*15*), who used the center deflection and a normalized deflection basin area bounded by the first four sensors to characterize pavement performance. We calculated the basin area bounded by the fourth, fifth, sixth, and seventh sensors and their respective deflection measurements. When the ratio of the basin area to the basin area before freezing was plotted with respect to time, the curves were similar to SSI.

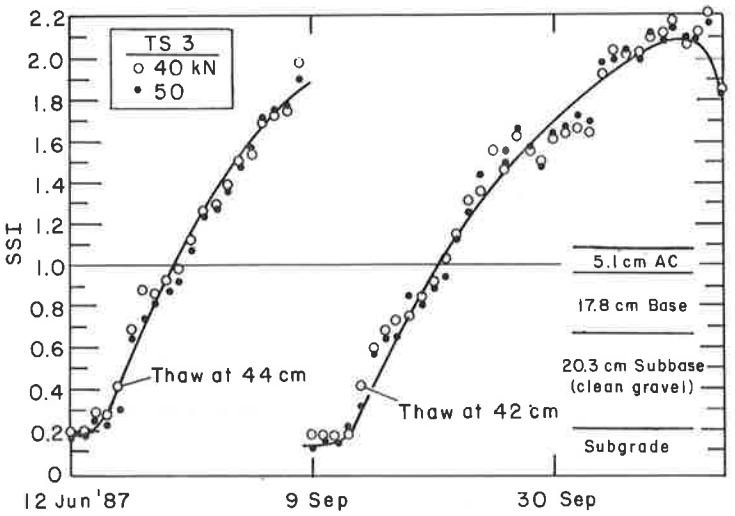

FIGURE 17 Change in the subgrade strength index (SSI) with time in TS-3.

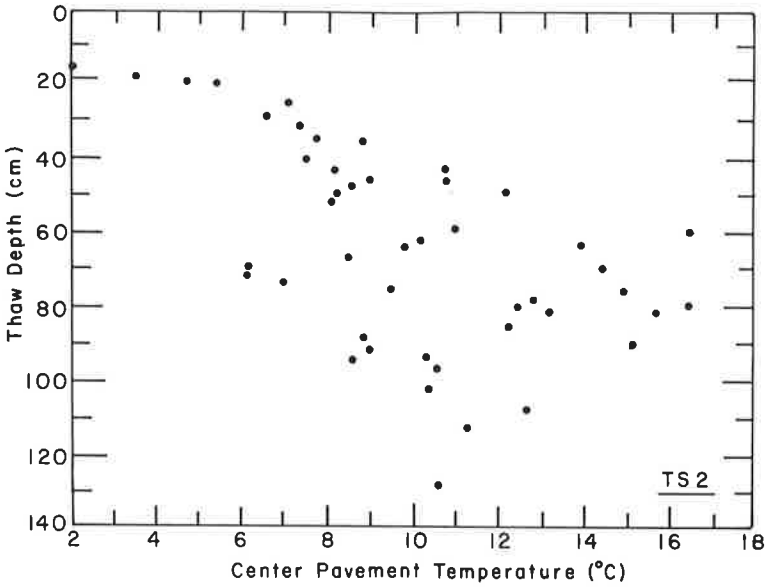

FIGURE 18 Variation in center pavement temperature with measured thaw depth in TS-2.

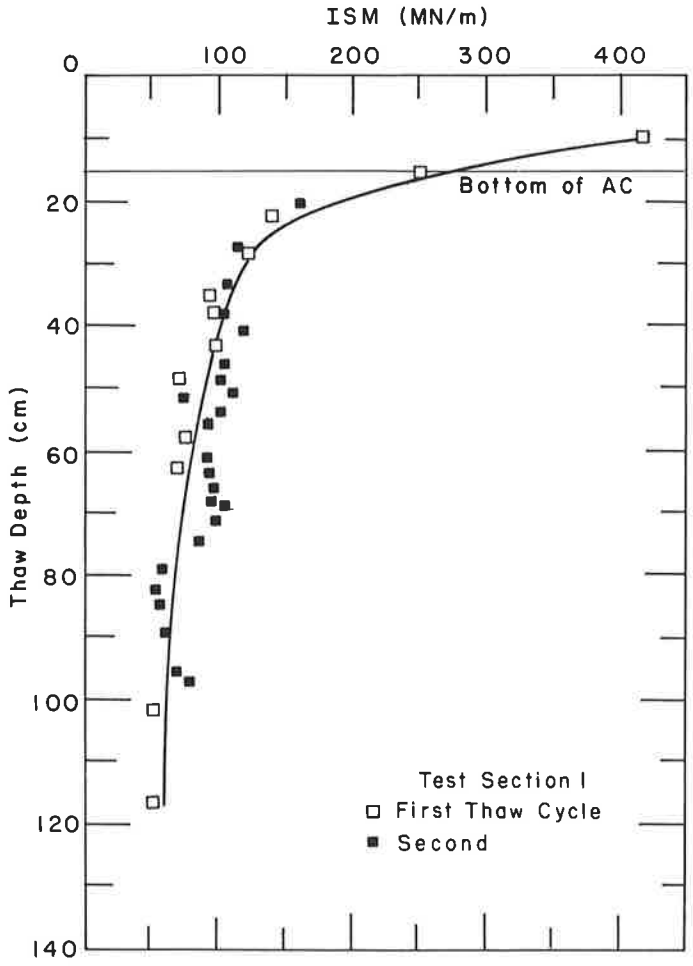

FIGURE 19 Change in ISM with measured thaw depth in TS-1.

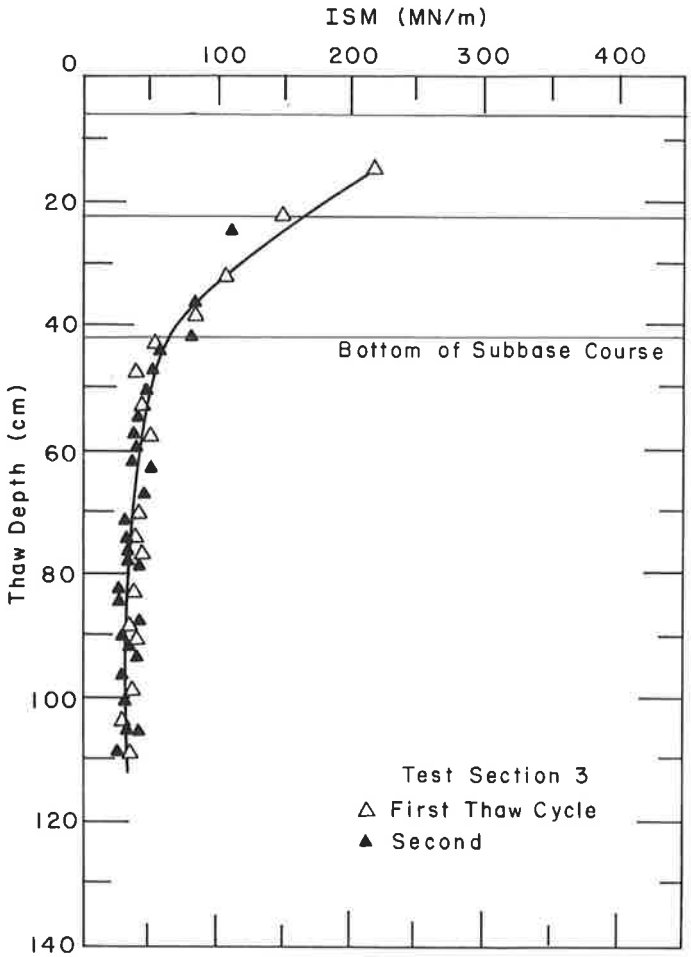

FIGURE 20 Change in ISM with measured thaw depth in TS-3.

ESTIMATING THAW DEPTH

The locations of the thaw depth have been used for imposing/removing load restrictions on pavements. Connor (*16*) found that, when back-calculating layer moduli in thawing pavement structures, knowing the location of the thaw depth was critical. The thickness of the thawed layer was found to affect the outcome of the back-calculated layer moduli. Currently there are no techniques for predicting thawed-layer thicknesses from NDT data (*16*). However, the authors feel that methods such as the modified Berggren equation or finite element or finite difference techniques could be used to estimate thaw depths. As an alternative, we investigated the possibility of using pavement temperatures and/or the deflection measurements (ISM, basin area, fourth-sensor deflections, or a combination of these parameters) to estimate thaw depth. In clay subgrades, especially with full-depth sections, the thawed-layer thickness will nearly correspond with the thaw depth because of the low permeability of the clay.

Pavement Temperature

The simplest prediction of thaw depth would be based on the pavement temperature. Figure 18 shows the variation of thaw depth with mid depth pavement temperature in TS-2. There was a poor correlation between pavement temperature and thaw depth; similar observations were made in TS-1 and TS-3.

Impulse Stiffness Modulus (ISM)

The ISM, as mentioned earlier, is equal to the FWD load divided by the center deflection; it has been used as an indicator of the bearing capacity of various pavement structures. The ISM, with respect to thaw depth for TS-1 and TS-3, is shown in Figures 19 and 20. A similar response was seen in TS-2 and TS-4. In TS-1, when thaw occurred in the subgrade, the ISM varied between 50 and 100 MN/m. The ISM dropped rapidly from about 300 to 100 MN/m, a factor of 3, when the thaw depth was between 15 and 30 cm. In TS-3, once thaw reached the subgrade, the ISM remained fairly constant at approximately 30 MN/m. It is interesting to note that the ISM changed the most, from about 200 to 30 MN/m, a factor of nearly 7, when thaw was in the base and subbase layer.

The ISM was found to distinguish between frozen and thawed pavements, but it remained fairly constant with thaw depth when thaw was in the subgrade. It was concluded that thaw depth in the subgrade cannot be determined using the ISM.

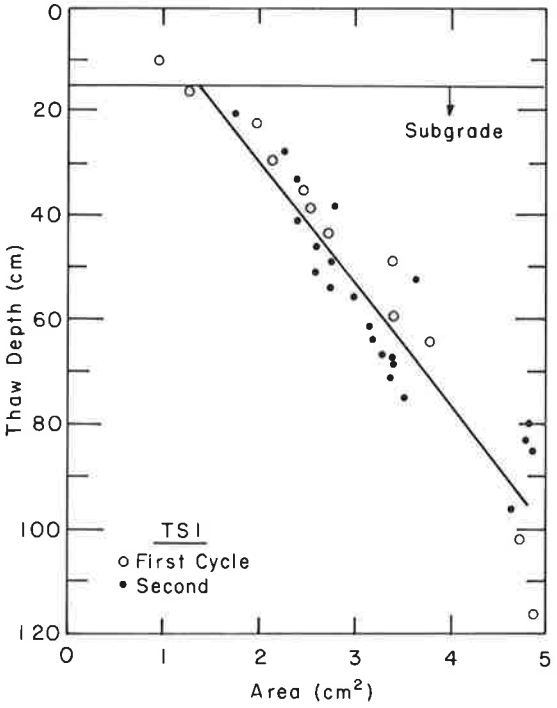

FIGURE 21 Change in total basin area with measured thaw depth in TS-1.

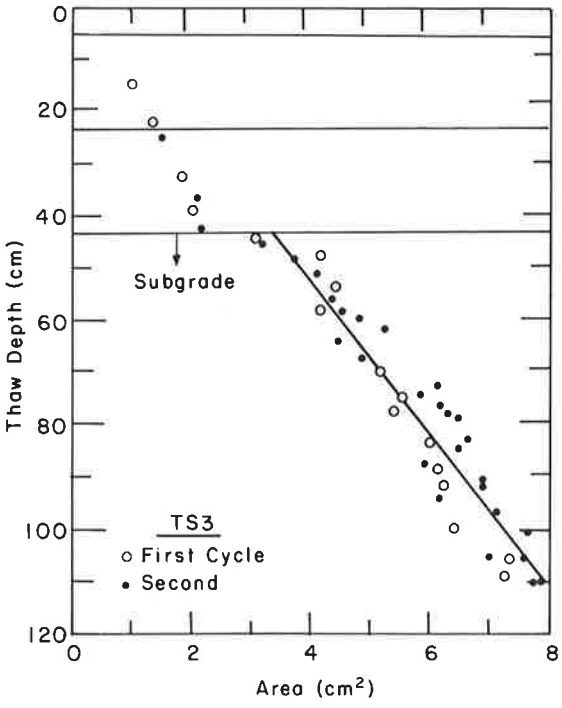

FIGURE 22 Change in total basin area with measured thaw depth in TS-3.

Area Of Deflection Basin

We studied whether the area of the deflection basin could be used as an indicator of thaw depth. The area was determined by summing the polygon enclosed by the seven sensors and the measured deflection in the vertical plane. The variations of the area of the deflection basin with thaw depth for TS-1 and TS-3 are shown in Figures 21 and 22. The figures show a strong correlation between thaw depth in the subgrade and basin area in all test sections. Figure 22 also shows a distinctive break in the relationship between area and thaw depth in the base/subbase courses and in the subgrade, which denotes a faster thaw rate in the base/subbase. With this method, estimation of thaw depth appears to be better at depths below 60 cm for full-depth sections and below 80 cm in conventional pavement structures.

Deflection Ratio

Finally, we looked at the possibility of using deflection ratios to predict thaw depth. Although using deflection ratios instead of deflections only will require taking FWD deflection measurements at other times of the year (summer or fall), easy comparison can be made of the strength of the pavement during spring thaw. Comparisons of the fourth-sensor deflection ratios (or SSI) with thaw depth in TS-1 and TS-3 are presented in Figures 23 and 24. From these figures, several observations can be made. First, the deflection ratios from the fourth sensor tend to increase with increasing thaw depth. Second, the fourth-sensor deflection ratios remain constant at 0.2 in the base and subbase, which further confirms that this sensor is sensing the deflection of the subgrade.

The SSI method appears to estimate the thaw depth reasonably well at thaw depths below 80 cm in the full-depth sections and below 95 cm in the conventional sections. The thaw depth in a clay soil subgrade can be estimated using either the basin area or the SSI (fourth deflection ratio). A graph for determining thaw depths using the basin area and SSI was developed, but it was found that two graphs were required, and the thaw depth depended on the pavement structure above the subgrade. Instead of using the total basin area, the area of the basin from the fourth sensor to the seventh sensor was used together with the SSI (Figure 25). In this case, the thaw depth in the clay subgrade was found to be independent of the pavement structure above the subgrade.

SUMMARY AND CONCLUSIONS

Four flexible pavement test sections, of which two were 152-mm full-depth asphalt pavements and two were 51-mm-thick asphalt pavements over a total of 381 mm of base and subbase courses, were constructed in the FERF and subjected to several freeze-thaw cycles. The subgrade was a clay classified as CH under the Unified Soil Classification System.

The test sections were instrumented with thermocouples and resistance gauges to determine the location of the 0°C isotherm, which was assumed to be the location of the freezing

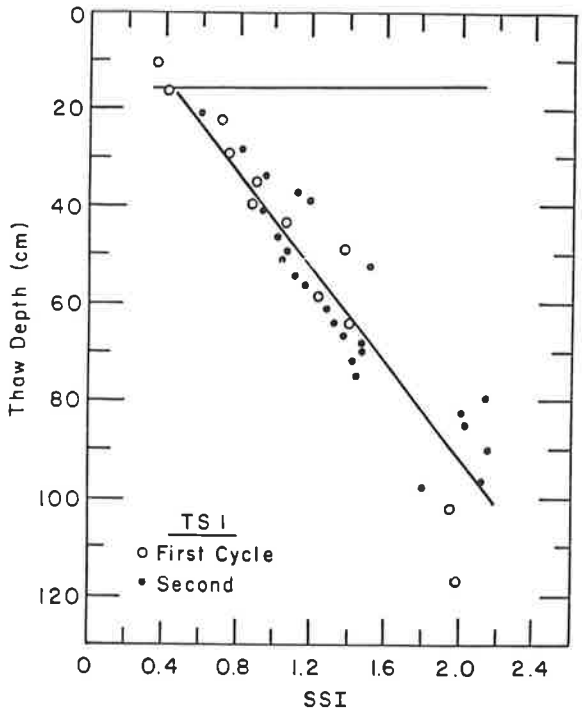

FIGURE 23 Variation in the SSI with measured thaw depth in TS-1.

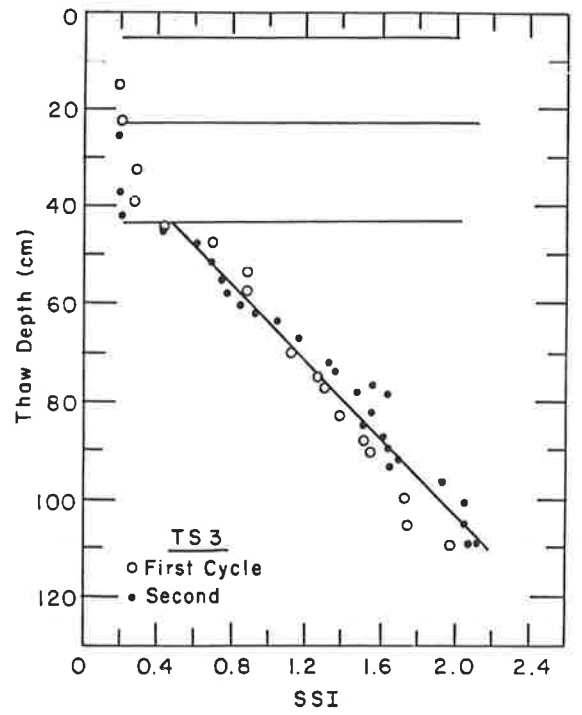

FIGURE 24 Variation in the SSI with measured thaw depth in TS-3.

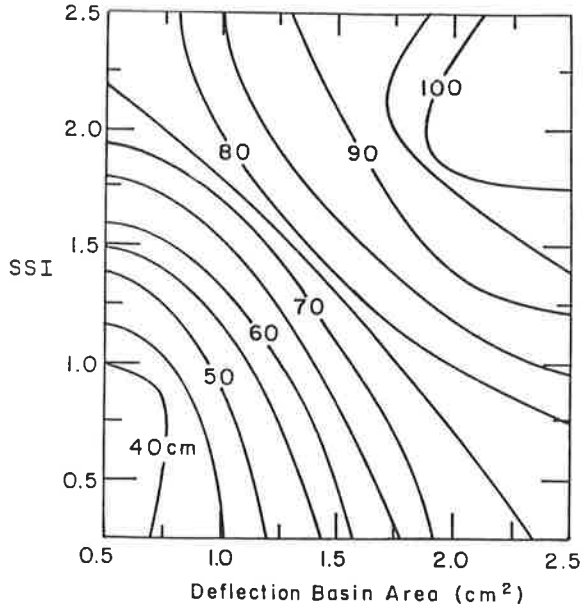

FIGURE 25 Nomograph for determining thaw depth using basic areas and SSI.

or thawing front. The resistance gauges were found to complement the temperature measurements and there was, as expected, a dramatic change in resistance when the soil water changed from frozen to the thawed state or vice versa.

It was found that the clay subgrade was weakened by a factor ranging from 2 to 2.2 when it was subjected to freeze-thaw. This information implies that a 50 to 60 percent reduction in the modulus of a CH subgrade is necessary in any mechanistic design procedure for determining damage (in terms of vertical strains) to pavement.

Because predicting thaw depth is considered a critical element in back-calculation of layer modulus procedures, an attempt was made to develop a method for predicting thaw depths in the subgrade based on FWD deflection measurements. Thaw depth could be estimated by using the area of the deflection basin and/or the fourth-sensor deflection ratio for a CH subgrade. It is recommended that this method be validated in the field. It is also recommended that similar studies be conducted with other fine-grained subgrades, thus enabling development of a thaw depth prediction model for all frost-susceptible soils based on FWD measurements.

Finally, the preliminary results from this study clearly show that, besides obtaining deflection basins from FWDs, in seasonal frost areas, additional information on the variation of the pavement strength and location of thaw depths can be developed. This additional information would not require any sophisticated analytical tools and could easily be incorporated in any pavement evaluation procedure.

REFERENCES

1. F. H. Scrivner, R. Peohl, W. M. Moore, and M. B. Philips. *NCHRP Report 67: Detecting Seasonal Changes in Load-Carrying Capabilities of Flexible Pavements*. HRB, National Research Council, Washington, D.C., 1969.

2. E. J. Chamberlain. *A Statistical Evaluation of Soil and Climate Parameters Affecting the Change in Pavement Deflection During Thawing of Subgrade*. CRREL Report 81-15. U.S. Army Cold Regions Research and Engineering Laboratory, Hanover, N.H., 1981.
3. R. S. Nordal. Detection and Prediction of Seasonal Changes of the Bearing Capacity at the Vormsund Test Road. *Proc., International Symposium on Bearing Capacity of Roads and Airfields*, Trondheim, Norway, pp. 374–382, 1982.
4. R. L. Berg. *Optimize Freeze-Thaw Design Of ALRS, Report for Air Force Engineering and Service Center*. Tyndall Air Force Base, Fla., December 1985.
5. R. N. Stubstad and B. Connor. *Prediction of Damage Potential on Alaskan Highways During Spring Thaw Using the Falling Weight Deflectometer*. Report AK-RD-83-11. Alaska Department of Transportation and Public Facilities, Fairbanks, 1983.
6. F. N. Finn, K. Nair, and J. Hillard. *NCHRP Report 195: Minimizing Premature Cracking in Asphaltic Concrete Pavements*. HRB, National Research Council, Washington, D.C., 1978.
7. *Manual of Pavement Structural Design, Managerial Summary*. Transport Canada-Air, Ottawa, July 1984.
8. J. F. Shook and J. A. Burton. Structural Design of Asphalt Pavements for Heavy Loads. *Proc., 6th International Conference on Structural Design of Asphalt Pavements*, Ann Arbor, Vol. 1, 1987.
9. V. C. Janoo and R. L. Berg. *Thaw-Weakening of Pavement Structures Founded on Fine-Grained Subgrade*. CRREL Report CR90-10. U.S. Army Cold Regions Research and Engineering Laboratory, Hanover, N.H., 1990.
10. E. J. Chamberlain. *A Freeze-Thaw Test To Determine the Frost Susceptibility of Soils*. Special Report 87-1. U.S. Army Cold Regions Research and Engineering Laboratory, Hanover, N.H., January 1987.
11. R. T. Atkins. *Determination of Frost Penetration by Soil Resistivity Measurements*. Special Report 79-22. U.S. Army Cold Regions Research and Engineering Laboratory, Hanover, N.H., July 1979.
12. L. Bjerrum. Embankment of Soft Ground. *Proc., ASCE Specialty Conference on Performance of Earth and Earth-Supported Structures*, Purdue University, West Lafayette, Ind., 1972, pp. 1–54.
13. D. J. D'Appolonia, H. G. Poulos, and C. C. Ladd. Initial Settlement of Structures on Clay. *Journal of the Soil Mechanics and Foundation Division*, ASCE, Vol. 97, No. SM10, 1971, pp. 1359–1377.
14. A. J. Bush III. *Development of a Pavement Evaluation Method for Low Volume Airfield Pavements*. Ph.D. dissertation. University of Illinois, Urbana-Champaign, 1987.
15. M. S. Hoffman and M. R. Thompson. *Mechanistic Interpretation of Non-Destructive Pavement Testing Deflections*. Transportation Engineering Series No. 32, University of Illinois, Urbana-Champaign, 1981.
16. B. Connor. Alaska's Experiences with Non-Destructive Testing. *Proc., Symposium on Instrumentation for Measuring Pavement Response*. U.S. Army Cold Regions Research and Engineering Laboratory, Hanover, N.H., 1989.

Publication of this paper sponsored by Committee on Frost Action.

Prediction of Damage to Flexible Pavements in Seasonal Frost Areas

W. ALLEN, R. BERG, AND S. BIGL

The U.S. Army Cold Regions Research and Engineering Laboratory (CRREL) is developing a mechanistic pavement design method for use in seasonal frost areas by the Corps of Engineers and the Air Force. The mechanistic method will employ results from a series of five computer programs that compute soil and pavement moisture and temperature conditions (FROST1), resilient modulus and Poisson's ratio (TRANSFORM), stresses and strains in the pavement system (JULEA and NELAPAV), and cumulative damage (CUMDAM). The model has been calibrated for the properties of six soils. Five fatigue equations, three based on horizontal strain at the bottom of the asphalt layer and two based on vertical strain at the top of the subgrade, are used to determine the cumulative damage for two-, three-, and four-layer pavement sections at Springfield, Missouri, and Rochester, Minnesota. Although all of the equations predicted failure during the design life for each pavement section modeled, significant jumps occurred during the spring, indicating that the thaw period is crucial in the fatigue life of a pavement.

In the development of a mechanistic design method for pavements subjected to annual freezing and thawing, seasonal variations must be considered. Seasonal variation in pavement strength manifests by (a) large increases in base and subgrade strengths when frozen, (b) loss in base and subgrade strengths during the spring when thaw weakens the layers, and (c) change in asphaltic concrete strength and modulus with temperatures.

The model in development at the U.S. Army Cold Regions Research and Engineering Laboratory (CRREL) in Hanover, N.H., is composed of a series of computer programs that are combined to provide a method for predicting the variation in the strength of flexible pavement structures throughout an annual temperature cycle. Variation in soil moisture content does not include an infiltration component and is based only on changing ground water levels. The emphasis of the work in this paper is on the spring thaw period.

The series of programs results in the computation of cumulative damage to the pavement structure attributable to vehicular loadings so that the remaining life of existing pavement systems can be evaluated. Results can also aid in the design of new pavements and overlays.

U.S. Army Cold Regions Research and Engineering Laboratory, 72 Lyme Rd., Hanover, N.H. 03755.

COMPUTER MODEL

The model includes five programs: FROST1, which computes frost heave and thaw settlement of the pavement structure and soil conditions throughout the depth of the structure (temperature, water content, ice content, density, etc.) at a given time increment; TRANSFORM, which uses FROST1 output files as input and produces files with layered or sublayered pavement systems with a resilient modulus, Poisson's ratio, and density assigned to each layer or sublayer; JULEA or NELAPAV, which calculates stress, strain, and deflection at given points within the pavement profile; and CUMDAM, which calculates incremental and cumulative damage to the pavement structure. Graphs are produced using commercially available plotting programs. The five programs do not work in a consistent system of units. FROST1 is metric, TRANSFORM converts from metric to English, and JULEA and CUMDAM work in English units. NELAPAV can work in either system. In this paper equations are in the units in which they were developed and used in a particular program. Conversion factors used are given in Table 1.

Soil constants and properties of six soils previously studied at a Winchendon, Massachusetts, test site were used for this study (*1*,*2*; E. Chamberlain, unpublished data, 1986). Some of the physical properties of these soils are given in Table 2; grain size distribution curves are shown in Figure 1. Additional properties and information required by each program are discussed later. Special laboratory tests on these soils were conducted at CRREL; test procedures are discussed in Ingersoll (*3*), Chamberlain (*4*), Cole et al. (*1*), and Tice et al. (*5*). Similar data from other soils will be added to the data base in the future.

FROST1

FROST1 was developed by the University of California, Irvine, for CRREL (*6*,*7*). The model assumes one-dimensional vertical heat and moisture flux and is based on a numerical solution technique termed the nodal domain integration method, which allows use of the same computer program to solve a problem by either the finite element method or the integrated finite difference method, or any other mass lumping numerical method. The program was developed for use on problems of seasonal freezing and thawing of nonplastic soils.

TABLE 1 UNIT CONVERSION FACTORS

Multiply	*By*	*To obtain*
inch	25.4	millimeter
lbf/in.^{2} (psi)	6894.757	pascal
degrees Fahrenheit	t °C = (t °F-32)/1.8	degrees Celsius
lb/ft^3	16.01846	kg/m^3

TABLE 2 PHYSICAL PROPERTIES OF WINCHENDON TEST SOILS

Soil	*Coefficients**		*Atterberg limits*		*Specific gravity*
	Cu	*Cc*	*LL*	*PI*	
Dense Graded Stone	32.8	7.1	23	3	2.81
Graves sand	39.1	1.6	0	0	2.70
Hart Brothers sand	8.0	0.92	0	0	2.76
Hyannis sand	4.7	1.2	0	0	2.67
Ikalanian sand	4.5	0.96	0	0	2.70
Sibley till	235	4.1	19	4	2.74

* Cu—coefficient of uniformity, Cc—coefficient of curvature.

The program is based on the following assumptions:

1. Darcy's law applies to moisture movement in both saturated and unsaturated conditions.
2. The porous media are nondeformable as far as moisture flux is concerned; that is, consolidation is negligible.
3. All processes are single valued; that is, hysteresis is not present in relationships such as the soil water characteristic curve.
4. Water flux is primarily as liquid; that is, vapor flux is negligible. Additional assumptions are reported by Berg et al. (*6*).

FROST1 requires the following input for initial and boundary conditions:

1. Upper and lower boundary temperatures,
2. Upper and lower boundary pore water pressures,
3. Initial temperature and moisture stress or moisture content, and
4. Surcharge pressure.

For each soil layer FROST1 requires

5. Gardner's coefficients for soil moisture characteristics,
6. Gardner's coefficients for hydraulic conductivity characteristics,
7. Porosity and density,
8. Coefficient of volume compressibility,
9. Freezing point depression,
10. Thermal conductivity and volumetric heat capacity of the dry soil, and
11. A hydraulic conductivity adjustment factor for the freezing zone.

From these inputs, FROST1 calculates frost heave and thaw settlement throughout a given period. In addition, the temperature, water content, ice content, moisture stress, density, and porosity in each element are determined for each time increment of the simulation.

The nodes are points that divide the column of material into vertical elements, as shown in Figure 2. In general, a 2-cm nodal spacing is used within the frost zone, whereas 5- to 20-cm spacings are used below. The water table is adjusted by assigning an appropriate pore water pressure to the bottom node.

TRANSFORM

TRANSFORM was developed at CRREL by Chamberlain (unpublished data, 1986) and Allen. Using the output file produced by the FROST1 program, TRANSFORM computes the moduli of homogeneous soil layers within the pavement profile. TRANSFORM initially divides the pavement structure into homogeneous layers on the basis of material type, ice content (which determines if the layer is frozen or unfrozen), pore water pressure, and temperature. A homogeneous layer consists of a single material type with the temperature, ice content, and pore pressure characteristics shown in Table 3.

The layers are then assigned a modulus value based on regression equations developed from laboratory resilient modulus results for the soils in frozen and thawed states. The equations relate the resilient modulus to temperature, pore water pressure, density, and stress conditions. These equations are shown in Table 4 (*1*). An approximation of the $f(\sigma)$ stress term was used, making this term a constant for each soil and thereby making the equations not dependent on stress. The equation for the resilient modulus of the asphalt layer is

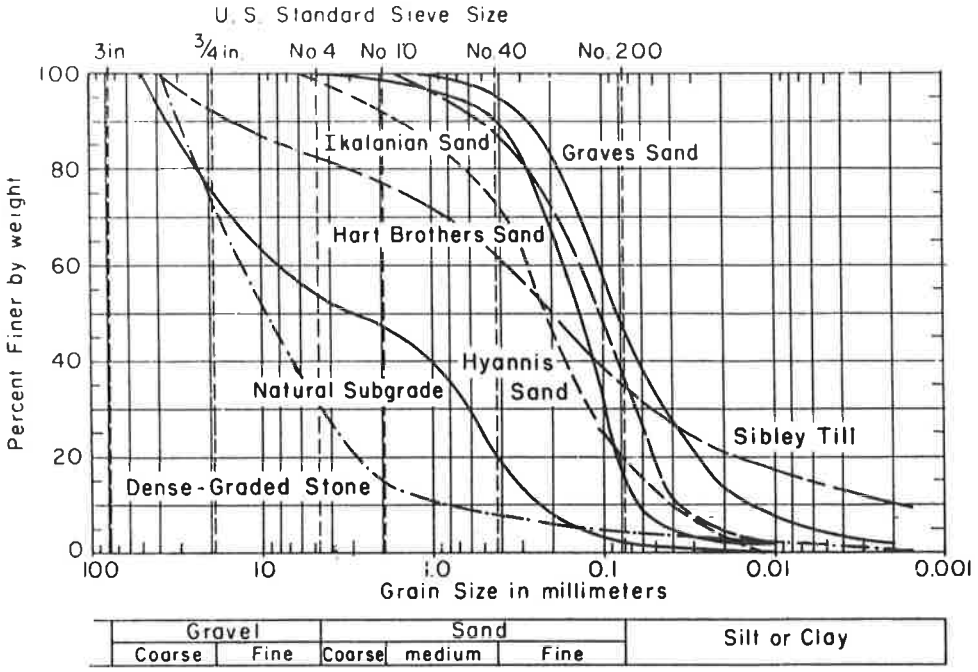

FIGURE 1 Grain size distribution of Winchendon test soils and natural subgrade.

based on a regression of data obtained by Schmidt (*8*) and is as follows:

$$E(\text{MPa}) = [10^{(6.285 - 1.931\times10^{-2}\ T - 3.275\times10^{-4}\ T^2 - 1.888\times10^{-5}\ T^3 + 1.175\times10^{-7}\ T^4 + 1.502\times10^{-8}\ T^5 - 2.022\times10^{-10}\ T^6)}] * 145$$

where T is the temperature of the top FROST1 node in degrees centigrade.

For pavement temperatures greater than 50°C, the asphalt modulus was set to 173 MPa; for temperatures less than −29°C, it was chosen at 33 389 MPa.

To reduce the number of layers, and thus simplify the profile and reduce the computer simulation time, adjoining sublayers were combined if modulus values were within ±20 percent of each other. The resulting modulus of the combined layer is a weighted average of the moduli of the component layers.

Two versions of TRANSFORM produce files appropriate for input into JULEA or NELAPAV. For JULEA this includes one load data file and a structural data file for each day of the simulation. NELAPAV requires a single file containing both load and structural data for each day of the simulation. Both of these programs use layered elastic methods.

JULEA

JULEA was developed by J. Uzan (unpublished data, 1986). Based on Boussinesq theory, JULEA will allow up to 25 layers and will provide a linear elastic solution for determination of stress, strain, and deflection at a point in the given pavement profile using layer modulus, Poisson's ratio, thickness, and area and magnitude of the load. JULEA allows multiple wheel loads.

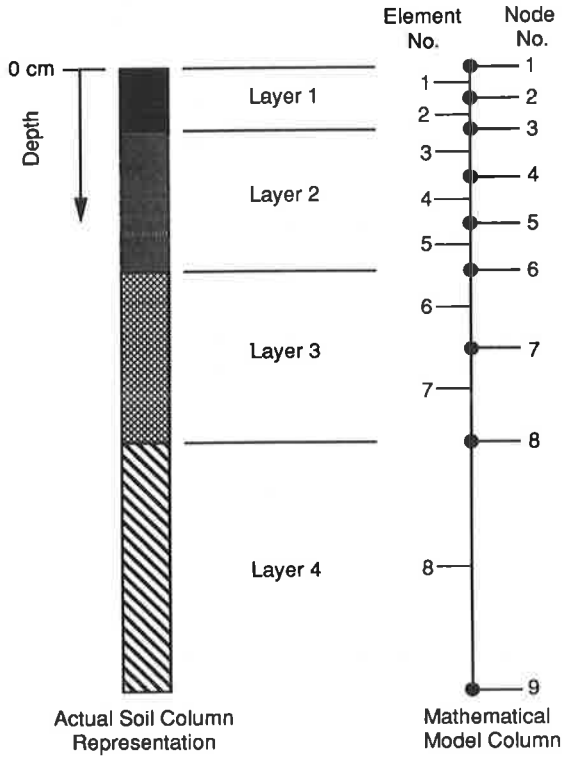

FIGURE 2 Example soil profile divided into finite elements.

TABLE 3 HOMOGENEOUS SOIL LAYERS PRODUCED BY TRANSFORM PROGRAM

Layer type	Description
1	Frozen, volumetric ice content greater than 0.002, with temperature less than -6.0°C.
2	Frozen, volumetric ice content greater than 0.002, with a temperature less than -1.0°C, divided into sublayers with a temperature difference across the layer of less than 1 degree for layers warmer the -6°C.
3	Frozen, with a temperature between -1.0 and -0.5°C.
4	Frozen, with a temperature greater than -0.5 and less than 0°C.
5	Frozen, with a temperature of 0°C.
6	Partially thawed, volumetric ice content greater than 0.002, and positive pore water pressure.
7	Unfrozen, with negative pore water press subdivided into additional layers if the difference in pore water pressure within a single layer is greater than 50 cm of water.
8	Unfrozen, with positive pore water pressure.

NELAPAV

NELAPAV was developed by Irwin and Speck (*9*) at Cornell University under a contract with CRREL. It is an adaptation of the Chevron Layered Elastic Systems program. NELAPAV has the ability to accommodate layers having moduli of elasticity that vary with the level of stress or strain in the layer and to produce both linear and quasi-nonlinear solutions with seven modulus models given in Table 5 (*10*). (Model 7 is not currently incorporated into the CRREL version of NELAPAV.) It will allow up to 25 layers in its present form. Initially, NELAPAV was run using the linear model 0 to compare its output with the linear JULEA solution. To investigate the nonlinear aspects of thawing soils, NELAPAV was then run using the linear model 0 for frozen layers, unfrozen layers with negative pore pressure and the asphalt layers, and model 3, which is dependent on the J_2/τ_{oct} stress term, for the thawed and partially thawed layers.

The solution computed by NELAPAV is an approximation to the exact solution. In reality, the stress state changes from point to point. Therefore, the modulus of a nonlinear material varies both vertically and horizontally. Whereas NELAPAV recomputes the set of compatible moduli to determine the states of points at various radii, it is bound by the assumption that the moduli are constant everywhere in the layers. A more exact theory for nonlinear materials would allow the modulus to vary horizontally within the layer in accordance with the nonlinear model.

CUMDAM

The program CUMDAM was developed at CRREL. It uses five fatigue equations—three based on horizontal strain at the bottom of the asphalt layer and two based on the vertical strain at the top of the subgrade. The equations are as follows.

Asphalt Strain

The Asphalt Institute (*11*):

$$N_a = 18.4\ C\ (4.325 \times 10^{-2})\ |\varepsilon_t|^{-3.291}\ (E_a^{-0.854})$$

where

N_a = number of load applications for cracking,
C = a function of the volume of the voids and the volume of asphalt (10^z),
z = $4.84\ [(V_b/V_v + V_b) - 0.69]$,
V_b = volume of asphalt (%),
V_v = volume of voids (%),
ε_t = tensile strain at the bottom of the asphalt layer (in./in.), and
E_a = modulus of the asphalt layer (psi).

TABLE 4 RESULTS OF REGRESSION ANALYSIS

Material	Regression equation	n	R^2	Std. error
Natural subgrade				
Frozen	$M_r(\text{MPa}) = 20.74\ f\ (\sigma)^{0.352}$	65	0.76	0.201
Graves sand				
Frozen	$M_r(\text{MPa}) = 39.1(w_u/w_t)^{-1.79}$	95	0.91	0.502
Thawed	$M_r(\text{MPa}) = 6.68\times10^4\ f\ (\psi)^{-2.2948} f\ (\sigma)^{0.414}$	186	0.89	0.144
Ikalanian sand				
Frozen	$M_r(\text{MPa}) = 86.4(w_u/w_t)^{-1.32}$	87	0.92	0.749
Thawed	$M_r(\text{MPa}) = 3.021\times10^4 f\ (\psi)^{-3.266} f\ (\gamma)^{11.634} f\ (\sigma)^{0.442}$	119	0.89	0.276
Hart Brothers sand				
Frozen	$M_r(\text{MPa}) = 4.085\times10^1\ (w_u/w_t)^{-1.59}$	99	0.92	0.623
Thawed	$M_r(\text{MPa}) = 1.269\times10^5 f\ (\psi)^{-3.089} f\ (\gamma)^{7.023} f\ (\sigma)^{0.453}$	172	0.87	0.185
Hyannis sand				
Frozen	$M_r(\text{MPa}) = 33.45\ (w_u/w_t)^{-2.03}$	69	0.95	0.617
Thawed	$M_r(\text{MPa}) = 7.147\times10^4 f\ (\psi)^{-1.782} f\ (\sigma)^{0.264}$	128	0.71	0.129
Dense Graded Stone				
Frozen	$M_r(\text{MPa}) = 82.27\ (w_u/w_t)^{-2.03}$	32	0.87	0.413
Thawed	$M_r(\text{MPa}) = 1.56\times10^5 f\ (\psi)^{-1.76} f\ (\sigma)^{0.136}$	64	0.65	0.202
Sibley till				
Frozen	$M_r(\text{MPa}) = 1.01\times10^2\ (w_u/w_t)^{-3.446}$	108	0.87	0.71
Thawed	$M_r(\text{MPa}) = 7.47\times10^6 f\ (\psi)^{-2.829} f\ (\sigma)^{0.192}$	118	0.63	0.283

Notes:

RPB = repeated-plate bearing apparatus waveform
n = number of points
M_r = resilient modulus
f = load wave frequency
$f\ (\sigma) = [(J_2/\tau_{oct})/\sigma_o]$
σ = stress (kPa)
J_2 = second stress invariant (kPa^2)
τ_{oct} = octahedral shear stress (kPa)
w_u = unfrozen water content
w_t = total water content
$T = \theta/\theta_o$
θ_o = 1°C
ψ = moisture tension
ψ_o = 1 kPa
$f\ (\gamma) = \gamma/\gamma_o$
γ_o = 1 mg/m^3
$f\ (\psi) = [(101.38-\psi)/\psi_o]$
γ = soil density (mg/m^3)

Witczak (*12*):

$$N_a = ab^{q^d}\ (1/\varepsilon_t)^c$$

where

$a = 1.86351 \times 10^{-17}$,
$b = 1.01996$,
$c = 4.995$,
$d = 1.45$, and
q = pavement temperature (°F).

The Army Corps of Engineers (*13*):

$$N_a = 10^{(5\ \log|\varepsilon_t| + 2.66\ \log E_a - 2.68)}$$

Subgrade Strain

The Asphalt Institute (*11*):

$$N_s = 10^{[1/m(\log l - \log\varepsilon_v)]}$$

where

N_s = allowable traffic based on subgrade strain,
m = a constant (0.25),
l = a constant (2.8×10^{-2}), and
ε_v = vertical strain at the top of the subgrade (in./in.).

The Federal Aviation Administration (Bush) (*14*):

$$N_s = 10^{\left(\frac{\log\varepsilon_v}{-0.17985} - 12.215\right)}$$

TABLE 5 RESILIENT MODULUS: NELAPAV MODELS

NELAPAV models		
Model no.	*Name*	*Specification*
0	Linear	E = constant
1	Bulk stress	$E = k_1\,\theta^{k_2}$
2	Deviator stress	$E = \begin{cases} k_2+k_3(k_1-\sigma_d) & \sigma_d < k_1 \\ k_2+k_4(\sigma_d-k_1) & \sigma_d \geq k_1 \end{cases}$
3	Second stress invariant	$E = k_1\,(J_2/\tau_{oct})^{k_2}$
4	Octahedral shear stress	$E = k_1\,\tau_{oct}^{k_2}$
5	Vertical stress	$E = k_1\,\sigma_v^{k_2}$
6	Major principal stress	$E = k_1\,\sigma_1^{k_2}$
7	First stress invariant octahedral shear stress and anisotropic consolidation ratio	$E = k_1(J_{1o}^2 + J_{1P}^2)^{k_2}\,(1 + \tau_{oct})^{k_2}\,k_c^{k_4}$

Notes:

θ = bulk stress
k_1, k_2, k_3, k_4 = constants
σ_d = deviator stress
σ_v = vertical stress
σ_v = major principal stress
J_{1o} = first stress invariant due to overburden only
J_{1p} = first stress invariant due to overburden and load
k_c = anisotropic consolidation ratio

For these calculations, the design traffic (n) is 685 loadings per day or a total of 5,000,000 passes of the equivalent standard axle load (ESAL) of 18,000 lb in 20 years. N_s or N_a were calculated daily using the above equations. The damage was accumulated as a summation of n/N incremented daily to match the time increment run in FROST1, starting on the first day of the freezing season at that site (Rochester, Day 13; Springfield, Day 69).

Although some of the equations are being applied outside of the original assumptions used in their development, they are representative of cumulative damage models currently available and are used for the initial analysis until more appropriate equations can be determined.

CALIBRATION OF THE MODEL

The model was calibrated by matching heave determined in FROST1 and deflection determined from JULEA and NELAPAV to field data from the Winchendon test site. Each of the six Winchendon pavement test sections contained 8 cm of asphalt over 1 to 1.5 m of a test soil. The sections were built for research only and never received significant vehicular traffic, but were tested using nondestructive equipment.

Data from the test site included temperatures from thermistors placed to a maximum depth of approximately 1.5 m, surface elevations to determine frost heave, and deflections from repeated-load plate bearing (RPB) tests performed during the winter and spring of 1978/1979. The RPB was a nondestructive testing apparatus used by CRREL before obtaining a falling weight deflectometer (*15*). This self-contained trailer-mounted apparatus generated successive load pulses in the 1- to 140-kip range at rates up to 20 repetitions per minute. The loading pulse profile from the RPB is the standard pulse used for laboratory resilient modulus tests at CRREL (Figure 3).

As mentioned, heave predicted by the FROST1 program was compared with the surface elevation data from the Winchendon test site. For each soil, the modifier of the hydraulic conductivity in the freezing zone was adjusted until the predicted heave most closely matched the observed heave, as shown in Figure 4.

Initial calculations by the model produced deflections during spring thaw that were generally much lower than those

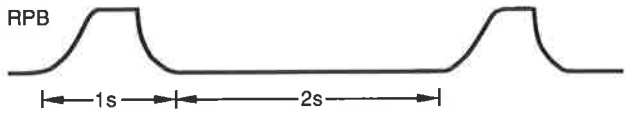

FIGURE 3 Typical RPB load pulse profile.

produced by the RPB for the same input load magnitude. These data indicated that, during spring thaw, the moduli values calculated by the programs were higher than those existing in the field.

An investigation of output from FROST1 during spring thaw indicated the presence of days when layers within the structure exhibited positive pore pressures, denoting saturation of the soil. Since the resilient modulus equations produced from the CRREL laboratory program (Table 3) were not intended for a saturated soil condition, a reduction factor (k) was applied to the modulus of saturated thaw layers, calculated in TRANSFORM, as follows:

$$M_r(\text{saturated}) = \frac{M_r(\text{thawed})}{k}$$

The magnitude of the k factor was determined by extrapolation of laboratory resilient modulus results to a 0 moisture tension case and refined with comparison to the field RPB data for each soil case. Model simulations using various k factors were made until the predicted deflection data closely matched data obtained in the field (e.g., Figure 5).

RESULTS

Pavement Response Models

Calibration of the programs to the Winchendon RPB deflection data indicated the following:

1. NELAPAV, using the linear model, gives approximately the same solution as JULEA (Figure 6).
2. The nonlinear model used in NELAPAV for the thawed layers produces closer agreement to the field data than the linear JULEA (or NELAPAV) solutions (Figure 7).

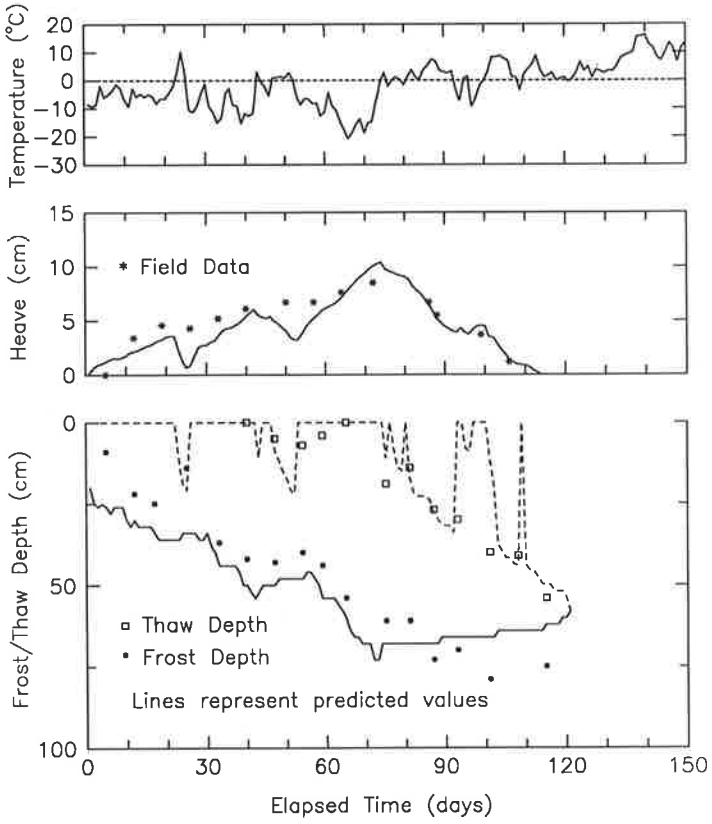

FIGURE 4 Example of comparison between field data and FROST1-predicted heave and frost depths. Case modeled is asphalt over Graves sand at Winchendon, Massachusetts, starting December 10, 1978.

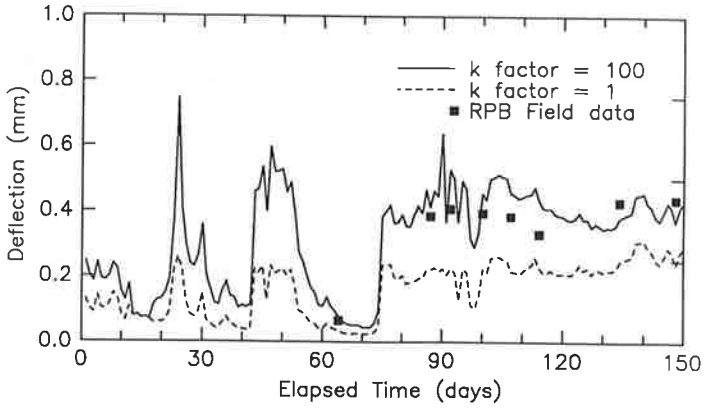

FIGURE 5 Example of *k* factor calibration. Case modeled is asphalt over dense graded stone at Winchendon, Massachusetts, starting December 10, 1978.

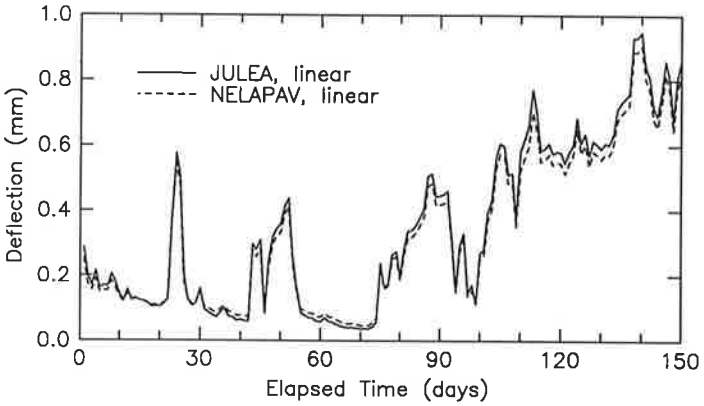

FIGURE 6 Comparison of JULEA and NELAPAV predicted deflections when NELAPAV is run with linear model. Case modeled is asphalt over Graves sand at Winchendon, Massachusetts, starting December 10, 1978.

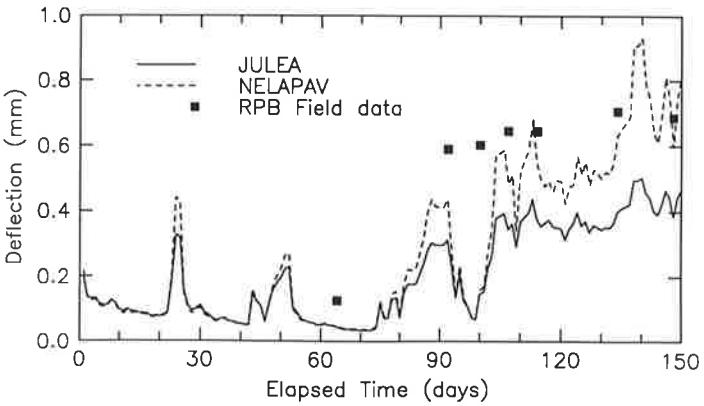

FIGURE 7 Comparison of JULEA and NELAPAV predicted deflections for typical Winchendon test site. Case modeled is asphalt over Ikalanian sand at Winchendon, Massachusetts, starting December 10, 1978.

Cumulative Damage

As part of developing a mechanistic design method for pavements in cold regions, we report the results from three pavement profiles for annual temperature cycles at two geographic locations. The pavement profiles, shown in Figure 8, result from the current Corps of Engineers reduced subgrade strength design method (*16*), except for the two-layer case, which is analogous to the Winchendon test site. The subgrade material, Graves sand, is an especially high-heaving material. The environmental conditions chosen were those at Springfield, Missouri, and Rochester, Minnesota, to represent typically warm and typically cold seasonal frost locations. The freezing indices used for the sites, the coldest in 30 years, were 702 and 2,805 degree Fahrenheit days, respectively. These cases are purely hypothetical and do not represent any existing field site.

Figures 9 and 10 show the mean daily temperatures, frost heave, frost penetration, and thaw penetration at the Springfield, Missouri, and Rochester, Minnesota, sites for the design years (1977–1978 and 1978–1979, respectively) for the two-

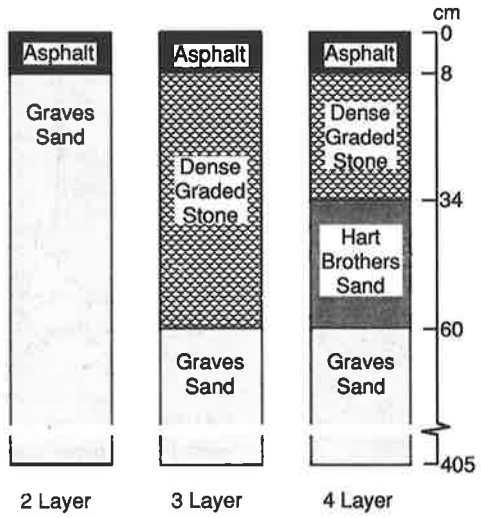

FIGURE 8 Pavement profiles.

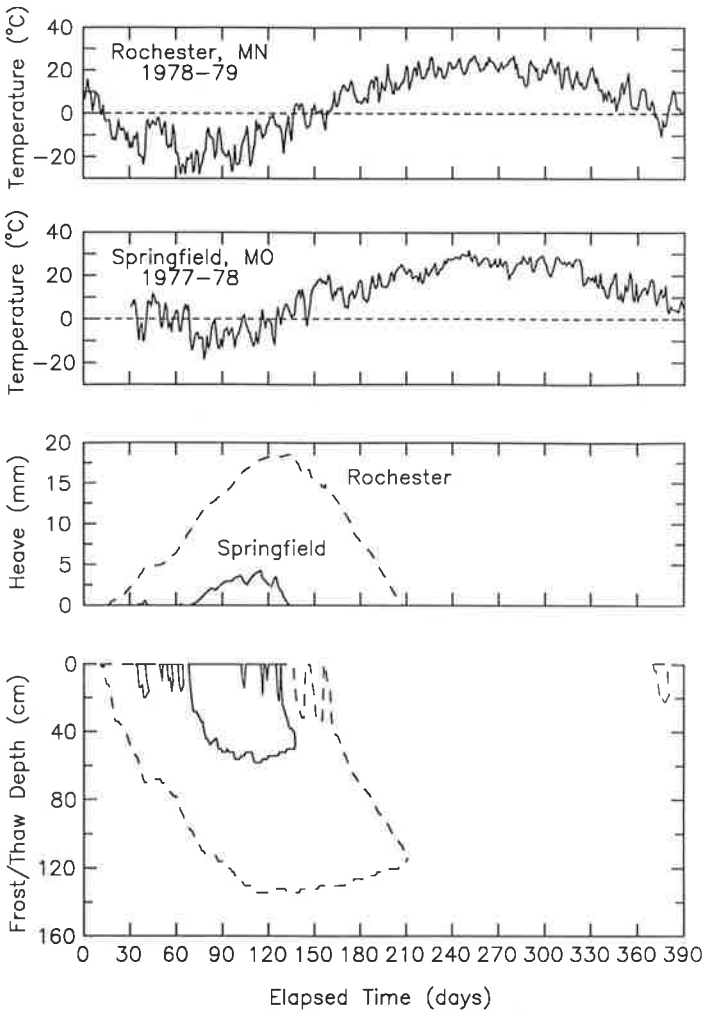

FIGURE 9 Predicted heave and thaw depths at Springfield, Missouri, and Rochester, Minnesota, during design cold year: two-layer pavement structure.

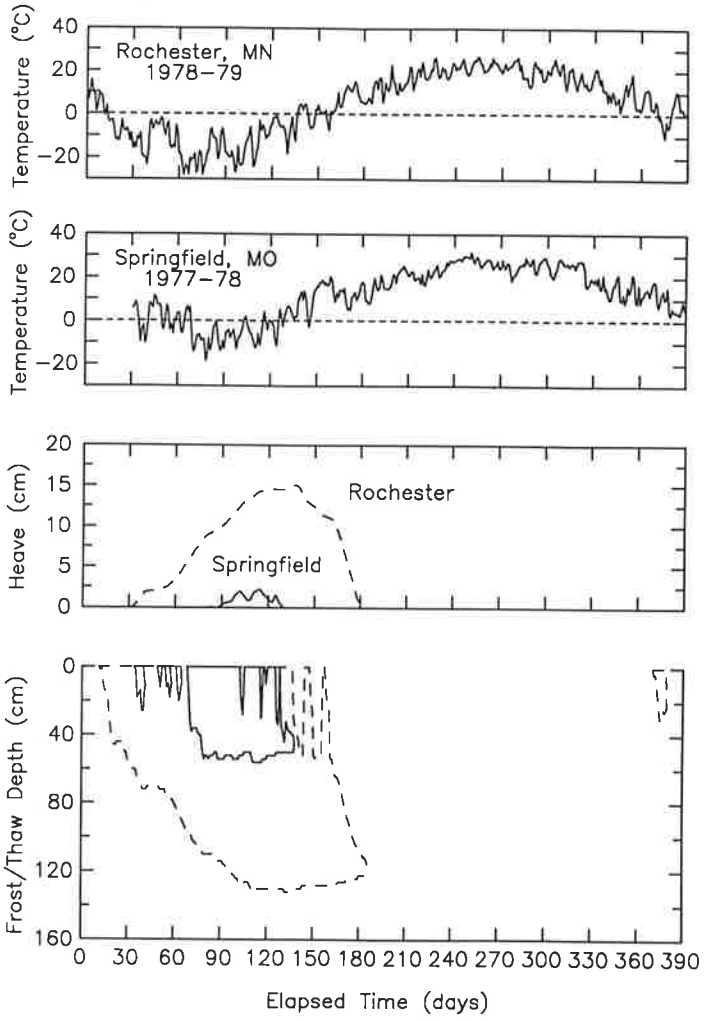

FIGURE 10 Predicted heave and thaw depths at Springfield and Rochester during design cold year: four-layer pavement structure.

and four-layer cases as depicted in Figure 8. The time plotted begins on November 1 of the design year; however, because Springfield has such a mild season, its simulation started on December 1.

Strains produced by JULEA for the four-layer case at each site are shown in Figures 11 and 12. Output from the fatigue equations for Rochester two-, three-, and four-layer cases is shown in Figures 13–15. A cumulative damage equal to 1.0 indicates pavement failure. Therefore, for a pavement system to last its design life, the amount of cumulative damage must be less than 1.0 for that period. For a 20-year design life, this indicates that the yearly cumulative damage should be less than 0.05 if the damage is assumed to be evenly distributed throughout the pavement life.

The figures produced during the simulations indicate the following:

1. For the two-layer case, failure of the pavement in less than 1 year was predicted by all five fatigue equations (Figure 13). For all cases, failure occurred during the thawing season, with a significant jump in the cumulative damage.

2. For the three-layer case, all the fatigue equations again predicted failure within the 20-year life span (Figure 14). Witczak and the Corps horizontal strain equations and the FAA vertical strain equation showed abrupt increases in the cumulative damage during the thawing period, resulting in failure within the first year. However, the Asphalt Institute equations for horizontal and vertical strain both showed a more gradual increase in cumulative damage, beginning in the spring and continuing through the rest of the period modeled. The Asphalt Institute horizontal and vertical equations predicted failure in approximately 2 and 6 years, respectively.

3. For the four-layer case, the pavement also failed, based on the horizontal strain criteria, with the Witczak equation predicting the earliest failure (Figure 15). Again, significant jumps in the cumulative damage were predicted during the thawing season by Witczak's and the Corps' horizontal strain equations and the FAA vertical strain equations. As in the

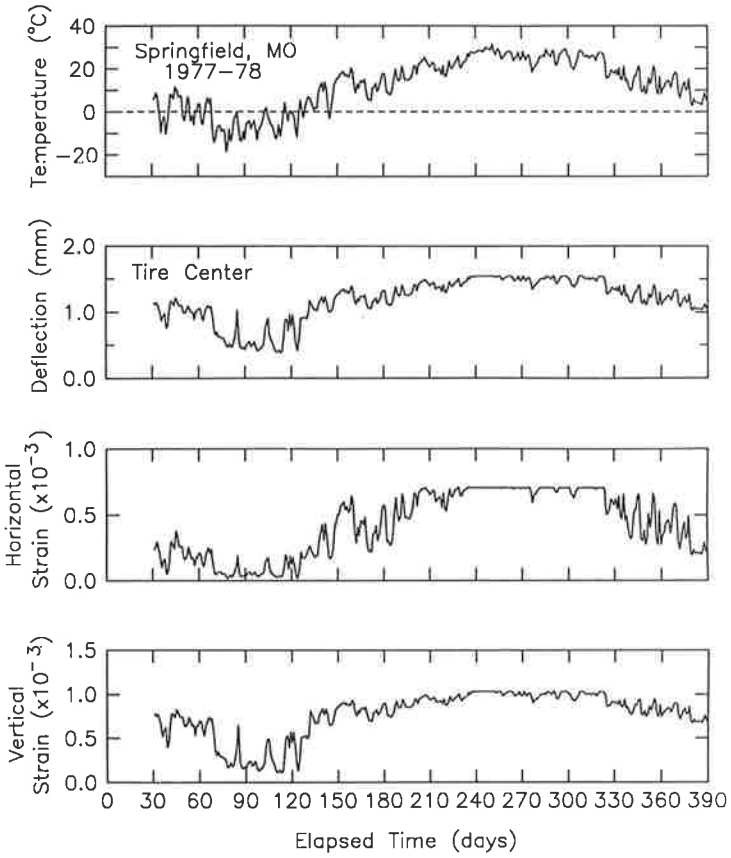

FIGURE 11 Engineering properties calculated by JULEA: surface deflections and strains at base of pavement and top of subgrade with four-layer pavement structure, Springfield.

three-layer case, the Asphalt Institute equations predicted more gradual failure in approximately the same time.

CONCLUSIONS

1. From the calibration effort, it was concluded that a nonlinear solution produces better correlation with observed repeated plate bearing test deflection data, especially during periods of thaw, than a linear elastic solution. Therefore, further simulations should concentrate on the nonlinear models with the addition of model 7 in NELAPAV.

2. The cumulative damage predictions produced the following preliminary conclusions:

- For the two-layer pavement structure, all of the cumulative damage equations predicted failure within the first thawing period. Failure was expected since the pavement modeled was designed for research and not for traffic.
- For the three- and four-layer cases, fatigue equations that use only one strain value for the entire subgrade layer may be misleading. FROST1 and TRANSFORM produce layered systems containing thin layers that may have substantially different moduli than the bulk of the subgrade. The current CRREL procedure uses the strain value at the point under investigation, typically less than 1 cm under the subgrade interface. If this layer has a particularly high or low modulus value, fatigue predictions will be affected accordingly. However, the significant rapid increases in the values for cumulative damage during the spring thaw period illustrate the amount of damage that the pavement may sustain in the thaw-weakened state.
- The cumulative damage equations are being applied outside the bounds of the original assumptions on which they are based, or beyond the data used in their development. For this preliminary study, several equations were incorporated into the CUMDAM program for comparison and evaluation. Further study on suitable damage equations is warranted.

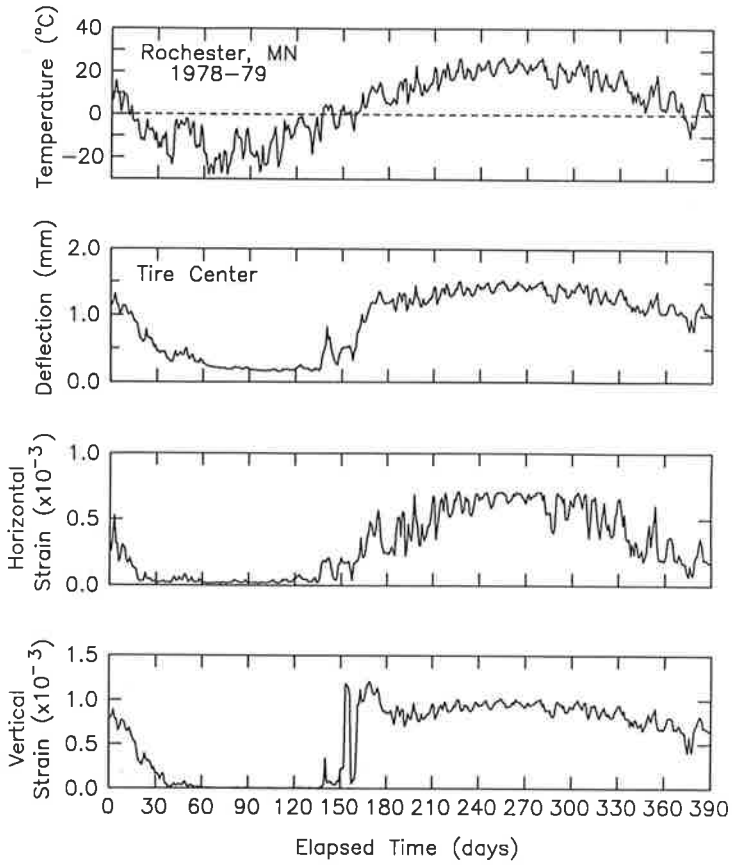

FIGURE 12 Engineering properties calculated by JULEA: surface deflections and strains at base of pavement and top of subgrade with four-layer pavement structure, Rochester.

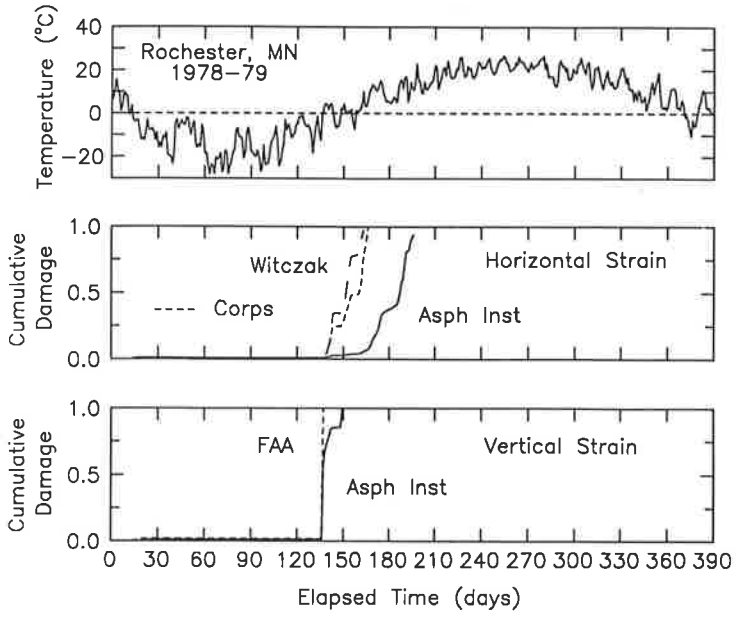

FIGURE 13 Cumulative damage through time during design year at Rochester: two-layer pavement structure.

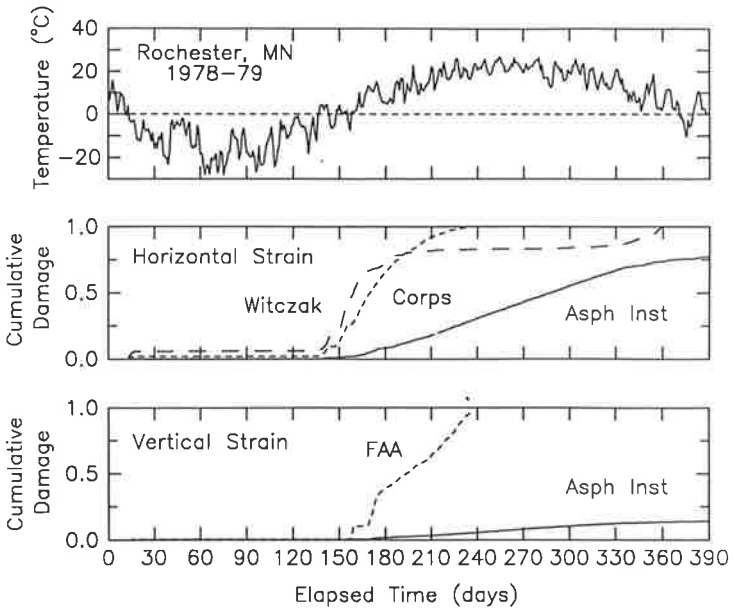

FIGURE 14 Cumulative damage through time during design year at Rochester: three-layer pavement structure.

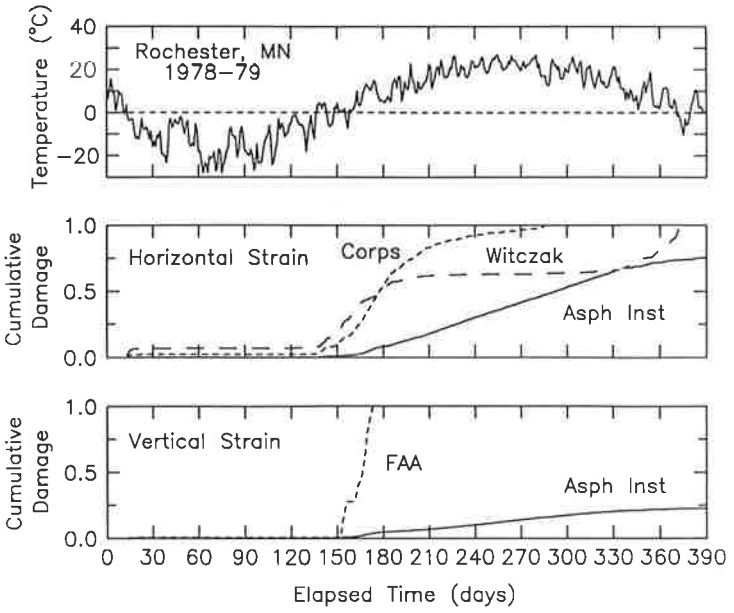

FIGURE 15 Cumulative damage through time during design year at Rochester: four-layer pavement structure.

REFERENCES

1. D. M. Cole, D. Bentley, G. Durell, and T. C. Johnson. *Resilient Modulus of Freeze-Thaw Affected Granular Soils for Pavement Design and Evaluation. Part 1. Laboratory Tests on Soils from Winchendon, Mass., Test Sections*. CRREL Report 86-4. U.S. Army Cold Regions Research and Engineering Laboratory, Hanover, N.H., July 1986.
2. T. C. Johnson, D. L. Bentley, and D. M. Cole. *Resilient Modulus of Freeze-Thaw Affected Granular Soils for Pavement Design and Evaluation. Part 2. Field Validation at Winchendon, Mass., Test Sections*. CRREL Report 86-4. U.S. Army Cold Regions Research and Engineering Laboratory, Hanover, N.H., Oct. 1986.
3. J. I. Ingersoll. *Method for Coincidentally Determining Soil Hydraulic Conductivity and Moisture Retention Characteristics*. CRREL Special Report 81-2. U.S. Army Cold Regions Research and Engineering Laboratory, Hanover, N.H., March 1981.
4. E. Chamberlain. A Freeze-Thaw Test to Determine the Frost Susceptibility of Soils. CRREL Special Report 87-1. U.S. Army Cold Regions Research and Engineering Laboratory, Hanover, N.H., Jan. 1987.
5. A. R. Tice, C. M. Burrows, and D. M. Anderson. Determination of Unfrozen Water in Frozen Soil by Pulsed Nuclear Magnetic Resonance. *Proc., 3rd International Conference on Permafrost*, Ottawa, Ontario, National Research Council of Canada, 1978, pp. 149–155.
6. R. Berg, G. Guymon, and T. Johnson. *Mathematical Model to Correlate Frost Heave of Pavements with Laboratory Predictions*. CRREL Report 80-10. U.S. Army Cold Regions Research and Engineering Laboratory, Hanover, N.H., 1980.
7. G. L. Guymon, R. L. Berg, T. C. Johnson, and T. D. Hromadka II. *Mathematical Model of Frost Heave and Thaw Settlement in Pavements*. CRREL Report. U.S. Army Cold Regions Research and Engineering Laboratory, Hanover, N.H., in press, 1990.
8. R. J. Schmidt. Use of ASTM Tests to Predict Low Temperature Stiffness of Asphalt Mixes. In *Transportation Research Record 544*, TRB, National Research Council, Washington, D.C., 1975, pp. 35–45.
9. L. Irwin and D. Speck. *NELAPAV User's Guide*. Cornell University Local Road Program Report No. 86-1. Cornell University, Ithaca, N.Y., Jan. 1986.
10. W. Yang. Mechanistic Analysis of Nondestructive Pavement Deflection Data. Ph.D. thesis. Cornell University, Ithaca, N.Y., Jan. 1988.
11. *Research and Development of the Asphalt Institute's Thickness Design Manual (MS-1)*. 9th ed. Research Report No. 82-2. The Asphalt Institute, College Park, Md., Aug. 1982.
12. M. W. Witczak. Design of Full Depth Asphalt Airfield Pavements. *Proc., 3rd International Conference on the Structural Design of Asphalt Pavements*, London, England, Vol. 1, pp. 550–567 Sept. 1972.
13. *Pavement Design for Roads, Streets, and Open Storage Areas, Elastic Layered Method*. Technical Manual 5-800-09. Department of the Army, Washington, D.C., Nov. 1988.
14. A. Bush. *Non-Destructive Testing for Light Aircraft Pavements*. U.S. Army Waterways Experiment Station, Vicksburg, Miss., Nov. 1980.
15. W. Allen, W. Quinn, D. Keller, and R. Eaton. *Response of Pavement to Freeze-Thaw Cycles: Lebanon, N.H., Regional Airport*. CRREL Special Report 89-2. U.S. Army Cold Regions Research and Engineering Laboratory, Hanover, N.H., Jan. 1989.
16. R. Berg and T. Johnson. *Revised Procedure for Pavement Design Under Seasonal Frost Conditions*. CRREL Special Report 83-27. U.S. Army Cold Regions Research and Engineering Laboratory, Hanover, N.H., 1983.

Publication of this paper sponsored by Committee on Frost Action.

Evaluation of Variables Affecting Flexible Pavement Thawing for Timing Spring Load Restrictions

MARY RUTHERFORD

A finite element analysis of pavement freezing and thawing was performed on four flexible pavement structures developed to represent typical pavements that receive spring load restrictions because of thaw weakening. The pavement structures consisted of 2- and 4-in.-thick asphalt concrete surface courses, 6- and 12-in.-thick granular base courses and fine- and coarse-grained subgrade materials. TDHC, a two-dimensional finite element heat transfer model, was used for the analysis. Air temperatures, short- and longwave radiation, and convection were included as the external variables driving the pavement thermal response. Latent heat, caused by the phase change of water during freezing and thawing, is included in the model. The results suggest that average daily pavement surface-air temperature differences vary from 2°F in February to 11°F in May. These data suggest that pavement thawing will be initiated during this time for average daily air temperatures of 30°F or less. In addition, it was found for the pavements analyzed that thawing reached the top of the subgrade, after pavement surface temperatures reached 32°F, in 1 to 4 days in thin pavements and in 4 to 9 days in thick pavements. The duration of thawing for total thawing to occur was correlated with the freezing index for all subgrade types combined with satisfactory results.

During spring thawing, the strength of the ground may be measurably weakened compared with its summer-fall state for one or both of the following reasons:

1. Moisture migration into the soil during the preceding freezing period and
2. Development of excess hydrostatic pressure in base and subgrade materials as moisture is liberated during thawing.

Recognition of seasonal variation in material properties is necessary for realistic estimates of pavement performance. For primary road facilities, it is necessary to minimize the detrimental effects of substantial thaw weakening because it is anticipated that these roads will perform at a high level of serviceability throughout the year under high traffic volumes. However, for many secondary roads with lower traffic volumes it is not economically feasible to provide adequate frost protection throughout for spring thawing. Agencies faced with secondary road maintenance in frost areas often choose to restrict vehicle or axle loads, or both, during some of the spring thaw period to reduce damage that may occur at this time.

Department of Civil Engineering, Seattle University, Seattle, Wash. 98122.

Studies performed in Alaska, Minnesota, and Washington (*1–3*) have shown that flexible pavements that were susceptible to spring thaw damage were weakened relative to summer stiffness levels when thawing had reached the bottom of the base course layer. Analytical studies of hypothetical pavement sections by Rutherford (*4,5*) resulted in similar findings. These field and analytical studies indicated that the time for base thawing to occur is short. However, because of radiation and the absorptive properties of the pavement surface, base thawing occurs before air temperatures warm to 32°F. The duration of the weakened period has been found to be variable and is a function of depth of freezing, soil type, lateral drainage potential, and surface thermal conditions. The end of ground thawing is important since it represents the end of the generation of excess moisture. However, there is not always enough time for sufficient recovery of stiffness of the unbound materials to warrant the removal of load restrictions.

The purpose of this study was to evaluate analytically when flexible pavement thawing occurs to gather information for use in timing spring load restrictions. Previous work (*4*) suggested that the following were of interest: (a) the start of pavement thawing, (b) the time for thawing to reach the top of the subgrade material, (c) the time for a small amount of subgrade thawing (4 in.) to occur, and (d) the time to total thaw. The analysis was performed on pavement cross-sections that were developed to represent "typical" pavement sections currently being restricted in the United States (*5*). In addition, it was desirable to develop pavement sections that represented a range of material types so that a range of performance could be observed.

ANALYSIS APPROACH

Two broad categories of variables required consideration to perform the analysis of pavement thawing: (a) climatic conditions or external variables and (b) layer material types and associated index and thermal properties. The choice of pavement cross-sections, climatic variables, and model selection will be discussed in this section.

Model Selection

The primary mode of heat transfer in pavement structures is conduction. However, two aspects of the ground thermal regime

warrant particular consideration for realistic results when modeling ground freezing and thawing. These include (a) consideration of ground surface effects, including radiation and convection and (b) the inclusion of latent heat effects caused by the phase change of the water in a pavement structure when it freezes and thaws. To adequately consider these effects, TDHC, a two-dimensional heat conduction finite element model developed by Goering and Zarling (*6*), was selected for the analysis.

Pavement Cross Sections

Hypothetical pavement cross sections were developed to represent to the best extent possible the types of road construction and subgrade materials existing in pavements currently being restricted. Data obtained from a survey of spring load restriction practices (*5*) were weighed heavily in the development of these sections. The data suggested that pavement cross sections on which load restrictions are currently being applied have the following ranges:

	Range	*Normal*
Asphalt surface (in.)	1½–6	2–4
Aggregate base (in.)	4–18	6–12

On the basis of this information, 2- and 4-in. asphalt surface courses and 6- and 12-in. unbound aggregate base courses were selected for the cross-sections for the analysis.

The predominant subgrade material present was clay, where load restrictions have reportedly been applied. Silts, gravels, granular materials, and tills were also mentioned as subgrade types requiring restrictions in the survey of current practice (*5*). Based on this information, both fine and coarse subgrade materials were modeled in the analysis. The pavement sections chosen for analysis are shown in Figure 1.

Material Thermal Properties

The thermal properties required for the analysis are the frozen and unfrozen thermal conductivity, the frozen and unfrozen volumetric specific heat capacity, and the latent heat. The values for the various materials are shown in Table 1. These properties are a function of the dry density of the material (γ_d) and the moisture content (w). Values for the thermal conductivity of the unbound materials were estimated using Kersten's equations (*7*) and assuming that all of the moisture is frozen at temperatures below 32°F, a reasonable assumption for granular materials. Fine-grained materials may contain unfrozen moisture at temperatures below 32°F; however, it was assumed for this analysis that all of the moisture was frozen during the freezing season. The amount of unfrozen water affects the volumetric latent heat, which is a significant variable in the rate of advancement of the thawing plane.

CLIMATIC VARIABLES

Previous work in pavement thermal analyses (*8–10*) has shown that the following surface thermal effects warrant consideration for realistic predictions of pavement thermal response:

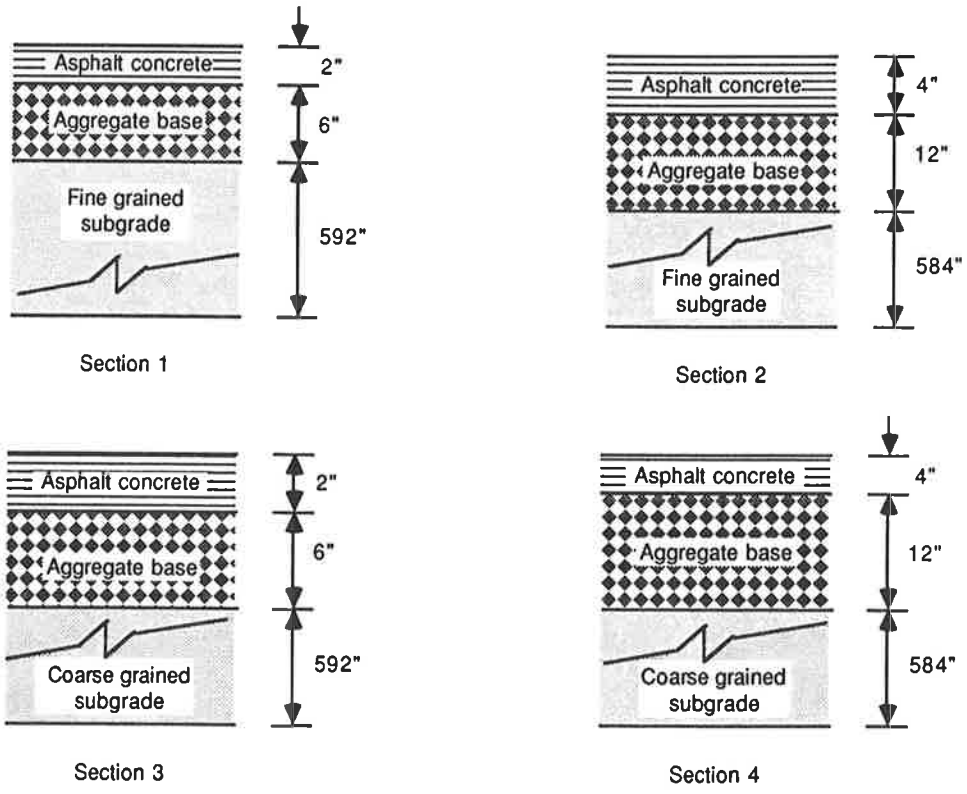

FIGURE 1 Pavement structures for thermal analysis.

TABLE 1 MATERIAL THERMAL PROPERTIES

Material	Dry Density d (lb/ft^3)	Moisture Content w (%)	Thermal Conductivity k_u, k_f (Btu/lb ft ^{0}F)	Volumetric Specific Heat C_u, C_f (Btu/ft^3)	Latent Heat L (Btu/ft^3)
Asphalt Concrete	138	0	0.84	21.0	0
Aggregate Base	130	4	1.15 f* 1.36 u*	24.7 f 27.3 u	749
Fine-grained Subgrade	95	15	0.71 f 0.64 u	23.3 f 30.4 u	2052
Coarse-grained Subgrade	105	10	1.06 f 1.03 u	23.1 f 28.4 u	1512

* The letters f and u denote frozen and unfrozen respectively.

- Air temperature,
- Shortwave radiation,
- Longwave radiation, and
- Convection.

These effects were included in the following analysis.

Air Temperature Functions

The TDHC model utilizes a sinusoidal temperature function to model annual air temperature variation. The sinusoidal air temperature functions were obtained by equating the area under discontinuous monthly air temperature functions, obtained from monthly temperature data, to the area under a sine curve with the same average annual air temperature.

Sinusoidal air temperature functions were obtained for 60 locations in frost areas in the United States (*11*). Locations in Alaska were excluded because of the existence of permafrost and extremes in solar radiation because latitude alters the ground thermal regime compared with that of the "lower 48" states. The data used included the average annual air temperature and average monthly temperatures for 30 years from 1941 to 1970.

From these results five air temperature functions were defined to represent a range of intensity of freezing conditions. Freezing index was used to indicate the intensity of freezing. It is defined as follows:

$$FI = \sum_{\substack{\text{freezing} \\ \text{season}}} (32 - T_{avg}) \times (1 \text{ day}) \quad (1)$$

where FI is the freezing index, in degree-days Fahrenheit, and T_{avg} is the average daily temperature, in degrees Fahrenheit.

The freezing index cases used in the analysis ranged from 500 °F-days to 2,500 °F-days. This range was selected on the assumption that freezing in cases of fewer than 500 °F-days would not be too critical because of the limited amount of frozen material and the brief duration of the thawing period. The upper limit was chosen on the basis of the air temperature data.

Regression analyses were performed for the freezing index, and for five air temperature variables—average annual temperature (T_m), amplitude of temperature variation (T_a), duration of the freezing season, start of thawing, and the phase lag of the sine function (ϕ)—to obtain the sinusoidal air temperature functions required for TDHC. The results are shown in Table 2.

Shortwave Radiation

The data used for estimating the shortwave radiation were also obtained from Cinquemani et al. (*11*). Data were collected from pyranometer measurements of shortwave radiation over a period of 24 or 25 years. No correlation between the shortwave radiation data with location (latitude) or freezing index was found. The primary dependent variable for solar radiation was solar declination or time of the year. Therefore, average values of surface solar radiation heat flux for the months from January through May were calculated from the data and used in the analysis. The absorbed shortwave radiant heat flux is equal to $1 - \alpha_s$ times the incoming shortwave radiation, where α_s is the surface albedo. Scott (*12*) reported a value of 0.1 for α_s.

Longwave Radiation

No data for the broad study area were found for longwave radiation. Therefore a quasi-theoretical approach was used

TABLE 2 AIR TEMPERATURE FUNCTION DATA FOR TDHC ANALYSIS

Freezing Index Case (^{0}F days)	Mean Annual Temperature (^{0}F)	Amplitude of Temperature Variation (^{0}F)	Phase Lag (days)	Duration of Freezing (days)	Start of Thawing (days from Jan 1)	Thawing Index (^{0}F days)
500	47.8	23.7	17	99	67	6276
1000	45.0	25.3	16	118	74	5770
1500	42.3	26.9	14	136	82	5265
2000	39.5	28.5	13	154	90	4760
2500	36.7	30.1	11	173	97	4254

for estimating longwave radiation flux at the pavement surface. Theoretically, the longwave radiation at the pavement surface emitted from the ground and the atmosphere for clear sky conditions is

$$Q_{RLO} = \sigma \varepsilon_s T_s^4 - \sigma \alpha_e \varepsilon_a T_a^4 \quad (2)$$

where

Q_{RLO} = longwave radiation at the pavement surface,
σ = Stefan Boltzmann constant,
ε_s = emissivity of the pavement surface,
ε_a = emissivity of the atmosphere,
α_e = absorptivity of the pavement surface, and
$T_{s,a}$ = temperature of the pavement surface and atmosphere, respectively.

Two temperatures, T_s and T_a, are required for evaluation of longwave radiation. Results obtained in preliminary analyses suggested that pavement surface-air temperature differences vary from about 1°F in January to about 10°F in May. The values used for T_s were based on these results.

The value used for the longwave emissivity of asphalt concrete was 0.93 in Equation 2, reported by Kreith (*13*). The value of the atmospheric emissivity used was obtained from the following expression formulated by Swinbank (*14*):

$$\varepsilon_a = 0.398 \times 10^{-5} T_a^{2.148} \quad (3)$$

where T_a is equal to the reference air temperature in degrees centigrade.

Finally, the net ongoing longwave radiation is reduced because of the presence of clouds in the atmosphere (*10,15*). The effect of cloud cover on outgoing longwave radiation was treated empirically using the following relationship proposed by Lunardini (*16*):

$$Q_{RLN}/Q_{RLO} = 1 - 0.8C_e \quad (4)$$

where

Q_{RLN} = net outgoing longwave radiation caused by cloud cover,
Q_{RLO} = clear sky outgoing surface radiation, and
C_e = 24-hr average fraction of sky covered by clouds.

The value of C_e was obtained from cloud cover data from Ruffner and Bair (*17*) for 33 locations in the frost area of the United States. These data were averaged for use in the above expression.

Convection

Vehrencamp (*18*) developed a formula for the convection coefficient (h) based on data collected on a dry lake bed. Because the conditions on which the formula is based are the closest available to a pavement surface, the Vehrencamp equation was selected for use in the analysis.

$$h = 122.93\,[0.00144\, T_m^{0.3} V^{0.7} + 0.00097(T_s - T_a)^{0.3}] \quad (5)$$

where

h = convection coefficient in Btu/hr ft^2 °F,
$T_{s,a}$ = pavement surface and air temperature, respectively, in °C,
V = average windspeed, in m/sec, and
T_m = $(Ts + Ta)/2 + 273.0$.

The air surface temperature differences given above for longwave radiation were used to evaluate the convection coefficient (h). Average monthly windspeeds were obtained from Ruffner and Bair (*17*) for January through May for 38 locations in the northern United States. The monthly averages for all of the data for January through May were 10.7, 10.7, 11.4, 11.5, and 10.2 mph, respectively. The convection coefficients obtained for these months were 2.9 Btu/hr ft^2 °F for January and February, 3.1 for March, 3.2 for April, and 3.0 for May.

ANALYTICAL PROCEDURE

Many different edge conditions exist in pavements, depending on local topography, embankment requirements for construc-

tion, and shoulder size. These conditions, as well as snow cover conditions, result in various boundary conditions and problem geometry for two-dimensional modeling. Aldrich (*19*) and Straub et al. (*20*) concluded that one-dimensional modeling of pavement freezing or thawing is satisfactory for cases in which the depth of frost penetration is small compared with the width of the pavement. This is generally the case in seasonally frozen ground.

TDHC uses triangular elements in the problem formulation. A 1-ft-wide strip was assumed for the one-dimensional analysis. Elements in the upper 2 ft of the pavement structure, which included the asphalt surface course, the granular base course, and from 4 to 12 in. of subgrade were 2 in. thick. From 2 to 6 ft (this is always in the subgrade layer) the element thickness was increased to 4 in. From 6 to 10 ft, element thicknesses were 6 in. From 10 to 50 ft, the elements were 5 ft thick.

To initialize the problem, a thermal analysis was performed on the pavement structure using air temperature as the only thermal driving force. This analysis was done for a period of 1 year starting at midfreezing season. After this, all surface thermal variables were included to evaluate the ground temperature variation throughout the remaining freezing season and the thawing period.

The heat flux at the surface caused by the net radiation and the convection coefficient changed abruptly at the beginning of each month since the values for radiant heat flux and the convection coefficient were obtained from monthly data. This resulted in some oscillation of the surface temperatures at the start of the month when the new values were introduced. For freezing index cases, in which the start of thawing and a step input occurred simultaneously, "flash" thawing occurred, resulting in up to as much as 2 ft of thawing in one day. These effects were mitigated by defining new sinusoidal temperature functions for surface temperatures that included the radiant heat and convective effects. These temperature functions were obtained from the stepped results and are given in Table 3. Using these revised temperature functions, all cases were reevaluated from midfreezing season until the end of the thawing period.

RESULTS

Comparison of Pavement Air/Surface Temperature

The net effect of solar and longwave radiation and convection occurring at the pavement surface is a net heat flux into the pavement causing surface temperatures to be higher than air temperatures. It was found that all pavement structures experienced the same surface temperatures during thawing (within 0.2°F) on the same day for a given freezing index case, suggesting that layer thicknesses and subgrade thermal properties have almost no effect on the surface temperatures. Air temperature, windspeed, and net radiation heat flux were the primary variables governing the pavement surface temperatures. The absorptive properties of the surface material also affect the amount of heat absorbed and the resulting surface temperature.

The air temperatures and surface temperatures obtained from the analysis for each freezing index case from midfreezing season to June 1 indicate that surface-air temperature differences are approximately equal at the same time for all freezing index cases. On February 1 the surface-air temper-

TABLE 3 SURFACE TEMPERATURE FUNCTIONS FOR TDHC ANALYSIS

Freezing Index FI (^{0}F days)	Mean Annual Temperature T_m (^{0}F)	Amplitude of Temperature Variation, T_a (^{0}F)	Phase Lag ϕ (days since Jan 1)
500	58.4	32.6	17
1000	54.0	32.3	16
1500	50.8	33.4	14
2000	48.1	35.1	13
2500	45.5	37.0	11

$$T = T_m - T_a \cos (2\pi t/365 - 2\pi \phi/365)$$

where
- T = the surface temperature at time t
- T_m = the mean annual temperature
- T_a = the amplitude of annual temperature variation
- t = the time in days after January 1
- ϕ = the phase lag of the temperature sine curve, in days after January 1

ature difference ranged from 2.0 to 2.4°F for the five freezing index cases. On March 1 the temperature difference varied from 3.9 to 4.2°F. On April 1 and May 1 the surface-air temperature differences ranged from 6.9 to 7.1 and 10.5 to 11.0°F, respectively. Figure 2 shows the average daily pavement surface-air temperature difference versus time.

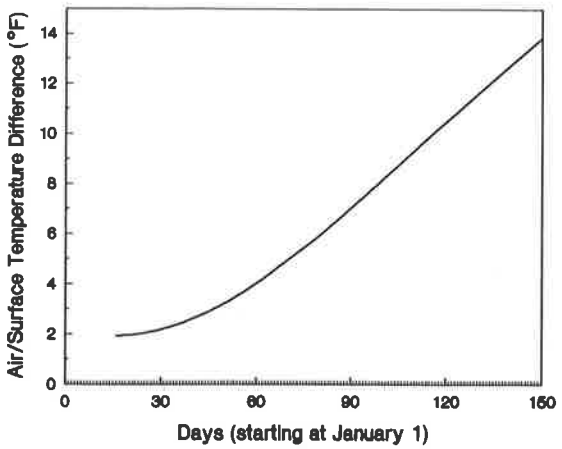

FIGURE 2 Average daily pavement surface/air temperature difference versus time.

Advancement of the Thawing Plane

In a previous work (*4*) the results of structural analyses on these pavement structures were reported. Based on this work and findings from other studies (*1–3*) the times selected for structural analysis of the pavement were base thawing, 4 in. of subgrade thawing, and complete thawing. The advancement of the 32°F isotherm, assumed to be coincident with the thawing plane, was obtained from the TDHC analysis. The results are given in Table 4. Included in this table is the day starting with day 1 on January 1 when (a) air temperatures reach 32°F, (b) pavement thawing begins, (c) base thaw occurs, (d) 4 in. of subgrade thawing occurs, and (e) complete thaw has occurred.

These results suggest that the intensity of the prior freezing season, date, and the type of subgrade have little effect on the time required for base thawing to occur for the range of climatic conditions studied. Thin pavements consisting of 2 in. of AC and 6-in. granular base courses took from 1 to 4 days to thaw through the base with an average of 2.7 days. The thick pavements analyzed consisted of 4 in. of AC and 12 in. of unbound base material. Base thawing for these pavements ranged from 4 to 9 days, with an average of 6.4 days. No trend of increasing duration of base thawing with increasing freezing index was evident from the results.

Four-Inch Subgrade Thaw

Early subgrade thawing also appeared to be unaffected by date or intensity of the previous freezing season. Thin pavements thawed more quickly to this level than did the thick pavements. The effects of the subgrade thermal properties were also apparent in the results. The time required for 4-in. subgrade thawing for pavement sections with thin pavement structures and fine subgrades ranged from 3 to 10 days, with an average of 6.8 days, whereas thin pavements on coarse subgrades thawed in an average of 5.8 days.

The thick pavements founded on the fine subgrades achieved 4 in. of subgrade thawing in 5 to 14 days in the analysis with an average of 12.4 days. By comparison, the coarse subgrade cases thawed in 6 to 13 days, with an average of 9.8 days. In the analysis of the thick pavements with fine subgrades an atypically short duration of thawing of 5 days was obtained from the results for a freezing index of 1,500 °F-days. If one were to eliminate this data point from the group, the average time for thawing would increase to 14.2 days.

Total Thaw

The results for total thawing suggested that the duration of thawing was dependent on the intensity of the previous freezing season and also on the subgrade thermal properties. The duration of thaw increased with increasing freezing index for all cases. In addition, the duration of thawing for similar structures and freezing indices for fine subgrades was usually longer than the comparable coarse-grained subgrade case caused by the lower thermal conductivity and increased latent heat of the subgrades. Table 4 shows the duration of total thaw for all cases. Total thawing for thin pavements with fine subgrades ranged from 16 days for an FI of 500 °F-days to 58 days for 2,500 °F-days. Thin pavements with coarse subgrades took from 20 to 54 days to thaw. Thick pavements with fine subgrades took 21 to 70 days to thaw for the range of freezing index cases. Similar pavements with coarse subgrades thawed in 16 to 51 days.

Duration of Thaw

The results for duration of total thawing were used to see if a relationship could be found between the freezing index and duration of thawing. A regression analysis was performed for all fine subgrade cases and all coarse subgrade cases. In addition, all cases analyzed were combined in a regression analysis. The results are shown in Figures 3 through 5. Also shown are the regression equations, correlation coefficients, and R^2 values for each regression performed. The regression equations obtained are as follows:

Fine-grained subgrade materials:

$$D = 0.0233FI + 8.0 \quad (6)$$

Coarse-grained subgrade materials:

$$D = 0.0176FI + 10.9 \quad (7)$$

All subgrade materials combined:

$$D = 0.02\ FI + 9.5 \quad (8)$$

where D is the duration of the thawing period in days and FI is the freezing index in °F-days.

TABLE 4 ADVANCEMENT OF THE THAWING PLANE

Freezing Index Case (^{0}F days)	Air Temperature = 32 ^{0}F (day from Jan 1)	Start Thaw (day from Jan 1)	Base Thaw (day from Jan 1)	4" Subgrade Thaw (day from Jan 1)	Total Thaw (day from Jan 1)
2/6 Fine*					
500	66	54	54	62	70
1000	76	64	67	67	96
1500	83	71	74	81	117
2000	89	77	81	84	125
2500	94	81	84	87	139
4/12 Fine					
500	66	54	61	70	75
1000	76	64	70	78	94
1500	83	71	76	76	110
2000	89	77	83	91	132
2500	94	81	88	94	151
2/6 Coarse					
500	66	54	54	60	74
1000	76	64	67	71	94
1500	83	71	75	77	110
2000	89	77	80	83	123
2500	94	81	83	87	135
4/12 Coarse					
500	66	54	62	64	70
1000	76	64	68	70	93
1500	83	71	76	80	108
2000	89	77	84	90	128
2500	94	81	90	92	132

* 2/6 Fine denotes 2" AC, 6" Base, Fine Subgrade.

The correlation coefficients for all fine subgrade cases combined and all coarse subgrade cases combined were 0.94 and 0.96, respectively. The results for all cases was 0.92. Although the regression of all cases combined resulted in the lowest correlation of all combinations, the results obtained from TDHC consistently reflect a relationship between freezing index and duration of thawing.

SENSITIVITY

Reference Case

The results reported apply to specific values for climatic variables, and pavement and subgrade material properties. It was of some interest to perform a sensitivity analysis to see how the results varied with changes in the values assumed for the external and internal variables.

The freezing index case of 1,000 °F-days was selected to perform the sensitivity analysis. The average *FI* for the locations from which climatic data were collected was 929 °F-days. Therefore, it was felt that this case would best represent the "typical" freezing intensity. The pavement structure selected was a thin pavement (2 in. AC and 6 in. base) with a fine subgrade because this case represented the most critical pavement sections with regard to timely application of load restrictions. Three thin pavements with coarse subgrades were also analyzed to consider the variation in thawing for coarse subgrades with varying thermal properties.

Variables Selected for Study

A total of 15 cases were included in the sensitivity analysis. They included the following variations:

1. Maximum and minimum latitude;
2. Maximum and minimum cloud cover;
3. Maximum and minimum windspeed;
4. Three fine subgrade thermal property cases;
5. Three coarse subgrade thermal property cases; and
6. Three location-specific temperature cases.

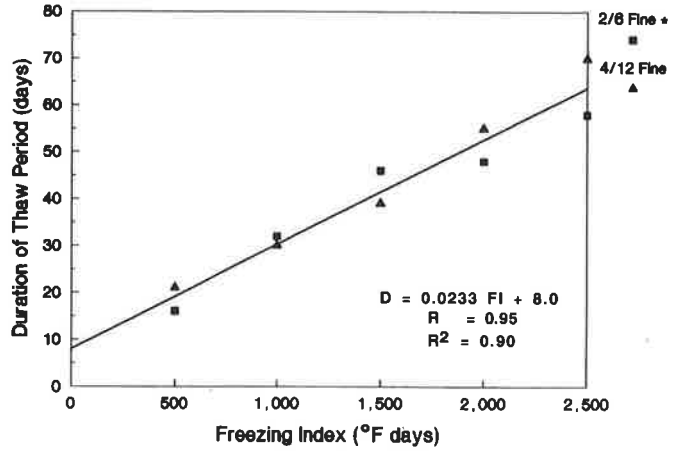

FIGURE 3 Duration of thaw versus freezing index, fine subgrades.* 2/6 fine denotes 2-in. AC, 6-in. base, fine subgrade.

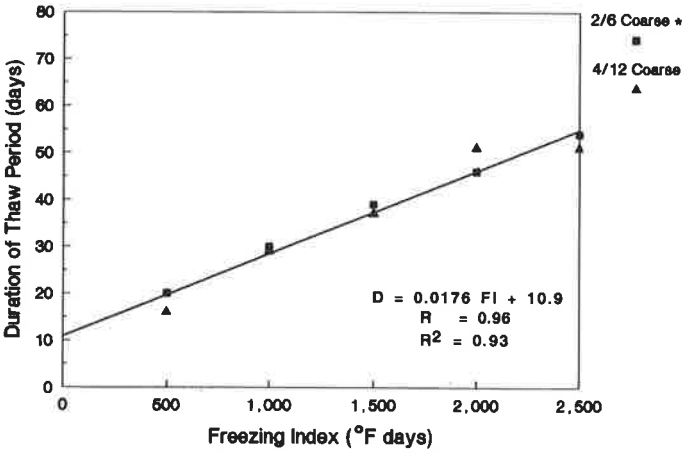

FIGURE 4 Duration of thaw versus freezing index, coarse subgrades.

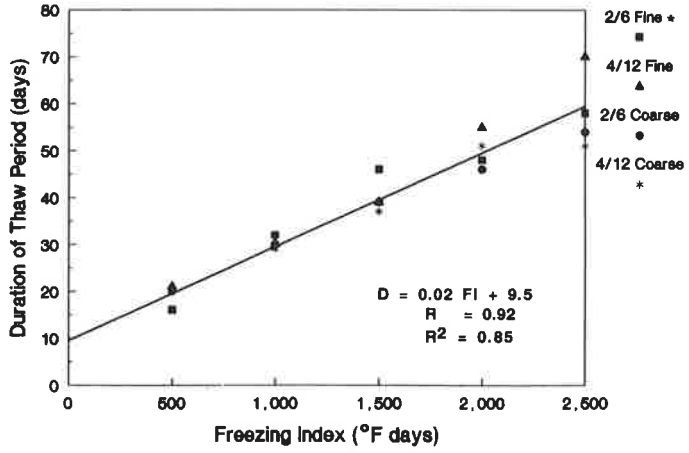

FIGURE 5 Duration of thaw versus freezing index, all cases.

The variables related to climate that were selected were chosen from an in-depth analysis of the primary variables that affect the radiation and convection coefficient at the surface (*21*).

Results

It was found that the smoothing procedure used to obtain the sinusoidal surface temperature functions could not be used for the sensitivity analysis. Therefore, the sensitivity results that will be presented for variations in external variables will be from stepped TDHC analyses.

Latitude Sensitivity

The variation in pavement surface temperature compared with the reference case for the minimum and maximum values of latitude assumed ranged from approximately 0.5°F to 1.5°F. The greatest variation occurred in February and March when the differences in heat flux caused by latitude variation are the greatest.

Thawing started on day 63 or March 4 for the maximum latitude case as compared with day 60 and day 62 for the minimum latitude and reference case, respectively. The duration of thaw ranged from 30 days for the minimum latitude to 33 days for the maximum latitude compared with 32 days for the reference case.

Cloud Cover Sensitivity

The effect of varying the amount of cloud cover on net radiant heat flux was found to increase with time into the thawing period. However, even during the late freezing season the effect of variations in the amount of cloud cover on net radiant heat was found to be rather small. Reductions in incoming solar radiation were approximately balanced by reductions in outgoing longwave radiation. During the thawing period, pavement surface temperatures for maximum and minimum cloud cover conditions varied by no more than +1°F.

Thawing started on day 63 or March 4 for the case of maximum cloud cover condition. Thawing for the minimum cloud cover assumed for analysis started on day 61. The duration of thawing for the minimum cloud cover case was 25 days compared with 32 days for maximum cloud cover.

Windspeed Sensitivity

Variations in windspeed that affect the convection coefficient caused the greatest variation in pavement surface temperatures. In early February, pavement surface-air temperature differences for maximum windspeed conditions were about 2.7°F. At the same time, minimum windspeed conditions produced surface-air temperature differences of about 4.5°F, compared with 3.5°F for the reference case. As thawing progressed into early April, pavement surface-air temperature differences ranged from 7.5 to 11.7°F for the maximum and minimum values of windspeed, respectively, compared with 8.7°F for the reference case.

The start of the thawing period and the duration of thawing were most significantly affected by the assumed variation in windspeed compared with the results from the other external variables considered in the sensitivity analysis. For the minimum windspeed case, thawing started on day 58 or February 27, as compared with March 3 (day 62) for the reference case and March 4 (day 63) for the maximum windspeed case. Thawing took 28 days under minimum windspeed conditions and 35 days for the maximum case.

Location-Specific Temperature Functions

It was also apparent from review of the sinusoidal temperature functions obtained for individual locations that some variation in mean annual temperature, amplitude of temperature variation, and phase lag could occur and still produce an equivalent freezing index. Therefore, three location-specific air temperature and freezing index cases were analyzed and compared to those of the reference case. The locations selected were Miles City, Montana; Burlington, Vermont; and LaCrosse, Wisconsin. The freezing indices computed for these locations were 1,022, 1,012, and 1,026 °F-days, respectively. When these location-specific temperature functions were analyzed, it was found that the pavement surface-air temperature differences varied by less than 1°F on any given date for the three locations studied compared with those from the reference case.

The start of thawing dates for LaCrosse, Miles City, and Burlington were March 4, 5, and 8, respectively. For all of these locations the start of thawing occurred after the start of thawing for the 1,000 °F-day reference case, which was on March 3. Total thaw occurred in 29 days in LaCrosse, 32 days in Burlington, and 36 days in Miles City.

Thermal Property Sensitivity

In the thermal property sensitivity portion of the sensitivity analysis, the air temperature functions and surface fluxes used were the same as those in the reference case. Therefore, no comparisons of surface temperatures or pavement surface-air temperature differences were made. The thaw period started on the same day, March 3, for all cases. Only the duration of thawing varied with changes in thermal properties. For the fine subgrade cases the duration of thawing ranged from 20 days for denser subgrades with lower moisture contents to 36 days for less dense materials with high water contents as shown in Table 5. The advancement of the thawing plane was similar for the third fine subgrade case analyzed, assumed to be 95 percent saturated, for the case in which the dry density was 80 lb/ft^3 and the reference case (γ_d = 95 lb/ft^3). The subgrade with a dry density of 110 lb/ft^3 thawed much more rapidly (20 days). This rapid thawing was probably caused by reduced conductivity and latent heat effects.

The duration of thaw for coarse subgrade cases is also shown in Table 5. The thaw period ranged from 16 days for denser subgrades with lower moisture contents to 36 days for looser subgrades with greater moisture contents compared with 30 days for the reference case. The 95 percent saturated case thawed in 34 days. The rapid thawing of the dense coarse subgrade case is evident in these results. It is also interesting

TABLE 5 THAW PLANE ADVANCEMENT FOR SENSITIVITY ANALYSIS OF EXTERNAL VARIABLES

CASE	Day Air Temperature = 32 °F (from 1/1)	Start Thaw (from 1/1)	Base Thaw (from 1/1)	4 Inches Subgrade Thaw (from 1/1)	Total Thaw (from 1/1)	Duration of Thaw (days)
Maximum Latitude	76	63	65	74	93	30
Minimum Latitude	76	60	60	60	93	33
Maximum Cloud Cover	76	63	63	66	95	32
Minimum Cloud Cover	76	61	65	71	86	25
Maximum Windspeed	76	63	64	70	98	35
Minimum Windspeed	76	58	58	64	85	28
Miles City, MT	84	64	61	70	100	36
Burlington, VT	83	67	69	76	99	32
LaCrosse, WI	75	63	64	64	92	29

to note the early rapid thawing of the 95 percent saturation case. It is not known if one could expect such rapid thawing in actual field conditions.

Conclusions on Sensitivity Analysis

The results of pavement surface-air temperature differences and the duration of thawing from the sensitivity analysis are of importance in developing guidelines (and their limitations) for timing load restrictions. The results reported suggest that latitude variations cause the greatest variation in pavement surface-air temperature differences in late February and early March (early thawing), and windspeed variations resulted in the greatest variation in pavement surface-air temperature differences in late March and early April (late thawing).

Figure 6 shows the variation in duration of thawing for all climatic variables and subgrade thermal properties for fine subgrades. The greatest range in response occurred because of variations in subgrade thermal properties. Variations in latitude had the least effect on the variation in duration of thawing. The remaining variables, cloud cover, windspeed, and air temperature functions resulted in variations of 6 to 7 days in duration of the thawing period compared with those of the reference case.

CONCLUSIONS AND RECOMMENDATIONS

The results of the thermal analysis suggest that pavement surface temperature relative to air temperature is primarily a function of date. The relationship of pavement surface-air temperature is of great importance in the timely application of load restrictions because it is apparent from the results that thawing will begin well in advance of air temperatures reaching 32°F. The minimum air temperature that will be sufficient to initiate pavement thawing on a given date in the spring is shown in Figure 7.

Further, it was found that the number of days required for pavement structures to thaw to the bottom of the base layer was 1 to 4 days for thin pavements and 4 to 9 days for thick

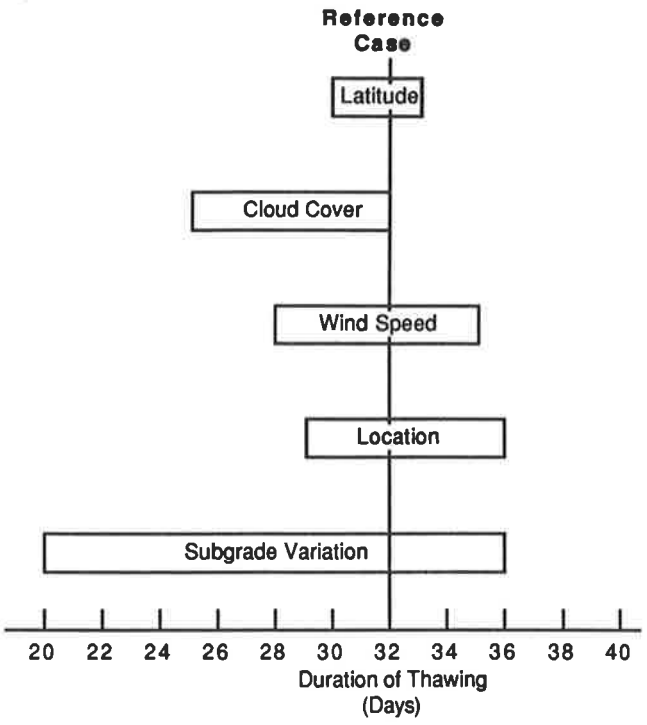

FIGURE 6 Sensitivity of duration of thawing of fine subgrades.

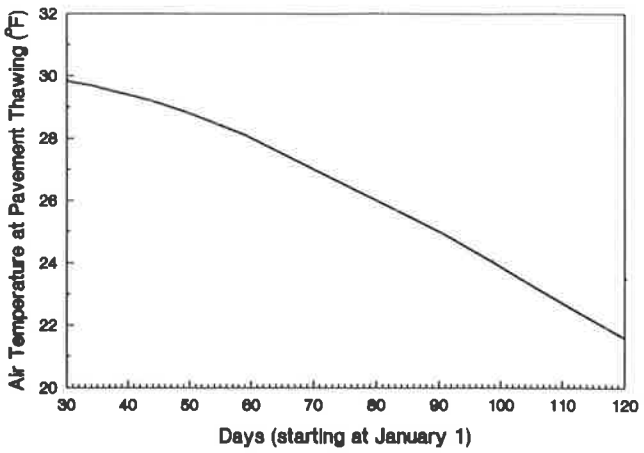

FIGURE 7 Air temperature at pavement thawing versus time.

pavements. When thawing proceeds into the subgrade, previous studies (*4*) suggest that asphalt tensile strains and subgrade vertical strains may be significantly increased; that is, the "critical" period has been reached.

Thawing proceeded into the subgrade at a slower rate because of greater moisture contents in these materials and the effects of latent heat. Equations 6 through 8 were presented for the duration of the thawing period as a function of freezing index for coarse subgrade materials, fine subgrade materials, and all subgrade material types combined.

It is intended that personnel involved with management of low-volume roads where spring load restrictions are typically applied could use Figure 7 to aid in determining when pavement thawing will begin. Further, these individuals could collect air temperature data during the freezing season to calculate the freezing index that could be used to estimate the duration of the thawing period using either Equation 6, 7, or 8.

However, the duration of thawing should not be confused with the duration of the critical period. Although the end of the thawing period indicates the limit of time when excess moisture is being generated from previously frozen materials, many pavements, particularly those with fine-grained subgrades, are not sufficiently recovered at this time to sustain normal load levels without damage.

In using the results presented, it is important to recognize that the greatest variation in the results occurred for variations assumed for dry density and moisture content of the subgrade materials in the analysis. Therefore, the results obtained for the duration of thawing are expected only to approximate the duration of the thaw period for an arbitrary pavement structure.

REFERENCES

1. R. N. Stubstad and B. Connor. *Prediction of Damage Potential on Alaskan Highways during Spring Thaw Using the Falling Weight Deflectometer*. Alaska Department of Transportation, Fairbanks, 1982.
2. *Recommended Guidelines for Imposing and Lifting Springtime Restrictions*. Minnesota Department of Transportation, St. Paul, 1985.
3. J. A. Lary, J. P. Mahoney, and J. Sharma. *Evaluation of Frost Related Effects on Pavements*. Report WA-RD 67.1. Washington State Department of Transportation, Olympia, May 1984.
4. M. S. Rutherford. Pavement Response and Load Restrictions on Spring Thaw Weakened Flexible Pavements. In *Transportation Research Record 1252*, TRB, National Research Council, Washington, D.C., 1989, pp. 1–11.
5. M. Rutherford, J. P. Mahoney, R. G. Hicks, and T. Rwebangira. *Guidelines for Spring Highway Use Restrictions*. Report WA-RD 80.1. Washington State Department of Transportation, Olympia, 1985.
6. D. Goering and J. Zarling. *TDHC Finite Element Program User's Manual*. University of Alaska, Anchorage, 1985.
7. M. S. Kersten. *Thermal Properties of Soils*. University of Minnesota Engineering Experiment Station, Minneapolis, Bulletin 28. 1949.
8. B. J. Dempsey and M. R. Thompson. A Heat Transfer Model for Evaluating Frost Action and Temperature Related Effects in Multilayered Pavement Systems. In *Highway Research Record 342*, HRB, National Research Council, Washington, D.C., 1970, pp. 39–56.
9. T. W. Miller. The Surface Heat Balance in Simulations of Permafrost Behavior. ASME Paper 75-WA/H7-86. Presented at Annual Meeting of American Society of Mechanical Engineers, Nov. 1975.
10. R. L. Berg. *Energy Balance on a Paved Surface*. CRREL Technical Report TR 226. Cold Regions Research and Engineering Laboratory, Hanover, N.H., 1974.
11. V. Cinquemani, J. R. Owenby, and R. G. Baldwin. Input Data for Solar Systems. National Oceanic and Atmospheric Administration Report to Department of Energy, November 1978.
12. R. F. Scott. *Heat Transfer at the Air-Ground Interface with Special Reference to Airfield Pavements*. MIT Department of Civil Engineering Technical Report 63, Massachusetts Institute of Technology, Cambridge, 1961.
13. F. Kreith. *Principles of Heat Transfer*. Intext Educational Publishers, New York, 1973.
14. W. C. Swinbank. Longwave Radiation from Clear Skies. *Quarterly Journal Research, Meteorological Society*, Vol. 89, 1963, pp. 339–348.
15. H. Wexler. *Observations of Nocturnal Radiation at Fairbanks, Alaska*. U.S. Weather Bureau, Monthly Weather Review, Suppl. No. 46, 1941.
16. V. J. Lunardini. *Heat Transfer in Cold Climates*. Van Nostrand Reinhold Company, New York, 1981.
17. J. A. Ruffner and F. E. Bair, ed. *The Weather Almanac*, Gale Research Co., Detroit, Mich., 1984.
18. J. E. Vehrencamp. Experimental Investigation of Heat Transfer at an Air-Earth Interface. *Transactions, American Geophysical Union*, Vol. 34, No. 1, 1953, pp. 22–29.
19. H. P. Aldrich. Frost Penetration Below Highway and Airfield Pavements. *Bulletin 135*, HRB, National Research Council, Washington, D.C., 1953, pp. 124–149.
20. A. L. Straub, H. N. Schenck, and F. E. Przybycien. Bituminous Pavement Temperature Related to Climate. In *Highway Research Record 256*, HRB, National Research Council, Washington, D.C., 1968, pp. 53–77.
21. M. Rutherford. *An Evaluation of Timing and Magnitude of Load Restrictions on Spring Thaw Weakened Flexible Pavements*. Ph.D. dissertation. University of Washington, Seattle, 1988.

Publication of this paper sponsored by Committee on Flexible Pavement Design.

Integrated Computer Model to Estimate Moisture and Temperature Effects Beneath Pavements

D. E. PUFAHL, R. L. LYTTON, AND H. S. LIANG

The Integrated Model, developed for highway engineers involved in pavement design and management, provides a computer simulation of climatic effects on the behavior of pavement materials and subgrade conditions or characteristics over several years of operation of either asphaltic concrete or portland cement pavements. The results indicate that reasonable predictions of moisture and temperature conditions, frost penetration and heave, thaw weakening, and the accompanying effect on pavement moduli can be achieved. An overview of the model is provided and some typical results for two climatic regions in the United States are presented. The input variables were reduced to a minimum number and were assembled so that they were input in a free format on input user screens that appear sequentially in the course of data entry. Climatic data have been assembled and processed within the files of the program so that users are relieved of obtaining and entering large quantities of this information. At the same time, users can enter their own data if available. Carefully selected default options that are representative of material properties of many typical highway pavement structures may be used, or a compendium of alternative data for a variety of soils based on texture and index properties is provided in the User's Manual. Deep ground temperatures and moisture conditions can be estimated from regional maps supplied in the Manual. These features should make the Integrated Model attractive to most highway design offices. The results of this simulation procedure will provide an important contribution to the complex process of assessing climatic effects on pavement design and management.

Rational methods of pavement management for America's massive, aging road system require sophisticated computer models capable of simulating not only load repetitions and configurations, and material properties, but perhaps more importantly the environmental factors that affect pavement design, performance, and longevity.

Although the importance of climatic influences on pavement performance has been recognized for the last 50 years or more, efforts to incorporate these parameters into pavement management in a comprehensive manner have been less successful than have load response models.

Traditionally, the worst-case scenario, usually the fully saturated case, for base course, subbase, and subgrade has been adopted for design purposes. Recent studies are showing that important climatic factors such as temperature, rainfall, wind speed, and solar radiation can be modeled accurately enough for design purposes by using a combination of deterministic and stochastic analytical methods.

These techniques provide the input into climatic-materials-structural, infiltration-drainage, and frost penetration-frost heave and thaw weakening models that result in meaningful simulations of the behavior of pavement materials and of subgrade conditions or characteristics over several years of operation.

The Integrated Model, developed by the Texas Transportation Institute under contract with FHWA, U.S. Department of Transportation, has been designed to perform these tasks. It can be applied to either asphaltic concrete pavements or portland cement pavements.

The model shown in Figure 1 is composed of four major components: the precipitation model [Precip Model (*1*)], the infiltration and drainage model [ID Model (*2*)], the climatic-materials-structural model [CMS Model (*3*)], and the U.S. Army Cold Regions Research and Engineering Laboratory (CRREL) frost heave-thaw settlement model [CRREL Model (*4*)]. A schematic interpretation of their interaction is shown in Figure 1.

For the most part, the component models were developed independently of one another to perform specific tasks. The purpose of the project in developing the Integrated Model was to combine these modules into one major pavement structure and subgrade analysis. As a result, portions of some of the original programs are no longer required, and methods of computations in some segments have been substituted for others. Significant modifications, additions, deletions, the assembly of data, and verification of the program have represented the major developments in the Integrated Model.

This paper is taken from a previously published report (*5*). The paper provides an overview of the model and presents some typical results for various climatic regions in the United States.

FEATURES

General

The Integrated Model has been modified to run on an IBM-compatible microcomputer with a minimum of 286 kilobytes of memory. Full-screen input processor capabilities now allow the user to enter data with considerably more ease and with substantially reduced opportunity for error. These modifications should make this program especially attractive to highway engineers.

D. E. Pufahl, Department of Civil Engineering, University of Saskatchewan, Saskatoon, Saskatchewan, Canada S7N 0W0. R. L. Lytton and H. S. Liang, Materials, Pavements, and Construction Division, Texas Transportation Institute, Texas A&M University, College Station, Tex. 77843.

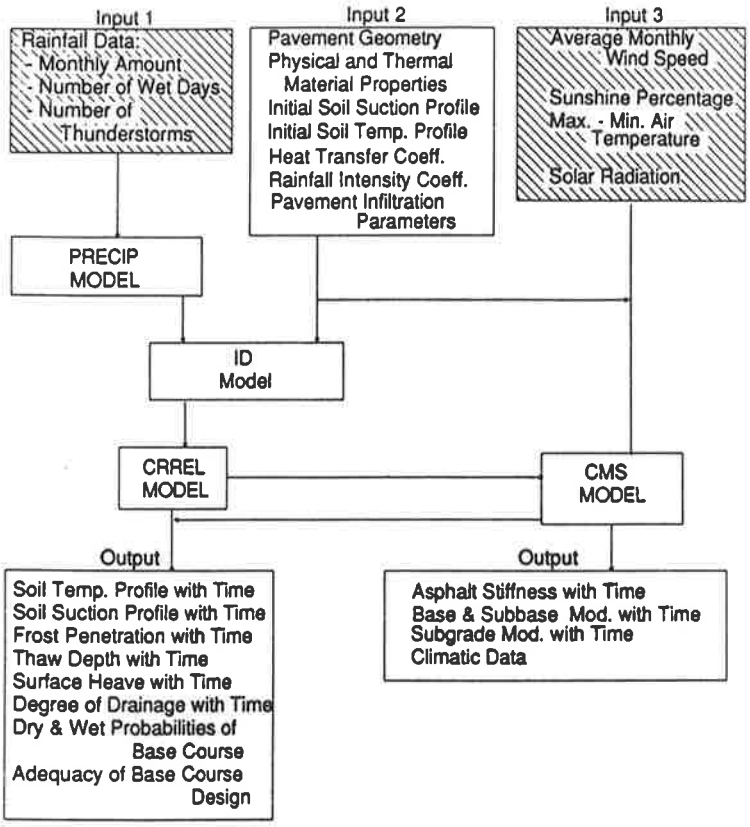

FIGURE 1 Integrated pavement model.

Input

Because a large quantity of climatic input data are required to obtain statistically significant results, users may elect to use representative data from any one of the nine climatic zones in the United States rather than entering their own data for a specific site (Figure 2 and Table 1).

The input data in Figure 1 is shown in three windows. The shaded windows represent data that have been provided in the files of the program. Input 1, which is required for the Precip Model, contains 30 years of precipitation data from the National Oceanic and Atmospheric Administration (NOAA) for each of the nine climatic zones shown in Figure 2. In some cases additional cities have been included, making a total of 15 specific sites. Where the data from more than one city in a region have been tabulated, the average values from the two weather stations may be selected for computations. The data consist of the average monthly rainfall, the number of wet days per month, and the number of thunderstorms.

Input screens allowing users to enter their own data appear sequentially in the course of entering data for the Integrated Model. This information may be obtained from U.S. Weather Bureau Data Summary Sheets for numerous locations throughout the United States.

Input 3 also appears as a shaded window and represents the data required to generate the heat flux boundary conditions at the surface of the pavement. The data in Input 3 consist of monthly averages of air temperature (maximum and minimum), wind speed, and sunshine percentage. Solar radiation is computed in a subroutine that requires only latitude as input. Because air temperature, wind speed, and sunshine percentage represent relatively large quantities of data, the user may prefer to use the information that is tabulated and stored in the program. However, because solar radiation requires only the latitude of the location, users are encouraged to input this value. Again the option of using site-specific data is provided in this input file.

Input 2, which is represented by the clear window in Figure 1, is unique to each site. It consists of pavement structure geometry, material components, physical and thermal material properties, surface heat transfer coefficients, pavement infiltration parameters, and initial soil temperature and suction profiles. Although this list of input variables may appear somewhat daunting at the outset, many of the values can be selected from a list of typical values, or the default options will often be acceptable.

Output

The amount of the level of detail of output from the Integrated Model may be selected by the user. For example, output from the Precip Model consisting of the amount of precipitation, the sequence of wet and dry days, the number of thunder-

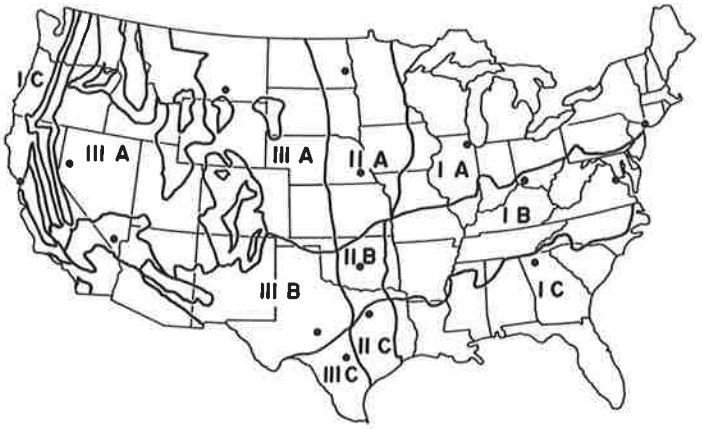

FIGURE 2 Locations of selected cities for each environmental region.

storms, and the distribution of wet days for each month of the analysis may not always be of interest. However this information may occasionally be relevant in assessing the reasonableness of the results. Similarly, the ID Model provides a variety of probabilistic events that generally will be of little interest to the typical user. As a result, either this output has been suppressed or it may appear at the user's discretion.

The output shown at the bottom of Figure 1 will prevail. Since the program will generally simulate conditions for a period of a year or more, monthly or bimonthly samples should be adequate. Provision is made to regulate the frequency of the output.

Although the output in Figure 1 is shown in two different windows, no distinction is made in viewing the results from the program. It is shown here in separate windows only to give the user a general idea of where the computations occur.

The output information is fairly self-evident and will not be reviewed here. Details of the output will be addressed in examples presented later in the paper. A variety of graphic displays allow the user to view many of the results in graphical form.

Pavement Segments In Which Component Models are Used

The four major components of the Integrated Model are used in individual regions of the pavement structure for various temperature and moisture conditions. Figure 3 shows where each of the component models is employed in a typical pavement structure during the course of calculations.

Figure 3 has been divided into two temperature zones: above freezing and below freezing. Additional divisions are based on moisture and temperature conditions.

1. The Precip Model provides the upper-boundary moisture conditions when temperatures are above freezing.
2. The ID Model accounts for the infiltration analysis and the moisture conditions in the materials above the subgrade.
3. Moisture conditions above the surface and infiltration into the base course are not considered when temperatures are below freezing.
4. The heat flux boundary condition at the surface and the temperature profile through the asphaltic or portland cement concrete layers are determined by the CMS Model.
5. All moisture and temperature calculations in the remaining segments of the pavement structure are performed by the CRREL Model.
6. The moisture and temperature conditions at the base of the bottom layer may be held constant with time or varied in a specified manner.
7. Values of resilient moduli depend on moisture content. The moisture contents are determined by the CRREL Model, but the CMS Model is responsible for all calculations of moduli in the base course, subbase, and subgrade.

TABLE 1 SELECTED CITIES FOR EACH ENVIRONMENTAL REGION

Moisture Region	Temperature Region		
	A	B	C
I	New York, NY Chicago, IL	Washington, D.C. Cincinnati, OH	San Francisco,CA Atlanta, GA
II	Fargo, ND Lincoln, NE	Oklahoma City, OK	Dallas, TX
III	Reno, NV Billings, MT	Las Vegas, NV San Angelo, TX	San Antonio, TX

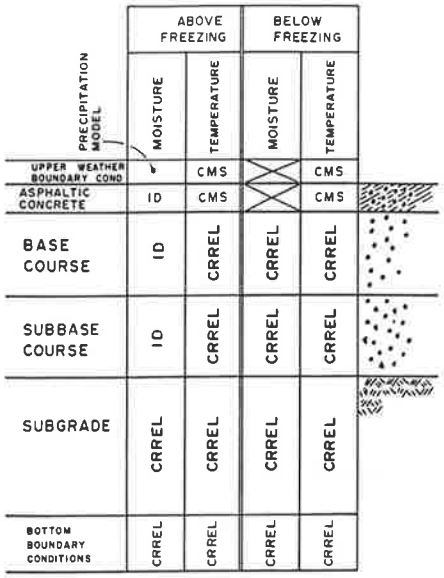

FIGURE 3 Pavement segments where component models are used.

INNOVATIONS IN THE INTEGRATED MODEL

Boundary Condition Subroutines

Surface Conditions

Temperatures throughout the pavement structure are dominated by atmospheric conditions at the surface. Although it is easy to monitor air temperatures, there is not a direct correspondence between air temperatures and surface temperatures. The Corps of Engineers (*6*) has used the surface correction factor (n) to relate air temperatures to surface temperatures. Although the Corps was cognizant of the shortcomings of this approach, a heat flux surface boundary condition was not incorporated into the CRREL Model before the assembly and development of the Integrated Model. The CMS Model is now used to generate a heat flux at the surface, which then establishes the temperature profile through the asphalt or portland cement concrete layers.

Top of Subgrade

In many regions west of the Mississippi River, highway subgrades are composed of fine-grained, low-permeability soils that remain unsaturated throughout the year.

Infiltration of water through the pavement during or after a rainstorm often will produce free water in the base course and subbase. Thus, an abrupt boundary between a positive water pressure in the subbase and a negative water pressure or suction in the subgrade will exist at the interface. The gradient at this boundary equals the sum of the positive pressure in the subbase plus the suction in the subgrade times a pore pressure transfer coefficient (r). The transfer coefficient has units of *l*/distance.

The concept has been adopted from the theory of an insulted, heated steel rod of initial uniform temperature with one end radiating heat to the air at a constant lower temperature. The physical and thermal properties of the rod compared with those of the air are vastly different, and the formulation reveals that the transfer coefficient in the case of the heated rod is a function of the Stefan Boltzmann constant of heat transfer—the absolute temperature of the rod and the thermal conductivity of the rod. The units of the transfer coefficient are *l*/distance.

Mitchell (*7*), using this analogy, showed that a cylinder of soil of known constant suction, enclosed on all sides but open on one end to the atmosphere at a higher suction, underwent increases in suction at the exposed surface and along its entire length in general accordance with the theory used to predict the cooling of the steel rod.

It is postulated here that changes in suction in the subgrade will occur because of changes in water pressure in the base course/subbase in general accordance with the theory of the cooling steel rod or with the changes in suction along the column of unsaturated soil with one end exposed to the atmosphere.

The appropriate range of values for r in the Integrated Model appears to lie between 1.0×10^{-6}/in. and 1.0/in. and is controlled by the magnitude of the permeabilities on each side of the interface. A suggested maximum value for r is numerically equal to the computed velocity of the water into the subgrade under a unit hydraulic gradient.

Bottom Boundary Conditions

Suction

Bottom boundary conditions of temperature and water pressure or suction are entered every 2 weeks for the period of 1 year.

Russam and Coleman (*8*) have found that, in arid climates, if the water table exists within a depth of 25 ft of the pavement surface it will dominate the moisture conditions in the subgrade. Thus, for initial conditions a linear hydrostatic variation of suction from the water table to the top of the subgrade is assumed unless data from locally instrumented sites indicate otherwise. Under the latter circumstances, the minimum depth of the water table must be taken as the maximum depth of the analysis because the CRREL Model is not designed to deal with moisture conditions extending below the water table. As the water table falls in drier periods of the year, suctions can be calculated and input to the lower boundary conditions as specified.

If the water table is below 25 ft, another technique has been adopted in which measured values of suction are not available. Russam and Coleman (*8*) have suggested that the Thornthwaite Moisture Index (*9*) may be used to predict equilibrium soil suction conditions. Figure 4 shows the relationship of soil suction and Thornthwaite Moisture Index for three different soils. Figure 5 provides contours of the Thornthwaite Moisture Index for the continental United States. Thus, an estimate of the bottom boundary moisture conditions can readily be determined from the two figures.

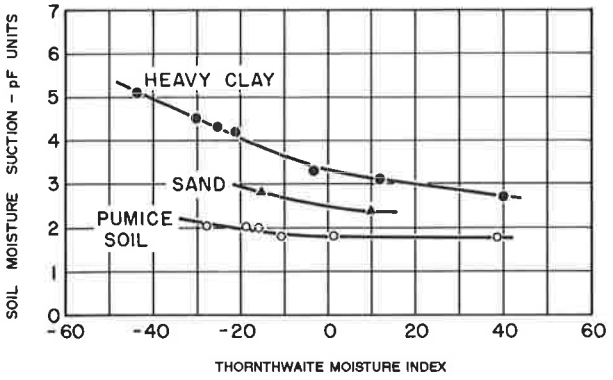

FIGURE 4 Variation of soil suction of road subgrade with Thornthwaite Moisture Index (*8*).

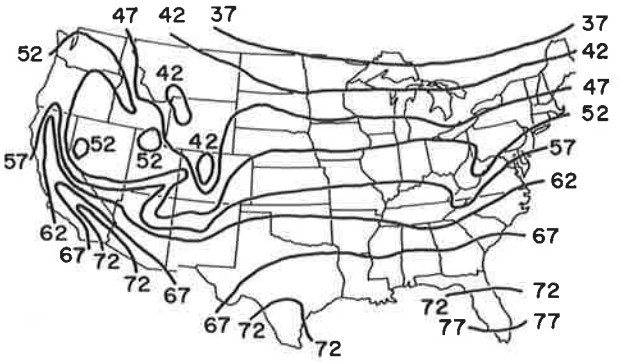

FIGURE 6 Temperature (°F) of water from nonthermal wells at depths of 30 to 60 ft (*11*).

An initial soil suction profile from the bottom boundary to the top of the subgrade on January 1 of the beginning year is required. Thus, an estimate of the position of the water table at that time of year must be made. If no water table is present, the equilibrium suction value may be used throughout the depth of the subgrade.

Temperature

Bottom temperature conditions are handled in much the same way as values of suction. It is desirable to extend the analysis to a depth of constant ground temperature. This value varies with location, but frequently it is on the order of 12 ft [Dempsey et al. (*3*), Fluker (*10*), and others]. Figure 6 provides a measure of bottom soil temperature values for the continental United States if local data are unavailable.

If the depth of the analysis is significantly less than 12 ft because of a high water table, some accommodation will have to be made for changing soil temperatures at the bottom nodes over the period of analysis. It is not possible to provide default options for every situation, and users will have to provide their best estimates based on data and local experience at their location.

An initial soil temperature profile is also required for January 1. A linear relationship between the January mean monthly air temperature at the surface and the bottom constant ground temperature may be assumed. This procedure is equivalent to using an n factor of 1 for surface conditions.

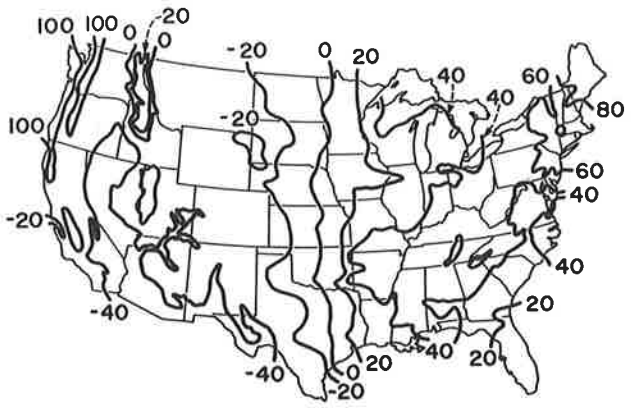

FIGURE 5 Thornthwaite Moisture Index distribution in the United States (*9*).

Base Course/Subbase Moisture Conditions

The drainage analysis in the ID Model considers an initially saturated subbase/base course and computes the time for varying degrees of drainage. However, it is unrealistic to assume that this pavement component ever becomes saturated, especially for free-draining base courses in the more arid regions of the nation. The depth of free water in the subbase/base course is estimated by multiplying the probability of having a wet base course for a given month (one minus the probability of having a dry base course) times the thickness of the subbase/base course. Values for intervening days are computed by linear interpolation.

Unsaturated, Unfrozen Permeability and Temperature-Vapor Pressure

Moisture flow in unsaturated soil conditions requires a model to characterize permeability with changing soil suction and with the formation of ice in the pore spaces of the soil.

The changes in unfrozen water content with time can be expressed as

$$\frac{\delta\theta_u}{\delta t} = \frac{\delta\theta_u}{\delta h_p} \cdot \frac{\delta h}{\delta t} \tag{1}$$

where

θ_u = volumetric water content (unfrozen),
h_p = pore water pressure (suction), and
h = total head (pressure head plus elevation head).

$\delta\theta_u/\delta h_p$ is the slope of the volumetric water content suction relationship or the moisture characteristic curve. This function can be linearized by plotting it on a log-log plot, resulting in

$$\theta_u = \frac{n}{A_w|h_p|^{X_w} + 1} \tag{2}$$

where n equals porosity. A_w and X_w are Gardner's coefficients (*12*), which can be characterized for specific soils based on grain size and plasticity characteristics.

The permeability is related to the soil suction in a similar manner.

$$K_h = \frac{K_s}{A_k|h_p|^{X_k} + 1} \tag{3}$$

where K_s is saturated permeability and A_k and X_k are Gardner's coefficients for permeability.

The original formulation of moisture flow in the CRREL Model divided a freezing column of soil into three zones: a "fully frozen zone," a "freezing zone," and an "unfrozen zone."

Moisture flow was not considered in the fully frozen zone, and Equations 2 and 3 were applied in the unfrozen zone. However, in the freezing zone, the CRREL Model required some method to account for the apparent decrease in permeability that accompanied the formation of ice in the pore spaces of the soil. In the freezing zone the permeability was described as

$$K_f = K_h|h_p|\ 10^{-E\theta_i} \tag{4}$$

where θ_i is ice content and E is a parameter required to reduce K_h accordingly. The E parameter was evaluated by trial and error until the model predicted what was observed in the laboratory or field for various soils.

The Integrated Model eliminates the E parameter by adopting the principle that changes in permeability in the freezing zone occur because of the high suctions that are developed in that zone rather than from ice blocking the pore spaces in the soil structure. This principle implies that Equations 2 and 3 remain applicable, and that a relationship between suction and temperature is required at temperatures below freezing.

This relationship has been developed from the original work by Washburn (*13*) and is described in equation form as

$$h_p = 2.3026\left(\frac{RT}{\nu}\right)\log_{10}\left(\frac{p_w}{p_0}\right) \tag{5}$$

where

h_p = the suction (in cm) of water at the Kelvin temperature (T),
R = the universal gas constant ($= 8.314 \times 10^7$ erg/°K-mole),
T = the absolute temperature (°K),
ν = 1.7686×10^4 gm-cm/mole-sec^2 for water,
pw/p_0 = the relative vapor pressure of water,

and

$$\log_{10}\left(\frac{p_w}{p_0}\right) = \frac{1.1389t + 2445.5646}{273.1 + t} + 8.2312\log_{10}(273.1 + t) - 11.09691 - 0.01019t - 0.12486 \times 10^{-5}t^2 + 9.084 \times 10^{-8}t^3$$

where

t = the temperature (°C),
p_w = the vapor pressure of unfrozen water at t°C, and
p_0 = the vapor pressure of water at 0°C ($= 4.579$ mm of mercury).

Thus, knowing the temperature allows the suction to be determined, and from the moisture characteristic curve, the unfrozen water is determined. Equations 2, 3, and 5 provide a continuous physical relationship among the variables of temperature, suction, and permeability. This addition has eliminated the need to identify zones as frozen, freezing, and unfrozen. A continuous process is now used to move from the unfrozen to the frozen condition.

Time Step-Depth Increment Relationships

The size of the time steps used in the program to march forward in time is of interest to the user for two reasons: (*a*) it controls the running time of the program to complete a full year and (*b*) if the time step is too large, it causes an unstable growth of the errors in computation. The CMS Model uses the forward difference method for which stability criteria are known. Experimentation with the CRREL Model has shown that it remains stable for much longer time steps than does the CMS Model. The maximum time steps that can be used in the Integrated Model are therefore controlled by the CMS Model and are summarized as follows:

Increment Size (in.)	*Time Step (hr)*
1.0	Unstable
2.0	0.125
4.0	0.50

TYPICAL OUTPUT RESULTS

The Integrated Model has been used at several sites to demonstrate both the accuracy and the discrepancies that may be expected between the predicted results and the actual observed values in the field. The source of the discrepancies is systematic errors in the Integrated Model. Such errors are introduced by assumptions that do not match the reality. They may be stated briefly as

1. The temperature and rainfall patterns generated by the Integrated Model.
2. The assumed water content-versus-suction relation in each soil layer, which does not include hysteresis.
3. The assumed permeability-versus-section relation in each soil.

4. The inability of the permeability relation to represent the effects of cracks in transmitting water in both liquid and vapor phases.

The Integrated Model does not "predict;" instead it computes expected results based on historical weather trends and is intended to be used for design purposes. In design, it is not essential to match exactly the measured temperatures, suctions, and layer moduli at the exact time they occur, but it is important to determine realistic ranges of these during each month and each season. This capability is more useful in design than any other; the comparisons made below demonstrate and compare typical results that can be expected from this computer model.

Measured field data from three sites were compared with the model, but because of space limitations only two are presented.

1. Amarillo, Texas, which represents a dry, freeze-thaw cycling climate with a clay subgrade.
2. Deland, Piatt County, Illinois, which represents a wet-hard freeze climate with a silty subgrade.

Comparisons at Amarillo, Tex.

The instrumented site in Amarillo has been built as a covered area analogous to a slab on an expansive clay subgrade with a 6-in. (15-cm) sand layer beneath a polyethylene plastic sheet 24 ft by 40 ft (7.3 m by 12.2 m) in plan dimensions. Surface elevations, suction, and temperature measurements to a depth of 8 ft (2.4 m) were made each month.

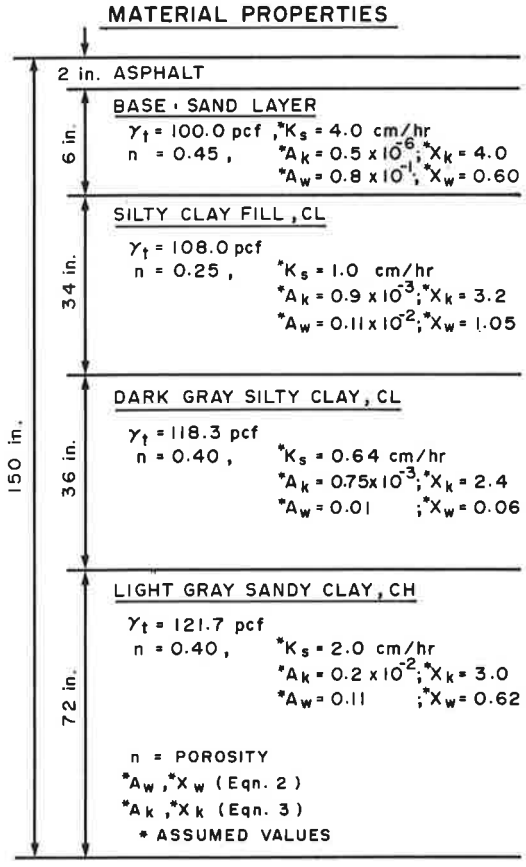

FIGURE 7 Amarillo, Texas: soil profile and properties.

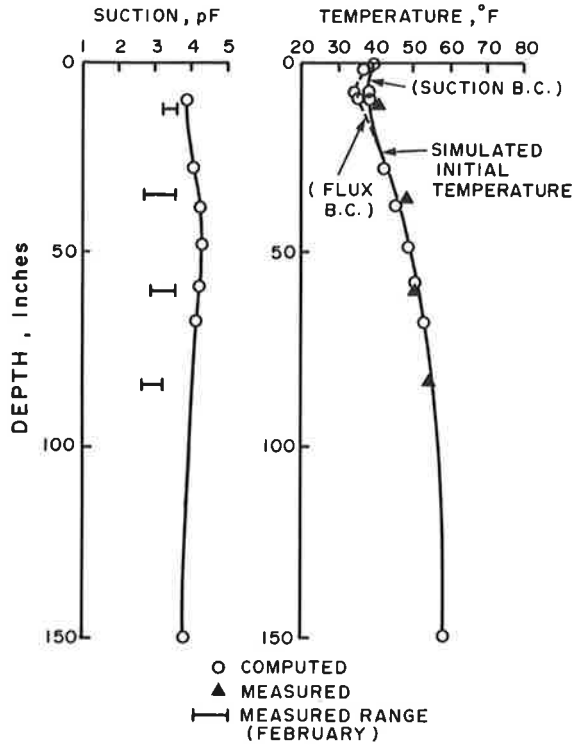

FIGURE 8 Amarillo, Texas: initial measured and simulated suction and temperature profiles, January 1.

The soil layers at the Amarillo test site are shown in Figure 7 along with the total unit weight, porosity, and assumed soil properties. Figure 8 shows the initial suction and temperature profiles assumed for a typical January 1 date along with measured values of the same profiles made in January. Figure 9 shows the measured and computed suction profiles at various times during the year. Figure 10 shows the measured and computed temperature profiles at the same times of the year. The difference in temperature profiles between the flux and suction boundary conditions brackets the actual measured temperatures, indicating perhaps that a different "*r*-value" for the flux boundary condition may be able to match the field temperature data very well while falling consistently within the measured suction range.

Comparisons at Deland, Piatt County, Illinois

The instrumented site in Piatt County, Illinois, near Deland was on a rural road, FAS Route 537. The pavement consists of a double bituminous surface treatment on an 8-in. (20-cm) aggregate base course that was 24 ft (7.3 m) wide with 6-ft (1.8-m) unpaved shoulders. Suction, temperature, and frost depth measurements were made periodically with the measurement dates spaced 3 to 4 months apart.

The soil layers and soil properties at the Piatt County site are shown in Figure 11. The water table fluctuated throughout

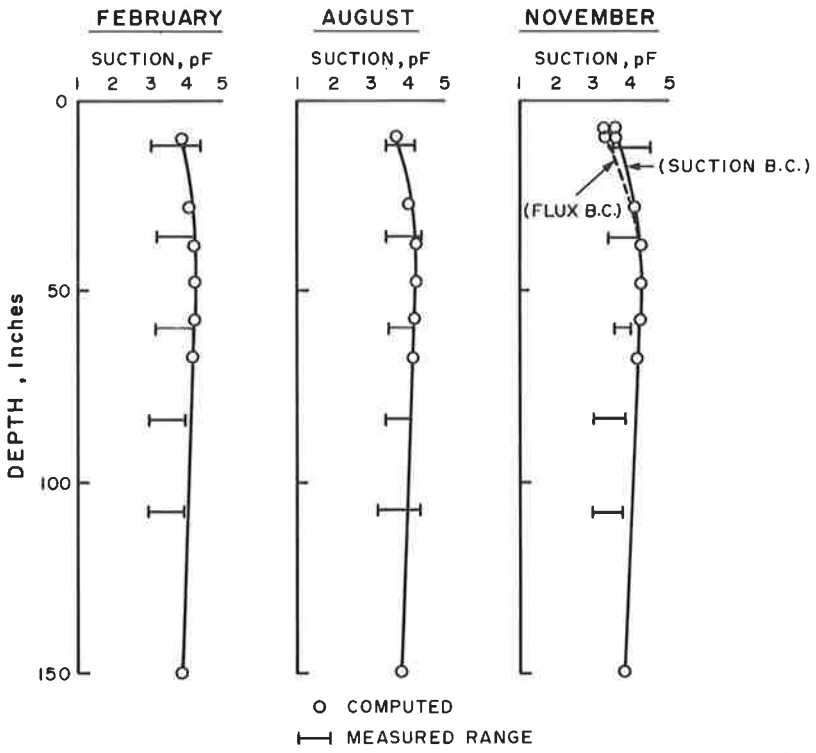

FIGURE 9 Amarillo, Texas: measured ranges and computed suction profiles at various times of the year.

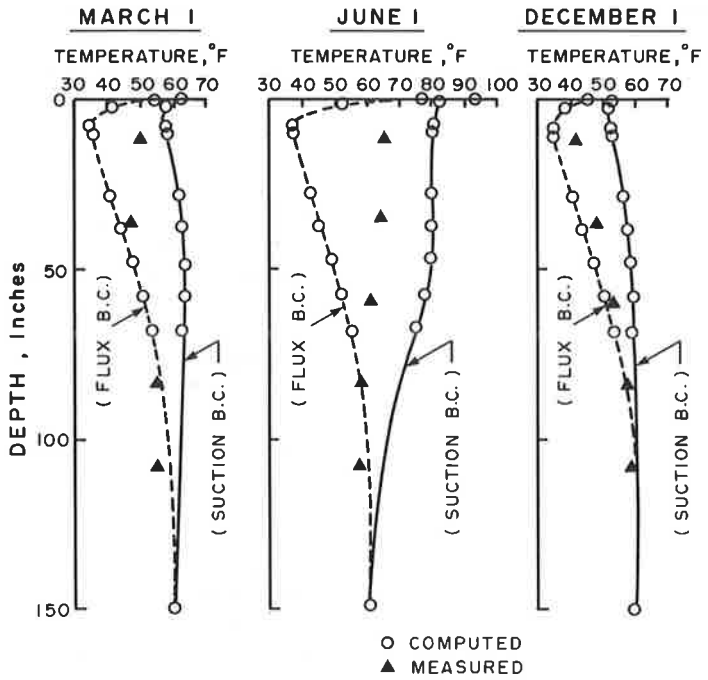

FIGURE 10 Amarillo, Texas: measured ranges and computed temperature profiles at various times of the year.

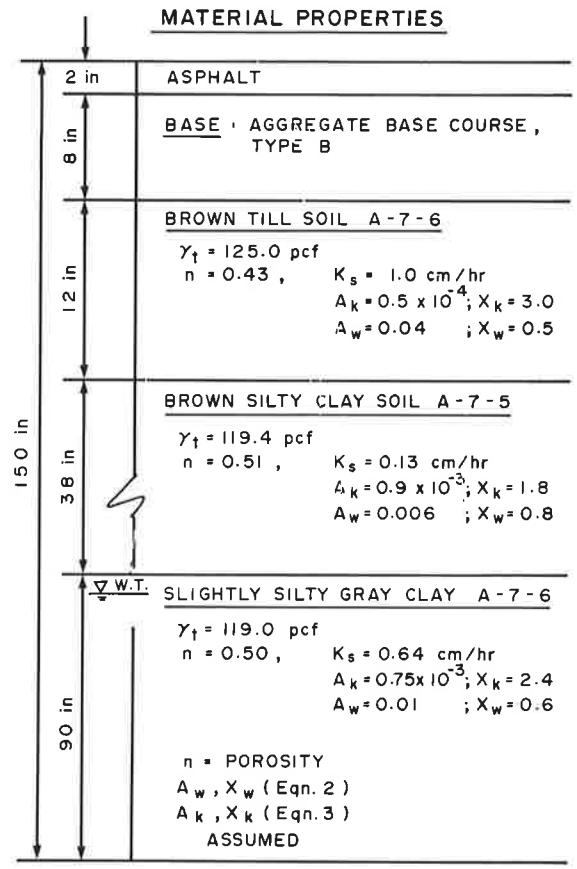

FIGURE 11 Deland, Piatt County, Illinois: soil profile and properties.

the year from a high elevation of 46 in. (1.2 m) below subgrade level to a low of 105 in. (2.7 m) below the subgrade. Figure 12 shows the assumed initial suction and temperature profiles for January 1 of the simulated year. In this case, both the flux and the suction boundary condition between the base course and subgrade provide practically the same pore water pressures as an initial condition. This is because of the small difference of negative pore water pressures at the interface between the base course and the subgrade. The initial temperature profile is virtually the same with both boundary conditions. Figure 13 shows the measured and computed pore water pressure profiles at two different times during the year. The computed pore water pressures are practically the same for both boundary conditions. Both have the same profile pattern and are nearly the same as the values measured with tensiometers.

Figure 14 shows the measured and computed temperature profiles at three different times during the year. The computed temperature profiles are the same to three significant figures for the two boundary conditions, unlike those for the Amarillo site. In the present case, both boundary conditions predict a temperature profile that is fairly close to the values measured in the field.

Evaluation of Simulations

The simulated temperatures using the two boundary conditions, flux and suction, commonly bracketed the measured values. The simulated suctions and pore water pressures followed the same patterns as in the measured data and were generally within the measured ranges. The temperature pro-

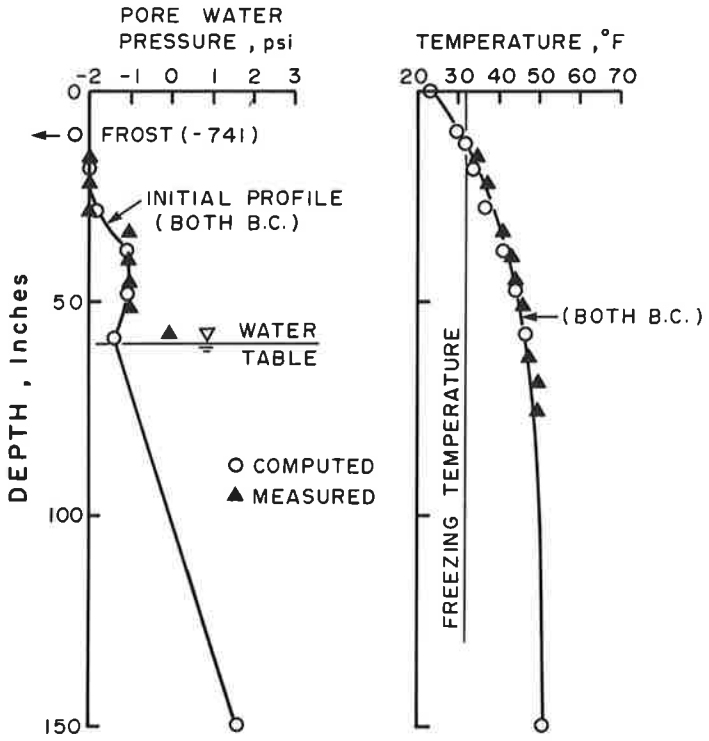

FIGURE 12 Deland, Piatt County, Illinois: initial measured and assumed pore water pressure and temperature profiles, January 1.

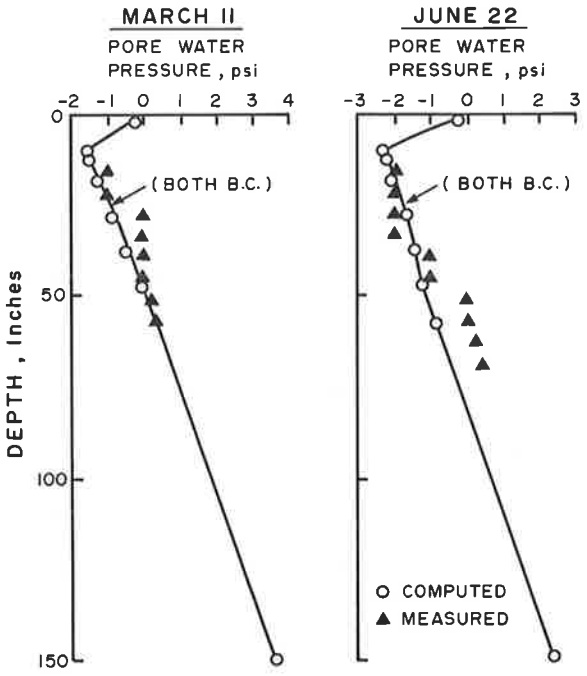

FIGURE 13 Deland, Piatt County, Illinois: measured and computed pore water pressure profiles at various times of the year.

files were particularly sensitive to the base course subgrade boundary condition. Because of this sensitivity, it is possible, by adjusting the flux by trial and error, to get the measured and computed temperatures to match as closely as desired, but there is no guarantee that the same boundary conditions and soil properties will provide as good a match to the temperature values observed in the following year. The measured suction values in Amarillo, Tex., had a much broader range at any given depth and time than the computed values. This range was undoubtedly because of the effects of the cracks in the clay soil subgrade that transmit water faster along specific paths than is estimated by the program. There is a tendency for the computed subgrade suction beneath pavements in these areas to become irreversibly wetter with time.

The positive and negative pore water pressures in Deland, Illinois, were predicted with reasonable accuracy.

As noted earlier, the objective of this program should not be to duplicate field measurements but rather to be able to generate patterns and ranges of the values that realistically match those measured in the field, for that is what is important in design. The program serves that purpose well.

CONCLUSIONS

The Integrated Model provides a simple, user-friendly simulation of weather patterns and computes temperature, suc-

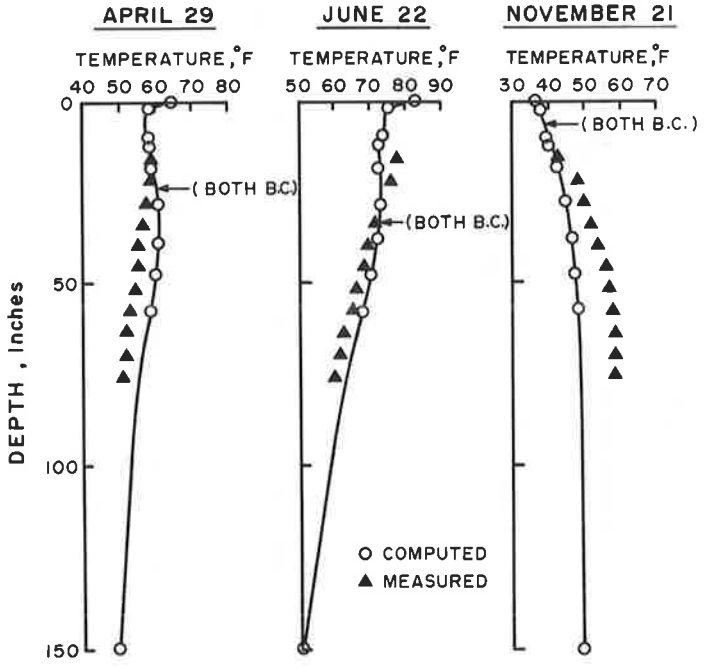

FIGURE 14 Deland, Piatt County, Illinois: measured and computed temperature profiles at various times of the year.

tion, and frost penetration profiles with depth that are realistic in their patterns and ranges when compared with those of actual field data. Because of this, the Integrated Model is expected to be a particularly useful method of simulating moisture and temperature conditions in pavements for use in design.

The final report, prepared for the Federal Highway Administration, provides a substantially more detailed description of the model, including additional simulations. In addition, the computer program is contained on IBM-compatible floppy disks. The final report, the computer program, and the user's Manual are available through the National Technical Information Service, Springfield, Virginia.

REFERENCES

1. H. S. Liang and R. L. Lytton. Rainfall Estimation for Pavement Analysis and Design. In *Transportation Research Record 1252*, TRB, Washington, D.C., 1989.
2. S. J. Liu and R. L. Lytton. *Environmental Effects on Pavement-Drainage*. FHWA, U.S. Department of Transportation, 1985, Vol. 4.
3. B. J. Dempsey, W. A. Herlach, and A. J. Patel. *The Climatic-Materials-Structural Pavement Analysis Program*. FHWA, U.S. Department of Transportation, 1984.
4. G. L. Guymon, R. L. Berg, and T. C. Johnston. *Mathematical Model of Frost Heave and Thaw Settlement in Pavements*. U.S. Army Cold Regions Research and Engineering Laboratory, Hanover, N.H., 1986.
5. *An Integrated Model of the Climatic Effects on Pavement*. Final Report. FHWA, U.S. Department of Transportation, 1990.
6. R. L. Berg. *Design of Civil Airfield Pavements for Seasonal Frost and Permafrost Conditions*. FAA Report No. FAA-RD-74-30. U.S. Department of Transportation, 1974.
7. P. W. Mitchell. *The Structural Analysis of Footings on Expansive Soil*, 2nd ed. Research Report No. 1. K.W.G. Smith and Associates, Adelaide, South Australia, 1980.
8. K. Russam and J. D. Coleman. The Effect of Climate Factors on Subgrade Moisture Conditions. *Geotechnique*, Vol. 3, No. 1, 1961, pp. 22–28.
9. C. W. Thornthwaite. Rational Classification of Climate. *Geographical Review*, Vol. 38, No. 1, 1948, pp. 55–94.
10. B. J. Fluker. Soil Temperatures. *Soil Science*, Vol. 86, No. 1, 1958, pp. 35–46.
11. *Water Supply Paper No. 520*. U.S. Geological Survey.
12. W. R. Gardner. Some Steady State Solutions of the Unsaturated Moisture Flow Equation with Application of Evaporation from a Water Table. *Soil Science*, Vol. 85, 1958, pp. 223–232.
13. E. W. Washburn. The Vapour Pressure of Ice and Water Below the Freezing Point. *Monthly Weather Review*, National Research Council, Vol. 52, Oct. 1924, pp. 488–490.

Publication of this paper sponsored by Committee on Environmental Factors Except Frost.